Phase Separation and Phase Preferences

in

Pigmented, Impact-Modified, PC/PBT Blends

VOLUME I

by

José Manuel Ribeiro Correia Afonso dos Santos

Submitted in accordance with the requirements for the degree of

Doctor of Philosophy

The University of Leeds

Department of Colour Chemistry

June 2003

ACKNOWLEDGEMENTS

I hereby acknowledge the invaluable support of my family and friends. Thank you for accompanying me throughout this endeavour and for your continuous support and understanding.

I am very grateful to my supervisor, Professor Jim Guthrie, for his friendship, guidance and encouragement. I owe a debt of gratitude to my colleagues Karen Fagelman and Carolyn Pearce for their patience and friendship. In addition, I acknowledge the help and collaboration of the members of staff of the Colour Chemistry Department and from the various Departments of the University of Leeds, without whom it would not had been possible to carry out this project.

Also, I am very thankful to the sponsors of this project, General Electric (Plastics), Bergen op Zoom (The Netherlands), for providing the opportunity to carry out this applied research study. I specially acknowledge the invaluable collaborations, discussions and guidance from the GE Plastics European Colour Technology group.

I also acknowledge the staff of the Department of Chemical Engineering of the University of Coimbra, Portugal, particularly Professor Helena Gil, for allowing me to use the facilities available in the Polymeric Materials Research Section.

A final thank you to my colleagues at the Polytechnic Institute of Bragança, Portugal, for their support during the writing-up process of this thesis.

ABSTRACT

Polycarbonate/poly(butylene terephthalate)/impact modifier (PC/PBT/IM) blends are a commercially important type of polymer blend. In recent years, pigmented PC/PBT/IM blends have been produced for specific applications, with particular attention being given to the method of mass coloration. The useful properties of these pigmented blends are determined, to a large extent, by the phase separation and phase preference phenomena that occur in these multi-component polymeric systems. In this study, the thermodynamic origins of the phase separation and phase preferences that exist in pigmented PC/PBT/IM blends have been assessed by means of inverse gas chromatography (IGC). Subsequently, in order to characterise these blends both physically and chemically, and to assess the influence of the pigment (C. I. Pigment Blue 28) on the physical properties, on the mechanical properties, and on the morphology of the blends, several analytical techniques and mechanical tests were used. These analytical techniques and mechanical tests, along with the controlled surface modifications of the pigment (which were achieved by means of a photo-sensitised grafting procedure), allowed for a rationalisation of the interactions that exist between the components of the pigmented blends as encountered in the phase separation, the phase preferences, the physical properties and the mechanical properties of these polymeric systems.

The Lewis acid/base interaction between the major components of these blends has been proven to influence decisively the physical properties and the mechanical properties of the pigmented PC/PBT/IM blends. Phase separation exists in PC/PBT/IM blends as the PBT molecules are preferentially involved in specific intermolecular, and intramolecular, interactions with themselves and other PBT molecules. Partial miscibility between the PC and the PBT has been interpreted on the basis of the Lewis acid/base attraction between these polymers, with contributions from the repulsion effect that exists between the Lewis basic centres in PBT. The impact modifier is shown to interact preferentially with the PC phase rather than with the PBT phase. This is due to the preference of the PBT molecules to interact with PBT molecules and to the strong Lewis base/base repulsion between the impact modifier PMMA shell and the PBT molecules. The fast crystallisation of PBT, favoured by the strong Lewis amphoteric character of this polymer, also contributes to the expulsion of the IM particles, and of the PC, from the PBT domains. The pigment interacts favourably with both the PBT and the PC, but preferentially with the PBT phase. This is because of the Lewis amphoteric properties of C. I. Pigment Blue 28.

The pigment under study, C. I. Pigment Blue 28, influences significantly the physical properties and the mechanical properties of the PC/PBT/IM blends. These effects differ for blends that have been processed in equipment and/or under conditions that lead to a lesser or greater degradation of the molecular weight of PC and of PBT. Also, the importance of the PBT-rich phase and of the PC-rich phase, in relation to the viscoelastic properties of the PC/PBT/IM blends,

depends on the magnitude of the molecular weights of PC and of PBT. The influence of the pigment on the physical and mechanical properties of the pigmented blends has both direct and indirect consequences. The direct consequences arise from the physical properties of the pigment (particle size and particle size distribution, surface area) and from the chemical properties of the pigment (inorganic nature, surface chemical composition). In particular, the surface chemical composition and the surface area determine the interaction potential of the pigment with the other components of the PC/PBT/IM blends. The indirect consequences stem from the influence the pigment has on the occurrence of transesterification, on the crystalline properties of PBT, and on the molecular weights of PC and of PBT. The influence of these factors on the physical properties and on the mechanical properties of the pigmented blends has been rationalised.

C. I. Pigment Blue 28 enhances the impact resistance of the blends by means of altering the mechanisms of absorption of the impact energy. The pigment decreases the crystallisation activation energy and increases the rate of crystallisation of PBT. The crystallinity degree is not directly affected by the presence of the pigment. At low loadings, the pigment enhances the transesterification reactions that occur between PC and PBT and the thermal degradation of the molecular weight of PBT. At greater pigment loadings, the pigment particles act as an inhibitor of the transesterification reactions and of the polymer chains thermal scission. The effect that C. I. Pigment Blue 28 has on the transesterification reactions is thought to be due mainly to the thermal conductivity differences between the inorganic pigment particles and the polymers.

Microscopic evaluations have established that the pigment is preferentially located at the PC/PBT interphase. This finding is in line with the predictions made from the IGC study and is substantiated by thermal analytical techniques and by mechanical testing of the pigmented blends. Control of the Lewis surface acid/base properties of C. I. Pigment Blue 28, by means of a photo-sensitised surface modification procedure, allows one to modify the preferential location of the pigment particles in the PC/PBT/IM blend. Accordingly, the physical properties and the mechanical properties of these pigmented blends are influenced. When the Lewis acidity of the pigment is significantly enhanced, the interaction of the inorganic particles with the PBT is improved. This results in a more significant nucleating effect of the pigment, an increased rate of crystallisation and an increased crystallinity degree of PBT. On subsequent reduction of the surface Lewis acidity of the modified pigment by neutralisation of the surface carboxylic acid groups, the interaction of the pigment particles with the PC phase is enhanced. The surface modifications lead to improved adhesion between C. I. Pigment Blue 28 and the polymeric matrix. This improvement in the adhesion, along with the changes to the phase preferences of the pigment, result in: 1) lower viscosity of the pigmented blends, due to improved dispersion of the modified pigments in the polymeric matrix; 2) very significant reduction of the transesterification reactions and of the thermal scission of the polymers, namely at the lower pigment loadings; 3) more consistent viscoelastic behaviour of the blends with varying pigment loading, and 4) less pronounced dependence of the impact resistance on temperature.

TABLE OF CONTENTS

VOLUME I

VOLUME II

LIST OF FIGURES

LIST OF TABLES

LIST OF ABBREVIATIONS

PC – Polycarbonate

PBT – Poly(butylene terephthalate)

IM – impact modifier

MBS – methyl methacrylate-butadiene-styrene

PE – poly(ethylene)

PVC – poly(vinyl chloride)

PET – poly(ethylene terephthalate)

EVA – ethylene-vinyl acetate copolymer

LLDPE – low pressure, low-density poly(ethylene)

EPR – ethylene-propylene rubber

EPDM – ethylene-propylene-diene rubber

NBR – nitrile rubber

PMMA – poly(methyl methacrylate)

MMA – methyl methacrylate

PS – poly(styrene)

MAA – methacrylic acid

TEA – triethylaluminium

PELTP – [pentaerythritol tetrakis(3-n-dodexyl thiopropionate)]

MZP – monozinc phosphate

C6 – n-hexane

C7 – n-heptane

C8 – n-octane

C9 – n-nonane

C10 – n-decane

C11 – n-undecane

TCM – trichloromethane

DCM – dichloromethane

DEE – diethyl ether

THF – tetrahydrofuran

Acet – acetone

EtAcet – ethyl acetate

hiwre – “Lewis acidic” pigment

hiwren – “neutralized” hiwre pigment

LCST – lower critical solution temperature

UCST – upper critical solution temperature

IGC – inverse gas chromatography

GC – gas chromatography

GPC – gel permeation chromatography

DMTA – dynamic mechanical thermal analysis

DTA – dynamic thermal analysis

DMA – dynamic mechanical analysis

DSC – Differential scanning calorimetry

TGA – thermogravimetric analysis

SEM – scanning electron microscopy

TEM – transmission electron microscopy

OM – optical microscopy

FTIR – Fourier transform infra-red spectroscopy

NMR – nuclear magnetic resonance (spectroscopy)

WAXS – wide angle X-ray scattering

XRD – X-ray difraction

EDX – Energy Dispersive X-ray Spectrometry

MAI – multi-axial impact

MVR – melt volume rate

VST – Vicat softening temperature

1. INTRODUCTION

1.1. Polymer Blends and the System Studied

Polymer blends, by definition, are physical mixtures of structurally different homopolymers or copolymers. In polyblends or polymer alloys, the mixing of two or more polymers leads to a new material with its own characteristic set of properties. The constituent polymers adhere together through the action of secondary bond forces only. In favourable cases, multiphase systems can display an interesting synergism of properties. The properties of immiscible and partially miscible blends are highly sensitive to their morphology: phase separation, (that is miscibility, connectivity and sizes of the phases, interface thickness), and phase preferences. These in turn strongly depend on the interactions between the blend components and on the processing conditions. Most polymers are mutually immiscible from the thermodynamic standpoint since the entropic contribution to the free energy of mixing is negligible (Delimoy *et al.* 1988; Favis 1991; Lyngaae-Jorgensen 1993; Al Saigh 1997b; Liang *et al.* 2000; Ryan 2002). Hence, most commercial polymer blends are multiphase systems.

Polymer alloys and polymer blends have been known since the 1940's. Such polymer alloys represent one of the faster growing sectors of the plastics industry (Utracki *et al.* 1989; Keskula and Paul 1994). In the recent past, research into polymer blends has increased significantly with more than 4500 patents being produced annually world-wide. In the 1980-1990 decade, the use of polymer blends in the market place was growing at approximately 10-15 % per year (Fayt 1989) compared to a growth of 4 % for all plastics (Favis 1991). The primary uses of polymer blends are in the automotive and business machine applications.

Blends can result in completely new materials that exhibit high degrees of synergism compared to the properties of the single components. In other cases, blends serve as materials with optimal cost/performance behaviour. Blending has several important economic advantages as it can: a) generate a material with unique properties and/or processability, b) extend the performance of expensive polymers, c) allow for the quick modification of performance, d) increase plant capacity since most polymer blends are processed on standard processing equipment, and e) be achieved through low capital investment and be accomplished much more rapidly than would developing a totally new polymer (Al Saigh and Chen 1991; Favis 1991; Mishra and Venkidusamy 1995). The major physical properties that are targeted for improvements in blending are: impact strength > heat deflection > cost/processability (Favis 1991).

In order to achieve the level of performance that is required of commercial polymers, additives are incorporated into formulations. Such additives include thermal stabilizers, UV

stabilisers, plasticizers, organic/inorganic pigments, other polymers to form blends and alloys, and reinforcing fibres to formulate high-performance material composites. Not infrequently, these additives are used in combination, thereby further complicating the composition of interfaces and their potential for interaction.

Particulate fillers, including glass beads and mineral fillers such as silicates, metal flakes and talc, are generally added to improve stiffness and compressive strength and to reduce shrinkages and the cost of the material. In most cases, the addition of these fillers tends to reduce the toughness of the thermoplastic matrix. However, a greater retention of the toughness can be obtained in fillers that have stronger interfacial adhesion with the matrix (Folkes and Hope 1993).

Commercial polymer blends or alloys normally consist of binary systems with partial solubility, thus containing more than two phases. Occasionally, a third component may be added to serve as a compatibiliser or as an impact modifier. Among the factors influencing the degree of solubility of the components and also the morphological structure of a moulded part, processing conditions play an important role (Bertilsson *et al.* 1988a; Ryan 2002).

Most commercial polymer alloys are prepared by mechanical mixing, largely because of the simplicity and low cost of such a procedure (Utracki *et al.* 1989). The preferred industrial method of mechanical mixing is to use a screw compounder or extruder that can operate continuously and can produce a product in a convenient form for further processing. Extrusion is, thus, the most common operation encountered in plastics processing.

Other methods for forming blends, such as by evaporation of a solvent or by polymerisation of a monomer in the presence of a polymer, involve at least three components in the preparation process, one of which is a solvent/polymerisation medium. These methods are not normally used commercially due to their being costly and the solvent being difficult to recover. There are also potential environmental hazards that are associated with handling large volumes of often toxic chemicals (Utracki *et al.* 1989).

Blends of thermoplastic polyesters with the polycarbonate of bisphenol-A constitute an important type of commercial blend. The alloys, usually with cocontinuous morphology, have good processability, heat and chemical resistance, elongation, low temperature impact and tensile strength. Most of these blends show high notched impact strength down to -40 ºC. From the commercial application point of view, it can be said that the major advantages of polycarbonate/poly(butylene terephthalate) (PC/PBT) alloys are increased stiffness, low susceptibility to stress cracking on contact with fuels and an improved resistance to chemicals and fuels (Utracki 1998).

PC/PBT blends are mainly used in the automotives industry for automotive body panels that require toughness at low temperatures, chemical resistance, heat resistance and dimensional stability, as encountred in dashboards, pillars, roof claddings, head lamp housings and luggage

racks. PC/PBT blends are also used in outdoor power equipment (tractor or lawn mower shrouds, consoles, grilles, trim and equipment parts), recreational applications, for the manufacture of consumer goods (vacuum cleaner housings and nozzles, utility locks, protective face guards, beverage containers, dishes, food transport bins, dinnerware, mixing bowls, salad tongs and swimming pool pump housings), telecommunications (radio housings, speakers and instrument housings) and many other applications (Utracki 1998).

PC/PBT blends are mainly processed by injection moulding. However, grades for extrusion, blow moulding as well as for transfer and compression moulding, solid state processing, and thermoforming are also available (Utracki 1998). The moulded parts can be painted, hot stamped, metalised and plated.

Commercial blends of PC and of PBT include Xenoy®, from General Electric Plastics, Makroblend®, from Bayer, Sabre® 1600 from Dow Chemical Company, Stapron® E from DSM and Ultrablend® KR from BASF.

The Xenoy® alloy, in particular, is commercially important, offering a very good balance of chemical and mechanical properties, good weatherability, low temperature impact strength, heat resistance, UV stability, colour retention, lubricity, and very good melt flow. Common applications of this alloy include automotive bumpers/ fascia, tractor hoods and panels, lawn mower decks, business equipment housings, outdoor recreational vehicle components, material handling pallets, cellular phones and large structural parts. Since its introduction as a bumper material on the Ford Sierra 1982 model, the Xenoy® alloy, a modified PC/PBT blend, has found wide use in automotive applications. Besides bumpers, painted as well as unpainted (Ford, Mercedes, BMW 7 series, Rover 4WD, Fiat Barchetta, Peugeot 2D coupe), substantial penetration has been achieved in other automotive applications such as cladding on trucks, trunklids (Volvo S80), doorhandles, tankflaps, and the like. In most of these applications, the Xenoy® PC/PBT blend has been chosen also for the obvious advantages over steel (weight reduction, design freedom, low cost forming/assembly) and also for its paintability, dimensional stability, high impact and fuel resistance and wide processing window. As far as the use of Xenoy® on the Smart car (commercialised by MCC Ltd.) is concerned, the applications consist of: door panels, front centre parts, front fenders, rear door panel, rear wheellarch cladding/bumper corner and rear bumper centre section.

References to studies carried out on Xenoy® blends can be found commonly in the literature. This literature demonstrates well the attention that academia has been giving to these commercial polymer alloys (Wahrmund *et al.* 1978; Birley and Chen 1984; Delimoy *et al.* 1988; Golovoy *et al.* 1988; Bertilsson *et al.* 1988a, 1988b and 1989; Dekkers *et al.* 1990; Bennekom *et al.* 1997b; Choi *et al.* 1998; Kakarala 1999; Umamaheswaran and Bax 1999; Tseng and Lee 2000b; Pickett 2001).

The polymeric system that is a major component of the current research is a mass-coloured thermoplastic alloy of a bisphenol A polycarbonate and a poly(butylene terephthalate) (Figure 1-1). A core-shell type elastomer (MBS rubber) is added to the polymer blend to improve its impact

toughness. The amorphous PC provides the impact resistance, the toughness, and the dimensional stability at elevated temperatures. The semi-crystalline PBT provides the chemical resistance and the thermal stability. The degree of chemical resistance of these blends is directly related to the relative percentage of PBT. In general, the higher the percentage of PBT the higher is the chemical resistance of the blend.

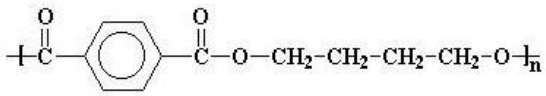

Poly(butylene terephthalate)

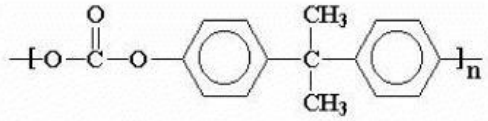

Bisphenol A Polycarbonate

Figure 1-1. Repeating unit in poly(butylene terephthalate) and in bisphenol A polycarbonate.

The matrix itself is created by extrusion of a mixture of the PC, of the PBT granulate, of a rubber based impact modifier and of additives (including anti-oxidants and a transesterification stabiliser). The blend displays a co-continuous morphology, with a designed miscibility level of the polymers of approximately 5-10 %.

Commercial, pigmented, impact-modified PC/PBT blends (for example Xenoy®, from GE Plastics) are currently commercialised in yellow, red, green, purple, brown, white and black colour forms, with an overlaid polyurethane clear coating to improve the weatherability. It has been stated by the manufacturers of mass-coloured Xenoy® that the colorant suppliers do not, currently, possess good knowledge with respect to this type of application (Timmerman, T. *et al.* 2001, Personal Communication). Thus, fundamental studies relating to the interactions between colorants and the remaining components of polymer blends, namely impact-modified PC/PBT blends, are of crucial importance to an understanding of the properties (physical, mechanical and coloristic) of these commercially important polymeric systems.

In the mass coloration of plastics, the pigment is added to the polymer matrix either during extrusion or during moulding. Some of the advantages of the mass coloration method over more traditional methods of decorating and/or coloration, such as painting or coating the plastic parts, include technological aspects, aesthetic aspects, lower cost factors and better environmental prospects. On the other hand, mass colouration can lead to a reduction in the material properties such as weatherability, physical properties, and mechanical properties. The effect of a pigment on such a system is dependent on the level of interaction between the various components of the blend.

A study of the effects of using C. I. Pigment Blue 28 on the mechanical properties and on the physical properties of mass-coloured PC/PBT/MBS rubber polymer blends constitutes a major component of the present programme. C. I. Pigment Blue 28 falls within the category of complex

inorganic coloured pigments, (also called mixed-metal oxide pigments), having a spinel structure (Figure 1-2).

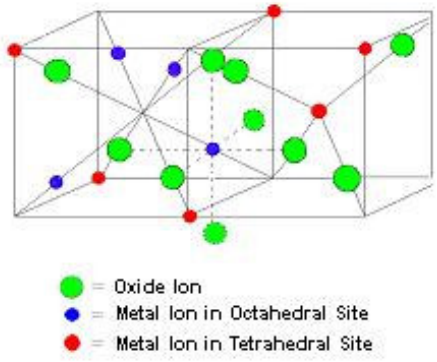

Figure 1-2. Spinel structure of C. I. Pigment Blue 28 ($CoAl_2O_4$).
The Al^{3+} cations are represented in blue, the Co^{2+} cations are represented in red and the O^{2-} anions are represented in green.

Inorganic coloured pigments have a widespread range of uses in applications such as paints, plastics, printing inks, building materials, and ceramics. This is due to their excellent hiding power, colour fastness and stability, heat resistance and their reasonable chemical resistance. These characteristics ensure that they are very suitable for use in plastic applications. However, there are some pigmentary exceptions to these performance characteristics. The application of inorganic pigments is influenced by their physical properties as well as their chemical properties. The particle size, shape, and surface properties are important in the pigment performance as is the surface chemical composition. The commercial form of C. I. Pigment Blue 28 is not surface treated.

1.2. Component Interactions in Polymer Systems

The strong correlations that exist between the morphology, the processing, and the physical properties in polymer blends are well recognised (Utracki *et al.* 1989; Ryan 2002). As the number of constituents in these blends increases, the ways in which the various components become dispersed and segregated during melt compounding become increasingly important. Among these added materials are the stabilisers, plasticizers, reinforcing fibres, pigments and other polymers.

It is well-known that, for polymer blends, the apparent properties and morphology often do not indicate an equilibrium situation (Schreiber 1993). In blends of an amorphous polymer and a semi-crystalline polymer, the phase behaviour is strongly dependent on blending and the cooling conditions. In the case of partial miscibility or of complete miscibility of the components in the

molten state, the cooling rate and the kinetics of non-isothermal crystallisation influence the final extent of phase separation at room temperature.

The morphologies of two-component polymer blends have been widely discussed in the literature as these represent the more common commercial form of polymer blends. In response to commercial pressures and to the need for precisely tailored physical properties, more complex blends that consist of multiple components are under active development. In such blends, morphological concerns go beyond questions concerned with the dispersed phase size, anisotropy, etc., to include more subtle issues such as why one of the dispersed polymer phases may spontaneously encapsulate another (Schreiber and Germain 1990) or encapsulate the filler particles (Premphet and Horanont 2000). Obviously, in multi-phase polymer systems, interfaces and interphases must exit. Therefore, it is reasonable to assume that under equilibrium conditions, such effects must arise from interfacial energy differences among the blend components. Surface and interfacial phenomena have been proven to influence:

i) The dispersion of minor phases in polymer matrices (Boluk and Schreiber 1986; Boluk and Schreiber 1989);

ii) The processability of polymer blends and composites (Malik *et al.* 1988; Trujillo *et al.* 1988), and

iii) The mechanical properties of polymer blends (Ishida 1984; Ratzsch *et al.* 1990).

The use properties of polymer blends depend strongly on the miscibility (compatibility) of the polymers. For the particular case of binary polymer blends, according to Raetzsch (1990), to state that two polymers are partially miscible implies that a two-phase structure is generated when they are mixed. Both phases contain different but limited amounts of each component. Miscibility occurs when specific interaction forces develop between the two polymers (Al Saigh and Chen 1991; Coleman *et al.* 1991). Specific interactions may be in the form of hydrogen bonding, charge transfer complexes, acid-base type interactions, dipole moments, and electron donor-acceptor complexes (Ponec *et al.* 1974; Huyskens *et al.* 1991; Israelachvili 1991; Lara and Schreiber 1991b; Stone 1998). These specific interactions are of a highly directional nature and are present in addition to the dispersive forces. A current view, pioneered by Fowkes (Fowkes and Mostafa 1978; Fowkes 1980, 1983a, 1983b and 1990; Lara and Schreiber 1991b; Nardin and Schultz 1993a; Liang *et al.* 2000), which is increasingly accepted, suggests that the totality of specific interactions may be viewed as acid/base forces. This approach has been supported by experimental results (Liang *et al.* 2000).

From the above description it is clear that there is a link between component interactions on the one hand and the rheological, physico-chemical and mechanical properties of the system, on the other.

1.2.1. Thermodynamic Requirements for Miscibility in Polymer Blends

The basic question when considering a polymer blend concerns the extent of thermodynamic miscibility. Several polymer pairs are known to be miscible or partially miscible, and many of these have become commercially important (Utracki *et al.* 1989). Considerable attention has been focused on the origins of miscibility and on binary polymer/polymer phase diagrams. It is usually observed that high molar mass polymer pairs, showing partial miscibility, exhibit phase diagrams that indicate a lower critical solution temperature (LCST) (Utracki *et al.* 1989; Bonner and Hope 1993; Cheng *et al.* 1996; Pompe 1997). In a polymer blend that exhibits LCST behaviour, the miscibility is higher at low temperatures. As temperature increases phase separation occurs because the intermolecular attractive forces responsible for the miscible behaviour tend to disappear as the internal energy of the molecules becomes high enough to overcome them.

The classic Flory-Huggins theory and extensions of this model, have been most helpful in providing an understanding of the phase behaviour of polymer blends (Ratzsch *et al.* 1990). Miscibility is understood to be the penetration of components on the molecular level, analogous to the behaviour of low molecular weight substances. Fundamentally, one thermodynamically describes the miscibility of two arbitrary components by the Gibbs free energy of mixing, ΔG_{mix}:

$$\Delta G_{mix} = \Delta H_{mix} - T\Delta S_{mix} \qquad (1\text{-}1)$$

Here ΔH_{mix} denotes the enthalpy of mixing and ΔS_{mix} denotes the entropy of mixing.

Any two components are mutually miscible if the mixing free energy of the systems meets the following conditions (Lyngaae-Jorgensen 1993; Al Saigh 1997b):

$$\Delta G_{mix} < 0 \qquad \text{Scheme 1-1}$$

$$\left(\frac{\partial^2 \Delta G_{mix}}{\partial \phi^2}\right)_{p,T} > 0 \qquad \text{Scheme 1-2}$$

Here ϕ is the molar fraction of a component.

For spontaneous mixing, the value of ΔG_{mix} must be negative. Thus, and bearing in mind the small contribution of the entropy of mixing to the free energy of mixing, exothermic mixtures ($\Delta H_{mix} < 0$) will mix spontaneously. On the other hand, for endothermic mixtures, miscibility will only occur at high temperatures. The condition expressed in Scheme 1-2 means that, mathematically, ΔG_{mix} (ϕ) is a convex function of the composition of the mixture (ϕ). This results in the well-known phase diagram with its lower critical solution temperature (LCST) or the upper critical solution temperature (UCST) either bimodal or spinodal. From the above it follows that the mixing process, in blends exhibiting LCST behaviour, is an exothermic process and that the mixing process of blends exhibiting UCST behaviour is an endothermic process. However, most polymers are not fully miscible, so that a complete thermodynamic description is not possible since the phase separation diagram cannot be determined. This apparent “chemical incompatibility” results, in

many cases, in the creation of a stable, finely dispersed distribution of the polymers in one another (Ratzsch *et al.* 1990).

In Equation 1-1, the combinatorial entropy of mixing of components 1 and 2 depends on the number of molecules present, according to Equation 1-2 (Utracki *et al.* 1989):

$$\frac{\Delta S_{mix}}{RT} = n_1 \ln \phi_1 + n_2 \ln \phi_2 \qquad (1\text{-}2)$$

Here, ϕ_1 is the molar fraction of component 1 in the mix and ϕ_2 is the molar fraction of component 2 in the mix. R is the gas constant and T is the temperature. The parameters n_1 and n_2 are the number of moles of molecules of components 1 and 2, respectively. Therefore, as the molar mass increases, the number of molecules per unit mass becomes small and the combinatorial entropy of mixing becomes negligibly small (Lyngaae-Jorgensen 1993).

In order to explain phase separation that occurs on heating, i. e. LCST behaviour, the effect of volume changes on mixing must be considered. This effect is described by equation-of-state theories such as that developed by Flory and co-workers (Utracki *et al.* 1989). The free volume contributions to the free energy are unfavourable and increase with temperature.

A question arises as to why miscible polymer pairs exist. In the case of polymers that are very similar physically and chemically, the occurrence of miscibility is comprehendible. If that is not the case, the major driving force for miscibility must be the enthalpic contributions to the free energy (Utracki *et al.* 1989). There are two ways, not mutually exclusive, of explaining favourable enthalpic contributions (Utracki *et al.* 1989; Lee *et al.* 2001):

a) Positive interactions between the two polymers, and

b) Unfavourable interactions between groups on the same polymer, causing an overall favourable interaction with another polymer.

Examples of favourable interactions between the polymer chains include specific intermolecular interactions, such as acid/base interactions involving hydrogen bonds. In these cases, phase separation that occurs on heating may be due to dissociation of the hydrogen bond matrix (Utracki *et al.* 1989).

If the groups within the same polymer chain have a large enough unfavourable interaction, they will prefer to mix with another polymer group, in order to minimise the number of unfavourable-unfavourable contacts (Bertilsson *et al.* 1988b; Lee *et al.* 2001). A copolymer is often found to be miscible with another polymer over some range of monomer composition. The use of a cross term in the free energy expression allows for the description of this phenomenon (Utracki *et al.* 1989). It should, however, be pointed out that in the above case, if one simply ascribes a single solubility parameter to each monomer, it is impossible to predict an overall negative enthalpy of mixing (Utracki *et al.* 1989). Furthermore, it has been noted that a window of miscibility can be

explained by the presence of a favourable specific interaction without recourse to a cross term. If one separates the normal dispersive forces from the specific interaction then, as a first approximation, when the solubility parameters of the two polymers are similar, the unfavourable dispersive interactions are small and the specific interactions yield miscibility.

Summarising, it can be said that for most miscible blends, the miscibility stems from specific interactions. However, the miscibility can also originate from reduction of unfavourable specific interactions between groups of the same polymer (Bertilsson *et al.* 1988b; Utracki *et al.* 1989; Lee *et al.* 2001).

1.2.2. The Solubility Parameter – Relevance to Interactions in Multicomponent Polymeric Systems

One widely used approach to the quantification of interactions that occur in multicomponent polymeric systems is through the determination of "solubility" or "cohesion" parameters, δ_T. The parameter is, in effect, the square root of a cohesive energy density, as defined by Hildebrand in Equation 1-3 (Jackson *et al.* 1994; Walker and Collyer 1994; Guthrie 1996):

$$\delta_T = \left(\frac{\Delta H_v}{V} \right)^{1/2} \tag{1-3}$$

Here ΔH_v is the molar vaporisation energy of the substance and V its molar volume.

The solubility parameter was originally intended to be applied to substances whose cohesion arises from dispersion forces (Fowkes *et al.* 1990). Consequently, this parameter seems to be of limited use with polymers that generally decompose before vaporisation enthalpies can be determined (Schreiber 1993). Since then, the concept underlying the use of solubility parameters has been greatly expanded. The overall δ_T can be divided into dispersion contributions and polar contributions. Often non-polar homomorphs of polar molecules can provide values for the dispersive contribution, δ_d, and the polar contributions, δ_p, can then be obtained from differences between δ_T and δ_d. Further refinements (Fowkes 1980 and 1983a; Schreiber 1993; Walker and Collyer 1994) due to Hansen, have introduced a three-component solubility parameter, which separates non-dispersive contributions into polar components and hydrogen bond components. This has been applied to organic liquids and some polymers (Walker and Collyer 1994). Calculations of δ_T for macromolecules can also be made from tabulated values of molar attraction constants, as carried out, for example, by Ryan and colleagues (1988). Extensive summaries of δ_T and of other cohesion parameters are readily available in the literature (Ryan *et al.* 1988; Walker and Collyer 1994).

Some researchers (Walker and Collyer 1994; Liang *et al.* 2000), consider that the use of solubility parameters is best restricted to the estimation of dispersion forces at interfaces, and is less

reliable as an indication of short-range polar, or acid-base interactions, for semi-crystalline polymers and for crosslinked polymers.

For solids, polymers, and many liquids, it is necessary to use indirect evaluation methods in the estimation of solubility parameters, as such materials have a vapour pressure that is too low to detect. Although these indirect methods are useful, they are also tedious and time consuming.

Furthermore, ultimately, the application of δ_T to polymer systems is impeded by the following factors (Hobbs *et al.* 1988a; Schreiber 1993; Liang *et al.* 2000):

1) No direct, experimental determinations of δ_T for polymers exist to corroborate the validity of calculations and inferences. Only relatively complex scattering techniques being promising in this regard;

2) Available solubility parameters generally apply to polymers as solutes at very high dilution. The concentration dependence of δ_T is difficult to assess;

3) Data generally apply to room temperature conditions. The evaluation of a temperature dependence of behaviour is problematic.

1.2.3. Interaction Parameters from Polymer Solution Theories

Polymer solution thermodynamics, as developed firstly by Flory and Huggins (Su *et al.* 1976; Galin and Rupprecht 1979a-c; Ward *et al.* 1980), express the interaction between a polymer and a liquid in terms of a dimensionless parameter, $\chi_{1,2}$. This can be written as Equation 1-4:

$$\chi_{1,2} = \frac{\mu_1 - \mu_2}{RT\varphi_1^2} - \left(\ln \varphi_1 + \left(1 - \frac{V_1}{V_2} \right) \varphi_2 \right) \varphi_2 \qquad (1\text{-}4)$$

The subscripts 1 and 2 denote the liquid (solvent) and the polymer (solute), respectively. μ is the chemical potential, φ are the volume fractions and V molar volumes. Miscibility occurs when $\chi_{1,2}$ is lower than a critical value, or lower than zero.

The parameter $\chi_{1,2}$, as expressed in this manner, indicates intermolecular forces between the components of any polymer-liquid mixture. Therefore, this parameter is not dependent on the choice of theory or theoretical model. Its usefulness in practice, however, is once more limited because $\chi_{1,2}$ is usually determined by methods such as vapour pressure lowering, osmotic pressure effects, equilibrium swelling of polymers by liquids, light scattering, etc (Liang *et al.* 2000). In all of these cases, the “interaction” describes systems in which the polymer is at very high dilution. The temperature range over which the data may be collected is narrow and often far removed from conditions of interest. Moreover, these methods do not lend themselves readily to evaluations of what often are the more important interaction data – those between the solid components of a polymer system.

The Flory-Huggins parameter, χ, can be measured from the surface tensions that operate in a melt and by inverse gas chromatographic evaluations (Lara and Schreiber 1991b). However, using the aforementioned techniques, it is not easy to measure χ exactly (Ratzsch *et al.* 1990). An alternative approach may be used to try to overcome that problem. This involves the calculation of the interfacial tensions from measurements of the thickness of the interfaces. This, in turn, is not easily achieved (Utracki *et al.* 1989). Nevertheless, using this method, an inverse proportionality of the interfacial tension to the thickness of the interlayer, as described by Raetzsch (1990), is obtained. Other approaches exist to determine χ for polymer blends. These include the use of the T_g (Kim and Burns 1989) and the use of T_m (Al Saigh and Chen 1991; Cheng *et al.* 1996), based on the effect of miscibility on these characteristic temperatures.

1.2.4. Work of Adhesion and Interfacial Tension

Researchers such as Raetzsch (1990) and Liang (2000) studied miscibility phenomena of polymer blends based on the presence of interfaces in multiphase polymer mixtures, employing the thermodynamic work of adhesion between two different solids and interfacial tension determinations. This specific thermodynamic adhesion energy (W_a) or, in the case of a known adhesion distance, the specific adhesion strength between two solids, can be determined from the respective surface tensions, γ_1 and γ_2 and the interfacial tension γ_{12}, Equation 1-5 (Dupré's equation):

$$W_a = \gamma_1 + \gamma_2 - \gamma_{12} \tag{1-5}$$

The surface tension is a manifestation of intermolecular forces. The molecules at the surface of a liquid or a solid are influenced by unbalanced molecular forces and, therefore, possess additional energy in excess of the bulk molecules of the solid or liquid phase, that is, surface free energy.

Interactions in liquids and at polymer and solid surfaces and interfaces arise essentially from two types of forces. The first are the comparatively weak van der Waals dispersion forces (London forces, Debye forces and Keesom forces), which are universal. The second type, the specific (non-dispersive) forces, often designated "polar" forces, are present solely in polar molecules.

The surface tension, γ, is the sum of the components γ_d and γ_p. Thus:

$$\gamma = \gamma_d + \gamma_p \tag{1-6}$$

Here γ_d is the apolar dispersive component and γ_p is the "polar" component. The polar component includes the contribution of the dipole forces (electrostatic in origin) and of the acid-base (electron donor/electron acceptor) forces.

The interfacial tension, γ_{12}, between the polymers can be calculated from the individual surface tensions and their component terms (Ratzsch *et al.* 1990), Equation 1-7:

$$\gamma_{12} = \gamma_1 + \gamma_2 - \frac{4\gamma_1^d \gamma^d}{\gamma_1^d + \gamma_2^d} - \frac{4\gamma_1^p \gamma_2^p}{\gamma_1^p + \gamma_2^p} \quad (1\text{-}7)$$

Fowkes has proposed that non-dispersive interactions should be represented quantitatively as Lewis acid/base, or electron acceptor/donor effects (Fowkes and Mostafa 1978; Fowkes 1980, 1983a, 1983b and 1990). Accordingly, the strength of an interface, as represented by the work of adhesion, can be written as:

$$W_a = W_d + W_{ab} \quad (1\text{-}8)$$

Here "ab" represents acid/base effects. W_{ab} can be estimated using the notion of acidic, γ^+, and basic, γ^-, components of the surface tension, according to the van Oss equation (Chehimi *et al.* 2002):

$$W_{ab} = 2(\gamma_1^+\gamma_2^-)^{0.5} + 2(\gamma_1^-\gamma_2^+)^{0.5} \quad (1\text{-}9)$$

The contribution of the dispersive forces to the work of adhesion can be quantified by means of the approach of Fowkes (Fowkes *et al.* 1990; Riddle and Fowkes 1990):

$$W^d = 2(\gamma_1^d \gamma_2^d)^{0.5} \quad (1\text{-}10)$$

In the same manner, the surface energy can be represented as:

$$\gamma = \gamma_d + \gamma_{ab} \quad (1\text{-}11)$$

The assumption is made that other non-dispersion (e.g. dipole) forces may be neglected. The total contribution of acid-base interaction to the surface tension is:

$$\gamma_{ab} = 2(\gamma^+\gamma^-)^{0.5} \quad (1\text{-}12)$$

It has been increasingly recognised that the convention adopted in first place by Fowkes for the non-disperive component of the free energy, γ_{ab}, is more adequate to the description of these forces than is the "old" concept of polar interactions, γ_p. This is due to the greater contribution of the acid/base forces, in comparison with the contribution of the dipole forces, to the total "polar" forces, in liquids, and at interfaces (Fowkes 1991).

Equation 1-6 is only valid provided that no reaction takes place between the polymers and is limited to polymers whose polar components and apolar components of the surface tension have been experimentally determined or theoretically estimated. Furthermore, knowledge of the surface tension components at wide temperature ranges is quite limited as far as published data are concerned. This is understood bearing in mind, for example, the commonly used contact angle method for the determination of surface tension values.

The quantitative measurement of the interfacial tension still remains a subject of controversy (Liang *et al.* 2000). Some of the approaches used include the acid-base rationalisation of surface and interfacial energies, pioneered by Fowkes (Fowkes and Mostafa 1978; Fowkes 1980, 1983a

and 1983b), and other such as alternative acid-base rationalisation due to Good and colleagues, equation-of-state arguments by Neumann and colleagues, and the association of surface and interfacial energies with the Gibbs-Thomson equation. Nevertheless, values of interfacial tension calculated by these various approaches can differ by more than two orders of magnitude (Liang *et al.* 2000).

Experimental methods for the determination of interfacial and surface tension include the abovementioned contact angle method, whose use must take into account the possible time-dependence of contact angle values, the relatively narrow temperature range limitation, and the influence of factors such as the surface roughness and heterogeneity, and bulk penetration of the liquid. Other experimental methods for the determination of the surface free energy include extrapolation of the surface tension of polymer melts to room temperature (Hobbs *et al.* 1988a) and also the pendant drop and the spinning drop methods (Liang *et al.* 2000). However, the latter two methods are complex equilibrium techniques and generally require long experimental times, putting in jeopardy the thermal stability of polymers (Liang *et al.* 2000).

1.2.5. Inverse Gas Chromatography and Some of Its Uses

The growing awareness of the importance of solid surfaces, interfaces and interphases in determining the useful properties of polymeric systems, has led to the development of inverse gas chromatography (IGC) as a useful technique in evaluating the potential for interaction of different components of polymer blends, composites, and multicomponent polymeric systems. The ability of the IGC technique to provide information concerning the acid/base interaction potentials of polymer surfaces is widely recognised in the literature· Data obtained from IGC experiments may, in favourable cases, correlate directly with observed performance criteria, such as colour development, gloss, rheological properties, adhesion and mechanical properties (Schultz and Lavielle 1989; Lee 1991; Mukhopadhyay and Schreiber 1993).

The first papers on IGC go back 30 years. Two papers were published in 1972 and from then the number of publications has increased significantly. In 1993, 93 papers were published and since then an average of 65 papers per year has been published. Most of the papers published, especially is the last 10 years, deal directly with assessment of practical problems, not just mere academic curiosities.

The fields of application of IGC include polymers, paper and other cellulosics, fillers and pigments, flavourings and perfumes, minerals and inorganic materials, food products and ingredients, packaging and coatings, pharmaceuticals and medical products, building materials, cosmetics, natural and artificial fibres, supported catalysts, and microporous materials.

The main difference between conventional gas chromatography (GC) and IGC lies in the fact that the species of primary interest are not the volatile components injected but the material acting as the stationary phase, typically a powder, fibre or film. This material may be packed directly into

the column, coated onto a suitable support or coated onto the walls of the column. This allows the investigation of the interactive nature via the degree of interaction with well-characterised volatile liquids/vapours ("probes"). Quantification of this interaction may be achieved by the determination of the retention time, t_r, for a given probe. In most uses, the quantity of probe vapour injected into the carrier gas is extremely small. Thus, the retention data relate to the thermodynamic interaction that occurs between polymer and the vapour when the polymer is highly concentrated, as in most practical situations. Furthermore, IGC experiments may be carried out over appreciable temperature ranges, so that the temperature dependence of thermodynamic interactions is no longer indeterminate.

The IGC technique has been extended to allow for measurements of interactions that occur between mixed stationary phase components (Su *et al.* 1976; El Hibri *et al.* 1989). Useful values of the Flory-Huggins parameter, χ, may be obtained for polymer blends and for mixtures of polymers with fibres, pigment, etc.

Further advantages of IGC over other methods include:

1) The ability to quantify strong interactions that occur between the support and the probe (strong interactions cannot be characterised by contact angle measurement because such interactions give rise to contact angles that are close to zero);

2) Nanorugosity and surface heterogeneity is not a problem as it is in the case of contact angle measurements;

3) The fact that this approach is less time consuming than other methods;

4) The fact that the method is accurate, versatile, with relatively easy sample preparation, and

5) The reality that there is no need for expensive equipment.

As well as providing thermodynamic information, the IGC technique is an excellent technique for determining phase transitions, for measuring adsorption properties, and so on. This is illustrated by the following list, in which are compiled parameters/phenomena that can be studied by the IGC technique, together with relevant information sources.

a) Flory-Huggins solubility parameters (Ward *et al.* 1981; Chen and Al Saigh 1989; Prolongo *et al.* 1989; Al Saigh and Chen 1991; Lara and Schreiber 1991b; Shi and Schreiber 1991 and 1992);

b) Crystallinity of semi-crystalline polymers (Lipson and Guillet 1982; Guillet *et al.* 1989; Shi and Schreiber 1991; Al Saigh 1997b);

c) Phase separation phenomena in immiscible polymer blends (Ward *et al.* 1981; Klotz *et al.* 1989; Mandak *et al.* 1989; Xu *et al.* 1999; Santos *et al.* 2002a);

d) Surface/bulk composition differences in polymeric systems (Lipson and Guillet 1982; Shi and Schreiber 1991 and 1992; Jones and Kramer 1993);

e) Surface roughness (nanorugosity) of solids (Brendle and Papirer 1997a and 1997b);

f) Surface areas of phase domains, and molecular areas (Lipson and Guillet 1982; Guillet *et al.* 1989; Qin and Schreiber 1994);

g) Surface energy of solids (dispersive and specific components of the surface free energy, enthalpy and entropy of adsorption) (Hegedus and Kamel 1993a and 1993b; Murakami 1994; Goss 1997; Santos *et al.* 2001; Santos *et al.* 2002a; Santos *et al.* 2002b);

h) Infinite dilution activity coefficients (Sadowski *et al.* 1997);

i) Glass transition temperature, T_g, and melting temperature, T_m, of polymers (Guillet *et al.* 1989);

j) Barrier properties of polymeric systems (Lipson and Guillet 1982).

Given this range of parameters/phenomena and the continued growth of material science, it is reasonable to conclude that IGC studies will continue to play an important role in furthering an understanding of the behaviour of polymeric materials, and in helping to design multicomponent systems that meet desired targets of performance and durability.

1.2.5.1. IGC and Quantification of Interactions in Multicomponent Polymeric Systems

The relationship between intermolecular interactions and system properties is particularly important in polymer compositions, bearing in mind the variety of polymers and additives that are used to achieve desired performance requirements.

Intermolecular forces that are operating between molecular segments of polymers and at particulate interfaces are frequently cited in the literature (Fowkes *et al.* 1990; Schreiber and Germain 1990 and 1991; Dwight *et al.* 1991; Finlayson and Shah 1991; Fowkes 1991; Huang *et al.* 1991; Jensen 1991; Lee 1991; Ma *et al.* 1991; Tiburcio and Manson 1991b) as being responsible for the properties of the system as a whole. Control of Lewis acid/base interactions has gained increasing significance in industrial practice (Schultz and Lavielle 1989; Lara and Schreiber 1991b; Mukhopadhyay and Schreiber 1993) for optimising the performance of polymer composites. This is because such intermolecular forces are known to dominate over dispersion intermolecular forces and dipole-dipole intermolecular forces (Boluk and Schreiber 1986; Fayt *et al.* 1989; Schultz and Lavielle 1989; Utracki *et al.* 1989; Fowkes *et al.* 1990; Al Saigh and Chen 1991; Coleman *et al.* 1991; Huyskens *et al.* 1991; Lara and Schreiber 1991b; Schreiber and Germain 1991; Tiburcio and Manson 1991b; Bonnerup and Gatenholm 1993; Mukhopadhyay and Schreiber 1993; Zhang and Leonov 2000). This is clear in the definition of specific interactions, given by Huyskens (1991): “Specific interactions are short-range, site-bounded cohesion forces that considerably weaken a

given chemical bond of one of the partners". Furthermore, from a thermodynamic point of view, specific interactions between chemical moieties are required in order to obtain a negative excess free energy by mixing (Pompe 1997). Some illustrative examples of the importance of Lewis acid/base interactions, quantifed by means of IGC, are described in the next paragraphs.

A strong correlation has been found by Liang and colleagues (2000) between the interfacial tension of polymer pairs and their acid-base pair interaction, as determined by IGC. The relationship is inverse, with interfacial tensions decreasing as acid-base interactions increase. The existence of acid-base interactions among the components of a polymeric system may also be cited as a source of compositional variation at the surface, or within the bulk, of the system (Shi and Schreiber 1992). Raetzsch (1990) demonstrated that a correlation exists between the difference of the polar component of the interfacial tension and the particle size of the dispersed phase and on the mechanical properties in polymer blends.

The interaction of a filler with itself, and with the fluid medium, influences to a large extent its state of dispersion and, in the end, the quality and the performance of the composition into which the filler is incorporated. If the acceptor and donor numbers of a filler are known, one can anticipate the behaviour of the filler with respect to the adsorption of polymers (Papirer *et al.* 1991; Wang *et al.* 1997), and to the mechanical properties of composites (Flour and Papirer 1983; Schultz and Lavielle 1989; Xu and Schreiber 1998) and film-forming polymers (Lara and Schreiber 1991a). Good examples can be found in the literature concerning the way in which IGC characterisation, associated with controlled surface modification, leads to a better knowledge of the surface physico-chemistry of fillers (Balard and Papirer 1993; Wang *et al.* 1997; Xu and Schreiber 1998).

Schreiber and colleagues used IGC for the evaluation of Lewis acid/base interaction parameters for PE, PVC, and $CaCO_3$ (Schreiber *et al.* 1982). The surface Lewis acid/base characteristics of the filler were controlled by microwave plasma surface treatments using acidic and basic vapours. It was concluded that the dispersion behaviour of the filler in the polymer matrixes, and the mechanical properties at large deformation, are influenced by the acid/base interaction balance in the polymer-filler pair, as determined by IGC.

The dispersion of surface-treated fillers in polymer matrixes as been studied by Boluk and Schreiber (1989) by means of assessing the acid-base interaction potential of the major components by IGC. In the case of pigmented, plasticized PVC, significant differences in rheological and mechanical properties have been observed (Schreiber 1993) when the interaction balance within the system was altered by substituting a basic rutile TiO_2 for one with acidic surface tendencies. Acid-base surface properties of TiO_2 particulates with surfaces modified with silica and/or alumina, and the surface modification influence on the dispersion of the filler in a polymeric medium, have been studied using IGC by Lee and co-workers (1992).

Ziani *et al.* (1999) studied the dispersion stability of pigments in paint formulations and concluded that a correlation exists between the ease of dispersion and acid-base interaction parameters, as determined by IGC.

1.2.5.2. The use of IGC on the Determination of Flory-Huggins Interaction Parameters and Solubility Parameters

The relationship between the basic information of IGC, the net retention volume, V_n, and the Flory-Huggins interaction parameter, χ, may be written as expressed in Equation 1-13 (Al Saigh 1994 and 1997b; Herrero *et al.* 1994; Jackson *et al.* 1994):

$$\chi = \ln\left(\frac{RTv_2}{V_n p_1^0 V_1}\right) - \left(1 - \frac{V_1}{V_2}\right)\varphi_2 - \frac{p_1(B_{11} - V_1)}{RT} \tag{1-13}$$

Here v_2, V_2 and φ_2 are the specific volume, the molar volume and the volume fraction of the polymer. V_1 and p_1^0 refer to the molar volume and the saturation vapour pressure of the molecular probe. B_{11} is the second virial coefficient of the probe and corrects for non-ideality in the vapour phase. R is the ideal gas constant and T (K) is the column temperature.

When χ values are determined for a given polymer or other non-volatile component of a polymer system and a series of vapours for which solubility parameter values are known, the IGC method provides a unique way to determine δ_T for the polymer phase. The method is based on the principle that the Flory-Huggins interaction parameter, χ, can be related to δ_T by combining Hildebrand-Scatchard solution theory with Flory-Huggins theory (Jackson *et al.* 1994):

$$\chi = \frac{V_1}{RT}(\delta_1 - \delta_2)^2 \tag{1-14}$$

Here V_1 is the molar volume of the probe, and δ_1 and δ_2 are the solubility parameters of the probe and stationary phase, respectively.

The necessary relationship, between χ and solubility parameters (Ito and Guillet 1979; Jackson *et al.* 1994; Li 1996), states that:

$$\frac{\delta_1^2}{RT} - \frac{\chi}{V_1} = \left(\frac{2\delta_2}{RT}\right)\delta_1 - \left(\frac{\delta^2{}_2}{RT} + \frac{\chi_s}{V_1}\right) \tag{1-15}$$

Here, δ_1 is the solubility parameter of component 1 and δ_2 is the solubility parameter of component 2. V_1 is the molar volume of the probe, χ_s is the entropic contribution to χ . A plot of the left hand side of Equation 1-15 vs. δ_1 should lead to a straight line, with δ_2 obtained from its slope.

The great advantage here is the ability to evaluate δ_2 for essentially pure polymers at temperatures that are relevant to identified applications. The generality and usefulness of the method has been demonstrated frequently in the work of Price (1989).

Thermodynamic interactions between mixed stationary phases may be obtained from IGC as first proposed by Su *et al.* (1976) and followed by other research laboratories (El Hibri *et al.* 1989; Mandak *et al.* 1989; Al Saigh 1994). The approach calls for the experimental determination of $\chi_{1,2}$ and $\chi_{1,3}$, using common vapour probes, to characterise any desired pure components 2 and 3. These solids may then be mixed to any suitable composition, a column prepared for IGC and an overall interaction parameter, $\chi_{1(2,3)}$ evaluated. The term $\chi_{1(2,3)}$ is related to compositional variables through use of an extension of Scott's ternary solution theory. The results are most frequently written as (Mandak *et al.* 1989; Al Saigh 1994):

$$\chi_{1(2,3)} = (\chi_{1,2})\varphi_2 + (\chi_{1,3})\varphi_3 + (\chi'_{2,3})\varphi_2\varphi_3 \qquad (1\text{-}16)$$

Here $\chi_{2,3}' = (\chi_{2,3})V_1/V_2$. The parameter for the interaction of mixed polymeric and/or non-polymeric solids is thereby normalised to the size of the vapour phase molecule.

The attractiveness of this flexible and relatively easy experimental route to valuable information concerning the miscibility of system components is evident. Difficulties arise however, in that $\chi_{2,3}'$ can vary with the selection of the vapour probe. This problem has been the subject of much discussion (Prolongo *et al.* 1989; Shi and Schreiber 1991 and 1992; Farooque and Deshpande 1992; Du *et al.* 1999a and 1999b). Shi and Shreiber (1991) state that the probe dependence of $\chi_{2,3}$ is due to two major contributing factors. Firstly, the surface composition of a mixed stationary phase will rarely, if ever, correspond to the composition of the bulk. Thermodynamic requirements to minimise the surface free energy of the stationary phase will favour the preferential concentration, at the surface, of the component with the lower (lowest) surface free energy (Shi and Schreiber 1991 and 1992; Jones and Kramer 1993; Mukhopadhyay and Schreiber 1993). Thus, the values of φ_2 and φ_3, as defined by the bulk composition of mixtures, are inapplicable to Equation 1-16. Instead, a graphical method was proposed by Shi and Schreiber (1991) to evaluate the effective volume fraction and to correct the problem. Secondly, since $\chi_{1,2}$ and $\chi_{1,3}$ will not usually be equal, it follows that the volatile phase will partition preferentially to the component that has the lower pertinent $\chi_{1,x}$ value. Thus, the partitioning must vary with each probe, inevitably affecting the $\chi_{2,3}'$ datum. Far from invalidating the IGC route to thermodynamic information, these considerations if approached logically, can shed new and valuable light on the nature of surface interactions in polymeric systems.

1.2.5.3. IGC and the Quantification of Lewis Acidity/Basicity Parameters

Due to the dynamic nature of IGC experiments, the retention time is dependent on the flow rate of the carrier gas. Therefore, the retention time is usually converted into a net retention

volume, V_n, which may be defined as the volume of carrier gas that is required to elute a given probe, as follows:

$$V_n = (t_r - t_o)\, F\, C\, J \tag{1-17}$$

Here, t_o is the retention time of a non-interacting probe species, either air, or more commonly, methane. F is the carrier gas flow rate in cm^3/s. J is a term correcting for the compressibility of the carrier gas, such that:

$$J = 1.5\frac{\left(\frac{P_i}{P_o}\right)^2 - 1}{\left(\frac{P_i}{P_o}\right)^3 - 1} \tag{1-18}$$

Here P_i and P_o are the inlet and outlet pressures of the carrier gas, respectively. C is a correction factor, allowing for the vapour pressure of the water at the temperature of the bubble flow meter used to determine the flow rate. Thus:

$$C = 1 - \frac{P_{H_2O}}{P_o} \tag{1-19}$$

Here, P_{H_2O} is the vapour pressure of the water in the flow meter, at the temperature of measurement.

The retention time, as defined by Equation 1-17, is known as the net retention volume. This may be normalised per gram of interacting material present in the stationary phase, yielding the specific retention volume:

$$V_g = \frac{V_n}{m} \tag{1-20}$$

Here, m is the mass of interacting stationary phase.

Thermodynamic Considerations

The net retention volume, V_n, is a measure of the time that the probe is adsorbed on the stationary phase and a measure of the time that the molecule is present in the carrier gas, under isothermal conditions. Therefore, the net retention volume is expressed by a partition function. Strictly, the net retention volume can be divided into two components: a term that is related to bulk absorption (and therefore, to the volume of adsorbate) and a term that is related to the surface adsorption, (and thus, to the adsorbate surface area) (Papirer *et al.* 1988a; Beaumont 1996). The relationship can be expressed, as:

$$V_n = k_a V + k_s A \tag{1-21}$$

Here, k_s and k_a are the partition coefficients, for the surface adsorption and the bulk absorption, respectively. V and A are the volume and surface area of the adsorbate, respectively. Equation 1-21 is used in gas-liquid chromatography. As far as pigments and glassy polymers are concerned, the bulk absorption can be, generally, disregarded. Thus, under such conditions, Equation 1-21 simplifies to (Papirer *et al.* 1988a; Mukhopadhyay and Schreiber 1995):

$$V_n = k_s A \tag{1-22}$$

k_s can be formally defined as a partition function that accounts for the probe excess concentration on the surface, Γ, and its concentration on the gas phase, c. Thus,

$$k_s = \left(\frac{d\Gamma}{dc} \right) \tag{1-23}$$

Under infinite dilution conditions, Henry's Law is obeyed. Thus,

$$\left(\frac{d\Gamma}{dc} \right)_{\Gamma \to 0} = \frac{\Gamma}{c} \tag{1-24}$$

Under these conditions, the partition coefficient, expressed by Equation 1-23, is independent of the probe concentration in the gas phase. Experimentally, this fact can be verified by obtaining constant retention times, injecting a probe amount that is lower than a certain limit. The probe concentration, under such conditions, can be expressed by:

$$c = \frac{p}{RT} \tag{1-25}$$

Here, p is the partial pressure of the probe and R is the universal gas constant. From Equations 1-23 to 1-25 one gets (Mukhopadhyay and Schreiber 1995):

$$k_s = \Gamma \frac{RT}{p} \tag{1-26}$$

Γ is related to the pressure on the surface through the Gibbs equation (Mukhopadhyay and Schreiber 1995):

$$\Gamma = \frac{1}{RT} p \left(\frac{d\pi}{dp} \right) \tag{1-27}$$

Here, π is the pressure of the probe on the surface and can be defined as the reduction in the surface free energy of the probe due to vapour adsorption. In the region where Henry's Law is valid, the reduction in the surface free energy of the stationary phase due to the probe, is a linear function of the probe's partial pressure. Thus,

$$\frac{d\pi}{dp} \rightarrow \frac{\pi}{p} \tag{1-28}$$

Combining Equations 1-26 to 1-28 one gets (Mukhopadhyay and Schreiber 1995):

$$k_s = \frac{\Gamma RT}{p} = \frac{\pi}{p} = \frac{V_n}{A} \tag{1-29}$$

The free energy of adsorption can be compared with the change in the surface free energy that is due to the adsorption of one mole of probe molecules, from a reference gas phase, to a reference adsorption phase, as expressed in Equation 1-30 (Mukhopadhyay and Schreiber 1995):

$$\Delta G_a = -RT \ln\left(\frac{P_s^s}{P_g^s}\right) \tag{1-30}$$

Here, ΔG_a is the difference in the free energy that is related to the isothermal adsorption of one mole of probe molecules in the reference gas phase, at a pressure P_g^s, in a reference adsorption phase, at a pressure P_s^s. The reference vapour pressure of the probe, in the gas phase, must be expressed such that its value corresponds to a surface pressure in the Henry's Law region. This can be attained by manipulating the relevant portion of Equation 1-29, i.e., $p=\pi/k_s$. Thus (Mukhopadhyay and Schreiber 1995):

$$\Delta G_a = -RT \ln\left(\frac{V_n P_s^s}{\pi A}\right) \tag{1-31}$$

Here, A is the adsorbate' surface area, P_s^s and π are the reference gas pressure and the reference surface pressure, respectively. DeBoer defined the surface pressure as the pressure at which the distance between two probe molecules is equal to the distance in the standard gas phase. Thus, π = 3.38 x 10^{-4} Nm^{-1} and P_g^s = 101.3 kPa (Papirer *et al.* 1988a; Balard and Papirer 1993; Mukhopadhyay and Schreiber 1995).

The surface area is constant between experiments and, therefore, Equation 1-31 can be reduced to (Mukhopadhyay and Schreiber 1995):

$$\Delta G_a = -RT \ln(V_n) + K \tag{1-32}$$

Here K is a term that includes all the constants that are present in Equation 1-31.

Dispersive Component of the Surface Free Energy of Solid Surfaces

Three approaches are commonly employed in the analysis of the dispersive component of the surface free energy of solid surfaces via IGC. These are due to Fowkes (Schultz and Lavielle 1989; Nardin *et al.* 1990; Riddle and Fowkes 1990; Lavielle and Schultz 1991; Lavielle *et al.* 1991; Nardin and Schultz 1993a-c; Brendle and Papirer 1997b; Goss 1997; Hamieh *et al.* 1997 and 1998)

(refered to as Schultz and Lavielle approach, by some authors), Dorris and Gray (1980), and Flour and Papirer (1982).

The approach of Fowkes is based on his definition of work of adhesion between two apolar species (Fowkes *et al.* 1990; Liang *et al.* 2000). Thus,

$$W_a = 2(\gamma_s^d \gamma_l^d)^{0.5} \quad (1\text{-}33)$$

Here, γ_s^d and γ_l^d are the dispersive component of the surface tension of a solid and of a liquid, respectively. According to Fowkes, the free energy of adsorption can be defined as:

$$-\Delta G_a = N_A a W_a + K' \quad (1\text{-}34)$$

Here N_A is Avogadro's constant and "a" is the molecular surface area of the adsorbed species. As defined by Equation 1-34, the molar free energy of adsorption, $-\Delta G_a$, is equal to the sum of the work of adhesion for the surface area occupied by one mole of molecules. Thus, it is equal and opposite to the work required to separate the area of interface created by one mole of molecules. The molar free energy of adsorption can be related to the retention volume using Equation 1-32. From Equations 1-32, 1-33 and 1-34 one obtains:

$$RT \ln(V_n) = 2N_A a(\gamma_s^d)^{0.5}(\gamma_l^d)^{0.5} + K'' \quad (1\text{-}35)$$

From the above equation, a plot of $RT\ln(V_n)$, (or $RT\ln(V_g)$), as a function $a(\gamma_l^d)^{0.5}$ will yield a slope of $2N_A(\gamma_s^d)^{0.5}$ and an intercept of K''. Values of $a(\gamma_l^d)^{0.5}$ can be found in the literature (Riddle and Fowkes 1990; Kamdem *et al.* 1993). Selected values are presented in Table 1-1 for the apolar probes that apply to the present study, corresponding to probe molecule surface area values reported (Schultz and Lavielle 1989; Riddle and Fowkes 1990; Kamdem *et al.* 1993).

The method, however, does not always yield reliable values of γ_s^d. The reason for this is the uncertainty of the molecular surface area values of the adsorbed species (Nardin and Schultz 1993a; Garnier and Glasser 1994; Mukhopadhyay and Schreiber 1995). Molecular areas of adsorbed molecules may be distorted by forces that are exerted by the surface. Non-shperical molecules such as alkanes may lie "flat" or "head-to-tail" in the interface. Furthermore, different methods are in use for the estimation of the molecular areas, which may result, in some cases, in different values (Hamieh *et al.* 1998). Also, the temperature influence on the molecular areas is not usually taken into account (Nardin and Schultz 1993a; Garnier and Glasser 1994). Consequently, IGC evaluations of γ_s^d, using this approach, must be viewed with some caution. Corrections for the values of the molecular area of adsorbed probes that take into account the aforementioned factors can be found in the references cited.

Table 1-1. Values of $a(\gamma_l^d)^{0.5}$ for several n-alkanes (Schultz and Lavielle 1989; Riddle and Fowkes 1990; Kamdem *et al.* 1993).

n-alkane	$a(\gamma_l^d)^{0.5}$ (cm^2 ($mJ\ cm^{-2}$)$^{0.5}$)
n-hexane	2.21E-16
n-heptane	2.57E-16
n-octane	2.91E-16
n-nonane	3.29E-16
n-decane	3.63E-16
n-undecane	3.99E-16

The approach of Dorris and Gray (Courval and Gray 1975; Gray 1977; Dorris and Gray 1980; Mukhopadhyay and Schreiber 1995; Goss 1997) is similar to that of Fowkes. This approach involves the use of molecular surface areas to elucidate the dispersive surface free energies, derived via the dispersive component of the work of adhesion.

The method is based on calculation of the incremental free energy of adsorption of a $-CH_2$ group, for which the dispersive component of the surface tension is known to be 35.6 mJ/m^2 at 20 °C (Mukhopadhyay and Schreiber 1995). The free energy of adsorption of a $-CH_2$ - group may be related to the dispersive component of the surface tension via (Mukhopadhyay and Schreiber 1995):

$$\gamma_s^d = \frac{\left(RT \ln \frac{V_n[C_{n+1}H_{2n+4}]}{V_n[C_nH_{2n+2}]} \right)^2}{4N_A{}^2 a_{CH_2}^2 \gamma_{CH_2}} \tag{1-36}$$

Here, $(V_n[C_{n+1}H_{2n+4}])/(V_n[C_nH_{2n+2}])$ corresponds to the difference in the free energy of adsorption arising from introducing an additional $-CH_2-$ into the carbon chain of a n-alkane probe. The other terms have the definition given earlier. Care should also be taken when using Equation 1-36 because the value of the molecular area of a CH_2 group, usually taken as 0.6 nm, may not be the more accurate value, as has been recognised by Dorris and Gray themselves (1980). This drawback has been studied by Goss (1997), who proposed corrections for the approach. Another frequently used approach for the determination of γ_s^d, is that of Schultz and Lavielle, which uses an equation that is equivalent to Equation 1-36, resulting in identical numerical values (Goss 1997).

The method of Papirer and Flour (Flour and Papirer 1982; Papirer *et al.* 1988a; Balard and Papirer 1993; Mukhopadhyay and Schreiber 1995) employs a different treatment to the retention times data. In this case, the free energy of adsorption of each probe is plotted as a function of the logarithm of the probe vapour pressure at the column temperature (or chosen reference temperature). The data for n-alkanes define a straight line of negative slope that may be used as a reference to define the potential of the surface to undergo dispersive interactions. The slope of the

reference line, in this case, is not related to the dispersive surface tension of the solid phase. The basis of the approach is empirical in nature.

Papirer argues (Papirer *et al.* 1988a; Balard and Papirer 1993) that the use of the vapour pressure of the probe in subsequent data manipulation is preferable, as it represents a readily determined macroscopic quantity and eliminates uncertainties that arise from the estimation of the molecular surface area of the probe and from the lack of data for γ_l^d at different temperatures. However, for surfaces with very high energy, such as graphite, this method has been shown to give unrealistic values (Goss 1997). This approach can, nevertheless, be used to determine the specific component of the energy of adsorption in an analogus procedure to that described below. Another approach, much less in use, is that of Sawyer and Brookman (Chehimi and Pigois-Landureau 1994; Mukhopadhyay and Schreiber 1995; Goss 1997) which makes use of the boiling point, T_b, of the probes instead of the logarithm of the saturated vapour pressure.

Other methods include the Dong approach (Voelkel *et al.* 1996a and 1996b; Brendle and Papirer 1997b; Andrzejewska *et al.* 1998) (based on the use of the molar deformation polarisation of the probe molecules), the Donnet approach (Donnet *et al.* 1992; Chehimi and Pigois-Landureau 1994; Voelkel *et al.* 1996a and 1996b; Andrzejewska *et al.* 1998) (based on the ionisation potential of the adsorbent and adsorbate, and on the deformation polarizability), the Chehimi approach (Chehimi and Pigois-Landureau 1994; Voelkel *et al.* 1996a; Brendle and Papirer 1997b) (based on the enthalpy of vaporisation of the probe molecules), and the Brendle and Papirer approach (Papirer *et al.* 1996; Brendle and Papirer 1997a and 1997b).

The Brendle and Papirer approach is based on the use of a topological index that accounts for the geometry of the probe. This topological index replaces $a(\gamma_l^d)^{0.5}$ in the determination of γ_l^d by Dorris and Gray approach. The other alternative approaches mentioned allow for the determination of quantities that are directly related to γ_l^d, from a plot of $RT\ln(V_n)$, (or $RT\ln(V_g)$), as a function of the mentioned probe properties and/or related quantities.

Of the methods mentioned, the approach of Fowkes has proven to be the most useful, due to its graphical approach and, most importantly, due to its provision of the dispersive component of the surface tension.

Quantification of the Lewis Acid/Base Interaction Capability of a Material

A Lewis acid is a molecule or ion whose incomplete electronic arrangement allows it to bind to another species by accepting an electron pair from that species. A Lewis base is a molecule or ion capable of donating an electron pair to a Lewis acid and resulting in the formation of coordination bonds (Gutmann 1978).

If a Lewis acid-base interaction occurs, as is the case with polar probes, there will be a corresponding specific component contribution to the overall free energy of adsorption, in addition to the dispersive component. Thus,

$$\Delta G_a = \Delta G_a^d + \Delta G_a^s \tag{1-37}$$

Here ΔG_a^d is the term that represents the dispersive Lifshitz-van der Waals contribution to the total free energy of adsorption, ΔG_a. ΔG_a^s represents the contribution to the free energy of adsorption by any Lewis acid/base (specific) interactions.

The determination of the non-dispersive, specific component of the free energy of adsorption is carried out graphically. The "Fowkes plot" (Figure 1-3) typically yields a straight line for a homologous series of n-alkanes, enabling linear regression to establish a relationship between $a(\gamma_l^d)^{0.5}$ and RTln(V_n) (or RTln(V_g)). Thus, any specific interactions result in a value of $-\Delta G_a$ that is greater than the value that is attributable to purely dispersive interactions for a species with a particular value of $a(\gamma_l^d)^{0.5}$.

If predominantly monopolar probes are used in the characterisation of the adsorbate, the interaction with a Lewis basic probe is a measure of the Lewis acidity of the surface. Conversely, a Lewis acidic species will undergo specific interactions with basic sites on the adsorbate.

From Equations 1-32 and 1-37, $-\Delta G_a^s$ may be defined as:

$$-\Delta G_a^s = RT \ln\left(\frac{V_n}{V_{n,ref}^d}\right) \tag{1-38}$$

V_n is the retention volume of the polar probe and $V_{n,ref}^d$ is the retention volume that is derived from the n-alkanes reference line. The procedure is illustrated in Figure 1-3.

Any of the aforementioned approaches used for the estimation of the dispersive component of the surface free energy, that differ in terms of the quantity RTln(V_n) is plotted against, can be used to determine the value of $-\Delta G_a^s$, according to the method expressed in Equation 1-38, and illustrated in Figure 1-3.

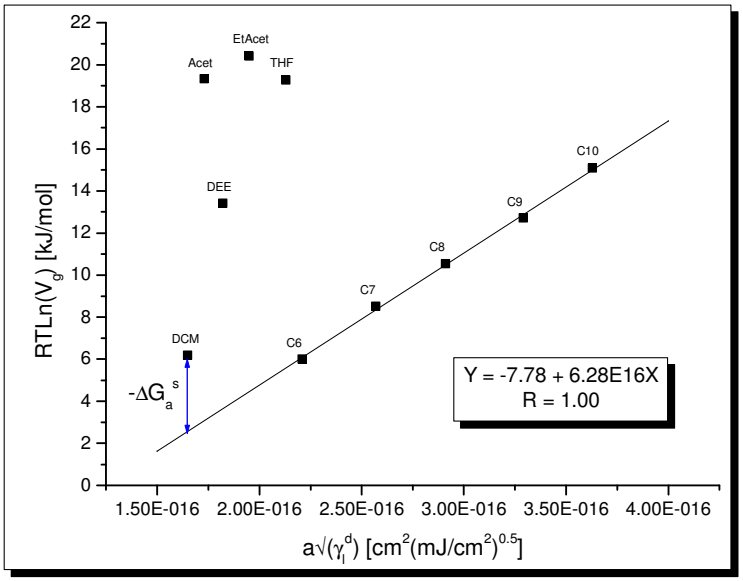

Figure 1-3. Typical Fowkes plot. Energy of adsorption ($RT\ln(V_g)$) versus $a\times\sqrt{\gamma_l^d}$ of n-alkanes and polar probes on the surface of C. I. Pigment Blue 28, at T = 313 K.

The van't Hoff equation,

$$\frac{d\ln k_s}{d(1/T)} = \frac{-\Delta H_a}{R} \tag{1-39}$$

shows that the change in the partition coefficient, k_s, (and, therefore, the free energy of adsorption) as a function of reciprocal temperature, must be constant to yield a single value of the enthalpy of adsorption, ΔH_a. Under the assumption of the temperature independence of the enthalpy component, the corresponding change in entropy is related to the change in the enthalpy of adsorption and the change in the free energy of adsorption, by:

$$\Delta G_a = \Delta H_a - T\Delta S_a \tag{1-40}$$

Here, ΔG_a, ΔH_a and ΔS_a are the corresponding free energy, enthalpy and entropy changes upon adsorption of a probe species by the adsorbate. The values of ΔH_a and ΔS_a, concerning a probe molecule, are determined plotting $\Delta G_a/T$ as a function of 1/T. The value of ΔH_a and of ΔS_a are determined from the slope and from the intercept, respectively. If the specific component of the surface free energy, ΔG_a^s, relating to a polar probe, is plotted against the reciprocal temperature, then the specific component of the enthalpy of adsorption, ΔH_a^s, and the specific component of the entropy of adsorption, ΔS_a^s, can be determined. Also, if the dispersive component of the surface free energy, ΔG_a^d, relating to a apolar probe, or a polar probe, is plotted against the reciprocal

temperature, then the dispersive component of the enthalpy of adsorption, ΔH_a^d, and the dispersive component of the entropy of adsorption, ΔS_a^d, can be determined.

Both the Lewis acidity and the Lewis basicity of a material contribute to the value of ΔH_a^s when that material is involved in intermolecular interactions. The approach of Gutmann (Chtourou *et al.* 1995) allows for the quantification of the Lewis acidity and of the Lewis basicity of a material, from ΔH_a^s values.

The value of the Lewis acidity constant, K_a, and of the Lewis basicity constant, K_b, is calculated using Equation 1-41 (Chtourou *et al.* 1995):

$$-\Delta H^s{}_a = K_a \times DN + K_b \times AN \qquad (1\text{-}41)$$

Here, DN and AN are Gutmann's donor and acceptor numbers, respectively, corresponding to the polar probes (Gutmann 1978; Riddle and Fowkes 1990; Kamdem *et al.* 1993). Gutmann (1978) defines DN as the molar enthalpy of mixing of a base with reference to the acceptor, $SbCl_5$. In contrast, AN is not an enthalpy parameter, but is defined as the relative ^{31}P-NMR shift in triethylphosphine oxide, when this substance is reacted with an acceptor solvent. AN is scaled arbitrarily, ranging from zero when the solvent is hexane to 100 when the solvent is a dilute solution of the reference acceptor, $SbCl_5$, in 1,2-dichloroethane.

A procedure has been suggested by Riddle and Fowkes (1990) to resolve the inconsistency in the units of DN and AN. They have shown that the ^{31}P-NMR shift of triethylphosphine oxide, Et_3PO, dissolved in acidic solvents, (the criterion used in Gutmann's approach for the definition of AN), can be divided into dispersive contributions and true acid/base contributions. These authors also found that the dispersive contribution to the NMR shifts is directly proportional to calorimetric determinations of the enthalpies of dispersive interactions between Et_3PO and acidic liquids. A new acceptor number AN^* is therefore obtained that has the same units as DN. Riddle and Fowkes suggest that AN^* be obtained from the simplified expression:

$$AN^* = 0.288(AN - AN^d) \qquad (1\text{-}42)$$

Here AN^d is the dispersive contribution reported by the authors (Riddle and Fowkes 1990). Thus, Equation 1-41 now becomes:

$$-\Delta H^s{}_a = K_a \times DN + K_b \times AN^* \qquad (1\text{-}43)$$

Plotting $\frac{-\Delta H^s{}_a}{AN^*}$ against $\frac{DN}{AN^*}$ gives K_a as the slope and K_b as the intercept. In Table 1-2 are summarised the values of AN^* and DN, the values of the surface area, and the values of $a(\gamma_l^d)^{0.5}$ for the polar probes used in the present study.

Table 1-2. Values of DN and AN*, of the surface area, and of $a(\gamma_l^d)^{0.5}$ for the polar probes used in the present study (Schultz and Lavielle 1989; Riddle and Fowkes 1990; Kamdem *et al.* 1993; Mukhopadhyay and Schreiber 1994; Belgacem 1995; Chtourou *et al.* 1995).

Probe	a (nm^2)	$a(\gamma_l^d)^{0.5}$ (cm^2 (mJ cm^{-2})$^{0.5}$)	AN* (kJ/mol)	DN (kJ/mol)
Trichloromethane	0.440	2.24E-16	22.7	0.0
Dichloromethane	0.315	1.65E-16	16.4	0.0
Diethyl ether	0.138	1.82E-16	5.9	80.6
Acetone	0.425	1.73E-16	10.5	71.4
Tetrahydrofuran	0.450	2.13E-16	2.1	84.4
Ethyl Acetate	0.397	1.95E-16	6.3	71.8

A commonly used alternative approach for the quantification of the Lewis acid/base character of a surface is due to Drago and co-workers (Drago *et al.* 1971; Fowkes *et al.* 1990; Jensen 1991). Here, acid/base pairs are equated to a set of four empirical parameters (C_a,E_a and C_b,E_b), based on enthalpies of mixing. The acidity of a substance and the basicity of a substance are given by parameters expressing covalent (C) and electrostatic (E) contributions. The Drago approach has been much favoured by Fowkes (Fowkes 1979, 1983a, 1983b, 1984 and 1990; Fowkes *et al.* 1980, 1985, 1988 and 1990). Using calorimetric data, C and E parameters have been obtained for a variety of organic solids and inorganic solids that are relevant to polymer systems. The fact that four parameters are needed, however, somewhat hinders the wide use of the Drago concept, and focuses attention on Gutmann's approach. Other reasons for the preference for the approach of Gutmann are that sufficient data are available for the volatile probes that are suitable for IGC experiments (larger than for Drago's scale) and, more importantly, the fact that the Gutmann's approach considers the amphoteric nature of most polar probes, which allows for the determination of K_a and K_b.

All of the above mentioned methods that allow the determination of ΔG_a^s, (and, thus, of ΔH_a^s and ΔS_a^s) of polar probes by the use of a n-alkanes reference line, can be used in the determination of K_a and of K_b. It has been shown (Panzer and Schreiber 1992) that nearly identical values of specific surface energy, of enthalpy of adsorption, and of K_a and K_b parameters are obtained with any of the options for data presentation, namely when the saturation vapour pressure, the normal boiling temperature or $a(\gamma_l^d)^{0.5}$ are used.

Other approaches exist such as the Goss approach (based on the van Oss approach) (Goss 1997). The Goss approach, and the van Oss approach, for the determination of the acid-base contribution to the surface energy are directly related to the free energy of the acid-base interactions, and not to the enthalpy as is the case with Gutmann's approach. This gives several advantages as it puts the acid-base surface parameters on the same (free energy related) basis as the

van der Waals parameters. Furthermore, the determination of the temperature dependence of the specific component of the free energy of adsorption is not necessary to any further extent.

A final remark regarding the interpretation of IGC results should be made. In order to favour the establishment of equilibrium conditions between the stationary phases and the mobile phases in an IGC experiment, the quantities of vapour that are injected are extremely small (e.g. nanolitre range of concentration). Surfaces are not generally energetically uniform. The small amounts of available vapour, therefore, will tend to adsorb on the most energetic fraction of available sites (Lara and Schreiber 1991b; Schreiber 1993; Mukhopadhyay and Schreiber 1995; Santos *et al.* 2001). Surface energy and acid/base characteristics, obtained from IGC, will, therefore, describe the performance of these surface fractions, and not necessarily the performance of the surface as a whole. More detailed descriptions of solid surfaces would necessitate the determination of adsorption isotherms of site energy distributions (Dorris and Gray 1979; Anhang and Gray 1982; Flour and Papirer 1982; Lipson and Guillet 1982; Grajek and Witkiewicz 1993; Filippova 1998; Bagreev *et al.* 1999). In many instances, however, the dominant surface interactions of a solid will be those involving the high-energy sites (Nardin and Schultz 1993a; Schreiber 1993).

Lewis Acid/Base Interaction Numbers from IGC Evaluations

The ability of the IGC technique to provide Lewis acid/base parameters for polymers and other materials used in polymeric systems, has lead to the development of Lewis acid/base pair interaction numbers. In this manner, an attempt to quantify the acid/base interactions at interfaces and/or interphases between a polymer matrix and additives present in the composition, making use of K_a and K_b, can be carried out. The lack of theory to guide such a calculation results in the use of empiricism. In this context, several Lewis acid/base interaction parameters, based on K_a and K_b, can be found in the literature (Lara and Schreiber 1991b and 1996; Mukhopadhyay and Schreiber 1995; Ziani *et al.* 1999; Liang *et al.* 2000; Wang *et al.* 2001):

$$I_{sp1} = (K_a)_1 \ (K_b)_2 \ + \ (K_a)_2 \ (K_b)_1 \tag{1-44}$$

$$I_{sp2} = [(K_a)_1 \ (K_b)_2]^{1/2} \ + \ [(K_a)_2 \ (K_b)_1]^{1/2} \tag{1-45}$$

$$I_{sp3} = (K_a)_1 \ (K_b)_2 \ + \ (K_a)_2 \ (K_b)_1 - (K_a)_1 \ (K_a)_2 \ - (K_b)_1 \ (K_b)_2 \tag{1-46}$$

Here, $(K_a)_1$ and $(K_b)_1$ correspond to the Lewis acidity/basicity constants of species 1, and $(K_a)_2$ and $(K_b)_2$, to those of species 2. All of these parameters are reported (Mukhopadhyay and Schreiber 1995) to correlate usefully with adhesion phenomena and with other properties that are influenced by the strength of Lewis acid/base intermolecular forces. Although the relations that are expressed in Equations 1-44 to 1-46 are empirical, the rationale for Equation 1-46 is that in a random mixing process there is a high probability of finding both unlike and like interaction sites of the two constituents in close contact (Ziani *et al.* 1999; Liang *et al.* 2000). However, several remarks (Santos *et al.* 2002a) must be made regarding the use of the interaction parameters that is represented by Equations 1-44 to 1-46.

Firstly, the parameters I_{sp1} and I_{sp2} do not take into account the Lewis base/base repulsion forces and the Lewis acid/acid repulsion forces. The Lewis base/base repulsions and the Lewis acid/acid repulsions, and the Lewis acid/base attractions, do not contribute equally to the overall specific interactions. The attractions have a greater contribution, according to Fowkes (1980) and Hegedus and Kamel (1993a). Lewis acid/acid repulsions and Lewis base/base repulsions do make a significant contribution in those particular systems were Lewis acid/base attraction does not exist or is very weak, as has been postulated, and experimentally proven, by Schreiber and coworkers (Schreiber and Germain 1990, 1991; Kloubek and Schreiber 1993; Ziani *et al.* 1999), and by Lee *et al.* (2001) and suggested by Utracki *et al.* (1989). Moreover, according to Kloubek and Schreiber (1993), Lewis acid-acid and Lewis base-base (repulsive) interactions do, in some cases, exceed the effects of Lewis acid-base attractive forces at interfaces, has is the case for interfaces between perfluorohydrocarbons and water. An example of the lack of acid/base attraction interaction due to predominant base/base repulsion is the incapacity of an acetone molecule to form H-bonds with another acetone molecule (Israelachvili 1991). This has lead to the proposal of a new parameter, I_{sp3} (Schreiber and Germain 1991; Kloubek and Schreiber 1993; Liang *et al.* 1999). In the formulation of parameter I_{sp3}, it is assumed that acid/acid and base/base repulsion make the same contribution as is provided by acid/base attraction for the overall interaction potential. However, when determining the interaction parameter involving the interaction of a hypothetical material with itself or between identical molecules (Table 1-3, values of K_a and K_b being presented as an example), the value of I_{sp3} is always negative or zero and, thus, interaction is not favoured. Consequently, no polar molecule would interact through acid/base intermolecular interactions (from the attractive point of view) with another molecule that is chemically identical.

Table 1-3. Value of I_{sp3}, for the acid/base interaction potential of a hypothetical material with itself. Values of K_a and K_b are given only as an example.

K_a	K_b	I_{sp3}
"low" (0.1)	"low"(0.1)	0.00
"low" (0.1)	"high" (1)	-0.81
"high" (1)	"low" (0.1)	-0.81
"high" (1)	"high" (1)	0.00

Secondly, the contribution of acid/base attraction and of acid/acid and base/base repulsion, to the total interaction potential, is a function not only of the intrinsic Lewis acidity of the molecules and the Lewis basicity of the molecules, but is also a function of the accessibility of such interaction sites (Ponec *et al.* 1974; Fowkes 1980; Huyskens *et al.* 1991; Goss 1997; Kim and Mai 1998; Ziani *et al.* 1999).

This factor is of considerable importance when long chains (as is the case with polymers) are present, or when particulates are involved. In such instances, conformational factors and configurational factors influence the accessibility of the interaction sites (Fowkes 1980; Kim and Mai 1998). Factors such as the localisation and the distribution of the Lewis acidic sites and of the

Lewis basic sites, and their accessibility by the Lewis acidic sites and the Lewis basic sites of the interacting species, influenced by the existence of bulky side groups, for instance, will affect the effectiveness of any acid/base interactions. Steric hindrance influences the interaction of the probe molecules that are used in IGC with the surface, and, thus, is quantified in K_a and K_b. However, when the material interacts with another surface (particulates, polymers), instead of with a probe molecule, the accessibility of the Lewis acidic sites and the Lewis basic sites in the materials involved is by far more influenced by conformational and morphological factors.

The thermodynamic properties determined are normalised per mole of adsorbate and per unit of surface area of adsorbent and, thus, are real indications of the likehood, strength, and stability of filler-polymer interactions. Nevertheless, as far as inorganic particles are concerned, the thermodynamic properties do not account for differences in the specific area of the particles that can vary noticeably from inorganic species to inorganic species, thereby determining the availability of interaction sites with respect to the other components of the polymeric mixture.

As the acid/base interaction most frequently found is the H-bond (alongside with the n-σ electron-donor-acceptor (EDA) bonding (Huyskens *et al.* 1991)) and, due to its highly directional and specific character (Ponec *et al.* 1974; Huyskens *et al.* 1991), the acid/base interaction will be strongly affected by the orientation and accessibility of the functional groups. Accordingly, and in conjunction with the acid/base properties of each material/molecule, the contribution of acid/acid repulsion and base/base repulsion to the interaction potential will vary with the chemical nature as well as with the spatial structure of the species involved. The repulsive interaction is expected to be significant in such cases where, in both materials, either the Lewis basic sites or the Lewis acidic sites are dominant to a large extent (Coleman *et al.* 1991), and are easily accessible.

Thirdly, in interactions between different materials that might be used as part of a multi-component polymeric system, the probability of acid/base interactions is a function, not only of the interaction potential, but also of the number of interaction opportunities, as defined by the relative presence of each species in the polymeric system.

Therefore, an interaction parameter that is considered to be suitable for multi-component polymeric systems, whose components are able to interact through specific interaction forces, would be influenced by the following factors:

a) K_a and K_b, the Lewis acidic and Lewis basic constants for each species;

b) The accessibility of the Lewis acidic sites and the Lewis basic sites in each species, relative to the Lewis acidic sites and the Lewis basic sites of the interacting species, due to the presence of bulky–side groups, molecular conformations, and morphological structural features of the species involved;

c) The larger contribution of acid/base attraction forces for the overall interaction;

d) The relative presence of each species in the blend.

In view of the above comments, an analysis of K_a and K_b, taking into account the chemical structure of the species involved, their relative amounts in the blend, and their physical properties (size, morphology), is thought to be the best way of predicting the acid/base interaction capability of the species that are present in multi-component polymeric systems.

Although acid/base interactions are known to be determinant, their importance should not be exaggerated. Dispersion forces still exercise a great influence on the behaviour of multi-component systems, and their contribution is not to be neglected when interpreting property data, and when selecting materials for polymeric compositions (Schreiber 1993; Mukhopadhyay and Schreiber 1995).

1.3. PC/PBT Blends

1.3.1. Development of PC/PBT Blends

The following summary is based on the extensive collection of information published by Utracki (1998) that relates to the development and technology of commercial polymer blends.

The blending of PC with PBT was first proposed in 1971 by Teijin Chemicals. PC was to be mixed with more than 50 wt% of PBT for 6 hr at 120 ºC. Development of these two-component blends was of little commercial consequence then, since the long cooking at low temperatures was considered to be rather expensive. Furthermore, as the transesterification process is sensitised by metallic salts (that were used to catalyse the polycondensation of the blend components), the process was difficult to control. In 1972, Teijin Chemicals discovered that three-component blends (PC, PBT and a core-shell impact modifier consisting of a methyl methacrylate-butadiene-styrene graft copolymer (MBS)), could be produced with good chemical resistance and impact strength.

The use of MBS rubber as a single, multicomponent compatibiliser and impact modifier constituted an important development in the evolution of PC/PBT blends. In 1974, BASF announced blends of PBT with 20 wt% PC. In 1978 and 1979 General Electric deposited several patent documents that were concerned with PET/PC blends and with PBT/PC blends. A later patent claimed that PBT could be blended with PET, PC and Al_2O_3. In 1980, General Electric announced moulding compositions that were characterised by their high impact strength and their heat resistance, prepared by blending 78.3 wt% PBT, with 10 wt% PC, and 10 wt% of a polyacrylate impact modifying rubber. In 1982, the company commercialised the highly successful Xenoy® alloys.

In 1981, Bayer deposited a series of applications that described blends of polyesters with either grafted elastomers or homopolymeric elastomers. These alloys were reported to have good toughness, hardness and stiffness. Thus, PET and/or PBT and/or PC, when blended with graft

copolymers of poly(butadiene) and methacrylic esters produced alloys that were commercially interesting (Tseng and Lee 2000b).

In 1982, another series of patent applications was submitted for blends of 1-100 wt% PC with either PET or PBT, and with 1-30 wt% of EVA. This work led to the commercialisation of Makroblend® alloys. Another patent from General Electric described high impact strength blends that were prepared from 39 parts PBT (or PET), with 48 parts PC, 4 parts LLDPE and with 8 parts of an acrylic elastomer. PC was also blended with PET or PBT and an acrylic impact modifier, such as PET with 10-15 wt% PC and 10-15 wt% Acryloid® KM 330, for improved impact strength.

In 1984, BASF filed a patent for high impact strength moulding compositions that could be prepared by blending PBT with PC and an ethylene-acrylic acid-butyl acrylate copolymer. In 1986, the same company disclosed high impact strength blends that comprised either PET or PBT, 40-65 wt% PC and 1-30 wt% of an acrylic rubber. These patents provide the basic formulations for the commercial PC/PBT blends from BASF, Ultrablend®. A Montedison patent, also deposited in 1982, describes similar effects from blends of 0-50 wt% PBT with PC and 50 wt% of modified ABS. In 1982, Bayer disclosed a patent of PC blends with 10-50 wt% PBT that were useful for preparation of uniaxially drawn shrink films. In the same year, Uniroyal Chemical Inc. reported the highly synergistic enhancement of impact strength of polyester/PC blends, by incorporating a proprietary impact modifier.

In 1987, patent applications from General Electric concerning new blends of PC with either PET or PBT were described. The overall properties of these alloys were improved by incorporating polyacrylate rubbers.

From 1987 onwards, variations of impact-modified PC/PBT blends were reported in the patent literature. These represent the introduction of new impact modifiers and/or compatibilisers in the basic PC/PBT blend compositions. One of the later developments in impact-modified PC/PBT blends was reported in 1993 by Allied Signal. This company applied for a patent protection for blends comprising a polyester, 20-60 wt% (either PET, PBT or PCT), 40-60 wt% PC, 10-20 wt% of an amine-functionalised elastomer (either EPR, EPDM, or NBR), and, optionally, an effective amount of a graft coupling agent. The resulting materials showed several qualities such as a relatively high impact strength, at both room temperature and lower temperatures. These materials also retained a substantial portion of their room temperature impact strength and their low temperature impact strength after annealing or heat treatment.

1.3.2. The PC/PBT Blends Studied in this Project

The polymeric system studied in this research project consists of a blend of approximately 50/50 %wt of a bisphenol A polycarbonate (PC) and a poly(butylene terephthalate) (PBT). The poly(butylene terephthalate) is itself a blend of two PBT forms that differ mainly in their average molecular weight, their carboxyl end-group concentration and their hydroxyl end-group

concentration. An elastomer, MBS rubber, is added to the polymer blend to improve its impact toughness. The MBS rubber is usually used as approximately 15-20 wt% of the final blend weight (Dekkers *et al.* 1988, Utracki 1998). As mentioned previously, the pigment studied was C. I. Pigment Blue 28, cobalt aluminate. Inorganic pigments are normally added as 0.1-2.0 wt% of the total blend. Additives such as thermal stabilisers and transesterification reaction inhibitors are also included formulations. The thermal stabiliser is added to prevent thermal degradation, indicated in the chain scission of the PC and of the PBT, and in the crosslinking (oxidative degradation) of the MBS rubber. These deteriorating effects are due to the formation of radicals by UV-light, heat and shearing (Bukman 1988). Heat stabilisers are added to quench the radicals that are formed during melting and moulding of the material.

In terms of what is described in the literature about research studies that have been carried out on these blends, the first scientific articles were published more than 20 years ago (Wahrmund *et al.* 1978). It is well established that the use properties of impact-modified PBT/PC blends are directly related to: 1) the molecular weight of the PC and of the PBT, 2) the degree of crystallinity of the PBT, 3) the miscibility (that is phase separation) of PC and PBT, 4) the degree of chemical reaction (transesterification) between the PC and the PBT (influences all of the above points), and 5) the phase preference of the impact modifier for the PBT phase and/or for the PC phase.

In this polymer blend, the PC and the PBT are physically mixed and the occurrence of transesterification, which results in the formation of PC-PBT copolyester, is designed to be avoided. Although a certain degree of transesterification could be desirable, as the impact toughness of the blend improves on transesterification, there is also a loss of chemical stability and of thermal stability of the blend.

Details of studies relating to the phase preferences of the pigment(s), and the consequences thereafter on the physical properties, and on the mechanical properties of these blends have not been found in the literature. Furthermore, studies regarding the analysis/interpretation of the phase separation and phase preferences, characteristic of these systems, based on the concept of Lewis acid/base interactions, could not be found in the literature.

1.3.2.1. Poly(butylene terephthalate)

PBT is one of the faster crystallising polymers (Nadkarni and Jog 1991; Mishra and Venkidusamy 1995; Cheng *et al.* 1996; Huang and Chang 1997; Pillin *et al.* 2001). The chemical nature of the repeat unit is shown in Figure 1-1. The high crystallisation rate is a consequence of the high mobility that is caused by the butylene unit in the chain. Usually, pure PBT has a crystallinity degree in the range 30-40 %. The enthalpy of fusion, ΔH_f^o, of the 100 % crystalline PBT is 142 J/g (Pompe *et al.* 1991 and 1996; Cheng *et al.* 1996; Pompe 1997). The melting temperature T_m is about 225 ºC and the crystallisation temperature is approximately 180 ºC (Dekkers *et al.* 1990).

In PBT, both normal (with a normal Maltese cross) and abnormal (with a Maltese cross rotated 45º relative to the normal position) spherulites have been reported (Pompe 1997). The crystalline structure of both types is the same. The normal spherulites are reported (Pompe 1997) to form preferentially at low crystallisation rates, and to melt at higher temperatures, than the abnormal ones, grown at high crystallisation rates. The crystallisation rate is reduced in blends, for instance with PC. The PBT crystalline structure has been extensively studied (Pillin *et al.* 2001). Two crystalline forms (α and β) have been observed, the β form existing only after drawing. Transition between the two forms takes place by stress and relaxation. If the strain is higher than 12 %, only the β form exists (Pillin *et al.* 2001).

The value of T_g of the semicrystalline state is about 40 ºC. The completely amorphous state of pure PBT is difficult to produce due to the high crystallisation rate of this polymer. Nevertheless, a value of -25 ºC has been determined for the T_g of the 100 % amorphous PBT (Ratzsch *et al.* 1990; Pompe 1997).

PBT has good mechanical properties and electrical properties, excellent solvent resistance, and good hydrolytic stability.

1.3.2.2. Bisphenol A Polycarbonate

The PC studied has the chemical nature that is implied in Figure 1-1. Normally PC is completely amorphous. The glass transition is in the range of 140-147 ºC. It has exceptional properties, such as good impact strength, ductibility, extreme toughness, transparency, resistance to burning, and maintenance of useful engineering properties over a temperature range of -200 to 140 ºC. A secondary motional transtion, β relaxation, exists at -40 ºC as determined by dynamic mechanical thermal analysis (DMTA) (Wetton and Corish 1989). The shortcomings of PC include its high melt viscosity, (creating difficulties in processing), and its high glass transition temperature (Mishra and Venkidusamy 1995).

1.3.2.3. Impact Modification of PC/PBT Blends

Owing to possible transesterification reactions, PC/PBT blends do not necessarily require additional compatibilisation (Utracki 1998). Nevertheless, controlling the extent of co-reaction is critical as too much co-reaction decreases the crystallinity of the PBT, reducing the mechanical performance as well as solvent resistance, chemical resistance and thermal stability, whereas too little co-reaction leads to poor interphase adhesion and brittleness. Therefore, the introduction of an impact modifier into the composition is preferable to the use of the transesterification reaction in the improvement of the impact resistance.

As mentioned, the PC/PBT alloy has been widely used in shaped articles because of its easy processability, good dimensional stability, heat resistance, and solvent resistance. However, the brittleness problem of the PC/PBT alloy results in a low impact strength at low temperatures and,

thus, limits its applications. Additives such as impact modifiers, compatibilisers, and glass fibres are used to improve the physical properties of these blends (Tseng and Lee 2000b).

Among these additives, MBS impact modifiers have demonstrated a significant impact-modifying effect at low temperatures (Dekkers *et al.* 1988; Hobbs *et al.* 1988b; Utracki 1998; Tseng and Lee 2000a and 2000b) and are used normally as 15-20 wt%. This impact modifier consists of a core of poly(styrene), an inner layer of poly(butadiene) and a shell of poly(methyl methacrylate). The PMMA-shell of this impact modifier gives good adhesion with the polycarbonate, in which the impact modifier is to be dispersed. The poly(butadiene) is the component that causes the higher impact strength. The poly(styrene) layer has an aesthetic function. It is used in the impact modifier to ensure the proper reflection of light.

It is well established that rubber particles with low moduli act as stress concentrators in both thermoplastic materials and in thermoset resins, favouring the dissipation of the impact energy by enhancing shear yielding and/or crazing, depending on the nature of the matrix (Folkes and Hope 1993), and, thus, improving the impact toughness of the blend. Also, the voids created by the cavitated rubber particles act further as stress concentrators (Walker and Collyer 1994).

Several papers have been published that deal with the inclusion of an elastomer in PC/PBT blends in order to improve the impact resistance of these blends (Dekkers *et al.* 1988; Hobbs *et al.* 1988b; Tseng and Lee 2000b). More details on the impact toughness mechanisms of PC/PBT blends with added MBS rubber are given below. The inclusion of rubber in polymers does, nevertheless, reduce the elastic modulus and the yield stress (McGrath 1994). The phase separation between the polymer and the rubber is an important requirement, and mechanical resistance increases if the rubber has low elastic modulus in relation to the matrix, good adhesion to the matrix, adequate crosslinking, optimised average particle size and distribution and low glass transition temperature (McGrath 1994).

Functional MBS impact modifiers for PC/PBT blends are also reported (Tseng and Lee 2000b). Tseng and Lee grafted three different kinds of functional-group containing monomers in the outer layer of the MBS: glycidyl methacrylate, acrylamide, and methacrylic acid. The introduction of a functional group to improve the adhesion between the MBS rubber and the PC/PBT alloy and, thus, to have an effect on the impact strength of these blends, as been realised. The impact strength was observed to improve if the amount of functional monomer was between 4 and 6 wt%, thus allowing a smaller amount of impact modifier to be used.

The MBS core/shell impact modifier is affected by heat (Bukman 1988). Poly(butadiene) is the most vulnerable component of the MBS impact modifier with respect to the thermal stability, because it still has double bonded carbon atoms. Crosslinking of the poly(butadiene) causes severe loss of impact strength. The poly(styrene) and the PMMA are much more stable towards heat. However, at significantly elevated temperatures PMMA is easily thermally degraded, essentially to the MMA monomer.

1.3.2.4. Mechanical Properties of PC/PBT Blends

One of the major advantages of blending PC with PBT is the retention, or improvement, of the favourable mechanical properties of these polymers. The mechanical properties of the blend are determined by the mechanical properties of the initial materials and by the overall blend morphology that is formed upon processing. The PC/PBT blend is an excellent example of the complex relationship that exists between structure and properties. Therefore, the analysis of the mechanical properties, in order to find a structure-properties relation, only makes sense if both the chemistry (transesterification reaction) and the morphology (phase separation, crystallinity, phase preferences) are well characterised. During processing, the temperature and the shearing influence the transesterification rate, the mechanical mixing/segregation and the breakdown of chain length. The cooling conditions, after processing, influence the overall crystallinity, the morphology of the crystallites, the phase components segregation and, consequently, the overall blend morphology.

Usually, the mechanical properties, such as impact strength and ductility of immiscible blends, lie below the additive line of the mechanical properties of the components and are a function of the composition (Pompe 1997), although some exceptions exist (Mishra and Venkidusamy 1995). In miscible blends, the values of the mechanical properties of the blend lie, normally, above the linear additive line (Mishra and Venkidusamy 1995). Synergistic effects that cause higher values than those of the pure components are rare.

In general, both for single polymers and for polymer blends, the molecular weight influences impact toughness and viscoelastic properties such as the tensile modulus and, thus, the toughness of the material. The degree of crystallinity determines the impact resistance and the viscoelastic properties such as the strain at break and, thus, the extendibility of the material. Furthermore, the miscibility level in polymer blends, both inherent and due to transesterification reactions, influences the impact resistance, the creep resistance and the aforementioned viscoelastic properties.

Sanchez and colleagues (1993) have suggested that transesterification-free PC/PBT compositions show a general improvement of the mechanical properties, with a mix of behavioural features that are close to linearity and are synergistic. Bertilsson and colleagues (1988b) state that additivity in mechanical properties is not likely to occur in PC/PBT blends since it is a partially miscible blend, consisting of two amorphous phases and one crystalline PBT phase.

Wu and Mai (1998 and 2000) have shown that the toughness of 50 PC/50 PBT blends lies on the additive line between the toughness of bulk PC and PBT, except when tested under non-plane strain condition (e.g. using thin samples or at high temperatures). In their reports, no information was given concerning transesterification stabilisation. It can then be said that improvement of impact toughness (assessed by means of Charpy impact testing) by blending PBT and PC, without rubbery impact modifiers, is not successfully attainable. The reason for this, in the case of 60/40 and 80/20 PBT/PC blends, is stated by Wu and colleagues (1998 and 2000) to be the very poor

interfacial adhesion between the two phases. The PC, in this case, does not bear the load and provides the propagating crack with an easy breakdown path. Furthermore, the PBT/PC interfaces reduce the effective fracture surface area. On the other hand, for PC-rich blends, the failure is thought to be due to a combination of factors including the fracture characteristics of PBT and PC, interfacial bonding and the applied load. The introduction of rubbery particles into the PC domains has been suggested as a means of eliminating the crack bridging effect of the PC domains, as the yield strength of the PC will be strongly diminished by the rubbery particles.

Pompe and coworkers (1997) studied the notched impact toughness of PC/PBT blends in which the copolyester content could not be detected within the limits of the analytical methods utilised. They concluded that the composition is not the main factor for the notched impact toughness. The blend morphology is characterised not only by the composition but also by the crystalline PBT content. Furthermore, the special morphology of the PBT crystallites also influences the mechanical properties. The substitution of 10 wt% of PC with PBT causes a rapid decrease of toughness from about 90 kJ/m^2 for pure PC to about 3 kJ/m^2 for the mixture. A sharp increase in the impact toughness, up to values above those of pure PC, are obtained if the crystallinity of the sample is in the range of 4-8 %. If the crystallinity in the sample increases above 12 %, the impact toughness decreases and is in the range of that of pure PBT. The authors also point out that, in the amorphous state, the modulus, strength, elongation at failure and notched Izod impact toughness are nearly linearly dependent on the composition.

The impact toughness of these blends can be increased by a factor of 16 as a consequence of a 20 % copolyester content (Pompe 1997). However, important properties such as the resistance to chemicals and heat distortion are reduced because of reduced PBT crystallinity. Furthermore, a yellow colour is developed due to the presence of aryl titanate residues, originating from the PBT manufacture (Hamilton and Gallucci 1993).

Hobbs *et al.* (1987, 1988 and 1988b) investigated PC/PBT blends that had been extruded with the addition of organic phosphates and a thermal stabiliser to inhibit transesterification and thermal degradation. Additionally, in some blend compositions a MBS rubber impact modifier was added. Assuming partial miscibility the authors concluded that shear deformation is the major toughening mechanism. Brittleness at low temperatures is caused by a reduction in the ability of the matrix to undergo shear deformation. The synergistic effect that was observed when mixing PBT with PC was attributed to the PC residing in the amorphous interlamellar regions of the PBT spherulites, thus facilitating interlamellar slip. The authors also found significant changes in mechanical properties of samples that were characterised by having the same PBT crystallinity but various microstructures of the PBT spherulites.

Wu *et al.* (1993) found that, for PC/PBT/MBS rubber blends, the increase in impact toughness with temperature is a consequence of the relaxation processes of the rubbery zones and the parent polymers, in a relatively low-temperature range and the thermal blunting of the crack tip

at higher temperatures. The mechanisms suggested (Wu and Mai 1993; Wu *et al.* 1993 and 1994) for the excellent impact resistance of this blend are multiple crazing, shear yielding, crazing with shear yielding and rubbery particle stretching and tearing. Wu and Mai (1992 and 1993) found that massive plastic deformation of the matrix occurred after rubber particle cavitation. This plastic deformation, shear yielding, was responsible for the drastic enhancement in fracture toughness, although the widespread cavitation did absorb a considerable amount of energy also. The sequence of toughening mechanisms is thought to be (Wu *et al.* 1992; Wu and Mai 1993):

i) Crazes formed in the PBT phase and at the crack tip;

ii) If the interfacial adhesion between PBT and PC and between PC and rubber and pigment particles, is good, then the crazes are stabilized by crazing and prevented from growing into critical cracks, otherwise, the crazes develop into cracks and result in fast unstable fracture;

iii) In the case of good interfacial adhesion, since the crazes are stabilized, the triaxial stress will rise until debonding occurs. Thus, debonding and cavitation occur. Localized voids are formed and expanded until the plane-strain constraint is relieved by the voids;

iv) Massive plastic deformation (shear yielding) occurs in the polymer ligament between neighbouring voids. This stage absorbs a tremendous amount of energy;

v) The crack propagates by breaking up the PBT domains. However, the two surfaces of the crack are still bridged by the highly deformed PC domains. Weak interfacial adhesion cannot stabilize the growing crazes and, consequently, there is no bridging effect. Thus, good adhesion is essential to promote slow crack propagation, cavitation, shear yielding and good impact resistance.

At room temperature, massive cavitation occurs inside the rubbery particles as well as at the boundary between the matrix and inclusions (Wu and Mai 1993). As soon as the rubber tearing strength or matrix-particle debonding strength is reached, cavitation occurs. Subsequently, the thickness of the polymer material between the neighbouring voids is reduced gradually until the thinnest part is totally broken so that the neighbouring voids form one big void. However, if the stress transfer efficiency is decreased, due to the lack of adhesion between the PC and, e.g. inorganic particles, cracking is inhibited due to the lack of stress concentration at the rubber/inorganic particles interfaces. Under an applied stress, rigid particles, such as inorganic pigments, induce tensile stress concentrations in the matrix. They become debonded from the matrix readily as they are unable to deform at any significant degree. Since there is limited adhesion between the rigid particulates and the matrix, the inorganic particles are not particularly effective craze or crack terminators, resulting in poorer toughening performance when compared to that achieved with well-bounded rubber particles (Keskula and Paul 1994).

1.4. Phase Separation and Phase Preferences in Impact-Modified PC/PBT Blends

Blends of PC and PBT represent an excellent example of the complex interplay between phase separation and phase preferences, crystallisation properties, thermal degradation and transesterification reactions.

With regard to the miscibility of PC and PBT, it is well documented that in approximately 50/50 % (w/w) PC/PBT blends, partial miscibility exists both in the melt and after melt blending, with phase separation occurring during PBT crystallisation (Wahrmund *et al.* 1978; Hobbs *et al.* 1987, 1988a and 1988b; Bertilsson *et al.* 1988b and 1989; Dekkers *et al.* 1990; Ratzsch *et al.* 1990; Pompe *et al.* 1991 and 1997; Sanchez *et al.* 1993; Wilkinson *et al.* 1995; Bennekom *et al.* 1997a). In such blends, and in the solid state, the PC phase is less than 10 % miscible in the PBT phase (Delimoy *et al.* 1995). Furthermore, the solubility of PBT in PC is better by a factor of 2 than the solubility of PC in PBT (Kim and Burns 1989). Conversely, Cheng *et al.* (1996) concluded that PC is more miscible in PBT than the opposite. Moreover, completely immiscible PC/PBT blends have been reported (Hanrahan *et al.* 1985; Pompe *et al.* 1996; Pompe 1997; Pompe and Haubler 1997). These disagreements arise from the complex behaviour of PC/PBT blends during melt processing, in which there is competition between liquid-liquid phase separation, interfacial transesterification reactions, crystallisation of PBT and reduction of the molecular weights of PC and of PBT.

The partial miscibility of the amorphous phases (amorphous PBT and amorphous PC) in this polymer blend has been attributed to various factors such as the morphology of the crystalline phase (Ratzsch *et al.* 1990; Pompe *et al.* 1996), transesterification reactions resulting in PC-PBT copolyester (Wilkinson *et al.* 1995 and 1997; Pompe *et al.* 1996; Hopfe *et al.* 1997; Pompe 1997) and the closeness of the solubility parameters of PC and PBT (Delimoy *et al.* 1995). Most of these studies have been based on:

a) Thermal analysis of the influence of the miscibility of PC and PBT on the T_g of PC and of PBT, and on the T_m, the crystallisation temperature (T_c) and crystallinity degree of PBT (**DSC** (Birley and Chen 1984; Hobbs *et al.* 1987 and 1988b; Bertilsson *et al.* 1988b; Golovoy *et al.* 1988; Kim and Burns 1989; Ratzsch *et al.* 1990; Folkes and Hope 1993; Hamilton and Gallucci 1993; Delimoy *et al.* 1995; Mishra and Venkidusamy 1995; Cheng *et al.* 1996; Pompe *et al.* 1996; Bennekom *et al.* 1997a; Hopfe *et al.* 1997; Tattum *et al.* 2000; Wilkinson *et al.* 2002), **DMTA** (Birley and Chen 1984; Bertilsson *et al.* 1988b; Golovoy *et al.* 1988; Kim and Burns 1989; Namhata *et al.* 1990; Ratzsch *et al.* 1990; Howelton and Letton 1991; Wu *et al.* 1992; Hamilton and Gallucci 1993; Memon 1994; Sepe 1995; Cheng *et al.* 1996; Bennekom *et al.* 1997a; Tattum *et al.* 2000;), **TGA** (Wahrmund *et al.* 1978; Ratzsch *et al.* 1990; Mishra and Venkidusamy 1995; Cheng *et al.* 1996));

b) Microscopic assessment of the influence of the miscibility of PC and PBT on the morphology of the blends (**SEM** (Hobbs *et al.* 1987 and 1988b; Kim and Burns 1989; Wu *et al.* 1992 and 2000; Tattum *et al.* 2000), **TEM** (Hobbs *et al.* 1987 and 1988b; Dekkers *et al.* 1988 and 1990; Delimoy *et al.* 1988; Wu *et al.* 1992, 1998 and 2000; Tattum *et al.* 2000; Wilkinson *et al.* 2002) and **OM** (Hobbs *et al.* 1988b; Delimoy *et al.* 1995; Hopfe *et al.* 1997);

c) Spectroscopic assessment of the influence of miscibility of PBT and PC on characteristic bands of PC, PBT and PC-PBT copolymer (**FTIR** (Birley and Chen 1984; Mishra and Venkidusamy 1995; Hopfe *et al.* 1997; Tattum *et al.* 2000) and **NMR** (Hopfe *et al.* 1997));

d) Other techniques such as solvent extraction methods (Birley and Chen 1984) and density measurements (Bertilsson *et al.* 1988b; Mishra and Venkidusamy 1995).

Evaluations based on the Lewis acidic/basic properties of the major components of these polymeric systems, as determined by IGC, and consequences to the establishment of specific intermolecular interactions and phase separation/preferences phenomena, have not been found in the literature.

Few studies have been undertaken where use was made of analysis of intermolecular forces to interpret interactions between the PC, the PBT, and the MBS rubber. Wahrmund and coworkers (1978) concluded from their studies that maximal interaction is achieved, and a miscible blend formed, at an optimum density of ester groups in the polyester (PET, PBT), when mixed with PC. Further evidence of the importance of specific interactions to the miscibility of PC and polyesters blends is given by Mishra and Venkidusamy (1995). In their paper, IR studies were shown to indicate that addition of PBT improves the intermolecular forces in PC, in particular, on the end-groups, the CH_3 groups and the C=O groups as indicated in the frequencies 1020, 1370, and 1770-1790 cm^{-1}. This effect was indicated also in the increased density that was obtained upon addition of PBT to PC. Moreover, addition of PBT was proven to hinder the C-H, C=O, and C-OH intermolecular interaction in PC. Blends of 90 PC/10 PBT (wt%) showed a single glass transition temperature, indicating the miscibility of the two polymers in the amorphous phase. If PBT was added at more than 6 wt% of the total weight, crystallisation and phase segregation occurred.

1.4.1. The Transesterification Reaction between PC and PBT

Interchange reactions in condensation polymers at elevated temperatures are well known, especially with polyesters (Birley and Chen 1984; Bertilsson *et al.* 1988b). Delimoy *et al.* (1988), Birley and Chen (1984), Bertilsson *et al.* (1988b), Hamilton *et al.* (1993), Hobbs *et al.* (1987), Kim and Burns (1989), Kong and Hay (2002b), Montaudo *et al.* (1998), Pellow-Jarman and Hetem (1995), Tattum and coworkers (1993 and 2000), Wilkinson and colleagues (1995, 1997, and 2002),

and Pompe and coworkers (Pompe 1991 and 1997; Pompe *et al.* 1996; Pompe and Haubler 1997) studied in detail the interchange reactions in PC/PBT blends.

It is known that PC/PBT blends may undergo three types of exchange reactions during melt processing (Pompe *et al.* 1991; Pellow-Jarman and Hetem 1995): acidolysis (reaction between carboxyl end-groups of PBT with carbonate groups of PC), alcoholysis (reaction between hydroxyl end-groups of PBT with carbonate groups of PC) and direct transesterification (reaction between ester groups of PBT with carbonate groups of PC). The main process is that of direct transesterification (Sanchez *et al.* 1993; Pompe and Haubler 1997) and, as a consequence of this, copolymers act as compatibilisers in these blends, making it difficult to characterise the inherent miscibility of PC and PBT in melt blends.

Some researchers believe that the transesterification reaction occurs only at temperatures that are greater than the T_m of PBT, approximately 220 ºC (Birley and Chen 1984; Cheng *et al.* 1996; Montaudo *et al.* 1998). Pompe (Pompe 1997; Pompe and Haubler 1997) has shown, nevertheless, that transesterification also occurs after "thermal treatment" at 200 ºC and 210 ºC (lower than the T_m of PBT).

The transesterification reaction is catalysed by Ti residues that are present in the PBT (Delimoy *et al.* 1988; Wilkinson *et al.* 1995; Hopfe *et al.* 1997; Pompe 1997), which can furthermore lead to the development of a yellow colour in the blend (Hamilton and Gallucci 1993). Wilkinson *et al.* (1995) varied the content of the catalyst (alkyl titanium compound) added to 50 PC/50 PBT blends. To inhibit further transesterification, an effective inhibitor was added after a desired mixing time. All of the observed results confirmed the changes expected as a consequence of increasing the copolyester content. Another factor that was noted in their study was the phase morphology of the blend as it determines the specific interfaces and, in this way, also influences the transesterification rate.

Consistent performance of PC/PBT blends can be achieved only through control of melt transesterification. If this reaction is not controlled, the properties of the blend will change with each thermal history. The transesterification process can be suppressed by added stabilisers (Delimoy *et al.* 1988; Wilkinson *et al.* 1995), but complete suppression cannot be proven (Pompe 1997; Pompe and Haubler 1997). The problem is that the analytical detection of a very small, *in-situ* formed copolymer content is limited by the sensitivity of the methods such as NMR and FTIR (Delimoy *et al.* 1995; Pompe 1997; Pompe and Haubler 1997), which is reported to be restricted to copolymer concentrations above 1 mol% (Delimoy *et al.* 1988). Even very low contents of block copolymers are known to influence the morphology of immiscible blends (Delimoy *et al.* 1988; Pompe and Haubler 1997). Furthermore, a correct estimation of the copolymer content is impossible, because the transesterification is influenced by many parameters. Additionally these parameters have an interaction. On this basis, Pompe and coworkers (Pompe 1997; Pompe and Haubler 1997) concluded that PC and PBT are inherently immiscible and that the partial miscibility

referred to in the literature by analysis of the glass transition behaviour is caused by the compatibilisation of both components by a small, virtually undetectable copolymer content. They also concluded that the transesterification is at first faster than the reaction between the stabiliser and the residual catalyst. Summarising, the direct proof of the complete absence of copolyester is virtually impossible.

Many additives have been used as stabilisers to prevent transesterification. These include phosphates, and phosphorus-containing acids (Hamilton and Gallucci 1993; Cheng *et al.* 1996). Stabiliser systems based on phosphoric acid can lead to a decrease of the hydrolytic stability of the blend (Bukman 1988). Di-n-octadecyl (Delimoy *et al.* 1988) and triphenyl phospite (Delimoy *et al.* 1995) are widely used as efficient transesterification inhibitors. However, Birley and Chen (1984) found that, even in a commercial PC/PBT blend (Xenoy® CL-100), that was stabilised against transesterification, small but significant reactions occurred after 3 min at 240 ºC. Large structural changes were observed after 30 min at 270 ºC.

Delimoy *et al.* (1988) reported that IR spectroscopy and NMR gave a very coherent picture of the PC-PBT copolyester structure that resulted from an exchange reaction of aliphatic ester and aromatic carbonate sequences. They found that the direct transesterification reaction is the most important exchange reaction between PC and PBT. The transesterification reaction can be described by (Delimoy *et al.* 1988; Hopfe *et al.* 1995):

$$A_1B_1 + A_2B_2 \rightarrow A_1B_2 + A_2B_1 \qquad \text{Scheme 1-3}$$

(Here A_1 refers to butylene units, A_2 refers to bisphenol units, B_1 to terephthalate units and B_2 to carbonate units.)

The copolymer A_1B_2 is a copolyester that is more stable than the formed aliphatic polycarbonate A_2B_1 and could be better detected by NMR and FTIR (Pompe 1997). With progressive transesterification, the initial homopolymers will be transformed into block copolymers and finally into random copolymers.

The transesterification rate increases with decreasing molecular weight of the PC (Pompe 1997). Therefore, the reported increased miscibility with lower molecular weight species can also have contributed to the greater transesterification rate.

Methods of Direct Detection

The chemical structure of the copolymers is connected to the appearance of new IR bands from the aromatic ester, at 1740 and 1070 cm^{-1} and from the aromatic-aliphatic carbonate group at 1770 cm^{-1} (Pompe *et al.* 1991; Pompe 1997; Tattum *et al.* 2000). The formed aliphatic-aliphatic carbonate group has an IR band at 1763 cm^{-1}. Hopfe *et al.* (1997) showed, by means of FTIR with NMR and DSC, that a low level of transesterification has a sensitive influence on IR bands that are connected with conformation states and/or crystallinity. These investigations lead to an

unambiguous interpretation of the IR spectra and a better understanding of the observed changes that arise with increasing transesterification. The carbonyl band at 1780 cm^{-1} for PC and 1720 cm^{-1} for PBT (Birley and Chen 1984; Pompe 1997) can be used to assess the PC-PBT proportion according to expectation (Tattum *et al.* 2000).

Tattum *et al.* (2000) calculated the degree of transesterification by relating the areas of the residual PC and PBT carbonyl absorbances to the volume fraction of the pure materials. However, it is recognised by the authors that low levels of transesterification are extremely difficult to detect using IR spectroscopy and that the results obtained should only be used as a qualitatively indication of the degree of transesterification. The lowest concentration for direct detection using the IR band at 1070 cm^{-1} was 3.5 mol%, as determined by NMR (Hopfe *et al.* 1997).

The copolyester content can also be determined by means of ^{1}H NMR as the ratio of the area of signal intensities of both A_2-B_1-A_2 and A_2-B_1-A_1 triads to all terephthlate triads (Pompe *et al.* 1991; Hopfe *et al.* 1995; Pompe 1997).

Methods of Indirect Detection

Some researchers (Birley and Chen 1984; Delimoy *et al.* 1988; Tattum *et al.* 2000) have used the solubility test to indirectly quantify the transesterification reaction degree. The change of the weight fraction of the blend that is soluble in methylene chloride (a good PC solvent) was related to progressive transesterification. This technique, although not strictly quantitative, is reported to be more sensitive than the spectroscopic methods since, according to some authors such as Delimoy (1988), only the PC homopolymer is soluble in methylene chloride. Conversly, Wilkinson and colleagues (1995 and 1997) report that the random copolymers, formed beyond a particular transesterification reaction degree, are soluble in methylene chloride, a fact that contributes to the incorrect evaluation of the soluble PC content of the PC/PBT blend and, thus, to the inaccurate determination of the transesterification degree.

Studies of the thermal properties of the components of a polymer blend can be useful. The melting point depression in a miscible blend depends on the concentration of the dissolved polymer and on the polymer-polymer interaction parameter (Al Saigh and Chen 1991; Bennekom *et al.* 1997a). Ester interchange and transesterification reactions can cause a reduction in the melting point as a consequence of high melt temperatures or prolonged heat treatment (Birley and Chen 1984; Bertilsson *et al.* 1988b; Pompe *et al.* 1991 and 1996; Hamilton and Gallucci 1993; Hopfe *et al.* 1997; Pompe and Haubler 1997; Wilkinson *et al.* 1997 and 2002; Tattum *et al.* 2000). These reactions result also in a lower PBT crystallinity (Bertilsson *et al.* 1988b; Wilkinson *et al.* 1997 and 2002) and in a decrease of the molecular weight (Bertilsson *et al.* 1988b), especially that of the PBT (Pompe *et al.* 1991; Hamilton and Gallucci 1993; Pillin *et al.* 2001). Both factors are also indicated in lower melting temperatures. The polymer chain length reduction, due to processing and not due to transesterification reaction, also contributes to the decrease of T_m as it also increases

the miscibility of PC and of PBT. Thus, T_m studies cannot be used to prove that there is no transesterification (Pompe 1997). If transesterification occurs, however, T_m values can provide a picture of how significant is the extent of transesterification (Hopfe *et al.* 1997). The heat of fusion, on the other hand, gives only qualitative information with regard to the transesterification reaction extension (Pompe 1997). According to Hamilton and Galluci (1993), a significant transesterification reaction is said to occur if T_m is reduced by more than 20 ºC, after heat treatment at high temperatures and/or a prolonged heat treatment time.

It has already been stated that the crystallisability and, in consequence, the crystallinity and the melting temperature of PBT decrease with progressive transesterification (Hamilton and Gallucci 1993; Pompe *et al.* 1996; Pompe 1997; Pompe and Haubler 1997). The initial homopolymer transforms into a random copolymer. The crystallinity decreases owing to dissimilarity of the chemical units of formed copolymers, and, eventually, all crystallinity is lost as a random copolymer is formed. As the transesterification reaction proceeds, the molecular chain length, especially that of PBT (Hamilton and Gallucci 1993), diminishes and, consequently the crystallisable content of PBT also decreases (Hopfe *et al.* 1997; Pompe 1997; Wilkinson *et al.* 1997). Pompe (Pompe *et al.* 1996; Pompe 1997; Pompe and Haubler 1997) uses the analysis of PBT crystallisation as the method of choice to assess the transesterification reaction extent.

Tattum *et al.* (2000) and Wilkinson *et al.* (1995, 1997 and 2002) studied blends in which increased miscibility of PC and PBT is achieved by increasing the transesterification rate. The latter is attained by incorporating an increasing amount of an alkyl titanium catalyst. Increasing transesterification resulted in a progressive reduction of the melting temperature, of the crystallisation temperature, and of the degree of crystallinity, with the development of a mixed-phase glass transition at around 90 ºC. It is clear from the DMTA plots that there is a reduction of the PC-rich phase T_g and a shift of the amorphous PBT peak to the PC-rich phase peak side. There is also an increase in the amorphous PBT content due to reduced crystallinity. A shoulder and peak that are indicative of the glass transition of PBT-rich phase and of the PC-rich phase, respectively, are visible for the stabilised blend. These merge into a broad peak as the level of Ti catalyst is increased, indicating an increase in phase mixing, presumably due to low levels of transesterification. TEM studies revealed distinct morphological changes in the blends as transesterification proceeded. Initially, a relatively coarse bicontinuous morphology developed into a more finely dispersed submicron scale bicontinuous morphology. The semi-crystalline structure of the PBT phase is nonspherulitic, with sheaf-like bundles of lamellae growing from nucleation points (Tattum *et al.* 2000). On further transesterification, the growth of the lamellae bundles acted to obscure any two-phase morphology within the blends. Finally, extensive transesterification inhibited PBT crystallisation and generated a homogeneous material.

An additional measure of the morphological stability of a blend is its Vicat temperature (Hamilton and Gallucci 1993). The Vicat temperature is proportional the degree of crystallinity in

PC/PBT blends. A large drop in the Vicat temperature indicates the formation of a PC-PBT copolymer. The Vicat temperature is also influenced by the molecular weight of PC and of PBT. Higher molecular weight PC and PBT result in higher Vicat values (Hamilton and Gallucci 1993).

1.4.2. Crystallisation Properties of PC/PBT Blends

The presence of a second component, either in the molten state or in the solid state, influences both the nucleation and crystal growth of semicrystalline polymers (Nadkarni and Jog 1991). Usually, the presence of the second component physically restricts the movement of the crystallising polymer molecules, and, thus, constrains the crystal growth. The extent of this effect is controlled by the blend composition, by the relative melt viscosities of the polymers involved, and by their miscibility. The effect of blending on nucleation is quite more complex, especially in the presence of the melt of the second component, namely with regard to the formation of critical size nuclei.

The crystallisation temperature of PBT is approximately 180 ºC (Dekkers *et al.* 1990). The crystallinity of the PBT in PC/PBT blends has been determined by Hanrahan *et al.* (1985) and by Cheng *et al.* (1996) to be 26 to 38 %. A maximum degree of PBT crystallisation of 40 % in these blends was observed by Ratzsch *et al.* (1990). In blends that are effectively stabilised against transesterification (that is within the instruments detection limits), the crystallinity of PBT has been determined to be about 38 % (normalised to the PBT content) by Pompe and coworkers (1997; Pompe 1997) and 33 % by Hobbs and coworkers (1988b). The overall degree of crystallinity is greater in cold-crystallised blends than in melt crystallised blends (Cheng *et al.* 1996). The formation of PBT crystals from within the PC-rich phase, as well as within the PBT-rich phase, leads to greater overall crystallinity, in the case of cold-crystallised blends.

With high T_g PC, the PBT crystallisation from the melt depends strongly on the "crystallisation window" (Bennekom *et al.* 1997a) and on the cooling rate (Pompe 1997). The "crystallisation window" of the blend is determined by the melting temperature (T_m) and the T_g of the PC phase, upon cooling (Nadkarni and Jog 1991). The crystallisation rate is at its maximum at the crystallisation temperature (T_c). This temperature for PBT is strongly dependent on the cooling rate (Bennekom *et al.* 1997a). The T_g of PC and that of PBT are a little dependent on the cooling rate. The crystallisation of PBT in a partially miscible PC blend can occur from the PBT-rich phase or from the PC-rich phase (Sanchez *et al.* 1993). The crystallisation from the PBT-rich phase is hindered by the presence of dissolved PC that as a higher T_g (Nadkarni and Jog 1991; Pompe 1997). The chain mobility is reduced. Also the crystallisation rate is slowed down (Nadkarni and Jog 1991). The rate of crystallisation from the PC-rich phase is strongly hindered by the high T_g of the phase. Here, the "crystallisation window" is small and the rate of crystallisation very slow.

The crystallisation of PBT from PC/PBT blends at low cooling rates (< 5 ºC/min) is independent of the PC content (Bennekom *et al.* 1997a). At higher cooling rates of blends with a

high PC concentration (e.g. 60/40 wt% blends), the PBT appears to crystallise in steps (Delimoy *et al.* 1995; Bennekom *et al.* 1997a). With a cooling rate of 10 ºC/min the first exotherm is at 187 ºC and the second at 105 ºC (Bennekom *et al.* 1997a). This second exotherm is below the T_g of the PC phase. This double crystallisation behaviour has been reported by several authors (Wahrmund *et al.* 1978; Bertilsson *et al.* 1988b; Wilkinson *et al.* 1995; Bennekom *et al.* 1997a), being ascribed to the crystallisation of PBT from the different phases. It is reported to start at 100 ºC and proceed to about 170 ºC for 50/50 wt% PC/PBT blends. The two distinct crystallisation kinetic profiles, one for the PBT-rich phase and the other for the PC-rich phase have also been reported (Delimoy *et al.* 1988).

For samples that are effectively stabilised against transesterification, Bertilsson *et al.* (1988b) found that processing temperatures that are higher than 260 ºC might have resulted in a higher degree of crystallisation due to lowering of the PC and PBT molecular weight by thermal degradation. Also, the molecular chain length decreases by eventual, non-detectable, transesterification. However, if the molecular chain is shorter than the critical length, that is necessary for crystallisability, the PBT crystallinity decreases. This is the reason why some authors, e.g. Hopfe *et al.* (1997), report decreased crystallinity with decreased molecular weight. Hamilton and Galluci showed (1993) that if low molecular weight PC and PBT are used in transesterification stabilised blends, the improvement of miscibility is also sufficient to reduce the rate of crystallisation.

Ratzsch *et al.* (1990) found that, in blends prepared by melt processing in an extruder, followed by injection moulding, the PC content strongly influences PBT crystallisation. Furthermore, if PBT crystallisation is excluded, by fast cooling the sample from melt, the miscibility of PBT and PC of the melt is retained in the solid state. Birley (Birley and Chen 1984) found that, in commercial PC/PBT blends (Xenoy® CL-100), the PBT retained its crystallinity.

Cheng and co-workers (1996) found from their studies of blends of PBT and PC, for a range of molecular weights and blend compositions, that addition of PC reduces the crystallisation kinetics of PBT so that the resulting crystals are more perfect than those which form in the homopolymer. Furthermore, the molecular weight of PBT is determinant as far as the crystallinity is concerned. The PBT degree of crystallinity increases with decreasing molecular weight of PBT, and of PC, due to increased molecular chains mobility, agreeing with the results of other authors such as Pompe (1991). The authors conclude that if the components have better miscibility (by decreasing the molecular weight of PC), this will serve to inhibit the formation of crystal nuclei, since initial phase separation is required for the PBT chains to locate one another. This results in slower crystallisation kinetics for systems with increased miscibility by decreasing the molecular weight of PC. On the other hand, the lower molecular weight, especially of PBT, will result in a more rapid crystallisation rate, as the fluidity of the melt is greater.

1.4.3. Phase Separation in PC/PBT Blends

The most commonly used method for establishing miscibility or partial phase mixing in polymer-polymer blends is the analysis of the behaviour of glass transition temperatures. T_g is dependent on blend composition. A blend of two miscible polymers will exhibit a single glass transition between the T_g's of the components with a sharpness of the transition that is similar to that of the components. In the case of limited miscibility, two phases exist and two separate glass transitions between those of the constituents are observed. The difference between the glass temperature of the partially mixed phase and that of the corresponding pure component gives information concerning the level of partial miscibility. It is important to note that a single T_g does not necessarily mean that miscibility exists on a molecular level. A single T_g also appears if the components are separated in phases whose size is smaller than a critical value. This critical value has been reported in the literature as ranging from ≤ 5 µm to 30-50 nm (Pompe 1997). Other commonly used methods to assess miscibility in polymer blends include the melting point depression method (Imken *et al.* 1976; Bertilsson *et al.* 1988b; Kumar and Yoon 1989; Schreiber and Lloyd 1989; Frensch *et al.* 1989; Al Saigh 1991, 1997a and 1997b; Al Saigh and Chen 1991; Nadkarni and Jog 1991; Herrero *et al.* 1994; Cheng *et al.* 1996; Bennekom *et al.* 1997a; Pompe 1997; Wilkinson *et al.* 2002), light scattering studies and X-ray scattering studies (Cheng *et al.* 1996).

The experimental results and interpretations found in the literature concerning phase separation in PC/PBT blends are contradictory.

Wahrmund *et al.* (1978) performed DTA and DMA measurements on PC/PBT blends. They found unambiguous and less unambiguous glass transition temperatures. In the interpretation of the results, one should note that the DTA and DMA measurements were carried out on differently pretreated samples. Thus, a comparison of the results will not lead to precise conclusions because the degree of PBT crystallisation varies. The authors concluded the existence of LCST as well as UCST behaviour. They assumed the existence of multiple phases (two amorphous phases and one PBT crystalline phase) whose amount and composition depended on the thermal pre-treatment. They found no evidence for any substantial reaction between PBT and PC during the high temperature melt processing, although multiple relaxation transitions, indicative of incomplete miscibility in the amorphous phase, were detected. In accordance with the classical mean field theory of polymer mixtures, they found a correlation between miscibility (at least partial) in the amorphous phase and a negative heat of mixing for low molecular weight analogues of Bisphenol A PC and polyesters (Wahrmund *et al.* 1978; Delimoy *et al.* 1988).

Bertilsson *et al.* (1988b) found LCST behaviour in PC/PBT blends, from an initial analysis of SEM imaging. However, from the analysis of the DMA and the DSC results, it was concluded that the initial interpretation was not correct.

Delimoy *et al.* (1988 and 1995), Bertilsson and colleagues (Bertilsson *et al.* 1989) and Abdeyev and Chalykh (cited by Cheng (Cheng *et al.* 1996)) reported UCST behaviour, suggesting that the mixture is miscible at temperatures above a critical temperature that depends on the composition.

Okamoto and Inoue (1994) found LCST behaviour in a PC/PBT (50/50 wt%) blend, by means of a time-resolved light-scattering study. A spinodal temperature of 198 ºC was determined. Consequently, if the blend temperature decreases below 198 ºC, phase mixing will occur and a homogeneous mixture will be formed.

Phase mixing is in kinetic competition with the crystallisation of the PBT (initiated at temperatures below T_m). This polymer has one of the highest rates of crystallisation of common polymers and, altough some retardation occurs, due to the presence of the PC in the PBT-rich phase, the crystallisation kinetics of the PBT-rich phase is still fast in most PC/PBT blends (Wilkinson *et al.* 1997; Tattum *et al.* 2000). According to these authors, structure development within these materials, therefore, tends to be dominated by the crystallisation of the PBT. This prevents extensive phase mixing and freezes the morphology that was developed during melt processing. The formation of a copolyester due to transesterification reduces the interfacial tension and contributes to the compatibilisation of the PC and the PBT. However, the occurrence of transesterification reduces the tendency of PBT to crystallise, further complicating structure development. Finally, the reductions of the molecular weight of the PC and of the PBT due to thermal degradation (Hobbs *et al.* 1988b; Pillin *et al.* 2001) and the occurrence of transesterification also contribute to miscibility of PC and PBT.

Summarising, it can be established that the construction of a phase diagram of the PC/PBT blend system from the thermodynamic point of view would very difficult, if at all possible (Pompe 1997).

Ratzsch *et al.* (1990) found that, in DMTA and DSC studies of blends prepared by melt processing in an extruder, followed by injection moulding, shifts of the PC T_g occur, indicating a certain degree of miscibility. Moreover, they concluded that PC and PBT are miscible if both components are liquid or completely amorphous.

A reduction of the main glass-transition temperature (T_g) of PC from 147 ºC to 100 ºC was observed by Birley and Chen (1984) for the commercial blend Xenoy® CL-100. This decrease was more or less stable at different thermal treatments, which is attributed to a stabiliser used during processing.

Kim and Burns (1989) published investigations of thermal behaviour in connection with the miscibility of PC/polyester blends. Melt PC/PBT blends and solution cast PC/PBT blends were investigated, by determining experimentally the glass transition temperatures, the melting temperature and the specific heat increment at T_g. In both cases, a change of the PC-rich phase T_g

that was dependent on the composition was found. Here, the change in melt blends was higher than that in solution cast blends. Therefore, PC and PBT were more miscible in the case of melt-extruded blends. These results agree with those of other published studies (Hobbs *et al.* 1987; Cheng *et al.* 1996; Bennekom *et al.* 1997b). The solubility of the PBT in the PC-rich phase was higher than that of PC in the PBT-rich phase. The transesterification reaction was proven to be non-existent as the T_g's and the T_m's of blends after remelting change insignificantly, as was the case with the studies of Hobbs and colleagues (Hobbs *et al.* 1987). Values of the Flory-Huggins polymer-polymer interaction parameter were determined by the T_g method and ranged from 0.042 to 0.033 for extruded blends at 250 ºC and from 0.054 to 0.039 for solution cast materials, at 25 ºC. The Flory-Huggins parameter decreases with increase of the PBT content for the investigated composition range.

The determination of the Flory-Huggins parameter calls for the existence of clearly defined T_g regions for both the PBT-rich phase and the PC-rich phase. This allows the determination of the apparent mass fractions in each phase. Also, the system must be at equilibrium. This state is difficult to prove and attain. Besides the proven dissolution of PBT in the PC-rich phase and of PC in the PBT-rich phase the authors concluded that, as the values of the Flory-Huggins parameter are greater than the critical value of this parameter, PC and PBT are immiscible for the investigated blend composition range.

Radusch and Androsch (1994) investigated PC/PBT melt blends by DSC and by wide angle X-ray scattering (WAXS). The glass transition temperature was investigated with respect to the composition and to the cooling rate. The change in the T_g of blends in comparison to the T_g of the pure components was discussed as partial miscibility. Especially, in the PC-rich blends, the T_g of the PC-rich phase, observed after cooling from the melt, decreases with increasing cooling rate. This can be explained, bearing in mind the influence of PBT crystallinity on T_g of the PC-rich phase. Very interestingly, the authors report the crystallisation of PC in 60/40 PC/PBT blends, after an intensive thermal treatment at 200 ºC for 4 hr. Pompe (1997) attributes this effect to an amorphous PBT content dissolved in the PC-rich phase and points out that such an intensive treatment is rare. Hence, the chance of crystallisation of PC under normal conditions is small.

According to several authors such as Hopfe *et al.* (1997), Pompe (1997) and Bennekom *et al.* (1997a), in most cases, the quoted decreasing glass transition temperature (T_g) of PC with increasing PBT content involves systems that have not been entirely stabilised against transesterification reactions. Even in blends that have been apparently stabilised against transesterification, other effects may by contributing for a decrease in the T_g of the PC-rich phase. For example, in PC/PBT blends, that were stabilised with 0.5 wt% triphenyl phospite, a decrease of the T_g was observed from 147 ºC (pure PC) to 130-135 ºC, by Delimoy (1995). Hobbs *et al.* (1987) give a possible second reason for this strong lowering of the T_g. This is the plasticizing effect of the

stabiliser. Pompe (1997) attributes the lowering of the T_g of the PC in these blends to a very low, non-detectable copolyester content formed during the processing.

Pompe (Pompe 1997; Pompe and Haubler 1997) reports that PC and PBT are immiscible in melt blends, provided that the copolyester content is exactly zero. The authors reached this conclusion following the determination of the T_g of the PC-rich phase at a copolyester content of zero (by extrapolation). This T_g was found to be identical to that of pure PC (146 and 147 ºC, respectively). Furthermore, the authors concluded that the initial transesterification has a much stronger influence on the glass transition temperature than on the melting temperature. However, Pompe's team also reported, in a prior paper (Pompe *et al.* 1991), that PC/PBT blends are miscible in the melt state and in the solid state, if it is possible to suppress the PBT crystallisation or to reduce the crystallite size. The miscibility is shown to be enhanced with decreasing degree of crystallinity. Variation of the PBT crystallisation properties was achieved by changing the cooling condition from the melt, and by addition of nucleating agents. For PBT crystallisation, the authors found that it is the crystallite size, rather than the degree of crystallinity, that determines de homogeneity/heterogeneity of the amorphous phases.

The immiscibility of PC and PBT found by Pompe (1997) is in agreement with the results of Hanrahan *et al.* (1985) and Hobbs *et al.* (1987), obtained on solution-cast blends. Nevertheless, as pointed out by Pompe (1997), these results can be influenced by the kinetics of evaporation of the solvent and therefore cannot be used for conclusions concerning inherent properties such as the miscibility of PC and PBT. Liquid-liquid phase separation during evaporation of the solvent can lead to different phase behaviour as in a quasi-equilibrium state (Hobbs *et al.* 1987; Pompe 1997). In this way, it is not clear whether the observed behaviour represents the inherent immiscibility or a special state of phase segregation.

Hobbs *et al.* (1987) published results of stabilised 50 PC/50 PBT wt% melt blends and of solution-cast blends formed from these stabilised formulations. A copolyester content was not found within the detection limit of ^{13}C NMR. The authors analysed the behaviour of the PC-rich glass transition. The observed decrease of the T_g of the PC-rich phase, by 20±2 ºC, in comparison to the T_g of pure PC was interpreted as proof of partial miscibility. After dissolution and drying, the T_g of the pure PC was found. Therefore, a transesterification reaction can be excluded as being the reason for the T_g shift. However, other authors such as Pompe (1997) interpret this strong decrease as being due to incompletely crystallised PBT content, dissolved in the PC-rich phase. The T_g of the PC in the PC-rich phase increased with the solution-casting of this melt blend and remained slightly below that of pure PC. The authors attribute this effect to a small undetectable copolyester content or to the presence of the stabiliser that was added to the mixed melt. Since the PBT is completely crystallised in the solution-cast blends, observed increases in the T_g of the PC-rich phase can be connected to the changed PBT crystallinity (Hobbs *et al.* 1987; Pompe 1997).

The decrease of the T_g of the PC by mixing this polymer with the PBT also has an influence of the degree of crystallinity of the PBT and is not just due to changes of the level of miscibility. This system has been studied by Pompe (1997) who found that in PC/PBT samples with different degrees of crystallinity, and stabilised against transesterification, the T_g of the PC varied but that of the PBT remained unchanged. Thus, the change in the glass transition temperature of the PC-rich phase was explained on the basis of the varying content of amorphous PBT in the PC-rich phase. The T_g of the amorphous PBT is then more affected by the presence of crystalline PBT than by the presence of PC in the PBT-rich phase. The greater the crystallinity of the PBT, both in the PBT-rich phase and in the PC-rich phase, the greater is the PC-rich phase T_g.

Delimoy *et al.* (1988) (TEM studies), reported that, during annealing at 220 ºC, the PBT lamellae were growing from the interface, inside the PC-rich phase, depleting the PC from the dissolved PBT. This fact is quoted as being direct evidence of the limited miscibility of PC in PBT, above the crystallisation temperature of the PBT. TEM imaging confirmed the reported (Wahrmund *et al.* 1978; Birley and Chen 1984) partial miscibility of the PBT in PC. Moreover, it can be concluded that the extent of PBT crystallisation also influences its solubility in a PC blend (Bennekom *et al.* 1997a). Ratzsch *et al.* (1990) found that phase separation occurs upon the appearance of PBT crystallisation and, therefore, is said to be entropically promoted. Delimoy *et al.* (1995) presented further evidence of the partial miscibility of PC and PBT in PC/PBT blends. Complete inhibition of transesterification was assumed as triphenyl phosphite was used as a stabiliser. However the authors pointed to the problem of the limits of analytical methods needed to prove the absence of a copolyester content. The partial miscibility was interpreted from the observed behaviour of the glass transition with respect to the composition. A change in the melting temperature was not found.

Cheng and co-workers (1996) studied blends of PBT and of PC, for a range of molecular weights and blend compositions. The molecular weight of PBT was determinant as far as the crystallinity and miscibility is concerned. The degree of crystallinity of PBT increases with the decreasing molecular weight of the PBT, and of the PC, agreeing with other researchers (Pompe *et al.* 1991). The T_g of the PC-rich phase was lower in blends that had a lower molecular weight of PC than in blends that had a higher molecular weight, but more pronounced lowering was seen when low molecular weight PBT was used. The investigated blend states were completely crystallised. Also, the T_g of the PBT-rich phase shifts to higher temperatures if low molecular weight PBT is used. The authors concluded that the compatibility would be better if the molecular weight of the PC, and of PBT, is smaller. Furthermore, in 40/60 wt% PBT/PC blends, the molecular weight of PBT affects more the amorphous phases than does the molecular weight of PC.

Bertilsson and co-workers (1988b) reported that processing at high temperatures (300 ºC) produced a significant reduction in molecular weight, the melt flow index increasing due to

injection moulding above 260 ºC. Significant transesterification effects were not observed. It was concluded that the PBT suffers a more severe degradation than does PC. The decreased molecular weight seems to be responsible for an increased crystallisation rate, and, consequently, a higher degree of crystallinity.

Hamilton and Gallucci (1993) studied the effect of molecular weight of the blend components on the viscosity and miscibility under conditions where transesterification was controlled. In 50/50 PC/PBT blends, the viscosity is determined primarily by the molecular weight of PBT. The use of lower viscosity PBT results in a lower T_g of the PC phase that is due to the increased solubility of the PBT phase in the PC. Increasing the molecular weight of the PC phase generally results in a decrease in miscibility between the two phases as indicated by the increase of the T_g of the PC phase.

Normally, thermal stabilisers are added to commercial PC/PBT polymer blends to prevent molecular weight degradation (Bukman 1988; Hobbs *et al.* 1988b).

When the PC/PBT blend is cooled fast from the melt, as is the case with injection moulding, part of the morphology is retained. As the blend is allowed to ”relax”, through ageing, this being accelerated at temperatures close to the T_g of PC, the morphology tends to complete phase separation. This effect has been studied by Bertilsson and coworkers (Bertilsson *et al.* 1988a, 1988b and 1989) and by Sepe (1995). When the solidified blend is subject to thermal ageing at 130 ºC, phase separation increases, followed by secondary crystallisation, which causes a denser polymer to be formed. The effect on properties is that the polymer blend becomes more brittle and loses part of its impact strength (Bukman 1988; Sepe 1995). As the ageing temperature is close to the T_g of PC (145 ºC), the thermal ageing accelerates the reaching of equilibrium (with respect to internal stresses and phase morphology). This results in a decrease of the mobility of the molecules. Since impact strength depends on the mobility, this mechanical property decays with the reduction of the free volume.

Further evidence of partial miscibility of PC and of PBT has been supported by tensile dilatometry (Dekkers *et al.* 1988), which indicated good interfacial adhesion between PBT and PC, resulting from complex interpenetration of the two polymers at the interface.

1.4.4. Phase Preferences in PC/PBT Blends

Another aspect of the polymer studied is the preferential presence of the impact modifier (IM) in the PC phase (Hobbs *et al.* 1987 and 1988b; Delimoy *et al.* 1988; Bertilsson *et al.* 1989; Dekkers *et al.* 1990; Memon 1994), although not to such an extent as was found for the studies relating to the partial miscibility of PC and PBT. This phase preference is thought to be caused partially by the expulsion of the impact modifier particles from the crystallising PBT, by “bad” interaction of the shell of the modifier with the molten matrix during blending, especially with the PC (Memon 1994), by mechanical stripping and partial dissolution of the PBT in the surrounding

PC (Dekkers *et al.* 1990) and by the values for the spreading coefficients of the blend components (Hobbs *et al.* 1988a ; Dekkers *et al.* 1990).

Memon states (1994) that PC and PMMA (the shell component of the MBS rubber) are not thermodynamically miscible, their interaction parameter being positive and small. The preferential location of the MBS particles in the PC phase is, thus, not justifiable solely by its interaction capability with PC.

Dekkers *et al.* (1990) concluded, from TEM evidence, that in PC/PBT/IM blends in which the IM (MBS rubber) is precompounded with PBT, spontaneous migration of the IM into the PC phase is observed during mixing with PC. Furthermore, it is observed that migration and subsequent retention of the IM in the PC phase is driven by the positive spreading pressure of the PC on the IM, and facilitated by the partial solubility of the PBT phase and the PC phase.

Although the use of spreading coefficients is based on the definition of surface tension, no study has been found in the literature, based on the analysis of surface Lewis acidic/basic properties of PC, PBT and MBS rubber, and consequences to the effectiveness of intermolecular forces, to explain this phase preference. Furthermore, no study was found in the literature that deals with phase preference of insoluble colorants in polymer blends, and consequences thereof to the physical properties, to the mechanical properties and to the colour properties of these systems.

1.5. Plastics Coloration

Several methods can be used to impart colour to a polymeric system: surface coating, surface dyeing, the introduction of colour-forming groups into the polymer molecules (Guthrie and Lin 1994) and mass coloration. However, for most applications of rubbers and plastics, the mass coloration method is preferred as the disadvantages overcome the advantages, as far as the alternative methods are concerned. Among the advantages of mass coloration are cost reduction and quality improvement with elimination of processing steps and finishing materials, if exterior surfaces using this technology are durable (Luxgrant and Vesey 1998; Anonymous 1999). Other advantages include technological aspects, aesthetic issues and environmental issues.

Weatherable, molded-in colour polymeric products are increasing in popularity due to their ability to match the surface finish, gloss and lustre, UV stability and overall durability of a painted metal part. For molded-in coloration, pigments are added to the polymer material during its compounding process, either during extrusion or in the moulding of the material.

The ability to achieve a particular colour of a material using a pigment is influenced by the nature of the base polymer, either by itself or in combination with other polymers, together with modifiers, additives or stabilisers. In the process of mass coloration, other performance properties, such as weatherability and mechanical properties may be adversely affected (Guthrie and Lin 1994). This is especially true in the case of toughness and ultimate elongation of filled polymers

(Boluk and Schreiber 1990). Composite property alterations are function of the quantity of pigment/filler added, dispersion quality and of the adhesion at polymer/pigment(/filler) interfaces.

From the several colourant forms that can be used in mass coloration, the most used is still the masterbatch concentrate. The major reasons are that, in this type of colour concentrate, it is possible to obtain a high concentration of colorant, and, thus, the greatest money value for the product. Another reason is that the less added vehicle reduces the effect on the physical or chemical properties of the polymer system. Furthermore, the traditional physical form of pellets mimics the form in which thermoplastic polymers are usually supplied, so making dosing and incorporation during extrusion a much simpler process.

To safeguard product properties it is necessary to ensure resistance to weathering. This, in turn, requires an optimisation of the entire system as all the components in the system interact and can be susceptible to weathering themselves. For instance, additives can also degrade upon weathering, affecting the dimensional stability of the polymeric system. Furthermore, the chemical structure of the polymer can contribute meaningfully to the lightfastness of the plastic product. The colourant itself interacts with the other components of the system and, therefore, its physical/chemical properties must be taken into account when designing a new or improved coloured plastic product. A particular polymer-colourant combination must be evaluated and tested in the final application after all of the processing steps have been carried out, to ensure optimum performance.

Three types of colorants exist: organic pigments, inorganic pigments and dyes. Pigments are particles that remain as such in the coloured plastic itself. Dyes dissolve in the plastic material and, therefore, have no particle size. Organic pigments are usually chosen for applications such as inks, coatings, films and fibers, in which transparency and high tinctorial strength are required, due to their intrinsic properties. On the other hand, inorganic pigments are preferred for applications in which hiding power or opacity and high lightfastness and weatherfastness are critical factors. Inorganic coloured pigments often have a better cost-benefit ratio than is possessed by organic pigments of similar shade. Their disadvantage is their much lower colour strength, which is particularly evident in colour reductions with titanium dioxide. Another example of a disadvantage, with the exception of lead chromate, bismuth vanadate, cadmium and ultramarine pigments, is their duller colour.

Frequently, the two types of pigment, organic and inorganic, are combined to take advantage of each economically. Also, blending inorganic pigments, with their excellent hiding power, with organic pigments with their colour strength can solve many of the problems associated with pigmentation.

The application of inorganic pigments is determined by their physical properties as well as by their chemical properties. The particle size, shape, and surface properties (surface heterogeneities, porosity) are as important to the pigment performance as is the chemical composition, namely the surface chemical composition. Extensive reviews on the physical-chemical aspects of pigment applications can be found in the literature (Guthrie and Lin 1994; Christie 2002).

Inorganic coloured pigments have very limited, if any, solubility in the surrounding medium and their optical effect is due to selective light absorption in conjunction with light scattering. These types of pigment have been used since prehistoric times. The main fields of application of inorganic coloured pigments include the coloration of paints, plastics, artist's colours, cosmetics, printing inks, leather, building materials, paper, glass and ceramic (Kirk 1978; Endrib 1998). This widespread range of uses is the consequence, with few exceptions, of the following advantages: excellent hiding power; extreme fastness to light and to weathering; outstanding colour stability and heat resistance; very good chemical resistance; fastness to solvents and to overspraying. Used in plastics, inorganic pigments offer the prospects of exceptional colour stability and resistance to heat and to ageing, extreme fastness to light and to weathering, total fastness to migration and absolute dimensional stability, i.e. absence of warping, even in the case of large-area injection mouldings. However, there are exceptions to the performance characteristics mentioned.

In complex inorganic coloured pigments, various metal cations are incorporated into a stable rutile or spinel host lattice, with well defined crystal structures (Endrib 1998). Most of the complex inorganic coloured pigments contain metal ions that are balanced by oxygen anions having structures that are similar to those of naturally occurring minerals. The major advantages of these pigments are their outstanding lightfastness and their resistance to high temperatures, (many are thermally stable up to 1,400 ºC), chemicals and weathering. Because of their stability and low toxicity, these compounds are suitable for colouring plastics as well as ceramics and building materials. These kinds of pigments cover a wide range of colours. Another important property is their intermixing ability, allowing the user a choice in creating many intermediate colours.

C. I. Pigment Blue 28, cobalt aluminate, is a particular example of a complex inorganic coloured pigment, being characterised by a spinel structure (Figure 1-2). It is offered in a wide range of blue shades, the variations being determined by the volume of alumina used or by the addition of chrome or silica. Such pigments have excellent resistance to heat, light and chemicals, and are moderately easy to disperse. They are commonly used in a wide range of thermoplastics and thermosets.

1.6. Uses, Properties, and Characterisation of C. I. Pigment Blue 28 (Cobalt Aluminate)

According to *The Colour Index* (1971), cobalt aluminate is classified as C. I. Pigment Blue 28. Its CAS No. is 1345-16-0. C. I. Pigment Blue 28 is also known as Kings Blue, Leyden Blue, Thenard's Blue and Leithner Blue.

1.6.1. Uses

Cobalt was used as a colouring agent by Egyptian artisans as early as 2000 BC and cobalt-coloured lapis or lapis lazuli was used as an item of trade between the Assyrians and Egyptians. In the Greco-Roman period cobalt compounds were used as ground coat frits and colouring agents for glasses. The common use of cobalt compounds in colouring glass and pottery led to the import of such compounds to China during the Ming Dynasty, under the name of Mohamedan Blue (Endrib 1998). In the sixteenth century, the ability of cobalt to colour glass a blue shade was rediscovered. Thenard synthesized pure cobalt blue at the beginning of the 19^{th} century (Endrib 1998).

Cobalt aluminate powders find industrial application as blue pigments and as heterogeneous catalysts, electrode coatings and magnetic devices (Pyke *et al.* 1998). As pigments, they are used in glazes, in the ceramic industry, in paint formulations, as well as in plastics coloration.

The spinel structure that characterizes cobalt aluminate is versatile in being able to accommodate a wide range of metal cations and oxidation states and is therefore a suitable candidate for optimising the performance in a range of particular applications, including plastics and paints.

The application of spinel pigments (as well as rutile pigments) in plastics results from their very good chemical resistance, complete fastness to migration, extremely high fastness to light and weathering and outstanding shade-temperate-time stability (Kirk 1978). For instance, in the case of pigmented poly(ethylene) there is no adverse effect on the strength of colour even after years of weathering.

Because of their heat resistance, these pigments are used as colorants in polyolefins and poly(styrenes) and are becoming increasingly important in the coloration of structural plastics, special plastics and polymer blends. These pigments have no tendency towards warpage in large injection mouldings and extruded products. This and their excellent fastness to weathering make rutile and spinel pigments particularly suitable for colouring bottle crates (Endrib 1998). Nevertheless, there are restrictions on the use of cobalt pigments for pigmenting binder systems that contain chlorine atoms, e.g. those based on PVC and chlorinated rubber, because weathering may cause the shades to darken.

Other examples of spinels that are used as pigments are the iron-containing pigments, zinc-iron browns and chromium-iron browns that are extremely fast to weathering, with appropriate

stabilizers, and can be used in PVC for outdoor applications. Furthermore, the iron-free brown pigment, manganese rutile brown, is particularly successful in PVC window frames (Endrib 1998).

As far as paints are concerned, cobalt pigments of the spinel type have superlative fastness properties. In particular, they have outstanding resistance to chemicals and fastness to weathering, even in very pale tints with titanium dioxide. In light pastel shades, they outperform all the well-known organic blue and green pigments. Typical applications are in coil coatings and in powder coatings, swimming-pool paints and electrophoretic systems (Kirk 1978). However, the use of these pigments in the paints industry is limited by the relatively high price of the raw materials.

Cobalt-based pigments can be dispersed in the stirred ball mills that are commonly used in the paints industry. Despite excellent fastness properties, other spinel pigments are of relatively little interest in the paints industry, for colouristic reasons.

1.6.2. Physical/Chemical Characterisation of Cobalt Aluminate

An important feature of the spatial structure of $CoAl_2O_4$, is the fact that eight Co atoms lie on one set of symmetry-related positions, with the sixteen aluminium atoms and the thirty-two oxygen atoms. The simplest way of analysing the spinel spatial structure is in terms of the approximately cubic close-packed array of oxygen atoms. The unit-cell contains eight formula units, i.e. $8CoAl_2O_4$. The oxygen array, assuming perfect cubic close-packing has a unit-cell edge equal to half that of the spinel unit-cell. There are, therefore, eight close-packed “oxygen sub-cells” in the spinel unit cell and hence 32 octahedral interstices and 64 tetrahedral interstices in the unit-cell. In a normal spinel, one half of the octahedral sites are occupied by aluminium ions and one eighth of the tetrahedral sites are occupied by cobalt ions.

The occupied sites are regularly disposed in such a manner that tetrahedra share corners only with octahedra and the octahedra share edges with another. A more detailed and elucidative description of spatial distribution of ions can be found in the literature (McKie and McKie 1974) and is illustrated in Figure 1-2. In the reference mentioned, it is shown that the spinel structure satisfies exactly the electrostatic valency rule.

Due to non-ideality of the cubic close-packing, in crystals of the spinel type AB_2O_4, as is the case of cobalt aluminate, the A^{2+} and B^{3+} cations are distributed over sites of tetrahedral and octahedral coordination (Becker and Rau 1988). The order parameter, λ, the so-called degree of inversion, characterises the distribution of cations over the two cations sublattices: $(A_{1-\lambda}B_{\lambda})[\ A_{\lambda}B_{2-\lambda}]O_4$. The parentheses and square brackets comprise ions on tetrahedrally and octahedrally coordinated sites, respectively. At sufficiently low temperatures, $CoAl_2O_4$ is almost a normal spinel in equilibrium (i.e. $\lambda \approx 0$). Under these conditions nearly all of the Co^{2+} ions are positioned on tetrahedral sites (Becker and Rau 1988), in the almost cubic close packed, face-centered oxygen lattice.

As mentioned, the cobalt(II) ion displays a variety of colours in a solid form or in a solution, ranging from pinks and reds to blues and greens. The pink or red colours are generally associated with Co^{2+} in an octahedral environment and the chromophore is typically $Co\text{-}O_6$. The tetrahedral cobalt ion, $Co\text{-}O_4$ chromophore, is sometimes green, but usually blue in colour (Kirk 1978). Furthermore, the surface Lewis acidity/basicity is influenced, to a significant extent, by the position (octahedral, tetrahedral) of the Co^{2+} cations and of the Al^{3+} cations.

In $CoAl_2O_4$, the order parameter is noticeably temperature dependent (Becker and Rau 1988; O'Neill 1994; He and Becker 1997). A typical value of λ is 0.16, but higher values are obtained for high surface area cobalt aluminate (Busca *et al.* 1992), or with increasing temperature (Becker and Rau 1988; He and Becker 1997). In the normal $CoAl_2O_4$, octahedral Al^{3+} ions predominate with respect to the tetrahedral ones, (as expected considering the given value of λ) (Busca *et al.* 1991) and the surface Lewis acidity is forecast to be weak, at least from the point of view of the abundance of sites. From previous observations, it can be expected that the surface Lewis acidity increases with increasing value of λ and, thus, with increasing concentration of Co^{2+} on octahedral sites. Table 1-4 contains a summary of several parameters that characterise the cobalt aluminate structure.

Table 1-4. Crystallographic data and magnetic nature of $CoAl_2O_4$ (Busca *et al.* 1991; Wu and Mai 1993; O'Neill 1994).

Parameter	Value
% Co^{2+} in tetrahedral environment	≥ 85%*
	80 %**
Magnetic nature	Paramagnetic
Unit cell , lattice parameter, a_o (nm)	0.810664
B_{tet} nm)	0.031
B_{oct} (nm)	0.033

* reference (Lenglet and Lefez 1996); ** reference (Busca *et al.* 1991)

As far as the particle size, the particle size distribution and the surface area of cobalt aluminate are concerned, (determinant for the use properties of any pigment), these vary with the preparation method. For instance, values of 1 to 5 m^2g^{-1} are obtained for the surface area when the "ceramic method" is utilised (Arean *et al.* 1999). By contrast, high surface areas (120-140 m^2/g) can be achieved if alternative synthesis methods are used.

1.6.3. Synthesis of Cobalt Aluminate

Generally speaking, spinel pigments (and rutile pigments) are manufactured by reacting finely divided metal oxides, hydroxides or carbonates in the solid state at a temperature of 800 to

1,400 ºC (ceramic route). Reaction sintering at the high temperature needed (about 1,400 ºC or higher) leads to very low surfaces areas, typically of the order of 1 to 5 m^2g^{-1} (Arean *et al.* 1999).

Several "ceramic" methods to produce cobalt aluminate can be considered (The Colour Index 1971):

a) Thenard's Blue: aqueous cobalt nitrate (free from iron and nickel) is precipitated with sodium phosphate. The violet precipitate of cobalt phosphate is washed well and mixed with freshly precipitated alumina. The mixture is dried and calcined until the requisite blue is obtained. The reddish blue product is ground with water and dried. The blue colour is improved by addition of sodium phosphate or ammonium magnesium phosphate. Greener hues are obtained by adding zinc oxide;

b) Leithner Blue is obtained similarly by using cobalt arsenate and alumina;

c) Alumina, zinc oxide and Co_3O_4 are fused at 1300 ºC;

d) A cobalt salt is precipitated with alum and sodium carbonate or sodium phosphate and the product is calcined;

e) Aluminum sulphate, cobalt sulphate and ammonium alum are fused at 1350-1700 ºC, wet ground, neutralized with ammonia if free sulfuric acid is present, dried and ground.

The reactions proceed more readily if the components are reactive, finely divided and intimately mixed. Adding mineralizers promotes solid-state reaction during calcination, which is performed either continuously in a rotary furnace, an annular furnace or a tunnel furnace, or batchwise in a directly fired car-bottom furnace or a rotary-hearth furnace. After calcination, the resulting clinker is wet-ground and any soluble salts are washed out. Surface treatment is also possible at this stage. The product is dried either in a spray-drying tower, when low dusting, free-flowing grades are required, or by standard means, which, however, necessitates subsequent grinding of the particles (Kirk 1978).

1.7. Surface Modifications of Inorganic Particles

A concern for a better understanding of intermolecular, specific interactions that occur in multicomponent polymeric systems calls for the ability to control these interactions beneficially. Consequently, the second part of this study relates to the controlled modification of the surface Lewis acidity/basicity of C. I. Pigment Blue 28, and consequences thereof to their interactions with the remaining components of pigmented, PC/PBT/IM blends and, as a result, to their physical properties and mechanical properties.

The more important, application-oriented, properties of pigments are the chemical constitution (surface and bulk), the crystal structure, the particle size and shape, the absorption and scattering characteristics (electromagnetic radiation) and the dispersibility (in a variety of different

vehicles). Many of the inorganic fillers and pigments that are manufactured for incorporation in paints, plastics, and other organic media, are surface-treated prior to their use. They are also used in conjunction with formulation additives that effectively modify the surfaces in the compounding processes (Solomon and Hawthorne 1983). Surface modification use may be aimed at different aspects of the application of inorganic particulates, such as improvement of their dispersion in organic media, modification of the rheology of a particulate dispersion and improvement of the mechanical properties of filled plastics compositions. Optimisation of adhesion characteristics is a widely used method of altering the application properties of inorganic particles (fillers and/or inorganic pigments) in polymeric media.

Schreiber and co-workers have published a significant number of papers on the use of surface-modified particulates to promote compatibility in polymer blends. Wang and colleagues (2001) studied the use of a diblock copolymer-modified rutile pigments on the morphology and mechanical properties of LLDPE/PVC blends. The surface treatment was meant to enhance the miscibility of these inherently immiscible blends. The mechanical and morphological characteristics of the blends were rationalised by the concepts of acid/base and dispersion intermolecular forces, as quantified by IGC. Optimisation of the Lewis acid-base interactions was beneficial to the dispersion of rutile on PVC and to the mechanical properties of resulting blends. Other researchers, such as Lipatov and Nesterov (2002) have shown that the introduction of suitable fillers improves the thermodynamic compatibility of particular polymer blends.

The appeal of controlling polymer surface properties and particulate surface properties has been evident for many years, and various strategies have been developed toward that end. An extensive literature search on surface treatment of inorganic particulates has been carried out. The major aspects regarding the surface modification of inorganic particles are outlined within the scope of this study. Details of the actual surface modification strategy that is used are given in the section on Experimental Procedures.

The major strategies used to modify the surface properties of inorganic pigments/particulates are:

a) Mechanical modifications, such as abrasion treatments;

b) Physical modifications, including surface deposition, and modification techniques using plasma and corona discharges;

c) Chemical modifications, making use of modifying or coupling agents, namely silanes and titanates;

Plasma and corona treatments are used in the surface activation for the introduction of functional groups or active species (Schreiber 1993; Jagur-Grodzinski 1999). This approach is also used as a first step for surface coating/grafting with organic species (Wertheimer *et al.* 1984; Richard *et al.* 1985; Schreiber *et al.* 1990; Schreiber and Germain 1990; Xue *et al.* 1990; Iriyama

and Ikeda 1994) and with inorganic species (Tsubokawa and Kogure 1991; Tsobokawa *et al.* 1994). As an example, Schreiber and co-workers (1982 and 1983) modified the Lewis acid-base interaction characteristics of $CaCO_3$ in filled PVC by surface treatment with microwave plasma (using acidic vapours and basic vapours). The dispersion characteristics of the filler in the polymer matrix, and the mechanical properties of the filled polymer, were strongly influenced by the surface treatment nature (Lewis acidic or Lewis basic). In another example, Xu and Schreiber (1998) treated a rutile pigment to air corona discharges, following the adsorption of monomers of acrylamide and of acrylic acid. These modifications resulted in pigments that showed differing surface Lewis acidity/basicity properties. Excellent reviews exist in the literature that relate to the use of corona and of low pressure plasmas in the control, and modification, of surfaces and interfaces (Wertheimer *et al.* 1984; Klemberg-Sapieha *et al.* 1993; Liston 1993).

The use of coupling agents is a common surface modification method (Ishida 1984; Saini *et al.* 1984; Malik *et al.* 1988; Papirer *et al.* 1988b; Vollenberg *et al.* 1988; Stori and Dahl 1990; Schreiber 1993; Wang *et al.* 1997). Extensive reviews exist on the use of coupling agents as modifiers of the surface chemical properties, and of the physical properties, of inorganic particulates. Examples include that by Ishida (1984) and that by Plueddemann (1985). Silanes and titanates may be coated onto the surface (Dasgupta 1991) or used as a preliminary stage for the surface coating, or surface grafting, of organic species (Vollenberg and Heikens 1989; Stori and Dahl 1990; Boven *et al.* 1991; Jagur-Grodzinski 1999). The use of coupling agents to modify the Lewis acid/Lewis base surface properties of pigments has been applied, for example, by Schreiber and colleagues (1993), by Papirer *et al.* (1988b), and by Fowkes *et al.* (1988).

Coating types can be divided into organic coatings and inorganic coatings. Typical organic coatings include copolymers, hydrophobic polymers (polyolefins) and hydrophilic polymers (Lewis acidic, Lewis basic and Lewis amphoteric) (Jagur-Grodzinski 1999). The coating material is either adsorbed at the surface from solution (Fowkes and Mostafa 1978; Fowkes 1980 and 1983b; Lara and Schreiber 1991b; Wang *et al.* 1997), polymerised after surface-treating the pigments with an appropriate initiator system (Boven *et al.* 1991; Tsubokawa and Kogure 1991), or after surface activation through cold plasma/corona treatment. In the case of a deposited polymer coating, this should be between 2 and 5 % of the weight of the inorganic particles (Jacobson and Wilmington 1995). The initiator systems include common polymerisation initiators and coupling agents. The initiator system is commonly immobilised at the surface of the particulates (Boven *et al.* 1990 and 1991; Tsubokawa and Kogure 1991; Tsobokawa *et al.* 1994). In some cases, used is made of surface functional groups, such as OH groups (Solomon and Hawthorne 1983; Tsobokawa *et al.* 1989 and 1994; Abboud *et al.* 1997; Jagur-Grodzinski 1999) and COOH groups (Jagur-Grodzinski 1999), to initiate the polymerisation reaction. Another coating method consists of milling the pigment in polymer melts. The advantage of this method is that complication of solvent competition for Lewis acidic and basic sites is avoided. A further example of a coating method is that of polymer coating in a dry form (Mizobuchi and Freed 1996). However, such a technique

causes secondary agglomeration of the pigment particles because of the adhesion that is generated by the heat, such as grinding energy, between the polymer coated surfaces.

The nature and amount of coating agent used depends on the type of pigment, as well as on the nature of the application medium. The choice of coating thickness is an important factor, which controls the effectiveness of the coating material (Kim and Mai 1998). In some cases, it is sufficient to cover part of the pigment surface with a monomolecular layer of coating agent, whereas, in other cases, complete coating with a multimolecular layer may be preferable. For optimisation of the properties of filled polymers, wide use is made of modification of the surface of the filler particles with polymeric species. In such a case, the particulates boundary layer will contain the modifying polymer (the entire polymer or only a part of it). Besides the properties of the polymer matrix and of the filler, one of the factors determining the properties of the composite is the state of this boundary layer of the filler. The adhesion interactions between the bulk polymer and the inorganic particles must have intermediate values since very strong adhesion interactions hinder the mobility of the inorganic particles while a weak adhesion decreases the reinforcement effect of the particles (Malik *et al.* 1988).

The use of inorganic coatings is a well-established method of surface modification and examples of compounds and ions that are precipitated, e. g. during the calcination of inorganic pigments, onto the surface of inorganic particulates include: sulphates, phosphates, $CaCO_3$, SiO_2, Al_2O_3, ZnO_2 (Schroder 1988). The surfaces of commercial inorganic pigments, such as rutile TiO_2 are usually modified towards acidity by surface coatings of SiO_2 or towards basicity by coatings of aluminium oxides (Lee *et al.* 1992; Schreiber 1993). In the case of pigmented, plasticized PVC, significant differences in rheological properties, and in mechanical properties, have been observed (Schreiber 1993) when the interaction balance within the system was altered by substituting a basic rutile TiO_2 for one with acidic surface characteristics. Similar studies on alumina and/or silica surface modification of TiO_2, and its influence on the dispersion of the filler (and, thus, interaction of the filler with itself), have been carried out by Lee and co-workers (1992).

Chemical treatments offer a less used approach. The oxidation (Bagreev *et al.* 1999 and 2000) and acidification (Fowkes and Mostafa 1978; Weber 1978; Jagur-Grodzinski 1999) of surfaces provide two options. In most cases, the chemical treatment is used to activate the surface for further treatment such as the introduction of polymeric species. The work of Papirer *et al.* (1988b) offers a good example. Silica was first treated with thionyl chloride at 200 ºC, and, after cooling at room temperature under a N_2 flow, the surface was reacted with alcoholates. Other chemical treatments can be used, such as rendering the surface of the inorganic particulates basic, by the use of calcium stereate (Lambla and Schreiber 1980) or by the use of NaOH (Dasgupta 1991), and modification of the surface, e.g., of calcium carbonate with phosphates (Nakatsuka 1985). Other treatments include the use of stearic acid to render the surface of, e.g. calcium carbonate, less Lewis basic and more Lewis acidic (Balard and Papirer 1993).

Two other types of surface modification can be identified. In the first instance, the inherent surface modifications due to chemical instability of the surfaces (Balard and Papirer 1993) can be identified. These derive mainly from processing operations, such as drying operations and milling operations, or by chemisorption of water, e.g. from the atmosphere during storage. The second type of modification concerns heat treatments, under which solids undergo miscellaneous surface modification that may originate from dehydration or dehydroxylation reactions, or from crystalline reorganisation of surface structure (Balard and Papirer 1993).

2. EXPERIMENTAL PROCEDURES

Several analytical techniques, and mechanical tests, were used in the physical and chemical characterisation of pigmented PolyCarbonate/Poly(Butylene Terephthalate)/Impact Modifier (PC/PBT/IM) blends prepared by extrusion. Moreover, the influence of the pigment (C. I. Pigment Blue 28, unmodified version and surface-modified versions) on their physical properties, their mechanical properties, and their morphology has been studied. Controlled surface modifications of the pigment, by means of a photo-sensitised grafting procedure, were carried out.

Differential scanning calorimetry was used to assess the effect of the introduction of the pigment, in the unmodified version and in surface-modified versions, on the phase transitions and on the bulk structural features of the pigmented PC/PBT/IM blends (enthalpy of crystallisation, non-isothermal crystallisation temperature, glass transition temperature, melting temperature). Image analysis (transmission electron microscopy, scanning electron microscopy) and energy dispersive x-ray spectrometry were used to assess the morphology of the blends and to locate the components, in particular the pigments, in the characteristic morphology observed. Dynamic mechanical thermal analysis and tensile testing were used to study viscoelasticity-related parameters such as the tensile modulus, the stress at yield, the strain at yield, the strain at break, the stress at break, the storage modulus, the loss modulus and the loss tangent. Izod notched impact testing and puncture impact testing, were used to assess the impact toughness of the PC/PBT/IM blends. A rheological assessment of the blends was carried out by means of the melt volume rate test. The thermal stability of the blends was evaluated by determining their Vicat softening temperature. Furthermore, PBT-based blends and PC-based blends, were prepared so as to perform the aforementioned analyses on samples that mimic each of the individual phases (PC-rich phase and PBT-rich phase).

The individual components of these polymeric systems were characterised in terms of their physical properties and their chemical properties. Differential scanning calorimetry was used in the characterisation of the phase transitions of the polymeric components (glass transition temperature, melting temperature, enthalpy of crystallisation, non-isothermal crystallisation temperature). The pigments studied were characterised by determining the average particle size, the particle size distribution, the surface area (BET), by analysing the surface chemical composition (by means of energy dispersive x-ray spectrometry analysis), the weight loss upon heating (by thermogravimetric analysis), and by assessing the particulates morphology (by means of scanning electron microscopy).

The molecular weight, and molecular weight distribution, of PC, and of PBT, in the processed blends, was determined by size exclusion chromatography (SEC/GPC). The surface

Lewis acidic/Lewis basic character of the polymers, impact modifier, and pigments was quantified by means of inverse gas chromatography and, therefore, the Lewis acid-Lewis base intermolecular interaction potential of the major components of the blends was evaluated.

2.1. Compounding

Extrusion is the most widely used processing operation in the plastics industry, either for the production of pipes, rods, tubes, films, and pellets, or as an intermediate step for mixing the components before moulding the material into the final form (e.g. for the dispersion of pigments). An extruder is a device that performs the functions of melting the formulation and pumping it through the die (Figure 2-1). In a typical extruder, the screw itself is divided into several sections, each performing a specific function in the processing. The feed section of the screw picks up the particulate or granular material from the feed hopper and conveys it into the barrel of the extruder. In the compression or transition section the feed is compacted, melted and formed into a homogeneous stream. The melt is then conveyed to the dye in the final metering section of the screw. The function of this section is to build sufficient pressure to maintain a uniform flow rate of compounded melt to the die. External heat is applied to the barrel during operation, but a considerable amount of frictional heating also occurs within the system. External heating is usually provided by heating bands that are positioned around the barrel. Twin screws are used in the case of materials that are difficult to handle or in dispersing and compounding operations, as agitation and mixing is more efficient. The twin-screw extruders are expensive but they provide flexibility for change, uniformity of mixing, short residence times and a narrow residence time distribution (Utracki *et al.* 1989). With single screw extruders, control is not as good. As far as the PC/PBT/IM blends are concerned, more intense mixing results in a higher miscibility in these systems (Bennekom *et al.* 1997a). In these reactive blends, the creation of a larger interphase between the components of the blend is a first step in increasing miscibility.

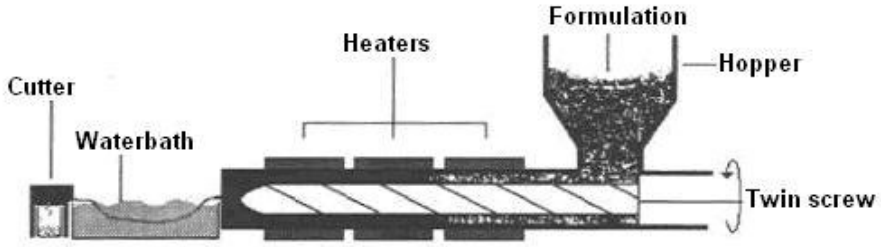

Figure 2-1. Cross section of an extruder.

A series of samples was prepared in order to assess the influence of C. I. Pigment Blue 28, and its surface-modified versions, on the mechanical properties and on the physical properties, of

PC/PBT/IM blends. A non-pigmented sample was prepared for use as a control, together with samples having the pigment loadings shown in Tables 2-4 to 2-10. PBT-based and PC-based samples, unpigmented and pigmented, were prepared to assess the effect of the pigments on each of the individual phases. The pigment loadings used are typically below, and up to, those used in commercial plastics applications.

Samples were prepared using two different extrusion systems. Extruder 1 (E1) was used to replicate the standard extrusion conditions and procedures used at the General Electric Plastics European facilities. Extruder 2 (E2) was used in order to study the influence of extrusion conditions, and of equipment specifications, on the physical properties, and on the mechanical properties, of the PC/PBT/IM blends. The major design difference between extruder E1 and extruder E2 is that the screw of E2 has a longer mixing area, and is equipped with more temperature control zones. Extruder E2 was operated at lower rpm (and, thus, lower throughput), and with a more controlled barrel temperature profile. The aforementioned differences in screw design, and operating conditions, resulted in a longer barrel residence time, and in a greater mixing energy being delivered to the blends, in the case of extruder E2. Also, due to greater mixing energy, and to the differences in the screw heating system, and temperature control facilities, the thermal history of the blends processed using extruder E1 or using extruder E2, was different.

The formulation of the blends consists of PBT (Valox® 195 and Valox® 315, from GE Plastics), PC (Lexan® 125, from GE Plastics), MBS rubber (the impact modifier Paraloid EXL 2600, from the Rohm and Haas Company), thermal stabilizers (Irganox® 1076, from CibaGeigy, and PELTP, from Sandoz B. V.), a transesterification inhibitor (monozinc phosphate (MZP), from Schmidt B. V.), and C. I. Pigment Blue 28 (Sicopal® Blue K6310, from BASF). All of the polymeric materials and additives were supplied through General Electric Plastics (Europe), Bergen op Zoom, The Netherlands. The PBT used in the compounding operations is a mix of the grades PBT 315 and PBT 195. These differ mainly in terms of the molecular weight, the carboxyl end-group concentration, and the hydroxyl end-group concentration (Table 2-3). The basic composition of the prepared blends is PC(45%)/PBT(45%)/IM(10%) (w/w). Additives (stabilisers and transesterification inhibitor) were added as 0.55 % (w/w) of the total blend weight. For the pigmented samples, the compositions were adapted to accommodate loadings ranging from 0.01 to 1.00 % (w/w).

Table 2-1. Some characteristics of the C. I. Pigment Blue 28 studied.

	BASF Sicopal® Blue K6310
Specific gravity (g/cm^3)$^+$	4.5
Average particle size (μm)	$1.18^+/0.40^*$
Specific surface area (m^2/g)	$20^+/22.8^{**}$

$^+$ from technical data sheets;

* determined using a Coulter N4M sub-micron Analyser (Section 2.8.);

** the BET surface area was determined using a Strentoline unit (Section 2.1.2.).

The major physical properties of the pigment, of the polymers, and of the impact modifier (IM) are summarised in Table 2-1 and in Table 2-2, respectively. The average particle size of the IM is 0.1 µm (source: GE Plastics Europe, Bergen op Zoom, The Netherlands).

Table 2-2. Weight-average molar mass ($\bar{M}_W$), polydispersity (D), and number-average molar mass ($\bar{M}_n$), of PC and of PBT, and T_g and T_m of the PC, of the PBT and of the IM.

	$\bar{M}_W$ (g/mol)$^+$	D$^+$	$\bar{M}_n$ (g/mol)$^+$	T_g (ºC)*	T_m (ºC)*
PC 125	37,000	2.30	17,000	145	n/a
PBT 195	46,000	2.70	17,000	45	230
PBT 315	108,500	3.18	34,100		
IM	not available	not available	not available	-70	132-149

$^+$ determined by GPC, source: GE Plastics, Bergen op Zoom, The Netherlands;

* determined by DSC (Section 2.4.1.).

Table 2-3. Carboxyl end-group concentration, and hydroxyl end-group concentration, of PBT 315 and of PBT 195, determined by FTIR. Source: GE Plastics, Bergen op Zoom, The Netherlands.

	-COOH (µeq/g)	-OH (µeq/g)
PBT 195	29	122
PBT 315	48	22

For samples extruded using extruder E1, the compositions of the formulations are described in Tables 2-4 to 2-9. Several sets of batches were produced, each batch weighing six kilograms. All the mixture components, except the PC (and the PBT 195 in the PBT-based blends) and the MBS rubber, were weighed in poly(ethylene) bags, mixed properly and put in a hopper, just prior to extrusion. The PC (or the PBT 195 in the PBT-based blends), and the MBS rubber, were delivered to the feed section of the screw by two separate hoppers, and, at the same time, mixed with the contents of the third hopper that contained the remaining blend components (Figure 2-2). Between samples runs, the extrudate was discarded until it appeared uniform (approximately 1 kg of material) and the following extrudate pelletised and collected.

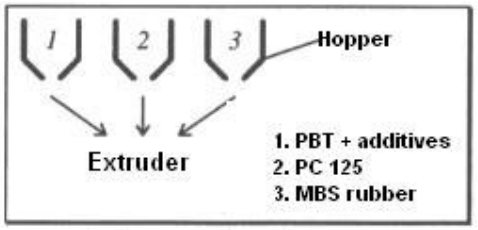

Figure 2-2. Hoppers system in extruder E1.

Extruder E1 is a Werner and Pfleiderer Supercompounder generation ZSK-30 twin-screw extruder (screw diameter: 25 mm). For the main operating conditions (average values), the screw

speed was 300 rpm, the flow rates were 40 kg/hr (Set 2), 25 kg/hr (Set 1, Set 3, Set 5 and Set 6), and 30 kg/hr (Set 4). The torque was 75 % (Set 1, Set 2, Set 5 and Set 6), 35 % (Set 3), and 70 % (Set 4). The temperature profile (ºC), ending at the nozzle, was: 50/100/200/260/270/255/255/275, slightly modified for the extrusion of the PBT-based samples and for the extrusion of the PC-based samples, due to the melt viscosity differences between these samples and the PC/PBT/IM blend samples.

Table 2-4. Summary of formulations (% w/w) extruded using extruder E1, Set 1.

Sample	B3	B4	B5
PBT 315	7.53	7.55	7.51
PBT 195	34.30	34.38	34.22
PC 125	45.32	45.42	45.21
IM	12.00	12.00	12.00
Irganox 1076	0.30	0.30	0.30
PELTP	0.05	0.05	0.05
MZP	0.20	0.20	0.20
C. I. Pigment Blue 28	0.30	0.10	0.50

Table 2-5. Summary of formulations (% w/w) extruded using extruder E1, Set 2.

Sample	Unpigmented blend (BX)	B6	B7	B8	B9	B10	B11
PBT 315	7.56	7.55	7.54	7.52	7.50	7.49	7.47
PBT 195	34.42	34.40	34.34	34.26	34.18	34.11	34.03
PC 125	45.47	45.45	45.37	45.27	45.16	45.06	44.95
IM	12.00	12.00	12.00	12.00	12.00	12.00	12.00
Irganox 1076	0.30	0.30	0.30	0.30	0.30	0.30	0.30
PELTP	0.05	0.05	0.05	0.05	0.05	0.05	0.05
MZP	0.20	0.20	0.20	0.20	0.20	0.20	0.20
C. I. Pigment Blue 28	0.00	0.05	0.20	0.40	0.60	0.80	1.00

Table 2-6. Summary of formulations (% w/w) extruded using extruder E1, Set 3.

Sample	Unpigmented PBT (PBTX)	B12	B13	B14
PBT 315	17.90	17.83	17.79	17.76
PBT 195	81.55	81.22	81.06	80.89
PC 125	0.00	0.00	45.27	45.16
IM	0.00	0.00	0.00	0.00
Irganox 1076	0.30	0.30	0.30	0.30
PELTP	0.05	0.05	0.05	0.05
MZP	0.20	0.20	0.20	0.20
C. I. Pigment Blue 28	0.00	0.40	0.600	0.80

Table 2-7. Summary of formulations (% w/w) extruded using extruder E1, Set 4.

Sample	Unpigmented PC (PCX)	B15	B16	B17
PBT 315	0.00	0.00	0.00	0.00
PBT 195	0.00	0.00	0.00	0.00
PC 125	73.21	45.06	44.95	0.00
IM	26.00	26.00	26.00	26.00
Irganox 1076	0.30	0.30	0.30	0.30
PELTP	0.05	0.05	0.05	0.05
MZP	0.20	0.20	0.20	0.20
C. I. Pigment Blue 28	0.00	0.40	0.60	0.80

Table 2-8. Summary of formulations (% w/w) extruded using extruder E1, Set 5.

Sample	B18	B19	B20	B21	B22
PBT 315	7.55	7.54	7.53	7.51	7.50
PBT 195	34.40	34.38	34.30	34.22	34.14
PC 125	45.45	45.42	45.32	45.21	45.11
IM	12.00	12.00	12.00	12.00	12.00
Irganox 1076	0.30	0.30	0.30	0.30	0.30
PELTP	0.05	0.05	0.05	0.05	0.05
MZP	0.20	0.20	0.20	0.20	0.20
C. I. Pigment Blue 28	0.05	0.10	0.30	0.50	0.70

Table 2-9. Summary of formulations (% w/w) extruded using extruder E1, Set 6.

Sample	B23	B24	B25	B26	B27
PBT 315	7.55	7.54	7.53	7.51	7.50
PBT 195	34.40	34.38	34.30	34.22	34.14
PC 125	45.45	45.42	45.32	45.21	45.11
IM	12.00	12.00	12.00	12.00	12.00
Irganox 1076	0.30	0.30	0.30	0.30	0.30
PELTP	0.05	0.05	0.05	0.05	0.05
MZP	0.20	0.20	0.20	0.20	0.20
C. I. Pigment Blue 28	0.05	0.10	0.30	0.50	0.70

For samples prepared using extruder E2, four kilogram batches, of the samples identified in Table 2-10, were prepared. The transesterification inhibitor (MZP) was added just prior to extrusion. The formulation components were mixed in a poly(ethylene) bag and energetically shaken to promote an even distribution. The powder samples were dried in a vacuum oven, for 4 hours at 120 ℃. After this time, the oven was switched off and the samples were left under vacuum

overnight to minimise degradation by water (Birley and Chen 1984; Delimoy *et al.* 1988; Kim and Burns 1989; Utracki 1998).

Samples were extruded within 24 hours of their preparation. The content of the poly(ethylene) bag was introduced in a single hopper that delivered the formulation to the feed zone of the screw. As with extruder E1, the extrudate was discarded between samples runs, until it appeared uniform (approximately 1 kg of material), and the resulting extrudate pelletised and collected.

Table 2-10. Summary of formulations (% w/w) extruded using extruder E2, Set 7.

Sample	Unpigmented blend (LX)	L7	L8	L9	L10
PBT 315	7.56	7.55	7.55	7.53	7.47
PBT 195	34.42	34.42	34.38	34.30	34.03
PC 125	45.47	45.47	45.42	45.32	44.96
IM	12.00	12.00	12.00	12.00	12.00
Irganox 1076	0.30	0.30	0.30	0.30	0.30
PELTP	0.05	0.05	0.05	0.05	0.05
MZP	0.20	0.20	0.20	0.20	0.20
C. I. Pigment Blue 28	0.00	0.01	0.10	0.30	1.00

Extruder E2 is an APV MP2000 extruder. It was noted that the mixing area of the screw was longer in this extruder than it was that of extruder E1. The average main operating conditions were as follows: the screw speed was 250 rpm, the flow rate was 10 kg/hr, the torque was close to 50 %. The temperature profile (ºC), starting at the feed section and ending at the nozzle was: 75/115/200/240/270/254/254/254/254/254/255/254/243/229/233. The temperature drift between the set-point and the actual temperature of the melt was up to 15 ºC.

2.1.1. Tape Extrusion

A laboratory-scale tape extruder (built in-house, Figure 2-3) was utilised to produce tape ribbons (thickness: 1 mm, width: 10 mm) from the extruded pellets. The tape extruder was operated at 265 ºC. The tape-extruded samples were used in DSC studies and in the TEM/SEM/EDX analysis of the blends.

An attachment was made so that the ribbon die, with the desired dimensions, could be used with the tape extruder. The samples were prepared from pellets of the abovementioned batches, dried in a vacuum oven at 80-100 °C, for 3 hours. The oven was then switched off and the pellets left under vacuum overnight, before proceeding with the tape extrusion.

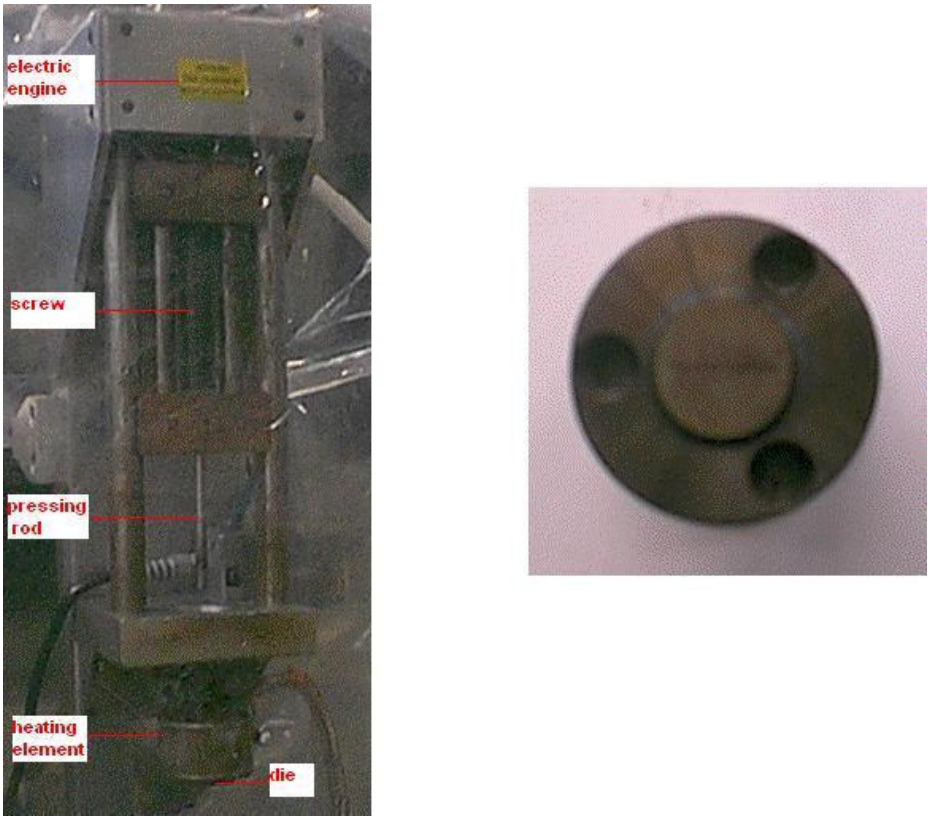

Figure 2-3. Tape-extruder (on the left-hand side) and detail of the die (on the right-hand side) used for the production of samples.

2.2. Injection Moulding

In the injection moulding process, the polymeric material is melted in a small screw and injected into a mould that has a specific design. Due to the temperature difference between the mould and the melt, the material can solidify and, after opening the mould, the shaped article is freed from the mould.

The injection moulding process is composed of different stages, in the following order: mould closing, injection of the melted material, cooling of the melted material, opening of the mould, and release of the moulded material. During the mould closing stage, both mould parts are kept together by high pressure in order to keep the material in the mould. Next, during the injection stage, the material previously melted in the screw is injected into the closed mould. During the cooling stage the material in the mould shrinks. The moulded article should have the same size as the inside mould size. To fulfil this requirement, the mould is filled with the proper amount of melted material. The cooling time should be sufficient for the article to be produced as fast as possible but not be damaged during the release of the mould. During the mould opening cycle, the cooled, shaped, material is pushed out of the mould. Before a new set of cycles begins, there is a pause. A safety valve prevents the material from returning to the back of the mould. The function

of the mould nozzle is to connect the mould and the injection unit and to ensure that material leakage does not occur.

The typical injection moulding machine (Figure 2-4) consists of two major sections: the injection unit and the holding unit. The injection unit is where the material is melted, transported by high pressure, and injected into the mould. The holding unit consists of the mould where the melted material is pressed, cooled and, thus, shaped. The screw consists of three zones: the feeding zone, the compression zone, and the pump zone. The screw functions are to melt the material and to transport it to the injection dye. Frictional heat arises by transport. External heating is also supplied.

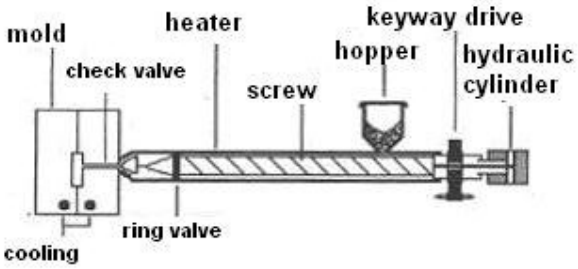

Figure 2-4. Cross section of an injection moulder.

The pelletised material was injection-moulded into impact testing bars, tensile testing bars and circular plaques, using a NETSTAL injection moulding unit. The extruded material was dried for 2 hours, at 110 ºC, prior to moulding. The screw speed was 30 rpm, the holding pressure 50 bar, the holding time 10 s, the injection time 10 s, the injection pressure 5 bar, the cooling time 20 s, the cycle time 41 s, the residence time 4 min, the mould temperature 60 ºC, and the temperature profile (ºC), ending at the nozzle: 40(intake)/250/255/265/255. The first five sets of moulded specimens, corresponding to the amount of melted polymer carried by the screw, were discarded, in order to ensure that there was no contamination from previous runs.

2.3. Mechanical Testing

2.3.1. Izod Notched Impact Testing

The purpose of impact testing is to obtain an indication of the ductility, or energy absorption capacity, of a material under high rate impact conditions. Izod is one of the pendulum-type impact tests. Other tests in this category include the Charpy impact test and the tensile impact test. The notched Izod impact test has become the standard for comparing the impact resistance of plastic materials (McGrath 1994). Although it has often been questioned as a meaningful measure of impact resistance (McGrath 1994; Timmerman, T. *et al.* 2001, Personal Communication), because

the test tends to measure notch sensitivity rather than the ability of plastic to withstand impact, the values are widely accepted as a guide for comparison of toughness between materials.

Izod impact testing was carried out according to the ISO 180 standard test method, and performed using a Zwick® 5110 unit (a pendulum impact testing machine). For more details on the test and on the experimental set-up, see Appendix G, following the presentation of essential results in the Appendix.

Test bars can vary in type and in the dimensions of the notches. The standard used was ISO 180/1A (specimen type I and notch type A). The bars were notched with a rotational single tooth miller (using a TMI 2205 unit, and according to ISO 2818). After notching, at least one hour elapsed before testing, in order to release possible stresses that might have been introduced by notching. The dimensions of specimen type I are 80 mm long, 10 mm high and 4 mm thick. The test samples were injection moulded to give specimens with the aforementioned dimensions.

The test temperatures used were: -20 ºC, -10 ºC, 0 ºC and 23 ºC. The samples were not all tested at all the temperatures mentioned: the temperature was decreased from 23 ºC until the sample exhibited brittle fracture. In order to reach the experiment temperature, the sample was conditioned at the desired temperature, for a sufficient length of time for temperature equilibrium to be reached. In this case, the time between taking the specimen out of the conditioning chamber and testing was kept as short as possible. Per batch, 5 bars were notched and tested.

Several break types can be distinguished: i) complete break; specimen breaks in two or more pieces; ii) hinge break; incomplete fracture such that both specimen parts are held together by only a thin peripheral layer in the form of a hinge having no residual stiffness; iii) partial break; any incomplete break that does not meet the definition of hinge break, and iv) non-break; no fracture at all, bending and stress whitening may be observed. Only in case of a complete break or a hinge break, was an Izod impact value reported. In the case of non-break, no value was reported.

2.3.2. Tensile Testing

Tensile properties are the most important single indication of strength in a material (McGrath 1994). In a tensile test, a specimen is extended along its major longitudinal axis (uniaxial deformation), at a constant velocity, until the specimen fractures, or until the stress (load) or the strain (elongation) reaches a predefined value. During the test, the load and the elongation are measured and utilised to calculate the tensile stress and the tensile strain, respectively. The parameters analysed are: the tensile modulus, the stress and the strain at yield, and the stress and the strain at failure. For more details on the theory, and experimental set-up of tensile testing, see Appendix H.

The test was performed according to the ISO 527 standard test method, using an automated Zwick® 1474 tensile testing machine, at room temperature and a test speed of 50 mm/min. The test

samples were injection moulded to give tensile testing specimens with the dimensions indicated in Table 2-11, according to the standard ISO 3167.

Table 2-11. Dimensions of the tensile testing specimen.

Dimension	Value in mm
width of narrow section	13
length of narrow section	57
overall width	19
overall length	165
gage length	50
distance between grips	115
Thickness	4

The thickness and width on each specimen were measured using a micrometer. The average value for several specimens was introduced as data for the computer prior to measurement. Per batch, 5 bars were tested.

2.3.3. Puncture Impact Testing

Puncture impact testing was carried out according to the ISO 6603-2 standard test method, in a Ceast® FractoVis unit. The multi-axial impact (MAI) test gives an indication of the ductility, and energy absorption capacity, of a material under high rate impact conditions. The testing system consists of a falling, or servo hydraulically driven mass that is used to move a dart through a plaque that is constrained by a clamp. A force-deflection, or force-time, curve is then integrated to quantify the area under this curve, which corresponds to the impact energy that is absorbed by the specimen as the dart passes through. The parameters determined are the energy to maximum force and the total puncture energy. Both parameters are reported in Joules (J). Visual inspection of the failed specimens can also be used to determine a percent ductility. This is defined by the percent of specimens, in a given sample, that exhibit ductile behaviour. There are three basic ways to characterize failure type: i) if the failure is a circular, clean hole where yielding is evident, the failure is counted as ductile, ii) if the hole exhibits any cracks but no part of the specimen is missing, the specimen is still counted as ductile and iii) if there are pieces missing from the specimen, the failure is counted as brittle.

The test specimen was an injection moulded disc of 60 mm diameter and 3.2 mm thickness. At least 5 specimens were tested and the average values reported. The actual test cycle consists of placing the specimen in the clamp so that the centre of the specimen is aligned with the centre of the clamp. The moulding cavity side of the specimen should be facing away from the dart. The falling (or driven) mass is then fired. The samples were tested at -20 ºC, at an impact velocity of 4.4 m/s.

2.4. Thermal Analysis

2.4.1. Differential Scanning Calorimetry

Differential scanning calorimetry, DSC, is defined as a technique in which the difference in energy inputs into a sample and reference is measured as a function of temperature, or time, while they are subjected to a controlled temperature programme. The instrument used was a DSC 2010 DSCalorimeter. All the studies were carried out under a nitrogen flow rate of 200 cm^3/min.

Initial studies were carried out on samples that were prepared by breaking a small piece from a single pellet. This sample preparation was found not to be the best. An improved sample preparation method was developed consisting of grinding the pellets (Section 2.11.). In this manner, the heat flow through the sample is greatly improved and the graphs obtained are more informative. An even more effective sample preparation procedure was developed using a tape extruder to produce the test specimen (Section 2.1.1.). The graphs obtained were even clearer and artifacts, due to movement of the sample in the aluminium pan when heating, were eliminated. This was the sample preparation procedure used thereafter.

In the DSC analysis of pellets, and of tape-extruded samples, mass sizes ranged from 20 to 30 mg, and from 4 to 10 mg, respectively. The typical sample mass for granulate and powder samples (relating to raw materials and blends) was 3-9 mg.

For the heating mode analysis, the samples were heated at a rate of 10 ºC/min, from 50 ºC to 440 ºC. From the thermograms obtained, the temperatures relating to characteristic exothermic relaxation processes, and to endothermic relaxation processes, were determined.

The non-isothermal crystallisation behaviour of the tape-extruded blends was studied using the following temperature program: heating the sample from room temperature to 250 ºC at 200 ºC/min; keeping the sample at this temperature for one minute, to release all the stresses within the material and to erase the thermal history; cooling the sample from 250 ºC at a constant rate (8 ºC/min) to 162 ºC. In practice, the sample was held at 250 ºC for approximately 2 minutes and 40 seconds, due to the temperature equilibration stage that was prior to the isothermal step. The typical mass of sample specimen was 7 mg. As no controlled cooling facilities were available, the sample was left to cool, inside the DSC cell, without cooling rate control. The cooling temperature profile was registered over time increments of 30 seconds. It was found that for all the samples analysed the cooling rate was effectively constant and equal to 8.3±0.2 ºC/min. The non-isothermal crystallisation properties determined were: the crystallisation on-set temperature, $T_{c,on\text{-}set}$, the crystallisation off-set temperature, $T_{c,off\text{-}set}$, the crystallisation temperature, T_c, and the enthalpy of crystallisation, $-\Delta H_c$. The thermogram was recorded so that the temperature scale was 175-230 °C. A designed data processing procedure was developed to determine $T_{c,on\text{-}set}$, $T_{c,off\text{-}set}$, T_c, and $-\Delta H_c$. Thus, the thermograms were digitalised and decomposed using the Microcal™ Origin® software for data analysis. The thermogram curve, (heat flow (mW) *vs* temperature (ºC)), was developed for

a temperature increment of 0.25 K. The heat flow data (mW) were then converted to heat capacity data (J/gK), using the mass of PBT present in the sample and the cooling rate, according to Equation 2-8:

$$C[J/(gK)] = \frac{q}{c \times x_{PBT} \times m} \qquad (2\text{-}8)$$

Here, C is the heat capacity of the sample (J/gK), q is the heat flow (mW), c is the cooling rate (K/s), x_{PBT} is the mass fraction of PBT in the sample, and m is the mass of sample (mg). Figure 2-5 is representative of the curves thereby obtained. Lines and tangents were constructed to determine $T_{c,on\text{-}set}$, $T_{c,off\text{-}set}$, and T_c, as demonstrated in Figure 2-5. The heat of crystallisation (J/g) was calculated from the area under the curve using the baseline defined, as shown in Figure 2-5. When calculating the enthalpy of crystallisation, the mass of PBT in the PBT-rich phase only should be used as the major crystallisation relates to this PBT. However, the contribution and the amount of the PBT in the PC-rich phase will not significantly affect the values obtained.

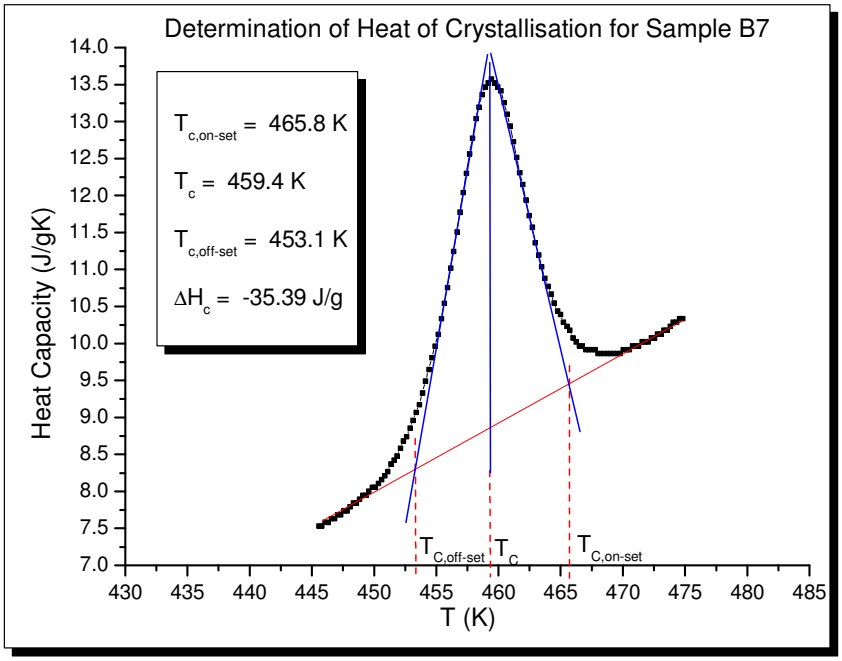

Figure 2-5. Graphical procedure for the determination of the crystallisation properties of the samples.

The melting behaviour of the blends was studied by heating the sample, typically 6 mg of tape-extruded blend, from room temperature to 270 ºC, at 10 ºC/min, and determining the T_m. The sample was held at 270 ºC for 5 minutes, cooled to room temperature at the fastest cooling rate, and re-heated to 270 ºC to determine the change, if any, in the value of T_m.

2.4.2. Thermogravimetric Analysis

For the polymer blends samples, thermogravimetric analysis (TGA) was used to investigate any weight loss occurring at temperatures up to 600 °C and, also, to aid with analysis of unknown events in the DSC thermograms. The weight loss and the temperature at which the curve presented significant slope changes were analysed. The instrument used was a TGA 2050 Thermogravimetric Analyser, the runs being carried out under a nitrogen flow. The heating rate was 10 °C/min, and the temperature scale 20 to 600 °C. The typical sample mass was 20-25 mg for pellets samples and 3-12 mg for powder samples. TGA was also carried out on the commercial pigment (BASF Sicopal® Blue K6310), in order to ascertain the presence of any manufacturer surface treatments. TGA was also carried out on the surface-modified pigments, in order to assess, qualitatively and quantitatively, the polymeric species that were fixed on the surface of the pigment after the surface treatment (i.e., surface photografting, see Section 2.13.). Thus, the weight loss at 600 ºC (the highest temperature allowed by the instrument) of a sample of surface-treated pigment was determined, along with that of control samples (non surface-treated pigment sample, photoinitiator sample, and homopolymer sample). The heating rate was 10 °C/min, starting at room temperature, and the sample was held at 600 ºC for 30 minutes. The runs for the pigments were also carried out under a nitrogen flow. A typical sample mass was 5-10 mg for the pigment samples and for the photoinitiator control sample and 1 mg for the homopolymer sample (see Section 2.13.).

2.4.3. Dynamic Mechanical Thermal Analysis

Dynamic mechanical thermal analysis (DMTA) is a technique in which the storage modulus (E') and the loss modulus (E'') of the sample, under an oscillating load, are recorded as a function of time, temperature, or frequency of oscillation, while the temperature of the sample, in a specified atmosphere, is varied. The storage modulus is related to the elastic response, and the loss modulus is related to the viscous response, of the polymeric system to a sinusoidally applied strain. Therefore, the stiffness and the damping properties of a material, over a specific temperature range, are measured. Further to the determination of the loss modulus and of the storage modulus, the loss tangent, tan δ, is determined. For more details on the theoretical background of DMTA see Appendix I.

The DMTA technique is particularly useful for evaluation of viscoelastic materials such as thermoplastic polymers that exhibit time and frequency dependent behaviour and temperature dependent behaviour. The DMTA technique has great sensitivity in detecting changes in internal molecular mobility and in probing phase structure and morphology. Secondary relaxations in the glassy state can be straightforwardly studied, along with the glass transition relaxation process. The secondary transitions at low temperature are important in affecting use characteristics, such as the impact strength and the ductility, at room temperature (Reading 1992). In comparison with the DSC (Wetton and Corish 1989; Wetton *et al.* 1991), the DMTA technique has the advantage of a

far greater sensitivity when studying glass transition phenomena and, more importantly, is able to detect all secondary motional transitions at low temperatures that influence the impact strength characteristics. Also, for example, the strength of adhesion between a filler and a polymer matrix, in a filled composite, can be correlated with the magnitude of the damping peak at the glass transition temperature (Reading 1992; Diez-Gutierrez *et al.* 1999). Moreover, the effects of processing, nucleating agents, and other fillers/additives, can be determined by parallel DSC and DMTA experiments, in which process conditions are simulated in the laboratory (Reading 1992).

One of the major uses of DMTA is the determination of T_g. At this temperature, the molecular chains of a polymer possess sufficient energy to overcome the energy barrier for bond rotation. The decrease in the storage modulus associated with T_g is typically three orders of magnitude for an amorphous polymer, large peaks occurring in the plots of the loss modulus and of the damping peak. These correspond to the onset of motion of the polymer chains and, thus, DMTA is a direct method for the determination of T_g. DMTA has been particularly useful in studies of miscibility of polymer blends (Wetton *et al.* 1991) through the analysis of changes in the T_g of the blends components due to miscibility. When blend components are compatible, a single loss peak is found for the polymer blends. The loss peak maximum temperature is intermediate between that of the loss peaks for the single components and shifts systematically with the composition of the blend. The T_g depends strongly on the frequency of deformation.

The samples were analysed in the bending mode. For more details on sample testing modes see Appendix I. In this mode, the sample is usually in the form of a rectangular bar that is clamped rigidly at both ends and with its central point vibrated sinusoidally by the drive clamp. The option exists of clamping the sample at one end only (single cantilever mode). This was the mode used (Figure 2-6) in the analysis of the polymer blends samples. The environment within the temperature enclosure is controllable. The coolant circulates in a separate jacket and an inert gas or controlled humidity air may be introduced from pipes in the rear bulkhead.

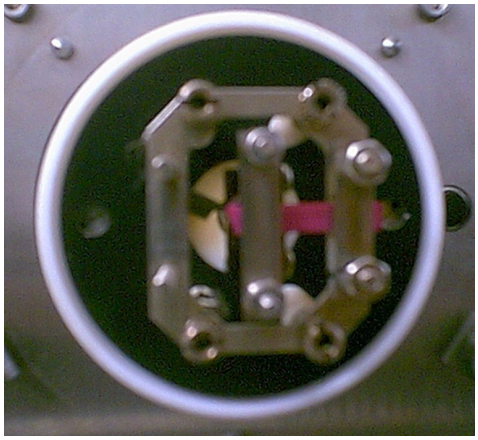

Figure 2-6. Sample clamped in the bending mode.

The instrument used was a Polymer Laboratories PL-DMTA MkII. The specimens were cut from injection-moulded tensile bars (Sepe 1995), with the dimensions: length = 30.0 mm, with = 4.0 mm and thickness = 2.0 mm, flow length. For the specimens relating to the PC-based samples, the thickness of the test specimen had to be increased to 5.0 mm due to movement of the clamped specimen in the frame, at temperatures above the T_g of the PC-rich phase.

The samples were not dried prior to test, to prevent the high drying temperature from causing morphology changes. The temperature range used was 20 ºC to 180 ºC, being extended to -150 ºC in the case of specific samples. It was considered important to include low temperature values as the secondary transitions occurring at low temperatures are known to correlate with impact strength and ductility, at room temperature. The strain used was 64 μ (n = 4) and the frequency was set to 5 Hz. The heating rate was 2 ºC/min, to allow the thermal equilibrium of the sample to be attained, and to avoid temperature gradients in the sample.

The strain level choice is influenced by samples size, sample non-linearity and sample stiffness. Usually, if a sample is being analysed in the bending mode, a strain level of x4 is selected. Large strain levels may lead to non-linear effects, particularly in semi-crystalline or filled systems (Wetton *et al.* 1991). Several frequency values have been tried and the one selected corresponds to that that allowed for the clearest distinction between the PBT-rich and the PC-rich phases, (that is better resolution), and the collection of an appropriate number of experimental data points. The instrument was calibrated before each new set of runs (once a day).

2.5. Microscopy

2.5.1. Scanning Electron Microscopy/Energy Dispersive X-ray Spectrometry

2.5.1.1. Scanning Electron Microscopy/Energy Dispersive X-ray Spectrometry on Blends

Scanning electron microscopy/energy dispersive x-ray spectrometry analysis (SEM/EDXA) studies were carried out using a JSM-820 Scanning Microscope unit, coupled with a Rontec GmbH Edwin energy dispersive spectrometer. The energy dispersive x-ray spectrometer (EDX) facility was used for elemental analysis, in an attempt to locate the pigment in the blend and to obtain an analytical composition of the “image”.

With regard to the analysis of tape-extruded samples, the surface of the samples was etched with dichloromethane (DCM) which selectively attacked the PC phase, prior to gold sputter coating and SEM/EDX examination. To etch the specimen, a 50 mm x 50 mm square of tape-extruded sample was left overnight in a closed vial in 25 cm^3 of DCM, under gentle agitation by a magnetic

stirrer. Similar strategies can be found in the literature that deals with blends of these types (Hobbs *et al.* 1988b; Sanchez *et al.* 1993). The rubber particles, which are swollen by the DCM, are not able to pass through the narrow passages which link many of the PC regions. As a result they may be retained in the matrix after extraction (Hobbs *et al.* 1988b). Accelerating voltages of 15 kV and of 20 kV were used, which allowed for a 3 μm deep surface analysis and, thus, included the zone from where the PC was extracted.

2.5.1.2. Scanning Electron Microscopy/ Energy Dispersive X-ray Spectrometry on the Unmodified Pigment and on the Surface-Modified Pigments

The objective of examining the pigments under the SEM/EDX was to analyse visually their shape, size and morphology, along with an assessment of their surface chemical composition. The instrument used was the same as that used for the polymer blends samples. The pigments were dispersed in distilled water with a non-ionic surfactant (Surfynol CT-141, from Air Products Plc, Hersam Place, Walton on Thames, Surrey, U.K.) and then subjected to ultrasonic dispersing for 2-3 minutes. The dispersed pigments were then dropped onto 0.025 μm (pore size) Whatman Anodiscs (aluminium membranes), and the aqueous medium removed (by means of a vacuum pump).

Sputtered gold coated specimens were examined by SEM, at accelerating voltages of 10 kV, 15 kV and 20 kV. Pigment samples for EDXA were not coated with sputtered gold nor dispersed with the help of Surfynol CT-141. EDXA was carried out on the pigments (unmodified and surface-modified), with an incident energy of 20.0 kV and duration of 35 cycles (approximately 30 minutes), in order to obtain an appropriate signal quality from the EDX instrument.

2.5.2. Transmission Electron Microscopy

In transmission electron microscopy (TEM), contrast arises from variations in electron density and can be most conveniently enhanced by incorporation of a heavy metal in one of the components (by chemical etching or by solvation (Vesely 1993)). The MBS rubber (IM) was differentiated from the PBT and the PC by reaction with OsO_4, which is known to form well-defined chemical complexes with double bonds (Delimoy *et al.* 1988; Hobbs *et al.* 1988b). The PC was distinguished from the other components as a result of its greater ability to absorb RuO_4. This chemical is a very powerful oxidising agent that reacts with macromolecules containing ether, alcohol, aromatic, amine or unsaturated moieties, among others. The darkening of the stained regions arises from the local precipitation of RuO_2, produced by the oxidation of the polymer (Delimoy *et al.* 1988).

The TEM analysis was carried out at the General Electric Plastics European facilities in Bergen op Zoom, The Netherlands, by TEM specialists. Ultrathin sections of the bulk specimens (approximately 50 nm thick) were obtained at room temperature using a microtome that was equipped with a diamond knife.

Approximately 1 % by weight of an aqueous solution of RuO_4 was prepared by dissolving a small vacuum-sealed RuO_4 crystal in freshly purified water. The sections supported on 400 mesh grids were exposed to RuO_4 vapours in a desiccator that contained a few millilitres of the solution.

Staining of sections with osmium tetraoxide was performed using the same procedure as that used with RuO_4 vapours. The specimens for TEM analysis were taken from the middle of the injection-moulded tensile bars as a cross-section with a thickness of 0.1 μm, or from tape-extruded samples. The samples were stained by RuO_4 and OsO_4 vapours for 10 minutes each. Tape-extruded samples of the blends were also analysed by TEM, after etching the surface with dichloromethane, as described in Section 2.5.1.1. The instrument used was a Tecnai 120 TEM unit, with an accelerating voltage of 100 kV.

2.6. Inverse Gas Chromatography

2.6.1. Materials Studied and Materials Used in the IGC Analysis

The materials analysed were: C. I. Pigment Blue 28 (BASF Sicopal® Blue K6310), Lexan® 125 (PC 125), Valox® 195 (PBT 195), Valox 315® (PBT 315), and the MBS rubber. For the IGC analysis, analytical grade probes were used without further purification. The apolar probes used were n-hexane (C6), n-heptane (C7), n-octane (C8), n-nonane (C9), and n-decane (C10). The polar probes used were tetrahydrofuran (THF), acetone (Acet), diethyl ether (DEE), trichloromethane (TCM), dichloromethane (DCM) and ethyl acetate (EtAcet). The chemicals used as probe molecules were obtained from Sigma-Aldrich Ltd, Poole, UK. Methane (Phase Separations Ltd, Deeside, UK) was used as a non-interacting reference probe and the carrier gas utilised was helium (99.999+ % purity, BOC Gases Ltd., Guildford, UK). Chromosorb® W AW DCMS (from Sigma-Aldrich Ltd, Poole, UK) was used as the column stationary phase support for the pigments and for the MBS rubber. Chromosorb® P AW DCMS (also from Sigma-Aldrich Ltd, Poole, UK) was used as the column stationary phase support for the PC 125.

2.6.2. Column Preparation

The columns were cut from stainless steel tubing and shaped in a smooth "U" shape to fit the detector/injector geometry of the instrument. The columns were 0.5 m in length, with an outside diameter and inside diameter of 6.4 and 4.4 mm, respectively. Cleaning was achieved via sequential rinsing with a hot aqueous detergent solution (Decon® 90 5%, from Sigma-Aldrich Ltd, Poole, UK), followed by acetone and drying at 150 °C, in a vacuum oven, for one day.

The column stationary phase was prepared using customary procedures, widely described in the IGC literature, for the study of polymers and particulates (Bolvari *et al.* 1989; El Hibri *et al.* 1989; Mandak *et al.* 1989; Hegedus and Kamel 1993a; Al Saigh 1997b). The materials under study can be coated or deposited onto commonly used support materials such as Chromosorb®, glass

beads and diatomaceous earth. The solid support should not interact with the material being studied because this will affect the interaction of the probe molecule with the stationary phase, as a consequence of preferential functional group orientation, and/or functional group blocking. Alternatively, the material being studied can be directly packed into the column.

The choice between packing the material directly and using another material as the supporting phase depends on: i) the surface area of the material (that influences the magnitude (too short/too long) of the retention times), ii) the form of the sample (fibres, granules, particles, etc) and iii) the pressure drop in the column. When the Chromosorb® support material is used, an acid-washed (AW), dimethyldichlorosilane treated (DCMS) grade should be used, in order to minimise interaction of the support material with the material under study, and interaction between the probe molecules and the support material.

The cobalt aluminate pigment column stationary phase was prepared by mixing the pigment with an "inert" support, Chromosorb® W AW DCMS, particle size 60-80 mesh. This procedure is necessary to avoid any undesirable pressure drop in the column, a consequence of the small particle size of the cobalt aluminate particles. Chromosorb® W AW DCMS is a white diatomite, prepared by the flux calcinations of diatomaceous earth. The support is acid washed (AW), with hydrochloric acid and afterwards with deionized water. The acid washing operation removes mineral impurities from the support surface and reduces surface catalytic activity. The support is also dimethyldichlorosilane-treated (DMCS), in order to convert the surface silanol groups to silyl ethers, which greatly reduces surface activity of the support and reduces peak tailing to a considerable degree. After weighing the support material (approximately 4 g) and pigment (in order to achieve pigment loadings ranging from 2 to 10 wt% (English 1995)), a 60 cm^3 screw top glass jar was used to mix both materials. Hexane (20 cm^3) was then added and the contents of the jar immersed in an ultrasonic bath for 30 minutes. Following this period of time, the hexane was removed in an oven at 80 °C and ambient pressure. Due to its inertness, hexane was used to coat the support material with the pigments. Thus, it was possible to avoid any undesirable adsorption if strong polar interacting solvents (e.g. acetone, THF) had been used, which could affect the IGC measurements if not completely removed.

The stationary phase columns for PC 125 were prepared by depositing the PC 125 onto Chromosorb® P AW DCMS, from a DCM solution. The use of this grade of Chromosorb®, instead of Chromosorb® W AW DCMS, stems from its larger surface area, which is required to optimise the exposure of the polymer to the molecular probes. Bearing in mind that the support material will be covered by a thin polymer layer, it is desirable to have the highest surface area available for adsorption. Chromosorb® P AW DCMS is a pink diatomaceous earth obtained from crushed firebrick, acid washed and dimethyldichlorosilane-treated. However, Chromosorb® P AW DCMS is more fragile than Chromosorb® W AW DCMS and must be handled more carefully, in order to avoid breakage of the particles and exposure of new surfaces, not covered with the polymer. In a

typical preparation, 10 grams of the polycarbonate were dissolved in 100 cm^3 of DCM. Known amounts of this solution were added to approximately 10 g samples of Chromosorb® P AW DCMS, to give theoretical loadings in 2.5 % increments between 5 and 15 % (Bolvari *et al.* 1989). Additional DCM was added to the support, as required, in order to obtain a thin slurry. Thereafter, the samples were dried at room temperature and atmospheric pressure, followed by drying under vacuum at 60 ºC for 24 hours. The free flowing powder that was obtained thereof was sieved through 125 µm filter gauzes and through 250 µm filter gauzes to remove any fine particles and any coarse particles. The concentration of PC 125 in solution was determined by evaporation and was 9.71 g/cm^3.

The polymer loading on the support was determined by TGA (Bolvari *et al.* 1989; Mandak *et al.* 1989). Samples of the column stationary phases for the PC, as well as the control samples of Chromosorb® P AW DCMS and of PC 125, were heated from room temperature to 600 ºC, at a rate of 10 ºC/min and under nitrogen flow, and held at this temperature for 60 minutes. The polymer loading was calculated knowing the sample weight loss, due to extensive oxidation, and corrected for the weight loss of the control samples (Chromosorb P® AW DCMS and PC 125).

For the columns containing PBT, due to the lack of an appropriate solvent, instead of coating a support material, the polymer was used as received, after grinding and sieving to achieve an appropriate particle size. To this end, the polymer particles were processed in a grinder while being cooled with liquid nitrogen, followed by sieving the material through 250 µm and 2 mm filter gauzes. The sieving operation aimed to exclude fine particles that would increase undesirably the pressure drop in the column. In the case where the material itself is used as the stationary phase, one can be sure that surface adsorption is the retention mechanism that prevails, as long as it is proven that the retention volume is not influenced by the carrier gas flow rate (Mukhopadhyay and Schreiber 1993).

The MBS rubber stationary phases were prepared by a procedure that is analogous to the one used for the columns containing the pigments (using Chromosorb® W AW DCMS as the support material).

Prior to packing, the columns were weighed. The stationary phase was introduced via a funnel, small additions being made alternately to each end of the column. The column was then tapped gently for several minutes to allow the support to achieve equilibrium packing, following each addition of the stationary phase. This procedure was continued until the column was filled to within approximately 6 mm of the ends. The stationary phase was then retained in the column by the introduction of small plugs of silanised wool. The column was then re-weighed and the mass of support obtained by difference. The columns studied, along with the quantities of support material, of stationary phase, and of material being analysed, are summarised in Table 2-12.

Table 2-12. IGC columns analysed.

Designation	Support material	Support weight (g)	Coating material	Coating weight (g)	Per cent coating (%)	Total weight (g)
RefW1	Chromosorb® W AW DCMS	2.020	n/a	n/a	n/a	2.020
RefW2	Chromosorb® W AW DCMS	1.475	n/a	n/a	n/a	1.475
RefP	Chromosorb® P AW DCMS	3.370	n/a	n/a	n/a	3.370
1	Chromosorb® W AW DCMS	2.582	C. I. Pigment Blue 28	0.129	4.76	2.711
2	Chromosorb® W AW DCMS	3.001	C. I. Pigment Blue 28	0.244	7.53	3.245
3	Chromosorb® W AW DCMS	2.735	C. I. Pigment Blue 28	0.070	2.51	2.805
4	Chromosorb® W AW DCMS	2.098	C. I. Pigment Blue 28	0.028	1.31	2.126
5	Chromosorb® W AW DCMS	2.022	C. I. Pigment Blue 28	0.126	5.87	2.148
6	Chromosorb® W AW DCMS	1.915	MBS rubber	0.055	2.81	1.970
7	Chromosorb® W AW DCMS	2.460	MBS rubber	0.137	5.27	2.597
8	Chromosorb® W AW DCMS	2.216	MBS rubber	0.188	7.80	2.404
9	Chromosorb® W AW DCMS	2.001	MBS rubber	0.231	10.33	2.232
10	Chromosorb® P AW DCMS	2.850	PC125	0.242	7.82	3.092
11	Chromosorb® P AW DCMS	3.389	PC125	0.299	8.11	3.688
12	Chromosorb® P AW DCMS	3.404	PC125	0.464	12.00	3.868
13	PBT 195	4.382	n/a	n/a	n/a	4.382
14	PBT 195	4.613	n/a	n/a	n/a	4.613
15	PBT 315	4.770	n/a	n/a	n/a	4.770
16	Chromosorb® W AW DCMS	3.952	C. I. Pigment Blue 28	0.248	5.90	4.200
17	Chromosorb® W AW DCMS	2.300	C. I. Pigment Blue 28	0.121	5.01	2.421

2.6.3. IGC Experimental Set-Up

Experimental work in IGC requires no specialised instrumentation and conventional GC equipment is generally used, with some adaptations. Prior to measurement, each column was conditioned at the highest temperature of measurement overnight, under a helium flow rate of approximately 10 cm^3/min. This pre-treatment of the column was aimed at ensuring the removal of any residual volatiles that could otherwise have affected the retention of the probes on the material being studied.

In the study of the BASF Sicopal® Blue K6310 pigment, a Perkin Elmer GC8410 unit (Perkin Elmer Ltd., Buckinghamshire UK), equipped with a FID detector, with a HS-101 headspace autosampler and coupled to a GP100 thermal printer/plotter, was used.

For the study of the PC 125, the PBT 195, the PBT 315, the MBS rubber, and the surface-modified versions of the pigment, the instrument used was a Fisons GC9100 unit (Fisons Scientific Equipment Ltd, Loughborough, UK), equipped with a FID detector. The experimental data were

acquired by coupling this GC with a personal computer that was equipped with a data acquisition card. This system has the advantage of providing a better data storage and manipulation.

In the experiments carried out using the Perkin Elmer GC8410 unit, typically, 0.1 µl of liquid probe was injected into each vial using a 1.0 µl Hamilton syringe. The injector was heated to 150 ºC and the FID detector to 200 ºC. The attenuation used was 2, with an off-set of 5 %. The equilibration time was set to 2 minutes. The HS-101 headspace autosampler allows reproducible extraction of the vapour probes from sealed headspace vials. Typically, the sample is extracted after initially pressurising the vial with the carrier gas, to a pressure that is equal to that of the head of the column (P_i). At the time of injection, the supply to the head of the column is momentarily transferred from the pressurised carrier supply, to the pressurised sample vial. This allows a small amount of probe to be transferred to the column, in order to ensure the Henry's infinite dilution region, a requirement for the applicability of the theory on which IGC is based. (It is assumed that only adsorption of isolated probe molecules on the solid surface is analysed, allowing one to neglect lateral interactions between adsorbed molecules.)

For the experiments that were carried out on the FISONS GC9100 unit, typically, the syringe was filled 0.1µl of gaseous probe, flushed with air around 10 times, in order to ensure the creation of a Henry's infinite dilution region, and injected manually. The injector was heated to 150 ºC and the FID detector to 180 ºC. The attenuation was set to 1. In both gas chromatographs, the flow rate was controlled using a needle valve pressure regulator and determined using a bubble flow meter that was equipped with a helium trap (Bolvari *et al.* 1989) and thermometer.

The inlet pressure, P_i, was measured using a pressure gauge and the atmospheric pressure, P_o, was obtained through the British Atmospheric Data Centre (www.badc.rl.ac.uk).

The temperatures, and carrier gas flow rates, used in the study of each material were different. This was due to the need to use a temperature range and flow rate that would not give rise to extremely short retention times or extremely long retention times, for all the apolar probes used and for all the polar probes used. Extremely short retention times (less than 10 seconds) or extremely long retention times (more than 45 minutes) are prone to a large experimental error, bearing in mind the Condor and Young method (Kamdem and Riedl 1992), (used in the determination of the probes retention time, Section 2.6.4.).

Also the values of T_g and of T_m (Table 2-2) were taken into account, as the aim was to determine the Lewis acidic/basic properties of the surface and not of the bulk of the material. If temperatures significantly greater than the T_g of the material are used, the opportunity for bulk absorption increases and the retention time of the probe would be affected. The temperature range and flow rate used in the determination of K_a and K_b of each material are summarised in Table 2-13.

Table 2-13. Temperature range and flow rate used in the determination of K_a and K_b.

	Temperature range (K)	Temperature increment (K)	Flow rate (cm^3/min)
Pigment (unmodified)	313 – 353	10	20
Pigments (modified)	323 – 373	10	20
PC 125	353 – 393	10	45
PBT 195^{+}	298 – 318	5	10
PBT 195^{++}	353 – 393	20	5 – 30
PBT 315^{+}	298 – 318	5	10
MBS rubber	333 – 373	10	30

$^{+}$ below T_g ; $^{++}$ above T_g

Preliminary studies concerning the influence of the carrier gas flow rate, and of the support materials (Chromosorb® P AW DCMS and Chromosorb® W AW DCMS), on the specific retention volumes of the probe molecules, were carried out. These involved the use of flow rates in the range 10-45 cm^3/min and varying the loading of the interacting material on the support. In addition, the influence of temperature of measurement on this study was evaluated. The probes used were n-decane for the pigments and the PBTs, n-hexane for the PC 125 and n-octane for the MBS rubber. Non-polar probes were chosen for the preliminary studies as they interact only through dispersive forces and, thus, the influence of specific interaction sites at the surface of the stationary phase is eliminated.

The absence of kinetic effects as well as diffusion phenomena on the column stationary phase was confirmed, in order to validate the use of Fowkes' approach (Garnier and Glasser 1996). The influence of the support material was found to be negligible. For the temperature ranges used, the net retention volume was independent of the carrier gas flow rate (thus, ensuring surface adsorption only) when this is included in the range 10-45 cm^3/min.

For the particular case of the study of PBT 195, at temperatures higher than its T_g, the net retention volume is a function of the flow rate. So, the flow rate was varied in order to extrapolate to the zero flow rate value (Mandak *et al.* 1989; Al Saigh 1997b; Xu *et al.* 1999). This way, the Lewis acidic/basic properties of the bulk PBT were assessed and compared to those of the surface of the PBT. The minimum loading value of the pigments and MBS rubber that ensures full coverage of the support material was found to be 5 %. For PC 125, if a loading of 7.5 % (or superior) is used, the support material is fully covered. This is critical to ensuring that the influence of the material support is negligible and, therefore, that one is quantifying solely the interactions of the probe molecules with the material being studied, and not with the support material (Bolvari *et al.*1989). A value of 7-9 wt% is commonly recognised as the minimum polymer loading that ensures full coverage of the available support surface (Ziani *et al.* 1999). As mentioned before, in the columns containing PBT, no column support (Chromosorb® P AW DCMS or Chromosorb® W AW DCMS) was used.

2.6.4. Determination of the Retention Time

The retention time was determined using the geometric technique outlined by Condor and Young (Kamdem and Riedl 1992; Jackson *et al.* 1994). This is necessary due to the "tailing" that is exhibited by some of the peaks that were obtained using polar probes. In those cases, the peak maximum method underestimates the interaction in the column between the probes and stationary phase. The Condor and Young technique allowed the determination of the peak mass centre, i.e., the time to 50 % elution, equivalent to the time of the peak maximum for symmetrical peaks. At least three retention times were obtained for each probe and the mean value used for further calculations, being the standard deviation inferior to 5 %. The procedure involves the definition of a baseline for the peak. Tangents are then drawn to the steepest part of the leading edge and the trailing edge of the elution profile, intersecting with the baseline, as exemplified in Figure 2-7.

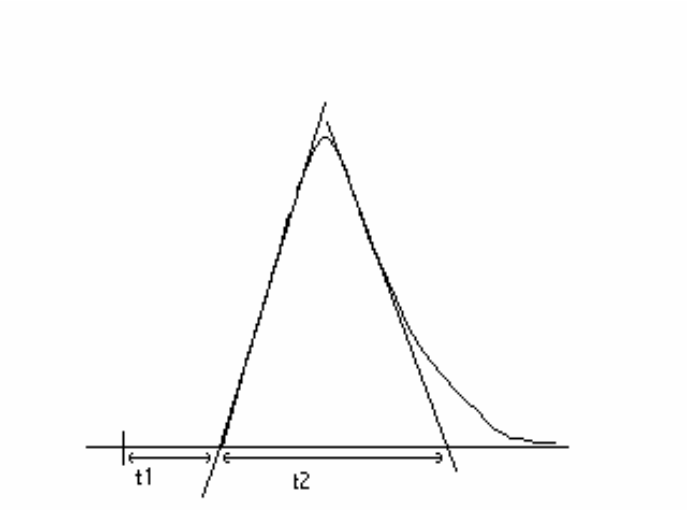

Figure 2-7. Exemplification of an asymmetric peak and determination of the retention time using the Condor and Young method.

The retention time is calculated using Equation 2-9:

$$t_r = t_1 + \frac{t_2}{2} \qquad (2\text{-}9)$$

In a general manner, the peak asymmetry increases as the interaction between the probe and the surface increases. The existence of a “tail” and asymmetry can be attributed to a non-uniform distribution of the potential interaction sites, or to the surface heterogeneity (Garnier and Glasser 1994).

In Figure 2-8 is represented a typical IGC chromatogram consisting of 3 runs (injections) for a sample of PC 125, at 100 ºC.

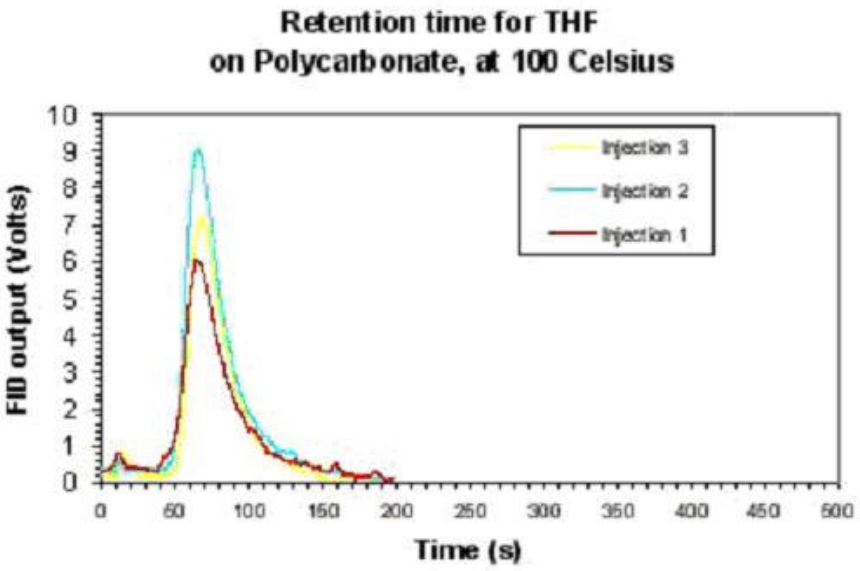

Figure 2-8. Typical IGC chromatogram.

Figure 2-8 shows that the "tailing" of the curves obtained for the chromatograms that relate to the probes that interact more strongly with the stationary phases, i.e. the polar probes, is not very pronounced.

2.7. Gel Permeation Chromatography

Gel permeation chromatography (GPC) was used to determine simultaneously the molecular weight of PC and of PBT, to assess how the molecular weight is affected by processing conditions and by the pigment, and to analyse the consequences thereof to the blend mechanical properties and physical properties. The GPC chromatogram is a single broad peak. The molecular weight is calculated after calibration using polymer standards.

The GPC analysis was carried out at the Polymer Characterisation Laboratories of the General Electric Plastics (Europe) company, by GPC specialists, using a method developed in that Laboratory. The reasoning behind the experimental procedure and respective description is given here.

The principle of applying GPC to determine simultaneously the molecular weight of PC and of PBT involves the specific absorption of PBT in the UV spectrum. Chromatograms are recorded at two wavelengths: at 270 nm both PBT and PC are detected, at the wavelength of 295 nm only PBT is recorded. The chromatogram at 295 nm is multiplied by a subtraction factor and subtracted from the chromatogram at 270 nm. The result is the PC chromatogram from which the molecular weight of PC can be calculated. The subtraction factor is calculated as expressed in Equation 2-10, using a standard PBT sample.

$$k_{sub} = Abs(270\ nm) / Abs(295\ nm) \quad (2\text{-}10)$$

The instrumentation used consists of a Hewlett Packard GPC 1100 series unit, a HP PL HFIP gel column, a Diode Array Detector (Agilent 1100 series), and a personal computer equipped with TurboChrom integration software and TurboGel size exclusion calibration software.

Twelve poly(styrene) (PS) calibration samples were used to set up a calibration curve, at 254 nm. With this curve the molecular weight of three standard samples and of a PC/PBT sample was determined (expressed as being PS). The molecular weight of PBT and of PC was determined using a solution of hexafluorisopropanol (5 %v/v) in chloroform, and a mixed bed column set. The mass of sample used was 80 mg.

2.8. Particle Sizing

Particle size analysis and particle size distribution analysis of the pigments was carried out in a Coulter N4M unit. The pigment was dispersed with the aid of Surfynol CT-141 (from Air Products Plc, Hersam Place, Walton on Thames, Surrey, U.K.) and the Erlenmeyer flask containing the dispersion was immersed in an ultrasonic bath for 15 minutes prior to measurement. The temperature of analysis was 20 °C. The viscosity was 0.977 cP, the refractive index was 1.333 and the scattering angle selected was the 90.0° angle.

2.9. Rheological Assessment (Melt Volume Rate)

The melt volume rate (MVR) determination is a rheological test that is used to investigate the flow of molten polymer through a die, with a specified length and diameter, under set conditions of temperature and load. The melt volume rate gives an indication of the viscosity of the material. The test was carried out according to the ISO 1133 standard test method. For more details on this method, see Appendix J.

The melt flow rate technique is based on the principle that flow increases with decreasing polymer viscosity for a given temperature and load test condition. A higher MVR value indicates a lower viscosity under an applied stress (load or weight in kg). The test temperature is usually set at or slightly above the melting region of the material being characterized. By keeping the shear stress constant (based on a loaded weight ranging from 1.2 to 21.6 kg depending on the stiffness of the material), the instrument used, a Goettfert MP-E unit, measures the time it takes for the piston to travel a specific distance, usually 25.4 mm, down the barrel. Approximately 5 grams of sample (pellets) are needed, and at least 3 replicates are obtained. The temperature used was 250 ºC and the load was 2.16 kg. Samples were dried before measurement because moisture in the samples can affect the measurement. The moisture level should be below 0.3 %. Samples were dried for two hours at 110 ºC in an air-circulating oven prior to testing.

2.10. Vicat Temperature Determination

The Vicat softening temperature is a parameter that is commonly used in the characterisation of polymeric materials as a measure of the upper limit of usable temperature for a short period. It has been shown (Namhata *et al.* 1990) that the Vicat softening temperature is a temperature at which a particular value of the material modulus is reached. The value is not simply related to the T_g of the material, as commonly believed. The Vicat temperature provides information that is related to the mobility of the whole polymer, whereas the T_g provides information that is restricted to the mobility of the amorphous phase (Rodriguez *et al.* 1997). The Vicat softening temperature is an additional measure of the morphological stability of a blend (Hamilton and Gallucci 1993).

The instrument used was a Coesfeld Vicat robot. The test was carried out according to the ISO 306 standard test method. This test gives a measure of the temperature at which a plastic starts to soften rapidly. A round, flat-ended needle of 1 mm^2 cross section penetrates the surface of a plastic test specimen under a predefined load, as the temperature is raised at a uniform rate. The Vicat softening temperature, VST, is the temperature at which the penetration reaches 1 mm. The test assembly is immersed in a heating bath (silicone oil) with a starting temperature of 23 ºC. After 5 minutes, the load is applied, being either 10 N or 50 N, depending on the material. The load applied in the present study was 50 N, and the heating rate was 120 ºC/hr. The temperature of the bath at which the indenting tip had penetrated by 1±0.01 mm was reported as the VST value of the material, at the chosen load and temperature rise. The standard specimen used was an injection moulded impact bar. The measurement was automatically performed in the centre of the specimen. Two specimens per sample were tested.

2.11. Sample Grinding

The aim of grinding the pellet samples, and the PBT granulates, was to obtain a finer sample form, to be used in some analytical techniques. The unit used was a Retsch ZM100 rock grinder. The system was cooled with liquid nitrogen (-196 °C), and continuous feeding of pellets was maintained.

2.12. BET Surface Area Determination

The BET surface area of the BASF Sicopal® Blue K6310 pigment was determined using a Strentoline unit. The value obtained, using liquid nitrogen, was 22.775±0.01005 m^2/g. This value is in agreement with data that are included in the technical data sheets for this pigment (20 m^2/g).

2.13. Surface Modifications of C. I. Pigment Blue 28

To support the observations that were made on the basis of the mechanical testing results, and of the physical characterisation of the pigmented blends, where use was made of the commercial C. I. Pigment Blue 28 (BASF Sicopal® Blue K6310), the surface Lewis acid/base properties of this pigment were "customised". The aim was to obtain two surface-treated pigments, such that the surface of one had dominant Lewis basicity and the surface of the other had dominant Lewis acidity, respectively. The "basic" pigment, hereafter designated **hiwren**, was expected to locate itself preferentially in the amorphous PC phase, and the "acidic" pigment, hereafter designated **hiwre**, in the PBT phase. If the surface acidity of **hiwre** was sufficient, this pigment would be expected to significantly influence the crystallisation properties of the PBT phase.

The physical properties and the mechanical properties of the blends that were prepared using the modified pigments are assessed. As a result, and in accordance with one of the major objectives of this project, a better understanding of the interactions occurring between the pigments and the polymer blend components, using the Lewis acid/base interaction concept, and subsequent consequences to the physical properties and to the mechanical properties of the polymeric system was attained.

The choice of the surface treatment type took into account the following factors: i) the nature of the polymeric system were it was to be included, ii) the specific processing conditions of the polymeric system (temperatures of up to 270 ºC, high shear stress), iii) the complexity of the experimental procedure in terms of experimental set-up and time consumption and iv) the facilities and equipment that were readily available.

In the light of the information gathered from the literature and the aforementioned constraints, a "photosensitised" grafting method was adopted. There are several different ways to achieve the grafting of a polymer chain onto a surface. These include:

a) Termination of a growing chain on an active group at the surface (**OH** groups (Solomon and Hawthorne 1983; Tsobokawa *et al.* 1994; Abboud *et al.* 1997; Jagur-Grodzinski 1999) and **COOH** groups (Tsobokawa *et al.* 1994; Jagur-Grodzinski 1999), for example);

b) Copolymerisation using a fixed double bond (Tsobokawa *et al.* 1994), and

c) Initiation of a polymerisation by an immobilised initiator.

The last method results in terminally attached polymer chains, with significant amounts of grafted polymeric species. Thus, bearing in mind the chemical nature of the surface of the pigment, a combination of method a) and method c) was the procedure adopted. Although no references could be found in the literature relating to the use of the surface OH groups in $CoAl_2O_4$ for grafting of polymeric species, a study by Abboud (1997) exists regarding the grafting of polymersable organic silane molecules onto the surface of Al_2O_3 *via* surface OH groups. Thus, bearing in mind

the chemical similarity between $CoAl_2O_4$ and Al_2O_3, the use of the surface OH groups for grafting of polymeric species was considered viable.

A variety of surface species can initiate the radical polymerisation of adsorbed monomers or contacted monomers (Solomon and Hawthorne 1983). These include adsorbed derivatives of conventional initiators, such as organic peroxides, benzoyl radical precursors, substituted benzoyl radical precursors, phosphinoyl radical precursors, azo compounds, and species formed by hydrogen abstraction or electron transfer (Solomon and Hawthorne 1983; Tsubokawa *et al.* 1989; Boven *et al.* 1991; Davidson 1999).

The photoinitiator system used was Speedcure® ITX, a mixture of 2-isopropylthioxanthone and 4-isopropylthioxanthone (Figure 2-9). This choice allowed the photosensitised grafting process to occur in an aqueous solution as this photoinitiator is water insoluble. This situation allows the initiator to demonstrate its preferential adsorption on the pigment. Due to the large amounts of reaction medium that was considered to be necessary to produce the desired quantity of modified pigment, distilled water was a very convenient reaction medium.

The monomer chosen for grafting was methacrylic acid (MAA), Figure 2-9. The use of this monomer allowed for the provision of carboxylic acid groups at the surface of the pigment. Furthermore, by neutralisation of the carboxylic groups with a base, such as NaOH, the Lewis acidity can be significantly reduced, compared with the non-neutralised carboxylic groups. In this fashion, the surface Lewis acidity/basicity of the pigment could be controlled by means of varying the extent of neutralisation of the carboxylic acid groups.

Figure 2-9. Structure of the photoinitiator, ITX (on the left-hand side), and of the monomer, MAA (on the right-hand side).

The photosensitised grafting mechanism consisted of the following steps:

a) Activation of the photoinitiator molecule by UV light (Figure 2-10);

b) Complex formation between the excited state of the photoinitiator molecules and the surface OH groups of the pigment, leading to the formation of surface radical species (Figure 2-11);

c) Initiation of polymerisation of the methacrylic acid monomer units by the surface oxy-radicals and by the thioxanthone radicals (dominantly on the pigment surface (adsorbed)) (Figure 2-12);

d) Termination of the polymeric chain growth at the surface of the pigment.

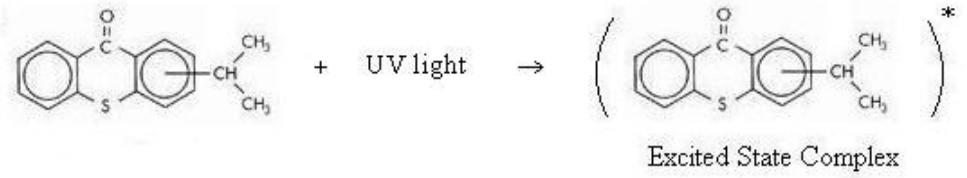

Figure 2-10. Activation of the photoinitiator (ITX) molecule by UV light (schematic).

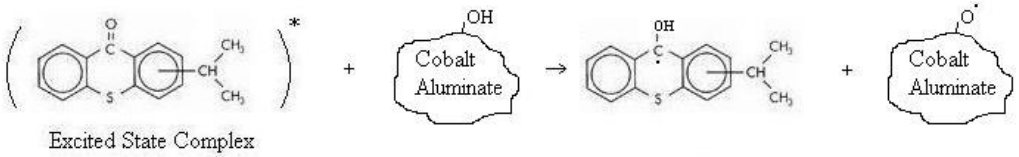

Figure 2-11. Complex formation between the excited state of the photoinitiator molecules and the surface OH groups of the pigment, leading to the formation of surface radical species (schematic).

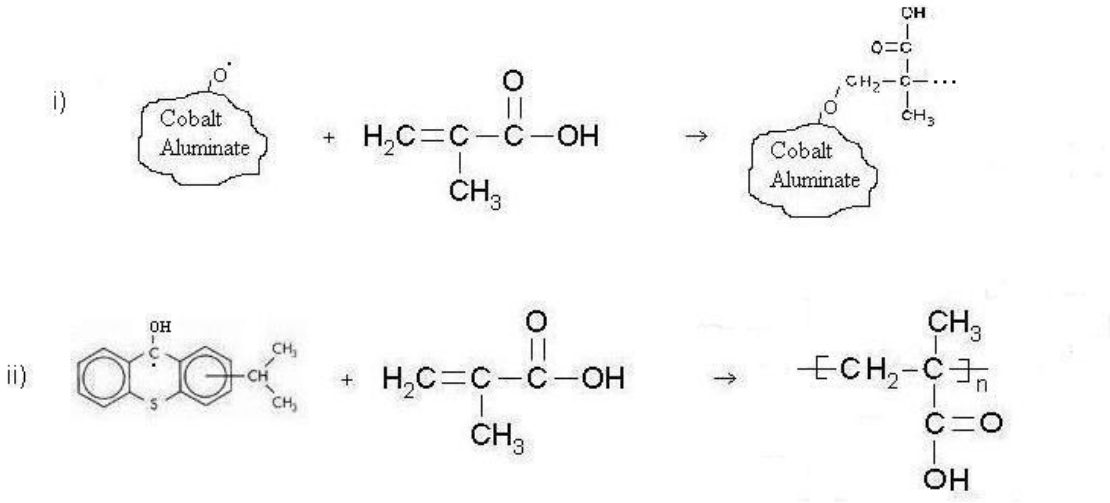

Figure 2-12. Initiation of polymerisation of the methacrylic acid monomer units i) by the surface oxy-radicals and ii) by the reduced, perhaps bound, ITX radical (schematic).

In brief, the experimental method that was implemented consists of the following stages: 1) adsorption of the photoinitiator, from solution, onto the surface of the pigment, 2) evaporation of the solvent and drying of the particles, 3) addition of the initiator-treated pigment to a monomer solution in which the photoinitiator is insoluble, and 4) conduction of the "photosensitised" grafting reaction in a photopolymerisation reactor.

Issues such as the thermal stability, the chemical stability, and the processing stability, were carefully assessed so that the modification success was optimised, from the point of view of the end-use of the modified pigment. To this end, techniques such as TGA, DSC, and solvent extraction were used as analysis supports. The physical characteristics of the modified pigment were determined by particle sizing. The surface chemistry was characterised by IGC and by EDXA.

Due to time restrictions that were related to the availability of the extruder facilities, no studies of the influence of factors such as the photoinitiator concentration, the monomer concentration and the reaction time, were carried out. Once it was established that the reaction scheme, the experimental set-up and procedure, the reagents quantities used, and the reaction parameters values chosen, successfully resulted in the fixation of MAA-based polymeric species onto the surface of the pigment, a total amount of 70 g of surface-modified C. I. Pigment Blue 28 was produced so that 2 kg batch samples of pigmented blends could be extruded with the pigment loadings that are presented in Tables 2-8 and 2-9 (Section 2.1.). Studies of the influence of the aforementioned factors on the effectiveness of the surface-treatment, along with an investigation of the nature of the pigment-polymer bonds are to be the subject of future work.

The amount of photoinitiator that is necessary for the complete abstraction of the hydrogen atoms from the hydroxyl surface groups was estimated from values reported in the literature for the surface concentration of hydroxyl groups. Methods for the quantification of surface OH groups in metal oxides include (Tamura *et al.* 1999):

1) Reaction with Grignard reagents;

2) Surface acid-base, ion-exchange reactions for saturation;

3) Dehydration by heating;

4) IR spectroscopy;

5) Tritium exchange with hydroxyl protons, and

6) Crystallographic calculations.

Thermogravimetry and chemical titration (with triethylaluminium (TEA)) are commonly used (Abboud *et al.* 1997) in the determination of the density of surface hydroxyl groups. No studies were found in the literature relating to the determination of the density of the surface hydroxyl groups in cobalt aluminate. Nevertheless, for alumina, Al_2O_3, values of 2-7 $\mu mol/m^2$,

10-20 μmol/m^2, and 40 μmol/m^2 are reported (Abboud *et al.* 1997; Tamura *et al.* 1999), by the use of different determination methods.

The TGA method does not distinguish between OH groups that are present on the particle surface from those within micropores (Abboud *et al.* 1997; Tamura *et al.* 1999). However, the OH grups that are located within micropores will have a reduced tendency to react with the photoinitiator and/or with the monomer, due to steric restrictions, and so are not relevant in the context of this study. Chemical titration may give overestimated OH surface densities owing to the presence of physisorbed water that is not completely removed during the initial drying process. Therefore, the estimated values reported are, most likely, overestimated (Abboud *et al.* 1997; Tamura *et al.* 1999). Conversly, other methods, such as proton or hydroxide ion-exchange techniques, are known (Tamura *et al.* 1999) to underestimate the surface OH density, being responsible for the lowest values reported. Bearing in mind these observations, a value of 1.9 μmol/m^2 is reported (Abboud *et al.* 1997) as being a more representative value of the actual density of OH groups accessible to chemical reagents, in Al_2O_3.

For different metal oxides (with di-, tri-, and tetravalent lattice metal ions), similar hydroxyl sites densities are reported (Tamura *et al.* 1999). The rationale suggested by Tamura and colleagues (1999) is that the lattice oxide ions are exposed to water at the oxide/water interface. Oxide ions are very strong bases and unable to exist unchanged in aqueous solutions, and, thus, they are neutralised by water to become two hydroxyl groups per molecule of water and per O^{2-} anion. On the oxide surface, terminal hydroxyl groups lie adjacent to each other. Their charges are not neutralised symmetrically by lattice cations, due to the local imbalance of anion and cation arrangements at the surface. The similar surface OH site density in different metal oxides corresponds to the closest packing of hydroxide ions, irrespective of the valence of the lattice metal ions.

Therefore, in the present study, it was not considered crucial to determine experimentally the concentration of surface OH sites in cobalt aluminate, bearing in mind the major objective of the surface treatment adopted. Instead, an excess of photoinitiator, relatively to the amount estimated as being necessary, was used in order to account for the estimative of surface hydroxyl groups, and to maximise the formation of active sites at the surface that would be necessary for the grafting process to proceed.

2.13.1. Materials and Apparatus

Distilled water was used throughout the experiments. The monomer (methacrylic acid, MAA), the organic solvent (acetone, analytical grade), and sodium hydroxide (NaOH, pellets, 98% pure) were obtained from Sigma-Aldrich Ltd, Poole, UK, and used without any purification step. The homopolymerisation inhibitor contained in the MAA (250 ppm hydroquinone monomethyl ether), is deliberately not removed. The objective was to reduce the tendency for the formation of

homopolymer in solution during the photografting process and, thus, maximise the amount of polymer species that would be chemically linked to the surface of the pigment, and minimise the adsorption of homopolymer from solution. A greater than estimated initiator concentration and monomer concentration were used to account for the inhibitor presence. The glassware was carefully cleaned prior to use, using a commercial detergent, followed by thorough rinsing with distilled water. The photoinitiator, Speedcure® ITX, was supplied by the Lambson Group Ltd., Castleford, West Yorkshire, U.K. Nitrogen, oxygen free and ultra pure, was supplied by BOC Gases Ltd., Guildford, UK.

Table 2-14. Selected properties of the monomer (MAA) and of the photoinitiator (ITX), from technical data sheets.

	Molecular weight (g/mol)	Melting point (ºC)	Boiling point (ºC)	Density
MAA	86.09	15	163	1.0153
ITX	254.30	63-77	n/a	n/a

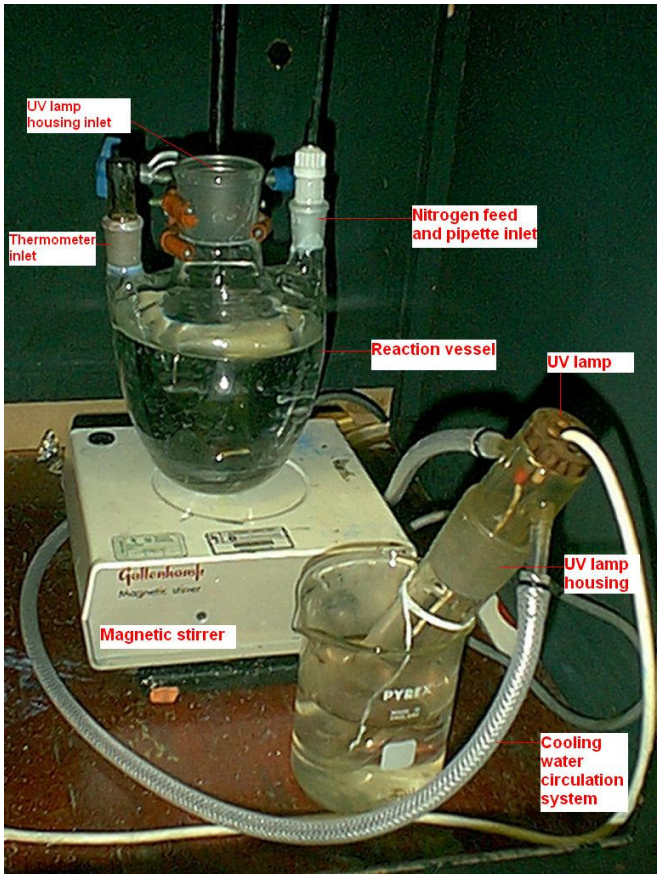

Figure 2-13. Experimental set-up relating to the photosensitised grafting reaction.

The experimental set-up is shown in Figure 2-13. The reaction vessel was fitted with a thermometer, a nitrogen feed, a magnetic stirrer, and an ultraviolet lamp (125 W/cm photochemical lamp system, medium pressure, 3 cm in length), that was designed for location within a silica jacket equipped with a water cooling system. The system was kept in a black box, to minimise UV light exposure and to ensure that the samples received the same UV dosage. The pH of the pigment dispersions was measured with an Extech Oyster pH/Conductivity meter. Glass microfibre filters, (obtained from Sigma-Aldrich Ltd, Poole, UK), were used in the filtration of the reaction mixture, and in extraction operations.

2.13.2. Surface Modification Experimental Procedure

2.13.2.1. Pre-treatment of the Pigment

In order to maximise the availability of surface OH groups, the pigment was hydrated. A slurry of pigment (15 g) in distilled water (250 cm^3) was prepared, followed by slow evaporation of the water, at 90 ºC overnight, followed by storage in a desiccator. The hydration procedure aimed the enrichment of the surface of the pigment with OH groups, originated from the dissociative chemisorption of water molecules (Tamura *et al.* 1999). This phenomenon has been proven to occur at both the lattice metal ion sites acting as a Lewis acid and at those sites acting as Lewis base. The drying temperature was limited to a maximum of 90 ºC to avoid the destruction of surface hydroxyl sites (Chehimi *et al.* 2001) or loss of water molecules.

The distilled water may also desorb some impurities at the surface of the pigment and reveal some adsorption sites (Tamura *et al.* 1999). This assists the interaction of the surface of the cobalt aluminate pigment with the photoinitiator molecules. An analogous procedure has been used by Chehimi *et al* (2001) for the creation of hydroxyl sites in alumina, prior to treatment with a silane. The hydration procedure was found not to change significantly the Lewis acid/base properties of the alumina, both Lewis acidity and Lewis basicity decreasing slightly. This effect was attributed to the disappearance of sodium (Lewis acid) ions and carbonate (Lewis base) ions, despite the fact that hydrating the surface creates acidic OH sites.

2.13.2.2. Treatment of the Pigment with the Photoinitiator

The amount of photoinitiator required to react with all the OH groups at the surface of the pigments was estimated as follows. It was assumed that the surface OH group concentration in the cobalt aluminate inorganic particles was close to that of alumina. On this basis, and from the abovementioned values reported, and observations made in the literature, a value of 2×10^{-6} mol of surface OH/m^2 was estimated. From the BET surface area value for the BASF Sicopal® Blue K6310 pigment, (22.775±0.01005 m^2/g, Section 2.12.), and for a mass of 10 grams of pigment, the number of moles of surface OH groups, accessible to reactants, was estimated to be 4.6×10^{-4} mol. As the molecular weight of ITX is 254.3 g/mol, and assuming that one photoinitiator molecule

reacts with one surface OH group, it follows that the mass of photoinitiator necessary to react with all the surface OH sites that were present in 10 g of pigment was 0.116 g. Bearing in mind the above comments, a mass of photoinitiator that was three times that of the estimated value was used.

Approximately 10 g of pigment were weighed and placed in a 50 cm^3 glass bottle. The photoinitiator solution was prepared by weighing the required mass of photoinitiator (approximately 0.35 g) in a 50 cm^3 stoppered Erlenmeyer flask and adding 25 cm^3 of acetone (in which the photoinitiator is soluble). The photoinitiator solution was added to the glass bottle containing the pigment so as to meet the ratio 0.35 g ITX/10 g pigment. The glass bottle was immersed in an ultrasonic bath for 3 hours. This procedure was designed to breakdown pigment agglomerates and to provide an even distribution of the photoinitiator at the surface of the pigment. The glass vessel was then opened and the solvent removed by rotary evaporation at a suitable temperature. The temperature was such that no thermal degradation of the photoinitiator occurred. Taking into consideration the melting temperature of ITX (Table 2-14), the drying temperature used was 70 ºC. It was noted that if the temperature was greater than 70 ºC, ITX started to darken (originally it is a yellow powder). The remaining solvent was evaporated by placing the glass vessel and its contents in a vacuum oven, overnight, at 70 ºC. Afterwards, the system was left to cool to ambient temperature, and atmospheric pressure.

Next, the photoinitiator-treated pigment was mixed with 25 cm^3 of reaction medium (distilled water). The excess initiator (not fixed to the surface of the pigment) was removed from the supernatant liquid, and the product dried at 70 ºC in the vacuum oven for 24 hours. The objective of this stage was to decrease the opportunity for excess photoinitiator to be transferred to the reaction medium (leading to homopolymerisation). It was determined that the maximum amount of photoinitiator that could be deposited onto the pigment, without resulting in ITX being released from the surface of the pigment when "washed" with distilled water, was 2.6 g ITX/10 g $CoAl_2O_4$ (20.5 % w/w). If a loading greater than 20 wt% was used, the ITX particles tended to agglomerate in the water and float. It was thought that this could increase the formation of homopolymer upon exposure to UV light, an event that was to be avoided. The mass of pigment plus initiator and, thus, the mass of adsorbed photoinitiator was determined by weighing the glass bottle after the final drying stage and subtracting the mass of the empty bottle.

This procedure was designed to reduce the prospects of involuntary homopolymer formation. It was recognised that the isopropyl thioxanthyl radical would be a by-product of the photochemical processes. It was anticipated that this by-product radical would, itself, be preferentially adsorbed on the pigment surface because of the presence of the aqueous system.

2.13.2.3. Photosensitised Grafting Method and Filtration of the Reaction Medium

The mass of monomer necessary for grafting was estimated from the number of surface radicals that originated from the surface OH groups. Thus, it was assumed that one monomer unit

reacts with one of the active O sites. From the estimated value of 4.6 x 10^{-4} mol of OH sites, and from the molecular weight of MAA (86.09 g/mol), it follows that the mass of MAA required was 0.040 g (that is approximately 0.040 cm^3, as d = 1.015). It was decided to use an excess of monomer. Thus, the volume of MAA used was of 2 cm^3 per 10 g of pigment (approximately fifty times the estimated value).

The mass of photoinitiator-treated pigment was added to the reaction vessel, followed by the addition of the appropriate volume of reaction medium (1 dm^3 of distilled water). The reaction medium selected was distilled water as the monomer, methacrylic acid, is soluble in water, whereas the ITX photoinitiator is insoluble in this solvent. Magnetic stirring was commenced and the air contained in the reaction vessel removed using the nitrogen feed. The nitrogen feed was then removed and replaced by a pipette through which the required volume of monomer was added. The monomer was added dropwise using the fitted pipette. When the addition of monomer was complete, the UV lamp was activated. It was ensured that the reaction vessel operated as a closed system, with no mass transfer to the exterior. The stirring of the reaction solution was regularly checked to ensure an even exposure of the system to the light source.

The silica glass UV lamp housing was effectively cooled by water circulation to avoid any "dangerous" temperature rise of the reactor system. The typical reaction temperature was 10 ºC. After the required reaction time, 30 minutes (previously determined), the treated pigment was recovered by filtering the reaction mixture via a glass microfibre filter, previously weighed. The filter was furthermore rinsed with "clean" monomer solvent (distilled water), to remove any traces of unreacted monomer, and low molecular weight oligomers, from the surface of the pigment. Typically, the filtration operation lasted 8 hours. The filter was dried overnight, at ambient temperature and atmospheric pressure, followed by drying in a vacuum oven at 120 ºC overnight.

Finally, the treated pigment was left to cool at room temperature and atmospheric pressure, to a constant weight. The mass of surface-treated pigment plus any eventual adsorbed homopolymer was then determined. In some cases, homopolymer could clearly be seen in the supernatant liquid after the reaction was terminated and the reaction medium transferred to the filter funnel. A distinct odour to MAA could still be noted when the allocated reaction time was ended.

2.13.2.4. Soxhlet Extraction

The surface-treated pigment (deposited in the glass fibre filter) was extracted by Soxhlet extraction with distilled water for 3 hr, to remove any monomer and homopolymer that was loosely fixed to the surface of the pigment. The water was then replaced by acetone, and the extraction of the excess photoinitiator carried out for 3 hours. The surface-treated pigment was introduced in the Soxhlet apparatus while still in the glass fibre filter that was closed to stop any pigment from being released from the filter. Furthermore, the filter was introduced in an extraction thimble. The glass

fibre filter plus the extracted surface-treated pigment were then dried in air overnight, followed by drying in a vacuum oven, at 120 ºC overnight and finally left to cool at room temperature and atmospheric pressure, to a constant weight, in a desiccattor. The mass of extracted surface-treated pigment (plus the mass of the glass fibre filter) was then determined. The residue remaining after evaporating the acetone used in the extraction consisted of a small amount of yellow particles (identified has being non-reacted photoinitiator).

A total of 70 g of modified pigment was prepared. A control sample was obtained using the experimental procedure described above but with no exposure to UV light. In addition, a sample of PMAA was produced by using the same reaction set-up but without the presence of pigment. Thus, a mass of 0.5111 g of ITX was reacted with 5 cm^3 of MAA monomer, with distilled water as the reaction medium, at 9 ºC, for 3 hours.

2.13.2.5. Neutralisation of the MAA-Modified Pigment

A solution of NaOH (0.039 M) was prepared by diluting 0.156 g of NaOH in 100 cm^3 of distilled water. Assuming that each surface OH site is occupied by a MAA unit, after surface treatment, the concentration of COOH groups present in the modified pigment was estimated to be 4.6×10^{-5} mol per gram of pigment. Thus, and as a very simple approximation, the volume of the dilute NaOH solution thought to be necessary to neutralise the COOH groups was 1.18 cm^3 per gram of modified pigment. An excess of the NaOH solution was used in order to maximise the extent of neutralisation of any carboxylic acid groups. Thus, a volume of 5 cm^3 of NaOH solution per gram of modified pigment was used.

3. RESULTS AND DISCUSSION

3.1. Study of Phase Separation and Phase Preferences Phenomena by IGC

Inverse gas chromatography (IGC), carried out at infinite dilution, was used to study the surface Lewis acid/base properties of the major components of the pigmented polycarbonate/poly(butylene terephthalate)/impact modifier (PC/PBT/IM) blends. Furthermore, the dispersive component of the surface tension of the materials studied was determined, allowing for an assessment of the interaction capability through dispersive forces.

These analyses provided the rationale for an interpretation of the phase separation and the phase preferences that exist in these polymer blends and of the consequences to their physical properties and to their mechanical properties. Furthermore, from the IGC characterisation of the pigment, the interaction potential of C. I. Pigment Blue 28 with the remaining components of the blends was evaluated.

The retention times of apolar probe molecules and of polar probe molecules were determined at specific temperatures, and the values of the retention volume, the energy of adsorption, the enthalpy and entropy of adsorption (dispersive and specific components) of the probes, and of the surface K_a and K_b, were computed.

3.1.1. Study of the Retention of Probe Molecules on the Support Material.

3.1.1.1. Chromosorb® W AW DCMS

A study of the retention of the apolar probes and of the polar probes on the support material, Chromosorb® W AW DCMS, was carried out using column RefW1 (Table 2-12, Section 2.1.2.) and the Perkin Elmer GC8410 unit. The objective of this study was to establish that the retention times obtained for the adsorption of the probe molecules on the stationary phase of columns containing C. I. Pigment Blue 28, and of columns containing MBS rubber, relates to the material being studied and not to the support material. One column, cut, shaped and cleaned as described in Section 2.6.2. was filled with 2.020 g of Chromosorb® W AW DCMS. This column was left overnight under a helium flow rate of 10 cm^3/min and at a temperature of 373 K to ensure that no solvent, from the column cleaning operation, remained, inside the column.

The retention times of n-alkanes ranging from n-hexane to n-decane, and of the polar probes: THF (basic probe), Acet, DEE, EtAcet (amphoteric probes), TCM and DCM (acidic probes) were determined at 313 K and at a flow rate of 20 cm^3/min. This experimental set-up allowed the determination of the dispersive component of the surface tension of Chromosorb® W AW DCMS,

at 313 K, as well as an evaluation of the specific component of the energy of adsorption relating to Lewis acidic probe molecules, Lewis basic probe molecules and amphoteric probe molecules.

Table 3-1. Retention time, t_r, net retention volume, V_n, energy of adsorption, $RTLn(V_n)$, and corresponding dispersive and specific components, $RTln(V^d_{n,ref})$ and $RTln(V^s_n)$, respectively, for the n-alkanes and polar probes on the surface of Chromosorb® W AW DCMS, at T = 313 K.

Probe molecule	t_r (s)	V_n (cm^3)	$RTLn(V_n)$ (kJ/mol)	$RT\ln(V^d_{n,ref})$ (kJ/mol)	$RT\ln(V^s_n)$ (kJ/mol)
CH_4	17.0	n/a	n/a	n/a	n/a
C_6H_{14}	19.9	0.9	-0.4	-0.4	n/a
C_8H_{18}	38.8	6.5	4.9	4.9	n/a
C_9H_{20}	67.9	15.1	7.1	7.1	n/a
$C_{10}H_{22}$	148.7	39.0	9.5	9.5	n/a
CH_4	30.4	n/a	n/a	n/a	n/a
Acet	98.1	19.2	7.7	-3.4	11.1
THF	114.0	23.7	8.2	-0.7	9.0
EtAcet	69.0	10.9	6.2	-1.9	8.2

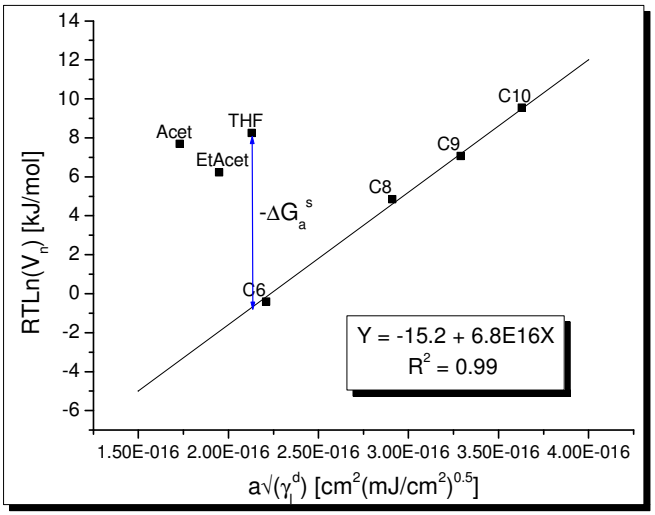

Figure 3-1. Energy of adsorption versus $a\times\sqrt{\gamma_l^d}$ for n-alkanes and polar probes on the surface of Chromosorb® W AW DCMS, at T = 313 K.

In Table 3-1 are summarised the experimental parameters and results concerning the adsorption of n-alkanes, and polar probes, on the surface of Chromosorb® W AW DCMS, at the measuring temperature of 313 K. Presented are the retention time, t_r, the net retention volume, V_n, the energy of adsorption, $RTLn(V_n)$, the energy of adsorption corresponding to the n-alkanes

reference line, $RT\ln\left(V_{n,ref}^{d}\right)$, and the specific component of the energy of adsorption, $RT\ln\left(V_{n,ref}^{s}\right)$. For the n-alkanes, the experimental parameters were as follows: F = 20.62 cm^3/min, J = 0.89, C = 0.97, P_i = 122.13 kPa, P_o = 99.00 kPa and $T_{flow\ meter}$ = 297 K. And for the polar probes: F = 19.38 cm^3/min, J = 0.90, C = 0.97, P_i = 118.69 kPa, P_o = 98.01 kPa and $T_{flow\ meter}$ = 296 K. In Figure 3-1 is presented the "Fowkes plot", where the energy of adsorption of the apolar and polar probes, at the temperature of measurement, is plotted as a function of $a\times\sqrt{\gamma_l^d}$.

The retention times of TCM, of DCM, and of DEE were too low (below 5 s) and, thus, could not be determined accurately with the current IGC system. The fact that the energy of adsorption of n-hexane is negative is a consequence of the relatively low surface area of adsorption and weak interaction with the probe that result in a retention volume value that is lower than 1.

From the linear regression of the experimental data relating to the energy of adsorption of the n-alkanes, it was established that the dispersive component of the surface tension, γ_s^d, is 33.4 mJ/m^2. Therefore, in line with expectation, there is interaction between n-alkanes and the column support by means of dispersive forces. From the interaction with polar probes, it can be concluded that Chromosorb® W AW DCMS does not interact with the acidic probes and that, thus, its surface does not possess a significant Lewis basic character. It does, however, interact with Lewis basic and amphoteric probes. Therefore, the surface of Chromosorb® W AW DCMS is Lewis acidic in nature. This is interpreted on the basis that, although the support is dimethyldichlorosilane-treated (DMCS) in order to convert the surface silanol groups to silyl ethers, there would still remain silanol groups, providing the surface with an electron acceptor character.

The question arose as to whether or not the ability of the material to interact with n-alkanes and basic/amphoteric probes would affect the retention times of the materials studied with Chromosorb® W AW DCMS as the stationary phase support. If the material being analysed covered completely the surface of the support, the retention time would be due solely to the interaction of the probe molecules with the material under analysis. In order to determine the minimum loading of C. I. Pigment Blue 28 and of MBS rubber, on the stationary phase, for which total surface coverage of the Chromosorb® W AW DCMS can be assumed, a study of the influence of the pigment, and of the MBS rubber loading on the support material of the column stationary phase was carried out (Sections 3.1.3.1. and 3.1.4.1., respectively).

3.1.1.2. Chromosorb® P AW DCMS

A study of the retention of the probe molecules on the stationary phase support material, Chromosorb® P AW DCMS, was carried out using column RefP (Table 2-12, Section 2.1.2.) and the Perkin Elmer GC8410 unit. The objectives of this study, and the probe molecules used, were the same as those relating to the study of Chromosorb® W AW DCMS. The measurement temperature was 353 K, and the carrier gas flow rate was set to 20 cm^3/min. This temperature was

selected because it is part of the temperature interval used in the analysis of PC 125 (deposited onto Chromosorb® P AW DCMS). The dispersive component of the surface tension was determined at 353 K and the specific component of the energy of adsorption for Lewis acidic, basic and amphoteric probe molecules was evaluated.

Table 3-2. Retention time, t_r, net retention volume, V_n, energy of adsorption, $RTLn(V_n)$, and corresponding dispersive and specific components, $RTln(V^d_{n,ref})$ and $RTln(V^s_n)$, respectively, for the n-alkanes and polar probes on the surface of Chromosorb® P AW DCMS, at T = 353 K.

Probe molecule	t_r (s)	V_n (cm^3)	$RTLn(V_n)$ (kJ/mol)	$RT\ln(V^d_{n,ref})$ (kJ/mol)	$RT\ln(V^s_n)$ (kJ/mol)
CH_4	17.1	n/a	n/a	n/a	n/a
C_6H_{14}	20.6	1.0	-0.1	-0.1	n/a
C_7H_{16}	24.8	2.1	2.2	2.2	n/a
C_8H_{18}	30.2	3.6	3.8	3.8	n/a
C_9H_{20}	46.8	8.1	6.1	6.1	n/a
CH_4	14.4	n/a	n/a	n/a	n/a
$C_{10}H_{22}$	64.6	14.7	7.9	7.9	n/a
TCM	18.6	1.2	0.6	0.1	0.5
DCM	20.0	1.6	1.4	-3.2	4.6
DEE	49.8	10.3	6.8	-2.2	9.1
Acet	382.3	106.7	13.7	-2.7	16.4
THF	254.5	69.7	12.5	-0.5	13.0
CH_4	13.0	n/a	n/a	n/a	n/a
EtAcet	167.0	46.0	11.2	-1.5	12.7

In Table 3-2 are summarised the experimental parameters and results concerning the adsorption of n-alkanes, and of polar probes, on the surface of Chromosorb® P AW DCMS, at the measuring temperature of 353 K. For n-hexane, n-heptane, n-octane and n-nonane, the experimental parameters were as follows: F = 19.27 cm^3/min, J = 0.87, C = 0.97, P_i = 127.84 kPa, P_o = 100.26 kPa, and $T_{flow\ meter}$ = 297 K. For n-decane, TCM, DCM, DEE, Acet, and THF: F = 20.67 cm^3/min, J = 0.87, C = 0.96, P_i = 127.83 kPa, P_o = 100.25 kPa, and $T_{flow\ meter}$ = 294 K. And for EtAcet: F = 21.33 cm^3/min, J = 0.86, C = 0.98, P_i = 131.28 kPa, P_o = 100.25 kPa, and $T_{flow\ meter}$ = 294 K. In Figure 3-2 is presented the "Fowkes plot" concerning the measurement temperature and the probe molecules used.

From linear regression of the data points concerning the n-alkanes, Figure 3-2, the dispersive component of the surface tension, γ_s^d, is calculated to be 21.6 mJ/m^2.

From the interaction of the stationary phase with polar probes it can be concluded that the Chromosorb® P AW DCMS does not interact strongly with Lewis acidic probes. Conversly, it interacts significantly with basic and amphoteric probes. This is an indication of the amphoteric character of the surface of Chromosorb® P AW DCMS, with predominant acidity. Consequently, it was considered to be necessary to find the minimum polymer (PC 125) loading that would provide total surface coverage of the Chromosorb® P AW DCMS. This point is dealt with in Section 3.1.5.1.

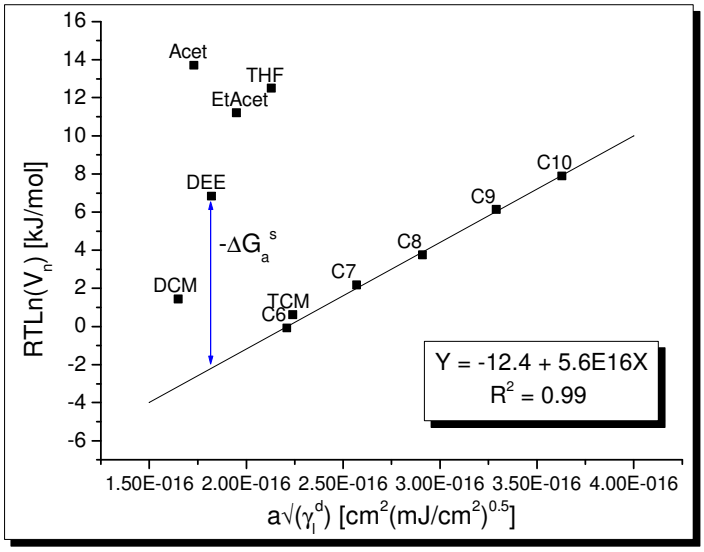

Figure 3-2. Energy of adsorption versus $a\times\sqrt{\gamma_l^d}$ for n-alkanes and polar probes on the surface of Chromosorb® P AW DCMS, at T = 353 K.

3.1.2. Study of the Reproducibility of Retention Times Determined Using Different IGC Units

Due to the fact that two IGC systems were used, it was thought essential that a study of the reproducibility of the results obtained was undertaken. Thus, the dispersive component of the surface tension of Chromosorb® W AW DCMS at 313 K was determined using column RefW2 (Table 2-12, Section 2.6.2.) and the Fisons GC unit. The flow rate used was 20 cm^3/min. In Appendix B are summarized the experimental parameters, the retention time, t_r, the net retention volume, V_n, and the energy of adsorption, $RTLn(V_n)$, for the surface adsorption of the n-alkane probe molecules. In Figure 3-3 is presented the "Fowkes plot", where the energy of adsorption of the apolar and polar probes, at the temperature of measurement, is plotted as a function of $a\times\sqrt{\gamma_l^d}$.

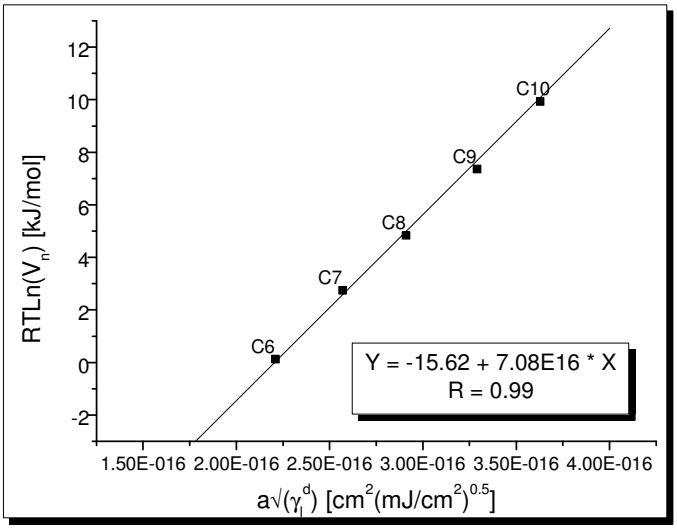

Figure 3-3. Energy of adsorption versus $a \times \sqrt{\gamma_l^d}$ of n-alkanes on the surface of Chromosorb® W AW DCMS , at T = 313 K.

From linear regression of the experimental data relating to the n-alkanes, γ_s^d was determined to be 33.2 mJ/m^2. In the following table are collated the values of γ_s^d determined at 313 K using the Perkin Elmer GC unit, the Fisons GC unit and those values that are reported in the literature (Schreiber *et al.* 1994).

Table 3-3. Dispersive component of the surface free energy of Chromosorb® W AW DCMS, at 313 K.

	γ_s^d (mJ/m^2)
Perkin Elmer GC unit	33.4
Fisons GC unit	33.2
Literature	31.6

The values of γ_s^d obtained using different IGC units are identical, and agree well with the literature value. It should be noted that the value taken from the literature refers only to Chromosorb, without further details regarding the grade. It was thus proven that both GC units could be used for inverse gas chromatographic studies, with excellent reproducibility of the results.

3.1.3. IGC Study of C. I. Pigment Blue 28

3.1.3.1. Preliminary Studies

Preliminary studies concerning the influence of the carrier gas flow rate on the energy of adsorption ($-\Delta G_a$) were carried out. These involved the use of flow rates in the range 10-30 cm^3/min. In addition, the influence of the temperature of measurement on this study was evaluated. The probe molecule used was n-decane and the pigment loading in the IGC column was 4.7 % (w/w) (column 1, Table 2-12, Section 2.6.2.).

The objective was to verify the absence of kinetic effects as well as diffusion phenomena on the pigment, for the carrier gas flow rate range used, in order to validate the use of the Fowkes approach.

The results are presented in tables in Appendix B and summarised in Figure 3-4. Here, the free energy of adsorption, $-\Delta G_a$, is plotted as a function of the flow rate of the carrier gas. The different series of data represented relate to the temperatures 313 K, 333 K, and 353 K.

Throughout the IGC studies, the standard deviation of the energy of adsorption values of the probe molecules was calculated as described in Appendix A, and is included, as an example, in Figures 3-4 and 3-5. The relative standard deviation in $-\Delta G_a$ was typically below 5 %.

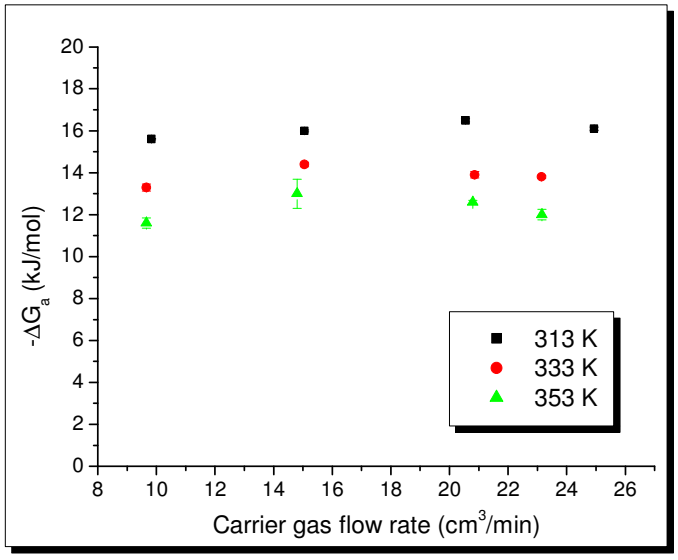

Figure 3-4. Influence of the carrier gas flow rate on the energy of adsorption of n-decane on the surface of C. I. Pigment Blue 28.

Figure 3-4 shows that the value of $-\Delta G_a$ can be considered to be independent of the carrier gas flow rate, in the range 10-30 cm^3/min, within experimental error. This behaviour is consistent

with the temperature variation. As the temperature increases, the free energy of adsorption decreases, in line with expectation. It can be concluded that kinetic effects as well as diffusion phenomena in the pigment can be disregarded for flow rate values that are within the range studied. Therefore, in further studies, the carrier gas flow rate was kept at approximately 20 cm^3/min.

In the study of the effect of the pigment loading on the retention time of probe molecules, several columns were prepared with increased C. I. Pigment Blue 28 loadings on the stationary phase. The probe molecule used in this study was n-decane. This was because n-decane interacts with both the pigment and the stationary phase. The measurement temperature was 313 K and the flow rate 20 cm^3/min. The columns used were columns RefW1, 1, 2, 3, 4, and 5 (Table 2-12, Section 2.6.2.). The results are presented in tables in Appendix B and summarised in Figure 3-5.

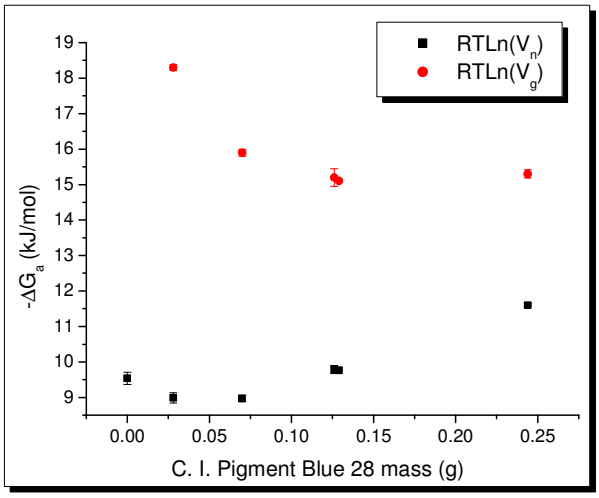

Figure 3-5. Energy of adsorption of n-decane *versus* pigment mass on the stationary phase.

The data curve of RTLn(V_n), shows that there is a decrease on the energy of adsorption when a small amount of pigment is added to the column support. This seems to continue until a point when, as the mass of pigment rises, the energy of adsorption rises proportionally. Thus, it can be concluded that the strength of interaction between n-decane and cobalt aluminate is lower than the interaction between this probe molecule and Chromosorb® W AW DCMS. From this, it is expected that the dispersive component of the surface tension of cobalt aluminate is lower than that of Chromosorb® W AW DCMS. Over a certain amount of pigment in the support material, the energy of adsorption rises and surpasses the values for Chromosorb® W AW DCMS (data point at 0.00 g pigment loading). This is due to an increase in the adsorption area as the amount of pigment in the stationary phase increases. Considering the mass-normalised values of the adsorption energy, RTLn(V_g), one can notice that its values decrease until a certain loading of pigment is reached, thereafter remaining constant. This behaviour supports the explanation given above and proves that

there is a minimum amount of pigment that covers completely the surface of Chromosorb® W AW DCMS. This amount was achieved in columns 1 and 11, corresponding to a pigment loading of approximately 5 % (w/w).

In conclusion, although the stationary phase used, Chromosorb® W AW DCMS, interacts with the n-alkanes and basic/amphoteric probe molecules, when a minimum pigment loading on the support is used (5 % w/w), this interaction is eliminated and only interactions between the pigment and probe molecules are encountered and measured.

For further studies the carrier gas flow rate used was 20 cm^3/min and the pigment loading on the column stationary phase was 5 % (w/w). The dispersive component of the surface tension was determined according to the procedure outlined in Section 1.2.5.3., using the Fowkes approach. The temperature was varied between 313 K and 353 K, in increments of 10 K, in order to follow the evolution of γ_s^d with temperature and to evaluate the surface Lewis acidic/basic characteristics. The results presented in the following sections concern column 1 (Table 2-12, Section 2.6.2.). The instrument used was the Perkin Elmer GC8410 unit.

3.1.3.2. Determination of the Dispersive Component of the Surface Tension

In Table 3-4 are summarised the experimental parameters and results concerning the adsorption of n-alkanes on the surface of the pigment, at a measuring temperature of 313 K. Presented are the retention time, t_r, the specific retention volume, V_g, and the energy of adsorption, $RTLn(V_g)$. The experimental parameters and results concerning the remaining measurement temperatures are summarised in tables in Appendix B. Figure 3-6 illustrates the determination of the dispersive component of the surface tension at the temperature of 313 K, according to the Fowkes approach.

Table 3-4. Retention time, t_r, specific retention volume, V_g, and energy of adsorption, $RTLn(V_g)$, of n-alkanes on the surface of C. I. Pigment Blue 28, at T = 313 K, F = 18.22 cm^3/min, J = 0.85, C = 0.98, P_{in} = 133.53 kPa, P_{out} = 99.06 kPa, and $T_{flow\ meter}$ = 290 K.

Probe molecule	t_r (s)	V_g (cm^3/g)	$RTLn(V_g)$ (kJ/mol)
CH_4	20.8	n/a	n/a
C_6H_{14}	25.9	10.0	6.0
C_7H_{16}	34.3	26.4	8.5
C_8H_{18}	50.1	57.2	10.5
C_9H_{20}	88.2	131.7	12.7
$C_{10}H_{22}$	189.3	329.0	15.1

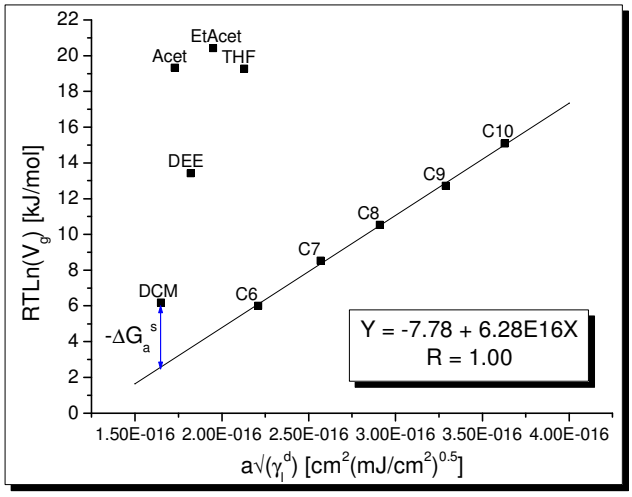

Figure 3-6. Energy of adsorption versus $a\times\sqrt{\gamma_l^d}$ of n-alkanes and polar probes on the surface of C. I. Pigment Blue 28, at T = 313 K.

From the slope of the linear relationship that is observed in Figure 3-6, it follows that the value of γ_s^d is 27.2±1.2 mJ/m^2, at 313 K. Following the same methodology, the value of γ_s^d at the temperatures of 323 K, 333 K, 343 K and 353 K was determined. It should be noted that a very good correlation factor was obtained for the linear regression of RTLn(V_g) *vs* $a\times\sqrt{\gamma_l^d}$, for the n-alkanes. Correlation coefficients for these functions were typically greater than 0.98, providing a good indication that the chromatographic method was being performed accurately (Hegedus and Kamel 1993a). Table 3-5 summarises the values that were determined for the dispersive component of the surface tension in the temperature range analysed.

Table 3-5. Values of the dispersive component of the surface tension, γ_s^d, for the surface of C. I. Pigment Blue 28.

T (K)	γ_s^d (mJ/m^2)	R^2
313	27.2 ± 1.2	1.00
323	23.2 ± 2.5	0.99
333	20.1 ± 2.2	0.99
343	19.7 ± 3.4	0.98
353	17.4 ± 3.2	0.98
$\frac{d\gamma_s^d}{dT}$	-0.23 ± 0.04	n/a

It should be noticed that the value of γ_s^d for cobalt aluminate is lower than that of the IGC column stationary phase, Chromosorb® W AW DCMS (γ_s^d = 33.4 mJ/m^2, Section 3.1.1.1.), as predicted from the preliminary studies at low pigment loadings in the stationary phase (Figure 3-5, Section 3.1.3.1.). This fact further supports the reasoning presented in the appropriate section.

Table 3-5, shows that the dispersive component of the surface tension decreases consistently with increasing temperature. This decrease is an expression of the entropic contribution of increasing temperature to the energy of adsorption. No values were found in the literature concerning the dispersive component of the surface tension of cobalt aluminate. Nevertheless, for alumina, the following values can be found in the literature: 109 mJ/m^2 (at 310 K) (Zhang *et al.* 1992), 60 mJ/m^2 (at 323 K), 40 mJ/m^2 (at 354 K), 20 mJ/m^2 (at 384 K), 10 mJ/m^2 (at 414 K), 5 mJ/m^2 (at 434 K), 7 mJ/m^2 (at 454 K) (Hamieh *et al.* 1998), and 51.8 mJ/m^2 (at 403 K) (Bogillo and Voelkel 1997). No further details on the surface characteristics of the aluminas studied are given in the references mentioned and the differences observed in the data presented may be due, e.g., to the presence of surface coatings, to differences in the crystalline structure, and to the presence of contaminants at the surface. Bearing in mind the different values found in the literature for aluminas, no comparisons can be made of the values obtained for γ_s^d in the present study, for cobalt aluminate, with those relating to (the chemically similar) alumina.

The enthalpy and the entropy of adsorption of the n-alkanes on the surface of C. I. Pigment Blue 28 were determined as described in Section 1.2.5.3. The procedure involves the plot of $-\Delta G_a/T$ as a function of 1/T. The value of $-\Delta H_a$ and of ΔS_a are determined from the slope and from the intercept, respectively. The results of the procedure are illustrated in Figure 3-7. The values determined are summarised in Table 3-6.

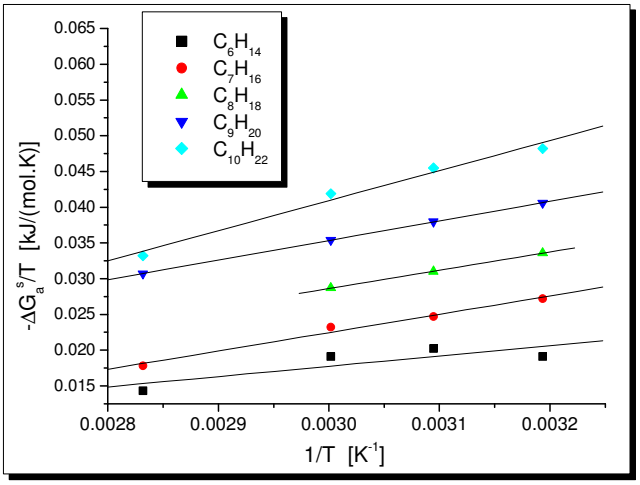

Figure 3-7. Determination of the enthalpy, and of the entropy, of adsorption of the n-alkanes on the surface of C. I. Pigment Blue 28.

Table 3-6. Enthalpy of adsorption, ΔH_a, and entropy of adsorption, ΔS_a, of the n-alkanes on the surface of C. I. Pigment Blue 28.

Probe molecule	$a(\gamma_l^d)^{0.5}$ (cm^2 (mJ cm^{-2})$^{0.5}$)	$-\Delta H_a$ (kJ/mol)	ΔS_a (J/molK)	R^2
C_6H_{14}	2.21E-16	14.5	-25.9	0.85
C_7H_{16}	2.57E-16	25.8	-54.8	0.99
C_8H_{18}	2.91E-16	26.1	-49.6	1.00
C_9H_{20}	3.29E-16	27.5	-47.1	1.00
$C_{10}H_{22}$	3.63E-16	42.2	-85.7	0.99

Table 3-6 shows that the value of the enthalpy of adsorption of the apolar probes increases with increasing value of $a\times\sqrt{\gamma_l^d}$. This is understood on the basis that the n-alkane molecules will interact only through dispersive forces. This type of intermolecular force increases of importance with increasing number of carbon atoms in the n-alkane molecule (indicated by the greater value of $a\times\sqrt{\gamma_l^d}$). With respect to the entropy of adsorption, it can be seen that, in a general manner, the change in the entropic component of the energy of adsorption is greater in the case of larger molecules.

3.1.3.3. Determination of the Energy, the Enthalpy and the Entropy of Adsorption of Polar Probes

The specific component of the free energy of adsorption, $-\Delta G_a^s$, corresponding to the polar probes, was determined by the method outlined in Section 1.2.5.3. The procedure is illustrated in Figure 3-6 and consists in determining the difference between the value of the energy of adsorption of a particular polar probe and the corresponding value in the n-alkanes reference line. The polar probes used were THF (basic probe), Acet, DEE, EtAcet (amphoteric probes), TCM and DCM (acidic probes).

In Table 3-7 are given the values of the retention time, of the specific retention volume, of the energy of adsorption, of the energy of adsorption corresponding to the n-alkanes reference line and of the specific component of the energy of adsorption, for the measurement temperature of 313 K. The data relating to the remaining temperatures (323 K, 333 K, and 353 K) are presented in Appendix B.

Table 3-7. Retention time, t_r, specific retention volume, V_g, energy of adsorption, $RTLn(V_g)$, and corresponding dispersive and specific components, $RTln(V^d_{g,ref})$ and $RTln(V^s_g)$, respectively, for the adsorption of polar probes on the surface of C. I. Pigment Blue 28, at T = 313 K, F = 21.77 cm^3/min, J = 0.85, C = 0.98, P_{in} = 134.31 kPa, P_{out} = 99.84 kPa, and $T_{flow\ meter}$ = 291 K.

Probe molecule	t_r (s)	V_n (cm^3)	$RTLn(V_n)$ (kJ/mol)	$RT\ln(V^d_{n,ref})$ (kJ/mol)	$RT\ln(V^s_n)$ (kJ/mol)
CH_4	23.8	n/a	n/a	n/a	n/a
DCM	28.4	10.7	6.2	2.6	3.6
DEE	98.0	173.1	13.4	3.7	9.8
Acet	743.0	1678.0	19.3	3.1	16.3
THF	729.0	1645.3	19.3	5.6	13.7
EtAcet	1116.0	2548.2	20.4	4.5	16.0

The retention time values corresponding to TCM were too low to be determined accurately with the current IGC system. The origin of the aforementioned limitation when using TCM arises from steric hindrance factors (Balard and Papirer 1993), due to the size of this molecule, hindering its adoption of a conformation that would be more favourable for interaction through the hydrogen atom (Lewis acidic centre).

When comparing the TCM acidic strength with that of DCM it can be seen that TCM is more acidic (AN* of 22.7 and 16.4 kJ/mol, respectively). The surface area of TCM is greater than that of DCM (0.440 and 0.315 nm^2, respectively). However, the existence of an additional chlorine atom in TCM makes the effectiveness of highly directional specific interactions more difficult. A solution would be to use a larger column or a higher pigment loading, providing an increase in the surface area available for adsorption and, thus, longer retention times of this probe on the stationary phase.

Table 3-7, shows that the values of the specific component of the energy of adsorption of basic/amphoteric probes are significantly greater than those relating to the acidic probes. It can be concluded that the surface of C. I. Pigment Blue 28 is Lewis amphoteric. Nevertheless, no absolute conclusions can be drawn from the analysis of the results, as far as dominant surface acidity or dominant surface basicity is concerned, as the acidity of the acidic probes is not comparable to the basicity of the basic probes (Table 3-8).

The enthalpy of adsorption, and the entropy of adsorption of the polar probes, along with the corresponding dispersive and specific components, were determined by the method explained in Section 1.2.5.3, and described in the previous section for the adsorption of apolar probes. Table 3-8 summarises the results obtained. The results of the procedure are illustrated in Figure 3-8.

Table 3-8. Dispersive and specific components of the enthalpy of adsorption, and of the entropy of adsorption, ΔH^d_a, ΔH^s_a and ΔS^d_a, ΔS^s_a, respectively, of the polar probes, on the surface of C. I. Pigment Blue 28.

Probe molecule	$a(\gamma_l^d)^{0.5}$ (cm^2 ($mJ\ cm^{-2}$)$^{0.5}$)	$-\Delta H^d_a$ (kJ/mol)	ΔS^d_a (J/molK)	R^2	AN* (kJ/mol)	DN (kJ/mol)	$-\Delta H^s_a$ (kJ/mol)	ΔS^s_a (J/molK)	R^2
DCM	1.65E-16	7.2	-13.6	0.73	16.4	0.0	12.9	-30.2	0.96
DEE	1.82E-16	9.9	-18.9	0.84	5.9	80.6	29.6	-64.2	0.98
Acet	1.73E-16	8.4	-16.1	0.79	10.5	71.4	20.7	-14.6	0.99
THF	2.13E-16	14.8	-28.6	0.94	2.1	84.4	29.2	-49.7	1.00
EtAcet	1.95E-16	11.9	-23.0	0.89	6.3	71.8	33.1	-56.2	0.95

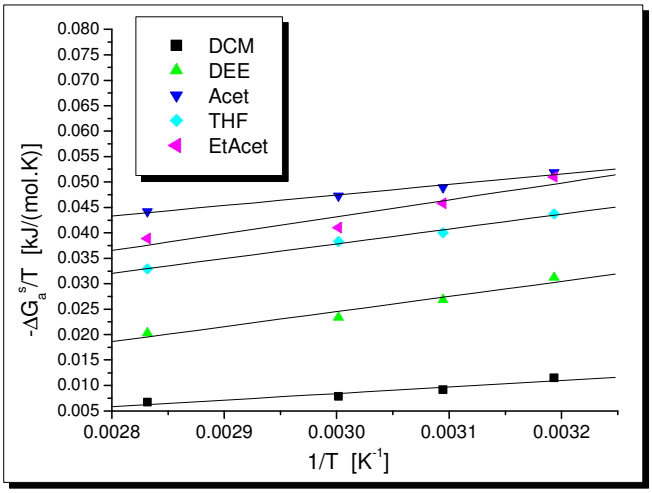

Figure 3-8. Determination of the specific component of the enthalpy, and of the entropy, of adsorption of polar probes on the surface of C. I. Pigment Blue 28.

Due to the above mentioned constraint relating to the use of TCM as a probe molecule it was not possible to determine the enthalpy and entropy of adsorption corresponding to this molecule. The values of the adsorption energy of the polar probes, at 343 K, were not used for the determination of $-\Delta H^s_a$, because they are significantly higher than they should be, considering the trend observed for the remaining temperatures. The propagation of an experimental error is thought to be the cause. This error could be derived from the flow rate measurement, determination of the retention time for methane and/or from the incorrect reading of the column inlet pressure.

As far as the dispersive component of the energy of adsorption is concerned, Table 3-8 shows that it increases with increasing $a\times\sqrt{\gamma_l^d}$ for the polar probe, and, thus, with increasing capability of interaction through dispersion forces. The change in the dispersive component of the

entropy of the system upon adsorption of the polar molecules also increases with increasing $a \times \sqrt{\gamma_l^d}$, and with increasing $-\Delta H^d_a$. This trend stems from the greater decrease of entropy associated with the greater dispersive component of the enthalpy of adsorption, and, thus, to the greater restriction of the molecules upon adsorption, for those probe molecules whose dispersive component of energy of adsorption on the surface is greater.

The greater the value of $-\Delta H^s_a$, the stronger is the interaction between the probe molecule and the surface of the solid. Therefore, the results presented in Table 3-8 are an indication of the amphoteric character of the surface of the cobalt aluminate pigment. They do not, however, indicate that the surface is predominately acidic (due to the greater value of ΔH^s_a for the basic/amphoteric probes, compared with that relating to the acidic probe, DCM), because the basic strength of THF and Acet, for example, is notably greater than the acidic strength of DCM (Table 3-8). Furthermore, the interaction with the amphoteric probes will indicate not only the acidity but also the basicity of the material. The analysis of $-\Delta H^s_a$ for the polar probes does, nevertheless, confirm the analysis of the specific component of the energy of adsorption for these probes.

It is clear that the specific component of the entropy of adsorption is lower for those probes that have the lower values of $-\Delta H^s_a$, in line with expectation, although a distinct trend is not observed. This indicates that the behaviour of the decrease of entropy of the system that is associated with the formation of specific intermolecular interactions is not as linear as that of the dispersive component (of the entropy of adsorption). Factors related to changes in the conformation of the probe molecules, and to changes in the conformation of the surface, upon adsorption, are thought to be more complex than when only dispersive forces are involved.

3.1.3.4. Determination of K_a and K_b

The observations relating to the specific component of the energy of adsorption and specific component of the enthalpy of adsorption can be compared with the values obtained for the surface Lewis acidity constant, K_a, and for the surface Lewis basicity constant, K_b. These constants were determined according to the procedure described previously (Section 1.2.5.3.). The procedure is illustrated in Figure 3-9. From the slope and from the intercept of $-\Delta H^s_a/AN^*$ *vs* DN/AN^* the values of K_a and of K_b are obtained, respectively.

From linear regression on the data presented in Figure 3-9, the values obtained for K_a and K_b are calculated as 0.33 and 0.60, respectively. From the values of K_a and K_b it can be concluded that the surface of cobalt aluminate is amphoteric, though predominantly Lewis basic. The results obtained for the C. I. Pigment Blue 28 pigment are in agreement with results published in the literature from studies of the Lewis acidity/basicity of alumina, as its surface has been shown to be amphoteric, predominantly basic (Ponec *et al.* 1974; Zhang *et al.* 1992). For C. I. Pigment Blue 28, the acidity is localised in the cations Co^{2+}, Co^{3+} (easily reducible (Busca *et al.* 1992)) and Al^{3+} (Ponec *et al.*1974; Busca *et al.* 1992) and, in the surface OH groups (Solomon and Hawthorne

1983; Busca *et al.* 1992; Tsobokawa *et al.* 1994). The basicity of this inorganic pigment is localized in the anion O^{2-}, and also in the surface hydroxyl groups (Ponec *et al.* 1974; Solomon and Hawthorne 1983; Fowkes *et al.* 1990; Busca *et al.* 1992; Tamura *et al.* 1999). The surface was predicted not to be strongly acidic, at least from the point of view of the abundance of sites, due to the fact that, on normal cobalt aluminate, octahedral Al^{3+} ions predominate with respect to the tetrahedral ones (Busca *et al.* 1991). This prediction was confirmed in the present study. Aluminium (Al^{3+}) cations in tetrahedral environments act as strong Lewis acid sites, whereas those in octahedral positions have a weaker Lewis acidic character.

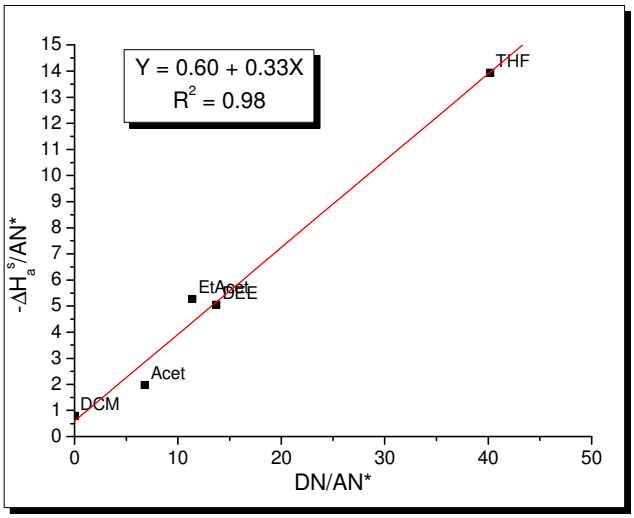

Figure 3-9. Determination of K_a and K_b of the surface of C. I. Pigment Blue 28.

There are two general classes of acidic species: those that can act as proton donors for basic molecules (e. g. surface hydroxyl groups), Bronsted acids, and those that can accept electron pairs from basic molecules, forming coordination bonds (e. g. Al^{3+}, Co^{2+}), Lewis acids. Lewis acids may form Bronsted acids on hydration, provided that the polarisation of H-O bonds of the coordinated water molecules is sufficient to enhance significantly their dissociation (Solomon and Hawthorne 1983). The surfaces of cobalt aluminate may contain both Lewis acidic species and Bronsted acidic species. The most important sources of Bronsted acidity are the polarised water molecules that are adsorbed on the inorganic surfaces, particularly those water molecules that are associated with polyvalent, compensating cations such as Al^{3+}. The dominating Lewis acidic species on the surface of inorganic particulates are usually the Al^{3+} cations (Solomon and Hawthorne 1983). In the presence of water, these Lewis acidic species are hydrated and their acidity masked. However, if the Al^{3+} cations have electronegative substituents such as halide or silicate ions, the coordinated water molecules may be sufficiently polarised to form strong Bronsted acidic species. The basic

centres include surface OH groups, exposed at the layer lattice edges that can accept protons from water molecules or other Bronsted acids.

Pigment processing parameters and procedures play a critical role in determining surface properties. Small concentrations of foreign species such as water or other chemicals, can significantly alter surface characterisitics (Hegedus and Kamel 1993a). Furthermore, the concentration of surface groups can vary. In the particular case of alumina, surface contamination by silica (SiO_2) and by other metal oxides (e.g. CaO, Na_2O and MgO) (Papirer *et al.* 1991; Chehimi *et al.* 2001) significantly influences the Lewis acid/base properties, namely the surface Lewis acidity, in the case of silica impurities (Papirer *et al.* 1991). Therefore, it is expected that the presence (intentional or unintentional) of such substances at the surface of the commercial C. I. Pigment Blue 28, may be contributing to the values of K_a and K_b. It should be noted that no surface coating was detected by TGA (Section 3.3.4.).

3.1.4. IGC Study of the MBS elastomer (IM)

3.1.4.1. Preliminary Studies

Preliminary studies concerning the influence of the carrier gas flow rate, and of the MBS loading on the support material (Chromosorb® W AW DCMS), were carried out using flow rate values in the range 25-50 cm^3/min and MBS rubber mass values ranging from 0.05 to 0.20 g (columns 6 to 9, Table 2-12, Section 2.6.2.). The probe molecule used was n-octane and the measurements were performed at 343 K. The instrument used was the Fisons GC unit. The results are presented in tables in Appendix B and are summarised in Figure 3-10.

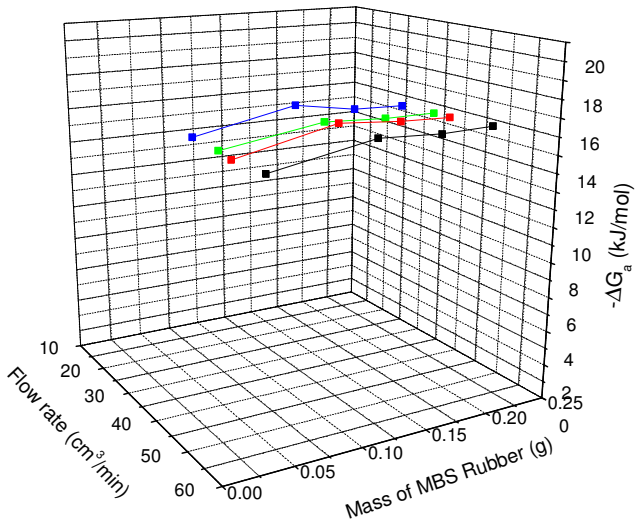

Figure 3-10. Effect of the carrier gas flow rate, and of the MBS rubber loading on the support material, on the value of the energy of adsorption of n-octane.

Figure 3-10, shows that neither the carrier gas flow rate nor the MBS loading in the stationary phase influence the adsorption energy of n-octane on the surface of the MBS rubber, within experimental error. The relative standard deviation associated with the determination of $-\Delta G_a$ was typically lower than 5 %. Bearing in mind that the measurement temperature is lower than the T_g of PMMA (383 K (Hamieh *et al.* 1998)), the shell material of the MBS rubber), it can be concluded that surface adsorption is the dominant mechanism, and absorption of the probe molecules into the bulk of the MBS rubber particles can be neglected. In what concerns the effect of the MBS rubber loading, the analysis of Figure 3-10 leads to the observation that there is no meaningful effect of the loading on the value of the energy of adsorption. It can be concluded that for the flow rate range and MBS rubber loading range studied, the adsorption energy of n-octane on the surface of the elastomer is not affected by the variation of those factors. Therefore, in further studies, the carrier gas flow rate used was 30 cm^3/min and the MBS rubber loading on the stationary phase was 7.80 % w/w (column 8, Table 2-12, Section 2.6.2.). The temperature was varied between 333 K and 373 K, in increments of 10 K.

3.1.4.2. Determination of the Dispersive Component of the Surface Tension

The experimental parameters and results concerning the adsorption of n-alkanes on the surface of the MBS rubber are presented in tables in Appendix B. Figure 3-11 illustrates the determination of the dispersive component of the surface tension at 333 K.

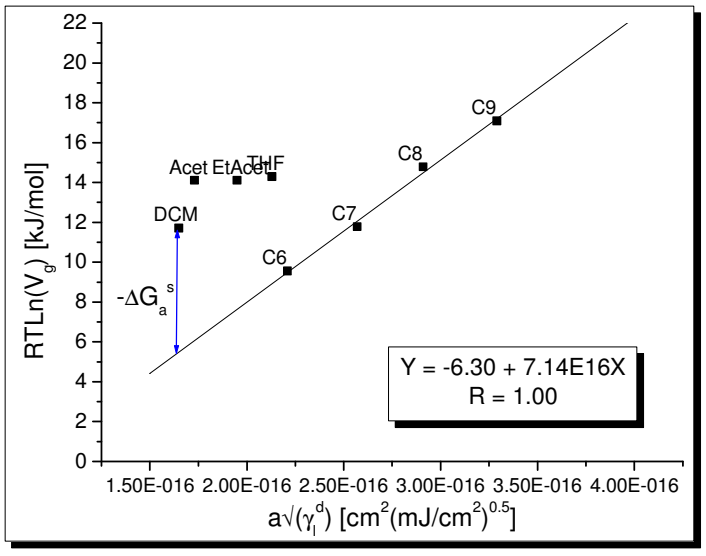

Figure 3-11. Energy of adsorption versus $a \times \sqrt{\gamma_l^d}$ for n-alkanes and polar probes on the surface of the MBS rubber, at T = 333 K.

Table 3-9 summarises the values determined for the dispersive component of the surface tension in the temperature range analysed.

Table 3-9. Values of the dispersive component of the surface tension of the MBS rubber.

T (K)	γ_s^d (mJ/m^2)	R^2
333	35.1 ± 3.7	0.99
343	37.5 ± 2.9	1.00
353	38.5 ± 6.6	0.99
363	39.1 ± 5.5	0.99
373	38.5 ± 5.5	0.97
Average	37.7 ± 1.6	n/a

Table 3-9 shows that the dispersive component of the surface tension remains reasonably constant, within experimental error, and equal to 37.7±1.6 mJ/m^2. The value of γ_s^d at the temperature of 333 K, falls slightly below expectation. This is thought to be due to a ß relaxation process known to occur in PMMA at this temperature (Hamieh *et al.* 1998). This ß transition is a consequence of the movement of the side chains (Figure 3-12).

It was noticed that, at 383 K, the apolar probes were able to penetrate into the bulk of the polymer as the value of γ_s^d was significantly different from the value obtained for lower temperatures. In order to check if experimental errors were involved, this determination was repeated. The same γ_s^d value was obtained on repetition. This behaviour is consistent with the value of T_g for PMMA (383 K (Hamieh *et al.* 1998)). Similar phenomena are found in the literature for the IGC characterisation of a SBR rubber, below it T_g and above its T_g (Mukhopadhyay and Schreiber 1993).

The value of γ_s^d for the surface of the MBS rubber is in good agreement with values found in the literature for PMMA: 38.8mJ/m^2 (at 295 K), 40.9 mJ/m^2 (343-383 K) (Abel and Chehimi 1994), 40.9/43 mJ/m^2 (343-383 K) (Hegedus and Kamel 1993a), 41.1mJ/m^2 (at 293 K) (Hobbs *et al.* 1988a), and 41.5mJ/m^2 (at room temperature) (Schreiber 1993).

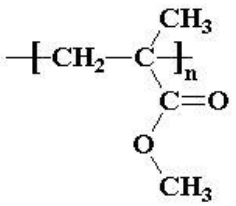

Figure 3-12. Repeating unit in poly(methyl methacrylate).

The enthalpy and the entropy of adsorption of the n-alkanes on the surface of the MBS rubber were determined as described in previous sections. The results are illustrated in Figure 3-13 and summarised in Table 3-10.

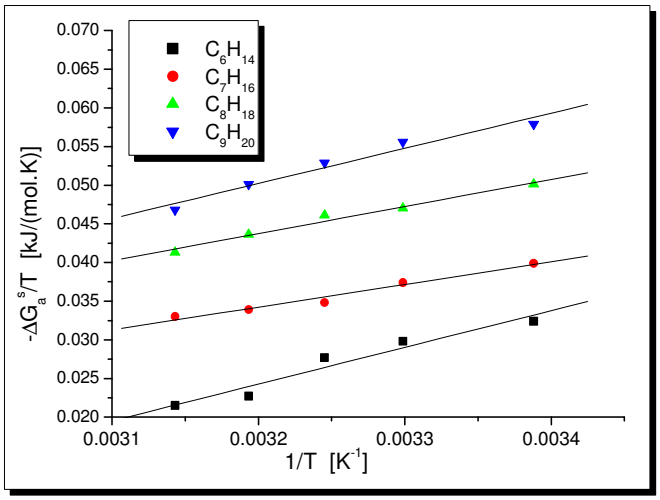

Figure 3-13. Determination of the enthalpy, and of the entropy of adsorption of n-alkanes on the surface of the MBS rubber.

Table 3-10. Enthalpy of adsorption, ΔH_a, and entropy of adsorption, ΔS_a, of the n-alkanes on the surface of the MBS rubber.

Probe molecule	$a(\gamma_l^d)^{0.5}$ (cm^2 (mJ cm^{-2})$^{0.5}$)	-ΔH_a (kJ/mol)	ΔS_a (J/molK)	R^2
C_6H_{14}	2.21E-16	47.6	-128.0	0.97
C_7H_{16}	2.57E-16	29.2	-59.3	0.98
C_8H_{18}	2.91E-16	34.9	-68.0	0.99
C_9H_{20}	3.29E-16	45.3	-94.6	0.98

Table 3-10 shows that the value of the enthalpy, and of the entropy, of adsorption of the apolar probes increases with increasing $a\sqrt{\gamma_l^d}$, with the exception of n-hexane. For this molecule, the values of -ΔH_a and of ΔS_a are greater than expected. This is thought to be due to experimental errors in the determination of the retention times of n-hexane at the higher temperatures, derived from their low values (4.3 and 4.8 s at 373 K and 363 K, respectively).

3.1.4.3. Determination of the Energy, the Enthalpy and the Entropy of Adsorption of Polar Probes

The determination of the specific component of the free energy of adsorption, -ΔG_a^s, corresponding to the polar probes is illustrated in Figure 3-11, for the temperature of 333 K.

In Table 3-11 are presented the results concerning this measurement temperature. The data relating to the remaining temperatures (343 K, 363 K, 363 K and 373 K) are presented in Appendix B.

Table 3-11. Retention time, t_r, specific retention volume, V_g, energy of adsorption, RTLn(V_g), and corresponding dispersive and specific components, RTln($V^d_{g,ref}$) and RTln(V^s_g), respectively, for the adsorption of polar probes on the surface of the MBS rubber, at T = 333 K, F = 35.29 cm^3/min, J = 0.86, C = 0.97, P_{in} = 131.87 kPa, P_{out} = 100.16 kPa, and $T_{flow\ meter}$ = 296 K.

Probe molecule	t_r (s)	V_n (cm^3)	RTLn(V_n) (kJ/mol)	$RT\ln(V^d_{n,ref})$ (kJ/mol)	$RT\ln(V^s_n)$ (kJ/mol)
CH_4	22.5	n/a	n/a	n/a	n/a
DCM	48.8	68.5	11.7	5.5	6.2
Acet	85.0	163.2	14.1	6.1	8.1
THF	89.5	175.0	14.3	8.9	5.4
EtAcet	85.7	164.9	14.1	7.6	6.5

The retention time values corresponding to DEE and to TCM were too low for a precise determination using with the current IGC system. This is thought to be due to structural restrictions, as explained in Section 3.1.3.3. for TCM, from both the adsorbate and the adsorbent, hindering these molecules from spatial conformations effective in terms of specific intermolecular interactions. The oxygen atom (Lewis basic centre) of DEE is more susceptible to shielding by the neighbouring hydrogen atoms (Tiburcio and Manson 1991a) than is that of, e.g. acetone, which is readily accessible for interaction. The bulkiness of the TCM molecule, due to the three chlorine atoms, hinders the access to the acidic centre in this molecule (the hydrogen atom). Furthermore, the side chain of the PMMA molecule (Figure 3-12) further decreases the probability of establishment of the highly directional, specific, acid/base intermolecular interactions with the probe molecules. The determination of the retention times corresponding to TCM and to DEE was repeated in order to establish the nature of any possible experimental errors. However, the values found were identical to those of the first determination. The fact that $a\sqrt{\gamma_l^d}$ for TCM is the highest of the polar molecules used, leads to the observation that the strong contribution of dispersive forces, and the occurrence of conformational changes on this molecule, upon adsorption, may be influencing the achievement of H-bonding with the surface due to the highly directional character of this bond. This effect would be more pronounced as the temperature increases.

The values of $-\Delta G_a^s$ (Table 3-11) show that the values for Lewis acidic probes are close to those of the Lewis basic/amphoteric probes. Bearing in mind the relative low acidity of the acidic probe (DCM), when compared to the basicity of the basic probes (e.g. THF), it can be concluded that the surface of the MBS rubber is amphoteric, with a strong Lewis basic feature.

The results concerning the determination of the enthalpy, and entropy, of adsorption of the polar probes, along with the corresponding dispersive and specific components, are summarised in Table 3-12, and illustrated in Figure 3-14.

Table 3-12. Dispersive and specific components of the enthalpy of adsorption, and of the entropy of adsorption, ΔH^d_a, ΔH^s_a and ΔS^d_a, ΔS^s_a, respectively, for the adsorption of polar probes on the surface of the MBS rubber.

Probe molecule	$a(\gamma_l^d)^{0.5}$ (cm^2 ($mJ\ cm^{-2}$)$^{0.5}$)	$-\Delta H^d_a$ (kJ/mol)	ΔS^d_a (J/molK)	R^2	AN* (kJ/mol)	DN (kJ/mol)	$-\Delta H^s_a$ (kJ/mol)	ΔS^s_a (J/molK)	R^2
DCM	1.65E-16	25.6	-60.4	0.99	16.4	0.0	14.4	-24.4	0.99
Acet	1.73E-16	25.9	-59.7	0.99	10.5	71.4	19.8	-34.5	0.97
THF	2.13E-16	27.7	-56.3	1.00	2.1	84.4	11.0	-16.5	0.97
EtAcet	1.95E-16	26.9	-57.8	1.00	6.3	71.8	16.6	-30.8	0.98

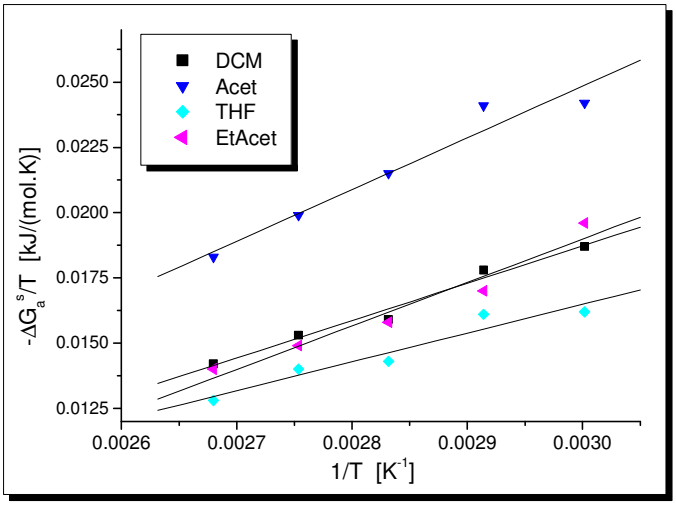

Figure 3-14. Determination of the specific component of the enthalpy, and of the entropy of adsorption of polar probes on the surface of the MBS rubber.

Due to the above mentioned constraints concerning the use of TCM and DEE probes, it was not possible to determine the enthalpy and entropy of adsorption corresponding to these probe molecules. With respect to $-\Delta H^d_a$, it can be seen, in Table 3-12, that the values increase with increasing value of $a\times\sqrt{\gamma_l^d}$ for the probe molecule. The dispersive component of the entropy of the system does not vary significantly with the probe molecule adsorbed.

The value of $-\Delta H^s_a$, is greater for the amphoteric molecules (Acet and EtAcet) and for the acidic molecule (DCM), than for the basic molecule (THF). Furthermore, Acet and EtAcet having similar basicity constants (71.4 kJ/mol and 71.8 kJ/mol, respectively), $-\Delta H^s_a$ is greater for the

adsorption of Acet, which has a greater acidic character (10.5 kJ/mol and 6.3 kJ/mol, respectively). Thus, bearing in mind the values of AN* and of DN of the polar molecules, it can be concluded that the surface of the MBS rubber is Lewis amphoteric, with strong Lewis basic features. This analysis confirms the observations made on the basis of the values that were obtained for the energy of adsorption (Table 3-11). As far as the values of ΔS^s_a are concerned, these follow the same trend as those for the determination of $-\Delta H^s_a$. The greater the enthalpy of adsorption, the greater would be the change in the entropy of the system probe-surface upon adsorption of the probe molecules.

3.1.4.4. Determination of K_a and K_b

The data relating to the determination of the surface Lewis acidity constant, K_a, and of the surface Lewis basicity constant, K_b, are illustrated in Figure 3-15.

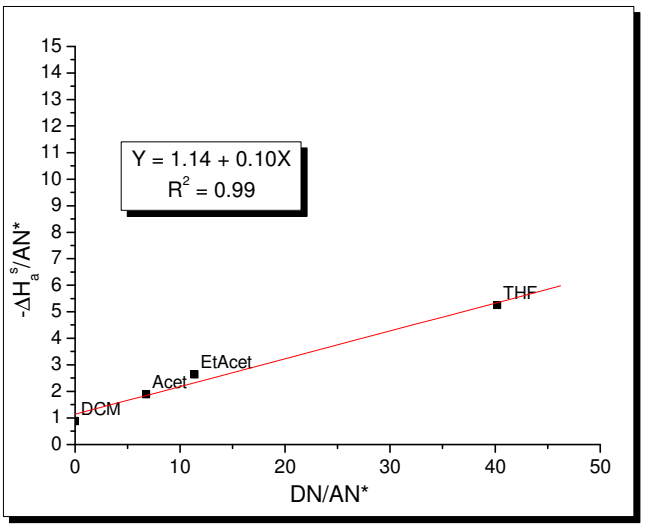

Figure 3-15. Determination of K_a and K_b of the surface of the MBS rubber.

From linear regression of the data presented in Figure 3-15, it follows that the values of K_a and K_b, are 0.10 and 1.14, respectively. Thus, the surface of the MBS rubber is amphoteric and predominantly Lewis basic, confirming the analysis of the enthalpy of adsorption and of the energy of adsorption of the polar probes. The conclusion that the MBS rubber has a Lewis amphoteric (predominantly Lewis basic) surface agrees with expectation from results of similar studies reported in the literature for PMMA (Fowkes 1980), and from an examination of the repeating unit in this polymer (Figure 3-12). The basic sites are identified with the ester functionality in the side chains. The weak Lewis acidic sites are localised in the terminal $-CH_3$ moiety in the side chain and also in the hydrogen atoms of the $-CH_2-$ moiety (this used to be controversial but is now recognized (Huyskens *et al.* 1991; Stone 1998)). Furthermore, each oxygen atom is able to interact with two hydrogen atoms and, thus, has a basic strength that is the double of the acidic strength of each

hydrogen atom. Consequently, the surface of the MBS rubber would be expected to be strongly basic and relatively weak acidic. It should be noticed that the presence of such a bulky side group (-CH_3) plus the lack of complete stereoregularity make this polymer amorphous. On the one hand, the acidity is not sufficient to overcome the steric hindrance and, on the other hand, the basicity is quite high. Thus, the repulsion between basic sites further contributes to the non-existence of intramolecular H-bonds and intermolecular H-bonds characteristic of the ordered phases, due to the fact that basic sites and acidic sites cannot get close enough, along with the directional character of the H-bond.

3.1.5. IGC Study of the PC 125

3.1.5.1. Preliminary Studies

Preliminary studies of the influence of the carrier gas flow rate on the energy of adsorption of the probe molecules on the surface of PC 125 were carried out. As with C. I. Pigment Blue 28 and with the MBS rubber, it was considered to be essential to study the influence of the support material and of increasing polymer loading, on the retention times of the probe molecules. Thus, several columns were prepared with increasing polymer loading on the stationary phase. The instrument used was the Perkin Elmer GC unit. The retention times of n-hexane at 353 K were determined for columns 10, 11 and 12 (Table 2.12, Section 2.6.2.), at carrier gas flow rates that ranged from 10 cm^3/min to 30 cm^3/min. The results are presented in tables in Appendix B and are illustrated in Figure 3-16.

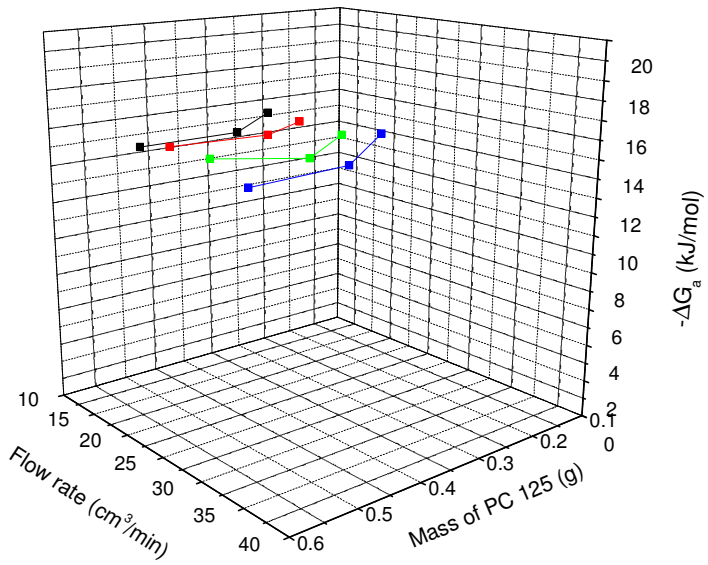

Figure 3-16. Effect of the carrier gas flow rate, and of the PC 125 loading on the support material, on the value of the energy of adsorption of n-hexane.

Figure 3-16, shows that the flow rate does not influence the adsorption energy of n-hexane on the surface of PC 125, within experimental error. Considering that the measurement temperature is lower than the T_g of PC (418 K, Section 2.1.), it can be concluded that surface adsorption was the dominant mechanism, and that absorption of the probe molecules into the bulk of the deposited polymer can be neglected.

With respect to the effect of polymer loading, the analysis of Figure 3-16 leads to the conclusion that there is no meaningful effect of the loading on the value of the energy of adsorption. It should be noticed that experimental errors, e.g. concerning the determination of the polymer loading by TGA, could be contributing to the slight variation of the adsorption energy for columns with different amounts of PC 125. Summarising, for the flow rate range and polymer loading range studied, the adsorption energy of n-hexane on PC 125 is not affected by the variation of these experimental parameters.

At the temperature of 353 K, the dispersive component of the surface free energy was determined at two carrier gas flow rate values: 30 cm^3/min and 45 cm^3/min. This was to check whether or not at 45 cm^3/min, the retention volume was still independent of the carrier gas flow rate. The value of γ_s^d did not vary significantly with the flow rate, with values of 33.9 mJ/m^2 at 30 cm^3/min and 33.7 mJ/m^2 at 45 cm^3/min. It was, therefore, concluded that at 45 cm^3/min the determination of the adsorption energy is not influenced by the carrier gas flow rate.

In subsequent studies, the temperature was varied between 353 K and 393 K, in increments of 10 K, and the carrier gas flow rate was kept at 45 cm^3/min. The temperature range and flow rate were chosen in order to provide retention times that were not excessively long, or short. Retention times that exceed 40 minutes tend to introduce large errors in the retention time due to the asymmetry of the chromatogram obtained and to the graphical method used to determine the retention times. This particular temperature range was selected so as to be lower than the T_g of PC 125, to avoid possible absorption of the probe molecules on the bulk of the polymer. The results presented in the following sections concern column 11 (Table 2-12, Section 2.6.2.)

3.1.5.2. Determination of the Dispersive Component of the Surface Tension

The experimental parameters and results associated with the adsorption of n-alkanes on the surface of PC 125, are summarised in tables in Appendix B. Figure 3-17 illustrates the results for the determination of the dispersive component of the surface tension at the measurement temperature of 353 K.

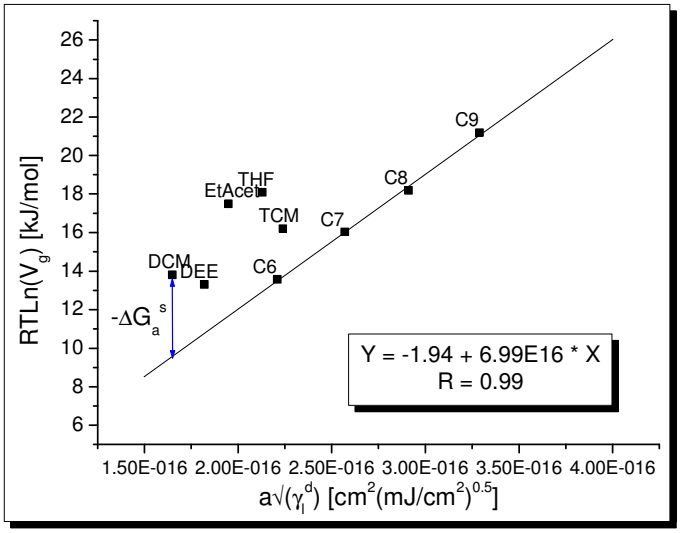

Figure 3-17. Energy of adsorption versus $a \times \sqrt{\gamma_l^d}$ for n-alkanes and for polar probes on the surface of PC 125, at T = 353 K.

Table 3-13 summarises the values determined for the dispersive component of the surface tension.

Table 3-13. Values of the dispersive component of the surface tension of PC 125, determined in the present study and from literature.

T (K)	γ_s^d (mJ/m^2)	R^2	T (K)	γ_s^d (mJ/m^2)*
353	33.7± 2.3	1.00	303	33.5
363	37.3± 2.6	1.00	313	33.0
373	33.1± 2.5	1.00	323	33.0
383	33.2± 1.9	1.00	333	32.6
393	29.3± 3.2	0.99	343	32.1
Average	33.3 ± 2.8	n/a	353	32.8
			Average	32.8 ± 0.5

* from literature (Champagne *et al.* 1994)

The value of γ_s^d for the surface of PC 125 was constant, within the temperature range studied, and equal to 33.3±2.8 mJ/m^2, agreeing well with values found in the literature (Champagne *et al.* 1994).

The enthalpy and the entropy of adsorption of the n-alkanes on the surface of PC 125 were determined as described. The procedure is illustrated in Figure 3-18 and the values determined are summarised in Table 3-14.

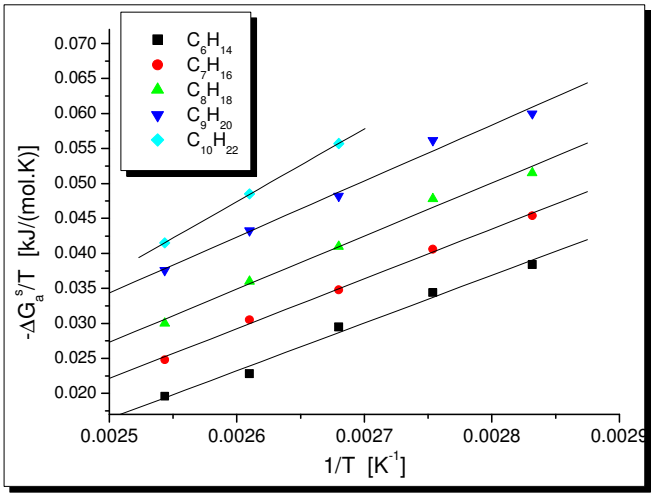

Figure 3-18. Determination of the enthalpy and of the entropy of adsorption, of n-alkanes on the surface of PC 125.

Table 3-14. Enthalpy of adsorption, ΔH_a, and entropy of adsorption, ΔS_a, of the n-alkanes on the surface of PC 125.

Probe molecule	$a(\gamma_l^d)^{0.5}$ (cm^2 ($mJ\ cm^{-2}$)$^{0.5}$)	$-\Delta H_a$ (kJ/mol)	ΔS_a (J/molK)	R^2
C_6H_{14}	2.21E-16	68.3	-154.0	0.99
C_7H_{16}	2.57E-16	71.2	-156.0	1.00
C_8H_{18}	2.91E-16	75.8	-162.0	0.99
C_9H_{20}	3.29E-16	79.9	-165.0	0.99
$C_{10}H_{22}$	3.63E-16	105.0	-225.0	1.00

In Table 3-14 it can be seen that the value of the enthalpy, and of the entropy, of adsorption of the apolar probes increases with increasing $a \times \sqrt{\gamma_l^d}$.

3.1.5.3. Determination of the Energy, the Enthalpy and the Entropy of Adsorption of Polar Probes

The determination of the specific component of the free energy of adsorption, $-\Delta G_a^s$, corresponding to the polar probes, is illustrated in Figure 3-17, for the temperature of 353 K. Table 3-15 summarises the value of the retention time, of the specific retention volume, of the energy of adsorption, of the energy of adsorption corresponding to the n-alkanes reference line, and of the specific component of the energy of adsorption, for the measurement temperature of 353 K. The data relating to the remaining temperatures (363 K, 373 K, 383 K and 393 K) are presented in Appendix B.

Table 3-15. Retention time, t_r, specific retention volume, V_g, energy of adsorption, $RTLn(V_g)$, and corresponding dispersive and specific components, $RTln(V^d_{g,ref})$ and $RTln(V^s_g)$, respectively, relating the adsorption of the polar probes on the surface of PC 125, at T = 353 K, F = 47.40 cm^3/min, J = 0.92, C = 0.98, P_{in} = 118.47 kPa, P_{out} = 101.24 kPa, and $T_{flow\ meter}$ = 291 K.

Probe molecule	t_r (s)	V_n (cm^3)	$RTLn(V_n)$ (kJ/mol)	$RT\ln(V^d_{n,ref})$ (kJ/mol)	$RT\ln(V^s_n)$ (kJ/mol)
CH_4	10.6	n/a	n/a	n/a	n/a
TCM	116.2	251.3	16.2	13.7	2.5
DCM	56.3	108.9	13.8	9.6	4.2
DEE	49.0	91.4	13.3	10.8	2.5
THF*	219.7	479.3	18.1	12.9	5.2
EtAcet**	181.5	394.2	17.5	11.7	5.9

* F = 46.04 cm^3/min, J = 0.92, C = 0.98, P_{in} = 118.53 kPa, P_{out} = 101.29 kPa, $T_{flow\ meter}$ = 293 K, $t_{r\ (methane)}$ = 11.4 s

** F = 45.80 cm^3/min, J = 0.92, C = 0.98, P_{in} = 115.99 kPa, P_{out} = 98.76 kPa, $T_{flow\ meter}$ = 291 K, $t_{r\ (methane)}$ = 9.8 s

Table 3-15 shows that the surface of PC 125 is Lewis amphoteric. When comparing the energy of adsorption of the basic/amphoteric probes with that of the acidic probes, it is noticed that those of the basic/amphoteric probes are relatively weak, bearing in mind the corresponding value of DN. This indicates that the surface is not strongly acidic. On the other hand, it can signify that the surface of PC 125 is strongly basic, as the energy of adsorption of the acidic probes is significantly high bearing in mind the value of AN* for these probes (TCM and DCM), when compared to the energy of adsorption of the basic/amphoteric probes (e.g. THF).

The enthalpy, and entropy, of adsorption of the polar probes, along with the corresponding dispersive and specific components, were determined by the method previously described. The results are summarised in Table 3-16 and illustrated in Figure 3-19.

Table 3-16. Dispersive and specific components of the enthalpy of adsorption and of the entropy of adsorption, ΔH^d_a, ΔH^s_a and ΔS^d_a, ΔS^s_a, respectively, of the polar probes on the surface of PC 125.

Probe molecule	$a(\gamma_l^d)^{0.5}$ (cm^2 (mJ $cm^{-2})^{0.5}$)	$-\Delta H^d_a$ (kJ/mol)	ΔS^d_a (J/molK)	R^2	AN* (kJ/mol)	DN (kJ/mol)	$-\Delta H^s_a$ (kJ/mol)	ΔS^s_a (J/molK)	R^2
TCM	2.24E-16	57.3	-124.0	0.99	22.7	0.0	4.1	-4.6	0.84
DCM	1.65E-16	60.8	-145.0	1.00	16.4	0.0	6.1	-5.4	0.98
DEE	1.82E-16	63.0	-148.0	1.00	5.9	80.6	12.1	-27.4	1.00
Acet	1.73E-16	62.9	-149.0	1.00	10.5	71.4	8.1	-3.6	0.95
THF	2.13E-16	66.6	-152.0	1.00	2.1	84.4	6.0	-2.7	0.94
EtAcet	1.95E-16	64.5	-149.0	1.00	6.3	71.8	10.1	-12.0	0.91

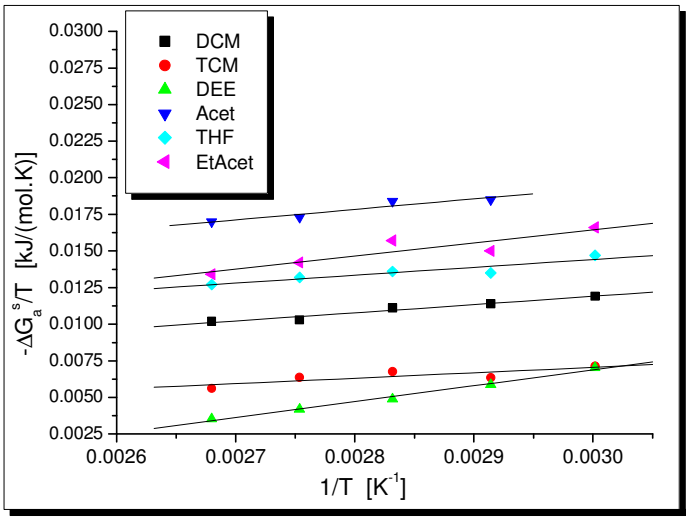

Figure 3-19. Determination of the specific component of the enthalpy and of the entropy of adsorption, of polar probes on the surface of PC 125.

Table 3-16 shows that $-\Delta H^d_a$ increases with increasing $a\times\sqrt{\gamma_l^d}$, with an exception occurring for TCM. This exception is thought to be caused by steric hindrance and structural factors. The dispersive component of the entropy of the system follows a trend that is analogous to that of the $-\Delta H^d_a$.

The trend observed for the energy of adsorption also applies to the behaviour of $-\Delta H^s_a$. The specific component of the enthalpy of adsorption of basic/amphoteric probes is low compared with that of the acidic probes, bearing in mind the corresponding values of DN and AN*. Thus, the surface of PC 125 is weakly acidic and moderately/strongly basic.

The determination of K_a and K_b allows one to deduce which of the possibilities is the most appropriate. The change in the entropic component of the specific adsorption energy is greater for DEE and EtAcet, amphoteric probes that are characterised by the greater values of $-\Delta H^s_a$. In a general manner, it can be said that ΔS^s_a increases with increasing strength of adsorption, $-\Delta H^s_a$.

3.1.5.4. Determination of K_a and K_b

The determination of the surface Lewis acidity constant, K_a, and of the surface Lewis basicity constant, K_b, is illustrated in Figure 3-20.

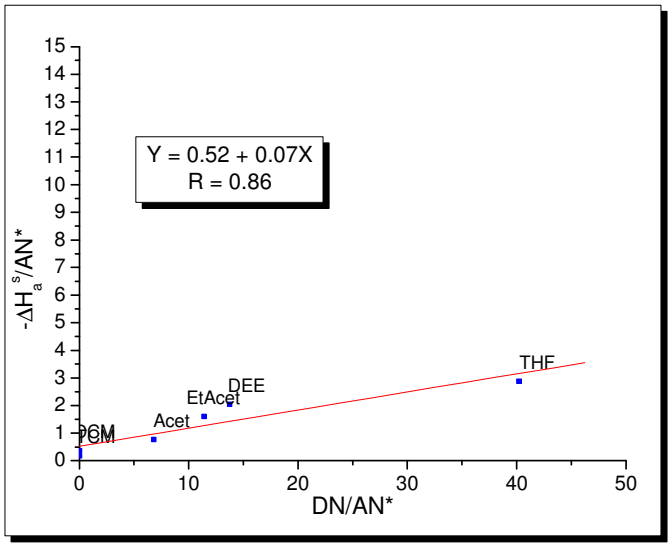

Figure 3-20. Determination of the K_a and of the K_b of the surface of PC 125.

From linear regression of the experimental data, the values obtained are 0.07 and 0.52, for K_a and K_b, respectively. Thus, the surface of PC 125 is amphoteric, being predominantly basic, and should be able to function as an electron donor as well as an electron acceptor. The values obtained for K_a and for K_b are in line with the previous discussion of the values of the energy of adsorption and of the enthalpy of adsorption for the polar probes, the surface being moderately Lewis basic. The results of the present study are analysed bearing in mind the structure of the repeating unit in this macromolecule (Figure 1-1) and the results that have been published in the literature for this type of polycarbonate (Bolvari and Ward 1989; Panzer and Schreiber 1992; Champagne *et al.* 1994; Xu *et al.* 1999). The Lewis basic sites derive from the carbonate groups, and the Lewis acidic sites from the OH end-groups. The higher basicity was expected due to the greater presence of oxygen donor sites and also due to the fact that the oxygen basic sites have a greater interaction potential than have the acidic sites mentioned (Huyskens *et al.* 1991), being able to interact with two hydrogen atoms. Furthermore, the bulky $-CH_3$ groups and benzene rings hinder the interaction with the acidic sites (and with the basic sites), which is reflected in the amorphous structure of PC, for most polycarbonates, as intra and intermolecular H-bonds are not favoured within the PC (the basic sites and acidic sites are not easily accessed, and there is the directional character of H-bonding).

3.1.6. IGC Study of PBT 195

Following the determination of the dispersive component of the surface tension and the evaluation of the surface Lewis acidic/basic characteristics, the bulk dispersive forces and non-dispersive forces interaction capability of PBT 195 was assessed determining the energy of adsorption of n-octane, TCM, and THF on the bulk PBT 195, at several temperatures. This allowed

a comparison of the surface Lewis acidic/basic properties, and a comparison of the thermodynamic nature of the interactions, with those of the bulk polymer. The measurement temperature used in the study of the surface was varied between 298 K and 318 K, in increments of 5 K, under a flow rate of 10 cm^3/min. These temperature interval and carrier gas flow rate were chosen in order to ensure that there was no absorption, and adsorption, of the probe molecules on the bulk of PBT 195. This was proven to be the case, as explained in the following section. In the study of the bulk PBT 195, the temperature range was 353 K to 393 K, in 20 K increments, and the flow rate was varied between 5 cm^3/min and 30 cm^3/min. The results concern column 13 (Table 2-12, Section 2.6.2.).

It is worth noting that no reference has been found in the literature that deals with the study of the surface properties (surface free energy, surface Lewis acidity and surface Lewis basicity) of poly(butylene terephthalate), by means of inverse gas chromatography. The only reference found in the literature, regarding surface tension studies of PBT, made use of contact angle measurements to determine the dispersive component of the surface tension and, from that value, the specific component of the surface free energy (without quantifying the contribution of the Lewis acidic sites and of the Lewis basic sites) was evaluated (Hobbs *et al.* 1988a).

3.1.6.1. Preliminary Studies

The retention times of n-decane on the surface of PBT 195 were determined using column 14 (Table 2-12, Section 2.6.2.). Carrier gas flow rates ranging from 3 cm^3/min to 35 cm^3/min were used to assess the influence of the flow rate on the retention times of n-decane, at 303 K and 313 K. The tables presented in Appendix B summarise the results, which are represented graphically in Figure 3-21. The instrument used was the Fisons GC unit.

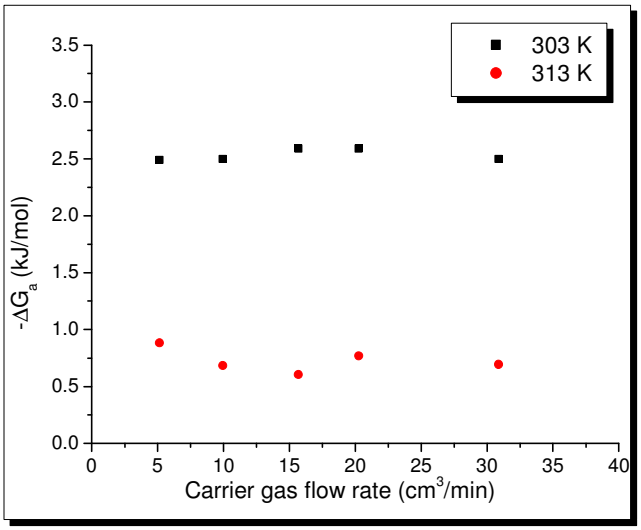

Figure 3-21. Influence of the carrier gas flow rate on the energy of adsorption of n-decane on the surface of PBT 195.

Figure 3-21, indicates that the carrier gas flow rate does not influence the adsorption energy of n-decane to a significant extent. Bearing in mind that the temperatures used are below the T_g of PBT (318 K, Section 2.1.), it can be concluded that surface adsorption is the dominant mechanism, and absorption of the probe molecules into the bulk of the polymer can be neglected, for the temperature range and flow rate range studied.

3.1.6.2. Determination of the Dispersive Component of the Surface Tension

The experimental parameters and results for the adsorption of n-alkanes on the surface of PBT 195, are summarised in tables in Appendix B. Figure 3-22 illustrates the determination of the dispersive component of the surface tension at 295 K, according to Fowkes approach.

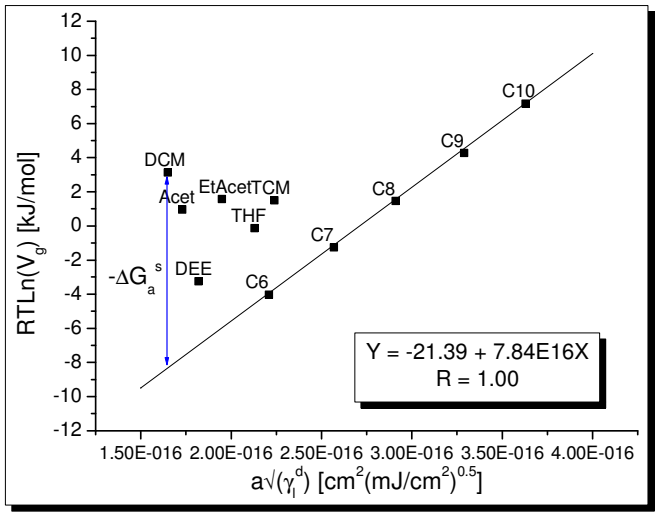

Figure 3-22. Energy of adsorption versus $a\times\sqrt{\gamma_l^d}$ for n-alkanes and polar probes on the surface of PBT 195, at T = 295 K.

Table 3-17 summarises the values determined for the dispersive component of the surface tension.

Table 3-17. Values of the dispersive component of the surface tension of PBT 195.

T (K)	γ_s^d (mJ/m^2)	R^2
295	42.4±1.0	1.00
303	42.5±2.8	0.99
308	41.4±2.6	1.00
313	40.7±1.3	1.00
318	44.7±9.9	0.99
Average	42.3±1.5	n/a

Table 3-17 indicates that the dispersive component of the surface tension remains constant, within experimental error, for the temperature range studied, equal to 42.3±1.5 mJ/m^2. The only reference found in the literature regarding surface tension studies on PBT is based on contact angle measurement producing an energy value of 52.4 mJ/m^2 at 293 K (Hobbs *et al.* 1988a). These authors have determined that the component derived from specific forces is 12.4 mJ/m^2, and the component resulting from dispersive forces is 40.0 mJ/m^2. Thus, the value found in the present study by means of IGC agrees very well with data published for this polymer obtained from contact angle measurements. The values of γ_s^d for poly(ethylene terephthalate) (PET), using IGC at infinite dilution and using contact angle measurements, are close to the value for PBT that was determined in the present study. This agrees with prediction bearing in mind the chemical similarity between these two polymers. For PET, using IGC at infinite dilution, the values of 44.6 mJ/m^2 at 293 K (Wu 1982), and 40 mJ/m^2 (Anhang and Gray 1982) (average value for the temperature range 288-313 K) were found. For the same polymer, from contact angle measurements, the values of 41 mJ/m^2 (Lavielle *et al.* 1991) and of 43.2 mJ/m^2 (Anhang and Gray 1982) have been reported in the literature.

The enthalpy of adsorption and the entropy of adsorption of the n-alkanes on the surface of PBT 195 were determined as described. The procedure is illustrated in Figure 3-23 and the values determined for all the n-alkane probes are summarised in Table 3-18.

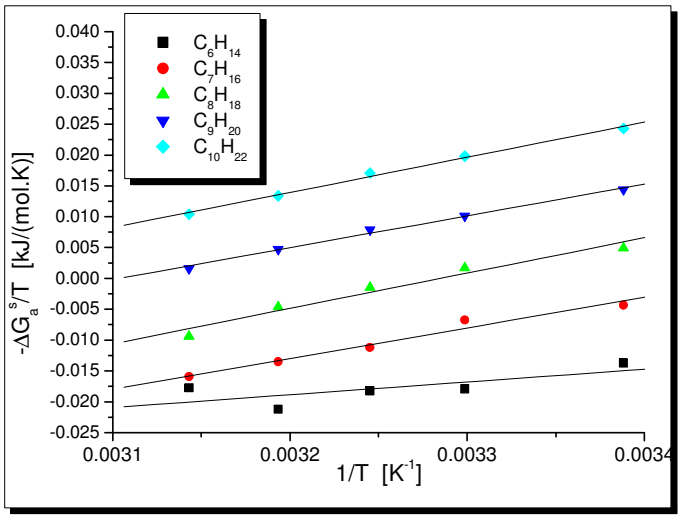

Figure 3-23. Determination of the enthalpy and of the entropy of adsorption of n-alkanes, on the surface of PBT 195.

Table 3-18. Enthalpy of adsorption, ΔH_a, and entropy of adsorption, ΔS_a, of the n-alkanes on the surface of PBT 195.

Probe molecule	$a(\gamma_l^d)^{0.5}$ (cm^2 ($mJ\ cm^{-2}$)$^{0.5}$)	$-\Delta H_a$ (kJ/mol)	ΔS_a (J/molK)	R^2
C_6H_{14}	2.21E-16	36.5	-137.0	0.98
C_7H_{16}	2.57E-16	49.6	-172.0	0.99
C_8H_{18}	2.91E-16	57.4	-189.0	0.98
C_9H_{20}	3.29E-16	51.7	-161.0	1.00
$C_{10}H_{22}$	3.63E-16	56.9	-168.0	1.00

Table 3-18 shows that the value of the $-\Delta H_a$ of the apolar probes increases with increasing $a\times\sqrt{\gamma_l^d}$, with the exception of n-octane. The value of ΔS_a, is generally greater for those probes whose value of the enthalpy of adsorption is greater.

3.1.6.3. Determination of the Energy, the Enthalpy and the Entropy of Adsorption of Polar Probes

The results for the determination of the specific component of the free energy of adsorption of polar probes, $-\Delta G_a^s$, are summarised in Table 3-19, for the measurement temperature of 295 K. The data relating to the remaining temperatures (303 K, 308 K, 313 K, and 318 K) are presented in Appendix B.

Table 3-19. Retention time, t_r, specific retention volume, V_g, energy of adsorption, RTLn(V_g), and corresponding dispersive and specific components, RTln($V^d_{g,ref}$) and RTln(V^s_g), respectively, for the adsorption of polar probes on the surface of PBT 195, at T = 295 K, F = 11.94 cm^3/min, J = 0.95, C = 0.97, P_{in} = 111.59 kPa, P_{out} = 101.25 kPa, and $T_{flow\ meter}$ = 295 K.

Probe molecule	t_r (s)	V_n (cm^3)	RTLn(V_n) (kJ/mol)	$RT\ln(V^d_{n,ref})$ (kJ/mol)	$RT\ln(V^s_n)$ (kJ/mol)
CH_4	34.7	n/a	n/a	n/a	n/a
TCM	78.3	1.8	1.5	-3.8	5.3
DCM	120.0	3.6	3.1	-8.5	11.6
DEE	41.0	0.3	-3.3	-7.1	3.9
Acet	69.8	1.5	1.0	-7.8	8.8
THF	57.2	1.0	-0.1	-4.7	4.6
EtAcet	80.0	1.9	1.6	-6.1	7.7

From the value of $-\Delta G_a^s$ it can be seen that the values for Lewis acidic probes are greater than/close to those of the Lewis basic/amphoteric probes. In the particular case of DCM, bearing in

mind the relative low acidity of this acidic probe (AN* of 16.4 kJ/mol), when compared to the basicity of the basic probes (e.g. THF, with a DN of 84.4 kJ/mol), it can be concluded that the surface of the PBT 195 is amphoteric, being a very strong Lewis base.

The values of the enthalpy, and entropy, of adsorption of the polar probes, along with the corresponding dispersive and specific components, are summarised in Table 3-20, and their determination is illustrated in Figure 3-24.

Table 3-20. Dispersive and specific components of the enthalpy of adsorption and of the entropy of adsorption, ΔH^d_a, ΔH^s_a and ΔS^d_a, ΔS^s_a, respectively, of the polar probes, on the surface of PBT 195.

Probe molecule	$a(\gamma_l^d)^{0.5}$ (cm^2 ($mJ\ cm^{-2}$)$^{0.5}$)	$-\Delta H^d_a$ (kJ/mol)	ΔS^d_a (J/molK)	R^2	AN* (kJ/mol)	DN (kJ/mol)	$-\Delta H^s_a$ (kJ/mol)	ΔS^s_a (J/molK)	R^2
TCM	2.24E-16	47.8	-147.0	0.97	22.7	0.0	-51.5	193.0	0.99
DCM	1.65E-16	43.8	-176.0	0.94	16.4	0.0	-34.2	155.0	0.95
DEE	1.82E-16	44.9	-176.0	0.95	5.9	80.6	-31.2	119.0	0.98
Acet	1.73E-16	44.3	-176.0	0.94	10.5	71.4	-31.2	135.0	0.95
THF	2.13E-16	47.0	-175.0	0.96	2.1	84.4	-44.9	167.0	0.95
EtAcet	1.95E-16	45.8	-175.0	0.95	6.3	71.8	-41.9	166.0	0.92

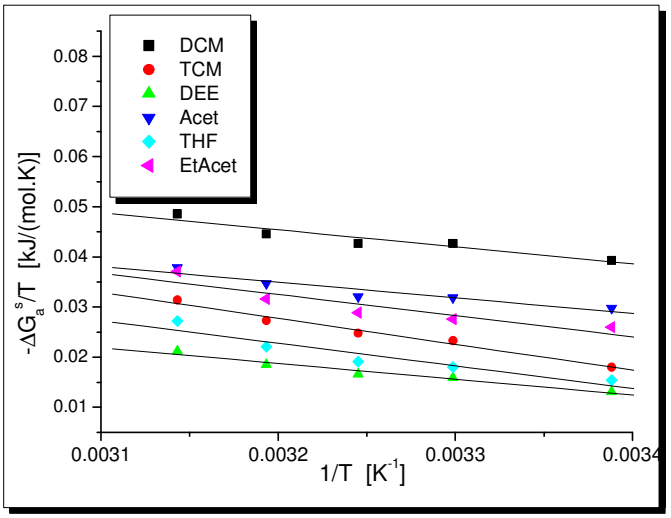

Figure 3-24. Determination of the specific component of the enthalpy and of the entropy of adsorption, of polar probes on the surface of PBT 195.

The specific component of the enthalpy of adsorption of polar probes on the surface of PBT 195 is endothermic. This is quite unusual. However, endothermic values of energy of adsorption are reported in the literature for the adsorption of polar probe molecules on surface treated titanium dioxide pigments (Lee *et al.* 1992; Hegedus and Kamel 1993a), and on a copolymer of vinyl acetate (94.8 mol %) and vinyl alcohol (Chen 1988).

The adsorption of polar probes on a surface occurs *via* dispersive and specific intermolecular forces. The specific interactions originate mainly from the interaction between the Lewis acidic sites and the Lewis basic sites of the interacting species. In the particular case of PBT, bearing in mind its molecular structure (Figure 1-1), the dominant specific interactions are H-bonds. Rearrangement of the surface upon chemisorption of polar molecules is thought to occur, in this case, leading to an increase on the entropy of the system (Ponec *et al.* 1974; Santos *et al.* 2002b). This is confirmed by the positive values of ΔS^{s}_{a}. An increase of the entropy of the system implies an increase in the number of degrees of freedom, and a considerable increase in the disorder of the system. This may be the case, if the entropy of the adsorbent increases sufficiently owing to adsorption. The experimentally verified phenomena of swelling, adsorbent expansion, dissolution of the adsorbate in the adsorbent structure and rearrangement of the surface layers due to chemisorption, support this thesis (Ponec *et al.* 1974).

Although the enthalpy of formation of individual hydrogen bonds is always negative, the overall enthalpy (and entropy) associated with the formation of hydrogen bonds will depend on the balance between three contributions (Coleman *et al.* 1991):

a) A positive contribution to the enthalpy (and entropy), the result of breaking hydrogen bonds in the self-associating polymer;

b) A negative contribution to the enthalpy (and entropy), the result of forming hydrogen bonds between the self-associating polymer and the adsorbent molecule;

c) Contributions from other interactions (van der Waals, dipole forces, etc).

The specific component of the energy of adsorption, Table 3-20, accounts for the contribution of breaking, and forming, H-bonds, alongside with the contribution of dipole-dipole forces. On the other hand, the dispersive component of the energy of adsorption accounts for the van der Waals forces. In the case of adsorption of polar molecules on PBT, the positive contribution to the enthalpy (and entropy) of adsorption, due to breaking hydrogen bonds in the self-associating polymer, is thought to dominate, resulting in an endothermic enthalpy of adsorption and increased entropy of the system. A necessary condition for adsorption of a molecule on a surface is a negative value of the free energy change, ΔG_a, of the entire system, between the initial state and the final state through adsorption. In the system under study, the value of $T\Delta S_a$ is greater than the value of ΔH_a and thus, the thermodynamic condition for adsorption to occur is obeyed. In the case of dispersive forces, ΔH_a is always negative and smaller than $T\Delta S_a$ (Ponec *et al.* 1974).

Exothermic adsorption ($\Delta H_a < T\Delta S_a < O$ or $\Delta H_a < O < T\Delta S_a$) was considered for a long time to be the only possible situation (Ponec *et al.* 1974) because, on adsorption, the molecule usually loses some of its degrees of freedom (thus, $\Delta S_a < O$) compared with the gaseous state. Therefore, the adsorbed state is characterised by a higher degree of order. In fact, it is the only possible case

for physical adsorption on an inert adsorbent. In most cases, conversely, endothermic adsorption phenomena exist (Ponec *et al.* 1974).

It should be noticed that the dispersive component of the energy of adsorption, ΔH^d_a, is exothermic, and the corresponding change in entropy, ΔS^d_a, negative, and similar for most of the polar probes, TCM being the exception. Furthermore, the value of $-\Delta H^d_a$ increases with increasing $a \times \sqrt{\gamma_l^d}$.

The ordered structure characteristic of the crystalline domains of PBT decreases to a large extent the opportunity of interaction of its acidic sites and its basic sites with acidic/basic probe molecules. Furthermore, the availability of the functional groups of PBT is much decreased as these are already involved in intramolecular forces and intermolecular forces within the PBT itself. Nevertheless, as the temperature of measurement is close to the T_g of PBT (318 K, Section 2.1.), the probes are thought to interact with the available functional groups that are more accessible to the probe molecules, due to an increase of the mobility of the polymeric chains. One can conclude that the surface of PBT interacts through specific forces with the probe molecules, but not to a large extent, resulting in relatively low values of the energy of adsorption, as the acidic/basic sites are either already involved in intramolecular associations and intermolecular associations within the PBT or not easily accessible due to the close packed structure of the crystalline domains. This agrees well with practical experience of the well-known chemical resistance of PBT.

An analysis of the specific component of the enthalpy of adsorption, leads to the following ranking (the more negative, the stronger the interaction, as it is endothermic): DEE = Acet < DCM < EtAcet < THF < TCM. This indicates that PBT 195 is amphoteric and K_b ought to be high, in line the analysis of the specific component of the energy of adsorption of the polar probes. The change in entropy upon adsorption is greater for those probes whose adsorption is characterised by the greater specific component of the enthalpy of adsorption.

The entropy change upon adsorption of polar probes is greater for PBT 195 than it is for the remaining materials. The value of ΔS^s_a increases in the following order: PC 125 < MBS rubber < C. I. Pigment Blue 28 << PBT 195. This observation supports the aforementioned events of reorganisation of the surface, breaking of strong bonds and forming of new bonds, all of these factors contributing to higher entropy changes upon adsorption in the case of PBT 195.

3.1.6.4. Determination of K_a and K_b

The determination of the surface Lewis acidity constant, K_a, and of the surface Lewis basicity constant, K_b, is illustrated in Figure 3-25.

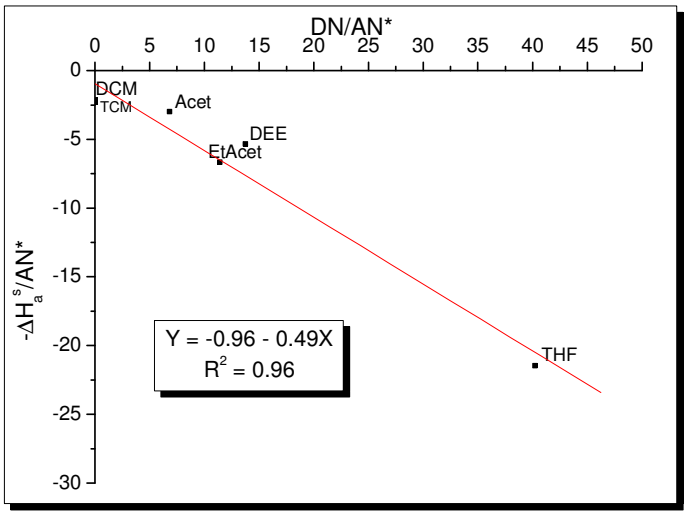

Figure 3-25. Determination of the K_a and of the K_b of the surface of PBT 195.

The values of K_a and K_b are -0.49 and -0.96, respectively. The determination of the surface K_a and K_b, measured below T_g, results in negative values due to the endothermic adsorption of the probe molecules. The surface of PBT 195 is shown to be Lewis amphoteric, though strongly Lewis basic, in line with the analysis of the energy and enthalpy of adsorption of polar probes. The values obtained agree well with the analysis of the structure of this molecule (Figure 1-1). The Lewis basic sites are identified with the ester moiety, the oxygen atoms in the carboxylic end-group, and also with the oxygen atom in the hydroxyl end-group (Huyskens *et al.* 1991); the Lewis acidic sites are identified with the hydrogen atoms in the -O-CH_2- moiety, and with the hydrogen atom in the hydroxyl end-group and in the carboxylic end-group.

The values of K_a and K_b for PBT 195 indicate that the polymer interacts strongly with itself, as it has both strong Lewis basic sites and strong Lewis acidic sites. These, together with the chemically regular structure of the molecule, the non-existence of bulky side-groups, and the high mobility that is caused by the butylene unit in the chain, provide the structural requirements for crystallinity, and, consequently, for the excellent solvent resistance and thermal stability possessed by PBT.

3.1.6.5. Determination of the Energy, the Enthalpy, and the Entropy of Adsorption on the Bulk PBT 195

The adsorption energy of n-octane, and of the polar probes (TCM, DCM, DEE, Acet, THF, ETAcet) on the bulk of the polymer (and therefore on both the amorphous and the crystalline domains of the bulk PBT 195) was determined by extrapolation to zero carrier gas flow rate, as described in the literature when the bulk of semi-crystalline polymers is to be studied (Mukhopadhyay and Schreiber 1993; Mukhopadhyay and Schreiber 1995; Garnier and Glasser

1996; Xu *et al.* 1999). To this end, the energy of adsorption of n-octane and of the polar probes was determined at several carrier gas flow rate values (Figure 3-26). Figure 3-26 shows that the value of the energy of adsorption is dependent of the carrier gas flow rate. This stems from contributions of diffusion, absorption, and adsorption of the probe molecules on the bulk polymer to the total energy of adsorption. If the flow rate is adequately high, the opportunity for interaction of the probe molecules with the bulk polymer can be neglected and surface adsorption becomes the dominant interaction phenomenon. In this case, the energy of adsorption is independent of the carrier gas flow rate. If the value of the adsorption energy is extrapolated to the zero carrier gas flow rate the interaction of the probe molecules with the bulk polymer will be measured, with no contributions of surface adsorption phenomena, provided that the temperature of measurement is high enough to allow for an appropriate value of the free volume of the polymer.

The measurement temperature range must be sufficiently greater than the T_g (318 K) to allow for the penetration of the probe molecules into the bulk polymer. Bearing in mind the temperature interval used in the IGC study of the remaining materials, and the value of T_g for PBT 195, it was decided to use a temperature range that began at 353 K and with 10 K increments. It was not possible to determine the dispersive component of the surface tension due to the very low retention time of n-hexane and of n-heptane, and due to difficulties relating to the penetration of large n-alkanes molecules as n-nonane and n-decane. The increase in the temperature of measurement and, thus, the increase in the mobility of the polymeric chains are overcome by the decrease in the adsorption energy with increasing temperature and by the decreasing opportunity for absorption and diffusion when increasing the flow rate. Consequently, as the temperature and the flow rate are increased, the larger molecules have more difficulty in penetrating into the bulk PBT 195 and, therefore, it was not possible to measure the energy of adsorption of those molecules in the bulk polymer. In order to overcome this problem, measurements were made at 423 K. However, the noise level of the measured signals, even after conditioning the column overnight at this temperature and at a high flow rate, was too high to allow for the accurate determination of the retention times. Furthermore, a new column was prepared and the procedure repeated. However, the problem prevailed.

To determine the specific component of the energy of adsorption of the polar probes it is necessary to use the n-alkanes reference line. The only adsorption energy value that could be obtained was that concerning n-octane. The dispersive component of the surface tension of PBT 195 was determined to be to 42.3±1.5 mJ/m^2, in the temperature range 295 K to 318 K. Bearing in mind that the temperature coefficient of γ_s^d for polymers is very low (e.g. -0.08 $mJm^{-2}K^{-1}$ for PMMA, between 293 K and 473 K (Riedl and Kamdem 1992)), the value of γ_s^d of the bulk PBT 195 is estimated to remain approximately constant when the temperature of measurement is increased from 295-318 K to 353 K. Therefore, the slope of the n-alkanes reference line in the Fowkes plot (Figure 3-27), is estimated to be approximately the same at 353 K than that

corresponding to the temperature interval of 295 K to 318 K. As it was possible to determine the energy of adsorption of n-octane in the bulk PBT 195, at 353 K, one can define an estimated n-alkanes reference line using the value of $RT\ln(V_g)$ for n-octane, and the estimated value of the slope of the n-alkanes reference line. The values of the adsorption energy of n-octane and of the polar probes, for the carrier gas flow rate values used, are summarised in Appendix B. The values determined for the energy of adsorption at zero flow rate are presented in Table 3-21. The extrapolation to zero flow rate procedure is illustrated in Figure 3-26.

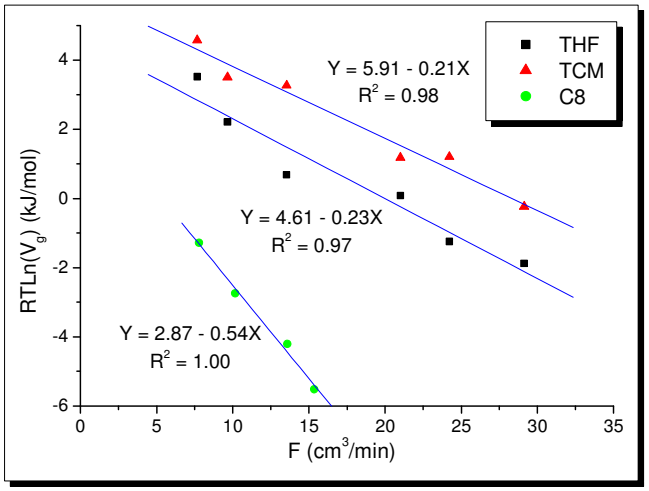

Figure 3-26. Determination of the energy of adsorption of n-octane, of TCM, and of THF on the bulk PBT 195, at zero carrier gas flow rate.

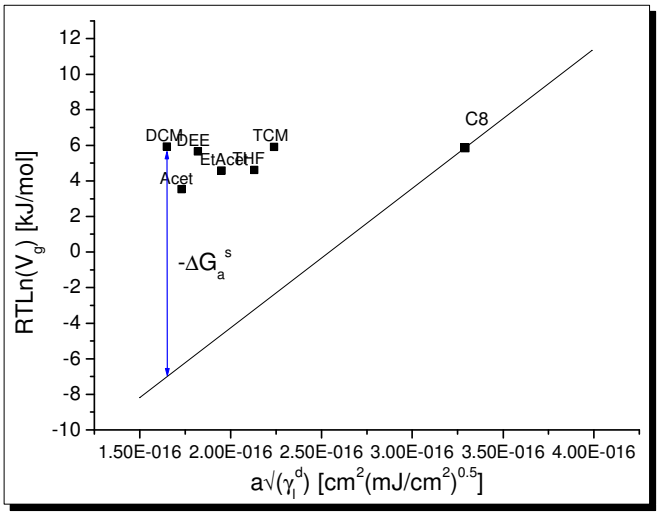

Figure 3-27. Extrapolated value of the energy of adsorption *versus* $a \times \sqrt{\gamma_l^d}$ for n-alkanes and polar probes on the bulk PBT 195, at T = 353 K.

Figure 3-27 gives a Fowkes plot that relates to the estimated n-alkanes' reference line (including the extrapolated value of the energy of adsorption of n-octane), and the extrapolated values of the energy of adsorption of the polar probes.

Table 3-21. Energy of adsorption at zero flow rate, $RTLn(V_g)$, and corresponding dispersive and specific components, $RTln(V^d_{g,ref})$ and $RTln(V^s_g)$, respectively, for the bulk PBT 195, at T = 353 K.

Probe molecule	$RTLn(V_g)$ (kJ/mol)	R^2	$RT\ln(V^d_{g,ref})$ (kJ/mol)	$RT\ln(V^s_g)$ (kJ/mol)
C_8H_{18}	2.9	1.00	n/a	n/a
TCM	5.9	0.98	-2.4	8.3
DCM	5.9	0.97	-7.0	12.9
DEE	5.7	0.87	-5.7	11.3
Acet	3.5	0.93	-6.4	9.9
THF	4.6	0.97	-3.2	7.9
EtAcet	4.6	0.87	-4.7	9.2

The results presented in Table 3-21 confirm the observations made for the values of the energy of adsorption of polar probes on the surface of PBT 195 (Table 3-19). In Figure 3-28 are compared the values of the specific component of the energy of adsorption of the polar probes at 353 K with those at 295 K.

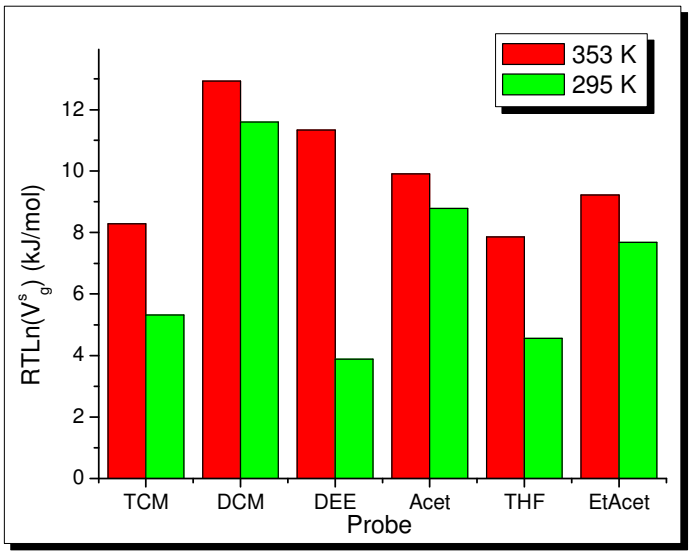

Figure 3-28. Comparison of the specific component of the energy of adsorption of the polar probes on the bulk PBT 195 (at 353 K) and on the surface of PBT 195 (at 295 K).

Figure 3-28 shows that $-\Delta G_a^s$ relating to Lewis acidic probes is greater than/close to that of the Lewis basic/amphoteric probes. Bearing in mind the relative low acidity of the acidic probes, when compared to the basicity of the basic probes, further evidence is presented of the Lewis amphoteric character of PBT 195 (both the surface and the bulk), and of very strong Lewis basic properties. Figure 3-28 shows that the values of $-\Delta G_a^s$ at 353 K are greater than those at 295 K. This indicates that the adsorption of the polar probes on the bulk PBT 195 is stronger than the adsorption at the surface of PBT 195, although the measurement temperature is increased from 295 to 353 K. The only exception to the very good correlation obtained between the results at 295 K and at 353 K relates to the adsorption of DEE. This is thought to be due to the comparatively lower correlation coefficient corresponding to the extrapolation of the adsorption energy of this probe to zero flow rate (Table 3-21), probably due to the relatively large size of this molecule, making more difficult the adsorption process.

The previous analyses lead to the conclusion that the procedure adopted to determine the energy of adsorption of the probes on the bulk PBT, and the estimation of the n-alkanes reference line, are valid. Furthermore, it is now possible to compare the Lewis acidic/basic properties of all the materials studied, using the values determined for the $-\Delta G_a^s$ of the polar probes, at 353 K.

The enthalpy of adsorption of TCM and of THF in the bulk of the polymer was calculated using the energy of adsorption of these probes, at different flow rates, and extrapolating to the zero flow rate, at each temperature of measurement. The major objective was to confirm the endothermic character of the adsorption of the polar probes on PBT 195. The results are summarised in Table 3-22.

Table 3-22. Enthalpy of adsorption, ΔH_a, and entropy of adsorption, ΔS_a, of TCM and of THF on the bulk PBT 195.

Probe molecule	$a(\gamma_l^d)^{0.5}$ (cm^2 ($mJ\ cm^{-2}$)$^{0.5}$)	$-\Delta H_a$ (kJ/mol)	ΔS_a (J/molK)	R^2
TCM	2.24E-16	-11.7	63.0	0.90
THF	2.13E-16	-14.5	68.0	0.99

The values presented in Table 3-22 correspond to the total (dispersive and specific) enthalpy of adsorption, and were determined using the net retention volume of TCM and of THF. Table 3-22 shows that the enthalpy of adsorption and entropy of adsorption of TCM and THF on the bulk PBT 195 are also positive, in line with the results concerning the analysis of the surface. It is thought that the probe molecules that were able to penetrate into the bulk of PBT 195 interacted with an interior crystalline layer, alongside with the amorphous phase. This is due to the column preparation. The PBT 195 stationary phase consists of 125-250 μm sieved polymer particles, and not Chromosorb® in whose surface, usually, the polymer is deposited for IGC analysis. No good

and safe solvent was found for PBT 195 and, thus, it was not possible to prepare the stationary phase depositing the polymer onto the surface of Chromosorb® as was the case with PC 125. Therefore, for the study of adsorption in the amorphous phase of PBT 195, temperatures close to or higher than T_m (503 K) should be used. This was not possible with the current IGC instrumentation and so the alternative procedure described above was used.

3.1.7. IGC Study of PBT 315

The temperature range and carrier gas flow rate values used in the analysis of the surface of PBT 315 were the same as those used in the study of the surface of PBT 195. The temperature was varied between 298 K and 318 K, in increments of 5 K, and the carrier gas flow rate was 10 cm^3/min. The results presented in the following sections concern column 15 (Table 2-12, Section 2.6.2.).

3.1.7.1. Determination of the Dispersive Component of the Surface Tension

The experimental parameters and results concerning the adsorption of n-alkanes on the surface of PBT 315 are presented in Appendix B. Figure 3-29 illustrates the determination of the dispersive component of the surface tension at 295 K.

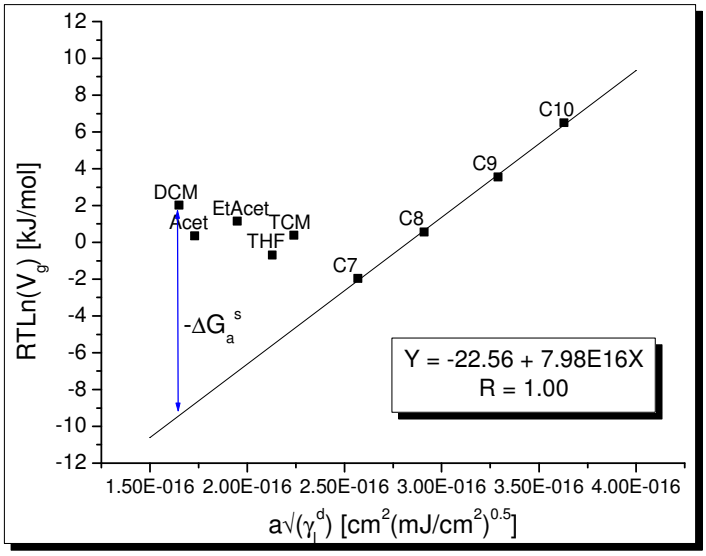

Figure 3-29. Energy of adsorption versus $a \times \sqrt{\gamma_l^d}$ for n-alkanes and polar probes on the surface of PBT 315, at T = 295 K.

Table 3-23 summarises the values determined for the dispersive component of the surface tension.

Table 3-23. Values of the dispersive component of the surface tension of PBT 315.

T (K)	γ_s^d (mJ/m^2)	R^2
295	43.9±2.1	1.00
303	40.7±1.9	0.99
308	42.8±2.4	1.00
313	40.0±0.6	1.00
318	40.7±2.1	0.99
Average	41.6±1.7	n/a

The average value of γ_s^d of the surface of PBT 315 is 41.6±1.7 mJ/m^2, in the temperature interval 295 K to 318 K. The value of γ_s^d for PBT 195 (42.3±1.5 mJ/m^2) and for PBT 315 are practically identical. This leads to the conclusion that the different end-group composition (Table 3-27) does not influence to a noticeable extent the dispersive component of the surface tension. Bearing in mind that the major difference between PBT 195 and PBT 315 is in the OH end-group concentration, the value found for γ_s^d confirms the observations found in literature (Zhang and Leonov 2000) with regard to the fact that this functional group, as a high-energy site, contributes mainly to the formation of specific intermolecular interactions.

The procedure for the determination of the enthalpy and of the entropy of adsorption of the n-alkanes on the surface of PBT 315 is illustrated in Figure 3-30. The values determined for all the n-alkane probes are summarised in Table 3-24.

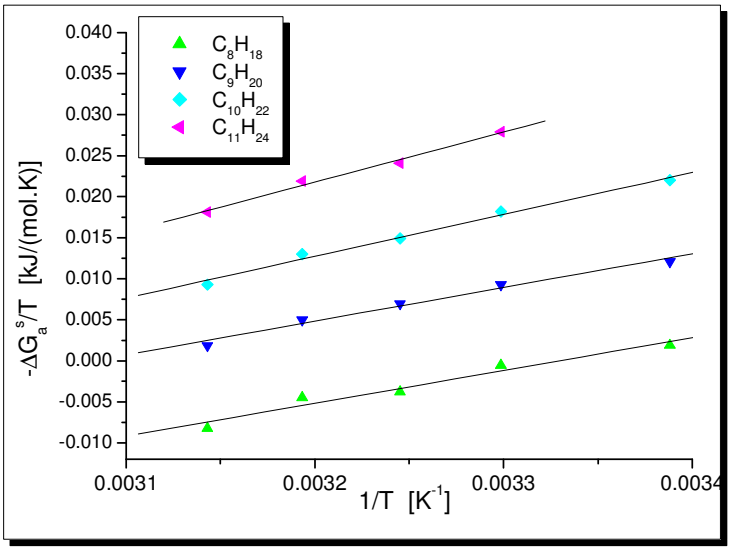

Figure 3-30. Determination of the enthalpy and of the entropy of adsorption of n-alkanes, on the surface of PBT 315.

Table 3-24. Enthalpy of adsorption, ΔH_a, and entropy of adsorption, ΔS_a, of the n-alkanes on the surface of PBT 315.

Probe molecule	$a(\gamma_l^d)^{0.5}$ (cm^2 ($mJ\ cm^{-2}$)$^{0.5}$)	$-\Delta H_a$ (kJ/mol)	ΔS_a (J/molK)	R^2
C_8H_{18}	2.91E-16	40.0	-133.0	0.98
C_9H_{20}	3.29E-16	41.0	-126.0	0.99
$C_{10}H_{22}$	3.63E-16	51.1	-151.0	0.99
$C_{11}H_{24}$	3.99E-16	60.9	-173.0	1.00

Table 3-24 shows that the values of $-\Delta H_a$ and of ΔS_a for the apolar probes increase with increasing value of $a \times \sqrt{\gamma_l^d}$.

3.1.7.2. Determination of the Energy, the Enthalpy and the Entropy of Adsorption of Polar Probes

The determination of $-\Delta G_a^s$ for the polar probes is illustrated in Figure 3-29 for DCM at a measurement temperature of 295 K. Table 3-25 summarises the results concerning the temperature of 295 K. The data relating to the remaining temperatures (303 K, 308 K, 313 K, and 318 K) are presented in Appendix B.

Table 3-25. Retention time, t_r, specific retention volume, V_g, energy of adsorption, $RTLn(V_g)$, and corresponding dispersive and specific components, $RTln(V^d_{g,ref})$ and $RTln(V^s_g)$, respectively, for the adsorption of the polar probes on the surface of PBT 315, at T = 295 K, F = 11.94 cm^3/min, J = 0.97, C = 0.98, P_{in} = 108.13 kPa, P_{out} = 101.24 kPa, and $T_{flow\ meter}$ = 291 K.

Probe molecule	t_r (s)	V_n (cm^3)	$RTLn(V_n)$ (kJ/mol)	$RT\ln(V^d_{n,ref})$ (kJ/mol)	$RT\ln(V^s_n)$ (kJ/mol)
CH_4	35.7	n/a	n/a	n/a	n/a
TCM	65.2	1.2	0.4	-4.7	5.1
DCM	93.3	2.3	2.0	-9.4	11.4
Acet	64.8	1.2	0.4	-8.7	9.1
THF	54.7	0.8	-0.7	-5.6	4.9
EtAcet	75.8	1.6	1.1	-7.0	8.2

From the values of $-\Delta G_a^s$ (Table 3-25), it can be seen that, like for PBT 195, the adsorption of the Lewis acidic probes on the surface of PBT 315 is as strong as, or stronger than, the adsorption of Lewis basic/Lewis amphoteric probes. Bearing in mind the relatively low acidity of the acidic probes, when compared to the basicity of the basic probes (e.g. THF), it can be concluded that the surface of PBT 315 is amphoteric, being a strong Lewis base.

In Figure 3-31 are compared the values of $-\Delta G_a^s$ for the polar probes on the surface of PBT 315 with those concerning the surface of PBT 195, at 295 K.

The retention times for DEE were very low and, therefore, prone to large experimental errors. Consequently, the determination of the energy of adsorption, and of the specific component of the enthalpy of adsorption of DEE, was not possible. This low retention time probably results from steric hindrance, as explained previously. Similar results have been observed when CCl_4 is used as a probe (Hegedus and Kamel 1993a).

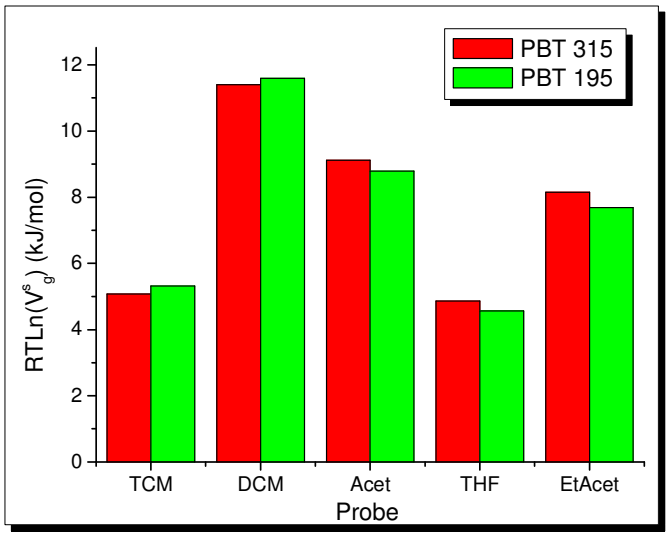

Figure 3-31. Comparison of the specific component values of the energy of adsorption of the polar probes on the surface of PBT 195 with those relating to the surface of PBT 315, at 295 K.

Figure 3-31 shows that the surface of PBT 315 is comparable to that of PBT 195 in terms of Lewis acidity/basicity. An analysis of the specific component of the enthalpy of adsorption will provide a better insight into the differences between the Lewis acidic/basic properties of the two PBTs.

The values of the enthalpy, and of the entropy of adsorption of the polar probes, along with the corresponding dispersive and specific components, are summarised in Table 3-26 and illustrated in Figure 3-32.

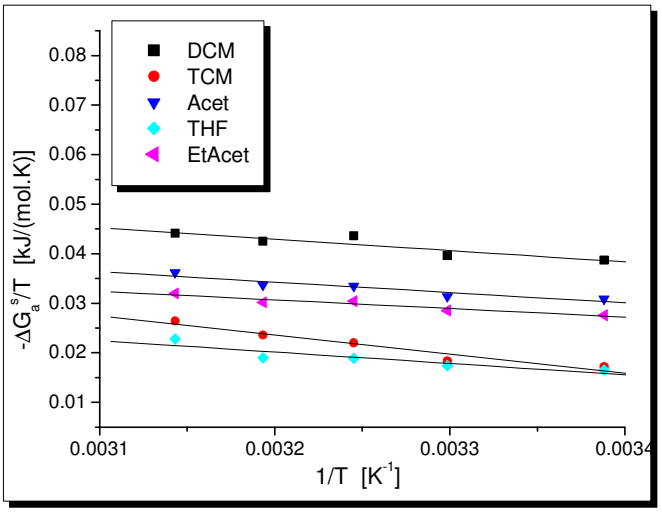

Figure 3-32. Determination of the specific component of the enthalpy and of the entropy of adsorption, of polar probes on the surface of the PBT 315.

Table 3-26. Dispersive and specific components of the enthalpy of adsorption and of the entropy of adsorption, ΔH^d_a, ΔH^s_a and ΔS^d_a, ΔS^s_a, respectively, of the polar probes, on the surface of PBT 315.

Probe molecule	$a(\gamma_l^d)^{0.5}$ (cm^2 ($mJ\ cm^{-2}$)$^{0.5}$)	$-\Delta H^d_a$ (kJ/mol)	ΔS^d_a (J/molK)	R^2	AN* (kJ/mol)	DN (kJ/mol)	$-\Delta H^s_a$ (kJ/mol)	ΔS^s_a (J/molK)	R^2
TCM	2.24E-16	33.0	-127.0	0.91	22.7	0.0	-38.4	147.0	0.94
DCM	1.65E-16	26.2	-120.0	0.81	16.4	0.0	-23.1	138.0	0.82
Acet	1.73E-16	27.1	-121.0	0.83	10.5	71.4	-20.9	101.0	0.89
THF	2.13E-16	31.8	-126.0	0.89	2.1	84.4	-23.0	93.7	0.81
EtAcet	1.95E-16	29.7	-124.0	0.87	6.3	71.8	-17.2	85.8	0.92

The specific component of the enthalpy of adsorption of polar probes on the surface of PBT 315 is endothermic. This finding confirms the results for the surface, and the bulk, of PBT 195. Agreeing with expectation, the dispersive component of the energy of adsorption, ΔH^d_a, is exothermic, and the corresponding change in entropy, ΔS^d_a, negative. Moreover, the values of $-\Delta H^d_a$ and of ΔS^d_a increase with increasing $a\times\sqrt{\gamma_l^d}$, also agreeing with expectation. The analysis of $-\Delta H^s_a$ is in line with the analysis of the energy of adsorption, and with the results relating to PBT 195. Thus, the surface of PBT 315 is amphoteric, being a strong Lewis base. Figure 3-33 gives a comparison of the values of ΔH^s_a of the polar probes on the surface of PBT 315 with those concerning the surface of PBT 195.

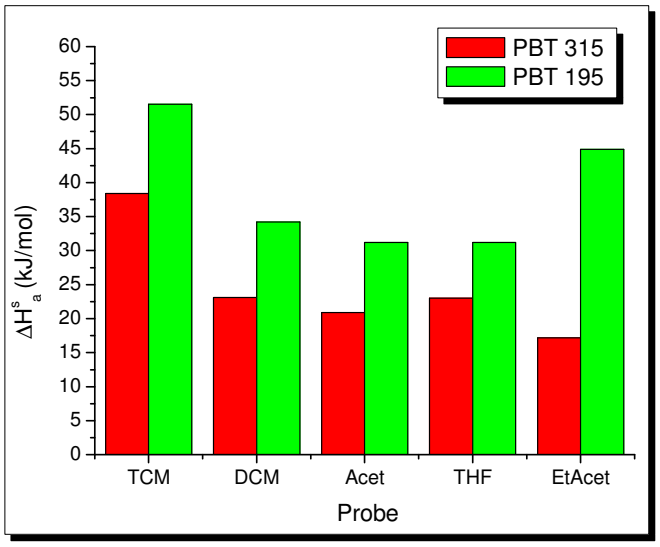

Figure 3-33. Comparison of the specific component values of the enthalpy of adsorption of the polar probes on the surface of PBT 195 with those relating to the surface of PBT 315.

Figure 3-33 suggests that the surface of PBT 315 should be less Lewis acidic and less Lewis basic, than that of PBT 195. The determination of K_a and of K_b provides a more complete description of the surface Lewis acidity/basicity.

3.1.7.3. Determination K_a and K_b

The surface Lewis acidity constant, K_a, and the surface Lewis basicity constant, K_b, were determined according to the procedure described previously, illustrated in Figure 3-34.

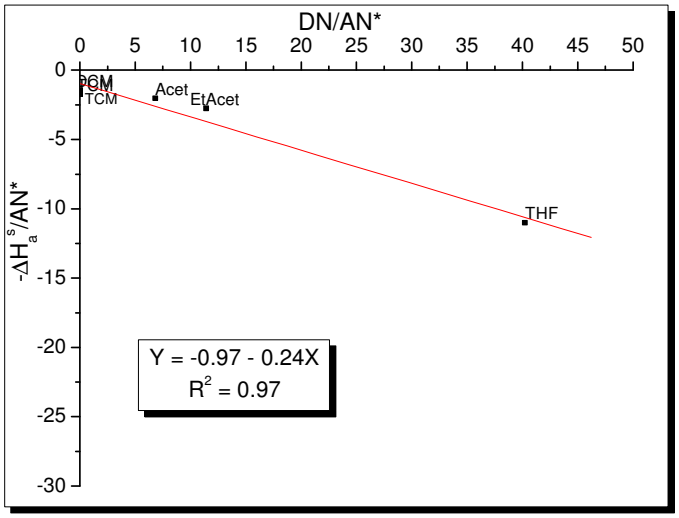

Figure 3-34. Determination of the K_a and of the K_b of the surface of PBT 315.

Table 3-27. Carboxyl end-group concentration, hydroxyl end-group concentration (source: GE Plastics, Bergen op Zoom, The Netherlands), and K_a and K_b, for PBT 195 and for PBT 315.

	-COOH (μeq/g)	-OH (μeq/g)	K_a	K_b	R^2
PBT 195	29	122	-0.49	-0.96	0.96
PBT 315	48	22	-0.24	-0.97	0.97

The poly(butylene terephthalate) PBT 315 is significantly less acidic than and as basic as PBT 195. The values obtained agree well with the structure of the repeating unit in PBT, as justified for the case of PBT 195. The fact that PBT 315 is significantly less acidic and slightly more basic than PBT 195 is understood on the basis of an analysis of the carboxyl end-group and hydroxyl end-group concentrations in both PBT 195 and PBT 315 as determined by FTIR (Table 3-27). The hydroxyl end-group and carboxyl end-group concentrations were determined using the -OH absorbance at 3550 cm^{-1} and the -COOH absorbance at 3290 cm^{-1}, respectively (Timmerman, T. *et al.* 2001, Personal Communication). The hydroxyl end-group concentration of PBT 315 is significantly lower than that of PBT 195, which is reflected in the lower acidic character of PBT 315. The carboxyl end-group concentration is higher for PBT 315, indicating the stronger surface Lewis basicity of this grade of PBT. Nevertheless, PBT 195 and PBT 315 have similar Lewis basicity constants. This may arise from the dominant contribution of the ester functionality to the surface basicity, alongside with the contribution of the basic oxygen atom in the hydroxyl groups. The fact that the K_b analysis for the two PBTs does not fully correlate with the analysis of the specific component of the enthalpy of adsorption of DCM and of TCM is thought to be related to the relatively low value of AN* for DCM and TCM, which is reflected in higher uncertainty associated with K_b, when compared to that associated with K_a.

PBT 195 would be expected to have a greater extent of crystallinity and higher crystallisation temperature than PBT 315, as a consequence of the described differences in the end-group type and concentration, and the consequences to differing effective formation of intramolecular, and intermolecular hydrogen bonds (assessed by IGC determination of K_a and K_b), along with differences in the average molecular weight of PBT 195 and PBT 315.

3.1.8. Intermolecular Interactions in Pigmented PC/PBT/IM blends

An analysis of the interaction potential between the major components of the blends studied was carried out. The interaction potential through dispersive and specific intermolecular forces between PC 125, MBS rubber, PBT 195, PBT 315, and C. I. Pigment Blue 28 has been assessed. The interaction potential by means of dispersive forces has been evaluated considering the values determined for γ_s^d, namely at 353 K. The interaction potential through specific interactions has been assessed by analysing the values obtained, for $-\Delta G_a^s$ (at 353 K), for $-\Delta H^s_a$, and for K_a and K_b,

for each material. The temperature of 353 K was chosen for the comparative study of γ_s^d and of $-\Delta G_a^s$ as this is a measurement temperature common to the IGC evaluation of all the materials.

Bearing in mind the Lewis acidic/basic properties of the polar probes used in this study, one cannot make absolute observations about the acidity of the materials studied, when analysing the values of $-\Delta G_a^s$ and of $-\Delta H^s_a$, as no purely basic probes were used. The interaction with these probes will reflect not only the acidity but also the basicity of the material. In this context the "best" probe is THF as it has the lowest AN* (2.1 kJ/mol) and the highest DN (84.4 kJ/mol). For the Lewis basicity of the materials under study, the aforementioned observation is not necessary as both TCM and DCM are "purely" Lewis acidic probes. Consequently, the interaction potential through specific forces has been carried out analysing the values of $-\Delta G_a^s$ and of $-\Delta H^s_a$, obtained for DCM and THF. The ratio of $-\Delta G_a^s$ (and of $-\Delta H^s_a$) for DCM and THF has been compared for the materials analysed. Bearing in mind the values of AN* and of DN for these probes, the lower the ratio, the more Lewis acidic sites exist relatively to the Lewis basic sites. Furthermore, the sum of $-\Delta G_a^s$ (and of $-\Delta H^s_a$) for DCM and THF, gives an indication of the total Lewis acid/basic interaction potential.

The determination of K_a and of K_b, independent of the AN* and DN values of the probes used, is the ultimate and more rigorous approach to be used when comparing the Lewis acidity/basicity of different materials. The ratio of K_b and K_a, along with the sum of these parameters, provides an indication of the relative existence of basic sites in comparison to the acidic sites, and of the total interaction potential through Lewis acid/base forces, respectively.

The interaction parameters currently in use (Equations 1-44 to 1-46, Section 1.2.5.3.) do not take into account the relative presence of each material in the polymeric system, the accessibility of the Lewis acidic and Lewis basic sites in relation to the Lewis acidic and Lewis basic sites available for interaction on the interactive species, and an appropriate balance of the contribution of the Lewis acid/acid and Lewis base/base repulsions to the overall Lewis acid/base interaction potential (Santos *et al.* 2002a). Therefore, in the analysis of the acid/base interaction potential of the materials studied, no use was made of the Lewis acid/base interaction parameters presently found in the literature. A semi-quantitative analysis of the Lewis acid/base interaction potential between the major components of these blends is carried out, taking into account:

a) The structure of the repeating units and end-groups in PC, PMMA (the shell component of the MBS rubber), PBT 195, and PBT 315;

b) The molecular structure of the C. I. Pigment Blue 28 pigment;

c) The relative surface Lewis acidity and surface Lewis basicity of these materials, as quantified by K_a and K_b, and

d) The relative presence of each material in the pigmented PC/PBT/IM blends.

Although different measurement temperature ranges were used in the determination of the values of $-\Delta H^s_a$, and of K_a and K_b, for the different materials, it is assumed that the enthalpy of adsorption is independent of the temperature. This was proven to be true by the very good correlation coefficient relating to the plots of $-\Delta G^s_a/T$ *versus* the reciprocal temperature. Only when "high" temperatures are involved, (for example temperatures greater than 583 K, for PC (Xu *et al.* 1999), and greater than 473 K for the system SAN/TPU (Ratzsch *et al.* 1990)), are the acid/base functionalities decreased substantially and, if the temperature is high enough, (above the temperature corresponding to the major motional transitions, namely the crystalline melting temperature), are suppressed, in particular the hydrogen bonds. Thus, for the measurement temperature ranges used, the values of K_a and K_b are not expected to vary significantly.

3.1.8.1. Dispersive Interactions in Pigmented PC/PBT/IM blends

The values determined for the dispersive component of the surface tension of the materials studied are summarised in Table 3-28, and agree well with data published in the literature for PBT (Hobbs *et al.* 1988a), PC (Champagne *et al.* 1994) and PMMA (Hobbs *et al.* 1988a; Hegedus and Kamel 1993a; Schreiber 1993; Abel and Chehimi 1994). No values were found in the literature for the dispersive component of the surface tension of cobalt aluminate pigments.

Table 3-28. Values of γ_s^d (mJ/m^2) determined for the surface of C. I. Pigment Blue 28, of the MBS rubber, of PC 125, of PBT 195, and of PBT 315.

T (K)	K6310	T (K)	IM	T (K)	PC	T (K)	PBT 195	T (K)	PBT 315
313	27.2±.2	333	35.0±3.7	353	33.7±2.3	295	42.4±1.0	295	43.9±2.1
323	23.2±2.5	343	37.5±2.9	363	37.3±2.6	303	42.5±2.8	303	40.7±1.9
333	20.1±2.2	353	38.5±6.6	373	33.1±2.5	308	41.4±2.6	308	42.8±2.4
343	19.7±3.4	363	39.1±5.5	383	33.2±1.9	313	40.7±1.3	313	40.0±0.6
353	17.4±3.2	373	38.5±5.5	393	29.3±3.2	318	44.7±9.9	318	40.7±2.1
$\frac{d\gamma_s^d}{dT}$	-0.23±0.04	Average	37.7±1.6	Average	33.3±2.8	Average	42.3±1.5	Average	41.6±1.7

The major observation from Table 3-28 is that γ_s^d is practically constant for the polymeric materials involved, in the temperature range studied. On the other hand, for the inorganic pigment, the value of γ_s^d decreases linearly with increasing temperature. The values presented in Table 3-28 show that both PBT 195 and PBT 315 have the greater interaction potential through dispersion forces, followed by the impact modifier, the PC 125, and the pigment, in this order.

As far as dispersion forces are concerned, the PBT 195 molecules and the PBT 315 molecules will interact preferentially *via* intramolecular forces, and intermolecular forces, with

other PBT molecules. The dispersive interaction ability of the MBS rubber is close to that of PBT 195 and to that of PBT 315, followed by that of PC 125. Therefore, it can be expected that the IM will interact to a larger extent with PC 125 rather than with PBT 195 or with PBT 315. C. I. Pigment Blue 28 has the lower interaction potential through dispersive forces, and is expected to interact more with the PC than with the PBTs.

3.1.8.2. Specific Interactions in Pigmented PC/PBT/IM blends

Figure 3-35 gives a comparison of the values of the specific component of the energy of adsorption of DCM, and of THF, on the surface of the C. I. Pigment Blue 28, of the MBS rubber, of the PC 125, and on the bulk of the PBT 195, at 353 K.

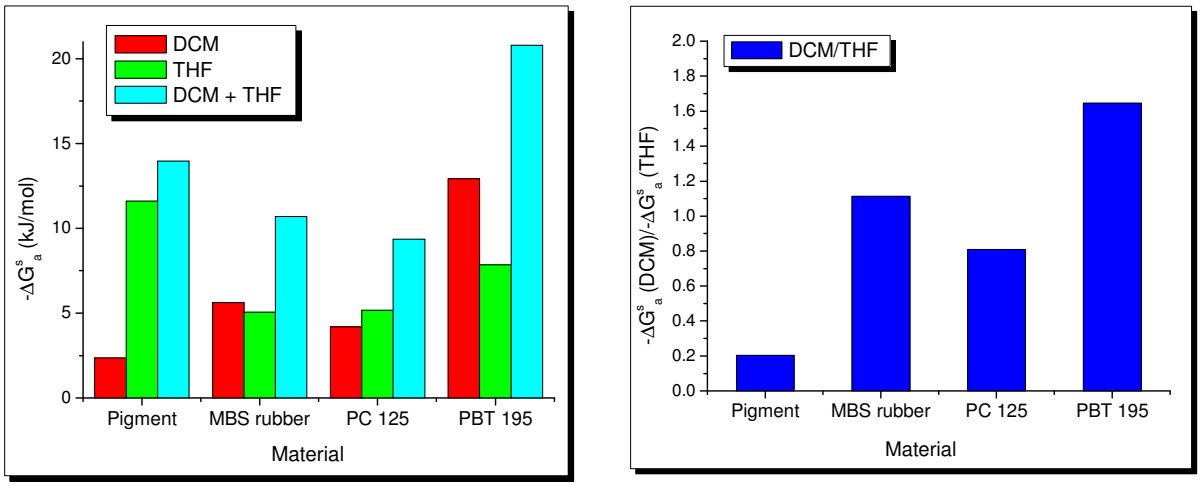

Figure 3-35. Comparison of the specific component of the energy of adsorption of DCM and of THF on the materials studied, at 353 K.

From Figure 3-35 it can be concluded that the Lewis basicity of the materials analysed (quantified in the value of $-\Delta G_a^s$ for DCM) increases in the following order: C. I. Pigment Blue 28 < PC 125 < MBS rubber < PBT 195. The Lewis acidity (quantified in the value of $-\Delta G_a^s$ for THF), increases in the order: MBS rubber ≈ PC 125 < PBT 195 < C. I. Pigment Blue 28. The total specific forces interaction potential increases in the order: PC 125 < MBS rubber < C. I. Pigment Blue 28 < PBT 195. The presence of basic sites, relative to the presence of acidic sites, increases in the following order: C. I. Pigment Blue 28 < PC 125 < MBS rubber < PBT 195.

If the ratio $-\Delta G_a^s$ (DCM)/$-\Delta G_a^s$ (THF) is quite low, then the surface interacts strongly with predominately basic probes, compared with the interaction with acidic probes. If the interaction with acidic probes is strong, then the value of the ratio is close to or greater than 1.

From the previous observations, bearing in mind the constraints related to the analysis of $-\Delta G_a^s$, it can be concluded that:

1) PBT 195 is the most interactive material, followed by the pigment and the MBS rubber;

2) PBT 195 and the MBS rubber have the greater predominance of basic sites, in relation to the acidic sites, and the pigment has the greater predominance of acidic sites in relation to the basic sites, and

3) PBT 195 is the more basic, followed by the MBS rubber, and the pigment is the more acidic, followed by PBT 195.

In Figure 3-36 are compared the values of the specific component of the enthalpy of adsorption of DCM, and of THF, on the surface of C. I. Pigment Blue 28, of the MBS rubber, of the PC 125, of the PBT 195, and of the PBT 315.

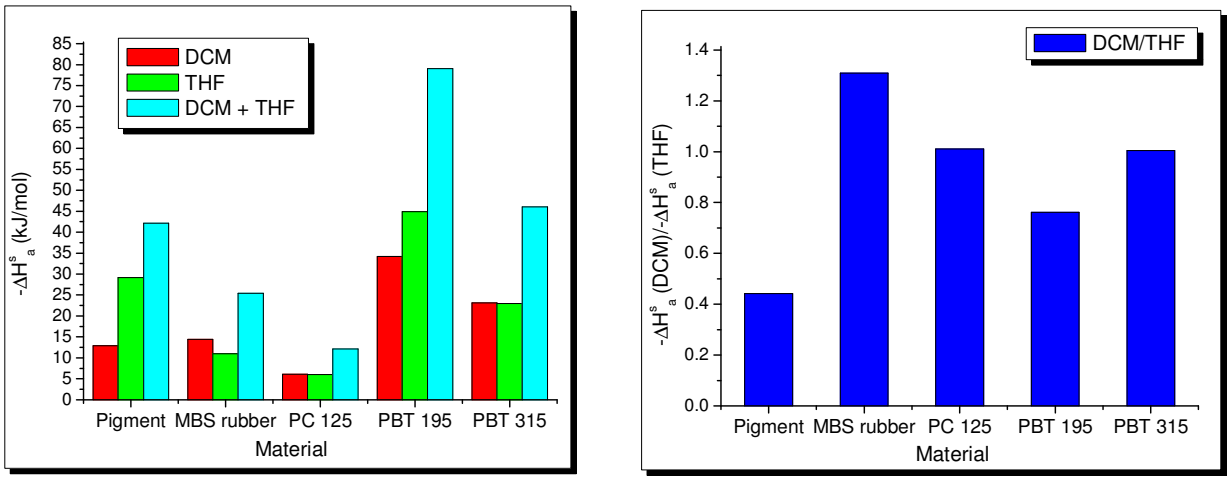

Figure 3-36. Comparison of the specific component of the enthalpy of adsorption of DCM and of THF on the surface of the materials studied. ΔH_a^s for PBT 195 and for PBT 315, $-\Delta H_a^s$ for the remaining materials.

From the analysis of the data that are presented in Figure 3-36, it can be concluded that the Lewis basicity of the materials analysed (quantified in the value of $-\Delta H_a^s$ for DCM) increases in the following order: PC 125 < C. I. Pigment Blue 28 < MBS rubber < PBT 315 < PBT 195. The Lewis acidity (quantified in the value of $-\Delta H_a^s$ for THF), increases in the order: PC 125 < MBS rubber < PBT 315 < C. I. Pigment Blue 28 < PBT 195. The total specific forces interaction potential increases in the order: PC 125 < MBS rubber < C. I. Pigment Blue 28 < PBT 315 < PBT 195. The presence of basic sites, relative to the presence of acidic sites, increases in the following order: C. I. Pigment Blue 28 < PBT 195 < PC 125 ≈ PBT 315 < MBS rubber.

Bearing in mind the constraints involved in the analysis of $-\Delta H_a^s$, it can be concluded that:

1) PBT 195 and PBT 315 are the more interactive materials, followed by the pigment and the MBS rubber;

2) MBS rubber has the greater predominance of basic sites, in relation to the acidic sites, and the pigment has the greater predominance of acidic sites in relation to the basic sites, and

3) PBT 195 and PBT 315 are the more basic, followed by the MBS rubber, and the PBT 195 is the more acidic, followed by the pigment.

The strength of a hydrogen bond can be as high as 30-40 kJ/mol (Hegedus and Kamel 1993a) so the heats of interaction determined are very significant, especially in the case of PBT 195, PBT 315 and C. I. Pigment Blue 28, decreasing of importance in that order. In the particular case of PBT 195, the value of ΔH_a^s relating to the adsorption of THF and of DCM is significantly high (44.9 kJ/mol and 34.2 kJ/mol, respectively). This agrees with the analysis of the repeating unit in PBT and of the OH end-group and COOH end-group concentrations, as discussed in Section 3.1.7.3. Since the enthalpy of interaction is directly related to the strength of the resulting bond, and a decrease in free energy will yield a spontaneous process, there is ample evidence that the acid-base interactions occurring in these systems are forming strong and stable associations between adsorbate and probe molecule.

In Figure 3-37 are compared the values of K_a and of K_b relating to the surface of C. I. Pigment Blue 28, of the MBS rubber, of the PC 125, of the PBT 195, and of the PBT 315.

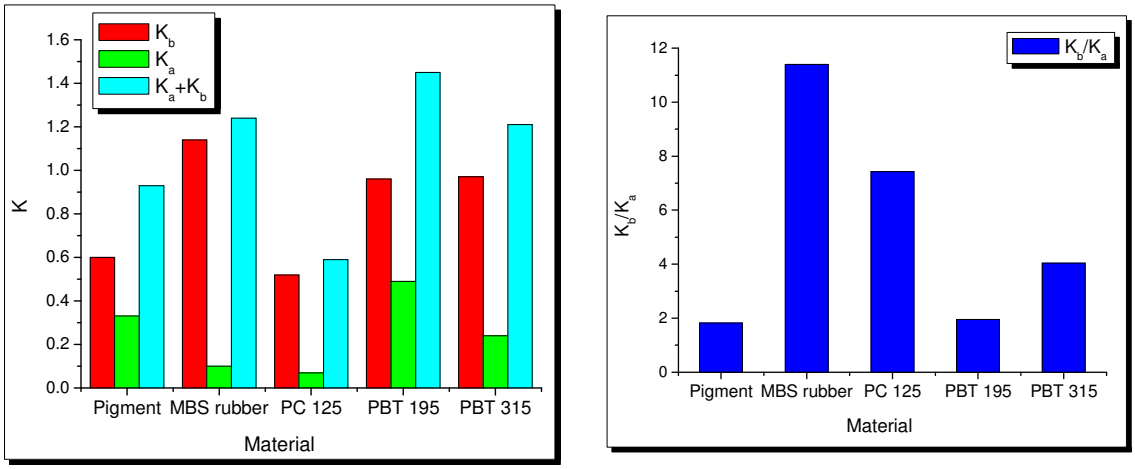

Figure 3-37. Comparison of the values of the K_a and of the K_b for the surface of the materials studied.

Figure 3-37 shows that all the materials are amphoteric, though predominantly Lewis basic. The predominant surface Lewis basicity is in line with the analyses of the structure of the

macromolecules and of the particulates involved. The Lewis acidity increases in the following order: PC 125 < MBS rubber < PBT 315 < C. I. Pigment Blue 28 < PBT 195. The Lewis basicity increases in the order: PC 125 < C. I. Pigment < PBT 195 ≈ PBT 315 < MBS rubber. The total interaction potential (quantified by the sum of K_a and K_b) increases in the following order: PC 125 < C. I. Pigment Blue 28 < PBT 315 < MBS rubber < PBT 195. The relative predominance of basic sites over the presence of the acidic sites increases in the order: C. I. Pigment Blue 28 < PBT 195 < PBT 315 < PC 125 < MBS rubber. It can then be concluded that:

1) The PBT 195, the PBT 315, and the MBS rubber are the most interactive materials and PC 125 is significantly less interactive that the remaining materials;

2) The MBS rubber has the greater predominance of basic sites, and C. I. Pigment blue 28 the lower, and

3) The MBS rubber, the PBT 195, and the PBT 315 are the more basic materials, and PBT 195 and C. I. Pigment Blue 28 are the more acidic materials.

The nature of K_a and K_b is, in a general manner, in accordance with the analysis of $-\Delta G_a^s$, and of $-\Delta H_a^s$. The small differences observed are due to the reasons pointed out earlier: the analysis of $-\Delta G_a^s$, and of $-\Delta H_a^s$ relies only on the adsorption of DCM and of THF, whereas that of K_a and K_b is based on the specific component of the enthalpy of adsorption of, at least, five polar probes. Furthermore, $-\Delta G_a^s$ concerns one measurement temperature, whereas the determination of $-\Delta H_a^s$, and of K_a and K_b, relates to a temperature interval. If the difference in the measurement temperature range between the studies of the different materials is very significant, ΔH_a^s will be affected, which may influence the comparative study. This would be particularly true as far as the study of the PBT 195 and of the PBT 315 is concerned. Nevertheless, the analysis of $-\Delta G_a^s$ for the temperature of 353 K, for all the materials, is consistent with the discussion of ΔH_a^s and of K_a and K_b.

From the observations made, it can be concluded that PBT 195 and PBT 315 are preferentially involved in intramolecular and intermolecular interactions with other PBT molecules, because PBT 195 and PBT 315 are characterised by both strong Lewis base and strong Lewis acid functionalities. It should also be noticed that no steric hindrance, due to bulky side-groups, is expected and, thus, the basic sites, and the acidic sites, are easily accessible to interaction through intermolecular forces and intramolecular forces. As far as the PC 125 is concerned, the strong base/base repulsion and weak acid/base attraction, alongside with the steric hindrance due to the $-CH_3$ side-groups and the aromatic ring, contribute to lower ability of this polymer in participating in specific interactions. A certain degree of Lewis acid/base attraction between PC 125 and the PBTs is expected as the PC 125, although being a weak Lewis acid, has some Lewis base character

and the PBTs have strong Lewis acidic sites. Moreover, the PBTs have strong Lewis basic sites and, thus, are able to interact to a certain extent with the Lewis acidic sites on PC 125. The PBT and the PC 125 account for 90 % (w/w) of the blend composition in an approximate 1:1 proportion and, therefore, the interaction opportunities are very considerable.

It has been shown that possibility of miscibility, and LCST behaviour, through the repulsion effect exists (Section 1.2.1.) (Bertilsson *et al.* 1988b; Utracki *et al.* 1989; Lee *et al.* 2001). The repulsion effect in the case of PC and PBT requires that at least one of the polymers be regarded as an alternating copolymer consisting of constituents with a large difference in polarity. Bearing in mind the repeating unit in PBT (Figure 1-1) one can identify the aforementioned constituents as being the ester functionality (strongly basic) and the hydroxyl groups (strongly acidic). As the number of ester groups per unit chain is significantly greater than the number of OH groups, it follows that base-base repulsion between the basic centres in the backbone of PBT is a probable event. Consequently, both PBTs, and namely PBT 315 (which has the lower K_a value of the two PBTs), and in view of the repulsion effect theory, are expected to interact with PC 125, although to a small extent. It can then be said that, although naturally phase-separated, PC and PBT may be miscible to a certain, low, extent.

The fast crystallisation kinetics of PBT also contributes to the expulsion of PC from within the PBT domains. This entropic effect has been observed by Ratzsch (1990).

Experimental evidence has been given by Sanchez and colleagues (1993), and by Dekkers *et al.* (1988) of good interfacial adhesion existing between PBT and PC in transesterification-free compositions. Mishra and Venkidusamy (1995) showed, by means of IR studies, that additions of PBT improves the intermolecular forces in PBT/PC blends, in particular, on the end-group and the $-CH_3$ and -C=O groups. These results further support the evidence given in the present study of the decisive role of Lewis acidic/basic centres on the partial miscibility of PBT with PC. In conclusion, the IGC analysis of the Lewis acidic/basic character of PBT and of PC, carried out in the present study, allowed for a rationalisation of the reported limited solubility of PC/PBT blends.

The MBS rubber interacts preferentially with the PC 125 rather than with the PBTs. This is due to two factors:

1) The preference of the PBTs molecules to interact with other PBT molecules, and

2) The Lewis base/base repulsion between the PBTs and the MBS rubber.

The second effect, i.e. predominant repulsion effect, is due to the fact that the PBT 195, the PBT 315 and the MBS rubber are very strong bases and the Lewis acidity of the MBS rubber is low (and, therefore, the impact modifier will interact mainly through the basic sites). As the PC 125 has the weakest Lewis basicity and weakest Lewis acidity, the base/base repulsion with the MBS rubber will not be as significant as between the impact modifier and the PBTs. Thus, acid/base attraction is thought to dominate in the pair MBS rubber/PC 125. Also, the PBTs and the PC 125

are used in an approximately 1:1 proportion, meaning that the interaction opportunities between the MBS rubber and the PC 125 are substantial. The interaction between PC and PMMA has been shown, by Nishimoto *et al.* (1991), to be weak but slightly favourable. Good adhesion between the PC and the MBS rubber has also been reported by Dekkers and colleagues (1988). The fast crystallisation of PBT also contributes to the expulsion of the MBS rubber from the PBT domains.

C. I. Pigment Blue 28 is thought to interact preferentially with the PBTs and then with the PC 125. This is due to the fact that the pigment is a strong Lewis acid and the PBTs are strong Lewis bases. Also, the PBTs, mainly PBT 195, are strongly Lewis acidic and the pigment is moderately Lewis basic. Nevertheless, as the PBT molecules prefer to interact with other PBT molecules, it is expected that some acid/base interaction between the pigment and the PC 125 would occur.

A practical example of modified PC/PBT solubility by alteration of the specific interactions potential of the polymers involved is the amide modification of PBT (van Bennekom *et al.* 1997a and 1997b; van Bennekom and Gaymans 1997). This modification leads to increased concentration of OH groups, thus promoting PBT crystallinity and phase separation of the PC and the PBT phases.

The phase segregation is due to an increase in the intramolecular and intermolecular interactions within the PBT. When the PBT is modified with 20-25 mol% amides, these PBT/PC blends were immiscible (van Bennekom *et al.* 1997a). The modified PBT has a higher melting temperature and a higher glass transition temperature, higher crystallisation rate and better solvent resistance than the unmodified PBT.

The solubility parameter, δ, for PC and PBT is about 21 $MPa^{0.5}$ and 22 $MPa^{0.5}$, respectively (van Bennekom *et al.* 1997a). With the incorporation of diamide units in the PBT, the $\Delta\delta$ is reported to increase. Consequently, the miscibility of the diamide-modified PBT with the PC decreases and the T_g of the PC phase will be less affected by the presence of the diamide-modified PBT. All of these aspects are well explained bearing in mind the values of the Lewis acidity constant and of the Lewis basicity constant determined in the present study.

Taking into account the values of K_a and K_b, for PBT 195 and PBT 315, (Table 3-31, Section 3.1.7.3.), an increase in the Lewis acidity of PBT, consequence of increased concentration of OH groups, will lead to stronger intramolecular and intermolecular specific interactions, namely hydrogen-bonds, between the OH groups and the Lewis basic sites (mainly oxygen atoms), resulting in an increase in the melting temperature, in the glass transition temperature, in the extent of crystallinity and associated properties such as solvent resistance.

3.2. Influence of C. I. Pigment Blue 28 on the Physical Properties and on the Mechanical Properties of PC/PBT/IM Blends

3.2.1. Gel Permeation Chromatography

Gel Permeation Chromatography (GPC) was used to assess the way in which the molecular weight distributions of PC and PBT are affected by the inclusion of C. I. Pigment Blue 28 into the composition of the blends, and consequences thereof to their mechanical properties and their physical properties. In Figure 3-38 are presented the weight-average molecular weight, $\bar{M}_w$, the number-average molecular weight, $\bar{M}_n$, and the polydispersity of PC and of PBT, for samples of Sets 1, 2 and 7 (Section 2.1.).

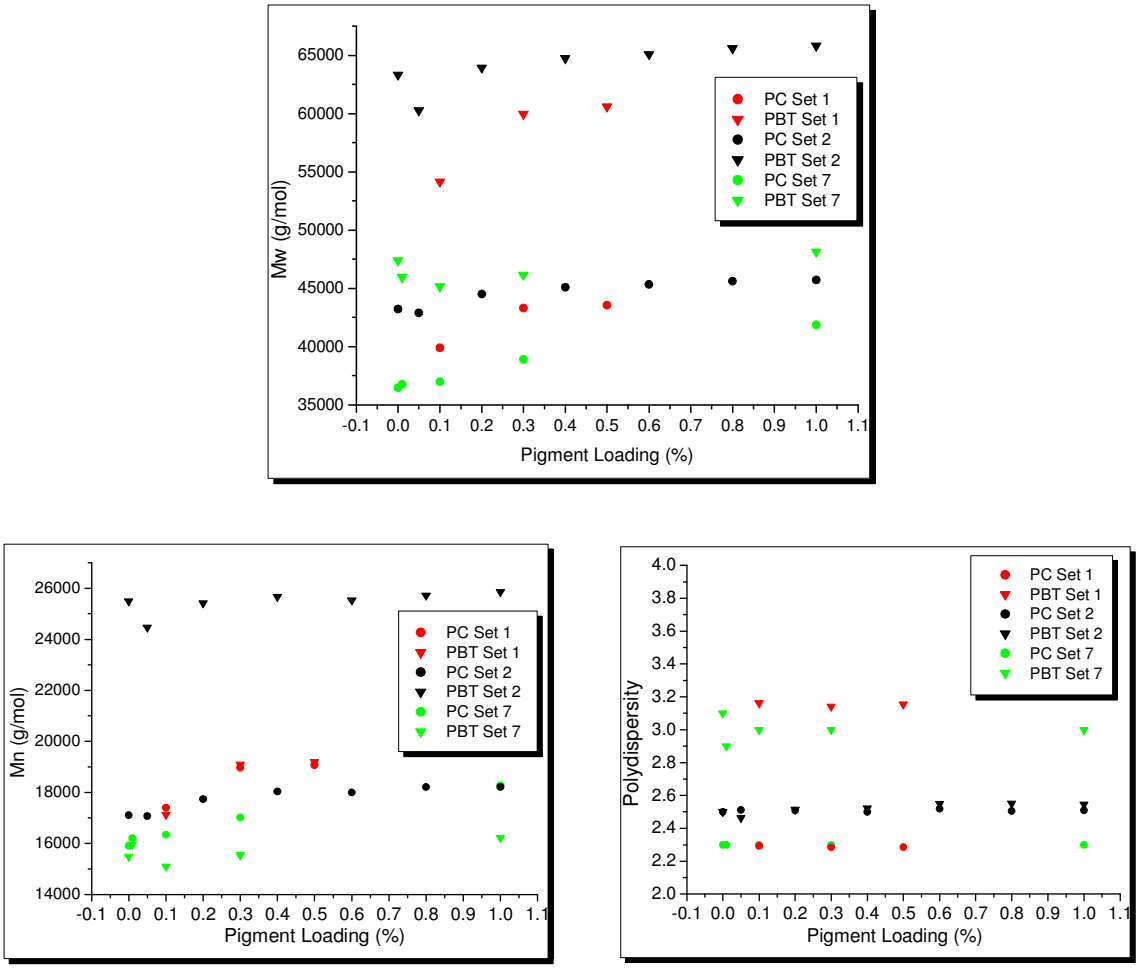

Figure 3-38. Weight-average molecular weight, number-average molecular weight and polydispersity of PC and of PBT in samples of Sets 1, 2 and 7.

From the analysis of the data that are presented in Figure 3-38, it can be concluded that the molecular weights of PC and PBT are influenced by C. I. Pigment Blue 28. The higher fraction of

the molecular weight distribution of PBT, represented by the weight-average molecular weight, is markedly more influenced by the pigment than is the lower fraction, represented by the number-average molecular weight, and markedly more influenced than is the PC. The fact that PBT is more prone to chain scission than is PC has been reported in the literature (Bertilsson *et al.* 1988b; Sanchez *et al.* 1993).

The effect of the pigment on the molecular weight of PBT is twofold. At lower pigment loadings, the presence of the inorganic pigment particles leads to a decrease of the average molecular weight. Above a particular pigment loading, the pigment particles show the opposite effect, that of inhibiting the chain scission of PBT. The decrease of the molecular weight of PBT is reported in the literature as being associated with the occurrence of transesterification and thermal degradation in PC/PBT blends (Bertilsson *et al.* 1988b; Cecere *et al.* 1990; Wu *et al.* 1994; Pompe 1997). Both factors are thought to contribute to a large extent to the behaviours observed in Figure 3-38, although they may not be the only factors involved. Further discussion of this subject is presented in subsequent paragraphs.

With PC, the inclusion of the pigment into the composition of the blends results in an increase of the average molecular weight, even at the lowest pigment loading used. This is in line with the blend morphology seen in TEM imaging of the blends (Section 3.2.10.) and with the DMTA results (Section 3.2.3.), as the greater the molecular weight of PC, the more well-defined are the PC-rich phase domains and the PBT-rich phase domains, along with increased phase separation.

The introduction of pigment decreases the polydispersity of PBT, at the lower pigment loading. This supports the inference that, at the lower pigment loadings, the effect the pigment has on the molecular weight of PBT is more pronounced than the effect it has on the PC. Moreover, it shows that, at that loading, the average molecular weight of the higher fraction of the molecular weight distribution of PBT is more affected than is the lower fraction. At pigment loadings that are greater than approximately 0.10-0.20 %, the polydispersity of PBT does not change significantly. Therefore, for pigment loadings above those values, the pigment is affecting both the higher and the lower fractions of the molecular weight distribution in a similar fashion. The polydispersity of PC remains essentially unchanged with increasing pigment loading. This indicates that the "stabilising" effect of the pigment, in terms of polymer chains degradation, is indicated in a similar manner on both the higher molecular weight PC and on the lower molecular weight PC.

As far as the samples of Set 7 are concerned, the polydispersity of the PBT is greater than that of the PC. This finding is in line with the use of two grades of PBT differing significantly in terms of their average molecular weight (Table 2-2, Section 2.1.). Also, the fact that the higher fraction of the molecular weight distribution of PBT is more affected than the PC, contributes to the greater polydispersity value for PBT. When comparing the GPC results with those relating to the determination of the non-isothermal crystallisation temperature, and of the degree of

crystallinity (Figures 3-41 and 3-42, respectively, Section 3.2.2.2.), it can be observed that the values of T_c show the same behaviour as those of the average molecular weight of PBT, with respect to the effect observed on increasing the pigment loading. Moreover, the trend observed for the $-\Delta H_c$ values follows the same pattern than that of the PBT polydispersity. The melting temperature depression method (Section 3.2.2.1.) shows that the trend that was observed for the molecular weight, and for the T_c and $-\Delta H_c$, of PBT, is in agreement with the estimation of the transesterification degree. Therefore, transesterification is proven to play a role on the physical properties of samples of Set 7, along with the thermal scission of the polymer chains. The transesterification, and the thermal degradation of the polymers in samples of Set 7, are shown to be directly influenced by the presence of C. I. Pigment Blue 28.

There is an increase in the number-average molecular weight of PBT at the lower pigment loading, when compared to the unpigmented blend. This is a consequence of the "milling effect" the pigment has, mainly on the higher fraction of the molecular weight distribution, leading to an enrichment of the lower fraction. This further supports the observation that the higher fraction of the molecular weight distribution (which refers mainly to PBT 315) is more responsive to the "milling" effect of the pigment on the PBT polymer chains, than is the lower fraction. The values of $\bar{M}_n$ for the PBT are lower than those corresponding to PC, which is not the case with samples of Set 2. This further supports the finding that the PBT is more sensitive to chain degradation than is the PC.

For the samples of Set 2, the trends observed are analogous to those relating to samples of Set 7, although in a less pronounced manner. The polydispersity values of PBT in samples of Set 2 are lower than those for samples of Sets 7 and 1. This indicates that the molecular weight distribution is more homogeneous in samples of Set 2. There is less difference between the average molecular weight of the higher fractions and of the lower fractions of the molecular weight distribution than for samples of Set 7. Therefore, the effect the pigment, and the extrusion conditions, have on the higher and lower fractions of the molecular weight distribution of PBT is more similar than in samples of Sets 7 and 1. In these samples, as discussed above, the higher fraction of the molecular weight distribution of PBT is significantly more affected than is the lower fraction. The polydispersity of PC is greater for Set 2 than in samples of Sets 1 and 7. This indicates that this polymer is less influenced by the pigment, and by the extrusion conditions, for the samples of Set 2.

Transesterification is known to broaden the molecular weight distribution of PBT (Timmerman, T. *et al.* 2001, Personal Communication). Therefore, it might be expected that samples of Set 2 would be less transesterified than those of Sets 7 and 1. The trend observed for the molecular weight of PBT, in samples of Set 2, is similar to that of ΔT_m (Figure 3-40, Section 3.2.2.1.). However, the trend observed for the non-isothermal crystallisation properties (Figures 3-41 and 3-42, Section 3.2.2.2.) differs from that observed for the molecular weight and from that

observed for ΔT_m. It is, therefore, concluded that the samples of Set 2 are not significantly transesterified as this does not affect the crystallisation properties of the PBT phase in the blends. Further discussion on the transesterification level in these samples is provided in Section 3.2.1.1. From the above inferences, it can be concluded that the major cause of the behaviour observed in the variation of the molecular weight, and of the ΔT_m, for samples of Set 2, is the thermal scission of the PBT.

For samples of Set 1, and the effect of the pigment loading, Figure 3-38 shows that the weight-average molecular weight, of both PC and PBT, increases with increasing pigment loading. The difference in molecular weight between the sample with 0.10 % pigment loading and the samples with 0.30 and 0.50 % loadings is significantly more marked than between the samples with 0.30 and 0.50 % loadings. This trend is analogous to that of samples of Set 2, which were processed in the same extrusion system, although with different throughput values (25 kg/hr for Set 1 and 40 kg/hr for Set 2). The average molecular weight values of PC and of PBT for samples of Set 1 are typically lower than those determined for samples of Set 2. This is thought to be caused by the longer residence time of the samples of Set 1 in the extruder barrel (due to lower throughput) which led to increased thermal degradation in these samples. The value of $\bar{M}_n$ of PBT is very close to that of PC, whereas $\bar{M}_w$ is significantly greater. This is in line with the expected greater polydispersity of PBT. It can be concluded that the $\bar{M}_w$ of PBT is mainly influenced by that of PBT 315, which is characterised by the greater value of average molecular weight (Table 2-2, Section 2.1.) and is more "stabilised" by the pigment against thermal degradation than is the higher molecular weight fraction of PC.

The comparison of the differences in values and trends between Sets 1, 2 and 7, gives important information concerning the differences in processing conditions and consequences thereafter to the breakdown of the PBT and PC polymeric chains and to transesterification reactions. From comparison of the results of samples processed in extruder E1 (Sets 1 and 2) with those processed in extruder E2 (Set 7), it can be concluded that the molecular weight of both the PC and the PBT in the samples of Set 7 is significantly lower. This difference is more striking for PBT due to the greater sensitivity of PBT to differences in processing conditions. It is known that the extruder that was used to process samples of Set 7 has a greater total mixing area and, thus, the melt blend is subject to greater shear stress during extrusion. Also, the residence time in the screw is significantly greater in extruder E2. The flow rate for samples of Set 7 was 10 kg/hr, whereas the flow rate for samples of Sets 1 and 2 was 25 kg/hr and 40 kg/hr, respectively. As the extrusion conditions become more aggressive towards the degradation of the molecular weight (longer mixing areas, more mixing energy, and longer residence time), the value of $\bar{M}_n$ of the PBT gets closer to that of PC and, in samples of Set 7, it is lower.

From the processing conditions, it can be concluded that longer residence times in the barrel, and greater mixing energies, lead to increased thermal degradation of the polymers and also to increased transesterification. The molecular weight of the polymers and the degree of crystallinity must be closely monitored due to their influence on the physical properties and on the mechanical properties of the blends. Interpretations of the GPC results contribute decisively, to an understanding of the effects of the pigment on the mechanical properties (such as the stress at break, the tensile modulus and the impact strength), on physical properties (such as the degree of crystallinity and crystallisation temperature), and on the morphological characteristics of the blends (namely phase separation and phase domain sizes). The following sections will illustrate these observations.

In Figure 3-39 are compared the average molecular weight, and the molecular weight distributions of PC and PBT with increasing pigment loading, for the blend samples (Set 2), and for the samples that mimic the PBT-rich phase, and the PC-rich phase (Sets 3 and 4, respectively).

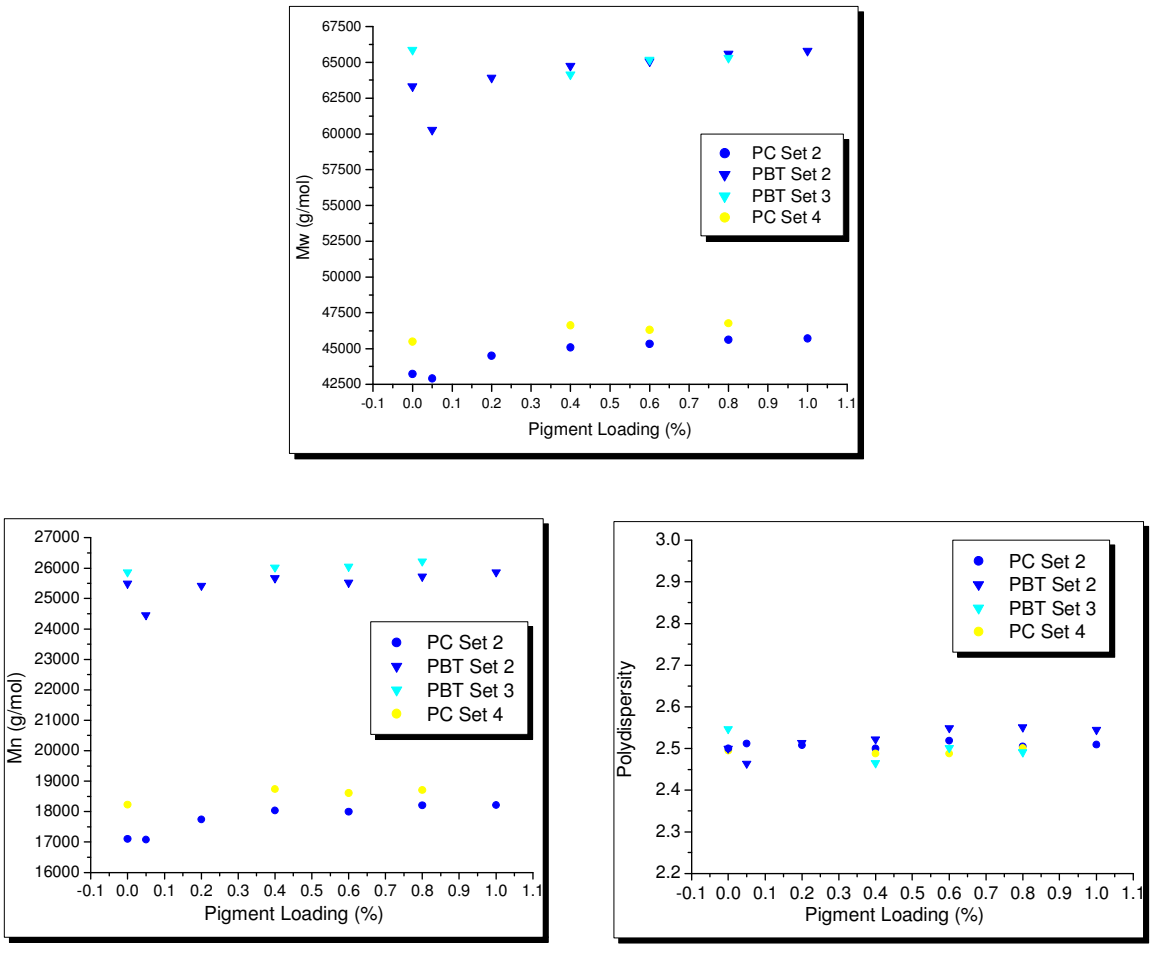

Figure 3-39. Weight-average molecular weight, number-average molecular weight and polydispersity of PC and of PBT in samples of Sets 2, 3 and 4.

Figure 3-39 shows that the values of $\bar{M}_w$ and $\bar{M}_n$ in the blend samples follow closely those concerning the PBT-based and the PC-based samples. It is interesting to note that the molecular weights of PBT and PC in the blend samples are slightly lower than those relating to samples of Sets 3 and 4. Therefore, blending PC with PBT leads to a decrease in the average molecular weight of both polymers.

3.2.2. Differential Scanning Calorimetry

3.2.2.1. Heating Mode

DSC analysis in the heating mode was carried out on samples of the polymeric raw materials (PC 125, PBT 195, PBT 315 and MBS rubber (IM)), in order to identify temperatures relating to characteristic exothermic and endothermic processes. A sample of tape-extruded PBT 195 granulate was also analysed. From the thermogram obtained for PC 125 (Figure C-1, Appendix C) it can be observed that the T_g of this polymer is 148 ºC, in line with values reported for this polymer (Birley and Chen 1984). No further significant thermal transitions are observed up to 270 ºC. As far as PBT 195 and PBT 315 are concerned, the T_g can be identified at 35-40 ºC (Figures C-2 and C-3, respectively, Appendix C), and the T_m at 225 ºC and 227 ºC, respectively. An exothermic phenomenon is identified at 180 ºC. These characteristic temperatures coincide with values found for this polymer (Birley and Chen 1984; Sanchez *et al.* 1993). The aforementioned exothermic phenomenon is more prominent for PBT 195 than it is for PBT 315 and is related to the crystalline melting transition of PBT (Dekkers *et al.* 1990). A smaller endothermic phenomenon is identified at 120 ºC for PBT 195. The higher T_m and the more evident exothermic phenomenon for PBT 195 are due to differences in crystallisation properties between this PBT grade and PBT 315, the PBT 195 being characterised by a greater crystallisation extent (Section 3.2.2.2.). In the MBS rubber thermogram (Figure C-4, Appendix C), a small endothermic phenomenon is identified at 110-120 ºC, and a significant exothermic phenomenon at 372 ºC. The small endothermic phenomenon is related to the T_g of PMMA (the shell component of the MBS rubber) (Hamieh *et al.* 1998), and the exothermic phenomenon to possible polymerisation (crosslinking of the poly(butadiene)) of the MBS impact modifier core.

From the DSC studies undertaken on the unpigmented, tape-extruded, blend sample (batch BX, Table 2-5, Section 2.1., thermogram: Figure C-5, Appendix C), the following observations can be made. The T_g of PBT is not clear, because it is affected by enthalpic relaxation processes occurring in the DSC cell. This finding is in line with observations reported for these blends (Huang and Chang 1997). At approximately 110-150 ºC, an exothermal phenomenon is identified. When performing the DSC evaluation in the cooling mode, and then reheating the sample, the exothermal transition peak disappeared in all the samples analysed. Thus, the exothermic transition is due to polymer chain orientation, resulting from processing (extrusion and tape-extrusion), and is related to the crystalline phase of PBT. The T_g of the PC-rich phase cannot be identified as it is

overlapped by the secondary crystallisation transition of PBT (Bertilsson *et al.* 1988b). At 180-200 ºC there is an exothermic peak, related to the crystalline melting transition of PBT. According to Huang and Chang (1997), this existence can be explained on the basis of the crystallisation of amorphous PBT molecules that are closely tied up to the crystallites. These authors concluded that crystallisation of partially melted, less perfect PBT crystallites, to form the better oriented crystallites and release the heat of crystallisation is not the major reason for the existence of the aforementioned exothermic phenomenon. This exothermic transition appears (and/or becomes more pronounced) upon reheating the sample in the DSC cell, which may be due to increased phase separation, that leads to a fraction of the PBT phase (characterised by lower molecular weight, and higher OH end-group concentration than the remaining PBT) crystallising at lower temperatures. The blend shows evidence of melting at 200-220 ºC, at a temperature range lower than that relating to pure PBT, coinciding with reports in the literature for these blends (Birley and Chen 1984).

With regard to the blend samples processed using extruder E1 (Sets 1 and 2, Tables 2-4 and 2-5, respectively, Section 2.1.), the following remarks can be made (Figures C-5 to C-24, Appendix C). In the heating cycle thermograms, the blends processing-driven exothermic phenomenon peak temperature increases with increasing pigment loading. Upon reheating the samples in the DSC cell, this exothermic trend remains, especially at the greater pigment loadings, although in a smaller expression. Thus, increasing the pigment loading, for these samples, leads to a more pronounced, blends processing-driven, PBT crystalline-related polymer chain orientation.

The recrystallisation exothermic peak, prior to melting of the sample, is not very pronounced in the heating cycle thermograms. Upon reheating the sample, the recrystallisation peak increases in importance and, as the pigment loading increases, remains approximately unchanged in terms of both peak maximum temperature and area under the peak. Thus, reheating the samples in the DSC cell leads to phase separation. However, the effect of the pigment on the phase separation is not very significant, for samples of Set 2. This inference is in agreement with there being an approximately unchanged degree of crystallinity with increasing pigment loading for samples of Set 2, which is subject of discussion in the following section.

Upon reheating the sample with the lower pigment loading (batch B6), a small endothermic change, just before the aforementioned recrystallisation exotherm, occurs. In the samples with higher pigment loadings, this endothermic transition is thought to be overlapped by the aforementioned recrystallisation exotherm. It is known (Huang and Chang 1997) that the PBT minor endothermic disappears, or decreases of importance, as miscibility, compatibilisation, increases. This inference leads to the conclusion that C. I. Pigment Blue 28 increases the miscibility of PC and PBT, in agreement with the DMTA results (Section 3.2.3.). The minor endotherm is not present in the heating thermogram but only in the reheating thermograms. Thus, it can be

concluded that reheating the sample leads to phase separation. The secondary endothermic event is followed by the PBT endothermic transition from the glass to the melt phase, at 224 ºC.

The observed double PBT melting peak is commonly interpreted in terms of reorganisation processes of the crystalline phase during heating in the DSC cell, related to the sequential melting of the two different crystalline structures of PBT (Birley and Chen 1984; Pompe *et al.* 1996; Huang and Chang 1997; Pompe 1997; Tattum *et al.* 2000). The reorganisation process is stronger in cold crystallisation than it is in melt crystallisation.

According to Pompe and colleagues (1996) and Huang and Chang (1997), the lower peak represents more or less the melting of crystallites with a lamellar thickness produced at T_c (referred to as less perfect crystallites). The upper peak, T_m, is related to more stable crystallites formed partially or completely during the reorganisation process. According to Wilkinson and colleagues (1995), the small melting endotherm peak may be ascribed to the melting of thin lamellae formed during secondary crystallisation.

For blend samples that were processed in extruder E2 (Set 7, Table 2-10, Section 2.1.), Figures C-25 to C-34, Appendix C, show that, for the heating cycle thermograms, the blends processing-driven exotherm temperature increases with increasing pigment loading more significantly than it does for samples of Set 2. Moreover, this transition occurs at significantly lower temperatures than those for samples of Set 2. Both trends are thought to be due to the lower molecular weights of the PBT and the PC for samples of Set 7 (Section 3.2.1). The results confirm that the pigment is affecting the crystalline properties of PBT. This effect is more pronounced for samples that are characterised by lower molecular weights of PBT and PC. The blends processing-driven exotherm disappears upon reheating, except for the unpigmented blend (sample LX). For samples of Set 2, this exotherm remains upon reheating. This difference in behaviour is thought to be due to more expressive phase separation, upon reheating, in the samples of Set 7, due to the lower PC and PBT molecular weights.

The secondary endotherm and the recrystallisation exotherm are not present in the heating cycle thermograms of samples of Set 7. On reheating the samples in the DSC cell, the minor endothermic transition appears, but is less significant than that which occurs for samples of Set 2. Thus, it can be concluded that the PC and PBT in samples that were processed in extruder E2 are more compatible than they are in the samples processed in extruder E1. As the pigment loading increases, the recrystallisation exotherm does not become distinctively more pronounced upon reheating. This would indicate that increasing the pigment loading does not lead to facilitated recrystallisation of the PBT upon increasing phase separation. This may be related to the higher degree of transesterification in samples of Set 7, mainly at the lower pigment loadings, compared to that of samples of Set 2. This point is considered below.

The level of transesterification in the blends has been assessed by the melting temperature depression method (Sections 1.4.1. and 1.4.3.). In Figure 3-40 are presented the values of the first

and second scan melting temperature (T_m), and the corresponding difference, ΔT_m, as a function of the pigment loading for the blend samples that were processed in extruder E1 (Set 2) and in extruder E2 (Set 7).

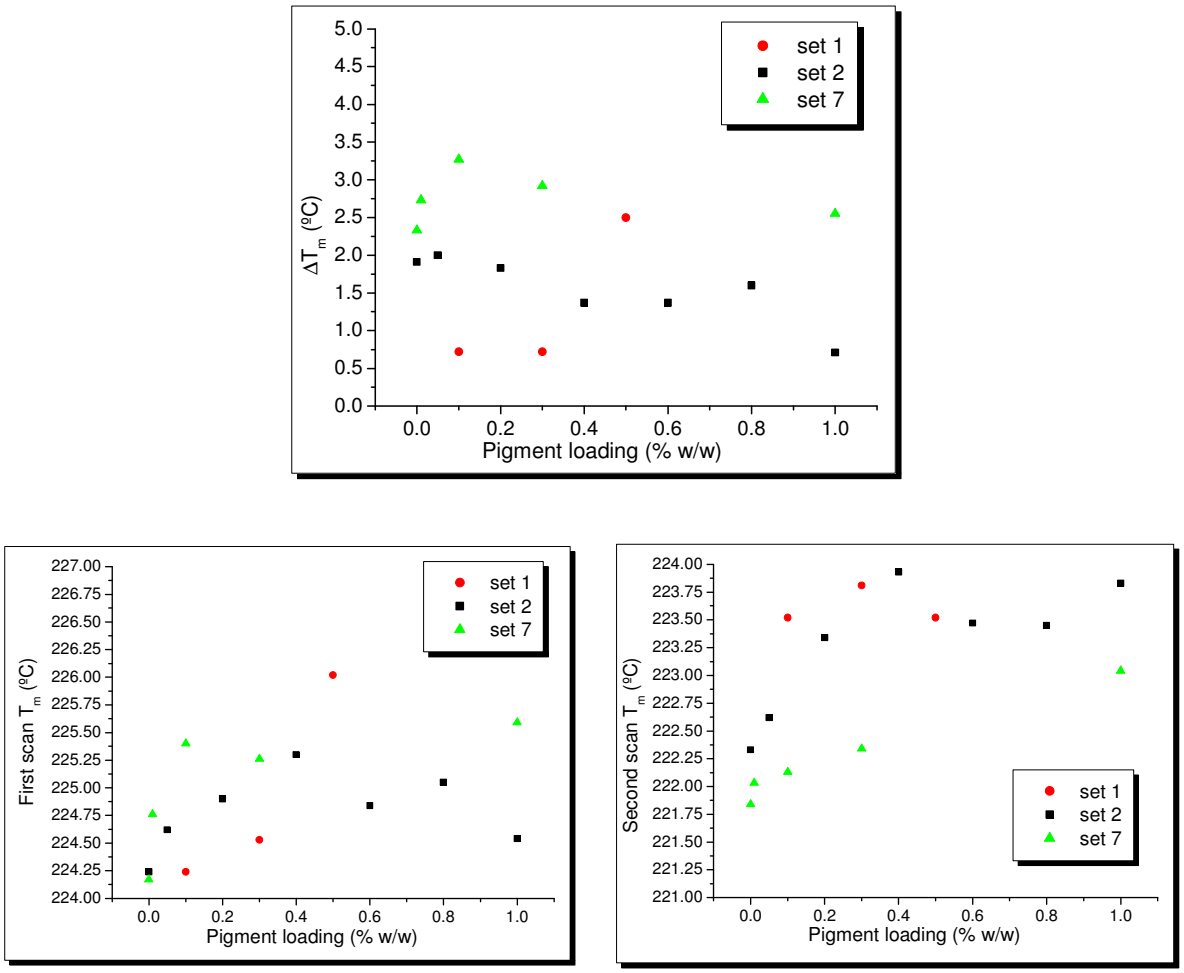

Figure 3-40. First scan melting temperature, second scan melting temperature and melting temperature variation from the first scan to the second scan, as a function of the pigment loading in samples of Sets 1, 2 and 7.

Figure 3-40 shows that the first scan T_m increases with increasing pigment loading (until a particular loading is reached for Set 2). The T_m for pigmented samples is always greater than that of the unpigmented sample. This applies for both the first scan and the second scan. Therefore, the introduction of C. I. Pigment Blue 28 into the blends leads to an increase in the melting temperature.

The factors influencing the values of the first scan T_m, with increasing pigment loading, include differences in the heat capacity between the pigment and the polymers, the level of interaction between the pigment and the polymers, the differences in the molecular weight of the polymers, the level of miscibility of PC and PBT (physical in character and due to

transesterification reactions), the processing operations (extrusion and tape-extrusion, which can induce complex polymer chains orientations and entanglements), the thermal history of the sample, and the degree of crystallinity of the PBT.

Therefore, an interpretation of the influence of increasing pigment loading on the values of T_m, namely those relating to the first scan, and the isolation of the influence of each of these factors, is not an easy task. Nevertheless, in Figure 3-40, the plot relating to the first scan T_m, shows that the increase in pigment loading, for samples of Set 7, follows a trend that is similar to that of the molecular weight of PC (Figure 3-38, Section 3.2.1.). The higher the average molecular weight of PC, the higher is the value of T_m. For the samples of Set 2, the behaviour of the first scan T_m with increasing pigment loading is more complex. Isolation of the contribution of one or each of the aforementioned factors is not attainable at this moment of the analysis.

The value of T_m for the data point that relates to the sample with 0.50 % pigment loading of Set 1 falls completely out of the expected range. This is thought to be due to a non-representative sample of this batch, bearing in mind the small size of the DSC sample. For example, artefacts consequence of processing (extrusion and tape-extrusion) could induce intricate polymer chain orientations and entanglements that would affect the vale of the first scan T_m. Therefore, the analysis of the first scan T_m and of ΔT_m relating to this batch was not carried out.

In Figure 3-40 are presented the values of T_m on reheating the samples (second scan), and the variation of T_m from the first scan to the second scan, ΔT_m. The plot for the second scan T_m, shows that the values corresponding to samples of Set 7 are lower than those relating to samples of Set 2. Therefore, bearing in mind the values of the first scan T_m, it is concluded that samples of Set 7 are more sensitive to the thermal treatment in the DSC cell than are samples of Set 2.

The values of the second scan T_m for samples of Set 1, are close to those of samples of Set 2. This is in line with the fact that these two sets of samples were processed in the same extrusion unit. The fact that the values of the second scan T_m are greater for the samples processed in extruder E1 (Set 2) agrees with the greater molecular weights of PC and PBT in these samples when compared to those of samples of Set 7 (Section 3.2.1.). Moreover, the degree of crystallinity in proven not to play a role in the above mentioned differences as it is approximately the same for the greater pigment loadings (Section 3.2.2.2.).

It can also be observed that the value of the second scan T_m increases with increasing pigment loading for samples of Sets 1, 2 and 7. This point may be related to increased crystallinity and/or with decreased degree of transesterification and/or with the molecular weight differences, mainly of the PC, observed for these blends (Section 3.2.1.), and/or to the presence of the rigid inorganic pigment particles.

The consistent increase in the values of the second scan T_m indicates, nevertheless, that the morphology of the crystalline PBT is basically the same in all the samples analysed (Sanchez *et al.* 1993).

The melting temperature in a partially miscible blend can be depressed. This melting point depression in miscible blends depends on the concentration of the dissolved polymer and on the polymer-polymer interaction parameter (Bennekom *et al.* 1997a). Also, ester interchange and transesterification, as a consequence of high melt temperatures, can cause a reduction in the melting point (Birley and Chen 1984; Bertilsson *et al.* 1988b; Tattum *et al.* 2000). The decrease in molecular weight, both due to thermal chain scission and transesterification, is also indicated in lower melting temperatures (Bertilsson *et al.* 1988b).

Clearly, in Figure 3-40, ΔT_m is greater for the samples of Set 7. This finding supports the evidence that PC and PBT, in samples processed in extruder E2, are more miscible than those processed in extruder E1, as can clearly be seen in the TEM imaging (Section 3.2.10.).

It should be noted that chain scission caused by the high shear stress during processing does not occur in the DSC cell. Thus, it can be concluded that samples extruded using extruder E2 are more prone to transesterification, and are characterised by a more extensive transesterification reaction degree, than those processed in extruder E1.

For samples of Set 7, the behaviour observed for ΔT_m with increasing pigment loading follows that of the crystallisation temperature (Figure 3-41, Section 3.2.2.2.), and of the weight-average molecular weight of PBT (Figure 3-38, Section 3.2.1.). The greater the ΔT_m, the more miscible PC and PBT are, the lower is the weight-average molecular weight of PBT, and the lower are the T_c and the $-\Delta H_c$. Thus, it can be concluded that the greater is the transesterification degree. As a result, it can be said that PBT 315 (the major component of the higher fraction of the molecular weight distribution of PBT, represented by $\bar{M}_W$), is more affected by transesterification than is PBT 195 and than is PC. Also, the physical properties of PBT are concluded to be a good indicator of the transesterification level in PC/PBT blends.

The transesterification rate is known to increase with decreasing molecular weight of PBT (Pompe 1997). Thus, decrease of the molecular weight of PBT (due to thermal scission) may also contribute to the greater transesterification rate at the lower pigment loadings.

For samples of Set 2, the behaviour observed for ΔT_m with increasing pigment loading follows that of the crystallisation temperature, but does not follow that of the crystallinity degree (Section 3.2.2.2.) nor that of the molecular weight of PBT (Section 3.2.1.). Thus, these samples are very significantly less transesterified than are those of Set 7. Also, the small decrease in the weight-average molecular weight of PBT at the lower pigment loading for samples of Set 2 is further proven to be mainly due to thermal cleavage of the polymeric chains, rather than to transesterification.

Pompe (1997) states that the value of T_m cannot be used to prove that there is no transesterification, but, in the existence of important transesterification T_m does provide an idea of how significant the transesterification is. Significant transesterification occurs if T_m is reduced, after heat treatment at high temperatures and/or prolonged time, by more than 20 ºC (Hamilton and Gallucci 1993). Thus, it can be said that although samples of Set 7 are shown to be transesterified, the extent of the transesterification reaction is not very significant.

Because of the low degree of transesterification in the samples of Set 7, a question arises with regard to the origin of such a phenomenon. The occurrence of transesterification and thermal scission is intimately related to the polymer blends processing conditions. During processing at elevated temperatures, hydrolytic, oxidative, and thermal degradation of PBT and of PC occurs, thermal degradation being the most important. The frictional heat that is generated during mixing of the polymer blend components in the extruder is expected to produce localised high-temperature zones. Therefore, the actual temperature of the molten polymer blend may be higher than the extruder barrel temperature. The localised high temperatures will accelerate transesterification between PBT and PC and produce PBT/PC copolymers.

The higher shear and elongational stresses, and the high temperatures, occurring in the mixing areas of twin-screw processing conditions, introduce severe polymer chain scission (Bertilsson *et al.* 1988b; Cecere *et al.* 1990) and also give the material system more energy to promote the exchange reaction between PBT and PC (Wu *et al.*1994).

The differences in transesterification level and sensitivity to thermal treatment between samples of Set 7 and samples of Set 2 are due to the use of different extrusion facilities and conditions. Thus, samples of Set 7, processed in extruder E2, are subject to a more intense mixing, more energy being delivered to the melt blend, and have a longer barrel residence time. This is because the screw of extruder E2 has a longer mixing area and because this extruder was operated at a lower throughput, than was extruder E1 (Section 2.1.). Consequently, the melt temperature and the shear and elongational stresses are greater for samples of Set 7, resulting in more acute polymer thermal scission and transesterification in these samples than in samples of Sets 1 and 2.

The pigment appears to influence the extent of transesterification. A number of reasons, direct and indirect, can be identified in attempts to understand the influence of the pigment on the transesterification degree and on the thermal scission of the polymers. Transesterification occurred in the samples with the lower pigment loadings, namely in those processed in extruder E2 (Set 7). Thereafter, the extent of formation of PBT-PC copolyester decreases with increasing pigment loading. The difference in thermal conductivity between the inorganic pigment particles and the polymers may contribute to this behaviour. At low pigment loadings, the inorganic particles, due to their greater thermal conductivity, act as heat concentrators, favouring the occurrence of transesterification and thermally induced polymer chain scission. At greater pigment loadings, the

transesterification degree and the polymer chain scission level decrease. This is because the pigment particles have the effect of lowering the local temperature.

The pigment particles can also be acting as a transesterification promoter at low pigment loadings, and as a stabilizer at higher pigment loadings, by scavenging the PBT catalyst. This idea is justified by the expected Lewis acidity of the PBT catalyst and the determined amphoteric, predominant Lewis basic, surface of the cobalt aluminate pigment (Section 3.1.3.). The pigment is located at the interphase of PC/PBT (Sections 3.2.3. to 3.2.8, 3.4.9. and 3.4.10.). Thus, increase of the degree of transesterification with increasing pigment loading is to be expected. This is because the PC and the PBT coexist and are intimately mixed at the surface of the pigment particulates. As the pigment loading increases, a dilution effect of the Ti catalyst would result in a decreased extent of transesterification. Inhibition of oxidative degradation may also occur at the greater pigment loadings.

3.2.2.2. Cooling Mode

The crystalline properties of PBT can change due to processing and blending with other polymers. During processing at elevated temperatures, hydrolytic, thermal, and oxidative degradation of PBT can occur with the formation of new carboxylic acid end-groups, along with the reduction in the molecular weight and alteration of the molecular weight distribution. These effects result in higher crystallisation rates and crystallisation degree (Bertilsson *et al.* 1988b; Pompe *et al.* 1991; Cheng *et al.* 1996; Pillin *et al.* 2001). The formation of PC-PBT copolyester results in a decrease of the molecular weight of PC and of PBT and in a reduction of the degree of crystallinity and of the crystallisation temperature (Hamilton and Gallucci 1993; Pompe *et al.* 1996; Huang and Chang 1997; Pompe 1997; Pompe and Haubler 1997; Wilkinson *et al.* 1997).

In polymer composites, additives may, intentionally or unintentionally, act as nucleating agents (e.g. $BaSO_4$, $ZnPO_4$ and Sb_2O_3), increasing the non-isothermal crystallisation temperature and reducing the size of the PBT spherulites. These alterations to the crystalline properties of PBT in the PC/PBT/IM blends have important consequences for the mechanical properties of the blends. To check if the pigment was having an effect on the crystalline phase, the non-isothermal crystallisation temperature and the enthalpy of crystallisation of PBT were determined from DSC experiments.

The experimental procedures and data handling methods were described in Section 2.4.1. In Table 3-29 are summarised the results obtained. The per cent crystallinity was calculated using the value of 142 J/g for the enthalpy of crystallisation of 100 % crystalline PBT (Kim and Burns 1989; Pompe *et al.* 1996).

Figure 3-41 summarises the variation of the crystallisation temperature, and of the difference between the crystallisation on-set and off-set temperatures, with increasing pigment loading for samples of Sets 1, 2, 3 and 7 (Section 2.1.).

Table 3-29. Values of the crystallisation on-set temperature ($T_{c,on\text{-}set}$), the crystallisation off-set temperature ($T_{c,\ off\text{-}set}$), the difference between $T_{c,on\text{-}set}$ and $T_{c,\ off\text{-}set}$ (ΔT), the crystallisation temperature (T_c) and the enthalpy of crystallisation ($-\Delta H_c$), relating to samples of Sets 1, 2, 3 and 7.

Blend sample	Pigment loading (%)	$T_{c,on\text{-}set}$ (K)	$T_{c,\ off\text{-}set}$ (K)	ΔT (K)	T_c (K)	$-\Delta H_c$ (J/g)	% Crystallinity
BX	0.00	463.1	449.5	13.6	456.2	35.1	24.7
B6	0.05	467.0	450.9	16.1	458.5	35.4	24.9
B7	0.20	465.8	453.1	12.7	459.4	35.4	24.9
B8	0.40	465.4	452.2	13.2	458.6	35.2	24.8
B9	0.60	465.9	452.9	13.0	459.1	35.5	25.0
B10	0.80	466.1	453.1	13.0	459.5	35.4	24.9
B11	1.00	465.4	453.3	12.1	459.5	35.6	25.0
PBTX	0.00	470.7	460.4	10.3	465.4	93.1	65.5
B12	0.40	471.1	462.2	8.9	466.8	93.1	65.5
B13	0.60	469.7	460.4	9.3	465.4	92.2	64.9
B14	0.80	470.5	461.3	9.2	466.2	92.1	64.9
LX	0.00	465.4	451.0	14.4	457.2	36.1	25.4
L7	0.01	466.8	447.2	19.7	456.3	32.5	22.9
L8	0.10	465.6	444.3	21.4	456.5	34.6	24.4
L9	0.30	466.5	451.1	15.4	458.0	35.7	25.1
L10	1.00	467.0	454.2	12.8	459.9	36.1	25.4
B3	0.30	466.0	455.5	10.5	460.6	33.2	23.4
B4	0.10	466.1	454.4	11.7	459.8	33.8	23.8
B5	0.50	466.2	455.1	11.1	460.5	33.4	23.5

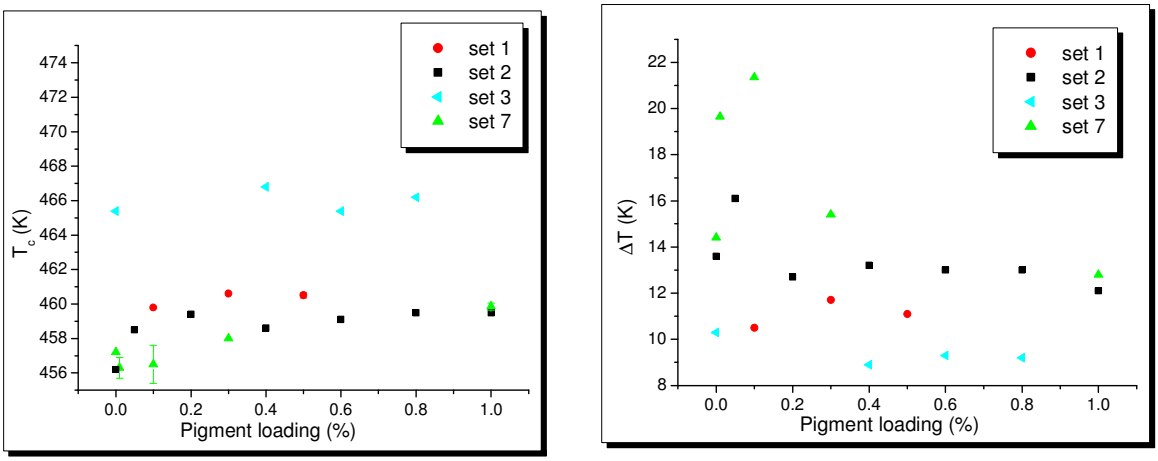

Figure 3-41. Non-isothermal crystallisation temperature, and ΔT, *versus* C. I. Pigment Blue 28 loading for samples of the PC/PBT/IM blends represented by Sets 1, 2, 3 and 7.

In Figure 3-42 are presented the values of the enthalpy of crystallisation, and of the crystallinity degree, as a function of C. I. Pigment Blue 28 loading for samples of Sets 1, 2, 3 and 7.

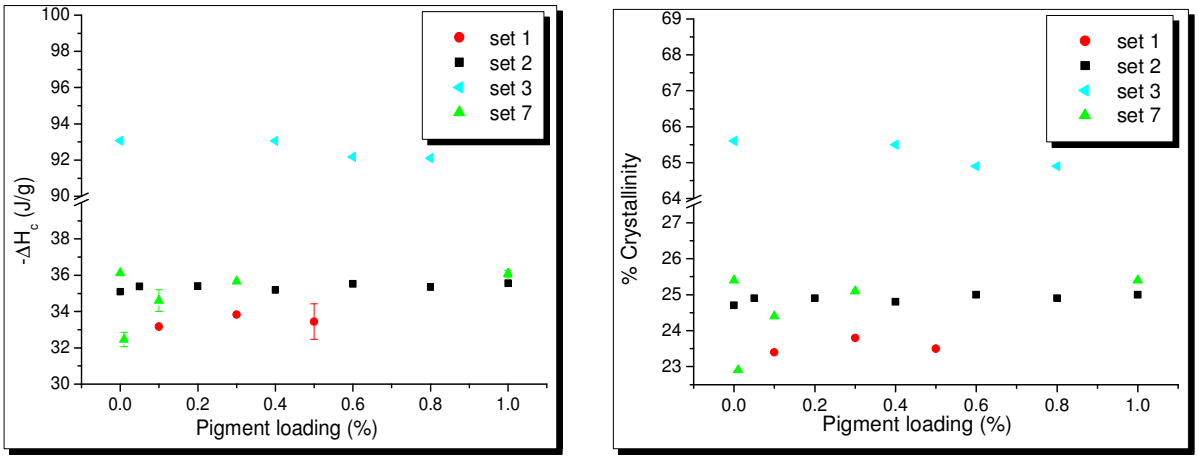

Figure 3-42. Enthalpy of crystallisation, and degree of crystallinity, *versus* C. I. Pigment Blue 28 loading for samples of the pigmented PC/PBT/IM blends represented by Sets 1, 2, 3 and 7.

Figures 3-41 and 3-42 show that the pigment has an effect on the PBT crystalline properties.

For the samples of Set 7, it can be said that the temperature of crystallisation follows the same trend, with varying pigment loading, as that of the average molecular weight of the higher fraction of the molecular weight distribution of PBT (Figure 3-38, Section 3.2.1.). The lower the $\bar{M}_w$ of PBT, the lower is the temperature of crystallisation. The enthalpy of crystallisation behaviour follows a trend that is similar to that of the polydispersity of PBT. Thus, the lower the polydispersity of PBT, the lower is the degree of crystallinity. ΔT follows a pattern similar to that of T_c. The greater the value of ΔT, the slower is the crystallisation (Joshi *et al.* 1991). The greater the non-isothermal crystallisation temperature, the lower is the crystallisation activation energy. Thus, for the lower pigment loadings, the rate of crystallisation and the degree of crystallinity are lower, and the crystallisation activation energy is higher, than that of the unpigmented blend, and than those of samples with higher pigment loadings.

The results obtained are in line with the proven occurrence of transesterification in these samples (Section 3.2.2.2.), and with the consequences thereof to the molecular weights of PC and of PBT (Section 3.2.1.). The decrease in the molecular weight of PBT, due to transesterification reactions, and due to thermal degradation of the polymers, does not contribute significantly to an increase of T_c and of $-\Delta H_c$. This observation contradicts expectation but is in line with reports in the literature for these blends (Bertilsson *et al.* 1988b). It has been shown by Hopfe *et al.* (1997) that if the molecular chain is shorter than the critical length necessary for crystallisability, the PBT

crystallinity decreases. Also, according to Pompe (1997), as the transesterification reaction proceeds, the molecular chain length diminishes and, consequently, the crystallisable content of PBT decreases. These factors will result in a decrease of the degree of crystallinity at the lower polymer loadings. The reduction of the T_c and ΔH_c of the PBT-rich phase may also have the contribution of increased miscibility of PC and PBT due to lower molecular weights of these polymers.

Figure 3-41 shows that, at the higher pigment loadings, cobalt aluminate lowers the crystallisation activation energy and increases the rate of crystallisation of PBT, when compared to the unpigmented blend.

Figure 3-42 shows that the degree of crystallinity of PBT increases with increasing pigment loading but never reaches the value for the unpigmented blend. This is in line with the transesterification level in these samples (Figure 3-40).

The lower degree of crystallinity at the lower pigment loadings may be influenced by the use of two grades of PBT in the blend (PBT 195 and PBT 315). These differ in their average molecular weight and in their carboxyl end-group and hydroxyl end-group concentrations (Table 2-3, Section 2.1.). To assess the influence of these differences in the crystallisation properties of the PBT phase, a series of PBT 915 plus PBT 315 granulate samples was prepared with increasing amounts of PBT 315. The values determined for the T_c and the $-\Delta H_c$ of these samples are presented in Figure 3-43.

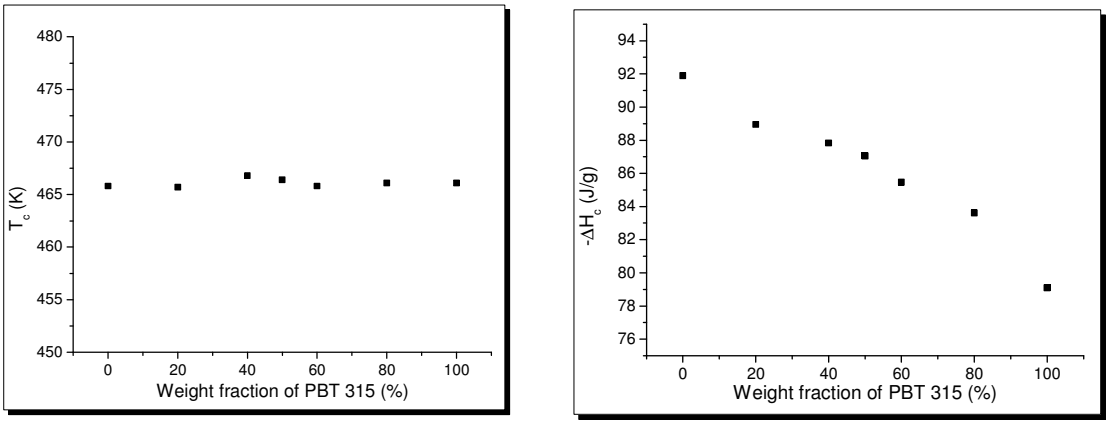

Figure 3-43. Non-isothermal crystallisation temperature and enthalpy of crystallisation *versus* PBT 315 loading in samples of PBT granulate.

Figure 3-43 shows that the non-isothermal crystallisation temperature is not significantly influenced by the weight fraction of PBT 315 in the sample. Conversely, the extent of crystallisation decreases with increasing amount of PBT 315 in the PBT granulate sample. The crystallinity degree of PBT 195 is 65 % and that of PBT 315 is 56 % (determined using the value of 142 J/g for the ΔH_c of 100 % crystalline PBT). Therefore, the behaviour observed for samples of

Set 7 can be interpreted on the basis that the lower the molecular weight of the PBT in the blend, the more miscible PBT 315 and PBT 195 are. As a result, the PBT phase in the blend will be characterised by a lower degree of crystallinity. This is indicated in the value of the polydispersity of PBT (Figure 3-38, Section 3.2.1.) as the more miscible the PBT 315 and the PBT 195 are, the lower is the polydispersity of the PBT. On the other hand, the greater the pigment loading, the more PBT 315 is adsorbed at its surface, and, thus, the greater is the relative amount of PBT 195 in the PBT phase, resulting in a greater degree of crystallinity.

The results presented in Figure 3-43 support the analysis of K_a and K_b for these grades of PBT and the predictions made in terms of differences in the degree of crystallinity between PBT 195 and PBT 315 (Section 3.1.7.3.). In contrast, the expectation of greater T_c for PBT 195 is not confirmed in Figure 3-43. Thus, it can be concluded that the differences in the end-group type and concentration, and in the average molecular weight, between PBT 195 and PBT 315, do not cause a decrease in the crystallisation activation energy.

Figures 3-41 and 3-42 show that the values of $-\Delta H_c$ of the PBT, in the samples that mimic the PBT phase (Set 3) in the PC/PBT/IM blends, are close to that of the PBT 195. This agrees with expectation from the 82/18 % (w/w) proportion of PBT 195 and PBT 315 in samples of Set 3 (and in the blend samples). With respect to the influence of cobalt aluminate on the physical properties of samples of Set 3, it can be seen that, for the pigment loading range used, the degree of crystallinity remains unchanged and equal to 65 %. The non-isothermal crystallisation temperature seems to increase, although slightly, and the rate of crystallisation (related to ΔT) decreases, although slightly as well, with the introduction of C. I. Pigment Blue 28 into the composition. Thus, it can be concluded that, for the pigment loading analysed, the increase in the pigment loading leads to a slight decrease of the crystallisation activation energy, and slight increase of the crystallisation rate, of the PBT-based samples.

For the samples of Set 2, Figures 3-41 and 3-42 show that the introduction of C. I. Pigment Blue 28 leads to an increase of the crystallisation temperature, this increasing slightly with increasing pigment loading. The degree of crystallinity remains unchanged with the introduction of cobalt aluminate into the composition of the blends, and with increasing pigment loading.

The value of ΔT decreases with increasing pigment loading with the exception of the sample with the lowest pigment loading (batch B6). From the above observations, and bearing in mind that samples of Set 2 are not significantly transesterified, it can be concluded that C. I. Pigment Blue 28 decreases the crystallization activation energy and increases the rate of crystallisation, without altering significantly the degree of crystallinity of PBT in the blend samples of Set 2. Bearing in mind the proposed origins of transesterification in the pigmented blends, the exception of sample B6 in terms of the trend observed for ΔT is thought to be due to a small transesterification extent. None-the-less, this extent of transesterification is greater than those of the remaining samples of

this set. Samples of Set 1 follow a trend that is analogous to that of samples from Set 2, concurring with expectation, as these two set of samples were extruded using the same extrusion facilities.

Comparison of samples of Set 2 with those of Set 7 shows that the degree of crystallinity behaviour is more consistent for the blends that were processed in extruder E1 (Set 2), at the lower pigment loadings. This has been interpreted in terms of the greater degree of transesterification, and lower average molecular weight of PC and of PBT for samples of Set 7. Moreover, as a consequence of this greater transesterification, the crystallisation activation energy is lower and the rate of crystallisation and the degree of crystallinity are greater, for the blends processed in extruder E1, at the lower pigment loadings.

The crystallinity of the PBT phase is reduced from 65 % in the PBT samples to 25 % in the blend samples, in good agreement with the values of 26 to 38 % found in literature for these blends (Hanrahan *et al.* 1985; Cheng *et al.* 1996). This reduction in degree of crystallinity is due to the fact that the chain mobility of PBT is reduced when PBT is mixed with PC. In this, the crystallisation rate also slows down (Bennekom *et al.* 1997a).

From the DSC studies, it can be concluded that the pigment has an effect on the crystallisation properties of the PBT in the blend samples. This effect has both indirect and direct contributions. The influence of C. I. Pigment Blue 28 on the transesterification reaction, and consequences thereof to the crystallisation properties, accounts for the indirect effects. Increasing transesterification results in a progressive reduction in the melting and crystallisation temperatures and in the degree of crystallinity. The nucleating effect of C. I. Pigment Blue 28, although small, accounts for the decreased crystallisation activation energy and the increased rate of crystallisation. The degree of crystallinity is not directly affected by the presence of C. I. Pigment Blue 28.

Thus, the pigment acts as a nucleating agent promoting crystallisation of PBT at its surface and, hence, leads to a composite that has higher T_c and lower ΔT values. The influence of the pigment upon T_c and ΔT strongly indicates that there is direct contact between the pigment and the PBT-rich phase in the PC/PBT/IM blends, as predicted from the IGC studies.

In the process of polymer crystallisation, two steps are usually required: formation of nuclei that are thermodynamically stable after they reach a critical size, and the growth of these nuclei to form spherulites. C. I. Pigment Blue 28 favours the formation of nuclei at higher temperatures. The rate of crystallisation is dependent on nucleation and on the growth of the nuclei (influenced by the molecular weight of the crystallising polymer). The effect of C. I. Pigment Blue 28 on the crystallisation rate is a consequence of the lower crystallisation activation energy caused by this pigment. Most inorganic particulates strongly affect the crystallisation of polymers in both primary nucleation and growth steps (Galeski 1990). It is, therefore, to be expected that the effect the pigment has on the rate of crystallisation may be favoured growth step.

The results of the present study are supported by findings in the literature. Pillin *et al.* (2001) studied the influence of several organic pigments (C. I. pigments Blue 16, Blue 60, Blue 15:3, Red 178, Yellow 138, Yellow 183 and Green 7), inorganic pigments (C. I pigments Yellow 53 and Blue 28) and fillers (talc and mica) on the crystallisation properties of PBT. The polymer, dried in a ventilated oven, was mixed with 0.1 % or 0.2 % of pigments and 0.1-1 % of talc or mica (w/w), in an opened mixer. The crystallisation kinetics was studied both isothermally and non-isothermally. All samples were first heated to 250 ºC for 5 minutes to erase the previous thermal history. The values of T_c and of T_m were measured from the respective peak maximum, and were determined with a standard deviation of ±0.5 ºC. Non-isothermal crystallisation and melting temperatures were determined in experiments at ±20 ºC/min heating/cooling rates.

An increase of the non-isothermal crystallisation temperature was observed for all the pigments and fillers used. The virgin PBT crystallised (non-isothermal crystallisation) at 185.6 ºC. The C. I. Pigment Green 7 (phthalocyanine derivative) had the greater influence on the T_c of PBT, along with the talc filler. The inorganic pigments (C. I. Pigment Yellow 53 and C. I. Pigment Blue 28) presented the smaller influence on PBT crystallisation properties. Nevertheless, C. I. Pigment Blue 28 is reported to increase slightly (T_c of approximately 188.1 ºC and, thus, an increase of around 2.5 ºC) the non-isothermal crystallisation temperature of PBT, at a pigment loading of 0.1 %w/w.

3.2.3. Dynamic Mechanical Thermal Analysis

The major factors that influence the response of polymeric systems to applied stress are:

a) The presence of inorganic particles (fillers, pigments);

b) The degree of crystallinity in semi-crystalline polymers;

c) The molecular weights of the species involved;

d) The miscibility for polymer blends, and

e) The presence of other additives/species such as elastomers and organic pigments.

In semicrystalline polymers, the crystals act as physical crosslinks and also as a filler. Small amounts of a suitable additive (< 1 %) are known to increase significantly the modulus of the blend. In complex multi-component polymeric systems it is not an easy task, in most cases, to distinguish the contribution of each of the factors ((a) to e)) to the viscoelastic properties of the system.

Analysis of the DMTA results involves the analysis of the loss tangent (qualitatively and quantitatively) and of the loss modulus (qualitatively and also quantitatively for those samples where the dimensions of the test samples do not vary significantly). The analysis of the storage modulus indicates the behaviour observed for the loss modulus and for the loss tangent.

The values of either the damping peak (tan δ) maximum, or shoulder values where the peak is indistinct, are taken as the T_g for the blend or for its individual components. For the broad peaks, the T_g values are estimates only (Cheng *et al.* 1996).

The extent of miscibility has been assessed by analysing the presence of two damping peaks located between the peaks of the pure components, indicating the existence of two amorphous mixed phases (Wahrmund *et al.* 1978; Bertilsson *et al.* 1988b; Bennekom *et al.* 1997a). The significant effects on the tan δ and on the dynamic modulus are seen in the α-transition because this change corresponds to the molecular micro-Brownian motions of long chain segments in the polymer structure rather than in motions in the side-groups, as is the case of the β-transition and the γ-transition. The glass transition phenomenon which occurs at the α-transition affects the peak height, the temperature of the α peak maximum, and the on-set of the transition.

Interpretations of the behaviour of the loss modulus and of the storage modulus for different samples must be undertaken with care as small changes in the geometry of the test samples can lead to differences in the value of these parameters. Nevertheless, the analysis of both parameters, side by side, in particular the shape of the loss modulus, provides important information relating to the viscous response of the system to the applied stress. In the cases were the dimensions of the test samples do not vary significantly, a quantitative comparison can be made of the loss modulus and of the storage modulus. The loss tangent values do not depend on the dimensions of the test samples. Thus, the loss tangent is the most commonly analysed parameter.

Comparison of the loss modulus for samples of Set 3 (that mimic the PBT-rich phase), of Set 4 (that mimic the PC-rich phase) and of Sets 1, 2 and 7 (blend samples) gives a good example of the care that must be taken when analysing loss modulus behaviour. The thickness of samples of the PC-based samples (Set 4) is the double of that of the remaining sets of samples (Section 2.4.3.). This is clearly indicated in the value of the loss modulus, and in the value of the storage modulus (Figure 3-44).

The following discussion will bear in mind the aforementioned points. It should be mentioned that the DMTA technique is significantly more efficient in detecting subtle differences in miscibility than is the DSC technique (Tattum *et al.* 2000).

The following figures relate to the variation of the storage modulus, the loss modulus and the loss tangent with temperature, for samples of Sets 1, 2, 3, 4 and 7. In Figure 3-44 are compared the results obtained for the unpigmented blend (BX), the unpigmented PBT-based sample (PBTX), and the unpigmented PC-based sample (PCX).

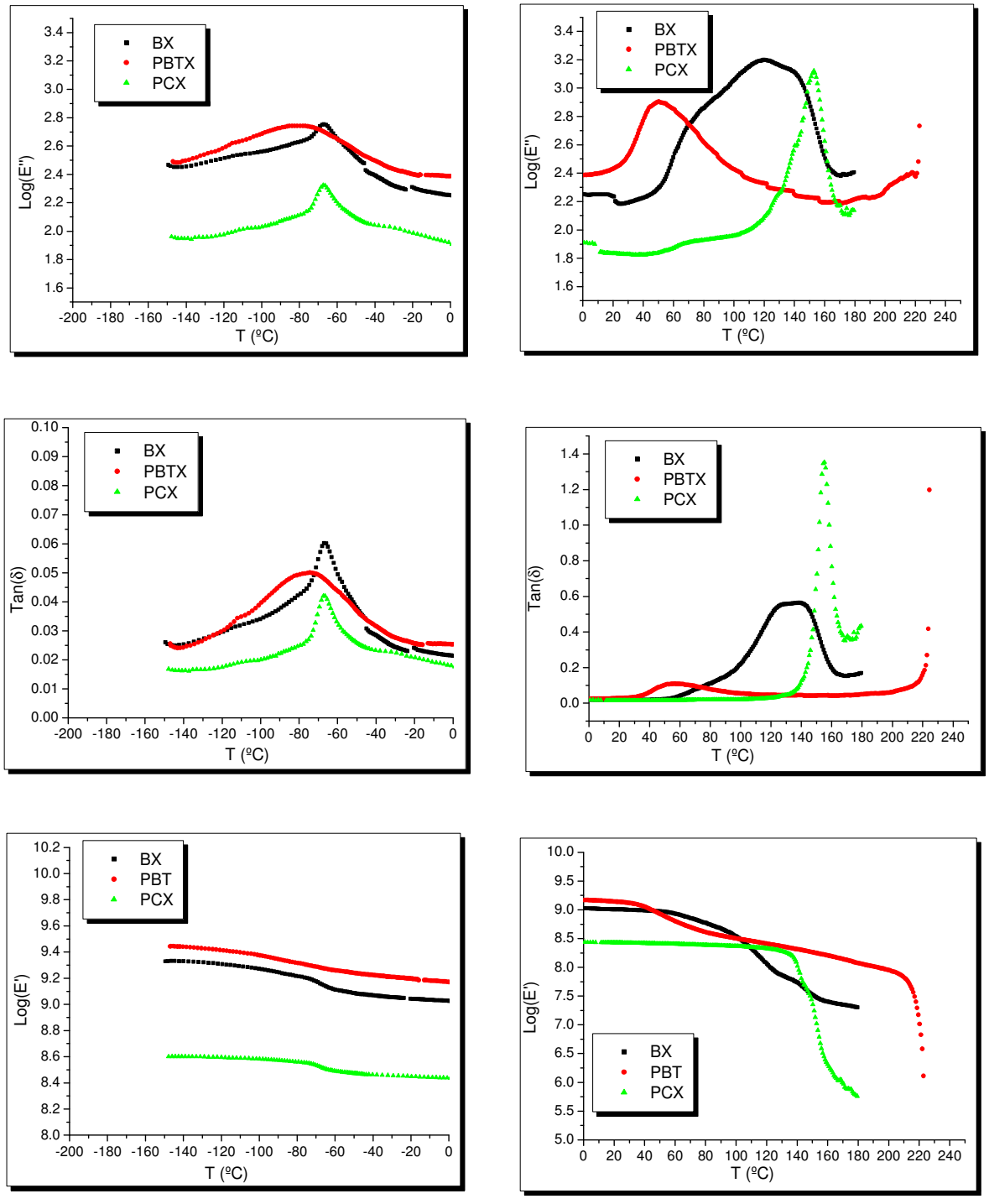

Figure 3-44. Loss modulus, loss tangent and storage modulus *versus* temperature, for the blend sample and samples that mimic the PBT-rich phase and the PC-rich phase.

From the loss tangent curve for samples PBTX and PCX, the T_g of the PBT is identified as being 57 ºC, and that of PC as being 155 ºC. In the loss modulus plot for PCX, a small peak can be identified at approximately 60-90 ºC, which is attributed to a β transition. Moreover, a small

shoulder is seen at around 120 ºC being identified as the T_g of the PMMA (MBS rubber shell component). For the viscoelastic response at low temperatures the following characteristic peaks, related to second order transitions phenomena, can be identified in the plots presented in Figure 3-44. For the PBT sample, a peak is identified at -74 ºC, as is a significantly smaller peak at -112 ºC. For the PC sample, a peak can be clearly identified at -66 ºC, and a small peak at -108 ºC. These values agree with those reported in the literature for PC (Birley and Chen 1984; Foreman and Blaine 1997) and for PBT (Birley and Chen 1984), and correspond to β relaxation processes.

It is clear (Figure 3-44) that the response of the blend sample to the applied stress is intermediate between that of the samples that mimic the PBT-rich phase and the PC-rich phase. Analysis of the loss modulus is more informative in relation to the existence of distinct characteristic regions than is the analysis of the loss tangent. Thus, for the blend sample, three regions can be identified:

a) A region corresponding to the PBT-rich phase, identified as a shoulder at around 85 ºC;

b) A region concerning the PC-rich phase, with its peak maximum at 139 ºC, and

c) A region where PC and PBT coexist, that is the PC/PBT interphase region, with its maximum at 127 ºC.

The existence of these three regions can also be seen in the plot for the loss tangent but in a less distinct manner than for the loss modulus. The temperatures of the characteristic transition peaks that were obtained by analysing the loss modulus are slightly different than those obtained from the loss tangent plot. In the literature, the values obtained from loss tangent plots are most commonly reported (Cheng *et al.* 1996). Nevertheless, the existence of the aforementioned three characteristic areas in the loss tangent plots for blend samples is confirmed at the temperatures of 140 ºC, 120 ºC and 80 ºC, respectively. In the loss modulus plot for sample PCX, an additional, small, peak is detected at 72 ºC, which is not clear in the plot obtained for sample BX. As mentioned previously, this peak suggests β-relaxation of the PC chains, whose expression (from the DMTA point of view) is reduced when this polymer is blended with PBT.

In the unpigmented blend sample (BX), the T_g of the PC is shifted towards that of the PBT and vice-versa. This is in line with the observation that the PC and the PBT are partially miscible. The different T_g values of the blends, relating to those of the pure components, indicate the presence of both components in each phase of the blend (Sanchez *et al.* 1993; Scherbakoff and Ishida 1997). The change in the T_g of the PBT-rich phase in comparison to the pure PBT is greater than is the change in the T_g of the PC in comparison to the pure PC. Thus, PBT is more miscible in the PC than the PC is in the PBT. These results confirm studies reported in the literature (Kim and Burns 1989; Pompe and Haubler 1997).

The response of the system to applied stress in the temperature range between -150 ºC and 0 ºC is also a combination of the plots of the PBT-based sample and the PC-based sample. A peak

can be identified at -67 ºC, a shoulder in the region of -100 ºC to -75 ºC, and a small peak at -110 ºC. These relaxation processes correlate with β relaxation phenomena of PC and PBT, which occur at almost the same temperature as that of the T_g of the MBS rubber (approximately -70 ºC) (Wu *et al.* 1992 and 1993). β-relaxation phenomena play an important role in PC/PBT/IM blends as they are related to the impact resistance of these blends at room temperature, due to effective absorption of impact energy by side groups in the polymeric species. It is interesting to note that the β-relaxation peak is clearer in the main relaxation peak of the loss modulus plot rather than in the storage modulus plot. This indicates that the β-relaxation is mainly related to the viscous properties of the system and, thus, to the ability of the blend to dissipate energy rather than to its ability to store energy. This inference supports interpretations that are based on second order transitions and the impact energy absorption capability of polymeric systems.

The observed partial miscibility of PC and PBT is supported by the Lewis acid/Lewis base interaction potential between the major components of the system, evaluated by means of inverse gas chromatography (Santos *et al.* 2002a), Section 3.1.8.

Evidence of partial miscibility in PC/PBT blends, as assessed by DMTA, is reported for this type of blend (Pompe *et al.* 1991; Tattum *et al.* 2000). In blends that are stabilised against transesterification, good miscibility is commonly attributed to the degree of crystallinity and/or to the size of the crystallites. The miscibility is reported to increase with decreasing degree of crystallinity and, for the same degree of crystallinity, with decreasing crystallite size (Pompe *et al.* 1991).

The influence of C. I. Pigment Blue 28 on the viscoelastic properties of the samples that mimic the PBT-rich phase and the PC-rich phase, PBTX and PCX, respectively, has been assessed and is illustrated in Figure 3-45.

The effect of the pigment on the PBT-based samples is shown in Figure 3-45. Thus, C. I. Pigment Blue 28 decreases the viscous response of this polymer, in the temperature interval -50 ºC to 50 ºC, between the major transitions temperatures. It does not, however, alter the temperature at which these characteristic transitions occur. As far as the PC-based samples are concerned, the viscoelastic behaviour is not significantly influenced by C. I. Pigment Blue 28, although a small shift of the characteristic peaks maxima to lower temperatures occurs.

The effects of increasing pigment loading on the viscoelastic properties of PC/PBT/IM blends processed in extruder E1 (Set 2) are illustrated in Figure 3-46. Measurement temperatures below zero ºC have not been included as no significant differences could be detected with increasing pigment loading. The same applies to samples of Set 7.

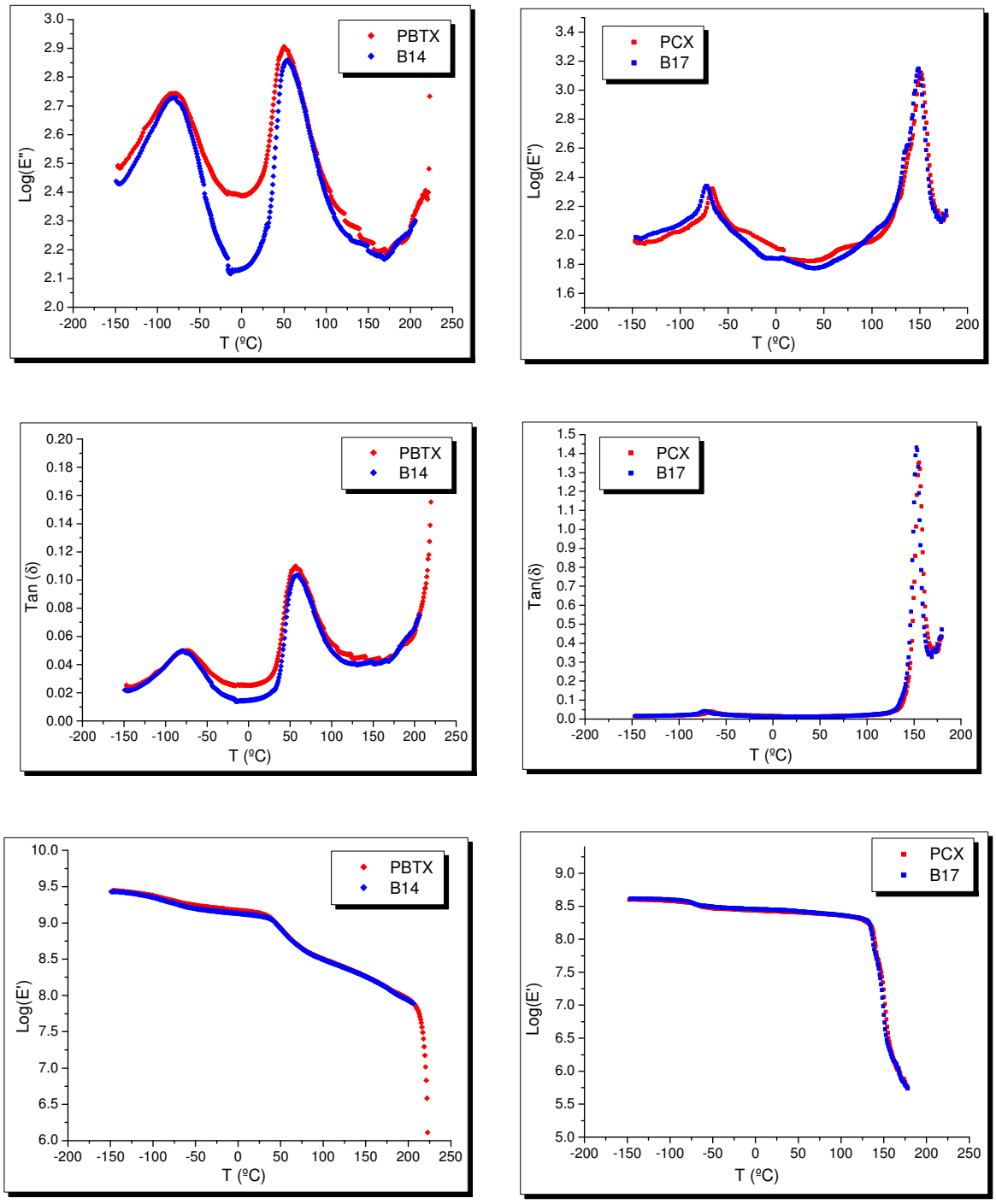

Figure 3-45. Loss modulus, loss tangent and storage modulus *versus* temperature, for the samples that mimic the PBT-rich phase and the PC-rich phase, PBTX and PCX, respectively.

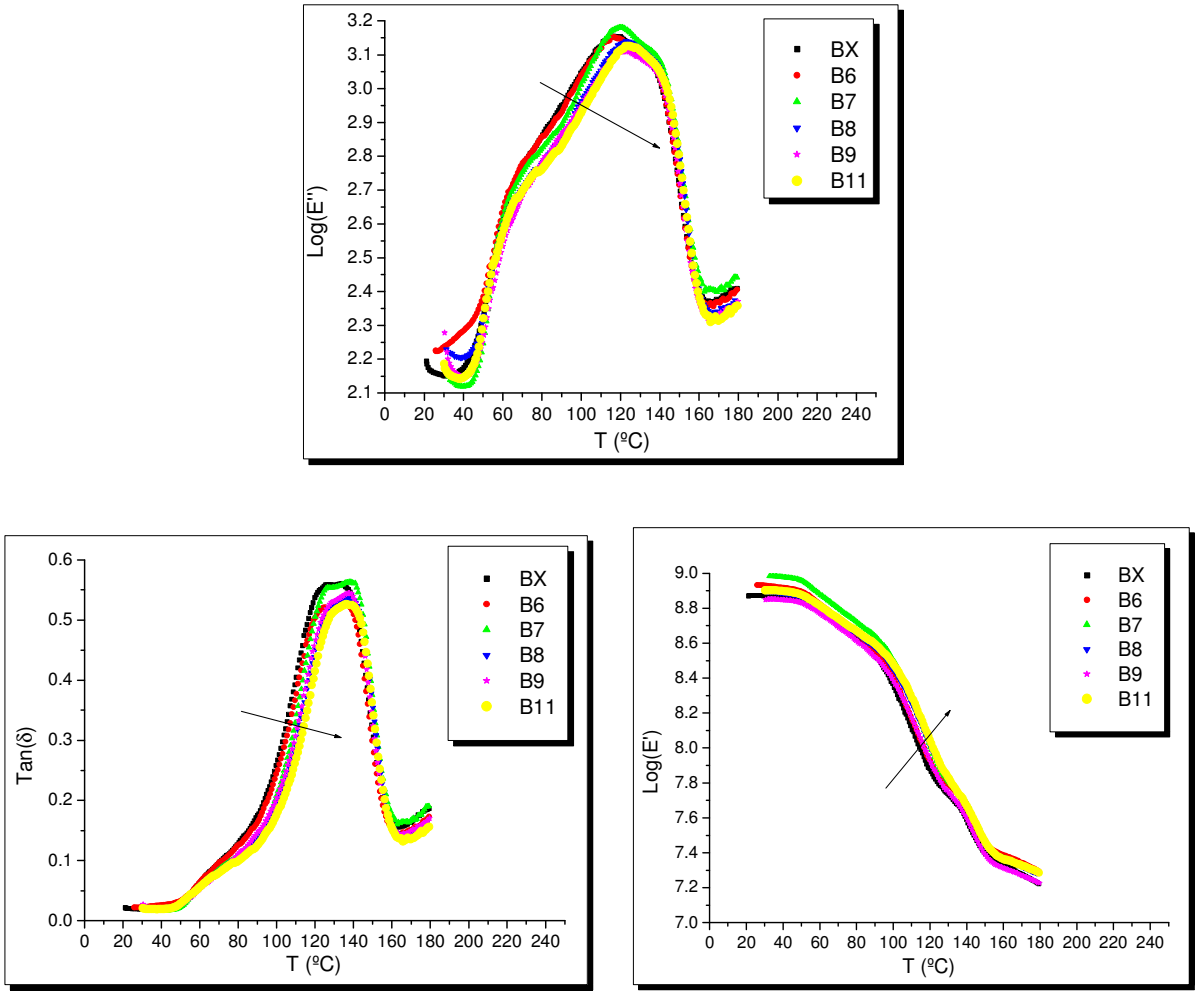

Figure 3-46. Loss modulus, loss tangent and storage modulus *versus* temperature, for samples of increasing pigment loading processed using extruder E1 (Set 2).

For the samples of Set 2, Figure 3-46 shows that there is an increase in the elastic response of the system with increasing pigment loading, mainly in the region concerning the PC/PBT interphase. This indicates that there is strong interaction between the pigment and the PC and the PBT, at the PC/PBT interphase, as predicted from the IGC studies. Increased miscibility of the PC and of the PBT at the PC/PBT interphase is thought to occur. This is more evident for samples of Set 7 (Figure 3-47), due to the lower molecular weight of the PC, and especially of the PBT, in samples of Set 7, and also due to existence of lower amorphous PBT content in samples of Set 2, mainly at the lower pigment loadings (Figure 3-38, Section 3.2.1.). Further discussion on increased miscibility of PC and PBT with increasing pigment loading is presented alongside the interpretation of the DMTA results for samples of Set 7 (Figure 3-47).

Although Figure 3-46 shows that there is no significant change in the T_g value the PBT-rich phase, there is evidence of phase separation with increasing pigment loading as the T_g of the PC/PBT interphase shifts towards that of the PC-rich phase, and the PBT-rich phase peak becomes more distinct as the pigment loading is increased. This is particularly clear in the plot of the loss modulus. Also, the T_g of the PC-rich phase is slightly increased with increasing pigment loading. The occurrence of phase separation is due to the increase of the molecular weight of the PC with increasing pigment loading, and of the PBT at the greater pigment loadings (Figure 3-38, Section 3.2.1.).

The height of the PC-rich phase peak in the loss tangent plot decreases with the introduction of the pigment but does not vary significantly with increasing pigment loading. This observation is in line with the trend observed for the PBT crystallinity in these blends (Figure 3-42, Section 3.2.2.2.).

Bearing in mind the definition of loss tangent, the lower the peak height, the greater is the energy that is absorbed elastically, in relation to the viscous response. The introduction of pigment leads to a decrease of the viscous response of the blend due to greater restriction in the motion of the polymers molecular chains. Thus, the stiffness and the hardness of the samples increase with the pigment loading. This finding is in accord with the results from the tensile tests where it was observed that the tensile modulus increases with increasing pigment loading (Section 3.2.8.), due to the presence of the rigid inorganic pigment particles, increased molecular weight of PC, and due to the adhesion of the PBT and of the PC to the surface of the pigment particles.

It should also be noted that the value of the loss tangent is always lower than 1, which means that the elastic response dominates over the viscous response, for the strain and frequency values used.

In general, the presence of an inorganic pigment results in an increase in the storage modulus because of the reinforcing effect of a relatively rigid inorganic inclusion (Chacko *et al.* 1982). The storage modulus also shows effects of the matrix-filler interactions (Boluk and Schreiber 1986). For samples that are characterised by a similar molecular weight and molecular weight distribution, the higher the storage modulus at 110 ºC the higher is the PBT crystallinity (Wilkinson *et al.* 1995). Figure 3-46 shows that the trend of the storage modulus with increasing pigment loading is a consequence of the presence of the inorganic pigment particulates but there is also a contribution from the degree of crystallinity. The degree of crystallinity has been shown to increase slightly with the inclusion of the pigment into the composition but not to change significantly with increasing pigment loading (Section 3.2.2.2.). This is the trend observed in Figure 3-46 for the storage modulus of the blends.

In Figure 3-47 are presented the DMTA results obtained for samples that were processed using extruder E2 (Set 7): C. I. Pigment Blue 28 pigmented PC/PBT/IM blends of increasing pigment loading.

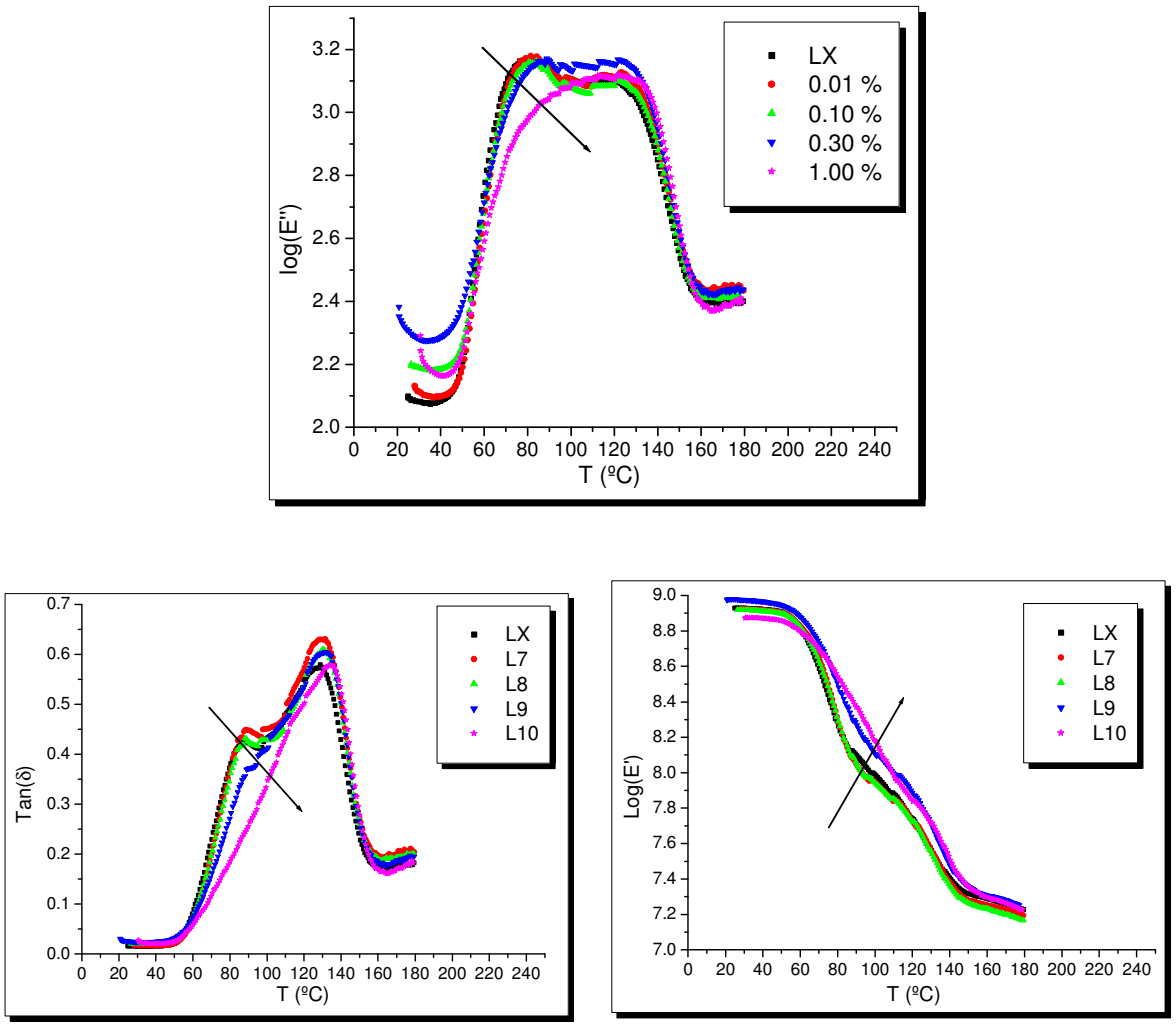

Figure 3-47. Loss modulus, loss tangent and storage modulus *versus* temperature, for the samples of increasing pigment loading processed using extruder E2 (Set 7).

One observation that can be made concerning the DMTA of blends that were extruded using extruder E2 is that, particularly for the loss modulus behaviour with increasing pigment loading, only two characteristic regions can be distinguished in the plots (Figure 3-47). These are the PBT-rich phase and the PC-rich phase. For samples of Set 2, a third region can be identified as being clearly related to the PC/PBT interphase. The fact that for samples of Set 7 the PC/PBT region cannot be identified as a peak in between that of the PC-rich phase and that of the PBT-rich phase, stems from the significantly lower molecular weights of the PBT and the PC, and from the lower

degree of crystallinity (at the lower pigment loadings), in these samples. Consequently, the amorphous phase and, in particular, the amorphous PBT phase, have a greater influence on the viscous response of the blend for samples of Set 7, and the peak corresponding to the PC/PBT interphase is not clearly separated from that of the PBT-rich phase. Also, the miscibility of PC and PBT is greater for samples of Set 7, due to the lower molecular weights of the polymers in these blend samples. The differences in the viscoelastic properties of samples of Set 2 and of Set 7 are clear in Figure 3-48, and are further discussed below.

Figure 3-47 shows that the elastic response of the amorphous PBT-rich region (along with that of the amorphous PC/PBT region) (samples of Set 7) is very significantly diminished with increasing pigment loading. Also, the T_g of the PBT-rich phase increases with increasing pigment loading. These facts indicate that the pigment particles are present in the interphase regions (were amorphous PBT and PC coexist), influencing the amorphous PBT-rich phase and the amorphous PC/PBT interphase. Furthermore, the observations are indicative of strong polymer-pigment interactions, as predicted from the IGC studies. The fact that the pigment does not influence very significantly the viscoelastic properties of the individual phases (Figure 3-44), but does influence viscoelastic properties of the PC/PBT/IM blends and the interaction between PC and PBT, further confirms the preferential location of the pigment particles at the PC/PBT interphase.

The effect of small amounts of inorganic particulates on the T_g is known to be slight. Nevertheless, increases in the glass transition temperature as a function of the filler content have been reported for composites that contain a wide variety of polymers and fillers. Such increases in T_g are attributed to polymer-filler interactions. The factors influencing the polymer-filler interactions include the interfacial forces between the filler and the matrix, the orientation of the polymer chains in the immediate vicinity of the filler surface, the formation of an interface, nucleation of crystallisation, and other physicochemical phenomena (Usaka and Shibayama 1978; Saini *et al.* 1984; Kim *et al.* 1991).

Good inorganic particulates-matrix adhesion results, in most cases, in a shift of T_g to higher temperatures and in a decrease of the tan δ peak height, as a combined result of the high surface area in inorganic particulates and of strong filler-polymer interactions (Saini *et al.* 1984; Boluk and Schreiber 1986; Malik *et al.* 1988; Scherbakoff and Ishida 1997). As the pigment loading is increased the more PC and the more amorphous PBT are adsorbed at the surface of the pigment particles. Therefore, bearing in mind the high surface area available for adsorption on the pigments, the PC/PBT interphase area is increased and so is the miscibility of PC and PBT. This phenomenon can clearly be seen in Figure 3-47 since the peak corresponding to the PBT-rich phase shifts towards the PC-rich phase with increasing pigment loading. In addition, the peak height decreases. It is also clear in Figure 3-47 that the damping curves become increasingly convoluted due to greater interfacial mixing as the level of miscibility increases with increasing pigment loading.

The occurrence of improved miscibility of PC and of PBT is further supported by the fact that, if the change in the PBT peak position and shape were related to the increasing phase separation (which is due to increased molecular weight of the polymers, mainly of the PC, and is clear in TEM imaging, Figure 3-64, Section 3.2.10.), the peak of the PBT-rich phase would move towards lower temperatures and would be more distinct as is the case of samples of Set 2 (Figure 3-46, particularly clear in the loss tangent plot).

The degree of crystallinity does not play a role in the phase separation, and in the PC/PBT miscibility at the interphase, as the extent of crystallisation of the unpigmented blend is greater than that of the pigmented samples (Table 3-29). The extent of the transesterification reactions decreases as the pigment loading is increased above 0.1 % (w/w) (Figure 3-40) and the miscibility of PC and PBT is still seen to improve, in the DMTA plots, beyond that pigment loading. The amorphous PBT peak height does not follow a trend that is analogous to that of the molecular weight of PBT or to that of the molecular weight of PC. These facts further support the idea that the increased miscibility is not due to a greater transesterification reaction extent and is not influenced by the degree of crystallinity or by the PBT and PC molecular weights, but is due to the presence of the pigment particles at the PC/PBT interphase.

For the lowest pigment loadings, the viscous response of the blend increases, in line with the decrease in the PBT crystallinity and decrease in the weight-average molecular weight of PBT. However, for the sample with the lowest pigment loading, the miscibility of the PBT and the PC in the PC-rich phase is not seen (in Figure 3-47) to be significantly improved. Although the occurrence of transesterification leads to improved miscibility of the PBT and the PC, the presence of a greater content of amorphous PBT (indicated in the greater viscous response) will contribute to a decrease of the PBT-rich phase peak maximum temperature (T_g). Thus, the presence of PBT-PC copolyester and of a greater amount of amorphous PBT have opposite effects with regard to the shape and position of the damping peak for the PBT-rich phase. This is thought to be the major reason why the damping peak curve for the sample with the lower pigment loading (L7) does not show clearly improved miscibility.

Also, the effect of improved miscibility due to the presence of the pigment particles loses importance for low loadings because the interactions favouring miscibility take place only in the surface layer at the interface with the pigment, whereas the greatest part of the blends stays in an unperturbed state. The absence of clearly improved miscibility of PBT and PC for the lowest pigment loadings is, furthermore, in line with the TEM image that is shown in Figure 3-61 (Section 3.2.10.). It can be concluded that the greater transesterification degree for samples L7 and L8, compared to that of sample LX (Section 3.2.2.1.), does not lead to an increase in miscibility of the PBT with the PC that is detectable by either DMTA or by TEM.

Due to the improved miscibility, it would be expected that the PC T_g peak maximum, of the PC-rich phase, should shift towards the PBT-rich peak side with increasing pigment loading. Such

a shift is not seen in Figure 3-47. Analogous results have been reported in the literature for these blends (Tjong and Meng 1999). In the present study, two factors are thought to be causing this lack of shift:

a) The greater contribution of the PC phase to the viscous response of the system, when compared to the contribution of the PBT amorphous phase, and

b) The increasing phase separation (less amorphous PBT content in the PC-rich phase) due to the increasing molecular weight of PC with increasing pigment loading, which leads to a shift of the PC T_g to higher temperatures.

Cheng *et al.* (cited by Pompe (Pompe 1997)) found that the T_g of the PC-rich phase is lower in blends that have a lower molecular weight of PC than in blends with a higher molecular weight. The investigated blend states were completely crystallised. The authors concluded that the compatibility would be better if the molecular weight of the PC was smaller. In fact, in the present study, a small shift of the T_g of the PC-rich phase to higher temperatures can be observed in the plot of the loss tangent (Figure 3-47) due to the increasing molecular weight of PC with increasing pigment loading (Figure 3-38, Section 3.2.1.).

Other factors are thought to contribute to the shift of the PC-rich phase T_g to higher temperatures. These include the finding that the PC-rich phase is less sensitive to the total weight fraction of PBT (Cheng *et al.* 1996), with contributions from the existence of a maximum content of PBT in this phase (Sanchez *et al.* 1993). Moreover, the greater change in the T_g of the PBT-rich phase is based on the higher solubility of PBT in PC than of PC in PBT (discussed in previous paragraphs). The direct effects of the inorganic pigment particles and of the degree of crystallinity on the value of T_g are of little significance.

It is interesting to note that the height of the PC peak follows a trend that is similar to that of the molecular weight of PBT, to that of the enthalpy of crystallisation, and to that of the degree of crystallinity. The lower the PBT molecular weight, the lower the enthalpy of crystallisation and the lower the degree of crystallinity, the greater is the peak height, because the greater is the viscous response of the major amorphous phase in the system.

An increase in the storage modulus is observed that is due to the inclusion of the rigid inorganic pigment, and to the effect of the pigment on the molecular weights of PC and PBT in these samples.

In Figure 3-48 are compared the viscoelastic properties of unpigmented PC/PBT/IM blends processed using extruder E1 (represented by sample BX) and using extruder E2 (represented by sample LX).

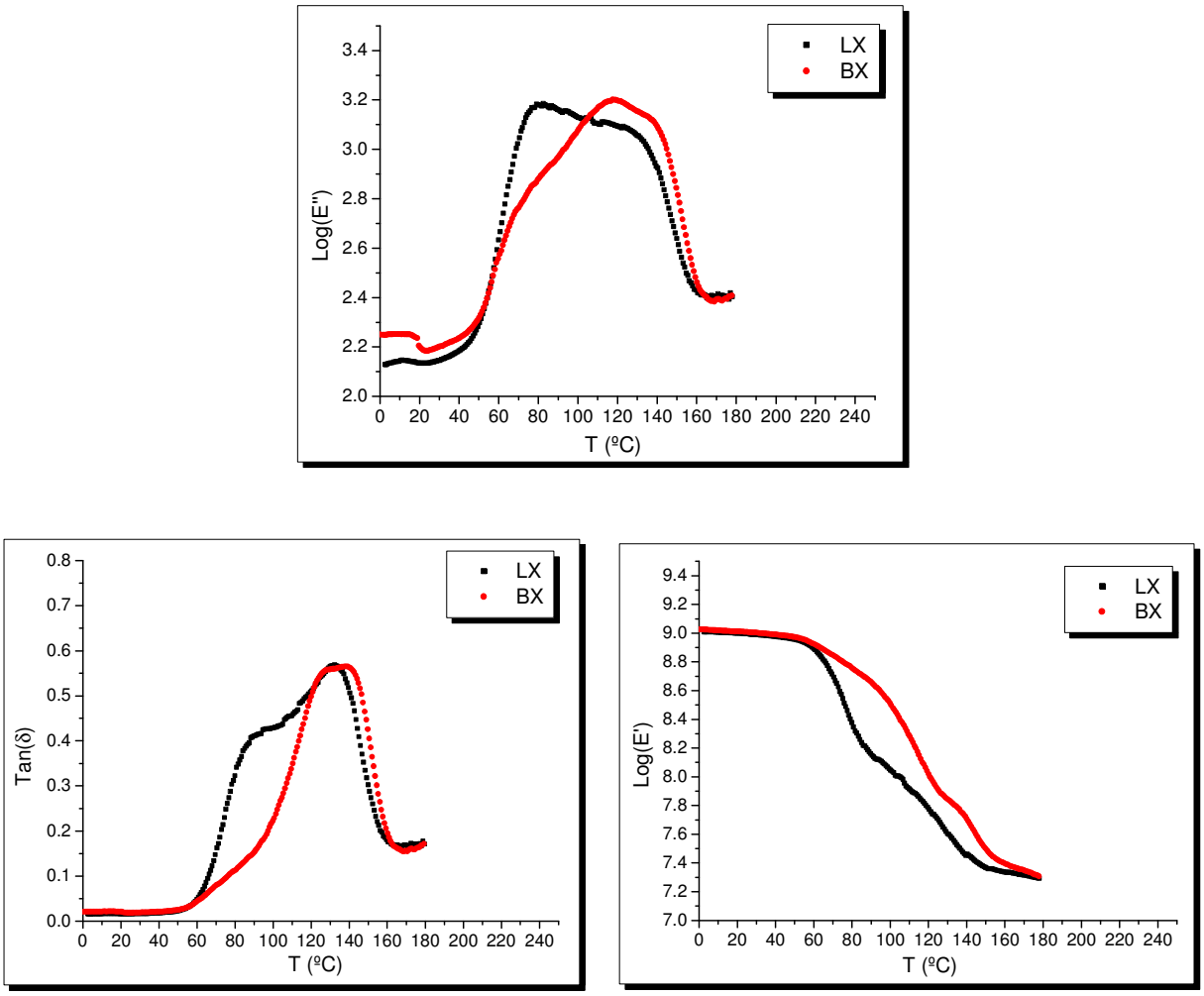

Figure 3-48. Loss modulus, loss tangent and storage modulus *versus* temperature, for samples BX and LX, processed in extruder E1 and E2, respectively.

Comparing the viscoelastic properties of samples of Sets 2 and 7, (Figures 3-46 and 3-47, respectively), bearing in mind the molecular weight of the PBT and of the PC in these blends (Section 3.2.1.), it can be stated that the greater molecular weight of PBT and of PC in the pigmented PC/PBT/IM blends represented by samples of Set 2, leads to a more distinct phase separation and not as clearly increased miscibility with increasing pigment loading. The more distinctive phase separation in samples of Set 2 is clear in Figure 3-48, for the unpigmented blends. Also, the lower molecular weight of the polymers, and mainly of the PBT, and the lower crystallinity for samples of Set 7 at the lower pigment loadings, lead to a more significant contribution of the amorphous PBT to the viscous response of the system for these samples. The effects of the greater molecular weight of PBT for samples of Set 2, which are particularly clear in Figure 3-48, result in not as distinct and/or not as significant, increased miscibility of the PBT and the PC with increasing pigment loading, for samples processed in extruder E2.

Summarising, from the DMTA results it can be stated that:

1) The pigment is located at the interphase of PC and of the amorphous PBT, and increases the miscibility of these polymers. This effect is particularly evident in the set of samples that is characterised by a lower molecular weight of PBT and of PC;

2) The pigment has an effect on the phase separation of PC and PBT as it influences the molecular weight of the polymers, in particular that of the PC.

Compatibilisation of binary blends by the addition of fillers has been studied by Lipatov and colleagues (2002). Miscibility improvement arising from the introduction of filler in an immiscible binary blend has been demonstrated by the reduction of the Flory-Huggins polymer-polymer interaction parameter, experimentally determined by IGC, at temperatures above the glass transition temperatures of the components. This effect was explained on the basis of the varying bulk composition due to preferential adsorption at the surface of the fillers, and also on the existence of a "quasi-ternary" system (polymer A-polymer B-filler surface), and consequences thereafter to the interaction parameter for the mixture.

Thus, the introduction of functional fillers, even for immiscible polymer pairs, may lead to the appearance of miscibility regions. At lower filler concentrations, the possible effect that is pointed out by the authors is the redistribution of the blend components according to their molecular masses between the filler surface and the bulk. According to the authors, usually, adsorption of high molecular mass fractions occurs. The effects of the filler on the phase behaviour were explained by the simultaneous action of two mechanisms: by changing the thermodynamics of interaction near the surface due to selective adsorption of one of the components and by the redistribution of components, according to their molecular masses, between the boundary region (near the surface) and in the matrix.

In face of the above reported results, the consequences of such phenomena in the composite system under study are expected to be visible in the physical properties and mechanical properties of the pigmented PC/PBT/IM blends as the composition of the interphase will differ from that of the bulk, with increasing pigment loading. For the PC/PBT/IM blends, preferential adsorption of PBT, mainly of the PBT 315 can be expected based on the greater molecular weight of this grade in comparison to that of PBT 195 and to that of PC 125, but also due to the specific interactions interaction potential as assessed by IGC (Section 3.1.8.2.).

3.2.4. Vicat Softening Temperature

The Vicat softening temperature (VST) corresponds to the temperature at which the polymer loses its "solid phase properties". The VST value is related to the dimensional stability and hardness of the material. In Figure 3-49 are summarised the VST results concerning Sets 1, 2, 3, 4 and 7 (Section 2.1.).

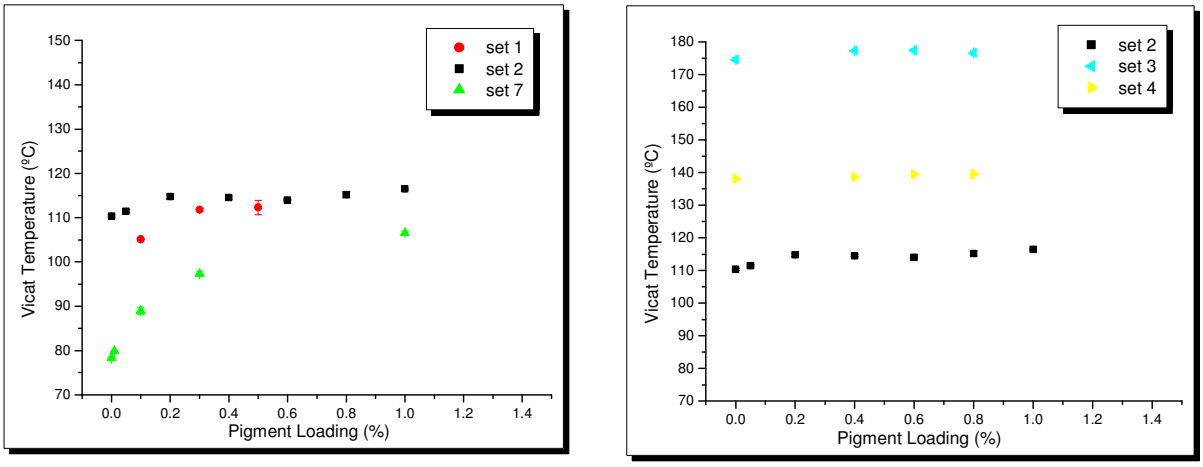

Figure 3-49. Vicat softening temperature as a function of pigment loading for samples of Sets 1, 2, 3, 4 and 7.

Figure 3-49 shows that the VST values increase with the inclusion of the pigment into the composition for all the tested samples. For the samples of Set 2 the VST value increases with the increase in the pigment loading, for loading values that are lower than 0.20 %. Thereafter, the VST remains constant, until a 0.60 % pigment loading is reached, increasing again beyond that loading. For samples of Set 1, the VST value is lower than that for the samples of Set 2, and follows an analogous trend with increasing pigment loading. For the samples of Set 7, the VST value increases proportionally to the pigment loading. Additionally, the values of the VST are lower than those for samples of Sets 1 and 2. The trend observed for the VST value with increasing pigment loading does not follow that of the average molecular weight of PBT, nor that of the crystallinity degree and that of the transesterification reaction extent. However, it follows the same trend as the average molecular weight of PC. This observation is in line with reports in the literature (Hamilton and Gallucci 1993). Thus, the improvement in the Vicat softening temperature with increasing pigment loading is attributed to the increase in the average molecular weight of PC, with a small contribution from the increasing presence of the rigid inorganic pigment particles. Accordingly, samples processed under conditions (extruder and screw design and/or operating conditions) that lead to greater molecular weight reduction show a lower value of VST. It should be noted that the degree of crystallinity for the unpigmented blend in Set 7 (batch LX) is greater than that of the unpigmented blend in Set 2 (batch BX) and the VST value of blend BX is greater than that of blend LX. Thus, the effect of the differences in molecular weight on the VST values overcomes the effect of the PBT crystallinity on this parameter. This finding supports the observation that samples with same VST value may have different crystallinity levels (Timmerman, T. *et al.* 2001, Personal Communication).

The VST values of the PBT-based samples are significantly greater than those of the PC-based samples and than those of the blend samples. This fact is due to the semi-crystalline nature of PBT and significantly greater degree of crystallinity in samples of Set 3.

For the pigmented PC samples (Set 4) and for the pigmented PBT samples (Set 3) an increase in the pigment loading does not influence significantly the value of the VST. For the samples of Set 3, it can be concluded that the small differences seen in the crystallinity degree and in the molecular weight of PBT do not influence significantly the value of the VST. The presence of the rigid inorganic particles does, nevertheless, raise the modulus of the samples, although not to a particularly notable extent. As far as the PC samples are concerned (Set 4) the behaviour observed in Figure 3-49 follows that of the molecular weight of this polymer. It can be said that both the molecular weight of PC and the presence of the pigment particles contribute to the observed trends. The value of the VST for the blend samples is lower than that of the PBT samples and than that of the PC samples. Thus, the blending of PC with PBT reduces the overall modulus when compared to that of the individual phases.

The trends observed are in line with those concerning the tensile modulus (Section 3.2.8.). The lower the molecular weights of PC and PBT the more consistent is the relationship between the VST values and the tensile modulus results.

The VST values also provide an indication of the extent of transesterification (Hamilton and Gallucci 1993). For these blends, if the VST value is lower than 110-115 ºC there is evidence of some transesterification (Timmerman, T. *et al.* 2001, Personal Communication), along with lowering of the molecular weight of the polymers, in particular of that of PC. Therefore, the VST results confirm those obtained from the melting temperature depression method, that indicate a greater transesterification level for samples of Set 7.

3.2.5. Thermogravimetric Analysis

Thermogravimetric analysis (TGA) was carried out on samples of blends that were processed in extruder E2. The corresponding thermograms are presented in Appendix D. The results are presented in Table 3-30. Here, T_d is the temperature at which decomposition of the polymers starts.

Table 3-30. Values of the decomposition temperature of the pigmented blends processed in extruder E2.

Sample	T_d (ºC)
L7	362.2
L8	352.0
L9	349.0
L10	337.3

It can be concluded that incorporation of pigment in the blend composition leads to a decrease in heat stability, blends beginning to decompose at lower temperatures. This is due to greater thermal conductivity of the pigment inorganic particles when compared to that of the polymers.

3.2.6. Izod Notched Impact Testing

The purpose of impact testing is to obtain an indication of the ductility, or energy absorption capacity, of a material under strong impact conditions. Figures 3-50 to 3-52 concern the variation of the impact energy absorption with pigment loading and with test temperature. Data are presented for the test temperatures of -20 ºC, -10 ºC, 0 ºC and 23 ºC. In Figure 3-50 is presented the variation of impact energy absorption as a function of the pigment loading, for samples processed using extruder E1 (Sets 1 and 2) and using extruder E2 (Set 7).

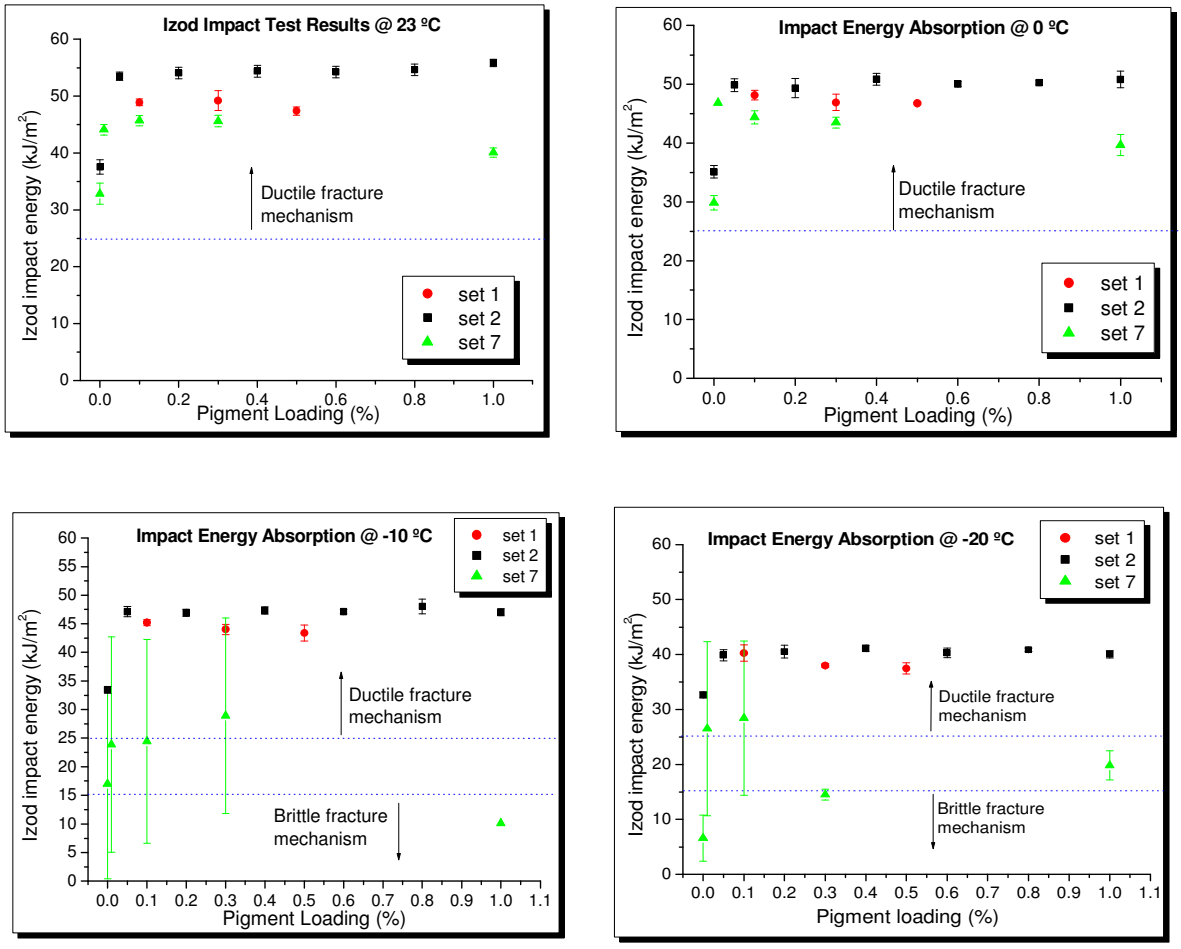

Figure 3-50. Variation of the notched Izod impact energy absorption for samples of Sets 1, 2 and 7, as a function of pigment loading and test temperature.

For the samples that were processed in extruder E2 (Set 7), Figure 3-50 shows that there is an improvement in the impact toughness of the PC/PBT/IM blends with the introduction of C. I. Pigment Blue 28 into their composition. This improvement continues until a pigment loading of approximately 0.10 % is reached, thereafter a reduction of the impact resistance of the blends occurs. This is clear from the ductile to brittle transition temperature for these samples (Table 3-31). The introduction of pigment reduces the value of $T_{D/B}$, (the ductile to brittle temperature). As the pigment loading is increased, the value of $T_{D/B}$ increases, reaching that of the unpigmented blend at a pigment loading of 1.00 %. From the values presented in Table 3-31, it can be concluded that the $T_{D/B}$ follows a similar trend to that of the PBT crystallinity. The greater the degree of crystallinity, the higher is the $T_{D/B}$.

Table 3-31. Ductile to brittle fracture mechanism transition temperature for samples of Set 7.

Sample	LX	L7	L8	L9	L10
Pigment loading (%)	0.00	0.01	0.10	0.30	1.00
$T_{D/B}$ (ºC)	-10	-	-	-20	-10

A more detailed analysis of the trends observed in Figure 3-50 for samples of Set 7 is given below.

Samples of Set 7 show that at the temperature of -20 ºC, after an initial improvement (at 0.01 and 0.10 % pigment loadings), the impact strength decreases with increasing pigment loading. The fracture mechanism is brittle for pigment loadings above 0.30 %. At -10 ºC, there is a continuous improvement in the impact strength with increasing pigment loading, until a pigment loading of approximately 0.20 % is reached. The high standard deviation for batches L7, L8 and L9 makes it difficult to assess how the increase in the pigment loading correlates with the greater impact strength. Two fracture modes, hinge and ductile, were identified for the tested specimens of blends L7, L8, and L9, indicating a temperature region of transition as far as the fracture mechanisms are concerned, that results in a bimodal distribution of the impact resistance. At 0 ºC and 23 ºC, the impact strength increases for the batches containing 0.00 % and 0.10 % pigment. Thereafter, a decrease is observed when the pigment loading is increased. All the batches showed a ductile fracture mode for the test temperatures of 0 ºC and 23 ºC.

Comparison of these results with those from the determination of the molecular weights of PBT and PC by GPC (Section 3.2.1.), allows one to conclude that, for samples of Set 7, a decrease of the average molecular weight of the higher fraction of molecular weight distribution of PBT corresponds to an improvement of the impact toughness of the blend. Also, as the average molecular weight increases, the impact toughness decreases. The trend observed is in line with that concerning the non-isothermal crystallisation properties of PBT in these blends (Section 3.2.2.2.). Thus, the lower the degree of crystallinity, and the lower the molecular weight of the higher

fraction of the molecular weight distribution of PBT, the greater is the impact energy absorption capability of the blend due to increase in the mobility of the macromolecular chains (Galeski 1990; Kong and Hay 2002a). Also, the greater the degree of crystallinity, the greater are the shear yielding phenomena (Bertilsson *et al.* 1989), that decrease the overall impact energy absorption. Furthermore, it can be concluded that the impact energy absorption increases with increasing transesterification (Section 3.2.2.1.). The greater the extent of transesterification, the better is the PC phase and PBT phase interconnection, due to the formation of PC-PBT copolyesters (bridging effect). Consequently, the stress transfer across the interphase is favoured by the occurrence of transesterification.

It can be concluded that the effect C. I. Pigment Blue 28 has on the impact resistance properties of the blends of Set 7 is a consequence of the changes in the molecular weight of PBT, in the degree of crystallinity and in the extent of transesterification. The trend observed is in line with the results concerning the strain at break (Section 3.2.8.), which derives from the effect the molecular weight, the degree of crystallinity and the transesterification reaction have on the ultimate elongation properties of these blends.

For samples of Set 2, it was observed that, for the pigment loading range used, the samples present a ductile fracture profile at all the test temperatures studied. The inclusion of pigment in the blends, improves their impact toughness. The increase in pigment loading has little effect on the test results. This behaviour does not follow that of the molecular weight of PC and PBT, nor is it analogous with that of the degree of crystallinity and that of the extent of transesterification in these samples. In the blend samples, the molecular weight of PC increases continuously with increasing pigment loading and that of PBT decreases for the lower pigment loading and then increases with increasing pigment loading. The increase in the molecular weight of PC would be expected to lead to an improvement of the impact resistance (Timmerman, T. *et al.* 2001, Personal Communication). This is not the pattern observed in Figure 3-50. The degree of crystallinity increases slightly with the introduction of the pigment and the extent of transesterification decreases. Both effects would be expected to lead to a decrease in the impact energy absorption capability of the blend. Thus, it can be concluded that the improvement of the impact resistance is due to changes in the impact toughening mechanisms. A possibility is the improvement of stress transfer between the PBT phase and the PC phase, due to strong adsorption, and improved miscibility, of these polymers at the surface of the pigment particles, and to the presence of the inorganic particulates at the interphase. Further discussion on this matter is presented in subsequent paragraphs.

The behaviour of the samples of Set 1 is intermediate between those of samples of Sets 2 and 7, but close to that of samples of Set 2. It can be concluded that the lower the molecular weights of PC and PBT, the more sensitive is the impact resistance to differences in the degree of crystallinity of PBT and in the extent of transesterification. Moreover, processing conditions that lead to a lower

breakdown of the polymer chains, and, thus, to a higher average molecular weight of both the PC and the PBT, lead to an improved impact toughness of the blend.

The fact that samples of Set 2 show better PC/PBT phase separation (Sections 3.2.3. and 3.2.10.), which reduces the interfacial area between the PC and the PBT, when compared to that of samples of Set 7, would be expected to lead to a lower impact resistance of the samples of Set 2. Thus, it can be concluded that the effect of the increased molecular weight of the polymers, mainly of the PC, overcomes the effect of reduced interfacial area, lower extent of transesterification and greater degree of crystallinity at the lower pigment loading, for samples processed in extruder E1.

The improvement in the impact resistance of the pigmented blends due to modifications (caused by C. I. Pigment Blue 28) in the fracture mechanisms does not prevail in the samples of Set 7. Thus, for lower molecular weight values of PC and PBT, the effects of varying the crystallinity degree, molecular weights, and extent of transesterification, dominate over those relating to the changes in the impact energy absorption mechanisms.

The following figures summarise the Izod notched impact testing results for different testing temperatures and pigment loadings, for samples of Sets 2 and 7.

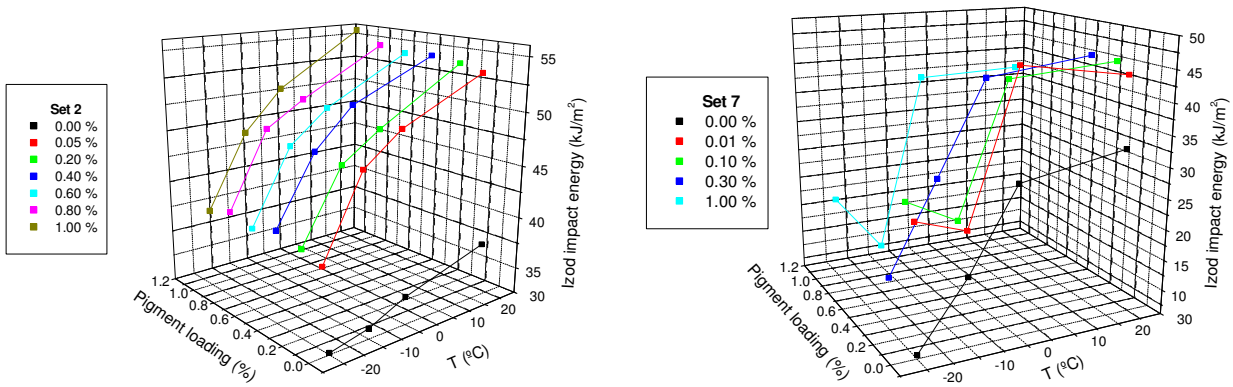

Figure 3-51. Izod impact testing results, as a function of test temperature and pigment loading, for samples of Sets 2 and 7.

For all of the samples, the energy needed to break the specimen increases with increasing testing temperature. This is in accord with expectation for the PBT/PC/IM blends, as the increase in impact toughness with temperature is a consequence of the relaxation processes of the rubbery zones and the parent polymers in a relatively low-temperature range and thermal blunting of the crack tip at higher temperatures (Wu *et al.* 1993).

Figure 3-52 concerns the notched Izod impact testing results for the blends (unpigmented and pigmented, Set 2), when compared to those of the unpigmented, and the pigmented, PBT-based, and PC-based samples, Sets 3 and 4 respectively.

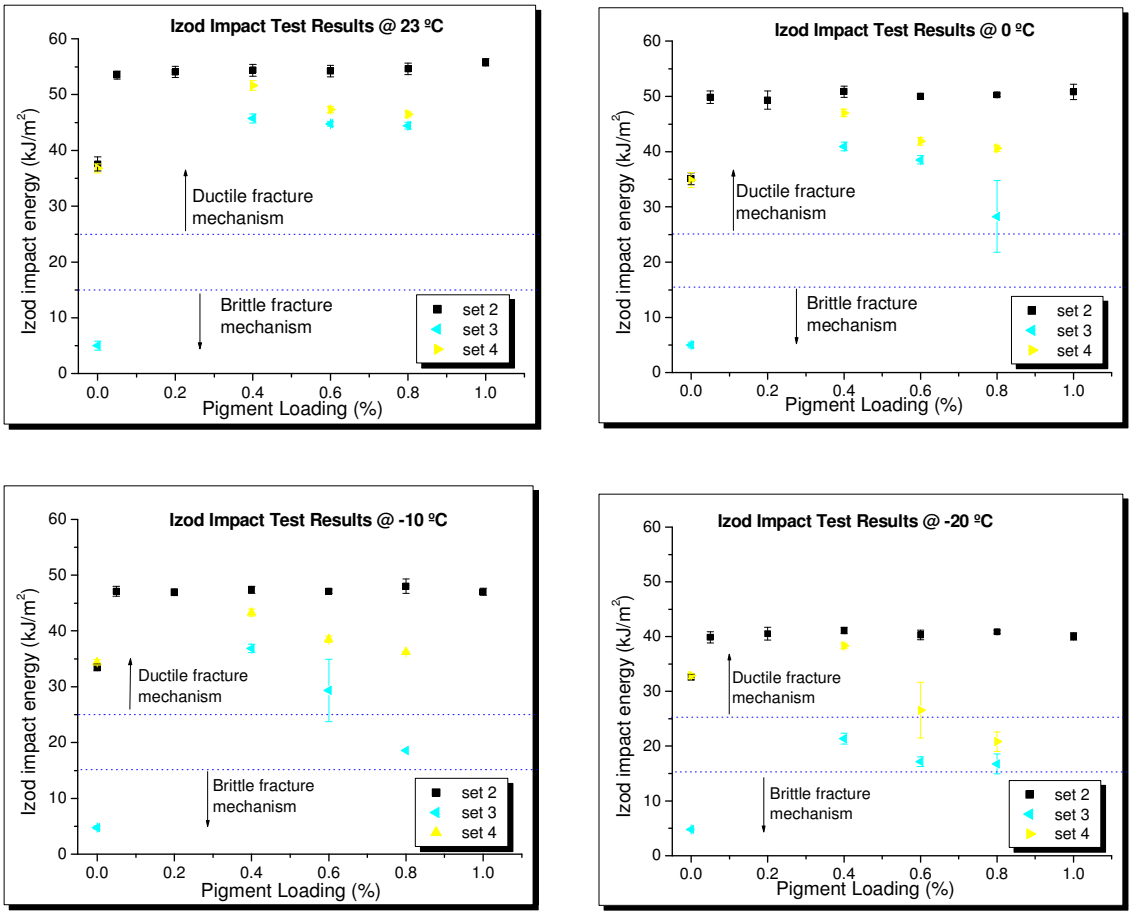

Figure 3-52. Variation of the notched Izod impact energy absorption for samples of Sets 2, 3 and 4 as a function of pigment loading and test temperature.

Figure 3-52, shows that the impact energy absorption of the PBT-based samples (Set 3) is the lowest of Sets 2, 3 and 4. This agrees with expectation due to the semi-crystalline nature of PBT. For the unpigmented samples, it has been observed that the impact toughness of the unpigmented blend is very close to that of the unpigmented PC-based sample, for all the test temperatures. Thus, in the unpigmented blend, the PC phase is determining the impact resistance of the blend. Consequently, it is expected that in the pigmented blends also, this phase plays an important role in terms of impact energy absorption. For the pigmented samples, the use of pigment at low pigment loadings, improves the impact toughness of the blend samples, of the PC samples, and of the PBT samples. This improvement is particularly marked for the PBT-based samples.

For all the test temperatures, the impact resistance of the pigmented blends is greater than that of the samples that mimic the PC phase (Set 4) and that mimic the PBT phase (Set 3). This realisation suggests that the total impact energy absorption of the blend is a sum of the effect of the pigment on the PC phase and on the PBT phase. Therefore, a synergistic effect is observed when PBT and PC are blended, this being enhanced when the pigment is introduced in the blends compositions. This is thought to be due to the striking improvement in the impact resistance of the PBT phase, originated by the pigment.

As the pigment loading is increased, the impact resistance of the blends does not change significantly, but that of Sets 3 and 4 decreases. Although the pigment loading range of the PBT and the PC samples is not complete, it can be said that the impact toughness, of both PC and PBT, is improved by the increase in the pigment loading, until a particular pigment loading is reached. For pigment loadings above this specific value, the increase in the pigment loading initiates a reduction of the impact resistance of both PC and PBT. This detrimental effect of the pigment on the impact resistance of the PC-based blends and of the PBT-based blends increases of importance as the test temperature decreases, approaching the impact toughness value of the unpigmented samples. For the PC-based samples, at a test temperature of -20 ºC, the impact resistance of the blend is lower than that of the unpigmented sample, at pigment loadings of 0.60 and 0.80 %.

For the PBT samples, the degree of crystallinity does not play a role in the abovementioned behaviour as it decreases slightly with the introduction of pigment and with increasing pigment loading, while the impact resistance also decreases. The decrease in the molecular weight of the PBT when the pigment is introduced into the blend is thought not to be the cause of the observed dramatic improvement in the impact resistance of the PBT-based samples. Furthermore, with increasing pigment loading, the molecular weight of PBT increases. This is not expected to initiate the observed decrease in the impact resistance. For the PC-based samples, the small increase in the molecular weight, when the pigment is included into the composition, would not be expected to cause the observed significant improvement of the impact resistance. Furthermore, with increasing pigment loading the molecular weight of PC does not change significantly. Thus, it is unlikely that this is the initiator of the decrease of impact resistance of these samples.

From the above observations, a change in the impact toughening mechanisms of the PC-based, PBT-based and PC/PBT/IM blends is concluded to be caused by the presence of C. I. Pigment Blue 28. The mechanisms suggested for the excellent impact resistance of these blends are: multiple crazing, shear yielding, crazing with shear yielding, and rubbery particle stretching and tearing (Section 1.3.2.4.). It has been suggested (Walker and Collyer 1994) that rigid inorganic particulate fillers can be used to increase the toughness of brittle polymers by initiating multiple crazing. Thus, on the one hand, the effect the pigment particulates may be related to improvement of the impact energy by crazing and cavitation. On the other hand, internal cavitation of the pigment particles may lower the impact resistance since, for optimum toughening, internal

cavitation is an undesirable deformation mechanism because the energy dissipation involved in this cavitation process is clearly lower than that involved in crazing and extensive shear deformation of the matrix (Dekkers *et al.* 1988). Thus, at the lower pigment loadings, crazing and cavitation may be contributing to the improvement of the impact toughness, whereas at the greater pigment loadings, the internal cavitation of the pigment particles may lower the impact resistance of the blends. This concept can be assessed through tensile dilatometry in order to determine if crazing and/or cavitation are being inhibited by the pigment particles.

The decrease of impact resistance with increasing pigment loading, beyond a critical value, for Sets 3 and 4, is thought to be related to the inter-particle distance. As this distance is reduced below a critical value, the toughening mechanisms are adversely affected since the particles act as crack initiators (Wang *et al.* 2001), increasing the level of shear yielding of the polymeric matrix and propagating the crazes. Consequently, the energy absorption due to the MBS rubber particles (crazing and cavitation), is reduced. A greater degree of agglomeration of the pigment at the higher loadings, may also initiate lower impact resistance (Wang *et al.* 2001). Also, the pigment-polymer matrix adhesion may not be high enough. This would inhibit crazing as debonding occurs readily, initiating cavitation and shear yielding, without stress transfer between particles and, thus, no crazing.

Under an applied stress, rigid particles induce tensile stress concentrations in the matrix but become debonded from the matrix readily as they are unable to deform to any significant degree. Thus, since there is limited adhesion between rigid particulate fillers and the matrix they are not particularly effective craze or crack terminators, resulting in poorer toughening performance compared with well-bonded rubber particles (Walker and Collyer 1994). Stronger interfacial bonding and/or improved dispersion may raise the impact resistance (Wang *et al.* 2001). Upon decreasing the test temperature, the toughening mechanisms lose importance as the macromolecular chain motion is significantly reduced. In the particular case of PC, at the greater pigment loadings and at -20 ºC, the changes in the toughening mechanisms due to the pigment particles are detrimental compared to those prevailing in the unpigmented PC.

For the PC/PBT/IM blends, the preferential presence of the pigment particles at the PC/PBT interphase, that results in impact energy transfer between phase domains (bridging effect), is thought to overcome the aforementioned detrimental effects of high pigment loadings on the impact resistance of the individual phases, namely for samples of Set 2.

For the pigmented blends, if the pigment was located totally in the PC phase or in the PBT phase, then the actual loading of the pigment in that phase would be approximately double. Thus, in the abovementioned case, the pigmented samples of PC and PBT would follow the same trend as that observed for the pigmented PC/PBT/IM blends with pigment loadings in the region of 0.20-0.40 %. The observation that the effect of increasing the pigment loading in the blend does not

follow that corresponding to the PC and that corresponding to the PBT, indicates that the pigment is not preferentially present in one of the phases (PC or PBT).

3.2.7. Puncture Impact Testing

The puncture impact test uses a falling weight to both initiate and propagate crack growth and, thereby, to evaluate the energy absorption capability of the material under high rate impact conditions. In Figure 3-53 are presented the values of the puncture energy and energy at maximum force, that result from testing of samples of Sets 1, 2 and 7.

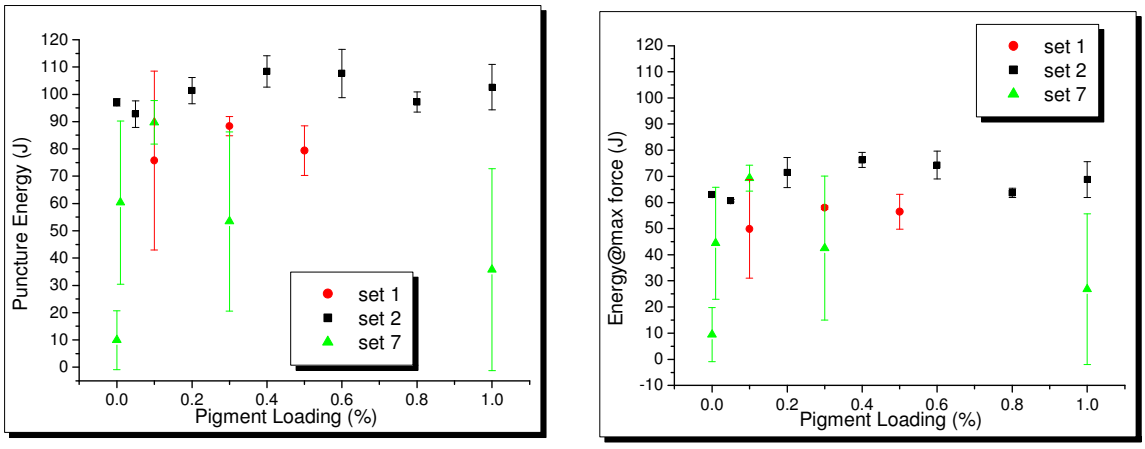

Figure 3-53. Puncture energy and energy at maximum force as a function of the pigment loading, for samples of Sets 1, 2 and 7.

For the samples of Set 7, the energy absorption capability of the blend increases with increasing pigment loading, until a particular value of loading is attained. Above that loading value, the impact energy absorption decreases with increasing pigment loading. This trend is in line with that relating to the notched Izod impact test. For samples of Set 2, the introduction of C. I. Pigment Blue 28 leads to an improvement of the energy absorption under high rate impact conditions. This improvement is not as clear as that observed for samples of Set 7. Thus, it can be concluded that the impact energy absorption mechanisms that improve the impact resistance of the pigmented blends when tested by means of the notched Izod impact tester are less significant when high rate impact conditions are applied.

It seems that also for the samples of Set 2 the impact energy absorption decreases when the pigment loading reaches a specific value. This indicates a change in the impact toughening mechanisms, suggested to be analogous to that relating to the notched Izod impact testing of samples of Sets 3 and 4 (Figure 3-52, Section 3.2.6.). The behaviour observed with increasing pigment loading follows a similar trend to that observed for the PC-based samples (Figure 3-52).

The results obtained for Set 1 are intermediate of those of Sets 2 and 7. Under these testing conditions, the lower the molecular weight of PC and of PBT the more significant are the effects of the varying degree of crystallinity, varying extent of transesterification and varying molecular weight of PC and PBT on the impact energy absorption, and the lower is the impact resistance.

Figure 3-54 relates to the comparison of the puncture impact testing results for the blend samples (Set 2) and for the samples that mimic the PBT phase (Set 3) and the PC phase (Set 4).

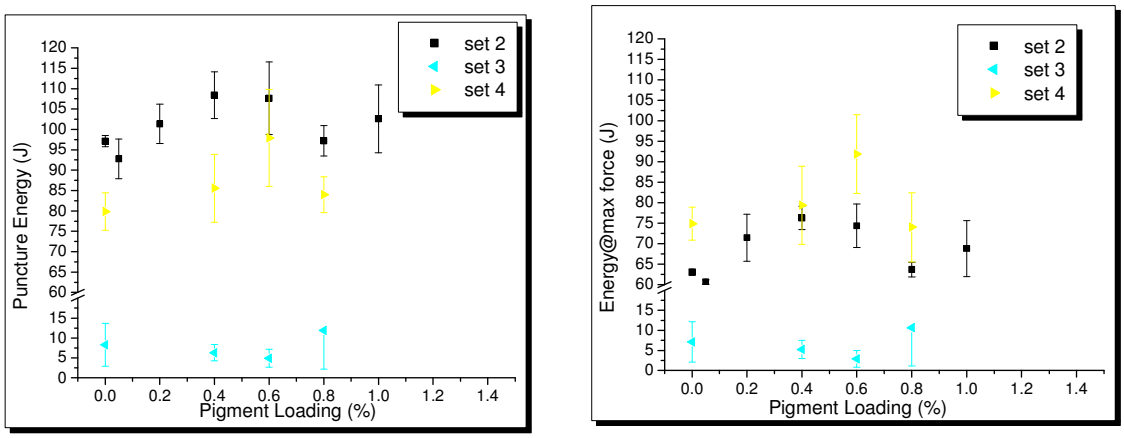

Figure 3-54. Puncture energy and energy at maximum force as a function of the pigment loading for samples of Sets 2, 3 and 4.

Figure 3-54 shows that the impact resistance, under high rate impact testing, of the PBT phase is the lowest of the PC and the PBT phases, agreeing with expectation due to the semi-crystalline nature of the PBT. For the puncture energy, the blend values are greater than those obtained for the individual phases. Therefore, the synergistic effect seen in the notched Izod impact testing, upon blending, is also indicated in the puncture impact test results. However, this synergistic effect cannot be attributed to the enhancement of the impact energy absorption of the PBT phase due to the pigment particles. For the PBT phase, in contrast to the effect the pigment has on the notched Izod impact test, the impact energy absorption under high rate impact situations does not improve upon the introduction of C. I. Pigment Blue 28 into the composition. Therefore, the toughening mechanisms in PBT that exist at high rate impact conditions are different than those that apply at lower impact rates. Multiple crazing originating in the pigment particles can occur, as can cavitation of the pigment particles themselves. For the PC phase, the inclusion of pigment increases the impact energy absorption, although not to a significant extent, bearing in mind the standard deviation.

Under high rate impact conditions, the PBT phase loses importance as far as the impact energy absorption is concerned.

Regarding the per cent ductility, all the samples of Sets 2 and 4 showed 100 % ductile fracture. Samples from the PBT-based batches, Set 3, all revealed 0 % ductility. As far as samples of Set 1 are concerned, the sample relating to the 0.10 % pigment loading showed 80 % ductility. The remaining samples showed 100 % ductility. The results obtained for samples of Set 7 are presented in Table 3-32.

Table 3-32. Percent ductility of samples of Set 7.

Sample	LX	L7	L8	L9	L10
Pigment loading (%)	0.00	0.01	0.10	0.30	1.00
% Ductility	0	80	100	60	40

The trend observed in Table 3-32 follows that observed for the puncture energy and that observed for the energy at maximum force. The discussions and interpretations concerning the values obtained for the puncture energy and for the energy at maximum force apply to the per cent ductility parameter.

3.2.8. Tensile Testing

The tensile properties of rubber filled polymer blends depend critically on the morphology and connectivity of the two phases (McGrath 1994). The more important parameters to be analysed are the modulus and strain at break (Timmerman, T. *et al.* 2001, Personal Communication). The elastic modulus represents the intrinsic capacity of the materials to resist an applied load. However, the elastic modulus is not as sensitive to the state of the interface as is a high strain type property such as the elongation at break or the impact strength (Leclair and Favis 1996). The elongation at break is a measure of the ductility of the blend (Sanchez *et al.* 1993).

In discussing these results, the assumption is made that interfacial factors, molecular weight factors, crystallinity factors and PC-PBT connectivity factors are responsible for the effects that were observed. It is, of course, possible that an additional contribution to the effects on the system properties arises from different degrees of dispersion, attained under the processing operations. Nevertheless, the quality of the dispersion is regarded as a property parameter of filled polymers that is sensitive to interfacial forces.

The following results summarise the tensile testing as a function of the pigment loading, for the batches extruded using extruder E1 (Sets 1, 2, 3 and 4) and using extruder E2 (Set 7).

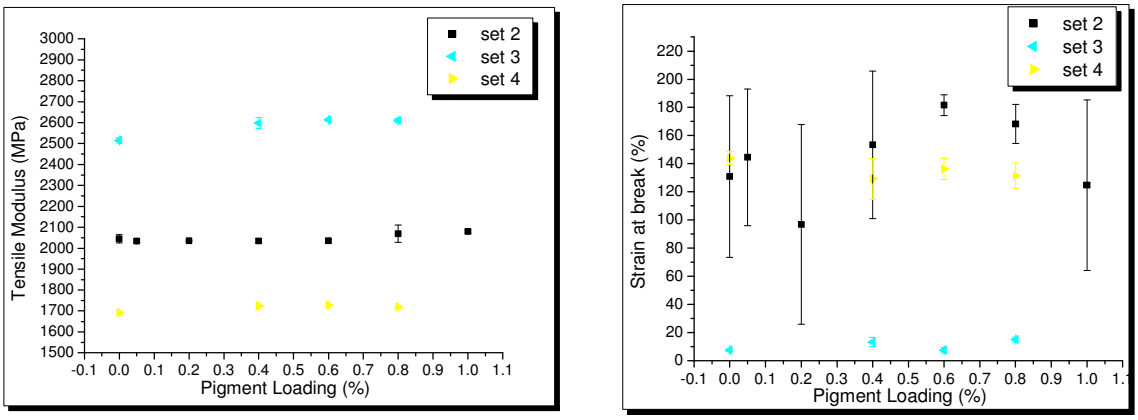

Figure 3-55. Tensile modulus and strain at break as a function of C. I. Pigment Blue 28 loading, for samples of Sets 2, 3 and 4.

Figure 3-55 shows the behaviour of the tensile modulus and of the strain at break, of blend samples (Set 2) and of the samples that mimic the PBT-rich phase and the PC-rich phase, Sets 3 and 4, respectively, with varying pigment loading.

Effect of Pigment Loading on the Tensile Modulus

Figure 3-55 shows that the tensile modulus of the PBT-based samples (Set 3) is higher than that of the PC-based samples (Set 4). The tensile modulus value of the blend lies between that of Set 3 and that of Set 4, slightly closer to that of the Set 4 samples. As the PC and the PBT are present in the formulation in a 1.08 ratio, it follows that the modulus of the blend results from the linear combination of the modulus of the PC phase and of the PBT phase, with greater contribution from the PC-rich phase.

For the PBT-based samples and for the PC-based samples, the introduction of pigment leads to an increase of the tensile modulus. This is more important for the samples of Set 3 (PBT-based samples). In this case, the tensile modulus increases slightly with increasing pigment loading. As far as the PC samples are concerned, the introduction of pigment leads to an increase of the modulus, with contributions from increased PC average molecular weight (Figure 3-38, Section 3.2.1.). On the other hand, with regard to the PBT samples, the introduction and increase of the pigment loading brings about a decrease of the average molecular weight in comparison to that of the unpigmented PBT. Thus, the increase of the tensile modulus of samples of Set 3 is thought to be due to good adhesion between the pigment particles and the PBT phase, as predicted from the IGC results analysis of the Lewis acid/base interaction potential (Section 3.1.8.).

The presence of pigment particles also influences the tensile modulus, if there is strong bonding at the polymer-filler interface (Richard *et al.* 1985; Schreiber and Germain 1990 and 1991; Scherbakoff and Ishida 1997). In this situation, the elastic deformability (ductility, large deformation) is reduced and the modulus increased. This is understandable bearing in mind that ductility is promoted by slippage at the polymer-filler interface (Schreiber and Germain 1991).

For the blend samples (Set 2), the use of pigment does not influence significantly the tensile modulus values, for the lower pigment loadings. Above a particular value of the pigment loading, the tensile modulus increases with increasing pigment loading, surpassing the value for the unpigmented blend. At the higher pigment loadings in the blend samples (Set 2), bearing in mind that the degree of crystallinity of the samples does not vary significantly, and the trend observed for the molecular weight of PC and of PBT in these samples, the presence of the rigid inorganic pigment particles at the interphase, which show good adhesion to PC and to PBT, is thought to contribute to the increase in the tensile modulus of the blend samples.

For the pigmented blend samples, if the pigment particles were solely in one of either the PBT-rich phase or the PC-rich phase, then the actual pigment loading in that phase would duplicate as PC and PBT are used in an approximate 1:1 proportion. Thus, bearing in mind the effect the pigment has on Sets 3 and 4, it can be concluded that the pigment particulates are not located preferentially on any of the phases (PC or PBT), nor in both. If that were the case, the inclusion of pigment in the blends composition would lead to an increase in the tensile modulus, at pigment loadings below 0.40 %, and not to the observed decrease. For pigment loadings above approximately 0.60 %, the effect of the pigment on the modulus of the blend shows behaviour that is closer to that of the presence of pigment in the PBT phase. This does not prove that, for pigment loadings greater than 0.60 %, pigment particles are located in the PBT phase. The trend observed is a consequence only of the greater influence of the pigment on the molecular weight of PBT, for pigment loadings above 0.60 %, in comparison to that on the molecular weight of the PC.

Effect of Pigment Loading on the Strain at Break

The strain at break results show that the values obtained for the samples of Set 3 (PBT-based samples) are lower than those obtained for the PC-based samples (Set 4), agreeing with expectation. The unpigmented blend has a value of strain at break that is between that of unpigmented PBT and that of the unpigmented PC, but closer to that of the unpigmented PC. For the pigmented samples, the strain at break of the blend is close to/greater than that of the PC samples. Thus, when the flow of the PBT component becomes significant at higher stresses, the PC-phase is the dominating one, in PC/PBT blends.

For the samples of Set 4, the introduction of the pigment results in a decrease of the strain at break value. The increase in pigment loading does not influence, to a notable extent, the value of this parameter. For samples of Set 3, the introduction of the pigment results in an increase of the strain at break value, and the increase in pigment loading does not influence significantly the strain at break. Thus, it can be said that the interaction between the pigment and the PBT is more effective than that between the pigment and the PC, as far as the strain at break is concerned.

For the blend samples, the strain at break increases with increasing pigment loading, for values below approximately 0.60 %. However, it can be argued that, for pigment loadings below 0.60 %, the behaviour of the strain at break is a combination of the effects of the pigment on the PC phase and on the PBT phase as the pigment is preferentially located at the PC/PBT interphase. This is thought to be the origin of the greater standard deviation, mainly at pigment loadings that are lower than approximately 0.60 %. At low pigment concentrations, ultimate properties (strain at break and stress at break) are known to be clearly affected by the condition of the polymer-filler interface (Boluk and Schreiber 1990).

As the pigment loading reaches 0.60 %, the strain at break shows behaviour (relative to that of the unpigmented blend) that is closer to that of the pigmented PBT samples. Above pigment loadings of 0.60 %, the strain at break decreases with increasing pigment loading. At those pigment loadings, the effect of the pigment on the blend is again a combination of the effects of the pigment on the PC phase and on the PBT phase. As the pigment loading reaches 1.00 %, the strain at break shows behaviour (relative to that of the unpigmented blend) that is closer to that of the pigmented PC samples.

From the above inferences, it can be concluded that, for the pigmented blends, the pigment particles are not located preferably either in the PC phase or in the PBT phase. Also it can be said that the contribution from the effect of the pigment on the PBT phase, for the blends strain at break values, reaches a maximum at a pigment loading of approximately 0.60 %.

The strain at break value for the blends with 0.05 %, 0.20 %, 0.40 %, and 1.00 % pigment loadings is characterised by a high standard deviation. It follows that the homogeneity of the blend, in terms of the effect the pigment has on the strain at break, increases until a pigment loading of approximately 0.60 % (where the effect of the pigment particles on the PBT is more distinct), thereafter becoming more heterogeneous with increasing pigment loading.

Figure 3-56 concerns the behaviour of the stress at break, the strain at yield and the stress at yield of blend samples (Set 2) and of the samples that mimic the PBT-rich phase and the PC-rich phase, Sets 3 and 4, respectively, with varying pigment loading.

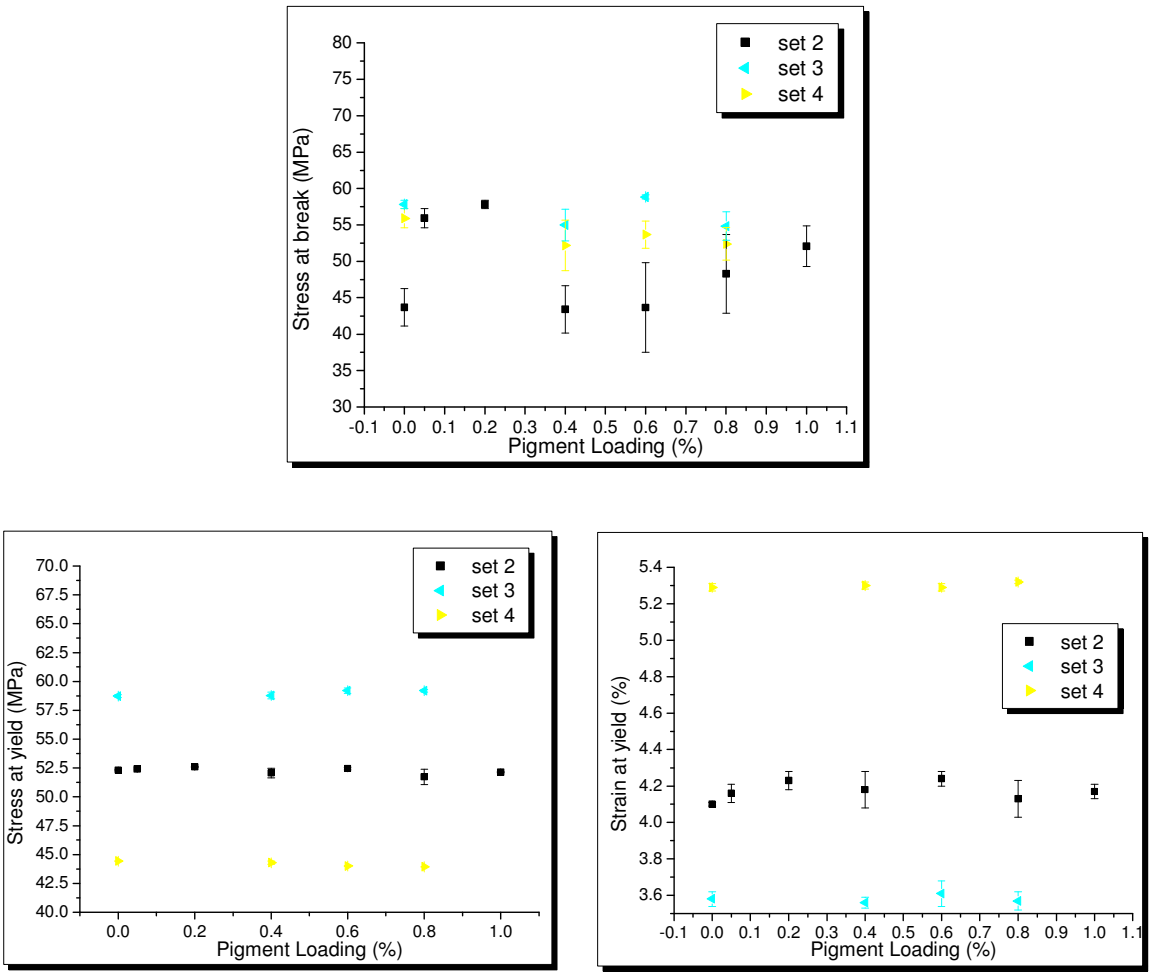

Figure 3-56. Stress at break, strain at yield and stress at yield as a function of C. I. Pigment Blue 28 loading, for samples of Sets 2, 3 and 4.

Effect of Pigment Loading on the Stress at Break

Figure 3-56 shows that the value of the stress at break for the samples of Set 3 is not noticeably influenced, by the introduction of the pigment or by the increase in the pigment loading. For Set 4 samples, the inclusion of the pigment lowers slightly the value of the stress at break. When the pigment loading is increased there is no significant alteration to the value of the stress at break of the pigmented PC-based samples. For the unpigmented blend, the value of the stress at break is lower than that of unpigmented PC and than that of unpigmented PBT.

On the other hand, the behaviour observed for the pigmented blends, when the pigment is included in the composition, and its loading increased, its quite complex. For the lower pigment loadings of 0.05 % and 0.20 %, the value of the stress at break is close to that of the PBT-based samples. At a pigment loading of 0.40 %, the value of the stress at break is close to that of the unpigmented blend, increasing thereafter with increasing pigment loading. These observations

show that the inclusion of the pigment, and the increase in the pigment loading, do not result in behaviour that is typical of either pigmented PC samples or pigmented PBT samples. Therefore, the pigment particles are thought not to be located preferentially on neither the PC phase nor the PBT phase. It is noteworthy that, for the pigmented blends, the greater standard deviation corresponds to the samples with 0.60 and 0.80 % pigment loadings, the samples that have the lowest standard deviation with regard to the strain at break.

Effect of Pigment Loading on the Strain at Yield

The strain at yield values of the PBT-based samples are lower than those of the PC-based samples. The values of the strain at yield for the blend samples lie between those corresponding to the PC samples and to those corresponding to the PBT samples, but are closer to those of the PBT samples. Thus, at low stresses the blend shows PBT-like behaviour. The effect of the pigment on the strain at yield values of the PC-based samples is not very marked. Nevertheless, at the pigment loading of 0.80 %, there occurs a small increase in the strain at yield values. The effect of the pigment on the strain at yield of the PBT-based samples is not significant.

The inclusion of the pigment in the blend leads to an increase in the strain at yield value of the blend samples (Set 2). Although the standard deviation for the pigmented blends cannot be ignored, an increase of the strain at yield with increasing pigment loading is seen, until a pigment loading value of approximately 0.60 % is reached. Above this loading value, the strain at yield decreases, but not significantly.

As mentioned previously, if the pigment were located fully in the PC phase or fully in the PBT phase, then the actual loading of the pigment in that phase would be approximately doubled. In that case, the pigmented samples of PC and PBT would follow the same trend as that observed for the pigmented blends with pigment loadings in the region of 0.20-0.40 %. Figure 3-56 shows that the trend observed on increasing the pigment loading, in the region 0.20-0.40 %, is similar to that of both the pigmented PC samples and the pigmented PBT samples.

Effect of Pigment Loading on the Stress at Yield

The stress at yield values of the PC-based samples are lower than those of the PBT-based samples. The values of the stress at yield for the blend samples lie between those corresponding to the PC samples and to those corresponding to the PBT samples, but closer to those of the PBT-based samples. Figure 3-56 shows that the effect of the pigment on the stress at yield of the blend samples, of the PC-based samples, and of the PBT-based samples, is not very significant. The pigment leads to a small decrease in the stress at yield of the PC-based samples, and to a small increase in the stress at yield of the PBT-based samples. For the blend samples (Set 2) the stress at yield does not vary significantly with increasing pigment loading.

The yield stress is usually reported to decrease with increasing content of an inorganic particulate which follows from the fact that the inorganic particles do not bear the load in the direction of deformation (Galeski 1990). This is thought to be the case when the interfacial adhesion between the filler and the polymeric matrix is weak. In the present case, from the specific interactions potential assessment by IGC (Section 3.1.8.), the adhesion between the inorganic pigment particles and the polymer matrix is considered to be significant, mainly in what concerns the PBT. Consequently, the value of the stress at yield of the samples is not directly influenced, to a significant extent, by the introduction of the pigment in the blends.

The following figures relate to the influence of C. I. Pigment Blue 28 on the tensile properties of blend samples processed using the same extruder but differing extrusion conditions, particularly the throughput (Sets 1 and 2), and processed using different extruders (Sets 1, 2 and 7).

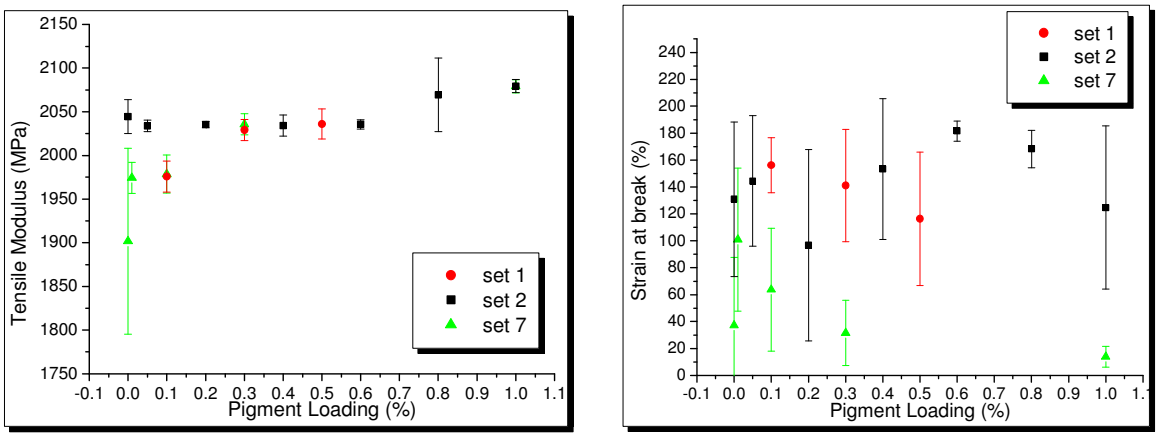

Figure 3-57. Tensile modulus and strain at break as a function of C. I. Pigment Blue 28 loading, for samples of Sets 1, 2 and 7.

Effect of Pigment Loading on the Tensile Modulus

For the samples of Set 7, the introduction of pigment in the blend causes a clear increase in the tensile modulus values. The tensile modulus increases with increasing pigment loading, though at 0.01 %, the improvement is more marked. This trend follows that observed for the behaviour of the average molecular weight of PC (Figure 3-38, Section 3.2.1.), and agrees with the Vicat softening temperature results (Section 3.2.4.). Thus, the modulus of the blend, in this set of samples, is influenced, to a large extent, by the molecular weight of the PC.

The trend observed is in accord with the DMTA studies carried out in these samples (Section 3.2.3.). The increase in pigment loading leads to an increase of the elastic absorption of energy. Thus, the stiffness and hardness of the sample are increased with increasing pigment loading. This is also indicated in the increasing value of the tensile modulus.

The lower degree of crystallinity for the lower pigment loadings would be expected to result in a decrease of the tensile modulus values (Galeski 1990; Leclair and Favis 1996; Foreman and Blaine 1997; Utracki 1998; Kong and Hay 2002a). However, for samples of Set 7, the effect of the molecular weight of the PC on the tensile modulus overcomes those of the degree of crystallinity and of the molecular weight of the PBT.

Among the parameters that possibly affect the modulus of elasticity of the blends, PBT crystallinity, free volume of the blends (density), molecular weight, PC-PBT connectivity, injection-moulding induced orientation and the presence of inorganic particulates should be considered.

There exist several equations, theoretical as well as semi-empirical, that predict the increase in tensile modulus with increasing filler concentration (Bohme 1968). Most of these equations are particle size dependent, and apply only to an amorphous matrix in thorough contact with a well-dispersed inclusion. With PBT, one is dealing with a semi-crystalline polymer. To a first approximation, the crystallites in the polymers represent one type of crosslink that contributes to the strength of the material. The miscibility level is a parameter that scarcely influences the modulus, particularly when at least partial miscibility is assured (Richard *et al.* 1985; Walker and Collyer 1994; Rodriguez *et al.* 1997).

From the results of the present study, it seems that the crystalline phase is not continuous enough to contribute to the modulus, and that the amorphous phase is mainly responsible for the deformations associated with the modulus, in line with interpretations given in the literature (Sanchez *et al.* 1993; Rodriguez *et al.* 1997). The lower the crystallinity degree, the greater is the contribution of the amorphous fraction of the PBT to increased tensile modulus. This realisation is thought to contribute to the prominent increase in the tensile modulus at the lower pigment loadings. Furthermore, the cobalt aluminate particulates replace, to some extent, the lost crystalline crosslinks, by strong adsorption of the polymers to their surface.

It can then be said that the specific volumes of the amorphous phases are more directly related to the modulus. These results are supported by similar observations for related materials (Rodriguez *et al.* 1997).

Samples of Set 2 have a value of the modulus that is greater than that of samples of Set 7, until a pigment loading of approximately 0.30 % is reached. Above this loading, the modulus attains the values corresponding to those of blends of Set 2, and follows the trend that is observed for these samples. The difference in the tensile modulus values of the blends of Sets 2 and 7, arising from the presence of the pigment and from an increase of pigment loading, is thought to derive from the differences in the molecular weight of the polymers, mainly in the molecular weight of the PC, between these two sets of samples.

For the set of samples that is characterised by lower average molecular weights of PBT and PC (Set 7 and also Set 1), at the lower pigment loadings, the tensile modulus is markedly more affected by differences (caused by the pigment) on the average molecular weight of PC. At the higher pigment loadings, the modulus is affected by the average molecular weight of both the PC and the PBT. For the set of samples with a higher average molecular weight (Set 2), the improvement in the modulus of the blend at the higher pigment loadings owes much to the major contribution from the molecular weight of PBT and of PC. As far as the lower pigment loadings are concerned, for this set of samples, the modulus is not affected notably by the increase in the pigment loading.

For Set 1 samples, the trend observed is the same as for samples of Set 2, at the pigment loadings greater than approximately 0.60 %. This observation is in agreement with previous comments on the effect of the pigment on the impact toughness, and on the tensile modulus, of samples of Sets 1 and 2. As was the case with the impact energy absorption, the behaviour of the tensile modulus of samples of Set 1 (pigment loadings between 0.10 and 0.50 %), resembles that of samples of Set 2, at pigment loadings above approximately 0.40 %, in terms of trend, and also in terms of the magnitude of the values.

Effect of Pigment Loading on the Strain at Break

For samples of Set 7, the inclusion of pigment in the blends leads to a quite marked increase in the strain at failure values. This is particularly true for pigment loadings that are lower than 0.30 %. At those loadings, larger standard deviation would be expected as uniform distribution of the pigment is not attained. As the pigment loading is increased, the strain at break decreases significantly and, thus, the blend responds more elastically to applied stress. The associated standard deviation decreases.

This behaviour can be understood bearing in mind the molecular weight distribution of PC and of PBT (Figure 3-38, Section 3.2.1.), the values of the non-isothermal crystallisation properties of PBT (Figure 3-42, Section 3.2.2.2.), and the degree of transesterification (Section 3.2.2.1.) in these blends.

The prominent increase in the strain at failure value at a pigment loading of 0.01 % coincides with the decrease of the PBT polydispersity, and with the decrease of the average molecular weight of the higher fraction of the molecular weight distribution of PBT. It also coincides with the lowest values of the crystallisation temperature and of the degree of crystallinity and with the greater values of the transesterification reaction extent.

As the pigment loading is increased, the strain at break value decreases, accompanying the increase in the average molecular weight of PBT, in the T_c and in the $-\Delta H_c$, and the decrease of the extent of transesterification.

It follows that there is a relationship between the average molecular weight of the higher fraction of the molecular weight distribution of PBT (which corresponds mainly to PBT 315), the non-isothermal crystallisation properties of PBT, the PC-PBT copolyester content, and the value of the strain at failure of the blend.

For large-strain fracture properties, the contribution of the crystalline phase is known to be significant. This is clear in the results presented in Figure 3-57. The greater the degree of crystallinity the more restrained is the motion of the polymeric chains and, thus, the lower is the extendibility of the PC/PBT/IM blend.

The lower the molecular weight of the polymeric species, the greater is the extendibility of the blends as the viscous response of the system is increased.

The greater the PC-PBT copolyester content, the greater the extendibility of the test specimen before breakage. This is because of the increased interconnection of the PC and PBT phases with increasing PC-PBT copolyester.

The set of samples that has a lower average molecular weight of PBT and of PC (Set 7) is characterised by a lower value of strain at break, than is the set of samples with higher average molecular weights (Sets 1 and 2), although the crystallinity of samples of Set 2 is greater than/equal to that of samples of Set 7. This is a consequence of the lower molecular weights of PBT and PC in samples of Set 7.

At the greater pigment loadings, for all the sets of samples, the inorganic pigment particles are thought to contribute to the decrease in the values of the strain at failure. This is because at high rates of deformation, as in stress-strain experiments, failure is often due to adhesive break down at the matrix-filler interface, occurring at interparticle boundaries, rather than to cohesive failure in the host polymer (Richard *et al.* 1985; Schreiber *et al.* 1990; Scherbakoff and Ishida 1997). This tendency increases with increasing filler loading.

Figure 3-58 relates to the behaviour of the stress at break, the strain at yield and the stress at yield of samples of Sets 1, 2 and 7, with varying pigment loading.

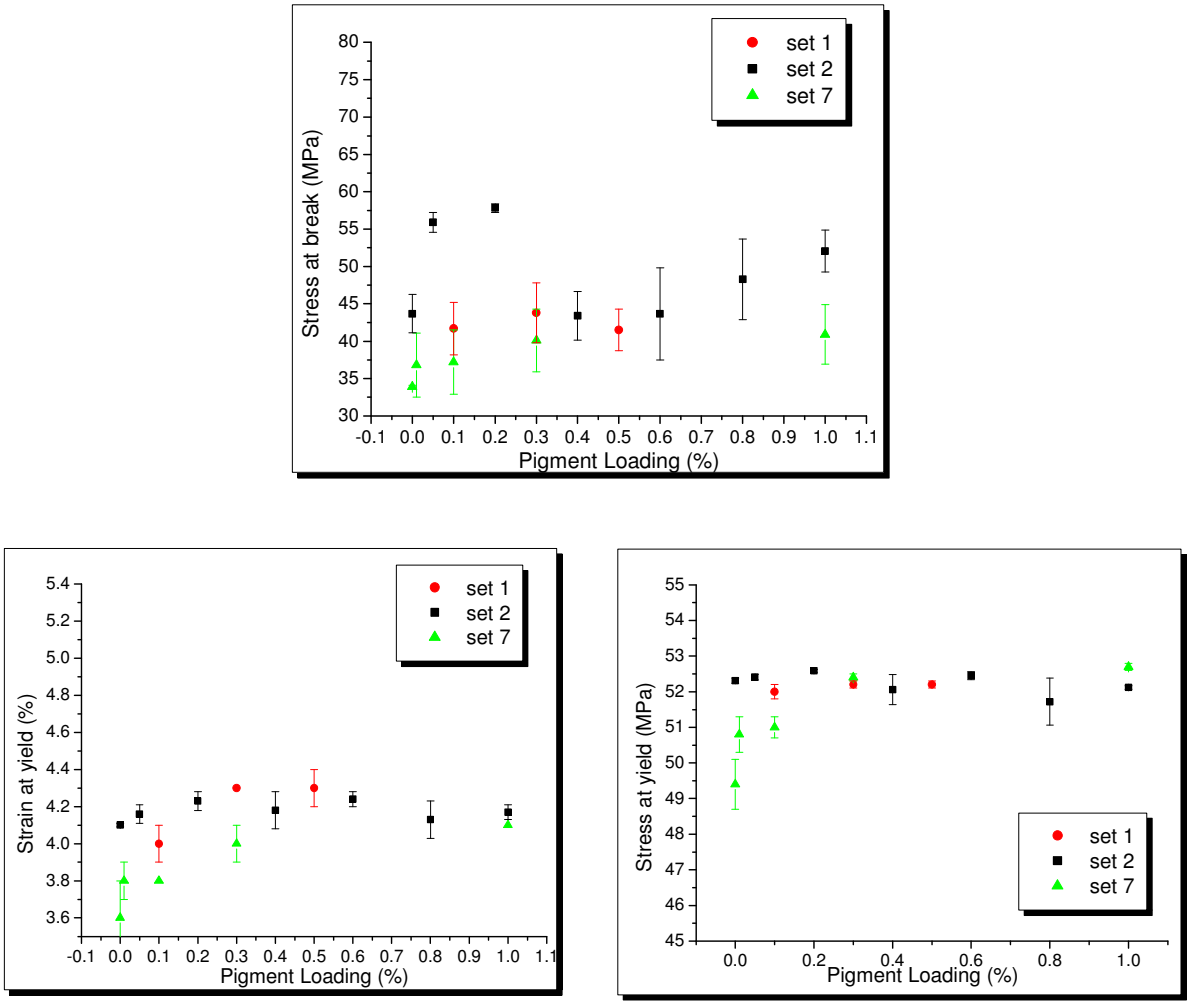

Figure 3-58. Stress at break, strain at yield and stress at yield as a function of C. I. Pigment Blue 28 loading, for samples of Sets 1, 2 and 7.

Effect of Pigment Loading on the Stress at Break

The values of the stress at break for samples of Set 1 are not affected significantly (bearing in mind the standard deviation), by the increase of the pigment loading. The values of the stress at break for these samples are lower than those for samples of Set 2, for the same pigment loading range. As far as samples of Set 7 are concerned, the introduction of the pigment in the blend, and the increase of its loading, initiates a marked increase of the stress at break values. This increase is evident even at the pigment loading of 0.01 %. This increase means that the stress needed to break the sample, when low deformation is applied, increases when C. I. Pigment Blue 28 is included in the blends. This trend follows the behaviour as that of the average molecular weight of PC (Figure 3-38, Section 3.2.1.) and, consequently, the stress at break values, for this set of samples, are influenced, to a large extent, by the molecular weight of the PC. This effect overcomes those due to

crystallinity differences, increasing presence of inorganic particles, differences in transesterification level, and differences in the molecular weight of PBT.

For the set of samples characterised by a higher average molecular weight of PC and of PBT (Set 2), the trend observed for the stress at break is not linear. After a pigment loading of approximately 0.40 %, the trend follows a similar trend to that of the set of samples with a lower average molecular weight of PC and of PBT (Set 7). The sets of samples characterised by lower values of the molecular weights of PC and of PBT have lower values of the stress at break. For samples of Set 7, the stress at break values follow a similar trend to that of the tensile modulus and to that of the yield stress, all stress-related properties.

Effect of Pigment Loading on the Strain at Yield

For the samples of Set 7, the trend observed is in line with that concerning the stress at break results and with that concerning the tensile modulus results. Thus, the strain at yield values for this set of samples are thought to be significantly influenced by the molecular weight of the PC. The strain range in which the blend behaves elastically is increased with increasing pigment loading due to increased average length of the PC chains.

The comparison of the values of the strain at yield of samples of Sets 1 and 7, with those obtained for samples of Set 2, leads to conclusions that are in line with those relating to the analysis of the tensile modulus. When compared to samples of Set 1 and 2, it can be seen that the value of the strain at yield is lower for samples of Set 7, until a pigment loading of approximately 0.30 % is reached. Above this loading, the strain at yield reaches the corresponding value in Sets 1 and 2.

The difference in the response of the blend to the presence and increase of pigment loading, between sets that were processed in extruder E1 (Sets 1and 2) and blends that were processed in extruder E2 (Set 7), is thought to derive from differences in the molecular weight of the polymers, mainly in the molecular weight of the PC. For the set of samples that is characterised by lower average molecular weights of PBT and PC (Set 7), at the lower pigment loadings, the strain at yield values are markedly more affected by differences in the average molecular weight of PC, derived from the presence of the pigment. At the higher pigment loadings, the strain at yield is affected by the average molecular weight of both the PC and the PBT.

For the set of samples characterised by a higher average molecular weight of PC and of PBT (Sets 1 and 2), the improvement in the strain at yield of the blend has a major contribution from the PC, at the lower pigment loadings. At the higher pigment loadings, the strain at yield is not so markedly affected by differences in the average molecular weight of both the PC and the PBT. The trend observed for samples of Set 1, is close to that of samples of Set 2, for the same pigment loading range.

Effect of Pigment Loading on the Stress at Yield

The values of the stress at yield for samples of Set 1 are not affected significantly by the increase of the pigment loading. Moreover, the stress at yield values of these samples are close to those of samples of Set 2, for the same pigment loading range. With regard to samples of Set 7, the trend observed is in line with that concerning the strain at yield, the stress at break and the tensile modulus. Hence, the stress range at which the blend behaves elastically increases with increasing pigment loading. Therefore, the molecular weight of the PC plays an important part with regard to the stress at yield, overcoming the effect of the degree of crystallinity, and the effect of the molecular weight of PBT, on this parameter.

The yield stress gives a qualitative guide to macromolecular chain mobility (Galeski 1990). The greater the molecular weight of PC, the lower is the chain mobility and, consequently, the greater are the values of the stress at yield. As is the case with the tensile modulus, the interfacial adhesion does not influence the yield stress values (Walker and Collyer 1994). From the above discussion it is concluded that the yield stress behaviour observed is due to the change of free volume of the polymer blend, a consequence of alterations in the molecular weight and, thus, the density, of the amorphous phase (Sanchez *et al.* 1993; Rodriguez *et al.* 1997).

3.2.9. Rheological Assessment (Melt Volume Rate)

In Figure 3-59 are presented the results concerning the melt viscosity assessment of samples of Sets 1, 2, 3, 4 and 7.

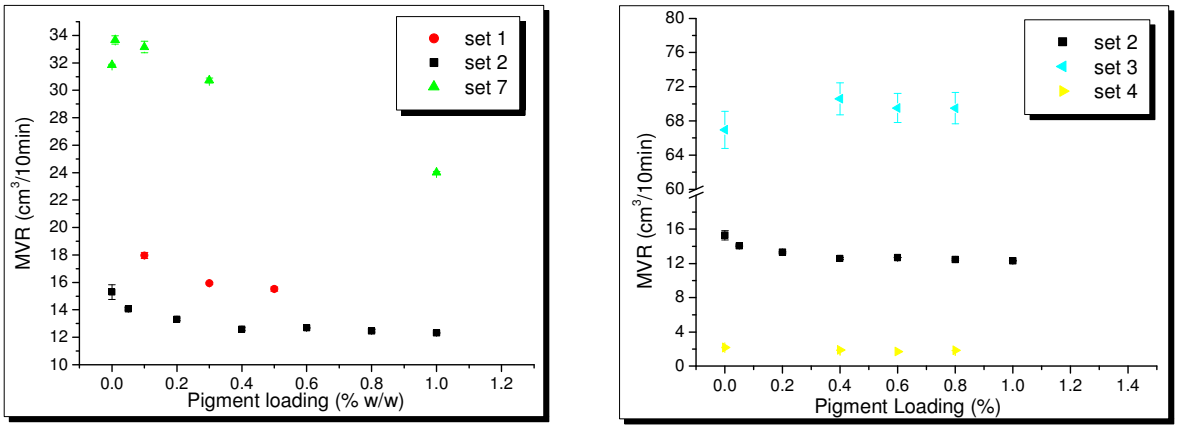

Figure 3-59. Melt volume rate as a function of the pigment loading for samples of Sets 1, 2, 3, 4 and 7.

Figure 3-59 shows that the inclusion and increase of C. I. Pigment Blue 28 loading in the PC-based samples (Set 4) does not lead to significant changes in the MVR values. Thus, for this set of samples, both the small differences in the molecular weight of PC in the pigmented samples and

the presence of C. I. Pigment Blue 28 do not influence significantly the melt viscosity of the PC phase.

For the PBT-based samples, the MVR change on the introduction and increase of the pigment loading follows the same trend as that of the molecular weight of PBT. Thus, the molecular weight of PBT, mainly that of the higher fraction of the molecular weight distribution, is determining the MVR values of the PBT phase.

The MVR values for the blend samples of Set 2 are intermediate between those of the individual phases (Sets 3 and 4), but closer to those of the PC-based samples. Therefore, it can be concluded that the PC phase is determinant as far as the melt viscosity of the blend is concerned.

The MVR value of the blend samples (Set 2) decreases with increasing pigment loading. This is in line with the increasing molecular weight of PC with increasing pigment loading in these samples. Therefore, it can be concluded that the greater the molecular weight of the PC in the PC-rich phase of PC/PBT/IM blends, the greater is the melt viscosity. This conclusion is in line with reports in the literature (Bertilsson *et al.* 1988b).

Samples of Set 1 follow a similar trend to that observed for samples of Set 2, but with greater values of MVR due to the lower molecular weight of PC, and PBT, in the samples of Set 2. The MVR values of Set 7 are significantly greater than those of samples of Sets 1 and 2. Therefore, further evidence is presented to the fact that the molecular weight of the polymers, mainly that of the PC, plays a decisive role in determining the melt viscosity.

For samples of Set 7 it can be seen that the trend observed in the MVR values with the introduction and increase in the pigment loading follows a trend that is similar to that observed for the PBT molecular weight. Thus, for this set of samples, and mainly for the lower pigment loadings, the molecular weight of the PBT phase is an important contributing factor to the melt viscosity values. Therefore, it is concluded that the lower the molecular weight of PC and PBT, the more important is the molecular weight of the semi-crystalline polymer in terms of the melt viscosity.

Temporary crosslinks in the melt due to particle-blend associations may also be contributing to the increase in viscosity with increasing pigment loading for the sets of samples that are characterised by a greater molecular weight of PC and PBT. The addition of solid particulates to a polymer increases the melt viscosity and decreases the melt elasticity (Scherbakoff and Ishida 1997).

3.2.10. Transmission Electron Microscopy

In Figure 3-60 is presented a typical TEM image of the PC/PBT/IM blends along with a schematic interpretation of the characteristic morphology observed. The TEM image corresponds to the cross-section of a tensile bar injection-molded using the unpigmented blend (BX).

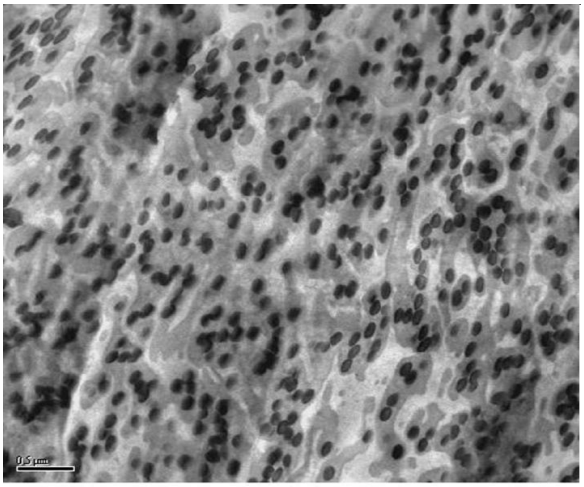

Unpigmented Blend - BX

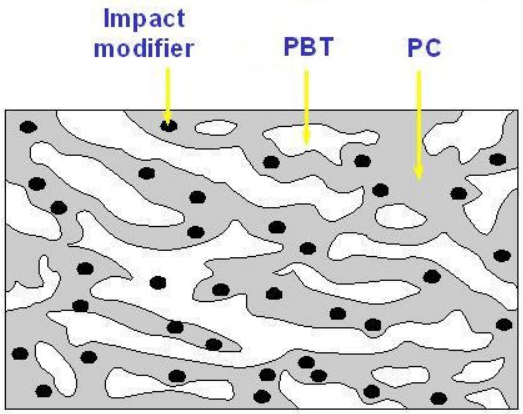

Figure 3-60. TEM image of the PC/PBT/IM blend corresponding to unpigmented blend BX.

In the TEM image presented in Figure 3-60, the PC domains can be identified with the darker areas and the PBT phase with the lighter areas. The IM particles are seen in the PC phase as small dark particles. In blends that are stabilised against transesterification, PC and PBT are only partially miscible (less than 10 %). This partial miscibility is clear in Figure 3-60. Figure 3-61 relates to samples processed in extruder E2 (Set 7).

In the images relating to pigmented blends, the pigment particles cannot be located in one or both of the phase domains. Even for the samples with 1.00 % pigment loading, it was not possible to locate the pigment in the blend morphology. This is thought to be due to the polymer phases being adsorbed at the surface of the pigment particulates, hindering these from TEM detection.

The images presented in Figure 3-61 show that with increasing pigment loading, the PC phase and the PBT phase become more distinct. The TEM images concerning the unpigmented blend and the blend with 0.01 % pigment loading are very similar but with somewhat coarser phase domains for sample L7. The morphology of the unpigmented blend is finer than that of the pigmented blends and, as the pigment loading increases, phase separation is more evident. These results are in line with the assessment of the molecular weight, and of the molecular weight distribution of the polymers, in particular those of the PC, by GPC (Section 3.2.1.).

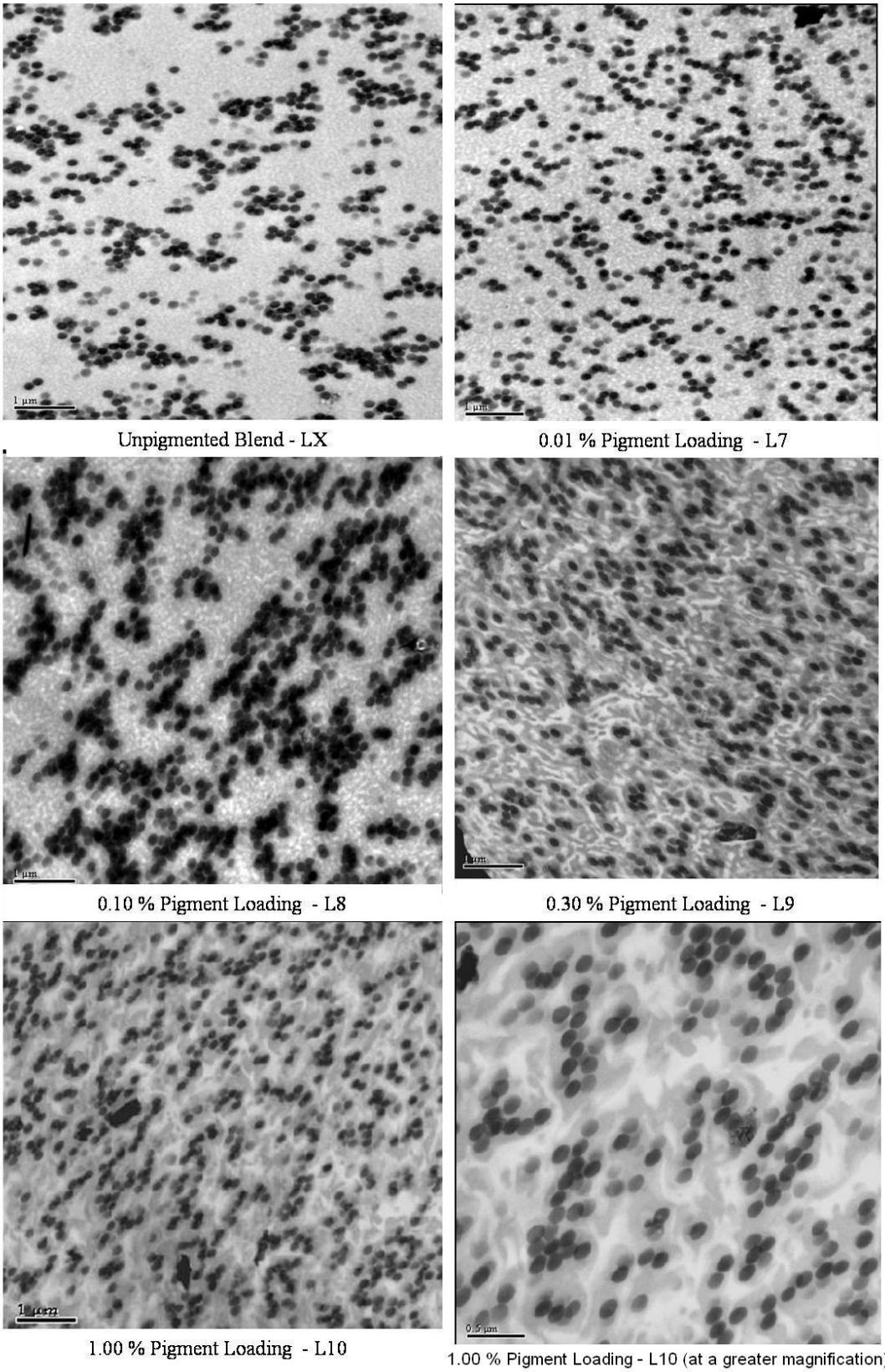

Figure 3-61. TEM images of samples of the blends processed in extruder E2 (Set 7).

For the sample with 0.10 % pigment, the impact modifier particles seem to be more clustered, and the phase domains coarser. The clustering of rubber (IM) particles is an evidence of transesterification. It can be concluded that this sample is more transesterified than the remaining. This agrees with the transesterification reaction assessment by means of the melting temperature depression method (Section 3.2.2.1.) and by means of the study of the crystallisation properties of PBT in these blends (Section 3.2.2.2.). In the image of the sample with 0.30 % pigment loading, a more defined phase separation is clearly seen. This increases thereafter with increasing pigment loading for sample L10.

Analysis of the TEM images of the samples of Set 7 show that the pigment has an effect on the morphology of the blend, by means of influencing the average molecular weights of the PC and PBT, and the degree of transesterification. Bearing in mind the analysis of the molecular weight distributions of PBT and PC, it can be concluded that the higher the average molecular weight of the PC, the more distinct is the phase separation of PBT and PC. These inferences are in line with the discussion of the DMTA results concerning these samples (Section 3.2.3.).

Figure 3-62 gives a comparison of the morphology of blend samples including 0.30 % of C. I. Pigment Blue 28, but processed in different extruders.

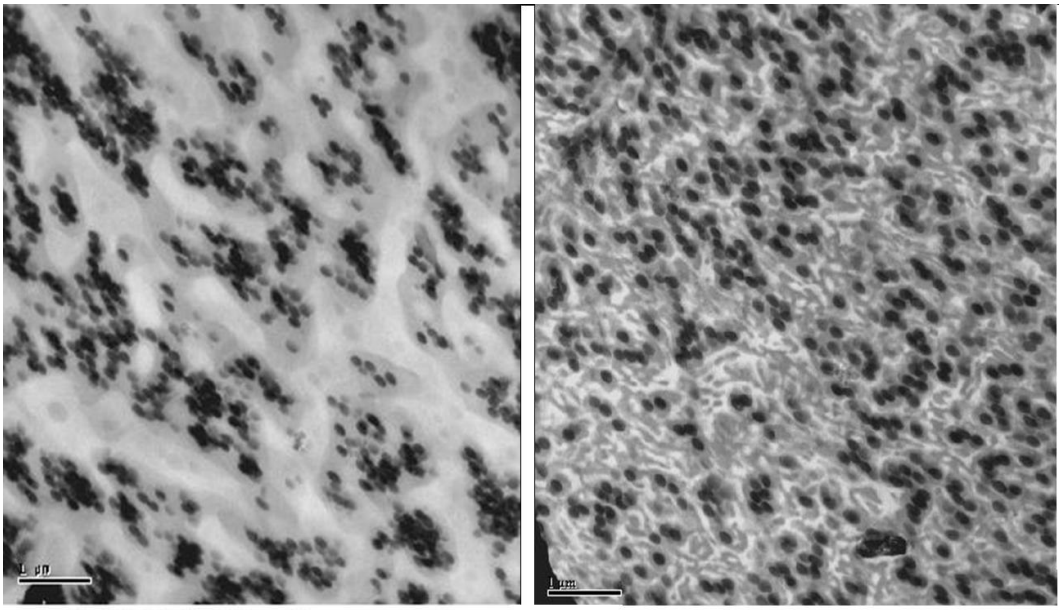

0.30 % Pigment Loading – B3 0.30 % Pigment Loading – L9

Figure 3-62. TEM images of blend samples pigmented with 0.30 % C. I. Pigment Blue 28 loading, processed in different extruders.

Sample B3 was processed in extruder E1 and sample L9 in extruder E2. It has been demonstrated that the processing conditions operating in extruder E2 lead to a more important thermal degradation of the polymeric chains and to increased levels of transesterification. This is clear in Figure 3-62. Bearing in mind the effects of different processing conditions on the

molecular weight distribution and transesterification reaction extent, it is clear from Figure 3-62 that a higher average molecular weight distribution of both the PC and the PBT, leads to a more well-defined phase separation, and larger PC, and PBT, domains. It should be noted that the degree of crystallinity in sample L9 is greater than that of sample B3 (Figure 3-42, Section 3.2.2.2.). Therefore, the effect of the lower molecular weight of PC and PBT, along with greater transesterification level, for sample L9 (Figure 3-40, Section 3.2.2.1.), overcome the expected effect of greater degree of crystallinity in the morpholgy observed.

Figures 3-63 and 3-64 relate to TEM imaging of tape-extruded samples of batches that were processed in extruder E1. The images represent samples of the unpigmented blend (BX) and of blends that are pigmented with low (0.05 %) and high (0.80 %) pigment loadings, batches B6 and B9, respectively.

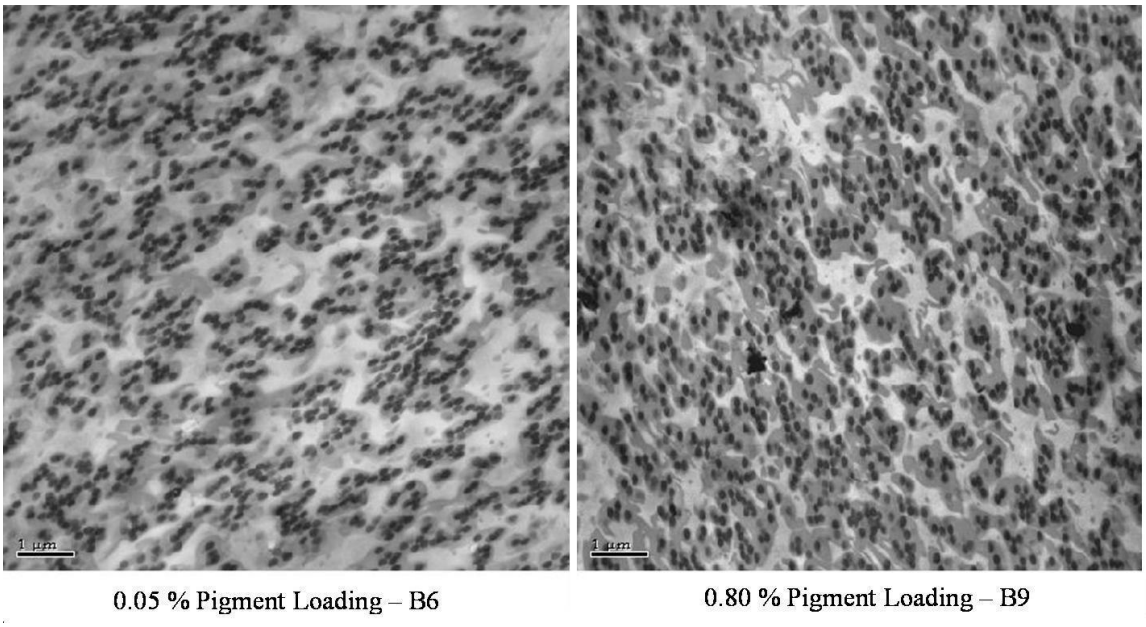

Figure 3-63. TEM images of blend samples (B6 and B9), processed in extruder E2.

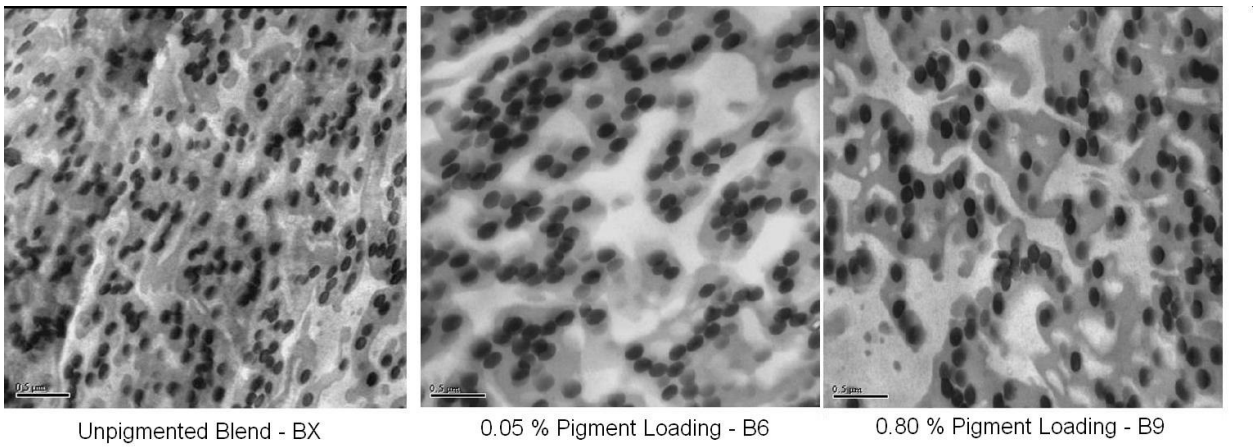

Figure 3-64. TEM images of blend samples (BX, B6 and B9), processed in extruder E2.

Figures 3-63 and 3-64 show that with increasing pigment loading there is better phase separation and more well-defined phase domains. When comparing the unpigmented sample with the pigmented samples it can be observed that the phase domains are larger and more well-defined for the pigmented samples. These results confirm the inferences made from the TEM images representing the samples of Set 7. Nevertheless, it can be said that the effects of better phase definition and increased phase separation with increasing pigment loading are not as striking in samples of Set 2 as they are for samples of Set 7, due to the greater molecular weights of PC and PBT for samples of Set 2. It can be concluded that for samples that were processed in extruder E1, the trend observed in Figures 3-63 and 3-64 is in line with the increase in the molecular weight of the polymers, mainly of the PC, with increasing pigment loading, as was the case with samples of Set 7.

3.3. Surface Modifications of C. I. Pigment Blue 28

3.3.1. Assessment of the Surfaces Interaction Potential by IGC

3.3.1.1. Determination of the Dispersive Component of the Surface Tension

The dispersive component of the surface tension of the modified pigments was determined using the approach of Fowkes, as described in Section 1.2.5.3. The results presented relate to columns 16 and 17 (Table 2-12, Section 2.6.2.), containing pigment **hiwre** and pigment **hiwren**, respectively.

The average carrier gas flow rate used was 65 cm^3/min and the pigment loadings on the columns stationary phase were 5.9 % and 5.0 % for columns 16 and 17, respectively. The temperature was varied between 323 K and 373 K, in increments of 10 K, in order to follow the changes in γ_s^d with temperature, and to evaluate the surface Lewis acidic/basic characteristics. The instrument used was the Fisons GC9100 unit.

The experimental parameters and results concerning the adsorption of n-alkanes on the surface of the surface-modified pigments are summarised in tables in Appendix B. Table 3-33 summarises the values that were determined for the dispersive component of the surface tension in the temperature ranges analysed.

It should be recalled that the acronym **hiwre** denotes the “Lewis acidic”, surface-treated C. I. Pigment Blue 28. The acronym **hiwren** denotes the pigment **hiwre** whose surface carboxylic acid groups have been neutralised with NaOH.

Table 3-33. Values of the dispersive component of the surface tension, γ_s^d (mJ/m^2), for the surfaces of the unmodified and surface-modified pigments.

T (K)	**Unmodified**	R^2	**Hiwre**	R^2	**Hiwren**	R^2
313	27.2±1.2	1.00	n/a	n/a	n/a	n/a
323	23.2±2.5	0.99	48.6±4.0	1.00	45.3±3.4	1.00
333	20.1±2.2	0.99	50.1±1.8	1.00	42.2±2.0	0.99
343	19.7±3.4	0.98	44.7±0.7	0.99	38.3±5.0	0.99
353	17.4±3.2	0.98	42.7±3.5	0.90	39.8±0.7	1.00
363	n/a	n/a	44.3±0.6	1.00	38.3±3.5	1.00
373	n/a	n/a	42.3±2.7	1.00	n/a	n/a
$\frac{d\gamma_s^d}{dT}$	-0.23±0.04	n/a	-0.15±0.01	n/a	-0.16±0.08	n/a

From observation of the data presented in Table 3-33 it can be concluded that the values of the dispersive component of the surface tension of the surface-modified pigments are greater than those of the unmodified pigment. Furthermore, the temperature coefficient, $\frac{d\gamma_s^d}{dT}$, is lower for the surface-modified pigments.

The values obtained for the γ_s^d of the surface-modified pigments correlate with the presence of organic species fixed onto the surface of these pigments. The values of γ_s^d in the case of **hiwre** and of **hiwren** decrease with increasing temperature, but in a less pronounced manner than for the unmodified pigment. This can also be attributed to a surface that shows a combination of characteristics of the original unmodified pigment and of the MAA polymeric species fixed to the inorganic surface.

The values of γ_s^d for the "Lewis acidic" pigment (**hiwre**) are greater than those for the "neutralised" pigment (**hiwren**). This difference is attributed to the fact that **hiwren** was obtained from **hiwre** by neutralisation of the surface carboxylic acid groups present in this surface-modified pigment. This process resulted in the replacement of the hydrogen atoms in the surface carboxylic acid groups by sodium atoms, which, in turn, increases the steric hindrance, that is unfavourable for the establishment of pigment-probe interactions.

The results presented in Table 3-33 indicate that the fixation of polymeric species onto the surface of C. I. Pigment Blue 28 was successful. Furthermore, it can be concluded that the surface-modified pigments have a greater potential to interact through dispersion intermolecular forces than does the unmodified pigment.

The enthalpy and the entropy of adsorption of the n-alkanes on the surface of the modified pigments were determined as described in Section 1.2.5.3. The results are summarised in Tables 3-34 and 3-35, for **hiwre** and **hiwren**, respectively.

Table 3-34. Enthalpy of adsorption, ΔH_a, and entropy of adsorption, ΔS_a, of the n-alkanes on the surface-modified pigment (**hiwre**).

Probe molecule	$a(\gamma_l^d)^{0.5}$ (cm^2 ($mJ\ cm^{-2}$)$^{0.5}$)	$-\Delta H_a$ (kJ/mol)	ΔS_a (J/molK)	R^2
C_8H_{18}	2.91E-16	52.0	-111.0	1.00
C_9H_{20}	3.29E-16	54.7	-110.0	1.00
$C_{10}H_{22}$	3.63E-16	59.7	-116.0	1.00
$C_{11}H_{24}$	3.99E-16	64.7	-122.0	1.00

Table 3-35. Enthalpy of adsorption, ΔH_a, and entropy of adsorption, ΔS_a, of the n-alkanes on the surface-modified pigment (**hiwren**).

Probe molecule	$a(\gamma_l^d)^{0.5}$ (cm^2 ($mJ\ cm^{-2}$)$^{0.5}$)	$-\Delta H_a$ (kJ/mol)	ΔS_a (J/molK)	R^2
C_7H_{16}	2.57E-16	31.1	-58.0	0.98
C_8H_{18}	2.91E-16	43.7	-87.0	0.96
C_9H_{20}	3.29E-16	47.1	-89.0	1.00
$C_{10}H_{22}$	3.63E-16	49.7	-89.0	1.00

Tables 3-34 and 3-35 show that the enthalpy and entropy of adsorption of n-alkanes on the surface of the modified pigments increase with increasing number of carbon atoms in the molecule. The values of $-\Delta H_a$ and of ΔS_a are greater for **hiwre** than they are for **hiwren**. This fact is in line with the results concerning γ_s^d (Table 3-33) and is due to the greater dispersive forces interaction potential of **hiwre**.

3.3.1.2. Determination of the Energy, Enthalpy and Entropy of Adsorption of Polar Probes

The specific component of the free energy of adsorption, $-\Delta G_a^s$, corresponding to the polar probes, was determined by the method outlined in Section 1.2.5.3. The polar probes used were DCM and THF, as representative of Lewis acidic probe molecules and of Lewis basic probe molecules, respectively. The average carrier gas flow rates were 20 cm^3/min and 80 cm^3/min for DCM and THF, respectively. Different values of the carrier gas flow rate had to be used for these probe molecules due to the significant differences in the magnitude of the retention times obtained.

In Tables 3-36 to 3-39 are presented the experimental parameters and results concerning the measurement temperature of 353 K. The experimental parameters and results concerning the remaining measurement temperatures are summarised in tables in Appendix B.

Table 3-36. Retention time, t_r, specific retention volume, V_g, energy of adsorption, RTLn(V_g), and corresponding dispersive and specific components, RTln($V^d_{g,ref}$) and RTln(V^s_g), respectively, for the surface-modified pigment (**hiwre**), at T = 353 K, F = 17.95 cm^3/min, J = 0.93, C = 0.98, P_{in} = 113.94 kPa, P_{out} = 100.15 kPa, $T_{flow\ meter}$ = 294 K.

Probe molecule	t_r (s)	V_n (cm^3)	RTLn(V_n) (kJ/mol)	$RT\ln(V^d_{n,ref})$ (kJ/mol)	$RT\ln(V^s_n)$ (kJ/mol)
CH_4	35.0	n/a	n/a	n/a	n/a
DCM	45.8	19.8	8.8	3.0	5.8

Table 3-37. Retention time, t_r, specific retention volume, V_g, energy of adsorption, RTLn(V_g), and corresponding dispersive and specific components, RTln($V^d_{g,ref}$) and RTln(V^s_g), respectively, for the surface-modified pigment (**hiwre**), at T = 353 K, F = 85.71 cm^3/min, J = 0.77, C = 0.97, P_{in} = 157.04 kPa, P_{out} = 100.16 kPa, $T_{flow\ meter}$ = 295 K.

Probe molecule	t_r (s)	V_n (cm^3)	RTLn(V_n) (kJ/mol)	$RT\ln(V^d_{n,ref})$ (kJ/mol)	$RT\ln(V^s_n)$ (kJ/mol)
CH_4	11.8	n/a	n/a	n/a	n/a
THF	381.7	2647.4	23.1	6.7	16.4

Table 3-38. Retention time, t_r, specific retention volume, V_g, energy of adsorption, RTLn(V_g), and corresponding dispersive and specific components, RTln($V^d_{g,ref}$) and RTln(V^s_g), respectively, for the surface-modified pigment (**hiwren**), at T = 353 K, F = 18.83 cm^3/min, J = 0.93, C = 0.98, P_{in} = 113.94 kPa, P_{out} = 100.15 kPa, $T_{flow\ meter}$ = 294 K.

Probe molecule	t_r (s)	V_n (cm^3)	RTLn(V_n) (kJ/mol)	$RT\ln(V^d_{n,ref})$ (kJ/mol)	$RT\ln(V^s_n)$ (kJ/mol)
CH_4	32.5	n/a	n/a	n/a	n/a
DCM	40.2	18.1	8.5	3.3	5.2

Table 3-39. Retention time, t_r, specific retention volume, V_g, energy of adsorption, RTLn(V_g), and corresponding dispersive and specific components, RTln($V^d_{g,ref}$) and RTln(V^s_g), respectively, for the surface-modified pigment (**hiwren**), at T = 353 K, F = 78.62 cm^3/min, J = 0.80, C = 0.98, P_{in} = 148.42 kPa, P_{out} = 100.15 kPa, $T_{flow\ meter}$ = 294 K.

Probe molecule	t_r (s)	V_n (cm^3)	RTLn(V_n) (kJ/mol)	$RT\ln(V^d_{n,ref})$ (kJ/mol)	$RT\ln(V^s_n)$ (kJ/mol)
CH_4	13.2	n/a	n/a	n/a	n/a
THF	150.8	1157.8	20.7	6.9	13.8

From the analysis of the data that are presented in Tables 4-36 to 4-39 it can be inferred that the surfaces of **hiwre** and **hiwren** are Lewis amphoteric. The enthalpy, and entropy, of adsorption of DCM and THF, along with the corresponding dispersive and specific components, were determined by the method outlined in Section 1.2.5.3. The results are summarised in Tables 3-40 and 3-41 for **hiwre** and **hiwren**, respectively.

Table 3-40. Dispersive and specific components of the enthalpy of adsorption and of the entropy of adsorption, ΔH^d_a, ΔH^s_a and ΔS^d_a, ΔS^s_a, respectively, of the polar probes, on the surface of the surface-modified pigment (**hiwre**).

Probe molecule	$a(\gamma_l^d)^{0.5}$ (cm^2 (mJ $cm^{-2})^{0.5}$)	$-\Delta H^d_a$ (kJ/mol)	ΔS^d_a (J/molK)	R^2	AN* (kJ/mol)	DN (kJ/mol)	$-\Delta H^s_a$ (kJ/mol)	ΔS^s_a (J/molK)	R^2
DCM	1.65E-16	30.2	-77.0	0.93	16.4	0.0	19.7	-39.0	0.83
THF	2.13E-16	40.6	-96.0	0.98	2.1	84.4	71.9	-164.0	0.91

Table 3-41. Dispersive and specific components of the enthalpy of adsorption and of the entropy of adsorption, ΔH^d_a, ΔH^s_a and ΔS^d_a, ΔS^s_a, respectively, of the polar probes, on the surface of the surface-modified pigment (**hiwren**).

Probe molecule	$a(\gamma_l^d)^{0.5}$ (cm^2 (mJ $cm^{-2})^{0.5}$)	$-\Delta H^d_a$ (kJ/mol)	ΔS^d_a (J/molK)	R^2	AN* (kJ/mol)	DN (kJ/mol)	$-\Delta H^s_a$ (kJ/mol)	ΔS^s_a (J/molK)	R^2
DCM	1.65E-16	22.3	-53.0	0.91	16.4	0.0	15.7	-116.0	0.84
THF	2.13E-16	31.8	-70.0	0.98	2.1	84.4	26.6	-37.0	0.94

With regard to the dispersive component of the enthalpy, and of the entropy, of adsorption of the probe-molecules, it can be observed that the values are greater for **hiwre** than they are for **hiwren**. This behaviour is in agreement with the analysis of $-\Delta H_a$, and of ΔS_a, for the adsorption of apolar probes, and of γ_s^d, for these pigments. The differences in the specific component of the enthalpy of adsorption of DCM and of THF on the surfaces of the modified pigments, and on the surface of the unmodified pigment, are discussed in the following section.

3.3.1.3. Consequences of the Surface Modifications to the Intermolecular Interactions Potential of the Pigments

The effects of the surface modifications of C. I. Pigment Blue 28 on the dispersive intermolecular interactions interaction potential has been discussed in Section 3.3.1.1. In the following paragraphs are considered the consequences of the surface modifications to the interaction potential of the pigment through specific interactions. In Figures 3-65 and 3-66 are compared the values of $-\Delta G^s_a$ and $-\Delta H^s_a$, respectively, relating to the adsorption of DCM and of THF on the surface of the unmodified and surface-modified pigments. Furthermore, the ratio, and

the sum of $-\Delta G_a^s$ (and of $-\Delta H^s_a$) for DCM and THF are used to assess the influence of the surface treatments on the relative, and total, specific interactions potential, respectively.

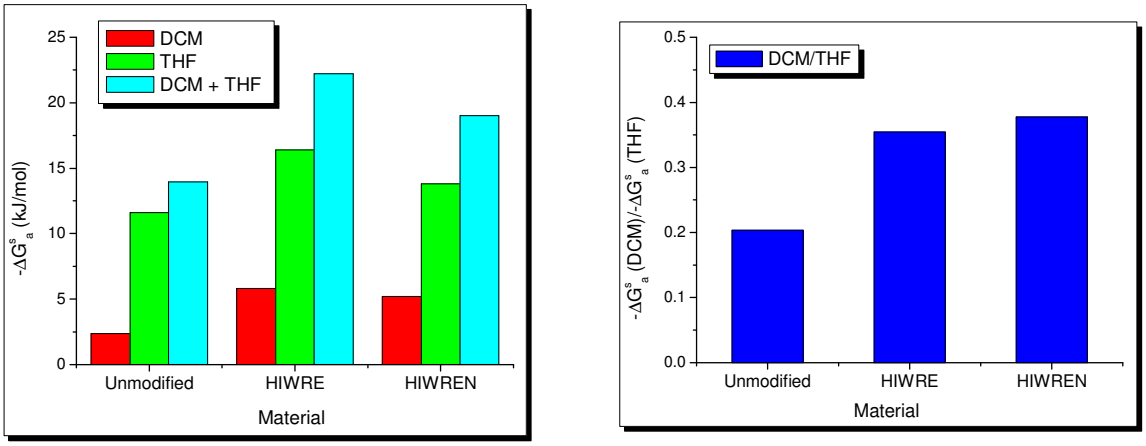

Figure 3-65. Comparison of the specific component of the energy of adsorption of DCM and of THF on the unmodified pigment and on the surface-treated pigments, at 353 K.

Figure 3-65 gives a comparison of the values of $-\Delta G_a^s$ for DCM and for THF on the surface-treated pigments, and on the suface of the unmodified pigment, at the measurement temperature of 353 K.

Figure 3-65 shows that the surface Lewis basicity, as quantified in $-\Delta G_a^s$ relating to DCM, is significantly greater for **hiwre** and **hiwren** than it is for the unmodified pigment. The surface Lewis acidity, as quantified in $-\Delta G_a^s$ relating to THF, increases in the order: unmodified pigment < **hiwren** < **hiwre**. The total Lewis acid/base interaction potential is greater for **hiwre**, followed by **hiwren**, and significantly lower for the unmodified pigment. The relative presence of Lewis basic sites to Lewis acidic sites increases in the order: unmodified pigment < **hiwre** < **hiwren**. It can be inferred that the modification of C. I. Pigment Blue 28 increases significantly the surface Lewis acidic and basic properties of this pigment. The neutralisation of the surface carboxylic acid groups present in **hiwre** results in a decrease of the surface Lewis acidity. The surface treatments also result in a significant increase of the surface Lewis basicity. The neutralisation of the surface carboxylic acid groups present in **hiwre** does not lead to a significant change in the surface Lewis basicity. The fixation of PMAA units onto the surface of the pigment results in an important increase in the total specific interactions potential. These inferences provide important information regarding the influence of the surface modifications on the surface chemistry of the pigments. Nevertheless, as discussed previously, the analysis of the specific component of the enthalpy of adsorption will supply a more complete and rigorous examination of the Lewis acid/base interaction potential of these pigments.

In Figure 3-66 are compared the specific component of the enthalpy of adsorption of DCM, and of THF, on the surface of the unmodified pigment and on the surface of the surface-treated pigments.

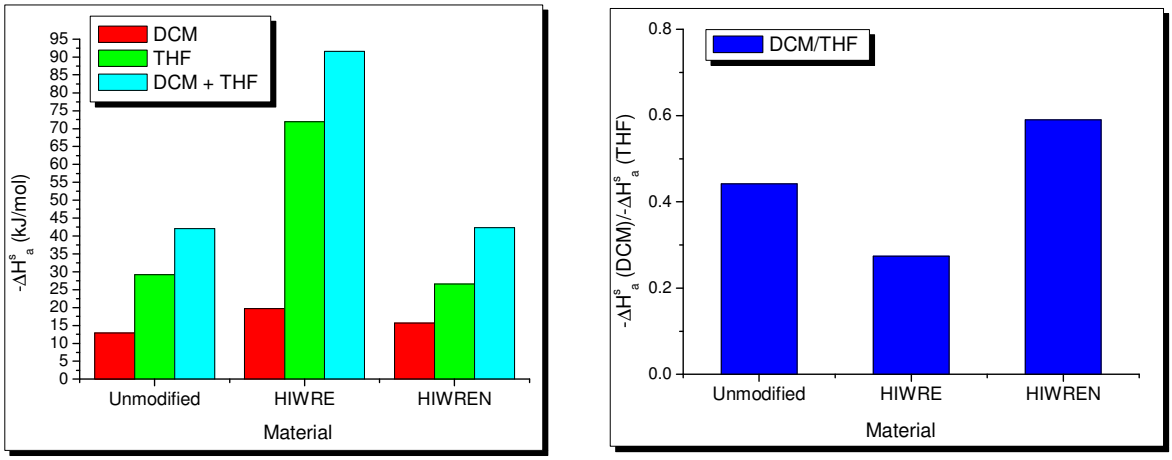

Figure 3-66. Comparison of the specific component of the enthalpy of adsorption of DCM and of THF on the unmodified pigment and on the surface-treated pigments.

The observation of Figure 3-66 leads to the conclusion that the surface Lewis acidity is greatly increased upon the surface treatment of C. I. Pigment Blue 28. When the surface carboxylic groups are neutralised, the Lewis acidity is significantly reduced, and is close to that of the unmodified pigment. The surface Lewis basicity increases due to the surface treatment and is slightly reduced after neutralisation of the surface carboxylic acid groups. The changes observed in terms of the surface Lewis acidity/basicity are in line with the presence of MAA-based polymeric species on the surface of the treated C. I. Pigment Blue 28. Bearing in mind the repeating unit in MAA (Figure 2-13, Section 2.9.), the important increase in the Lewis acidity is related to the presence of the side carboxylic acid group units, and is localised in the hydrogen atom. The increased Lewis basicity is related to the presence of the oxygen atoms in the carboxylic acid groups. After neutralisation of the carboxylic acid functional groups, the Lewis acidity is reduced due to the abstraction of the hydrogen atom. The Lewis basicity is slightly reduced due to the greater steric hindrance caused by the replacement of the hydrogen atom by the more bulky sodium atom, that increases the hindrance in the access to the oxygen atoms by an interacting species.

The total interaction potential of the surface of C. I. Pigment Blue 28 is greatly increased by the surface photosensitised grafting, and is reduced after the neutralisation process. The relative presence of Lewis basic sites to Lewis acidic sites is decreased due to the surface treatment, and increases upon the neutralisation procedure, in relation to that of the unmodified pigment.

A difference of at least 8 kJ/mol between the enthalpies of acid/base interactions from the retention behaviour of basic or acidic probes with two surface-modified inorganic fillers is considered to be sufficient to produce a corresponding difference in the interfacial behaviour of the two surface modification types (Tiburcio and Manson 1991a). Thus, it can be concluded that the surface modification, consisting of fixing PMAA onto the surface of the pigment, was successful, and is expected to influence significantly the physical properties and the mechanical properties of pigmented PC/PBT/IM blends. The surface-treated pigment was further modified in order to achieve a significant decrease in the surface Lewis acidity. This modification step was also found to be successful.

The influence of the changes of the surface Lewis acidity/basicity on the physical properties and on the mechanical properties of pigmented PC/PBT/IM blends is discussed in Section 3.4. Further to the influence of the surface Lewis acidic/basic properties, the existence of polymeric chains fixed onto the surface and the physical properties (particle size and particle size distribution) of the pigments will also be considered when analysing the influence of the surface modifications on the properties of the pigmented blends.

In the following sections the presence of the fixed organic species on the surface of the pigments is assessed using thermal, gravimetric, microscopic and other analytical techniques. It should be mentioned that the per cent fixation to be determined using the above mentioned techniques does not correspond solely to grafted material but to any material that is fixed to the surface of the pigment, upon surface treatment, and that is not released after the extensive washing and extraction operations.

3.3.2. SEM/EDXA on the Unmodified C. I. Pigment Blue 28 and on the Modified C. I. Pigment Blue 28

Figure 3-67 gives SEM images of dispersions of the pigments (unmodified and surface-treated) in distilled water.

Images (a), (d) and (g) correspond to the control sample, images (b), (e) and (h) to **hiwre**, and images (c), (f) and (i) to **hiwren**. Images (a), (b) and (c) relate to magnification level of x50, images (d), (e) and (f) to magnification level of x1000, and images (g), (h) and (i) to magnification level of x5000.

The experimental protocol is described in Section 2.5.1.2.

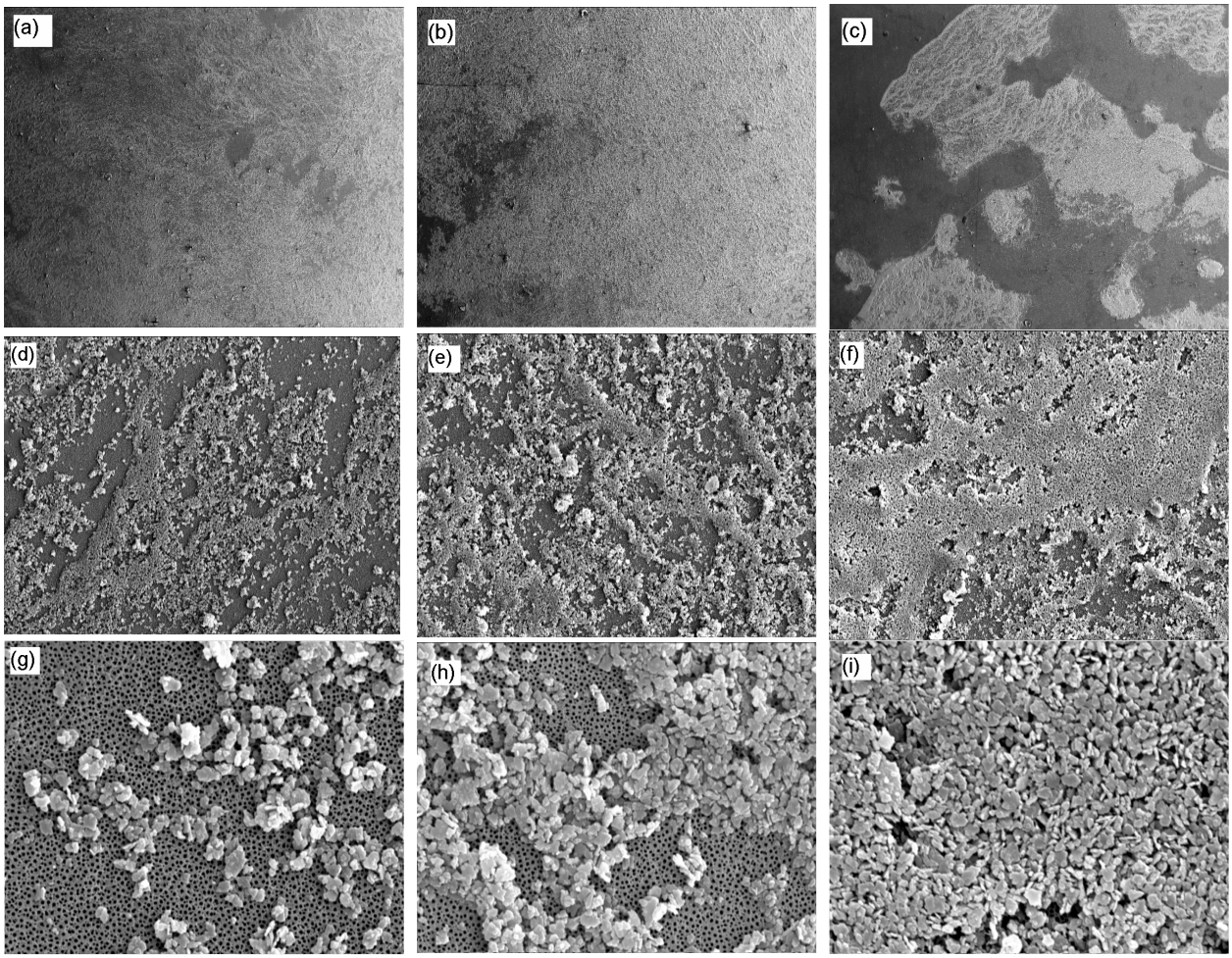

Figure 3-67. SEM imaging of aqueous dispersions of the unmodified pigment and of the surface-treated C. I. Pigment Blue 28.

It is clear from the images presented in Figure 3-67 that the dispersability of the pigment changes after the surface modification. The level of aggregation, after removal of the dispersion medium, increases in the following order: unmodified pigment **< hiwre < hiwren**. Thus, in the case of the "neutralised" pigment, the inter-particle, Lewis acid/base interactions are stronger than for the unmodified pigment and than for the "Lewis acidic" pigment. This is understood on the basis of the significantly predominant Lewis acidic character of **hiwre** (and, thus significant Lewis acid/acid repulsion), and bearing in mind the fact that the neutralisation of the carboxylic acid groups in **hiwre** is not complete and, consequently, there will be stronger interaction between the acidic and the basic moieties, and lower acid/acid repulsion, at the surface of **hiwren**. In conclusion, upon removal of the dispersion medium, the inter-particle interactions are stronger in the case of the surface-modified pigments, in line with the IGC analysis of the interaction potential of these pigments (Section 3.3.1.).

EDX analysis was carried out on the surface-modified pigments, and on control samples, to confirm the presence of fixed organic material at the surface of the pigments, and in an attempt at quantification of the organic coating attained. The experimental procedure was described in Section 2.5.1.2. The results are presented in Appendix E and summarised in Table 3-42 and Figure 3-68.

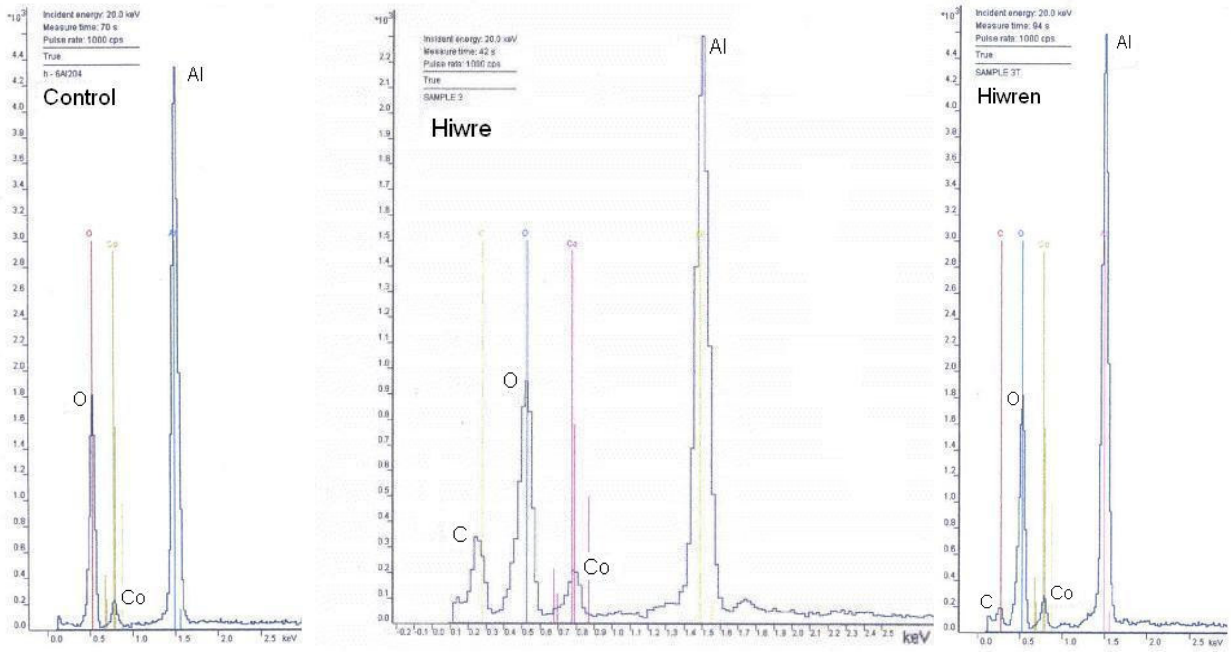

Figure 3-68. Spectra relating to EDX analysis of the surface of the unmodified pigment and of the surface-modified pigments.

Figure 3-68 shows that the surface of pigment BASF Sicopal® Blue K6310 contains oxygen, cobalt and aluminium in the approximate proportion 51:23:26 (Table 3-42). The surfaces of the modified pigments, **hiwre** and **hiwren**, show the presence of carbon, in addition to the aforementioned species. These results further confirm the success of the fixation of MAA-based polymeric species onto the surface of C. I. Pigment Blue 28.

Table 3-42. Percentage of carbon, aluminium, cobalt and oxygen elements present at the surface of the unmodified and surface-modified pigments, as determined by EDXA.

	% C	% Al	% Co	% O
Control Sample	0.00	25.63	22.89	51.48
Hiwren	5.74	28.33	29.65	36.27

The signal relating to carbon in the **hiwre** sample was not strong enough to allow for quantification of this element. This indicates the existence of sample heterogeneity, with regard to

the surface treatment. Therefore, the per cent fixation determined using the EDXA results concerning **hiwren** must be interpreted with care.

The percentage of fixed MAA units was calculated on the basis of the mass of carbon in each monomer unit. Thus, bearing in mind the molar mass of MAA and that of carbon, and the molecular formula of MAA, the mass of MAA, m_{MAA}, is given by: $m_{MAA} = m_c/0.558$, were m_c is the mass of carbon as determined by EDXA. From the values presented in Table 3-42, the amount of organic material fixed to the surface of the surface-modified pigments is estimated to be 5.2 % (w/w).

3.3.3. Determination of the pH of Dispersions of the Unmodified and Modified Pigments in Water

The pH values of aqueous dispersions of the pigments give an estimate of the extent, and nature, of the surface modifications. Thus, the pH values of the surface-modified pigment dispersions are compared to that of the unmodified pigment. It was considered that the greater the difference, the stronger would be the indication that modification of the surface had taken place.

The quantity expressed in Equation 3-1, E, is the surface modification effectiveness:

$$E = \frac{pH - pH_{H_2O}}{m} \qquad (3\text{-}1)$$

Here, pH denotes the pH of the pigment dispersion, pH_{H_2O} denotes the pH value for the dispersion medium (distilled water) and "m" is the mass of dispersed pigment. The lower the value of E, the more extensive would be the surface treatment of the pigment towards acidity. On the other hand, the greater the value of E, the more basic is the surface of the pigment.

Table 3-43 gives the values of E for the control samples (non-hydrated and hydrated C. I. Pigment Blue 28) and for the surface-modified pigments (**hiwre** and **hiwren**).

Table 3-43. Effectiveness of the surface treatment of C. I. Pigment Blue 28 as quantified by the pH of aqueous dispersions of the pigments.

	E (g^{-1})
Control sample	16.04
Hydrated control sample	15.28
Hiwre	0.97
Hiwren	21.80

The E parameter of hydrated $CoAl_2O_4$ is lower than that of the non-hydrated $CoAl_2O_4$, confirming the formation of acidic OH surface groups upon hydration of C. I. Pigment Blue 28. From the values presented in Table 3-43 it can be observed that the acidity of C. I. Pigment Blue 28 has been significantly enhanced due to the surface treatment employed. Moreover, the

neutralisation of the surface carboxylic acid groups leads to a marked decrease of the surface acidic properties and an increase of the surface basic character. The values observed for the surface-modified pigments clearly differ from those obtained for the control samples, and are in line with the results and discussion presented in Section 3.3.1.3., concerning the consequences of the surface treatments to the surface Lewis acidity/basicity.

3.3.4. Thermogravimetric Analysis

The weight losses of samples of the photoinitiator (ITX), of the grafting polymer (PMAA), and of the pigments (control sample, hydrated control sample, and surface-modified versions of C. I. Pigment Blue 28) were determined as described in Section 2.4.2. A qualitative, and quantitative, evaluation of the polymeric species fixed to the surface of the pigment was carried out. From the weight loss that occurred on heat treating the pigment sample at 600 ºC for 30 minutes in the TGA cell, taking into account the results concerning the control samples, the amount of material fixed to the surface of the pigment was estimated. The thermograms are presented in Appendix D and the results summarised in Table 3-44.

Table 3-44. Weight losses of the photoinitiator (ITX), PMMA, and pigments (C. I. Pigment Blue 28 and surface-modified versions: **hiwre** and **hiwren**), after heat treatment at 600 ºC for 30 minutes.

	Weight loss (%)
ITX	99.83
PMMA	32.49
C. I. Pigment Blue 28	0.87
Hydrated C. I. Pigment Blue 28	0.93
Hiwre*	1.74±0.02
Hiwren	1.98

*average of three samples

The results indicate that no organic surface coating is present in the commercial C. I. Pigment Blue 28 (BASF Sicopal® Blue K6310), as the mass loss relating to this pigment is not in line with the presence of such industrial coating. From the values presented in Table 3-44 it can be argued that the hydration of the commercial pigment does not lead to a significant, TG detectable, increase in the total mass loss of water molecules present at the surface of the pigment. However, evidence of significant physisorbed water molecules on the surface of the hydrated pigment is displayed in the TG plot (Appendix D). The mass loss for the non-hydrated pigment curve is significant only above 202 ºC, while, in the hydrated pigment, significant mass loss starts occuring at 190 ºC, corresponding to physisorbed water molecules. Moreover, once significant mass loss occurs, it is more pronounced in the case of the hydrated pigment. It can be concluded that the hydration of C. I. Pigment Blue 28 led to an increase in the extent of physisorbed water molecules.

The results concerning the modified pigments (**hiwre** and **hiwren**) confirm the presence of fixed material on the surface of the modified C. I. Pigment Blue 28, a consequence of the photosensitised grafting procedure. The differences observed between **hiwre** and **hiwren** are not very significant. This is in agreement with expectation, bearing in mind that **hiwren** differs from **hiwre** in that in the former the surface carboxylic acid groups have been neutralised with NaOH. From the values presented in Table 3-44, the amount of fixed material on the surface of **hiwre** is 2.59 % (w/w). The temperatures at which significant mass loss occurs are 200 and 195 ºC for **hiwre** and **hiwren**, respectively. Once significant mass loss begins, it is more pronounced for the modified pigments than it is for the non-hydrated and for the hydrated commercial pigment. This signifies that the amount of physisorbed water is greater in the surface-modified pigments. This is tought to be a consequence of the presence of fixed polymeric species that provide the surface of the modified pigments with greater interaction potential, as discussed in Section 3.3.1.3. No significant differences exist, with regard to the intensity of the mass loss, between **hiwre** and **hiwren**, although the thermogram weight loss scale makes it difficult to reach definitive conclusions.

3.3.5. Gravimetric Studies

The mass of grafted polymer (and of homopolymer firmly fixed to the surface) can be calculated using the expression:

$$\% \text{ fixation} = (W_f - W_c)/W_c \times 100\% \qquad (3\text{-}2)$$

Here, W_f is the mass of dried, extracted, surface-treated pigment, as determined from Section 2.13.2.4., and W_c is the mass of pigment prior to the surface treatment. Typical values for the extent of surface treatment that were obtained were 6.8±1 % (w/w). The high standard deviation (15 % relative standard deviation) could be due to incomplete pigment drying, which would alter the values determined in the weighing operations. Thus, the data arising from this method of determining the amount of fixed material should be treated with care.

3.3.6. Titration of the Carboxylic Acid Groups Fixed to the Surface of the Modified Pigments

In order to quantify the carboxylic acid groups fixed to the surface of the pigment, the MAA surface-modified pigments were titrated with solutions of NaOH of increasing concentration. Solomon and Hawthorne (1983) have shown that measurement of the acidity of inorganic particles in aqueous suspension does not give a valid indication of their potential acidity because of the effect of water molecules on the nature of the inorganic particles surface and because of the levelling effect of the solvent on the activity of the strongly acidic species.

Several factors are thought to contribute to the impossibility of quantifying the carboxylic acid groups content of the modified pigments. These include:

i) Dissociative chemisorption of water molecules at the uncovered pigment surface;

ii) Interaction of water molecules with the MAA-based polymeric species fixed at the surface of the pigment, and

iii) Interaction of the OH^- ions, originated from the NaOH solution, with the covered and uncovered surface.

Because of the above observations no further titration experiments were carried out.

3.3.7. Particle Sizing of the Unmodified Pigment and of the Modified Pigments

The particle size and the particle size distribution of the control (unmodified) pigment, BASF Sicopal® Blue K6310, and of the surface-modified pigments, **hiwre** and **hiwren**, were determined as described in Section 2.8. The results are summarised in Table 3-45.

Table 3-45. Average particle size and 95 % limits of the particle size distribution of the control samples and of the surface-modified pigments.

	Average particle size (μm)	95 % limits (μm)
Control sample	0.497	0.460-0.533
Hiwre	0.420	0.392-0.449
Hiwren	0.489	0.454-0.525

The average particle size of the surface-modified pigments is lower than that of the control sample. Moreover, the average particle size of the "Lewis acidic" pigment is lower than that of the "neutralised" pigment. These realisations are thought to be due to improved pigment dispersion in the aqueous medium, a consequence of the surface modification.

The strong surface Lewis acidic properties of **hiwre** cause decreased particle-particle interaction due to decreased Lewis acid-base interaction and increased Lewis acid-acid repulsion, between the pigment particles.

For **hiwren**, the slight improved pigment dispersion, in relation to that of the control sample, is thought to arise from greater interaction steric hindrance originating from the MAA polymeric chains fixed to the surface of the pigment.

The spatial hindrance caused by the fixed polymeric species also causes the average particle size of the **hiwre** pigment to be the lowest. The analysis of the 95 % limits of the particle size distribution supports this point. Thus, the particle size distribution of the surface-modified pigments

is narrower than that of the control sample. Furthermore, that corresponding to the "Lewis acidic" pigment is narrower than that of the "neutralised" pigment.

It is observed that the particle size and particle size distribution differences due to the pigment surface modification procedure ought not to influence significantly the physical properties and the mechanical properties of the pigmented PC/PBT/IM blends.

3.4. Influence of the Surface Modifications of C. I. Pigment Blue 28 on the Physical Properties and on the Mechanical Properties of PC/PBT/IM Blends

The major physical properties of inorganic particles that influence the properties of the polymeric matrixes in which they are incorporated are the average particle size, the particle size distribution, the surface area, and the surface chemical properties. The particle size and size distribution results presented in Section 3.3.7., suggest that the consequences of the differences observed in these pigment characteristics on the physical properties and on the mechanical properties of pigmented PC/PBT/IM blends, are not expected to be dominant.

The steric factors inherent to the presence of fixed polymeric chains on the surface of the treated pigments are also thought to influence the interaction of these pigments with other materials. The adhesion bond between the polymer and the inorganic particulates depends not only on chemical factors, such as ionic and hydrogen bonds, but also on physical factors such as mechanical links (anchoring effects).

Surface area changes through surface modification are thought not to be significant from the point of view of the physical properties and of the mechanical properties of the pigmented composites. This inference is based on the small changes in average particle size, particle size distribution, and the estimated relatively low (in terms of weight per cent) amount of polymeric species fixed on the surface of the surface-modified pigments.

In the next sections are considered the direct and indirect effects of the surface modifications of C. I. Pigment Blue 28 on the physical properties and on the mechanical properties of pigmented PC/PBT/IM blends.

3.4.1. Gel Permeation Chromatography

In Figure 3-69 are presented the values of the average-molecular weight, $\bar{M}_w$, number-average molecular weight, $\bar{M}_n$, and polydispersity of PC and PBT in samples of Sets 1, 2, 5 and 6. Samples of Sets 5 and 6 relate to blends incorporating the "Lewis acidic" pigment, **hiwre**, and the "neutralised" pigment, **hiwren**, respectively.

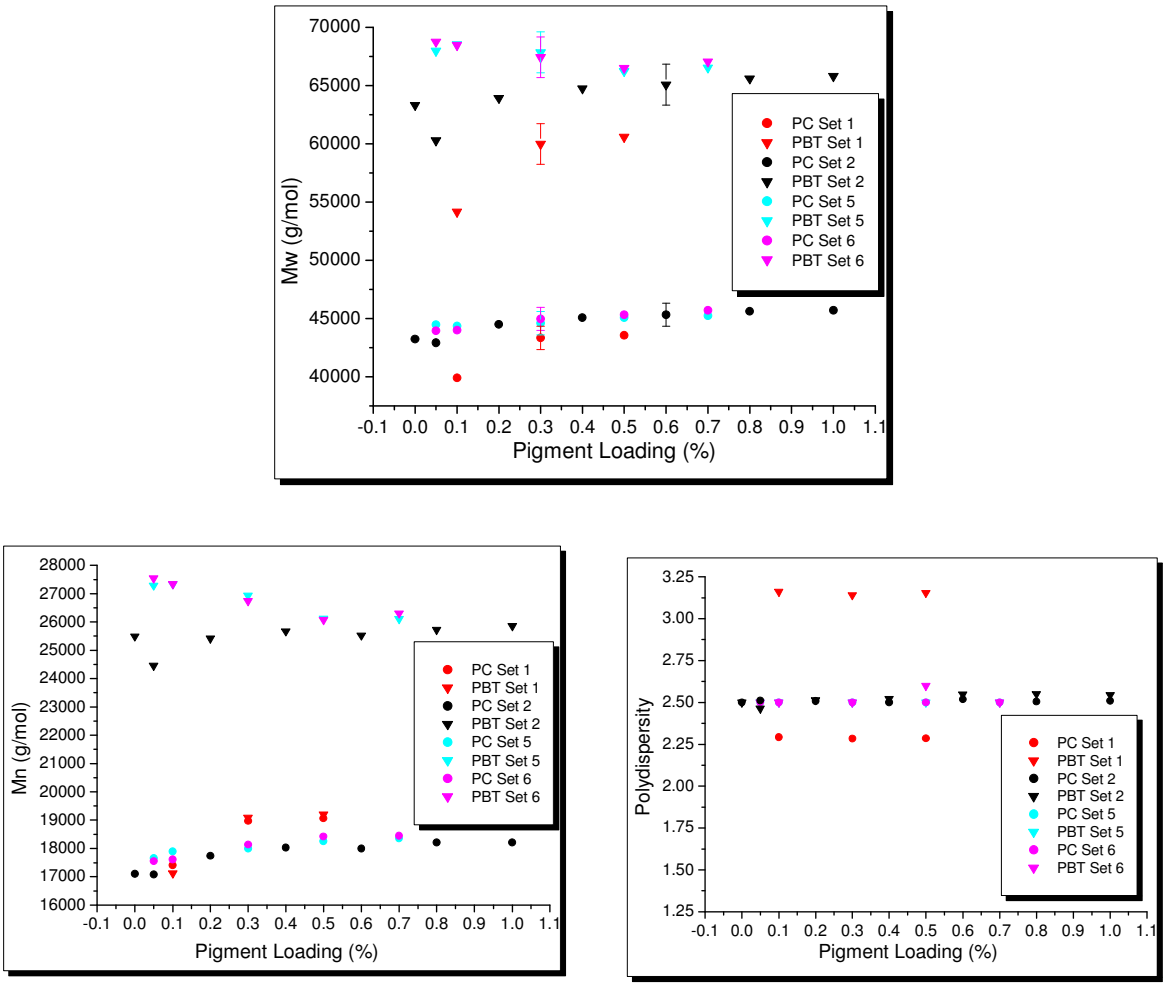

Figure 3-69. Weight-average molecular weight, number-average molecular weight and polydispersity of PC and of PBT in samples of Sets 1, 2, 5 and 6.

From Figure 3-69, it is clear that the average molecular weights of PBT and of PC in the blends that include the modified pigments (Sets 5 and 6) are greater than those corresponding to the blends in which the unmodified pigment was used (Sets 1 and 2). This difference is particularly striking for the blends that were extruded using the same extrusion settings (rpm and throughput), Sets 1, 5 and 6. Moreover, the aforementioned effects are more pronounced in the case of the PBT, and at the lower pigment loadings.

With respect to Sets 5 and 6, the molecular weight values of PC increase, although only slightly, with increasing pigment loading. The molecular weight of PBT is greater at the lower pigment loadings, decreasing slightly with increasing pigment loading. This behaviour is completely different from that oberved for the samples that include the unmodified pigment. The molecular weight change with increasing pigment loading is more consistent in the blends where

the modified pigments were used. This conclusion is very important, from the point of view of the application and processing of these blends.

It can also be concluded that the surface modifications of the pigment reduce very significantly transesterification/polymer chain scission at the lower pigment loadings. The reason for this resides in the surface chemistry differences due to the surface modifications. Improved adhesion between the pigment and the polymers, namely the PBT, leading to a better wetting of the surface of the pigments by the polymers and, thus, less pronounced differences in the heat transfer capacity between the pigment particles and the matrix polymers, is thought to contribute to the observed behaviour.

In extrusion operations involving PBT, the average molecular weight of this polymer decreases slightly with increasing number of processed batches, without following any relation with pigment type and loading (Timmerman, T. *et al.* 2001, Personal Communication). This point indicates that the small decrease observed in the values of $\bar{M}_W$ for PBT in samples of Sets 5 and 6 (Figure 3-69) is due to the continuous processing operations, that slightly decrease the PBT $\bar{M}_W$, probably consequence of higher temperatures in the extruder, and not due to the presence of the pigment.

3.4.2. Differential Scanning Calorimetry

3.4.2.1. Heating Mode

Heating mode DSC thermograms were obtained following the protocol that is described in Section 2.4.1. The thermograms relating to samples of Sets 5 and 6 are presented in Appendix C. With regard to samples of Set 5 (Figures C-35 to C-44), the following observations can be made. In the heating cycle thermograms, the extrusion-driven, crystalline phase-related, exotherm peak temperature increases with increasing pigment loading. Moreover, this increase is more significant than it is for samples of Set 2. In the reheating cycle thermograms, this exotherm is not present. From the previous inferences, the effect of the surface modifications of the pigment on the crystalline phase is confirmed and correlates well with the greater degree of crystallinity and with the greater non-isothermal crystallisation temperature for samples of Set 5, (discussed in the next section). The recrystallisation peak temperature increases with increasing pigment loading. This indicates that there is a more significant influence of the modified pigment on the phase separation of PC and PBT and on the degree of crystallinity, when compared to the effect of the unmodified pigment. Upon reheating the sample in the DSC cell, this exothermic phenomenon is thought to be overlapped by the secondary melting process, whose characteristic temperature increases with increasing pigment loading. This endothermic phenomenon (the secondary melting process) is not present in the heating cycle thermograms. Therefore, further evidence is presented, concerning the

significant influence of the surface modifications of the pigment on the crystalline properties, and on the phase separation phenomena, upon reheating of the sample in the DSC cell.

As far as samples of Set 6 are concerned, (Figures C-45 to C-53), the trends observed for the tape-extrusion driven exothermic change, for the recrystallisation exothermic change, and for the minor endothermic change, are analogous to those observed for samples of Set 5, although in a less well-defined manner. This is in agreement with the lower degree of crystallinity and with the lower non-isothermal crystallisation temperature for these samples when compared to those obtained for samples of Set 5 (Section 3.4.2.2.).

In Figure 3-70 are represented the values of the first and second scan T_m, and the corresponding difference, ΔT_m, as a function of the pigment loading for the samples of Sets 1, 2, 5 and 6.

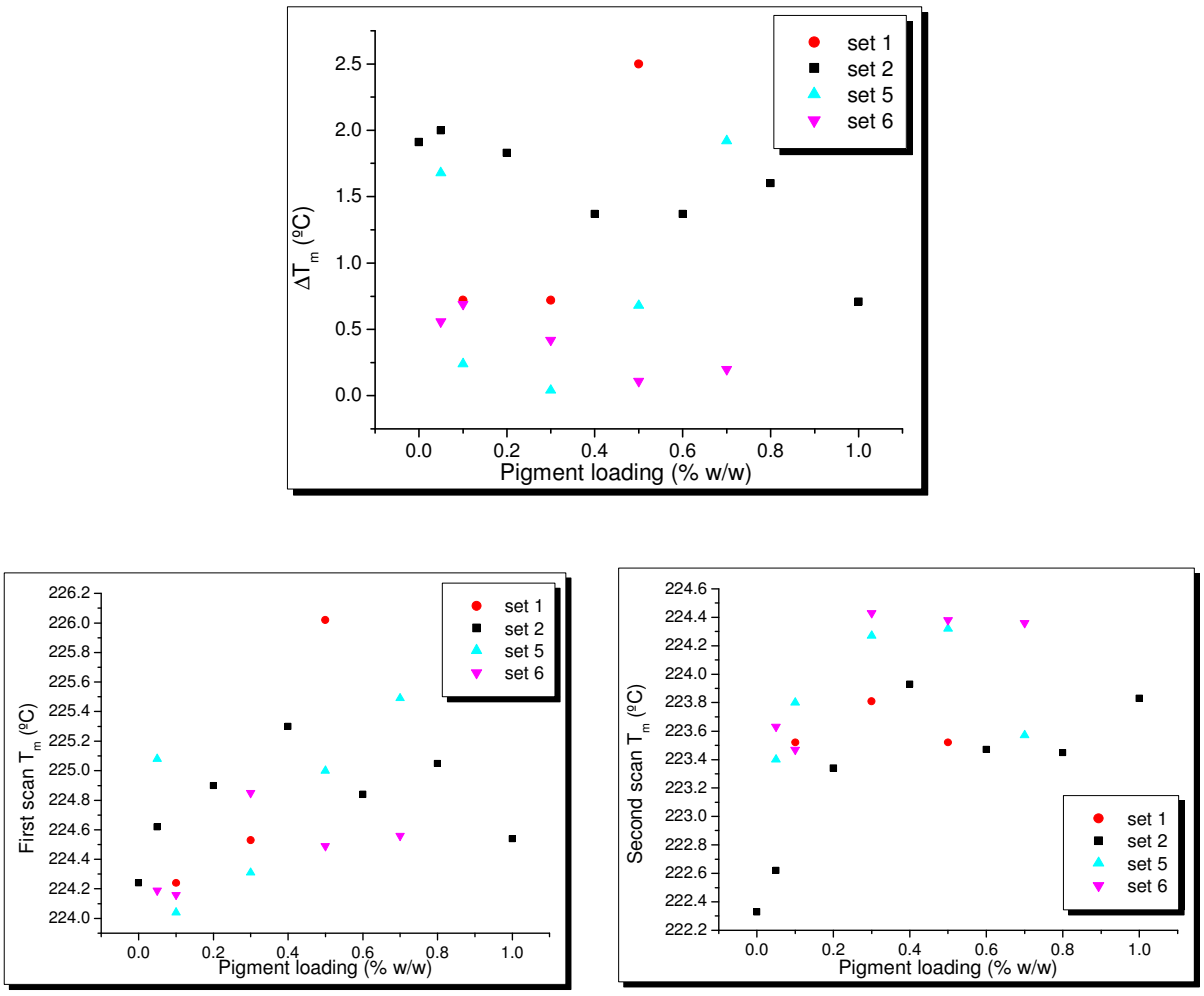

Figure 3-70. Melting temperature, second scan melting temperature and T_m variation from the first scan to the second scan, as a function of the pigment loading in the PC/PBT/IM blends represented by Sets 1, 2, 5 and 6.

As mentioned in Section 3.2.2.1., the number of factors influencing the values of the first scan T_m does not allow for an interpretation of the complex behaviour observed. The comments made regarding the 0.50 % pigment loading sample of Set 1 (Section 3.2.2.1.) apply to the 0.05 % pigment loading sample of Set 5. As far as samples of Set 5 are concerned, it can be observed that the second scan T_m follows a trend that is similar to that of samples of Sets 1 and 2. The major difference is in the greater values for the samples that include the modified pigment.

The results obtained for samples of Sets 5 and 6 are in line with the greater molecular weight of the polymers, mainly of the PBT (Section 3.4.1.), and with the greater degree of crystallinity in the samples of Sets 5 and 6 (Section 3.4.2.2.), when compared to the values obtained for samples of Sets 1 and 2.

With regard to the values of ΔT_m, samples of Sets 5 and 6 are characterised by lower values than those corresponding to samples of the sets containing the unmodified pigment. Therefore, the surface modification of the pigment influences the extent of transesterification.

The presence of the unmodified pigment particles at the PC/PBT interphase is thought to play a role in the transesterification level. Thus, it is expected that alterations to the preferential presence of the pigment particles in the blend morphology contribute to the behaviour observed for ΔT_m, in the case of the surface-modified pigments. In fact, the modified version of the pigment that is included in samples of Set 5 is preferentially located in the PBT-rich phase, and the surface-modified version that is used in the blends of Set 6 is shown to be preferentially located in the PC-rich phase (Sections 3.4.9. and 3.4.10.).

Also, better adhesion between the polymers and the surface-modified pigment particles, as predicted from the interaction potential analysis by IGC (Section 3.3.1.), leads to better wetting and, thus, to improved thermal isolation of the surface-modified particles. This would reduce the heat concentration/dilution effect of the pigment particles, and have consequences thereof to the transesterification level and to the thermal degradation of the polymers.

The surface-modified versions of the pigment do not cause thermal degradation of the polymers molecular weight (Section 3.4.1.), and lead to increased non-isothermal crystallisation temperatures and to higher degrees of crystallinity (Section 3.4.2.2.). Both factors support the results concerning ΔT_m, and confirm the lower degree of transesterification in samples of Sets 5 and 6.

3.4.2.2. Cooling Mode

The values determined for the non-isothermal crystallisation properties of samples of Sets 5 and 6 are summarised in Table 3-46 and represented graphically in Figure 3-71.

Table 3-46. Values of the crystallisation on-set temperature ($T_{c,on\text{-}set}$), the crystallisation off-set temperature ($T_{c,\ off\text{-}set}$), the difference between the latter (ΔT), the crystallisation temperature (T_c) and the enthalpy of crystallisation ($-\Delta H_c$), relating to samples of Sets 5 and 6.

Blend sample	Pigment loading (%)	$T_{c,on\text{-}set}$ (K)	$T_{c,\ off\text{-}set}$ (K)	ΔT (K)	T_c (K)	$-\Delta H_c$ (J/g)	% Crystallinity
B18	0.05	469.6	458.2	11.4	463.7	-37.0	26.0
B19	0.10	470.9	458.8	12.1	464.6	-37.2	26.2
B20	0.30	471.7	460.5	11.2	466.3	-37.0	26.0
B21	0.50	472.9	462.3	10.6	467.7	-36.8	25.9
B22	0.70	473.0	462.8	10.2	468.0	-37.1	26.1
B23	0.05	469.1	458.6	10.5	463.5	-36.0	25.4
B24	0.10	469.9	458.2	11.7	463.9	-35.5	25.0
B25	0.30	471.3	460.3	11.0	465.8	-35.6	25.1
B26	0.50	472.5	461.2	11.3	466.9	-35.8	25.2
B27	0.70	472.3	461.9	10.4	467.0	-36.3	25.6

For the key to these samples see Section 2.1.

Figure 3-71 summarises the variation of the crystallisation temperature, and of the difference between the crystallisation on-set and off-set temperatures, with increasing pigment loading for samples of Sets 1, 2, 5 and 6.

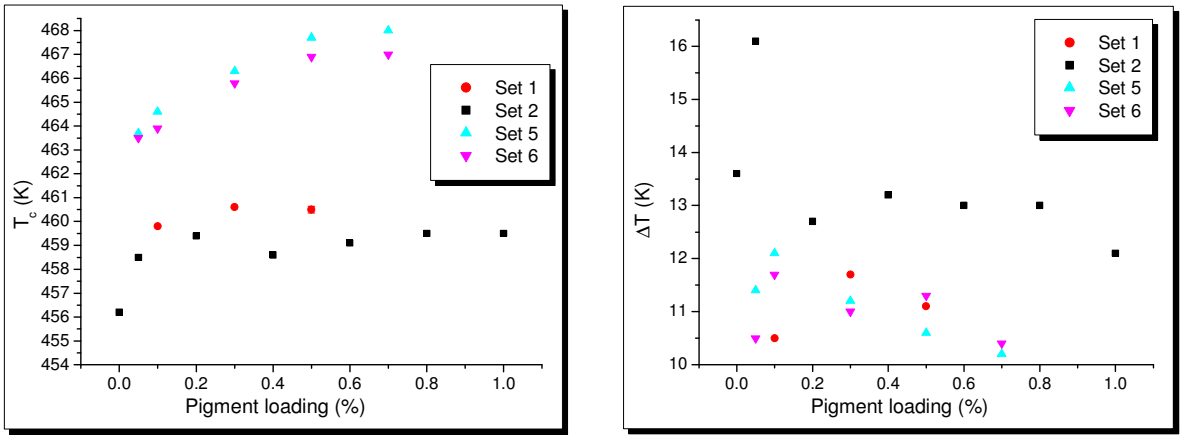

Figure 3-71. Non-isothermal crystallisation temperature and ΔT, *versus* pigment loading for samples of the PC/PBT/IM blends represented by Sets 1, 2, 5 and 6.

In Figure 3-71 it is evident that there is a very significant increase in the crystallisation temperature of the blends that include the surface-modified versions of C. I. Pigment Blue 28. A change of up to 12 K occurs for the samples having a pigment loading of 0.50 % (w/w), Sets 1 and 5. Moreover, the value of T_c increases with increasing pigment loading. The surface modifications of the pigment particles lead to a decrease of the crystallisation activation energy. The crystallisation activation energy decreases further with increasing pigment loading. The crystallisation temperatures for samples of Set 6 are lower than those for samples of Set 5. The

differences between the two sets increase with increasing pigment loading. This behaviour is due to the fact that samples of Set 6 correspond to the surface-modified pigment in which the grafted PMAA units have been neutralised with NaOH, thus reducing significantly the Lewis acidity of the surface, as quantified by IGC analysis of these pigments (Section 3.3.1.). Bearing in mind that the samples of Sets 5 and 6 have greater average molecular weights of PC and PBT than the samples of Sets 1 and 2, the nucleating effect of the surface-modified pigments is concluded to be very prominent.

Analysing the plot involving ΔT, and comparing Sets 2, 5 and 6, it can be inferred that the surface-modifications of C. I. Pigment Blue 28 lead to increased rates of crystallisation, when comparing sets that are characterised by having similar average molecular weight values of PC and PBT (Sets 2, 5 and 6 at pigment loadings that are between 0.40 and 0.80 %).

The rate of crystallisation of samples of Set 1 is comparable to that of samples of Sets 5 and 6. This is thought to be due to the lower average molecular weight of PC and PBT for samples of Set 1, which leads to increased rate of crystallisation. For samples of Sets 5 and 6, there is a slow down of the rate of crystallisation when the pigment loading is increased from 0.05 to 0.10 %, thereafter the rate of crystallisation increasing with increasing pigment loading. Bearing in mind the significantly low pigment loading of 0.05 %, the value determined for ΔT may be due to pigment dispersion issues, resulting in sampling heterogeneity. If, at that pigment loading, the pigment particles are agglomerated, the observed decrease in the rate of crystallisation could be due to the strong interaction between the PBT and the surface of the pigments.

Strong interactions between macromolecules and the surface of inorganic particles lower the macromolecular chain mobility. This, in turn, slows down the growth rate of polycrystalline aggregates and also the overall crystallisation rate (Galeski 1990). If the interaction between the pigment and the matrix is too strong, the polymer density close to the surface of the pigment will increase largely and may inhibit crystallisation by restricting too much the movement of the polymeric chains.

The rate of crystallisation of the samples of Set 5 is comparable to that of samples of Set 6. Therefore, the differences in the surface Lewis acidity/basicity between the surface-treated pigments do not cause changes in the rate of crystallisation.

In conclusion, the stronger interaction between the surface-modified pigments and the PBT leads to intense nucleation and an increased rate of crystallisation, when compared to the unmodified pigment. These could, in turn, result in transcrystallinity phenomena (Galeski 1990) originating at the surface of the pigment.

In Figure 3-72 are presented the values of the enthalpy of crystallisation, and of the crystallinity degree, with increasing pigment loading, for samples of Sets 1, 2, 5 and 6.

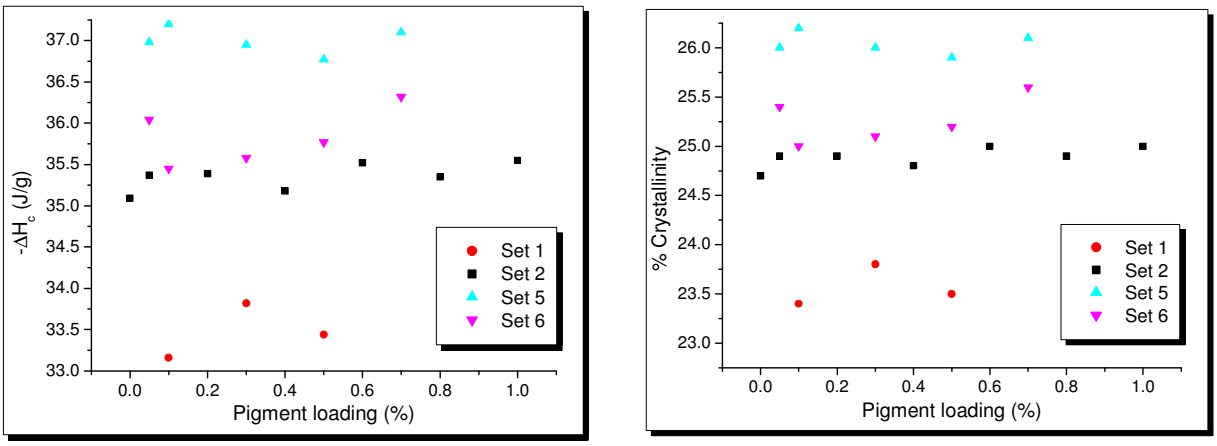

Figure 3-72. Enthalpy of crystallisation and degree of crystallinity, *versus* pigment loading for samples of the pigmented PC/PBT/IM blends represented by Sets 1, 2, 5 and 6.

From Figure 3-72 it can be concluded that the surface modifications of C. I. Pigment Blue 28 lead to a greater degree of crystallinity. Increasing the pigment loading does not lead to a clear change in the degree of crystallinity of the samples containing the surface-modified pigments.

The degree of crystallinity of samples of Set 5 is greater than that of samples of Set 6. Thus, the surface modification that provides the surface of the pigment with the greater Lewis acidic character causes a higher degree of crystallinity. This finding is in line with the IGC characterisation of PBT 195, of PBT 315, and of the pigments (Sections 3.1.6., 3.1.7. and 3.3.1., repectively).

In terms of the influence of the pigment particles properties on the crystallisation of PBT, the major aspects to consider are the particle size, the surface area, and the surface chemistry. From the particle size and particle size distribution analysis results, presented in Section 3.3.7., it can be concluded that these physical characteristics do not contribute significantly to the differences observed in the crystallisation properties of PBT. The surface chemistry differences between the pigments are thought to be the major factor influencing the crystallisation properties of PBT in the blends in which these pigments were incorporated.

As a final remark it is inferred that, from the industrial processing point of view, the accelerated nucleation is a process desirable to reducing cycle times in injection moulding operations.

3.4.3. Dynamic Mechanical Thermal Analysis

Figure 3-73 relates to the variation of the storage modulus, the loss modulus and the loss tangent with temperature, for samples of Sets 1, 2, 5 and 6. In Figure 3-73 are compared the results relating to the unpigmented blend (BX), and blends with 0.30 % pigment loading (unmodified, and

surface-modified pigments), processed in the same extruder and using the same extrusion settings. Sample B3 concerns the commercial C. I. Pigment Blue 28, and samples B20 and B25 concern the "Lewis acidic version" and the "neutralised version" of the surface-modified pigments, respectively.

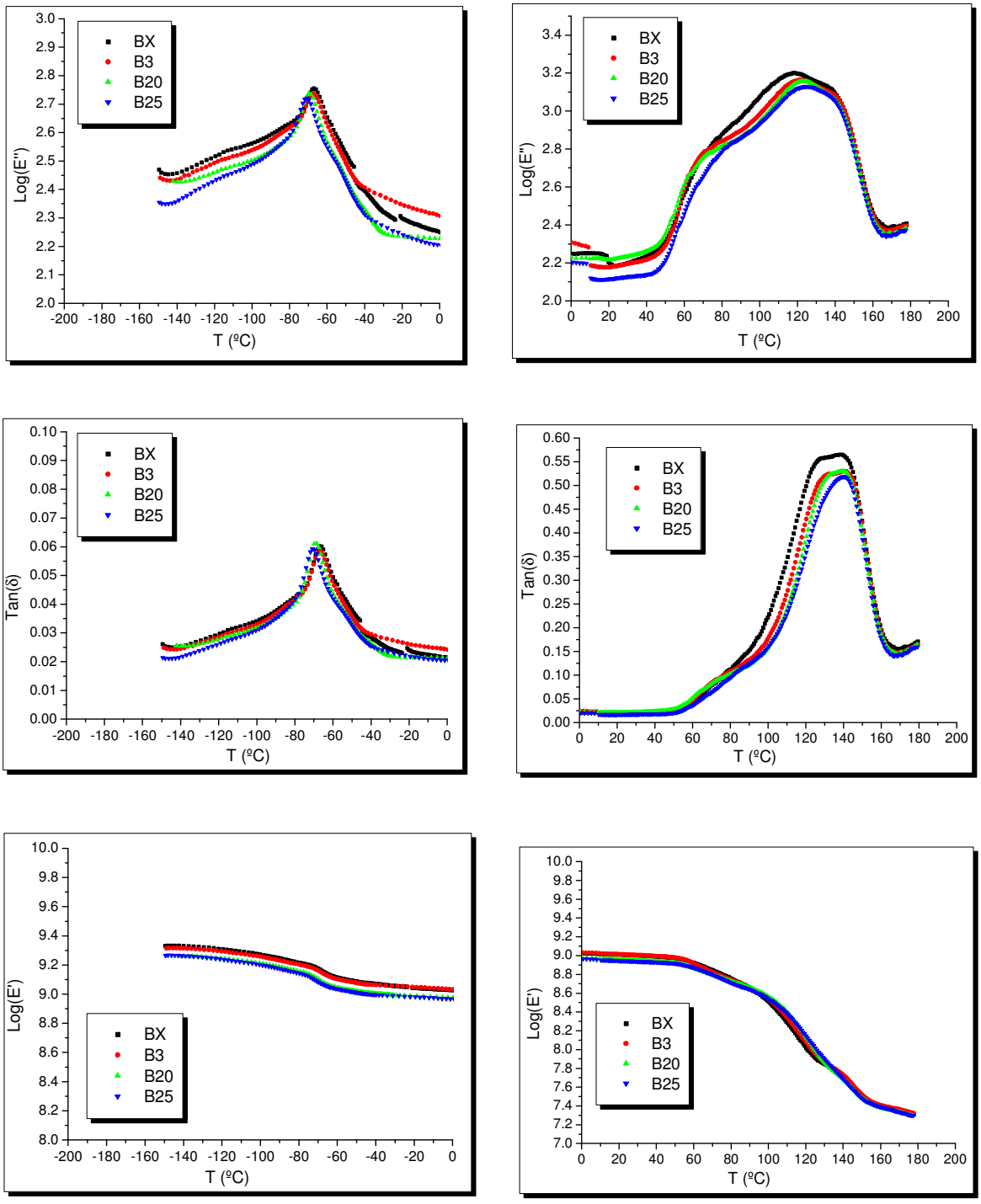

Figure 3-73. Loss modulus, loss tangent and storage modulus *versus* temperature, for the unpigmented blend, and pigmented blend samples relating to unmodified and modified pigments.

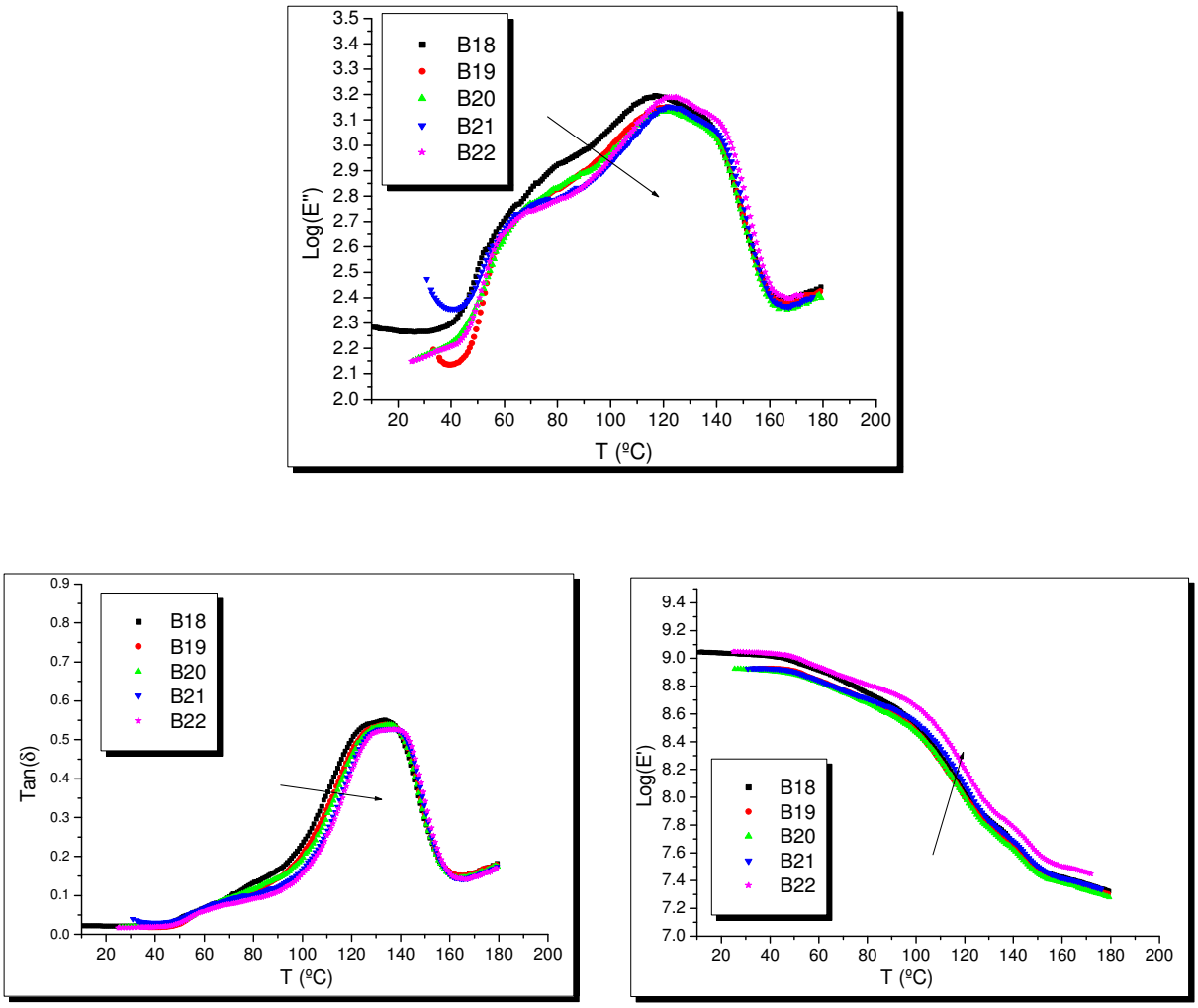

Figure 3-74. Loss modulus, loss tangent and storage modulus *versus* temperature, for samples of increasing pigment loading relating to Set 5.

The effects of the surface modifications on the viscoelastic properties of the blend are illustrated in Figure 3-73.

Sample B3, corresponding to the use of the unmodified pigment, is characterised by a lower molecular weight of PC and of PBT, along with a lower degree of crystallinity, than are samples of blends B20 and B25. These factors result in a greater viscous response of the blend to the applied stress, in the case of batch B3. This can be seen in the loss modulus plot and in the loss tangent plot as the area under the curve is greater for sample B3, than it is for the samples of blends B20 and B25.

The interaction between the pigment and the PC and the PBT, is greater in the case of the modified pigments. This is indicated by the higher degree of crystallinity of the modified pigment samples when compared to that of the unmodified pigment samples. The improved interactions, along with increased crystallinity, are thought to contribute to the more elastic response of the blends that include the modified versions of C. I. Pigment Blue 28.

A comparison of sample B25 with sample B20 shows that the height of the PC-rich peak is lower for blend sample B25. This is thought to be due to the preferential presence of pigment particles in the PC phase, for the samples of Set 6 (from which blend B25 is representative). The effects resulting from the phase preference of the pigment particles for the PC-rich phase in the case of the samples of Set 6 (Sections 3.4.9. and 3.4.10.), dominate over the effect of the greater crystallinity for the samples of Set 5. This would lead to a lower height of the PC-rich peak in these samples when compared to that that is observed for samples of Set 6.

The viscous response of sample B3 would be expected to be greater than the viscous response of the formulation B20, as the blend B3 has a lower average molecular weight of PBT and of PC, along with a lower degree of crystallinity. However, it must be taken into account that the pigment particles for blend B20 are preferentially located in the PBT-rich phase (Sections 3.4.9. and 3.4.10.), whereas in sample B3 the particles are preferentially located at the PC/PBT interphase. Thus, in blend B3, the effect of the pigment particles on the PC phase (reduction of the viscous response) is greater than that for sample B20, and overcomes the effects on the amorphous phase that arise from the differences observed between these blends with regard to the molecular weight and crystallinity degree.

The plots comparing the viscoelastic properties of the remaining samples of Sets 5 and 6 are presented in Appendix F. These confirm the above observations.

The effects of increasing pigment loading on the viscoelastic properties of the blends that include the “Lewis acidic” surface-modified pigment are illustrated in Figure 3-74.

For the samples of Set 5, the trend observed is similar to that corresponding to the samples containing the unmodified pigment that were processed in the same extruder (Set 2). The degree of crystallinity does not change significantly. The average molecular weight of the PBT decreases, although only slightly, with increasing pigment loading. Thus, the behaviour observed is due to the increase in the average molecular weight of the PC and consequent increased phase separation, with increasing pigment loading.

The effect of increasing pigment loading on the viscoelastic properties of the blends containing the “neutralised” surface-modified pigment is illustrated in Figure 3-75.

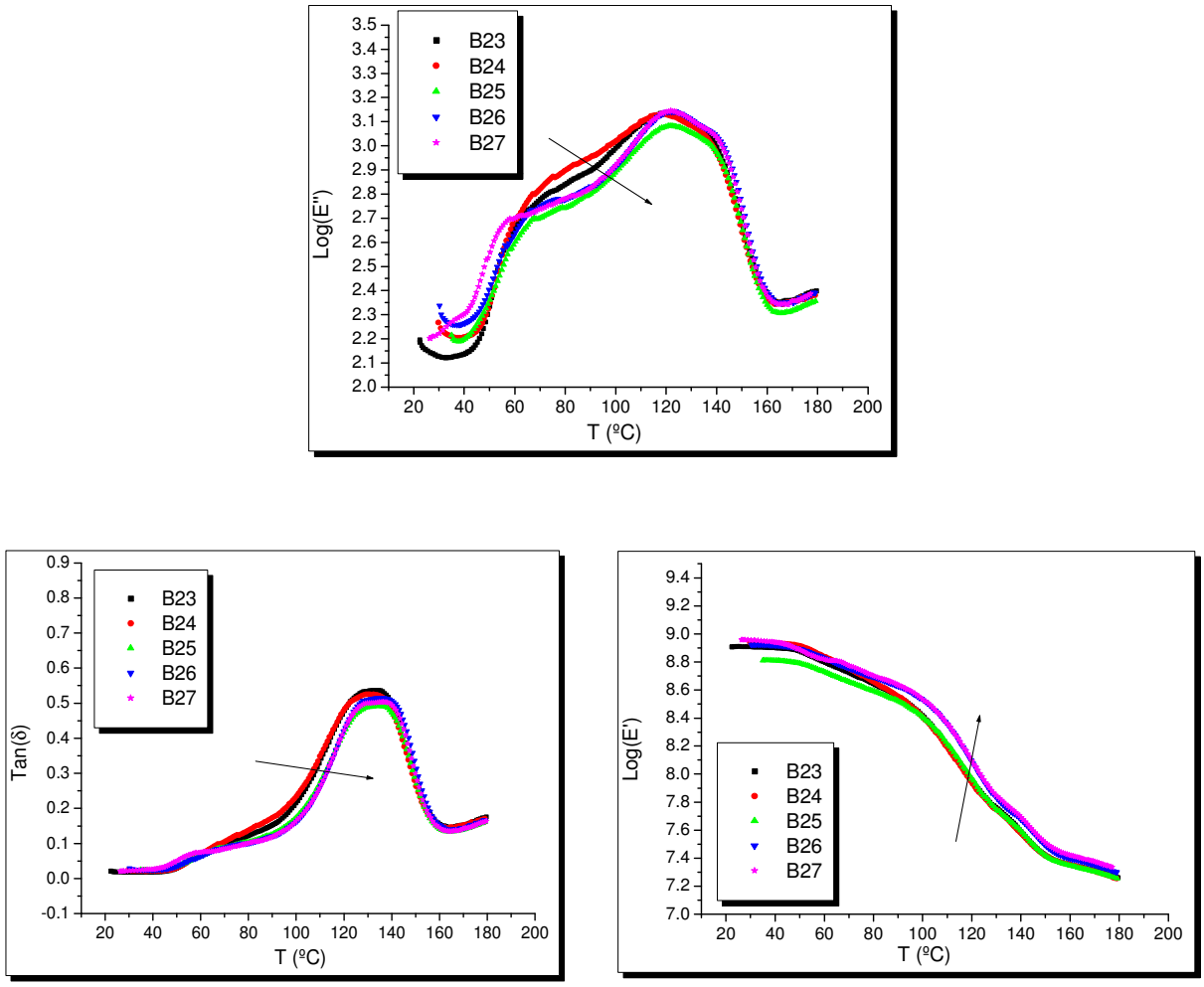

Figure 3-75. Loss modulus, loss tangent and storage modulus *versus* temperature, for samples of increasing pigment loading relating to Set 6.

The samples of Set 6 follow the same trend with increasing pigment loading as that oberved for the samples of Set 5.

From the analysis of the DMTA results it can be concluded that the pigment surface modifications lead to a lower viscous response of the blend due to increased average molecular weights of PBT and PC, increased crystallinity and increased interaction between the pigments and the polymers. The differences in phase preference of the modified-pigments particles are indicated by the viscoelastic properties of the blend. For the samples containing the "neutralised" pigment, and due to the greater presence of the pigment particles in the PC-rich phase, the viscous response of this phase is lower than that it was in the samples where the "Lewis acidic" pigment was used.

3.4.4. Vicat Softening Temperature

In Figure 3-76 are summarised the Vicat softening temperature (VST) results for samples of Sets 1, 2, 5 and 6.

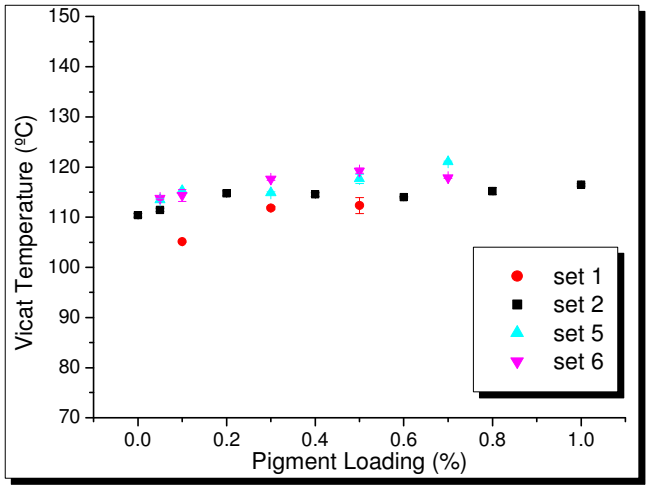

Figure 3-76. Vicat softening temperature as a function of pigment loading for samples of Sets 1, 2, 5 and 6.

From Figure 3-76, it can be concluded that the VST values for the samples containing the modified pigments are greater than those for the samples containing the unmodified pigment. This difference is greater for the samples that were extruded using the same parameters settings (Sets 1, 5 and 6), reaching 10 ºC for the samples with 0.10 % pigment loading. The observed differences are due to the greater average molecular weights of PC and PBT, and the greater degree of crystallinity, for the samples in which use was made of the surface-modified pigments.

3.4.5. Izod Notched Impact Testing

Figure 3-77 considers the variation of the impact energy absorption with pigment loading and with test temperature. Data are presented for the test temperatures of -20 ºC, -10 ºC, 0 ºC and 23 ºC, for samples of Sets 1, 2, 5 and 6.

From Figure 3-77, is it clear that samples that were pigmented with the unmodified pigment have a greater impact resistance than those containing the modified pigments. This is a consequence of the greater degree of crystallinity of the samples of Sets 5 and 6.

It is interesting to note that the dependence of the impact resistance on the test temperature is less pronounced for the samples that were pigmented with the modified pigments. Alterations to the impact toughening mechanisms due to changes in 1) the phase preferences of the modified pigments, 2) pigment dispersion, i.e., differences in interparticle-distance, and 3) matrix-pigment adhesion, are thought to be in the origin of the observed behaviour.

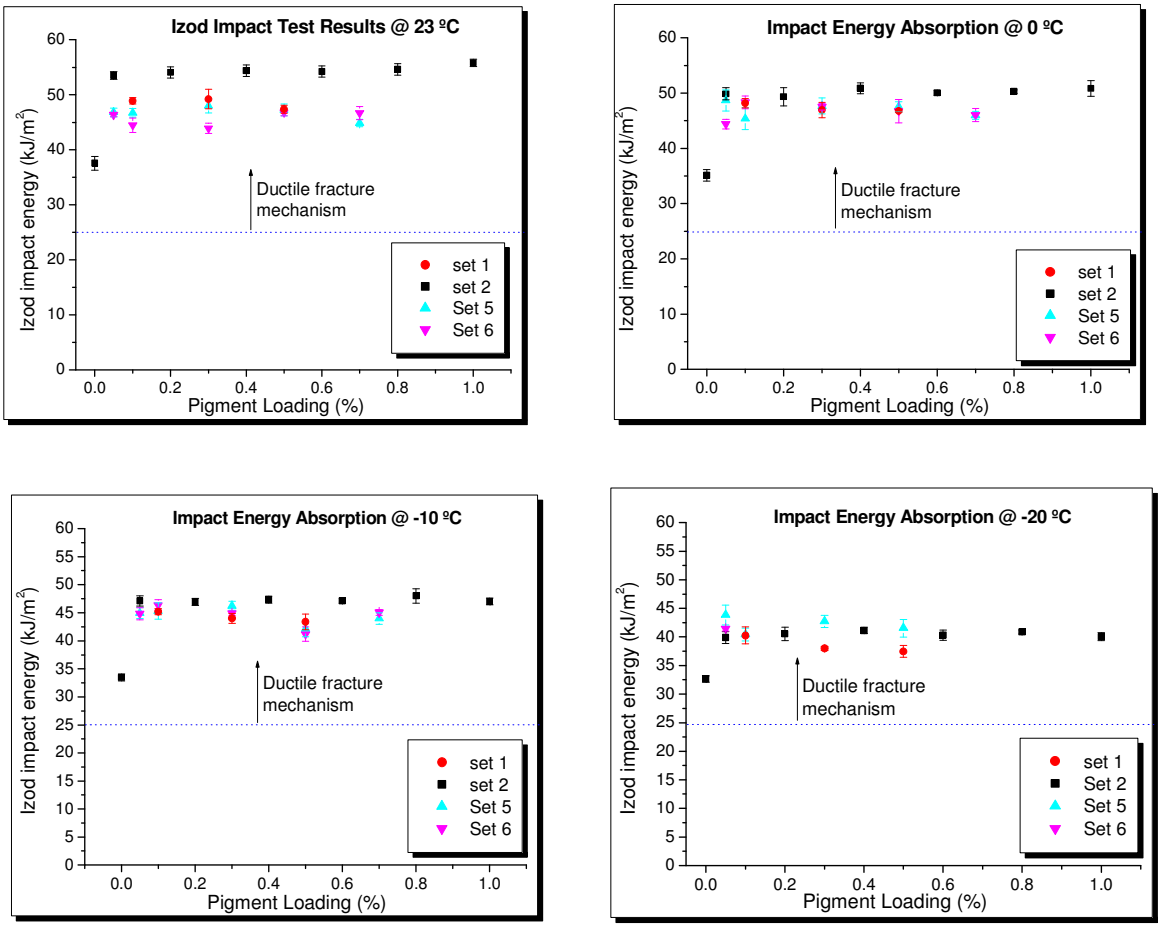

Figure 3-77. Variation of the notched Izod impact energy absorption for samples of Sets 1, 2, 5 and 6, as a function of pigment loading and test temperature.

It is known that strong interaction or chemical bonding between inorganic particles and a semi-crystalline polymer causes often the loss of toughness of the system (Marosi *et al.* 1987; Galeski 1990). Improved dispersion is reported to raise the impact resistance (Wang *et al.* 2001). Thus, it is inferred that the surface-treated pigment particles show better adhesion to, and are better dispersed in, the polymeric matrix. The improved dispersability of the surface-treated pigments is supported by the MVR test results (Section 3.4.8.), and the improved adhesion is indicated by IGC analysis of the interaction potential of **hiwre** and of **hiwren** (Section 3.3.1.).

The decreased impact resistance arising from the very strong adhesion between the inorganic particulates and the polymeric matrix has its origins in the rigid interphase that may be formed. The mechanical properties of the rigid polymer layer that surrounds the inorganic particles become closer to those of the inorganic particulates rather than to those of the polymeric matrix. Consequently, the apparent volume of the inorganic particulates increases and, as a result, the filled

polymers become hard but brittle (Marosi *et al.* 1987). Thus, increasing the adhesion to a very high level may decrease the extent of energy dissipation.

The unmodified pigment particles have been shown to be located preferentially at the PC/PBT interphase, and the "Lewis acidic" and "neutralised" pigments in the PBT-rich phase and in the PC-rich phase, respectively (Sections 3.4.9. and 3.4.10.). This change of phase preferences for the pigment particles will also bring about changes in the impact toughening mechanisms as these are inherently different between the PC phase and the PBT phase.

In polymers such as PC that deform predominantly by shear yielding, the effect of the size of inorganic particulates on the mechanical properties of the composites is believed to be minimal. This opinion applies as long as a sharp interface between the dispersed and continuous phase exists. However, as shear yielding is enhanced by the cavitation of particles, the ability of a particle to void or cavitate in relation to its size is unclear at present (Folkes and Hope 1993). Nevertheless, bearing in mind the particle size and particle size distribution results (Section 3.3.7.), alterations of these pigment properties, due to the surface modifications, are thought not to contribute to changes in impact energy absorption mechanisms.

From the observation of the results at the testing temperature of - 20 ºC, it can be argued that the impact resistance of samples of Set 5 is slightly greater to that of Set 2. Thus, the "Lewis acidic" pigment gives better impact resistance at that test temperature than do the samples containing the unmodified pigment. It is concluded that the changes in impact energy absorption mechanisms due to the surface modification of C. I. Pigment Blue 28 are favourable to the improved impact resistance of the blends at -20 ºC. For samples of Set 6, it was not possible to complete the testing of all the batches produced, due to the limited number of impact testing bars.

Figure 3-78 summarises the Izod notched impact testing results for all the testing temperatures and pigment loadings, for samples of Sets 5 and 6.

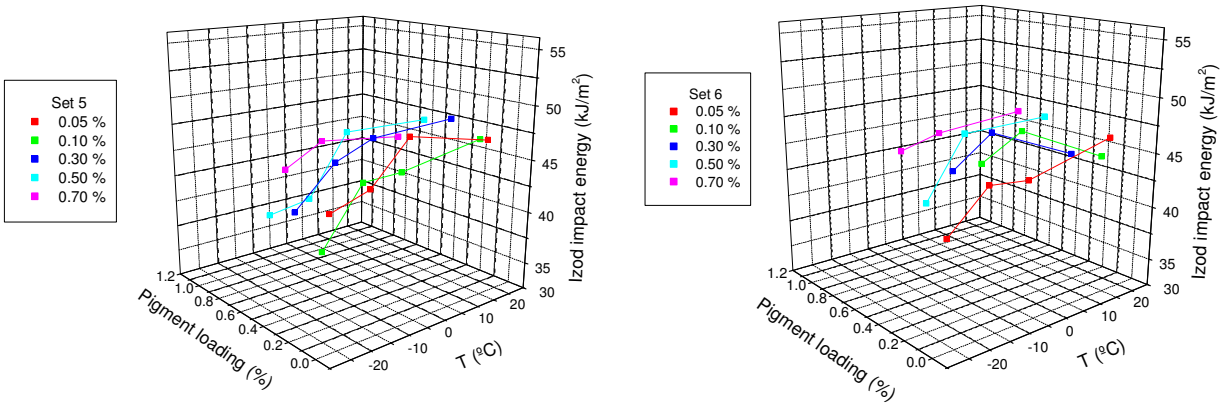

Figure 3-78. Izod impact testing results, as a function of test temperature and pigment loading, for samples of Sets 5 and 6.

For all of the samples tested, the energy needed to break the specimen increases with increasing temperature, agreeing with expectation, as explained in Section 3.2.6.

3.4.6. Puncture Impact Testing

Figure 3-79 gives the puncture energy values, and energy at maximum force values, for samples of Sets 1, 2, 5 and 6.

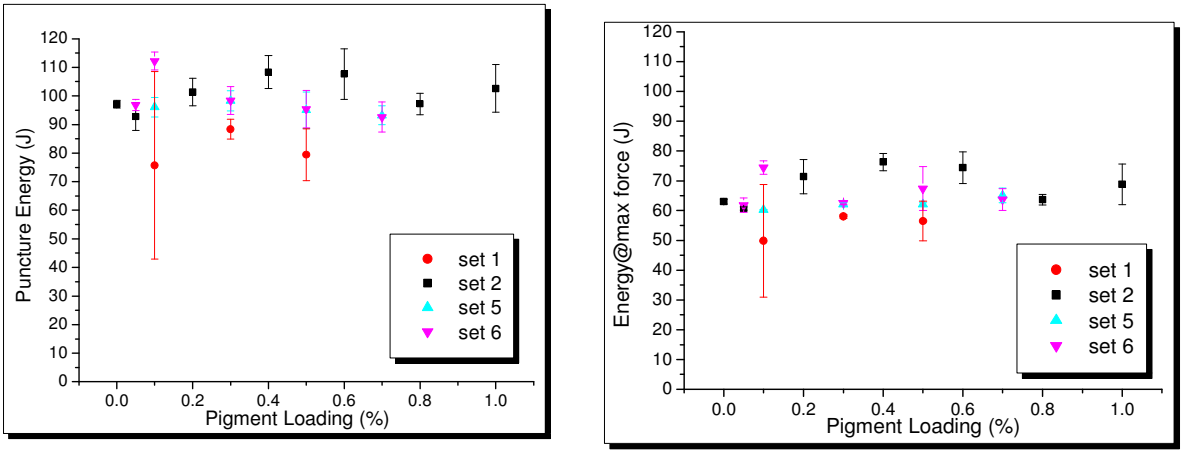

Figure 3-79. Puncture energy and energy at maximum force as a function of the pigment loading, for samples of Sets 1, 2, 5 and 6.

From Figure 3-79 it is concluded that the sets of samples with the greater molecular weights of PC and PBT (Sets 2, 5 and 6) have a greater impact energy absorption capability. From comparisons of samples that have similar molar mass values (Sets 2, 5 and 6, at pigment loadings between 0.40 and 0.80 %), it can be concluded that the samples containing the modified pigments have a lower impact energy absorption capability. This corresponds with the higher degree of crystallinity of these samples. With regard to the variation of the puncture energy and of the energy at maximum force, for the samples containing the modified pigments, the values of these parameters do not follow a trend with increasing pigment loading. All the samples of Sets 5 and 6 showed 100 % ductility.

3.4.7. Tensile Testing

The following figures summarise the results of tensile testing as a function of the pigment loading, concerning the batches of Sets 1, 2, 5 and 6. Figure 3-80 relates to the behaviour of the tensile modulus and of the strain at break of samples with varying pigment loading.

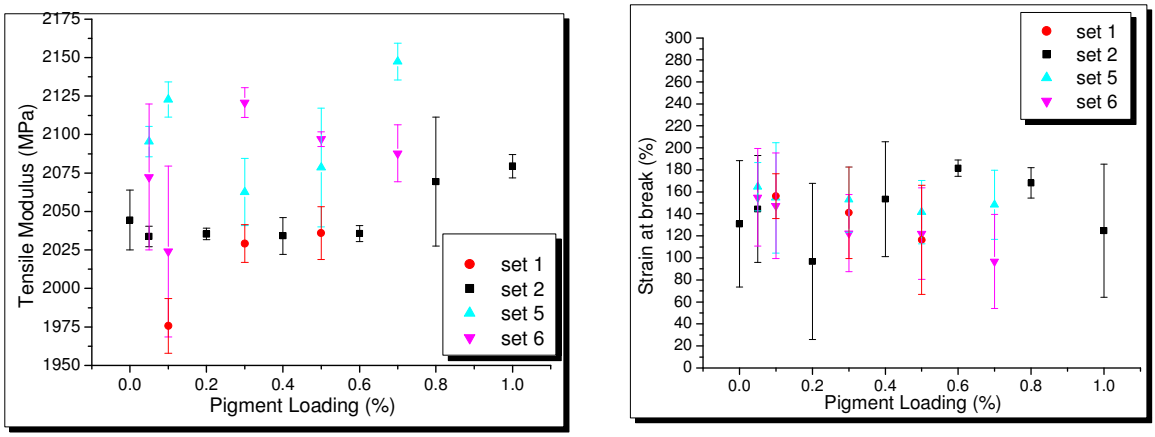

Figure 3-80. Tensile modulus and strain at break as a function of pigment loading, for samples of Sets 1, 2, 5 and 6.

Effect of the Surface Modifications of the Pigment on the Tensile Modulus

Figure 3-80 shows that the tensile modulus values for samples that were pigmented with the surface-modified pigments are greater than are the values for samples containing the unmodified pigment. The greater degree of crystallinity of samples of Sets 5 and 6 is thought to be a determining factor, leading to the greater tensile modulus of these samples. Improved adhesion between the polymer matrix and the surface of the modified pigments (Section 3.3.1.), and the greater values of the average molecular weights of PC and of PBT (Section 3.4.1.) are thought further to contribute to the aforementioned behaviour. In terms of specific interactions, it has been shown (Richard *et al.* 1985; Schreiber and Germain 1991) that strong acid/base coupling enhances the relative gain in the modulus of filled polymers. On the other hand, Lewis acid/acid repulsion is reported to initiate favourable elongational properties, while reducing the gains in elastic moduli.

Improved pigment particle dispersion is also reported to lead to increased values of the tensile modulus (Xu and Schreiber 1998). Therefore, it is to be expected that the pigment particles would be better dispersed in samples of Sets 5 and 6. This inference is supported by the MVR results (Section 3.4.8.). The changes in the preferential location of the pigments (Sections 3.4.9. and 3.4.10.) may also be contributing to the observed differences in the tensile modulus values. In Figure 3-80, no trend with increasing pigment loading can be observed for samples of Sets 5 and 6.

Effect of the Surface Modifications of the Pigment on the Strain at Break

With regard to the strain at break values, the results are difficult to analyse due to the high standard deviation. Nevertheless, for the higher pigment loadings the strain at break is lower for the samples containing the modified pigments. This finding is in line with the greater degree of crystallinity of these samples. For the samples of Sets 5 and 6, the behaviour of the strain at break value with increasing pigment loading is more consistent than it is for samples of Set 2.

Increased interaction strength between the inorganic particles and the polymeric matrix are reported to result in decreased extendibility (Schreiber *et al.* 1982; Schreiber and Germain 1991; Bokobza *et al.* 2002). In particular, at low pigment concentrations, ultimate properties have been shown to be clearly affected by the condition of the polymer-filler interface (Boluk and Schreiber 1990). Consequently, improved adhesion between the polymeric matrix and the surface of the modified pigments is also thought to contribute to the greater consistency and lower values of the strain at break, when compared to the samples incorporating the unmodified pigment.

Figure 3-81 concerns the behaviour of the stress at break, of the strain at yield and of the stress at yield of Sets 1, 2, 5 and 6, with varying pigment loading.

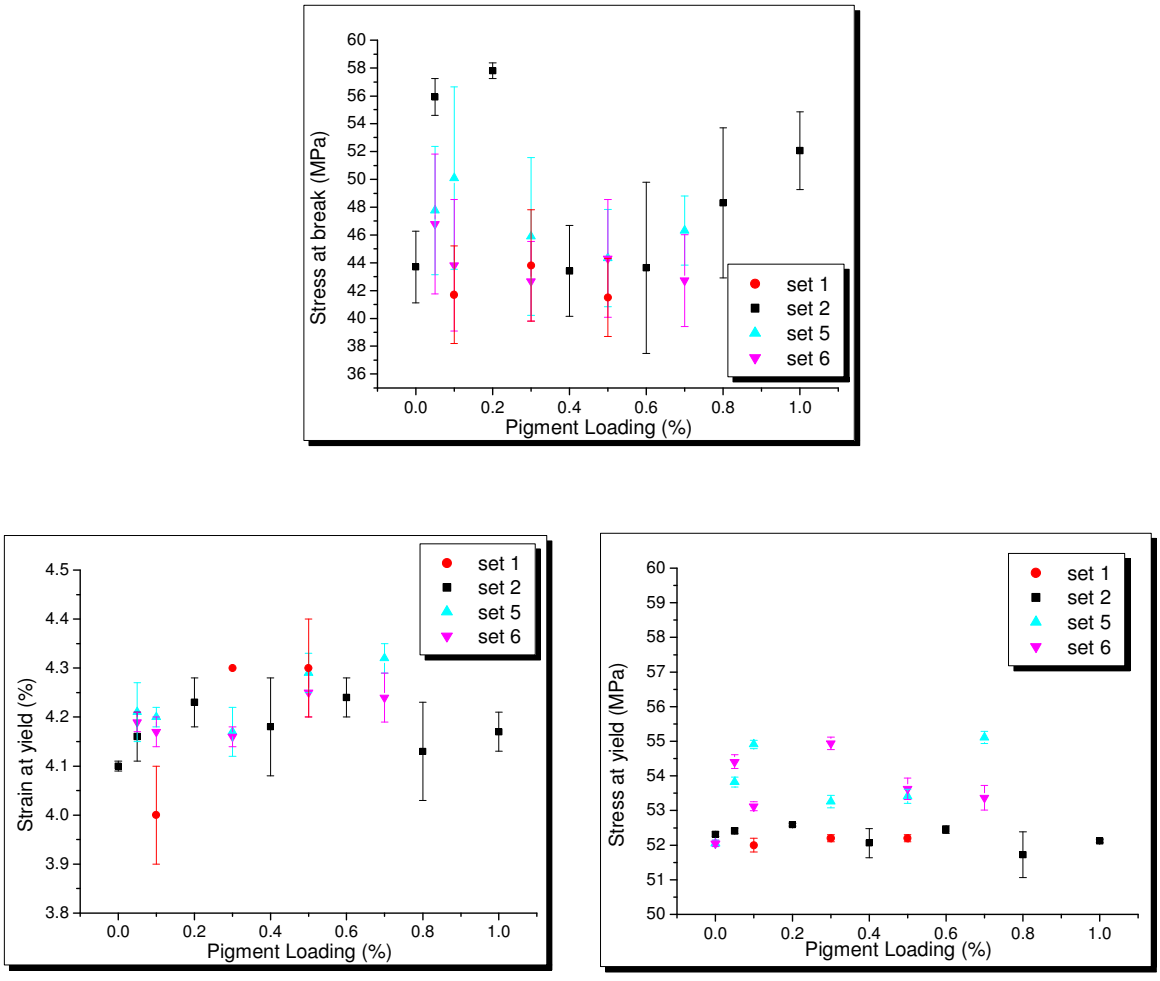

Figure 3-81. Stress at break, strain at yield and stress at yield as a function of pigment loading, for samples of Sets 1, 2, 5 and 6.

Effect of the Surface Modifications of the Pigment on the Stress at Break

Figure 3-81 shows that the differences in the average molecular weight between the different sets of samples do not influence significantly the values of the stress at break. It is interesting to

note that the change in this parameter with increasing pigment loading is more consistent in the case of the samples that were pigmented with the modified pigments. As there is not an effect of the average molecular weight of PC and PBT on the stress at break, and the crystalline phase loses importance at large test specimen elongation, the aforementioned difference is thought to be related to improved adhesion of the PC and of the PBT to the surface of the modified pigments.

Effect of the Surface Modifications of the Pigment on the Strain at Yield

As far as the values of the strain at yield are concerned, there are no significant differences between samples of Sets 2, 5 and 6, within experimental error. Thus, it can be concluded that the modification of the surface of the pigment does not influence, to a noticeable extent, the strain at yield. Furthermore, there is no trend with increasing pigment loading.

Effect of the Surface Modifications of the Pigment on the Stress at Yield

From Figure 3-81 it is clear that the stress at yield is greater for the samples that contain the modified pigments. This is thought to be related to the greater degree of crystallinity and to the greater average molecular weight of PC and PBT, in these samples. It is also related to improved adhesion between the polymers and the surface of the modified pigments. Stronger adhesion has been reported to lead to increasing yield stress values (Galeski 1990).

3.4.8. Rheological Assessment (Melt Volume Rate)

Figure 3-82 contains the results of the melt viscosity assessment of samples of Sets 1, 2, 5 and 6, with increasing pigment loading.

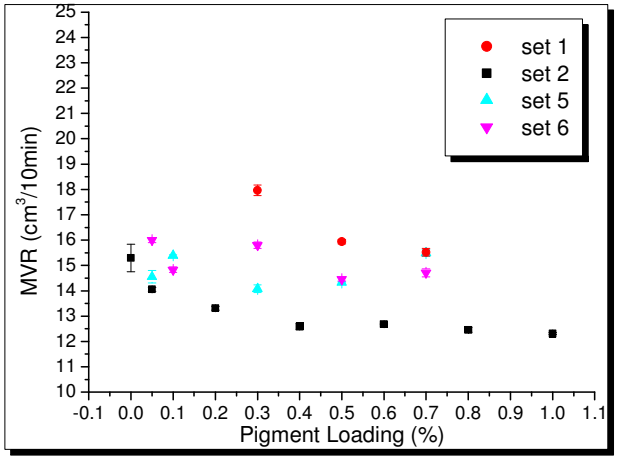

Figure 3-82. Melt volume rate as a function of the pigment loading, for samples of Sets 1, 2, 5 and 6.

Figure 3-82 shows that the melt volume rate (MVR) values of the samples containing the surface-modified pigments are greater than the values of MVR of the samples of Set 2. Thus, the melt viscosity of samples containing the surface-modified pigments is lower than that of samples that include the commercial C. I. Pigment Blue 28 in their composition. This fact is thought to be due to improved dispersion of the pigment particles, caused by the surface treatments, for the blend samples represented by Sets 5 and 6.

The MVR values of samples of Set 1 are greater than those values of samples of Sets 5 and 6. For these samples, the effect of the molecular weight differences on the MVR values is thought to overcome the effects of the surface modifications of the pigment. Conversely, for samples of Set 2, the effect of differences in the molecular weights of PC and PBT on the melt volume rates, are overcome by the effects of better pigment dispersion for the samples of Sets 5 and 6.

The samples of Sets 5 and 6 do not show significant differences with increasing pigment loading, except at the 0.30 % pigment loading. Nevertheless, the MVR values decrease with increasing pigment loading for samples of Set 6. This decrease is less prominent than it is in the case of samples of Sets 1 and 2. This is an important result from the point of view of the processing of these blends as it allows a more consistent rheological behaviour of blends with varying pigment loading. The values of MVR for samples of Set 5 do not show a clear decreasing trend with increasing pigment loading.

The surface modifications of C. I. Pigment Blue 28 reduce the particle-particle interactions in the polymer matrix and improve the filler dispersion, reducing the viscosity of the blend. The reason behind these effects lies in the strong acid/base coupling between the polymeric matrix and the surface-modified pigments, as discussed in Section 3.3.1. Similar results can be found in the literature. Strong acid/base coupling has been proven by Schreiber and colleagues (Schreiber *et al.* 1982) to result in better dispersion of basic surface-treated $CaCO_3$ in the acidic PVC matrix.

In the present study, for samples of Set 5, the decrease in viscosity is thought to have an important contribution from the significant Lewis acidity (Section 3.3.1.). This contribution leads to significant particle-particle Lewis acid/acid repulsion and significant particle-polymeric matrix Lewis acid/base attraction.

The change in phase preferences of the pigment particles according to the nature of the surface modification may also be influencing the MVR results. The improvement of the dispersability of the surface-modified pigments, namely of the “Lewis acidic” pigment, is further supported by the analysis of the average particle size and of the particle size distribution of the unmodified and surface-modified pigments (Section 3.3.7.).

3.4.9. Scanning Electron Microscopy/EDXA

Figures 3-83 to 3-88 relate to the SEM/EDXA imaging of tape-extruded samples of batches BX (unpigmented blend), B10 (0.80 %, unmodified pigment), B22 and B27 (0.70 % modified pigments, **hiwre** and **hiwren**, respectively), Section 2.1. These pigmented samples were chosen as being representative of the blends containing the unmodified pigment and containing the surface-modified pigments, respectively.

Samples were extracted with DCM prior to imaging and analysis, as described in Section 2.5.1.1. Thus, the PC has been removed from the polymeric matrix, namely from the region were SEM/EDXA is effective. In Figure 3-83 are presented SEM images of the unpigmented blend (BX) at magnification levels of x1500 (image (a)), x5000 (image (b)), and x20000 (image (c)).

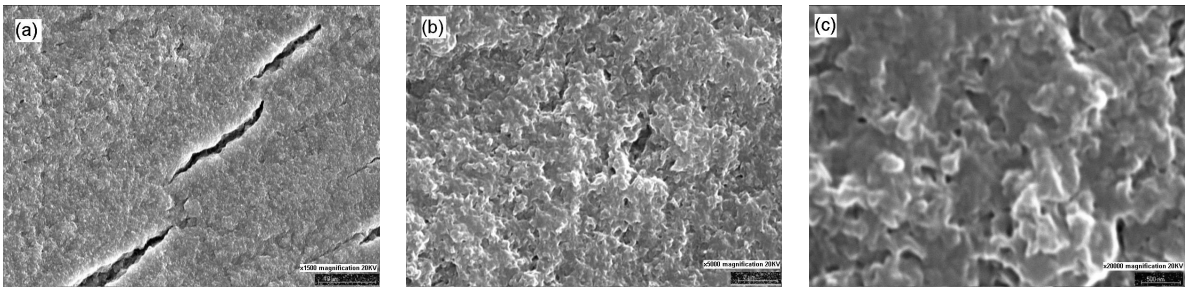

Figure 3-83. SEM images of tape-extruded, DCM-extracted, sample of unpigmented blend (BX).

The images in Figure 3-83 show a heterogeneous morphology. As the polymeric phases cannot be distinguished by SEM imaging, no further inferences can be made from the images that are presented. Below, the morphology observed for the DCM-extracted unpigmented sample is compared to that observed for the pigmented blends.

After removing the PC from the tape-extruded samples, it was possible to obtain Co and Al elements signals that were sufficiently strong to allow mapping of these elements by EDX. All of the samples were subject to the same signal acquisition conditions (Section 2.5.1.1.).

In Figure 3-84 are presented the SEM images, and the Al and Co EDX mapping images, of DCM-extracted sample of batch B10. Images (a), (b) and (e) correspond to SEM images. Images (c) and (f) correspond to Al EDX mapping. Images (d) and (g) correspond to Co EDX mapping. Image (a) corresponds to a SEM image at a magnification level of x1500. Images (b) to (d) correspond to a magnification level of x5000, and images (e) to (g) to a magnification level of x20000.

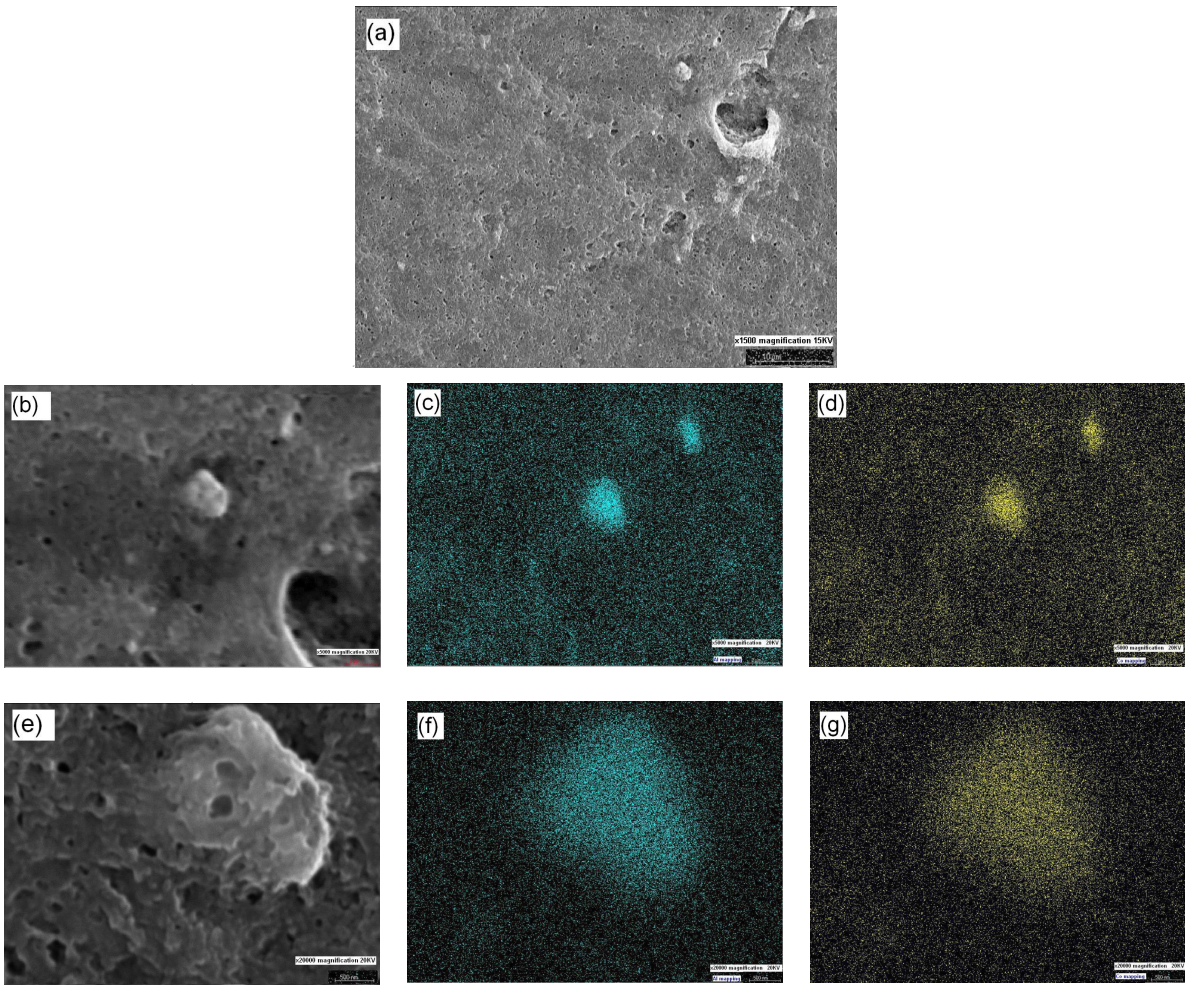

Figure 3-84. SEM/EDX images of tape-extruded, DCM-extracted, sample of blend B10.

From the observation of the SEM images at x5000 and x20000 magnification levels, it can be inferred that the surface of the DCM-extracted sample of B10 is more homogeneous and smoother than that of the unpigmented blend. This indicates more well-defined and larger phase domains, and, thus, better phase separation. These observations are supported by TEM imaging (Section 3.4.10.).

Figure 3-84 shows that it was possible to detect pigment particulates in the blend samples where PC had been removed from the surface of the specimen by dissolution in DCM. The pigment particles are observed to be encapsulated by the polymer matrix. If one assumes that the entire PC has been removed from the surface of the samples, it can be concluded that in samples containing the commercial C. I. Pigment Blue 28, the PBT shows very good adhesion to the pigment particles,

confirming expectations based on the IGC analysis of the interaction potential between the pigment and the polymers (Section 3.1.).

In Figure 3-85 are presented SEM images of a DCM-extracted sample of batch B22. The image on the left-hand side corresponds to a magnification level of x1500, and the image on the right-hand side to a magnification level of x5000.

In samples of batch B22 it was very difficult to find pigment particulates that were sufficiently exposed to allow for EDXA mapping of the Al and Co elements. It was observed that in samples of Set 5, the pigment particulates are very significantly more encapsulated by the polymer that is not soluble in DCM, i.e., the PBT phase, than in samples that contain the unmodified pigment. These inferences are clear in the images presented in Figures 3-86 and 3-88.

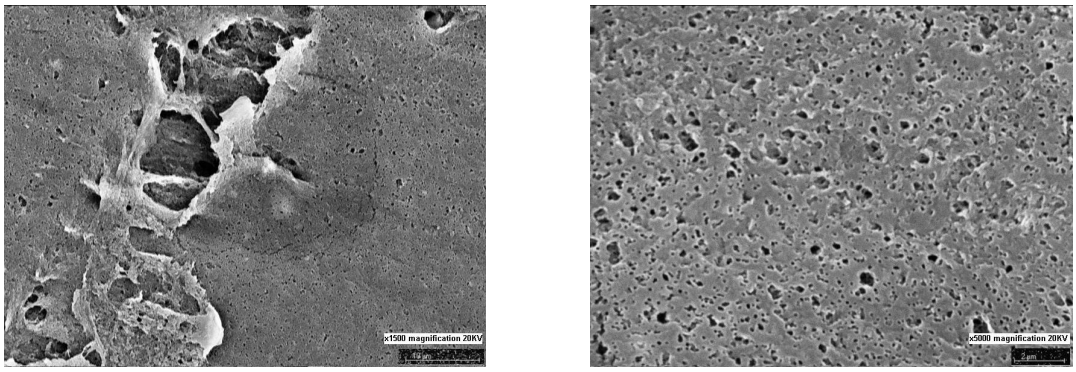

Figure 3-85. SEM images of tape-extruded, DCM-extracted, sample of blend B22.

From the images presented in Figure 3-85, it is clear that the surface is characterised by smaller, more well-defined and regular cavities than it is for samples BX and B10. It can be concluded that the phase domains are more well-defined than they are in blend B10. Also, the phase separation if more expressive in sample B22 than it is in samples BX and B10.

After many attempts, relatively weak Co and Al signals were obtained on the DCM-extracted sample of B22. The images presented in Figure 3-86 correspond to SEM images, Al EDX mapping images, and Co EDX mapping images, of DCM-extracted sample of batch B22. Images (a) and (d) correspond to SEM imaging at magnification levels of x5000 and x20000, respectively. Images (b) and (e) correspond to Al EDX mapping imaging at magnification levels of x5000 and x20000, respectively. Images (c) and (f) correspond to Co EDX mapping imaging at magnification levels of x5000 and x20000, respectively.

From the images presented in Figure 3-86 it is clear that the pigment particulates are significantly less exposed than they are in sample B10. Thus, the encapsulation of the surface-modified pigment particulates by the PBT phase is more prominent than it is for the unmodified C.

I. Pigment Blue 28. This indicates better adhesion and confirms the analysis of, and expectation from the IGC assessment of the Lewis acid/base interaction potential of the unmodified and modified pigments (Sections 3.1.8. and 3.3.1., respectively).

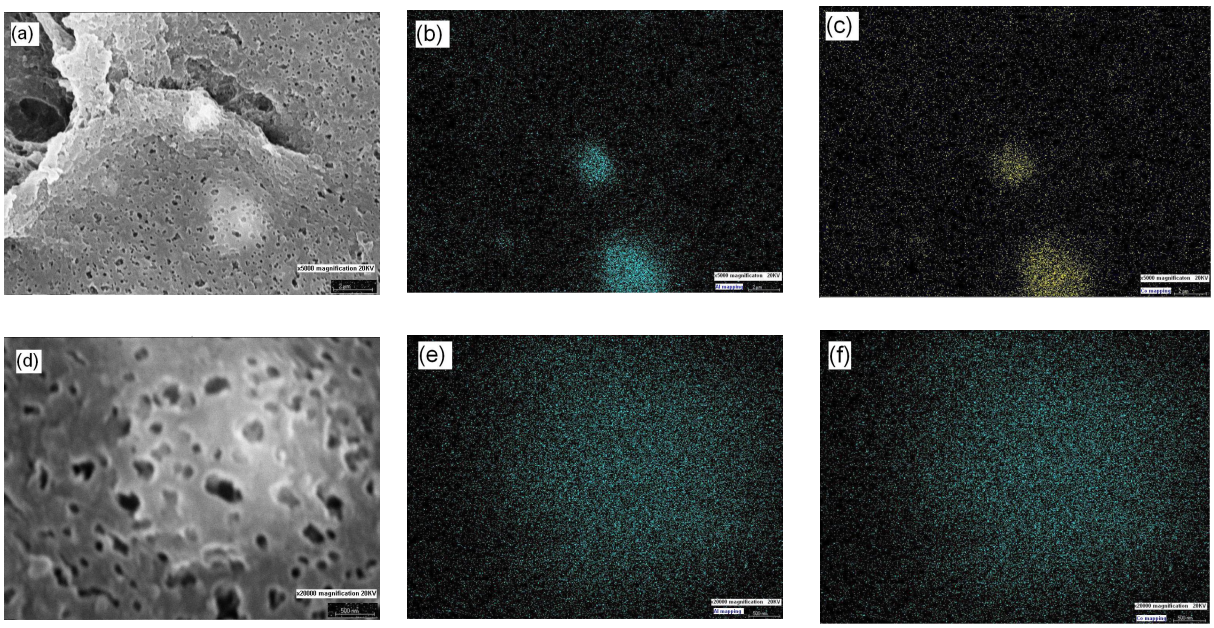

Figure 3-86. SEM/EDX images of tape-extruded, DCM-extracted, sample of blend B22.

In Figure 3-87 are presented the SEM images, and Al and Co EDX mapping images, of DCM-extracted sample of batch B27. Images (a), (b), and (e) correspond to SEM imaging at magnification levels of x1500, x500, and x20000, respectively. Images (c) and (f) correspond to Al EDX mapping at magnification levels of x5000 and x20000, respectively. Images (d) and (g) correspond to Co EDX mapping, at magnification levels of x5000 and x20000, respectively.

Figure 3-87, shows that the morphology is more similar to that of sampe B10 than to that of sample B22. The images in Figure 3-87 are clear in showing notably stronger Co and Al signals for blend B27 than was the case for blends B10 and B22. Thus, the pigment particles are more exposed than are the unmodified pigment particles and than are the “Lewis acidic” pigment particles. This is particularly evident in the images that are presented in Figure 3-88, and in the TEM images that are presented in Section 3.4.10.

In Figure 3-88 are compared the SEM images ((a), (d), and (g)), Co EDX mapping images ((b), (e), and (h)) and Al EDX mapping images ((c), (f), and (i)), at a magnification level of x20000, relating to samples B10 ((a), (b), and (c)), B22 ((d), (e) and (f)), and B27 ((g), (h) and (i)).

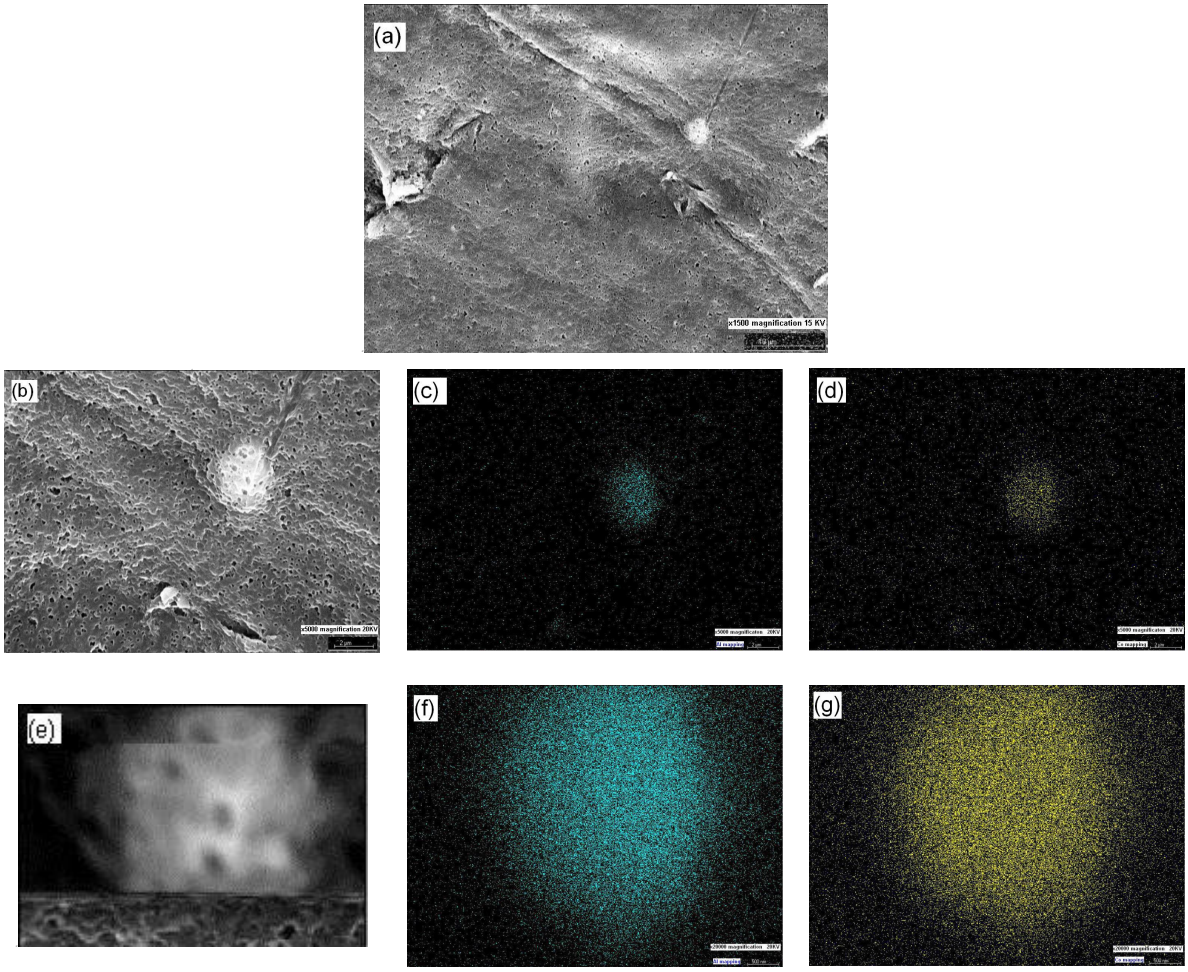

Figure 3-87. SEM/EDX images of tape-extruded, DCM-extracted, sample of blend B27.

Analysing the images that are presented in Figure 3-88 one can conclude that the pigment particles are more exposed in sample B27, followed by sample B10, and, finally by sample B22. Thus, the "neutralised" pigment is the less wetted, and the "Lewis acidic" pigment the more wetted, by the PBT phase. The unmodified pigment shows a level of PBT adhesion that is intermediate with that of the surface-modified pigments.

These observations are in line with predictions from the IGC results (Sections 3.1.8. and 3.3.1.), and are further confirmed by the TEM imaging of the DCM-extracted samples, (Section 3.4.10).

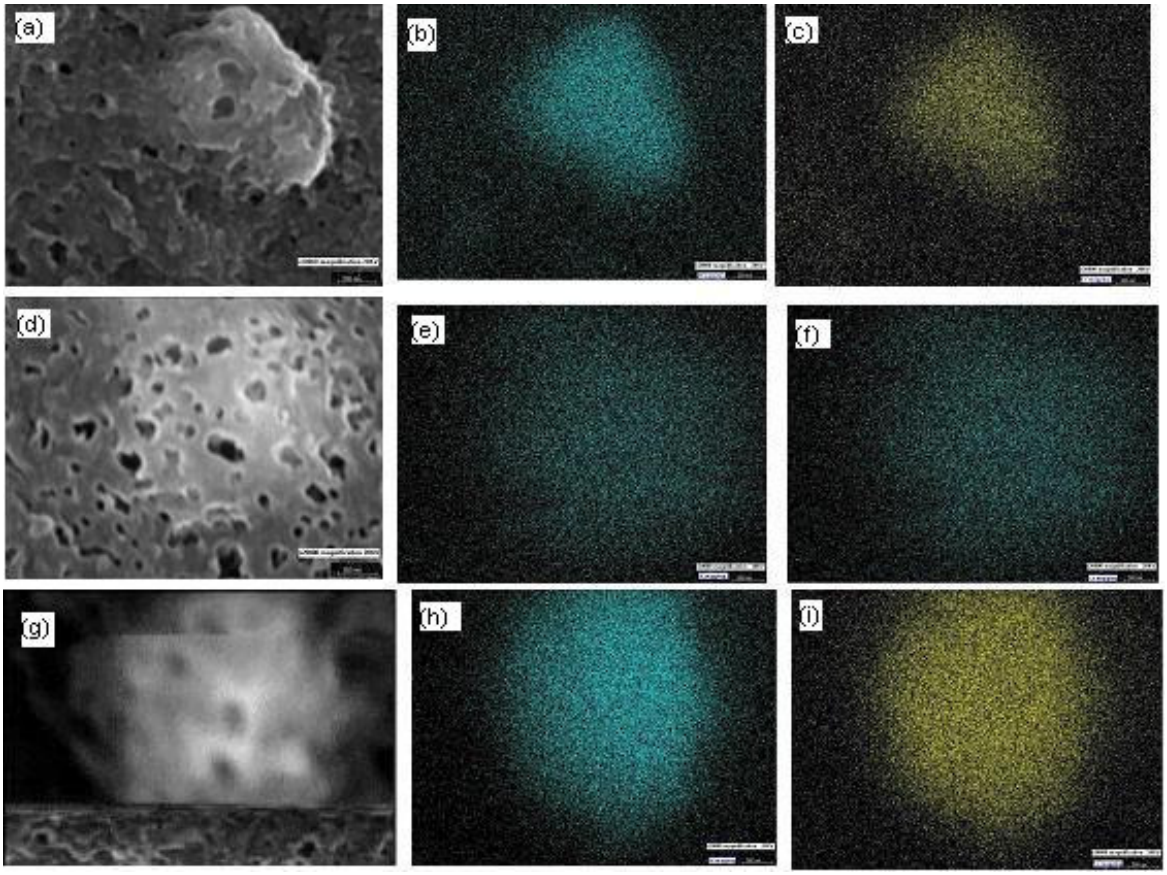

Figure 3-88. SEM/EDX images of tape-extruded, DCM-extracted, samples of blends B10, B22 and B27, at a magnification level of x20000.

3.4.10. Transmission Electron Microscopy/Photography Imaging

TEM imaging was carried out in the tape-extruded, DCM-extracted, samples of blends BX, B9, B22 and B27. The protocol is described in Section 2.5.2.

Figures 3-89 and 3-90 give images concerning the blends BX, B9, B22 and B27, prior to extraction of the PC. Images (a), (b) and (c) correspond to a 1.0 μm scale. Images (d), (e), (f) and (g) correspond to a 0.5 μm scale.

Figures 3-89 and 3-90 shows that the phase domains are more well-defined, and, thus, the phase separation is more pronounced, in samples B22 and B27 than it is in samples B9 and BX.

The PC and PBT phase domains are clearly more well-defined in the pigmented samples. These results confirm the inferences made in the previous section and are due to the greater crystallisation degree and greater molecular weights of the polymers (namely of the PC), for samples of the pigmented blends, and in particular for blends B22 and B27.

The phase domains in sample B22 appear to be larger than they are in sample B27. This is in agreement with the greater degree of crystallinity of blend B22.

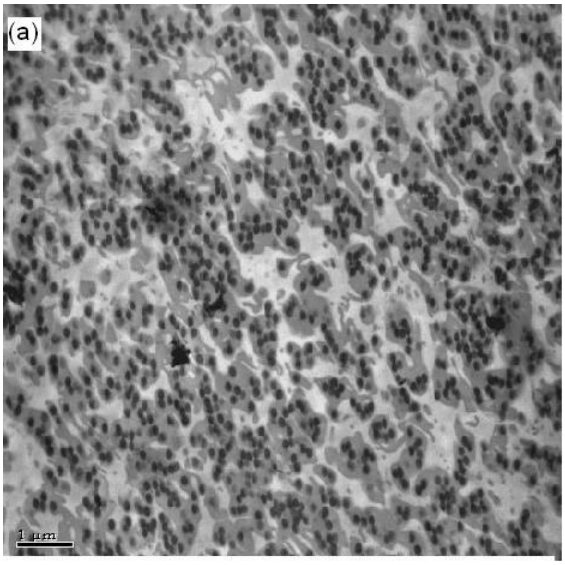

Blend B9 – Before Extraction with DCM

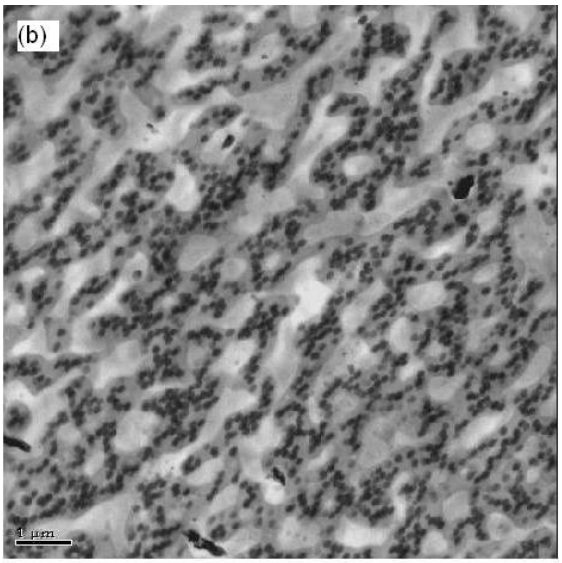

Blend B22 – Before Extraction with DCM

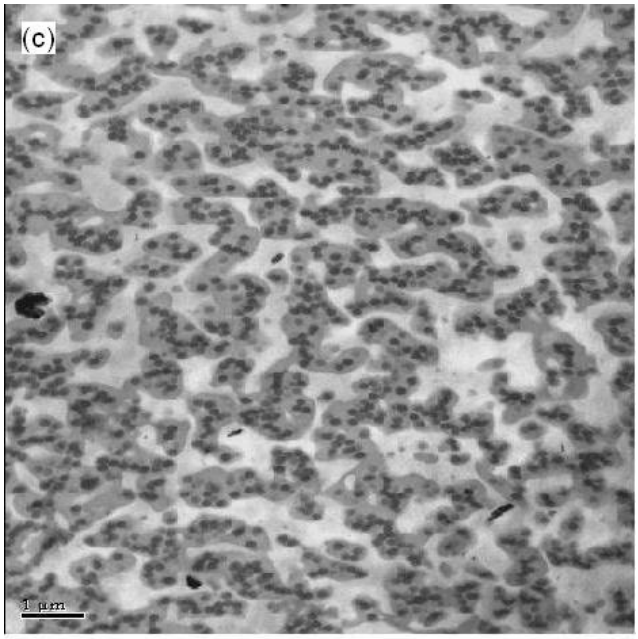

Blend B27 – Before Extraction with DCM

Figure 3-89. TEM images of tape-extruded samples of blends BX, B9, B22, and B27, prior to DCM extraction of PC, at a scale of 1.0 µm.

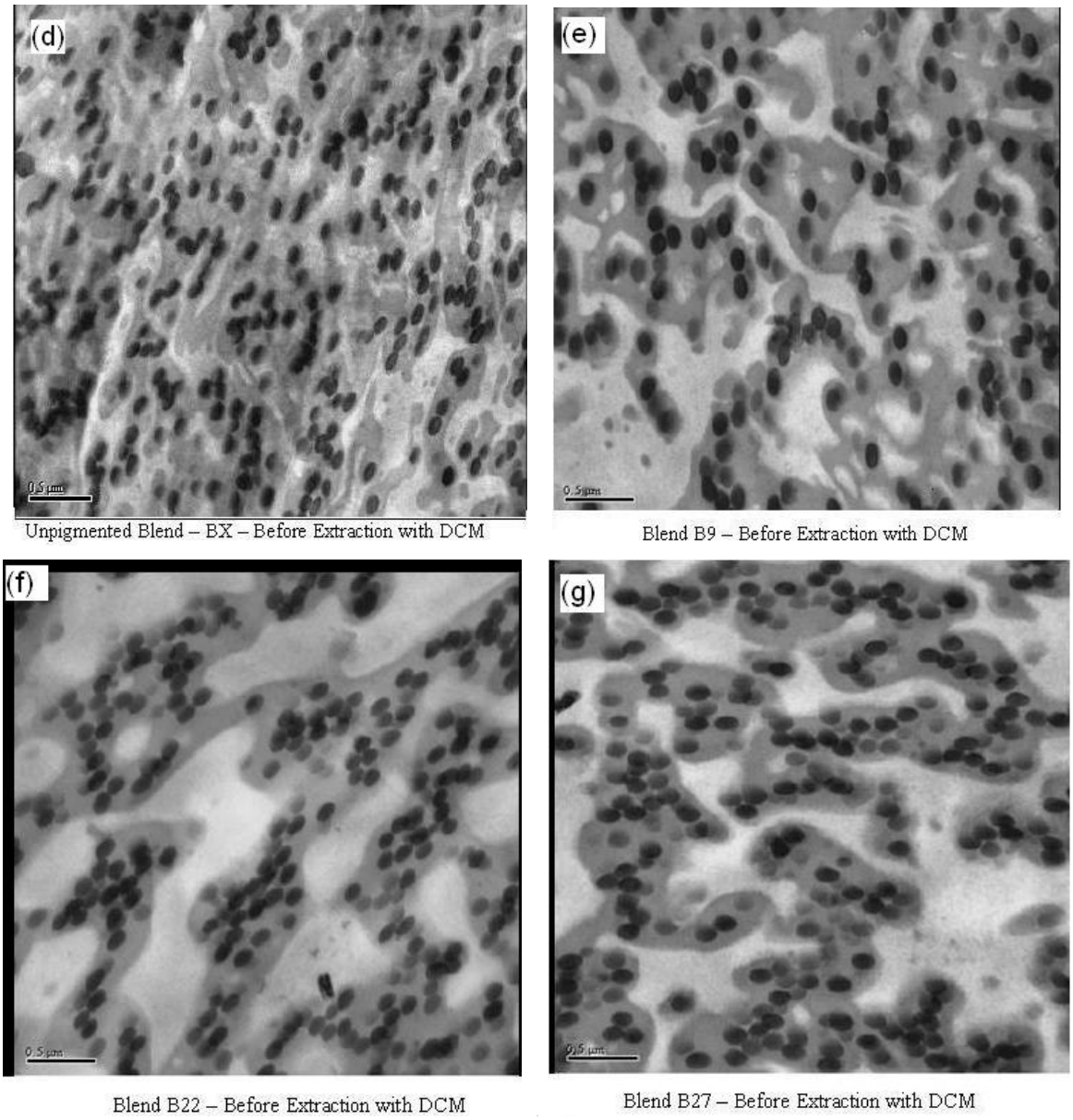

Figure 3-90. TEM images of tape-extruded samples of blends BX, B9, B22, and B27, prior to DCM extraction of PC, at a scale of 0.5 μm.

The morphologies observed for the pigmented blends, upon extraction of the PC, are considered below. Figures 3-91 to 3-93 contain TEM images of tape-extruded, DCM-extracted, samples of blends BX, B10, B22 and B27, at increasing magnification levels.

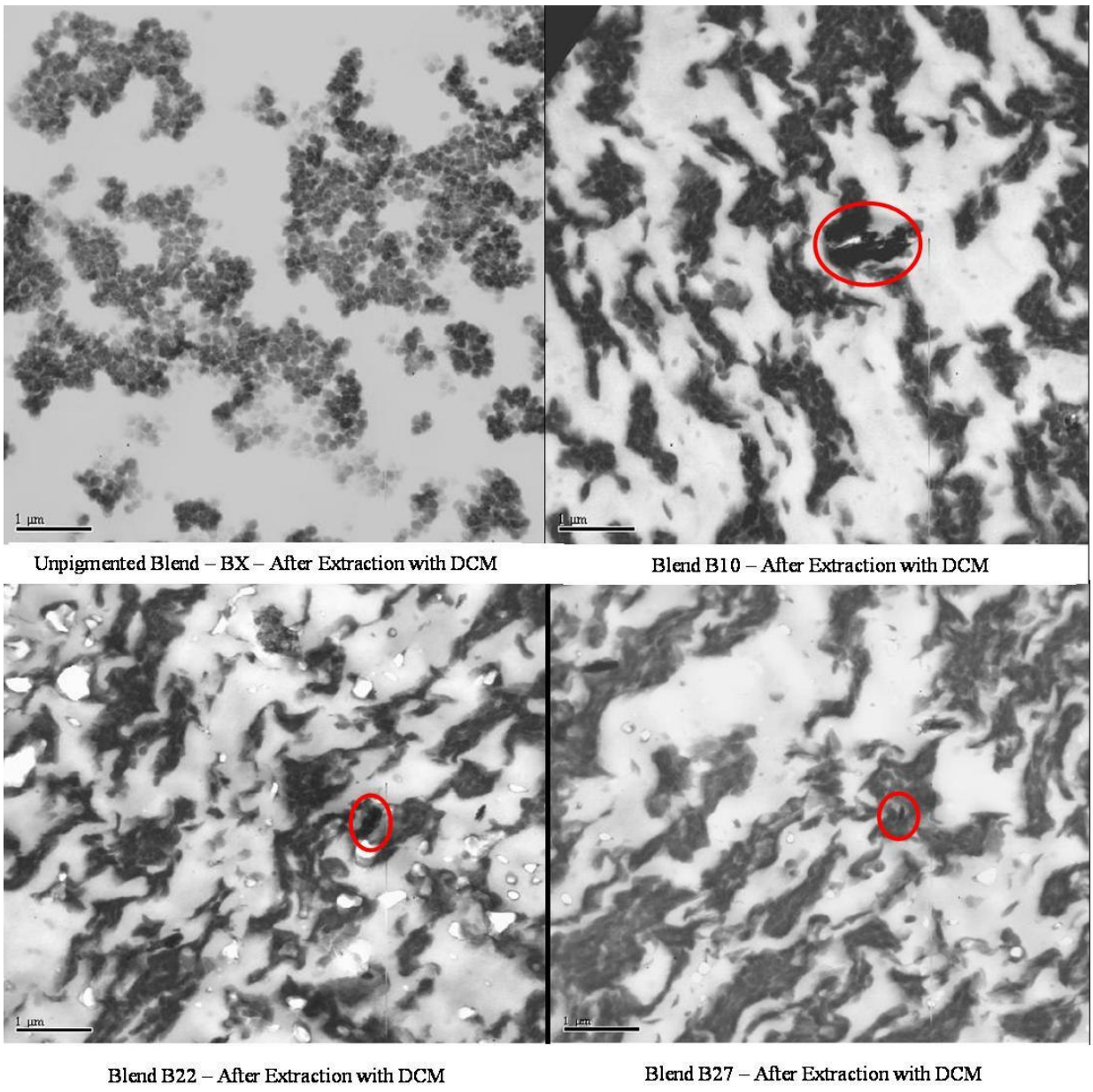

Figure 3-91. TEM images of tape-extruded samples of blends BX, B10, B22 and B27, after extraction of PC with DCM. The red circles indicate the location of pigment particles.

The darker areas in the images that are presented in Figure 3-91 correspond to the MBS rubber, and to any PC that was not removed by DCM, due to its being trapped in the PBT crystalline phase. Pigment particulates have been identified as the darker particulates, indicated by the red circles. The images shown are representative of the TEM imaging of the samples analysed. The shape, density, colour intensity and morphology of the pigment agglomerates are different from those of the MBS rubber particle agglomerates, a fact that allowed their identification.

From the images presented in Figure 3-91 it is clear that blend B22 presents significantly larger and more well-defined PBT domains. This results from the greater degree of crystallinity of this sample. The location of the pigment agglomerates is shown more in detail in Figure 3-92.

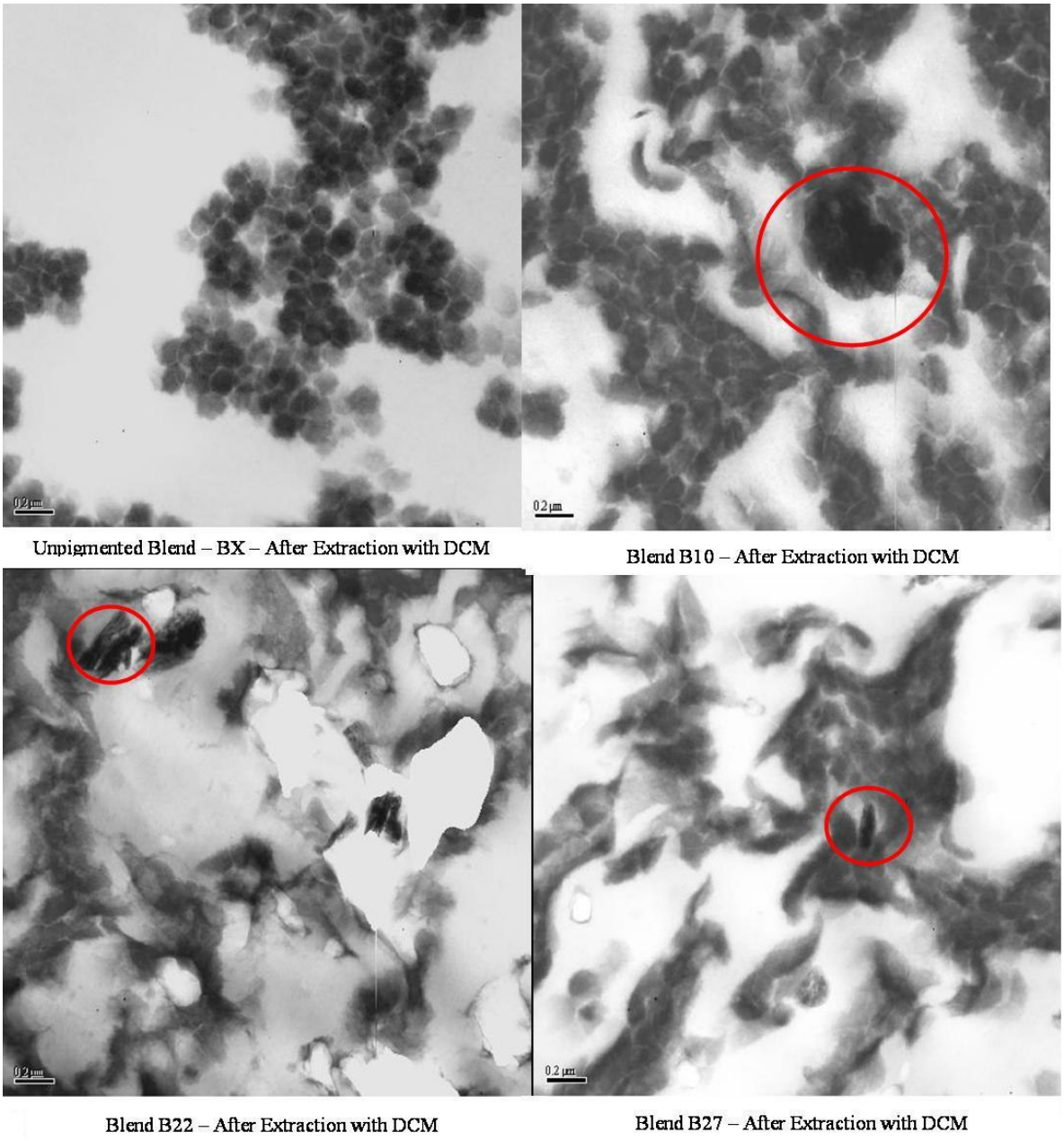

Figure 3-92. TEM images of tape-extruded samples of blends BX, B10, B22 and B27, after extraction of PC with DCM, at a greater magnification than in Figure 3-91.

From the observation of the images presented in Figure 3-92 it is clear that the phase preferences of pigment particles are as follows. The unmodified pigment particles (sample B10), are located in the interphase of the PC and PBT domains. The “Lewis acidic“ pigment particles are integrated in the PBT crystalline phase. The “neutralised” pigment particles are preferentially located in the PC phase.

Nevertheless, for the blend samples that contain the pigment **hiwren**, it is expected that a fraction of the particles will be located in the PBT-phase. This is a consequence of the incomplete neutralisation of the surface carboxylic acid groups present in the surface of the pigment **hiwre**. This fact is indicated in the greater non-isothermal crystallisation temperature and in the greater degree of crystallinity of samples of Set 6, when compared to the values of these parameters corresponding to samples of Sets 1 and 2.

Figure 3-93 shows in more detail the pigment particles, identified in the PBT phase, for sample B22.

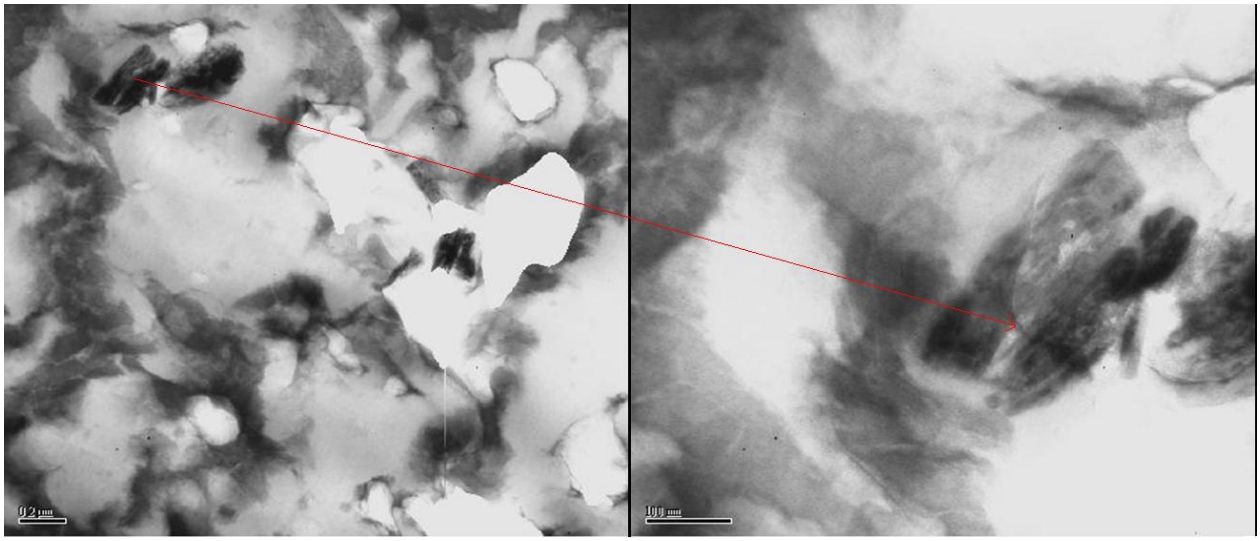

Figure 3-93. TEM images of tape-extruded sample of blend B22, after extraction of PC with DCM, at a greater magnification than was represented in Figure 3-92.

In Figure 3-93, the image on the left-hand side and the image on the right-hand side correspond to a scale of 0.2 µm and of 100 nm, respectively. Figure 3-93 shows that the pigment particulates are completely incorporated in the PBT crystalline phase.

The preferential locations of the unmodified pigment and of the modified pigments, and consequences thereof to the exposure of the pigment particulates after removal of the PC, are clear in the photographic image presented in Figure 3-94.

The effects of the surface modifications of the commercial C. I. Pigment Blue 28 on the colour properties are evident in the image presented this figure, the colour intensity increasing in the order: B10 > B27 > B22. Thus, the surface modifications of C. I. Pigment Blue 28 lead to decreased exposure of the pigment particles due to improved adhesion with the PBT phase, and due to increased degree of crystallinity.

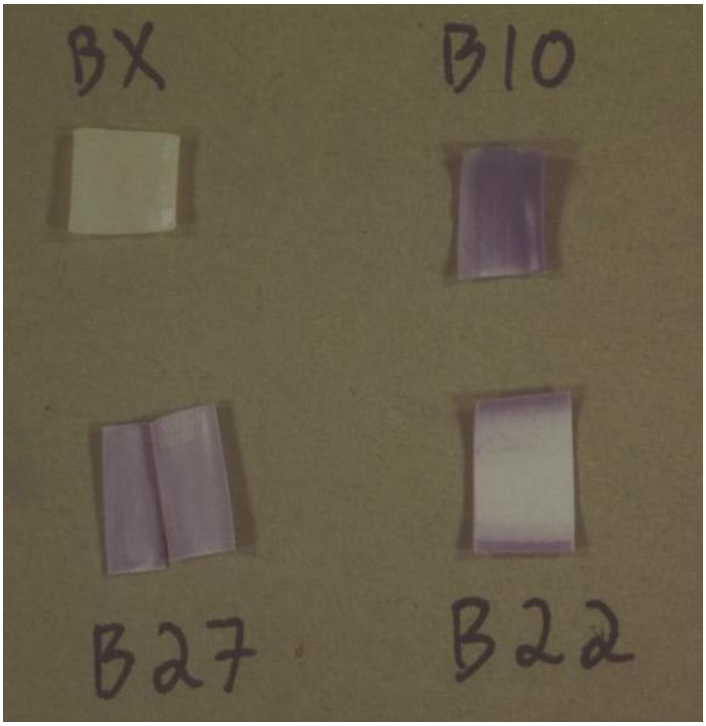

Figure 3-94. Photographic image of tape-extruded samples of blends BX, B10, B22 and B27, after extraction of PC with DCM.

The above discussions on the TEM and photo-imaging confirm the inferences made regarding the SEM/EDX imaging. Furthermore, the predictions and expectations in relation to the phase preferences of the pigment particles (unmodified and modified), are confirmed and supported.

4. GENERAL DISCUSSION OF RESULTS

The interaction potential of the major components of the pigmented PC/PBT/IM blends has been assessed by means of inverse gas chromatography. From the values determined for the dispersive component of the surface tension, Section 3.1.8.1., it is concluded that both PBT 195 and PBT 315 have the greater interaction potential through dispersion forces, followed by the impact modifier, the PC 125, and the pigment. Thus, each of PBT 195 and PBT 315 will interact, through dispersive forces, preferentially with PBT molecules. The dispersive forces interaction potential of the MBS rubber (IM) is close to that of PBT 195 and to that of PBT 315, followed by that of PC 125. Therefore, it can be expected that the IM will interact to a larger extent, through dispersive forces, with PC 125. The pigment, C. I. Pigment Blue 28, has the lower interaction potential through non-specific forces.

The determination of the surface Lewis acidity and basicity constants, K_a and K_b, respectively, showed that all the materials analysed are able to interact through specific intermolecular forces. These dominate over the dispersive forces. Therefore, the tendency for interaction between the major components of the system under study will be determined by their electron donor/electron acceptor interaction potential. The results obtained (Section 3.1.8.2.) show that the PBT 195, the PBT 315 and the MBS rubber are the most interactive materials. PC 125 is significantly less interactive than the remaining materials. The MBS rubber has the greater predominance of basic sites, and the C. I. Pigment blue 28 the lower predominance of basic sites. The MBS rubber, the PBT 195, and the PBT 315 are the more Lewis basic materials. PBT 195 and C. I. Pigment Blue 28 are the more Lewis acidic materials.

Taking into account:

1) The structure of the repeating units and end-groups in PC, PMMA (the shell component of the MBS rubber), PBT 195, and PBT 315;
2) The molecular structure of the C. I. Pigment Blue 28 pigment;
3) The relative surface Lewis acidity and surface Lewis basicity of these materials, as quantified by K_a and K_b, and
4) The relative presence of each material in the pigmented PC/PBT/IM blends,

the following conclusions can be drawn.

The PBT 195 and the PBT 315 interact preferentially intramolecularly, and intermolecularly, with PBT molecules, as they are characterised by both strong Lewis base and strong Lewis acid functionalities. The PC 125 has the lower ability to participate in specific interactions. This is due to the strong base/base repulsion and weak acid/base attraction, alongside with the steric hindrance

that is due to the -CH_3 side-groups and to the aromatic ring. The fast crystallisation kinetics of PBT contributes to the expulsion of PC from within the PBT domains. This fast crystallisation kinetics is interpreted as the contribution of the strong Lewis basic sites and of the strong Lewis acidic sites, of the chemically regular structure of the molecule, of the non-existence of bulky side-groups and of the high mobility that is caused by the butylene unit in the chain. These aspects provide the structural and chemical requirements for crystallinity and, consequently, for the excellent solvent resistance and thermal stability that is possessed by PBT.

A certain degree of Lewis acid/base attraction between PC 125 and the PBTs is expected as the PC 125, although being a weak Lewis acid, has some Lewis base character and the PBTs have strong Lewis acidic sites. Furthermore, the PBTs also have strong Lewis basic sites and, thus, are able to interact to a certain extent with the Lewis acidic sites on PC 125. One must also bear in mind that the PBT and the PC 125 account for 90% (w/w) of the blend composition in an approximate 1:1 proportion and that, therefore, the interaction opportunities are very considerable. Moreover, the partial miscibility has a contribution from repulsion effects (Section 1.2.1.). As the number of ester groups (Lewis base centres) per unit chain is significantly greater than the number of OH groups (Lewis acidic centres), it follows that base-base repulsion between the basic centres in the backbone of PBT is a probable event. Consequently, both PBTs, particularly PBT 315 (which has the lower K_a value of the two PBTs), and in view of the repulsion effect theory, are expected to interact with PC 125, although to a small extent. Thus, while being naturally phase-separated, PC and PBT may be miscible to a small extent.

The preference of the MBS rubber for interaction with the PC 125 rather than with the PBTs is interpreted in terms of the preference of the PBTs to interact intramolecularly and intermolecularly with PBT molecules, and of the Lewis base/base repulsion (predominant repulsion effect) between the PBTs and the MBS rubber. The fast crystallisation of PBT also contributes to the expulsion of the MBS rubber from the PBT domains.

C. I. Pigment Blue 28 is predicted to interact preferentially with the PBTs and then with the PC 125. This is due to the fact that the pigment is strongly Lewis acidic and the PBTs are strong Lewis bases. Also, the PBTs, particularly PBT 195, are strongly Lewis acidic and the pigment is moderately Lewis basic. Nevertheless, as the PBT molecules interact preferentially with other PBT molecules, it is expected that some acid/base interaction between the pigment and the PC 125 would occur.

The adsorption of polar molecules on PBT is an endothermic process. The results have been interpreted assuming the presence of a predominant contribution, to the enthalpy (and entropy) of adsorption, from the breaking of hydrogen bonds in the self-associating polymer, in relation to the formation of hydrogen bonds between the polar probe molecules and the PBT molecules.

In order to assess the influence of the pigments (C. I. Pigment Blue 28, **hiwre** and **hiwren**) on the physical properties, on the mechanical properties and on the morphology of the

polycarbonate/poly(butylene terephthalate)/impact modifier (PC/PBT/IM) blends, several analytical techniques, and mechanical tests, were used. These, together with the controlled surface modifications of the pigment (photo-sensitised grafting of MAA units), resulted in a rationalisation of the associations that exist between the components' interaction, the phase separation and the phase preferences, the physical properties, and the mechanical properties of these blends.

Three sets of PC/PBT/IM blends, of increasing pigment loadings, were prepared using different extruders and different extrusion conditions. The influence that C. I. Pigment Blue 28 has on the physical properties and on the mechanical properties of this polymeric system was assessed for blends characterised by lower degradation (Sets 1 and 2) and greater degradation (Set 7) of the molecular weights of PC and of PBT, a consequence of the extrusion conditions and facilities used.

The molecular weights of PC and of PBT are influenced by C. I. Pigment Blue 28, (Section 3.2.1.). The GPC results show that the higher fraction of the molecular weight distribution of PBT is distinctly more influenced by the pigment than is the lower fraction and than is the PC. Blending PC with PBT leads to a decrease in the average molecular weight of both polymers in the blend.

The addition of the pigment to the composition of the blends results in an increase of the average molecular weight of PC. From the TEM imaging of the blends (Section 3.2.10.) and from the DMTA results (Section 3.2.3.) it is concluded that the greater the molecular weight of PC, the more well-defined are the PC-rich phase domains and the PBT-rich phase domains, and the more expressive is the phase separation of PC and PBT.

The effect of the pigment on the molecular weight of PBT does not follow a linear relationship. At lower pigment loadings, the presence of the inorganic pigment particles leads to a decrease of the average molecular weight. Above a particular pigment loading, the pigment particles show the opposite effect, that of inhibiting the chain scission of PBT.

For the samples characterised by a lower molecular weight of PC and of PBT, consequent on the processing conditions, Set 7, a correlation exists between the crystalline properties of PBT (Section 3.2.2.2), the transesterification level (as assessed by the melting temperature depression method, Section 3.2.2.1.) and the average molecular weight of PBT. The lower the molecular weight of PBT, the lower is the crystallisation temperature and the greater is the transesterification level. Therefore, transesterification, along with the thermal scission of the polymer chains, has been proven to have an important effect on the physical properties of the blends that are characterised by a lower molecular weight of PC and of PBT. Moreover, the transesterification and the thermal degradation of the polymers in these samples are directly influenced by the presence of C. I. Pigment Blue 28.

The molecular weight distribution of PC and of PBT, in the blends that are characterised by greater average molecular weights of PC and of PBT (Set 2), is more homogeneous than it is in the blends represented by Set 7. The trends observed for Set 2 are analogous to those relating to

samples characterised by lower average molecular weight of PC and of PBT, but in a less pronounced manner. The trend observed for the molecular weight of PBT, with increasing pigment loading in these samples, is similar to that observed for the melting temperature depression (ΔT_m, Section 3.2.2.1.). The behaviour observed for the non-isothermal crystallisation properties (Section 3.2.2.2.) differs from that observed for the molecular weight and for the ΔT_m. Thus, these samples are not significantly transesterified as this does not affect the crystallisation properties of the PBT phase in the blends. It can be concluded that the major cause of the behaviour observed in the variation of the molecular weight, and of the ΔT_m, for samples that have a greater molecular weight of PC and of PBT, is that of thermal scission of the polymers.

The DSC analysis (in the heating mode, Section 3.2.2.1.) of the blends prepared, confirms the increased phase separation due to increased molecular weight of PC (supported by DMTA and TEM analysis), and increased miscibility (supported by DMTA) with increasing pigment loading. The results also confirm that the pigment affects the crystalline properties of PBT. These effects are more pronounced for samples that are characterised by lower molecular weights of PBT and PC (Set 7). The introduction of C. I. Pigment Blue 28 into the blends leads to an increase in the melting temperature of the blends. The blends that have a lower average molecular weight of PC and of PBT are more sensitive to the thermal treatment in the DSC cell and the corresponding values of the second scan T_m are lower.

The depression in the melting point, ΔT_m, is greater for the blends that are characterised by a lower molecular weight of PC and of PBT. This finding supports the evidence (TEM imaging, Section 3.2.10.) that, in these samples, PC and PBT are more miscible. Moreover, these samples are more prone to transesterification, and are characterised by a more extensive transesterification reaction degree, than are those that have a greater average molecular weight of PC and of PBT. The physical properties of PBT are concluded to be a good indicator of the transesterification level in PC/PBT blends.

The pigment appears to influence the extent of transesterification. Transesterification occurred in the samples with the lower pigment loadings, namely in those of Set 7. At greater pigment loadings, the transesterification degree and the polymer chain scission level decrease. Several reasons can be identified as the origin of these occurrences. The first is the difference in thermal conductivity between the inorganic pigment particles and the polymers. At low pigment loadings, the inorganic particles, due to their greater thermal conductivity, act as heat concentrators, favouring the occurrence of transesterification and of thermally induced polymer chain scission. The lower transesterification at greater pigment loadings is due to the fact that the pigment particles have the effect of lowering the local temperature. The second reason is the hypothesis that the pigment particles can act as a transesterification promoter at low pigment loadings and as a stabilizer at higher pigment loadings, by scavenging the PBT catalyst. This idea is supported by favourable Lewis acid/base interaction between the catalyst and the PBT, a consequence of the expected Lewis acidity of the PBT catalyst and of the predominant Lewis basic

surface of the cobalt aluminate pigment (Section 3.1.3.). As the pigment loading increases, a dilution effect of the titanium-based catalyst would result in a decreased extent of transesterification. The location of the pigment particles at the interphase of PC and PBT (Sections 3.2.3. to 3.2.8, 3.4.9. and 3.4.10.), where the polymers are intimately mixed at the surface of the inorganic particles, contributes to the occurrence of transesterification.

The blends represented by Set 7 are subject to a more intense mixing regime, more energy being delivered to the melt blend, and have a longer barrel residence time (Section 2.1), than samples of Set 2. As a result, the melt temperature and the shear and elongational stresses are greater for these blends than they are for those samples that are represented by Set 2. This results in more severe polymer thermal scission and transesterification in samples of Set 7.

A detailed study was carried out to assess the influence of C. I. Pigment Blue 28 on the crystalline properties of the PC/PBT/IM blends (Section 3.2.2.2). For samples of Set 7, the results obtained are in line with the proven occurrence of transesterification in these samples and with the consequences therefrom to the molecular weights of PC and of PBT. Thus, for the lower pigment loadings, the rate of crystallisation and the degree of crystallinity are lower and the crystallisation activation energy is higher, than that of the unpigmented blend, and than those of samples with higher pigment loadings. The degree of crystallinity of PBT increases with increasing pigment loading but never reaches the value for the unpigmented blend, in accord with the transesterification level in these samples. The reduction of the T_c and of the ΔH_c of the PBT-rich phase may also have the contribution of increased miscibility of PC and PBT, due to lower molecular weights of these polymers, at the lower pigment loadings. At the higher pigment loadings, the cobalt aluminate lowers the crystallisation activation energy and increases the rate of crystallisation of PBT.

For the samples of Set 2, characterised by a greater molecular weight of PC and of PBT, it can be concluded that C. I. Pigment Blue 28 decreases the crystallisation activation energy and increases the rate of crystallisation, without altering significantly the degree of crystallinity of PBT in the blend samples.

From the DSC studies, it can be concluded that the pigment has an effect on the crystallisation properties of the PBT in the blend samples. This effect has both indirect and direct consequences. The influence of C. I. Pigment Blue 28 on the transesterification reaction, and consequences thereof to the crystallisation properties, accounts for the indirect effects. Increasing transesterification results in a progressive reduction in the melting temperature, in the crystallisation temperature, and in the degree of crystallinity. The nucleating effect of C. I. Pigment Blue 28 accounts for the decreased crystallisation activation energy and the increased rate of crystallisation. The degree of crystallinity is not directly affected by the presence of C. I. Pigment Blue 28. The influence of the pigment on T_c and on ΔT strongly indicates that there is direct contact between the pigment and the PBT-rich phase in the PC/PBT/IM blends, in line with prediction from the IGC analysis.

The DMTA results (Section 3.2.3.) are clear in showing the existence of three characteristic regions in the morphology of the blend: the first corresponds to the PBT-rich phase, the second to the PC-rich phase, and a third region where PC and PBT coexist, that is the PC/PBT interphase region. This shows that the PC and the PBT are partially miscible. The differences between the T_g values of the PC-rich phase and of the PBT-rich phase, and the T_g values of the pure components, indicate the presence of both components in each phase of the blend. PBT is more miscible in the PC than the PC is in the PBT. The observed partial miscibility of PC and PBT is supported by the Lewis acid/Lewis base interaction potential between the major components of the system, evaluated by means of inverse gas chromatography, Section 3.1.8.2.

There is an increase in the elastic response of the system with increasing pigment loading, mainly in the region concerning the PC/PBT interphase. These observations are indicative of strong PC-pigment and PBT-pigment interactions. Increased miscibility of the PC and of the PBT at the PC/PBT interphase with increasing pigment loading is thought to occur. This is more evident for samples of Set 7, due to the lower molecular weight of the polymers, and also due to existence of greater amorphous PBT content in this set of samples, in particular at the lower pigment loadings. The degree of crystallinity does not play a significant role in the phase separation and in the PC/PBT miscibility at the interphase, observed in the DMTA results. The fact that the pigment does not influence very significantly the viscoelastic properties of the individual phases, but does influence those of the PC/PBT interphase, further confirms the preferential location of the pigment particles at the PC/PBT interphase, as predicted from the IGC studies.

The decrease of the viscous response of the blend due to the introduction of pigment is in line with the results from the tensile tests. In these, it was observed that the tensile modulus increases with increasing pigment loading, due to increased molecular weight of the PC, due to the presence of the rigid inorganic pigment particles, and due to the good adhesion of the PBT and of the PC to the surface of the pigment particles. This good adhesion causes increased restrictions in the movement of the polymeric chains (as is the case with increasing crystallinity).

The DMTA results show, nevertheless, phase separation with increasing pigment loading. The occurrence of phase separation is due to the increase of the molecular weight of the polymers, in particular that of the PC at the lower pigment loadings. The behaviours implied by the height of the peak representing the PC-rich phase and by the height of the peak representing the PBT-rich phase, (related to the viscoelastic behaviour of the blend), are in line with the trend observed for the PBT crystallinity in these blends.

Comparing the viscoelastic properties of samples of Sets 2 and 7, it can be stated that the greater molecular weight of PBT and of PC in the pigmented PC/PBT/IM blends, as represented by samples of Set 2, leads to a more distinct phase separation and not as clearly increased miscibility with increasing pigment loading.

There is an increment in the Vicat softening temperature, (VST, Section 3.2.4.) with increasing pigment loading in the pigmented PC/PBT/IM blends. This is attributed to the increase in the average molecular weight of PC, with a small contribution from the increasing presence of the rigid inorganic pigment particles. Accordingly, samples processed under conditions (extruder and screw design and/or operating conditions) that lead to greater molecular weight reduction show a lower value of VST. Blending of PC with PBT reduces the overall modulus when compared to that of the individual phases. This is due to the reduction the molecular weight of PC and of PBT upon blending of these polymers. The VST values also provide an indication of the extent of transesterification, and the results confirm those relating to the melting temperature depression method, that indicate a greater transesterification level for samples of Set 7. As a general observation, it can be said that the trends seen in the VST data are in line with those concerning the tensile modulus.

From the TGA studies carried out, Section 3.2.5., it can be concluded that inclusion of pigment in the PC/PBT/IM blend leads to thermal decomposition at lower temperatures. This is due to the greater thermal conductivity of the pigment inorganic particles when compared to that of the polymers.

In the unpigmented PC/PBT/IM blend, the PC phase determines the impact resistance of the blend (Section 3.2.6.). Consequently, it is expected that in the pigmented blends, this phase also plays an important role in terms of impact energy absorption. The total impact energy absorption of the pigmented blends is a sum of the effects of the pigment on the PC phase and on the PBT phase. Therefore, a synergistic effect is observed when PBT and PC are blended, if the pigment is included in the blend compositions. The effect of increasing the pigment loading in the blend does not follow that corresponding to the PC-based samples and that corresponding to the PBT-based samples. This suggests that the pigment is not preferentially present in one of the phases (PC or PBT), in agreement with the DMTA results.

For the blends that are characterised by a lower average molecular weight, Set 7, a decrease of the average molecular weight of the higher fraction of molecular weight distribution of PBT corresponds to an improvement of the impact toughness of the blend. Also, as the average molecular weight of PBT increases, the impact toughness decreases. The trend observed is in line with that concerning the non-isothermal crystallisation properties of PBT in these blends. Thus, the lower the degree of crystallinity and the lower the molecular weight of the higher fraction of the molecular weight distribution of PBT, the greater is the impact energy absorption capability of the blend due to increase in the mobility of the macromolecular chains. The ductile to brittle transition temperature, $T_{D/B}$, follows a similar trend to that of the PBT crystallinity. The greater the degree of crystallinity, the higher is the $T_{D/B}$. Furthermore, it can be concluded that the impact energy absorption increases with increasing transesterification. The greater the extent of transesterification, the better is the PC phase and PBT phase interconnection, due to the formation of PC-PBT

copolyesters (bridging effect). Consequently, the stress transfer across the interphase is favoured by the occurrence of transesterification.

It can be concluded that the effect C. I. Pigment Blue 28 has on the impact resistance properties of the blends of Set 7 is a consequence of the changes in the molecular weight of PBT, in the degree of crystallinity and in the extent of transesterification. The trend observed is in line with the results concerning the strain at break (Section 3.2.8.), which derives from the effect the molecular weight, the degree of crystallinity and the transesterification reaction have on the ultimate elongation properties of these blends.

For samples of Set 2, characterised by a greater molecular weight of PC and of PBT than the blends represented by Set 7, it was observed that, for the pigment loading range used, the samples present a ductile fracture profile at all the test temperatures studied. The incorporation of pigment in the blends improves their impact toughness. The increase in pigment loading has little effect on the Izod notched impact test results. This behaviour does not follow that of the molecular weight of PC and PBT, nor is it analogous with that of the degree of crystallinity or that of the extent of transesterification in these samples. Thus, it can be concluded that the improvement of the impact resistance is due to changes is the impact toughening mechanisms, a consequence of the presence of the pigment particles. A possibility is the improvement of stress transfer between the PBT phase and the PC phase, due to the adsorption, and improved miscibility, of these polymers at the surface of the pigment particles, and to the presence of the inorganic particulates at the interphase. At the lower pigment loadings, crazing and cavitation may be contributing to the improvement of the impact toughness, whereas at the greater pigment loadings, the internal cavitation of the pigment particles may lower the impact resistance of the blends. Nevertheless, the preferential presence of the pigment particles at the PC/PBT interphase, that results in impact energy transfer between phase domains (bridging effect), is thought to overcome the aforementioned detrimental effects of high pigment loadings on the impact resistance of the individual phases.

It can be concluded that the lower the molecular weights of PC and PBT, the more sensitive is the impact resistance to differences in the molecular weight of PBT, in the degree of crystallinity, and in the extent of transesterification. Moreover, processing conditions that lead to a lower breakdown of the polymer chains, and, thus, to a higher average molecular weight of both the PC and the PBT, lead to an improved impact toughness of the blend. The improvement in the impact resistance of the pigmented blends, due to modifications (caused by C. I. Pigment Blue 28) in the fracture mechanisms, does not prevail in the samples of Set 7. For lower molecular weight values of PC and PBT, the effects of varying the crystallinity degree, molecular weights and extent of transesterification, dominate over those relating to the changes in the impact energy absorption mechanisms.

When the samples of blends of Set 7 are tested by means of the puncture impact test, Section 3.2.7., the trend observed is in line with that relating to the notched Izod impact test. From testing

of samples of the blends that are represented by Set 2, it can be concluded that the impact energy absorption mechanisms that improve the impact resistance of the pigmented blends when tested by means of the notched Izod impact test are less significant when high rates of impact conditions are applied. Under these testing conditions, the lower the molecular weight of PC and of PBT the more significant are the effects of varying degree of crystallinity, extent of transesterification, and molecular weight of PC and PBT on the impact energy absorption and the lower is the impact resistance. For the puncture energy, the blend values are greater than those obtained for the individual phases. Therefore, a synergistic effect upon blending of PC with PBT is indicated in the puncture impact test results. Under high rate impact conditions, the PBT phase loses importance as far as the impact energy absorption is concerned.

The tensile modulus of the blend, Section 3.2.8., results from the linear combination of the modulus of the PC phase and of the PBT phase, with greater contribution from the PC-rich phase. The effect that the pigment has on the pigmented blends that are represented by Set 2, does not clearly follow the same trends observed for the molecular weight and molecular weight distribution of PC and of PBT, for the non-isothermal crystallisation properties, or for the transesterification degree. Thus, in these samples, the effect that the pigment has on the tensile modulus is concluded to be a consequence of the presence of the rigid pigment particles at the interphase of PC and PBT, and of the good adhesion between the pigment particulates and the polymers.

For the samples of Set 7, the trend observed for the tensile modulus values follows the behaviour of the average molecular weight of PC and is in line with the Vicat softening temperature results (Section 3.2.4.). Thus, the modulus of the blend, in this set of samples, is influenced, to a large extent, by the molecular weight of the PC. The trend observed is in accordance with the DMTA results for these samples (Section 3.2.3.) as the increase in pigment loading leads to an increase of the elastic absorption of energy. Thus, the stiffness and hardness of the sample are increased with increasing pigment loading, a fact that is also indicated in the increasing value of the tensile modulus. For samples of Set 7, the effect of the molecular weight of the PC on the tensile modulus overcomes those of the degree of crystallinity and of the molecular weight of the PBT. The miscibility level (inherent or due to transesterification) is a parameter that scarcely influences the modulus, particularly when partial miscibility exists. The results of the present study show that the crystalline phase is not sufficiently continuous to influence the modulus and that the amorphous phase is determining the deformations related to this viscoelastic property.

From the strain at break results, it is concluded that, in the PC/PBT/IM blends, the PC-rich phase dominates over the PBT-rich phase. This is because, at higher stresses, the flow of the PBT-rich component becomes significant. Nevertheless, changes to the crystalline content of the blend have effects on the values of the strain at break. The significant standard deviation that is associated with the strain at break values, in particular at pigment loadings that are lower than

approximately 0.60 %, is thought to have a contribution from the preferential location of the pigment particles at the PC/PBT interphase.

For samples of Set 7, a correlation exists between the average molecular weight of the higher fraction of the molecular weight distribution of PBT (which corresponds mainly to PBT 315), the non-isothermal crystallisation properties, the PC-PBT copolyester content, and the value of the strain at failure of the blend. The lower the average molecular weight of PBT, the lower the T_c and the $-\Delta H_c$, and the greater the transesterification level, the greater are the values of the strain at break. The greater the PC-PBT copolyester content, the more increased is the PC-PBT interconnection. In turn, the increased PC-PBT interconnection leads to greater extendibility of the polymer matrix.

The set of samples that has a lower average molecular weight of PBT and of PC (Set 7) is characterised by a lower value of strain at break than are the sets of samples with higher average molecular weights (Sets 1 and 2). The crystallinity of samples of Set 2 is greater than/equal to that of samples of Set 7. Thus, the lower values of the stain at break for samples of Set 7 are a consequence of the lower molecular weights of PBT and PC in these samples.

For the stress at break values, the introduction of the pigment and the increase of its loading, in the blends characterised by lower average values of PC and of PBT, results in a trend that follows that of the average molecular weight of PC. Thus, the stress at break values, for this set of samples, are influenced, to a large extent, by the molecular weight of the PC. This effect overcomes those due to crystallinity differences, increasing presence of inorganic particles, differences in transesterification level and differences in the molecular weight of PBT. The set of samples that are characterised by lower values of the molecular weights of PC and of PBT (Set 7) shows lower values of the stress at break than do the blends that are represented by Sets 1 and 2.

The values of the strain at yield and of the stress at yield, for the blend samples lie between that corresponding to the PC samples and that of the PBT samples, but are closer to the values obtained for the PBT samples. Thus, at low stresses the blend shows PBT-like behaviour. The inclusion of the pigment in the blend leads to an increase in the strain at yield of the blend samples that are represented by Set 2. For the samples of Set 7, the trend observed is in line with those concerning the stress at break results and the tensile modulus results. Thus, the strain at yield values for this set of samples are thought to be significantly influenced by the molecular weight of the PC. It can be said that the strain range in which the blend behaves elastically is increased with increasing pigment loading due to increased average length of the PC chains.

For the blend samples of Set 2, the stress at yield does not vary significantly with increasing pigment loading. For samples of Set 7, the trend observed is in line with that concerning the strain at yield, the stress at break and the tensile modulus. Therefore, the molecular weight of the PC plays an important part with regard to the stress at yield, overcoming the effects of the degree of crystallinity, of the transesterification, and of the molecular weight of PBT. The greater the

molecular weight of PC, the lower is the chain mobility and, consequently, the greater are the stress at yield values. It can be concluded that the yield stress trends that are observed are due to the change of free volume of the polymer blend, a consequence of alterations in the molecular weight and, thus, in the density, of the amorphous phase.

As a general observation, it can be said that the amorphous phase governs the mechanical response at low strains, while the crystalline content appears to be the most important parameter for break properties. The viscous response of the blend to applied stress increases when the pigment is introduced in the blend. As the pigment loading increases, the blend responds more elastically to applied stress. Bearing in mind the molar mass analysis of PC and PBT, it can be concluded that the molar mass of PC plays a dominant role in so far as the strain at yield, stress at yield, stress at break and the modulus are concerned. The degree of crystallinity, transesterification level and PBT molecular weight are decisive as far as the strain at break is concerned.

From the tensile testing results, it is also concluded that the pigment particles are located preferentially at the PC/PBT interphase.The good adhesion of PC and of PBT to the surface of the pigment and the presence of the pigment particulates at the PC/PBT interphase, also play a decisive role in determining the viscoelastic properties of the pigmented blends. C. I. Pigment Blue 28 affects indirectly the tensile properties of the blends due to its influence on the molecular weight of PC, on the transesterification reactions and on the crystalline properties of PBT.

The melt volume rate (MVR) values for the blend samples of Set 2, Section 3.2.9., are intermediate between those of the individual phases, but closer to those of the PC-based samples. Therefore, it can be concluded that the PC phase is determinant as far as the melt viscosity of the blend is concerned. The MVR value of the blend samples that are represented by Set 2 decreases with increasing pigment loading. This is in line with the increasing molecular weight of PC with increasing pigment loading in these samples. Therefore, it can be concluded that the greater the molecular weight of the PC in the PC-rich phase of PC/PBT/IM blends, the greater is the melt viscosity.

The MVR values of Set 7 are significantly greater than those of samples of Sets 1 and 2. This is due to the lower average molecular weight of PC and of PBT in the blends of Set 7. For samples of Set 7, the trend observed in the MVR values with the introduction and increase in the pigment loading follows a behaviour that is similar to that of the PBT molecular weight. Thus, for this set of samples and mainly for the lower pigment loadings, the molecular weight of the PBT phase contributes significantly to the melt viscosity values. Therefore, it is concluded that the lower the molecular weight of PC and PBT, the more important is the contribution of the molecular weight of the semi-crystalline polymer to the melt viscosity. Thus, C. I. Pigment Blue 28 influences the melt viscosity of the blend due to the effects it has on the molecular weights of PC and of PBT.

In the TEM images relating to pigmented blends, Section 3.2.10., the pigment particles cannot be identified in one or both of the phase domains. This is thought to be due to the polymer

phases being adsorbed at the surface of the pigment particulates, hindering these from TEM detection. For the set of blend samples that is characterised by a lower average molecular weight of PC and of PBT (Set 7), as the pigment loading increases, the PC and PBT phases become more distinct. These results are in line with the assessment of the molecular weight, and of the molecular weight distribution of the polymers, mainly of the PC. The greater the average molecular weight of the PC, the more distinct is the phase separation of PBT and PC. These inferences are in line with the discussion of the DMTA results concerning these samples. Visual evidence is found of greater transesterification in batch L8 (0.10 % pigment loading). This agrees with the transesterification reaction assessment by means of the melting temperature depression method and by means of the study of the crystallisation properties of PBT, in these blends.

Comparing samples that were processed in extruder E1 (Sets 1and 2) with those that were processed in extruder E2 (Set 7), it can be concluded that a higher average molecular weight distribution of both the PC and the PBT, leads to a more well-defined phase separation and larger PC, and PBT, domains. The effect of better phase definition and better phase separation, with increasing pigment loading for samples of Set 2, is not as evident as those for samples of Set 7, due to the lower molecular weights of PC and PBT for the blends represented by Set 7.

A series of techniques was used to assess the success of fixation of MAA-based units at the surface of C. I. Pigment Blue 28, a consequence of the surface treatment developed and applied to this pigment. From the IGC characterisation of the dispersive component of the surface tension, Section 3.3.1.1., the surface of the modified pigments shows a combination of characteristics of the original unmodified pigment and of MAA polymeric species fixed to the surface. The results indicate that the fixation of polymeric species onto the surface of C. I. Pigment Blue 28 was successful. Furthermore, it can be concluded that the surface-modified pigments have a greater potential to interact through dispersion intermolecular forces than does the unmodified pigment.

From the IGC characterisation of the surface Lewis acid/base properties of the modified pigment (**hiwre**), Section 3.3.1.2., it has been shown that the surface Lewis acidity is greatly increased upon the surface treatment of C. I. Pigment Blue 28. When the surface carboxylic groups are neutralised, to provide the pigment **hiwren**, the Lewis acidity is significantly reduced, and close to that of the unmodified pigment. The surface Lewis basicity increases due to the surface treatment and is slightly reduced upon neutralisation of the surface carboxylic acid groups. The changes observed in terms of the surface Lewis acidity/basicity are in line with the presence of MAA-based polymeric species on the surface of the treated C. I. Pigment Blue 28. The significant increase in the Lewis acidity is related to the presence of the pendant carboxylic acid group units of the MAA units, and is localised in the hydrogen atom. The increased Lewis basicity is related to the presence of the oxygen atoms in the carboxylic acid groups. Upon neutralisation of these functional groups, the Lewis acidity is reduced due to the abstraction of the hydrogen atom. The Lewis basicity is slightly reduced due to the greater steric hindrance that is caused by the

replacement of the hydrogen atom by the more bulky sodium atom that reduces the access to the oxygen atoms. The total interaction potential of the surface of C. I. Pigment Blue 28 is greatly increased by surface photosensitised grafting, and is reduced after the neutralisation process. The relative presence of Lewis basic sites to Lewis acidic sites is decreased due to the surface treatment. It increases upon neutralisation of the surface carboxylic acid groups of **hiwre**, relative to that of the unmodified pigment.

It can be concluded that the surface modifications of C. I. Pigment Blue 28, that consist of fixing PMAA onto the surface of the pigment (pigment **hiwre**), and neutralising the carboxylic acid groups of the treated pigment obtained in this first modification (pigment **hiwren**), was successful, and is expected to influence significantly the physical properties and the mechanical properties of pigmented PC/PBT/IM blends.

From SEM imaging of the pigments, Section 3.3.2., the inter-particle interactions for the surface-modified pigments are shown to be stronger than are those for the unmodified pigment. This is in line with the IGC analysis of the interaction potential of these pigments (Section 3.3.1.). By means of EDXA, the surfaces of the modified pigments, **hiwre** and **hiwren**, show the presence of carbon, in addition to the aforementioned species. These results further confirm the success of the fixation of MAA-based polymeric species onto the surface of C. I. Pigment Blue 28. From the EDXA quantitative results, the amount of organic material fixed to the surface of the surface-modified pigments is estimated to be approximately 5.2 % (w/w).

The measurement of pH values of aqueous dispersions of the pigments, Section 3.3.3., leads to the observation that the acidity of C. I. Pigment Blue 28 has been significantly enhanced due to the surface treatment used. In addition, the neutralisation of the surface carboxylic acid groups leads to a marked decrease of the surface acidic properties and to an increase of the surface basic character. The values observed for the surface-modified pigments clearly differ from those relating to the control samples and are in line with the results that arose from the IGC analysis, (consequences of the surface treatments to the surface Lewis acidity/basicity).

Thermogravimetric analysis carried out on the pigments, Section 3.3.4., indicates that no organic surface coating is present in the commercial C. I. Pigment Blue 28 considered in the present study. The pre-treatment of the pigment by hydration was successful, leading to an increase in the extent of physisorbed water molecules. The results confirm the presence of fixed material on the surface of the modified C. I. Pigment Blue 28. The differences observed between **hiwre** and **hiwren** are not very significant. The amount of physisorbed water is more proiminent for the surface-modified pigments. The amount of fixed material on the surface of **hiwre** is estimated to be 2.6 % (w/w).

By means of gravimetric studies, Section 3.3.5., the amount of fixed material is estimated to be 6.8±1 % (w/w). This value must, nevertheless, be analysed with care, due to the associated high standard deviation (15 % relative standard deviation). The estimatives of fixed material obtained by

the use of different techniques are different. The value obtained by TGA is tought to be more accurate and, thus, the successful fixation of MAA-based units at the surface of C. I. Pigment Blue 28 is estimated to be 2.6 % (w/w). It is, however, concluded that the surface treatment was not uniform.

The average particle size of the surface-modified pigments, Section 3.3.7., is lower than that of the control sample. Moreover, the average particle size of the "Lewis acidic" pigment is lower than that of the "neutralised" pigment. This is thought to be due to improved pigment dispersion in the aqueous medium, due to the surface modifications. Nevertheless, the relatively small differences observed for the average particle size of the pigments lead to the conclusion that these ought not to influence significantly the physical properties and the mechanical properties of the pigmented PC/PBT/IM blends.

The influence of the changes of the surface Lewis acidity/basicity on the physical properties and on the mechanical properties of pigmented PC/PBT/IM blends has been studied. The analysis of the molecular weights of the PC and of the PBT in the PC/PBT/IM blends that contain the modified pigments, Section 3.4.1., shows that the average molecular weights of PBT and PC in these blends are greater than those corresponding to the blends in which the unmodified pigment was used. This difference is particularly prominent for the blends that were extruded using the same extrusion facilities and extrusion settings. Moreover, the aforementioned effects are more pronounced for the PBT and at the lower pigment loadings. At those loadings, the decrease in the molecular weight of the PBT, caused by the unmodified C. I. Pigment Blue 28, was eliminated. The molecular weight change with increasing pigment loading is more consistent for the blends that contain the modified pigments. This conclusion is very important, from the point of view of the application and processing of these blends.

From the molecular weight analysis and from the DSC studies (heating mode, Section 3.4.2.1), the surface modifications of the pigment are shown to reduce very significantly transesterification and polymer chain scission at the lower pigment loadings. Alterations to the preferential presence of the pigment particles in the blend morphology (Sections 3.4.9. and 3.4.10.) are thought to contribute to the behaviour observed. Improved adhesion between the pigment and the polymers, namely the PBT, as predicted from the interaction potential analysis by IGC (Section 3.3.1.), leading to a better wetting of the surface of the pigments by the polymers and, thus, less pronounced differences in the heat transfer capacity between the pigment particles and the matrix polymers, is thought to further contribute to the observed behaviour. The improved adhesion would reduce the heat concentration/dilution effect of the pigment particles and have consequences for the transesterification level and for the thermal degradation of the polymers.

The DSC studies in the cooling mode, Section 3.4.2.2., show that there is a very significant increase in the crystallisation temperature of the blends that contain the surface-modified versions of C. I. Pigment Blue 28. A change of up to 12 ºC for the samples having a pigment loading of 0.5

% (w/w) is observed. The value of T_c increases with increasing pigment loading. Thus, the surface-modifications of the pigment particles lead to a decrease of the crystallisation activation energy, this decreasing further with increasing pigment loading. The crystallisation temperatures for samples of the blends that include the "Lewis acidic" pigment are greater than those for samples of the blends that include the "neutralised pigment". This is in line with the prediction of the differences in the interaction potential of these pigments from IGC studies. The nucleating effect of the surface-modified pigments is concluded to be very important. The surface-modifications of C. I. Pigment Blue 28 lead to increased rates of crystallisation. The differences in the surface Lewis acidity/basicity between the **hiwre** and the **hiwren** pigments do not cause changes in the rate of crystallisation.

The surface modifications of C. I. Pigment Blue 28 lead to a greater degree of crystallinity. Increasing the pigment loading does not lead to a clear change in the degree of crystallinity of the samples containing the surface-modified pigments. The degree of crystallinity of blends that contain **hiwre** is greater than that of samples that contain **hiwren**. Thus, the surface modification that provides the surface of the pigment with the greater Lewis acidic character causes a higher degree of crystallinity. This finding is in line with the IGC characterisation of PBT 195, of PBT 315 and of the pigments (Sections 3.1.6., 3.1.7. and 3.3.1., respectively).

From the particle size analysis and from the particle size distribution analysis, Section 3.3.7., it is concluded that these physical characteristics do not contribute significantly to the differences that were observed in the crystallisation properties of PBT. The surface chemistry differences between the pigments are thought to be the major factor in influencing the crystallisation properties of PBT in the blends in which these pigments were included. It is inferred that, from the industrial processing point of view, accelerated nucleation is a process that is desirable for reducing cycle times in injection moulding operations.

From the DMTA results for blend samples that include the modified pigments, Section 3.4.3., it is shown that the interaction between the pigment and the PC and between the pigment and the PBT, is greater for the modified pigments. The improved interactions, along with increased crystallinity and increased average molecular weights of PBT and PC, contribute to the more elastic response of the blends that contain the modified versions of C. I. Pigment Blue 28. The differences in phase preference of the modified-pigments particles are indicated by the viscoelastic properties of the blend. For the samples containing the pigment **hiwren**, due to the greater presence of the pigment particles in the PC-rich phase, the viscous response of this phase is lower than it is in the samples where the pigment **hiwre** was used.

The Vicat softening temperature values for the samples containing the modified pigments, Section 3.4.4., are greater than those for the samples that contain the unmodified pigment. This difference is greater for the samples that were extruded using the same parameters settings, the difference reaching a maximum value of 10 ºC. The observed differences are due to the greater

average molecular weights of PC and PBT, and to the greater degree of crystallinity, for the samples in which the surface-modified pigments were used.

The PC/PBT/IM blends that were pigmented with the unmodified pigment have a greater impact resistance than those containing the modified pigments (Section 3.4.5.). This is a consequence of the greater degree of crystallinity of the blends that contain **hiwre** and **hiwren**. The dependence of the impact resistance on the test temperature is less pronounced in the case of the samples that were pigmented with the modified pigments. This is thought to be due to changes to the impact toughening mechanisms. These changes would results from alteration to: 1) the phase preferences of the modified pigments, 2) pigment dispersion tendencies, i.e., differences in interparticle-distance and 3) matrix-pigment adhesion. From this, it is inferred that the surface-treated pigment particles show better adhesion to, and are better dispersed in, the polymeric matrix. The improved dispersability of the surface-treated pigments in the polymeric matrix is supported by the MVR test results (Section 3.4.8.). Also, the improved adhesion is indicated by IGC analysis of the interaction potential of **hiwre** and of **hiwren** (Section 3.3.1.). The changes in the impact energy absorption mechanisms that are due to the surface modifications of C. I. Pigment Blue 28 are favourable to the observed better impact resistance of the blends at -20 ºC, when compared to that of the blends that contain the unmodified pigment.

The results of puncture impact testing of the blends, where use was made of the modified pigments, are in line with those concerning the Izod notched impact testing. The sets of samples with the greater molecular weights of PC and PBT have a greater impact energy absorption capability. The samples containing the modified pigments have a lower impact energy absorption ability, due to the higher degree of crystallinity of these samples.

The tensile modulus values for blends that were pigmented with the surface-modified pigments, Section 3.4.7., are greater than are the values for blends containing the unmodified pigment. The greater degree of crystallinity, improved adhesion between the polymer matrix and the surface of the modified pigments and the greater values of the average molecular weights of PC and of PBT for the blends that include the modified pigments, contribute the higher value of the tensile modulus for these blends. Improved dispersion of the modified pigments (Section 3.4.8.) and changes to the preferential location of the pigments (Sections 3.4.9. and 3.4.10.) may also be contributing to the observed differences in the tensile modulus values.

For the blends that contain the modified pigments, the behaviour of the strain at break with increasing pigment loading is more consistent than it is for blends that contain the unmodified pigment. The improved adhesion between the polymeric matrix and the surface of the modified pigments and the greater degree of crystallinity are thought to contribute to the greater consistency and lower values of the strain at break (for the higher pigment loadings), when compared to values for the blends that include the unmodified pigment.

The change in the stress at break with increasing pigment loading is more consistent for the samples that were pigmented with the modified pigments. This is thought to be related to improved adhesion of the PC and of the PBT to the surface of the modified pigments. The stress at yield is greater for the samples that contain the modified pigments. This is thought to be related to the greater degree of crystallinity, to the greater average molecular weight of PC and PBT and to the improved adhesion between the polymers and the surface of the modified pigments, in these samples.

The melt viscosity of samples containing the surface-modified pigments is lower than that of samples that include the unmodified C. I. Pigment Blue 28 in their composition (Section 3.4.8.). This is due to improved dispersion of the pigment particles, caused by the surface modifications. The surface modifications of C. I. Pigment Blue 28 reduce the particle-particle interactions in the polymer matrix and improve the filler dispersion, reducing the viscosity of the blend. This is due to strong Lewis acid/base coupling between the polymeric matrix and the surface-modified pigments. The improvement of the dispersability of the surface-modified pigments, namely of the "Lewis acidic" pigment, is supported by the analysis of the average particle size and of the particle size distribution of the unmodified and surface-modified pigments (Section 3.3.7.).

From SEM imaging of tape-extruded samples, from which the PC was removed by extraction with DCM (Section 3.4.9.), the following observations can be drawn. The surface of the blend sample that includes the unmodified pigment is more homogeneous and smoother than that of the unpigmented blend. This indicates the presence of more well-defined and larger phase domains and, thus, better phase separation. The pigment particles are observed to be encapsulated by the polymer matrix. If one assumes that most of the PC has been removed from the surface of the samples, it can be concluded that in samples that include the unmodified pigment, the PBT shows good adhesion to the pigment particles, confirming expectations that are based on IGC analysis, of the interaction potential between the unmodified pigment and the polymers.

For the sample that contains the "Lewis acidic" pigment (**hiwre**), the pigment particles are significantly less exposed than they are in the sample that contains the unmodified pigment. Thus, the encapsulation of the surface-modified pigment particulates by the PBT phase is more prominent than it is with the unmodified C. I. Pigment Blue 28. This indicates better adhesion and confirms the analysis of, and expectation from, the IGC assessment of the Lewis acid/base interaction potential of the unmodified and modified pigments (Sections 3.1.8. and 3.3.1., respectively).

The morphology of the blend samples that contain the "neutralised" modified pigment (**hiwren**), is more similar to that of the blend corresponding to the unmodified pigment than to that of the blend containing the pigment **hiwre**. Markedly stronger Co atom signal and Al atom signal are obtained for the blend that contains the pigment **hiwren**. The exposure of the pigment particles follows the order: **hiwren** > unmodified pigment > **hiwre**. Thus, the **hiwren** pigment is the less wetted and the **hiwre** pigment the more wetted, by the PBT phase. The unmodified pigment shows

PBT adhesion that is intermediate with that of the surface-modified pigments. These observations are in line with predictions from the IGC results (Sections 3.1.8. and 3.3.1.) and are further confirmed by the TEM imaging of the DCM-extracted samples.

TEM imaging of tape-extruded blends, Section 3.4.10., shows that the phase domains are more well-defined, and that the phase separation is more pronounced, in the blends that contain the modified pigments than it is in the unpigmented blend and than it is in the blend pigmented with the unmodified pigment. The PC and PBT phase domains are clearly more well-defined in the pigmented samples. These results confirm the SEM observations, that the effects are due to the greater crystallisation degree and to the greater molecular weights of the polymers (especially that of the PC), for samples of the pigmented blends and, in particular, for those polymersthose where the modified pigments were used. The phase domains in the blend sample that contains **hiwre** are larger than they are in the blend sample that contains **hiwren**. This is in agreement with the greater degree of crystallinity of the blend that is pigmented with **hiwre**.

From scruting of the TEM imaging results for the tape-extruded samples that were extracted with DCM, it is clear that the blend that was pigmented with **hiwre** presents significantly larger and more well-defined PBT domains, than do the blends pigmented with the unmodified pigment and pigmented with the **hiwren** pigment.

Furthermore, the unmodified pigment particles are located at the interphase of the PC domains and the PBT domains. The “Lewis acidic“ pigment particles are integrated in the PBT crystalline phase. The “neutralised” pigment particles are preferentially located in the PC phase. Nonetheless, for the blend samples that contain the pigment **hiwren**, it is expected that a fraction of the particles will be located in the PBT-phase. This follows from incomplete neutralisation of the surface carboxylic acid groups of pigment **hiwre** and is indicated in the greater non-isothermal crystallisation temperature and in the greater degree of crystallinity of samples of the blends that contain **hiwren**, when compared to the values of these parameters corresponding to samples of blends that contain the unmodified pigment.

Photographic imaging of the DCM-extracted blends shows that the surface modifications of C. I. Pigment Blue 28 lead to decreased exposure of the pigment particulates. This is due to improved adhesion of the modified pigments with the PBT phase, to increased degree of crystallinity and to changes in the preferential location of the pigments in the characteristic morphology of these blends.

It should be noted that the persistence of effects that are attributable to the pigment surface modifications, following extended shearing and heating (as in the preparation of specimens for mechanical property testing), shows that the PMAA polymeric species are strongly anchored to the pigment surface. Furthermore, the surface treatments that were applied have not necessarily produced the optimum surface modification and, thus, the maximum changes in the mechanical properties and in the physical properties of systems that contain the inorganic pigment particles.

5. CONCLUSIONS

From the data and from the discussions that have been presented, concerning the analysis of the Lewis acid/base interaction potential between the major components of the pigmented PC/PBT/IM blends, the following conclusions can be drawn:

1. Phase separation exists in PC/PBT/IM blends as the interaction sites of PBT are preferentially involved in specific intermolecular (and intramolecular) interactions within PBT;
2. Partial miscibility between the PC and the PBT has been interpreted in terms of the Lewis acid/base attraction between these polymers, with contributions from the repulsion effect that exists between the Lewis basic centres in PBT;
3. The impact modifier interacts preferentially with the PC phase rather than with the PBT phase. This is due to the preference of PBT to interact with itself and to the strong Lewis base/base repulsion between the impact modifier and the PBT;
4. C. I. Pigment Blue 28 is predicted to interact preferentially with PBT and then with PC;
5. The enthalpy of adsorption of polar probe molecules on the PBT is endothermic. This finding is not a common observation (in the IGC literature);
6. The analysis of the surface Lewis acidity and of the surface Lewis basicity, as quantified by K_a and K_b, alongside with the analysis of the physical structure of these polymers, has been useful in the interpretation of the existence of crystallinity in PBT, of the excellent solvent resistance and thermal stability of PBT, and also in interpretations of the amorphous properties of PC and of PMMA.
7. The fast crystallisation of PBT contributes to the expulsion of the PC and of the MBS rubber (IM) from the PBT domains.

From the GPC analysis of the average molecular weight, and of the molecular weight distribution of PC and of PBT in pigmented PC/PBT/IM blends, C. I. Pigment Blue 28 is shown to influence importantly the alterations to the polymers chain length. For PBT, this influence is not simple but complex. The trend observed for low pigment loadings, that is, the reduction of the PBT molecular weight with increasing pigment loading, is the opposite of that which is observed for greater pigment loadings. For PC, the introduction and increase of pigment loading leads to an increase in its average molecular weight. C. I. Pigment Blue 28 affects the molecular weight of the PC and of the PBT by a combination of the effects that it has on the transesterification reactions and on the thermal degradation that occur in these polymer blends.

From the DSC study of the crystalline properties of PBT and of the melting properties of the pigmented PC/PBT/IM blends, it can be concluded that:

1. The differences in the end-group type and concentration and in the average molecular weight, between PBT 195 and PBT 315, do not cause a change in the crystallisation activation energy.
2. C. I. Pigment Blue 28 affects the crystallisation properties of the PBT by influencing the transesterification reaction, by decreasing the crystallisation activation energy and by increasing the rate of crystallisation;
3. The degree of crystallinity is not directly affected by the presence of C. I. Pigment Blue 28;
4. The physical properties of PBT are a good indicator of the transesterification level in PC/PBT blends;
5. The effect that C. I. Pigment Blue 28 has on the transesterification reactions is thought to be due mainly to the thermal conductivity differences between the inorganic pigment particles and the polymers and to the location of the pigment particles at the PC/PBT interphase.

The effects of the presence of the pigment, the degree of crystallinity, the transesterification reactions and the molecular weight, on response to applied stress to the PC/PBT/IM blends (by means of DMTA) have been successfully rationalised, providing a clearer image of the direct influence and of the indirect influence of the pigment on the viscoelastic properties of these polymer blends. The direct effects arise from the inorganic nature of the pigments associated with its surface chemical properties. The surface chemical properties influence the degree of crystallinity, the degree of miscibility of PC with PBT, and the level of interaction of the pigment with the PC and with the PBT. The indirect effects result from the influence the pigment has on the molecular weight of the PC and of the PBT. Moreover, the DMTA studies of the viscoelastic properties of the pigmented PC/PBT/IM blends, lead to the following conclusions:

1. PBT is more miscible in PC than PC is in PBT;
2. The pigment is located at the PC/amorphous PBT interphase. The pigment increases the miscibility of these polymers. The lower the molecular weight of the PBT and of the PC, the more pronounced is this effect;
3. The pigment has an effect on the phase separation of the PC and the PBT as it influences the molecular weight of the polymers, in particular that of the PC. Increasing the molecular weight of PC leads to an increased phase separation.

Pigmented PBT/PC/IM blends that were tested for their impact resistance, and for their tensile properties, revealed that there was an effect of the pigment on the mechanical properties of

the blend, namely on the strain at failure, on the tensile modulus and on the impact toughness. A general conclusion that was drawn from mechanical testing of the pigmented PC/PBT/IM blends is that the pigment particles are not preferentially located in any of the PC-rich phase or the PBT-rich phase.

From the tensile testing of pigmented PC/PBT/IM blends it can be concluded that:

1. The amorphous phase governs the mechanical response at low strains;
2. The crystalline content is the most important parameter for break properties;
3. The modulus is determined by the molecular mass of the amorphous polymer. This effect increases in importance as the breakdown of the polymers increases.
4. Good adhesion between C. I. Pigment Blue 28 and the polymers and the increased molecular weight of PC with increasing pigment loading, lead to an increased modulus of the pigmented blends;
5. There is a correlation between the Vicat softening temperature values and the tensile modulus values;
6. The strain at break is strongly influenced by the degree of crystallinity and by the extent of transesterification. Increased PC-PBT interconnection leads to a greater extendibility of the polymer matrix as does a decreased degree of crystallinity.
7. The molar mass of PC plays a dominant role with respect to the strain at yield, the stress at yield, the stress at break, and the tensile modulus.
8. C. I. Pigment Blue 28 affects the tensile properties of the blends indirectly, due to its influence on the molecular weight of PC, its influence on the transesterification reactions and its influence on the crystalline properties of PBT. Direct effects of the pigment arise from its inorganic nature and its presence at the PC/PBT interphase.

The results from impact testing of the pigmented PC/PBT/IM blends lead to the following conclusions:

1. The impact resistance is influenced mainly by the molecular mass of the amorphous polymer and by the crystallinity degree. These influences increase in importance as the average molecular weights of the PC and of the PBT decrease. The greater the molecular weight of the PC the better is the impact energy absorption.
2. C. I. Pigment Blue 28 enhances the impact resistance of the blends by means of altering the impact toughness mechanisms, due to its preferential presence at the PC/PBT interphase;

3. The pigment also influences indirectly the impact resistance of the blend, due to its influence on the transesterification reaction and to its effects on the crystallisation properties.

From the rheological study of the polymer melts, it is concluded that the PC phase is determinant as far as the melt viscosity of blends is concerned. However, the lower the molecular weight of the PC and the PBT, the more important is the contribution of the molecular weight of the semi-crystalline polymer to the melt viscosity. C. I. Pigment Blue 28 influences the melt viscosity of the blend due to the effects it has on the molecular weights of the PC and of the PBT.

From an analysis of the TEM images of samples of the blends, it can be concluded that the pigment has an effect on the morphology of the blend, because it influences the average molecular weights of the PC and of the PBT, and also because it influences the extent of transesterification. The greater the average molecular weight of the PC, the more distinct is the phase separation of the PBT and the PC. The greater the transesterification level, the more clustered are the MBS rubber particles.

Methacrylic acid-based units have been successfully grafted onto the surface of C. I. Pigment Blue 28. The techniques of EDXA, TGA, and pH value measurements of aqueous dispersions of the pigments, support the success of the fixation of MAA-based units to the surface of the C. I. Pigment Blue 28. The fixation efficiency is estimated to be 2.6 % (w/w).

The surface treatments employed changed significantly the dispersive component and the Lewis acidic/Lewis basic components of the surface free energy of the pigments. The surface-modified pigments have a greater potential to interact through dispersion intermolecular forces than does the unmodified pigment. The surface treatment provided the surface of C. I. Pigment Blue 28 with a considerably stronger Lewis acidic character. This was reduced by the neutralisation of the carboxylic acid groups with NaOH. Thus, two modified pigments were obtained, with different levels of surface Lewis acidity.

The specific forces interaction strength of the pigment with the major components of the PC/PBT/IM blends is influenced by the surface modifications of C. I. Pigment Blue 28. The total interaction potential of the surface of the C. I. Pigment Blue 28 through specific forces was greatly increased by the surface photosensitised grafting procedure. The relative presence of Lewis acidic sites to Lewis basic sites, in relation to that of the unmodified pigment, is greater due to the surface treatment, and is reduced after the surface carboxylic acid groups neutralisation procedure. The surface chemistry differences between the pigments are the major factor influencing the interaction of these pigments with the polymers.

From SEM imaging of the modified pigments, the inter-particle interactions for the surface-modified pigments were shown to be stronger than for the unmodified pigment. The modified pigments showed better dispersability in aqueous medium and in the polymeric matrix. The melt

viscosity of the blends pigmented with the modified pigments was lower than that of the blends that were pigmented with the unmodified pigment, due to the improved dispersion in the polymeric matrix.

The general behaviour of the physical properties and of the mechanical properties of the PC/PBT/IM blends that contain the modified pigments was more consistent with increasing pigment loading than it was when the unmodified pigment was used.

The decrease in the molecular weight of the PBT, at low pigment loadings, caused by the use of C. I. Pigment Blue 28, was eliminated after the surface treatments. The molar mass of the PC and of the PBT in the blends was greater and the molar mass change with pigment loading was more consistent, when compared to the situation where the unmodified pigment was used. The transesterification reactions are importantly decreased upon the surface modification of the pigment, especially at the lower pigment loadings. This results from changes in the preferential location of the modified pigments and from improved adhesion of these pigments to the polymeric matrix. This improved adhesion causes better thermal isolation of the pigment particles by the polymers.

Stronger interaction between the surface-modified pigments and the PBT leads to intense nucleation and an increased rate of crystallisation, compared to those that occur through use of the unmodified pigment. Consequently, the crystallisation degree and the crystallisation temperature of PBT are increased due to the surface modifications of C. I. Pigment Blue 28.

Comparison of the tensile properties of the blends that were pigmented with the modified pigments with those of the blends pigmented with the unmodified pigment, leads to the following conclusions:

1. The tensile modulus was greater, due to increased molecular weight of the amorphous phase, to increased degree of crystallinity and to better adhesion of the pigment to the polymeric matrix;
2. The strain at break was lower, due to the increased crystallinity degree. The behaviour of this viscoelastic property with increasing pigment loading was more consistent due to improved adhesion between the modified pigments and the polymers.

When the modified pigments are used, the impact resistance of the blends is slightly reduced, a consequence of the increased crystallinity degree. In addition, the dependence of the impact resistance on temperature is less pronounced, a consequence of changes to the impact toughening mechanisms and of better adhesion between the pigments and the polymers.

From SEM imaging of DCM-extracted blends, the PBT showed good adhesion to the unmodified pigment particles. However, the adhesion of the **hiwre** pigment was superior. The pigment **hiwren** showed less adhesion to the PBT than did either the unmodified pigment or the

hiwre pigment. The results confirm expectations based on IGC analysis of the interaction potential between the pigments and the polymers.

The predictions and expectations in relation to the phase preferences of the pigment particles (unmodified and modified), have been confirmed and supported by TEM imaging. Thus, the unmodified pigment was shown to be preferentially located at the PC/PBT interphase, the **hiwre** pigment in the PBT-rich phase and the **hiwren** pigment in the PC-rich phase. The DMTA study of the viscoelastic properties of the PC/PBT/IM blends that contained the surface-modified pigments confirmed the preferential locations for these pigments.

Finally, it can be stated that in systems of the type that were studied here:

1. The molecular weight of the polymers and the degree of crystallinity must be closely monitored due to their influence on the physical properties and on the mechanical properties of blends;
2. Interpretations of the GPC results contribute decisively to an understanding of the effects of the pigment on the mechanical properties (such as the stress at break, the tensile modulus and the impact strength), on physical properties (such as the degree of crystallinity and crystallisation temperature), and on the morphological characteristics of the blends (namely phase separation and phase domain sizes);
3. C. I. Pigment Blue 28 can influence significantly the physical properties and the mechanical properties of the PC/PBT/IM blends by affecting the thermal degradation of the polymers, the transesterification reaction and the crystalline properties of PBT. Direct contributions arise from the physical properties and from the chemical properties of the pigment;
4. The importance of the PBT-rich phase and of the PC-rich phase on the physical properties, and on the mechanical properties, of the PC/PBT/IM blends depends on the magnitude of the molecular weights of the PC and of the PBT;
5. Lewis acid/base interactions have proven to be determinant to the physical properties and to the mechanical properties of the pigmented PC/PBT/IM blends;
6. Evidence of phase separation and phase preferences has been rationalised in the light of the interaction ability by means of Lewis acid/base intermolecular interactions;
7. Control of the Lewis acid/base properties of C. I. Pigment Blue 28 permitted the alteration of the preferential location of the pigment particles in the characteristic morphology of these blends. These changes in phase preferences lead to alterations to the physical properties and to the mechanical properties of the blends.

6. REFERENCES

1971, *The Colour Index*, 3rd edn, The Society of Dyers and Colourists, Bradford, UK.

Abboud, M., Michelle, T., Duguet, E., and Fontanille, M. 1997, *Journal of Materials Chemistry*, vol. 7, no. 8, pp. 1527-1532.

Abel, M. L. and Chehimi, M. M. 1994, *Polymer*, vol. 35, pp. 1789-1790.

Al Saigh, Z. 1997a, *Trends in Polymer Science*, vol. 5, no. 3, pp. 97-102.

Al Saigh, Z. Y. 1991, *Macromolecules*, vol. 24, pp. 3788-3795.

Al Saigh, Z. Y. 1994, *Polymer News*, vol. 19, pp. 269-279.

Al Saigh, Z. Y. 1997b, *Int.J.Polym.Anal.Charact.*, vol. 3, pp. 249-291.

Al Saigh, Z. Y. and Chen, P. 1991, *Macromolecules*, vol. 24, no. 13, pp. 3788-3795.

Andrzejewska, E., Voelkel, A., Andrzejewski, M., and Maga, R. 1998, *Polymer*, vol. 39, no. 15, pp. 3499-3506.

Anhang, J. and Gray, D. G. 1982, *Journal of Applied Polymer Science*, vol. 27, pp. 71-78.

Anonymous 1999, *Automotive Body International*, Spring 99, pp. 9-12.

Arean, C. O., Mentruit, M. P., Platero, E. E., Xamena, F. X. L., and Parra, J. B. 1999, *Materials Letters*, vol. 39, pp. 22-27.

Bagreev, A., Adib, F., and Bandosz, T. J. 1999, *Journal of Colloid and Interface Science*, vol. 219, pp. 327-332.

Bagreev, A. and Bandosz, T. J. 2000, *J.Phys.Chem.B*, vol. 104, pp. 8841-8847.

Balard, H. and Papirer, E. 1993, *Progress in Organic Coatings*, vol. 22, pp. 1-17.

Beaumont, A. 1996, PhD Thesis, University of Leeds, Leeds, UK.

Becker, K. D. and Rau, F. 1988, *Solid State Ionics*, vol. 28-30, pp. 1290-1293.

Belgacem, M. N. 1995, *Cellulose*, vol. 2, pp. 145-157.

Bennekom, A. C. M., Berg, D., Bussink, J., and Gaymans, R. J. 1997a, *Polymer*, vol. 38, no. 20, pp. 5041-5049.

Bennekom, A. C. M., Pluimers, D. T., Bussink, J., and Gaymans, R. J. 1997b, *Polymer*, vol. 38, no. 12, pp. 3017-3024.

Bertilsson, H., Franzen, B., and Kubat, J. 1988a, *Plastics and Rubber Processing and Applications*, vol. 10, pp. 137-144.

Bertilsson, H., Franzen, B., and Kubat, J. 1988b, *Plastics and Rubber Processing and Applicatons*, vol. 10, pp. 145-153.

Bertilsson, H., Franzen, B., and Kubat, J. 1989, *Plastics and Rubber Processing and Applicatons*, vol. 11, pp. 167-173.

Birley, A. W. and Chen, X. Y. 1984, *British Polymer Journal*, vol. 16, pp. 77-82.

Bogillo, V. I. and Voelkel, A. 1997, *J.Adhesion Sci.Technol.*, vol. 11, no. 12, pp. 1513-1529.

Bohme, R. D. 1968, *Journal of Applied Polymer Science*, vol. 12, pp. 1097-1108.

Bokobza, L., Garnaud, G., and Mark, J. E. 2002, *Chem.Mater.*, vol. 14, pp. 162-167.

Boluk, M. Y. and Schreiber, H. P. 1986, *Polymer Composites*, vol. 7, pp. 295-301.

Boluk, M. Y. and Schreiber, H. P. 1989, *Polymer Composites*, vol. 10, pp. 215-221.

Boluk, M. Y. and Schreiber, H. P. 1990, *Journal of Applied Polymer Science*, vol. 40, pp. 1783-1794.

Bolvari, A. E. and al., e. 1989, "Experimental Techniques in IGC," in *Inverse Gas Chromatography, Characterization of Polymers and Other Materials*, D. R. Lloyd, T. C. Ward, and H. P. Schreiber, eds., A.C.S., Washington, pp. 12-19.

Bolvari, A. E. and Ward, R. C. 1989, "Determination of Fiber-Matrix Adhesion and," in *Inverse Gas Chromatography, Characterization of Polymers and Other Materials*, D. R. Lloyd, T. C. Ward, and H. P. Schreiber, eds., A.C.S., Washington, pp. 217-229.

Bonner, J. G. and Hope, P. S. 1993, "Compatibilisation and reactive blending," in *Polymer Blends and Alloys*, M. J. Folkes and P. S. Hope, eds., Blackie Academic and Professional, London, pp. 46-65.

Bonnerup, C. and Gatenholm, P. 1993, *Journal of Adhesion Science and Technology*, vol. 7, pp. 247-262.

Boven, G., Folkersma, R., Challa, G., and Schouten, A. J. 1991, *Polymer Communications*, vol. 32, no. 2, pp. 50-53.

Boven, G., Oosterling, M. L. C. M., Challa, G., and Schouten, A. J. 1990, *Polymer*, vol. 31, pp. 2377-2383.

Brendle, E. and Papirer, E. 1997a, *Journal of Colloid and Interface Science*, vol. 194, pp. 207-216.

Brendle, E. and Papirer, E. 1997b, *Journal of Colloid and Interface Science*, vol. 194, pp. 217-224.

Bukman, F. 1988, *Xenoy/Valox product development* Bergen op Zoom.

Busca, G., Lorenzelli, V., and Bolis, V. 1992, *Materials Chemistry and Physics*, vol. 31, pp. 221-228.

Busca, G., Lorenzelli, V., Escribano, V. S., and Guidetti, R. 1991, *Journal of Catalysis*, vol. 131, pp. 167-177.

Cecere, A., Greco, R., Ragosta, G., Scarinzi, G., and Taglialatela, A. 1990, *Polymer*, vol. 31, pp. 1239-1244.

Chacko, V. P., Karasz, F. E., and Farris, R. J. 1982, *Polymer Enginnering and Science*, vol. 22, no. 15, pp. 968-974.

Champagne, F., Li, J. F., Schreiber, H. P., and DiPaola-Baranyi, G. 1994, *Journal of Applied Polymer Science*, vol. 54, pp. 743-752.

Chehimi, M. M., Abel, M. L., Watts, D. C., and Digby, R. P. 2001, *Journal of Materials Chemistry*, vol. 11, pp. 533-543.

Chehimi, M. M., Cabet-DEliry, E., Azioune, A., and Abel, M. L. 2002, *Macromolecular Symposia*, vol. 178, pp. 169-181.

Chehimi, M. M. and Pigois-Landureau, E. 1994, *J.Mater.Chem.*, vol. 4, no. 5, pp. 741-745.

Chen, C. T. and Al Saigh, Z. Y. 1989, *Macromolecules*, vol. 22, pp. 2974-2981.

Chen, F. 1988, *Macromolecules*, vol. 21, no. 6, pp. 1640-1643.

Cheng, Y.-Y., Brillhart, M., Cebe, P., and Capel, M. 1996, *Journal of Polymer Science: Part B: Polymer physics*, vol. 34, pp. 2953-2965.

Choi, N. S., Takahashi, K., Oschamann, D., Karger-Kocsis, J., and Friedrich, K. 1998, *Journal of Materials Science*, vol. 33, pp. 2529-2535.

Christie, R. 2002, *Pigments, their Propertie and Applications,* The Royal Society of Chemistry, Cambridge, UK.

Chtourou, H., Riedl, B., and Kokta, B. V. 1995, *J.Adhesion Sci.Technol.*, vol. 9, no. 5, pp. 551-574.

Coleman, M. M., Graf, J. F., and Painter, P. C. 1991, *Specific Interactions and the miscibility of Polymer Blends*, 1st edn, Technomic Pub. Co, Lancaster, Pa., U.S.A.

Courval, G. and Gray, D. G. 1975, *Macromolecules*, vol. 8, pp. 326-331.

Dasgupta, S. 1991, *Progress in Organic Coatings*, vol. 19, pp. 123-139.

Davidson, S. 1999, *Exploring the Science, Technology and Applications of U.V. and E.B. Curing*, 1st edn, SITA Technology Ltd., London.

Dekkers, M. E. J., Hobbs, S. Y., Bruker, I., and Watkins, V. H. 1990, *Polymer Engineering and Science*, vol. 30, no. 24, pp. 1628-1632.

Dekkers, M. E. J., Hobbs, S. Y., and Watkins, V. H. 1988, *Journal of Materials Science*, vol. 23, pp. 1225-1230.

Delimoy, D., Baily, C., Devaux, J., and Legras, R. 1988, *Polymer Engineering and Science*, vol. 28, no. 2, pp. 104-112.

Delimoy, D., Goffaux, B., Devaux, J., and Legras, R. 1995, *Polymer*, vol. 36, no. 17, pp. 3255-3266.

Diez-Gutierrez, S., Rodriguez-Perez, M. A., de Saja, J. A., and Velasco, J. I. 1999, *Polymer*, vol. 40, pp. 5345-5353.

Donnet, J. B., Qin, R. Y., and Wang, M. J. 1992, *Journal of Colloid and Interface Science*, vol. 153, no. 2, pp. 572-577.

Dorris, G. M. and Gray, D. G. 1979, *Journal of Colloid and Interface Science*, vol. 71, no. 1, pp. 93-106.

Dorris, G. M. and Gray, D. G. 1980, *Journal of Colloid and Interface Science*, vol. 77, no. 2, pp. 353-362.

Drago, R. S., Vogel, G. C., and Needham, T. E. 1971, *Journal of the American Chemical Society*, vol. 93, no. 23, pp. 6014-6026.

Du, Q., Chen, W., and Munk, P. 1999a, *Macromolecules*, vol. 32, pp. 1514-1518.

Du, Q., Chen, W., and Munk, P. 1999b, *Macromolecules*, vol. 32, pp. 1514-1518.

Dwight, D. W., Fowkes., F. M., Cole, D. A., Kulp, M. J., Sabat, P. J., Jr., L. S., and Huang, T. C. 1991, "Acid-base interfaces in fiber-reinforced polymer composites," in *Acid-Base Interactions: Relevance to Adhesion Science and Technology*, K. L. Mittal and J. Anderson, eds., VSP, Utrecht, The Netherlands, pp. 243-256.

El Hibri, M. J. and al.et. 1989, "Inverse Gas Chromatography of Polymer Blends," in *Inverse Gas Chromatography, Characterization of Polymers and Other Materials*, D. R. Lloyd, T. C. Ward, and H. P. Schreiber, eds., A.C.S., Washington, pp. 120-133.

Endrib, H. 1998, *Inorganic coloured pigments today* Vincentz.

English, R. J. 1995, *PhD Thesis* Ph.D. Thesis, University of Leeds, Leeds, UK.

Farooque, A. M. and Deshpande, D. D. 1992, *Polymer*, vol. 33, no. 23, pp. 5005-5018.

Favis, B. D. 1991, *The Canadian Journal of Chemical Engineering*, vol. 69, pp. 619-625.

Fayt, R., Jerome, R., and Teyssie, P. 1989, "Interface Modification in Polymer Blends," in *Multiphase Polymers: Blends and Ionomers*, ACS, ed., ACS, pp. 38-66.

Filippova, N. L. 1998, *Journal of Colloid and Interface Science*, vol. 197, pp. 170-176.

Finlayson, M. F. and Shah, B. A. 1991, "The influence of surface acidity and basicity on adhesion of poly(ethylene-co-acrylic acid) to aluminium," in *Acid-Base Interactions: Relevance to Adhesion Science and Technology*, K. L. Mittal and J. Anderson, eds., VSP, Utrecht, The Netherlands, pp. 303-311.

Flour, C. S. and Papirer, E. 1982, *Ind.Eng.Chem.Prod.Res.Dev.*, vol. 21, pp. 666-669.

Flour, C. S. and Papirer, E. 1983, *Journal of Colloid and Interface Science*, vol. 91, no. 1, pp. 69-75.

Folkes, M. J. and Hope, P. S. 1993, "Toughened Polymers," in *Polymer Blends and Alloys*, M. J. Folkes and P. S. Hope, eds., Blackie Academic and Professional, London, pp. 170-194.

Foreman, J. A. and Blaine, R. 1997, *Plastics Engineering*, vol. 53, no. 10, pp. 31-34.

Fowkes, F. M. 1979, *Organic Coatings and Plastics Chemistry*, vol. 40, pp. 13-18.

Fowkes, F. M. 1980, "Donor-Acceptor Interactions at Interfaces," in *Adhesion and Adsorption of Polymers*, 12A edn, L. H. Lee, ed., Plenum Press, London, pp. 43-80.

Fowkes, F. M. 1983b, *Rubber Chemistry and Technology*, vol. 57, pp. 328-343.

Fowkes, F. M. 1983a, in *Physicochemical Aspects of Polymer Surfaces*, K. L. Mittal, ed., Plenum Press, New York, pp. 583-604.

Fowkes, F. M. 1984, *Polymer Mat.Sci.Eng.*, vol. 51, pp. 522-527.

Fowkes, F. M. 1990, *Journal of Adhesion Science and Technology*, vol. 4, pp. 669-691.

Fowkes, F. M. 1991, "Quantitative characterisation of the acid-base properties of solvents, polymers, and inorganic surfaces," in *Acid-Base Interactions: Relevance to Adhesion Science and Technology*, K. L. Mittal and J. Anderson, eds., VSP, Utrecht, The Netherlands, pp. 93-115.

Fowkes, F. M., Dwight, D. W., Cole, D. A., and Huang, T. C. 1990, *Journal of Non-Crystalline Solids*, vol. 120, pp. 47-60.

Fowkes, F. M., Manson, J. A., Lloyd, T. B., Tischler, D. O., and Shah, B. A. 1988, D. M. Mattox and e. al, eds., pp. 223-234.

Fowkes, F. M., McCarthy, D. C., and Mostafa, M. A. 1980, *Journal of Colloid and Interface Science*, vol. 78, no. 1, pp. 200-206.

Fowkes, F. M., McCarthy, D. C., and Tischler, D. O. 1985, in *Molecular Characterisation of Composite Interfaces*, H. Ishida and G. Kumar, eds., Plenum Press, London, pp. 401-411.

Fowkes, F. M. and Mostafa, M. A. 1978, *Ind.Eng.Prod.Res.Dev.*, vol. 17, pp. 3-7.

Frensch, H., Harnischfeger, P., and Jungnickel, B. J. 1989, "Fractionated Crystallisation in Incompatible Polymer Blends," in *Multiphase Polymers: Blends and Ionomers*, ACS, ed., ACS, pp. 101-125.

Galeski, A. 1990, in *Controlled Interfaces in Composite Materials*, H. Ishida, ed., Elsevier Science Publishing Co., Inc., pp. 623-635.

Galin, M. and Rupprecht, M. C. 1979a, *Macromolecules*, vol. 12, pp. 506-511.

Galin, M. and Rupprecht, M. C. 1979c, *Macromolecules*, vol. 12, pp. 506-511.

Galin, M. and Rupprecht, M. C. 1979b, *Macromolecules*, vol. 12, no. 3, pp. 506-511.

Garnier, G. and Glasser, W. G. 1994, *Journal of Adhesion*, vol. 46, pp. 165-180.

Garnier, G. and Glasser, W. G. 1996, *Polymer Engineering and Science*, vol. 36, no. 6, pp. 885-894.

Golovoy, A., Cheung, M. F., and van Oene, H. 1988, *Polymer Engineering and Science*, vol. 28, no. 4, pp. 200-206.

Goss, K. U. 1997, *Journal of Colloid and Interface Science*, vol. 190, pp. 241-249.

Grajek, H. and Witkiewicz, Z. 1993, *Polish Journal of Chemistry*, vol. 67, pp. 911-921.

Gray, D. G. 1977, *Prog. Polym. Sci.*, vol. 5, pp. 1-60.

Guillet, J. E. and al., e. 1989, "Studies of Polymer Structure and Interactions by IGC," in *Inverse Gas Chromatography, Characterization of Polymers and Other Materials*, D. R. Lloyd, T. C. Ward, and H. P. Schreiber, eds., A.C.S., Washington, pp. 20-32.

Guthrie, J. T. 1996, "Intermolecular Forces in Coatings", *Surface Coatings International*, vol. 6, pp. 268-273.

Guthrie, J. T. and Lin, L. 1994, *Physical-Chemical Aspects of Pigment Applications* Oil and Colour Chemists' Association, Wembley.

Gutmann, V. 1978, *Donor-Acceptor Approach to Molecular Interactions* Plenum Press, New York.

Hamieh, T., Rageul-Lescouet, M., Nardin, M., Rezzaki, M., and Schultz, J. 1997, *J.Chim.Phys.*, vol. 94, pp. 503-521.

Hamieh, T., Rezzaki, M., and Schultz, J. 1998, *Journal of Thermal Analysis*, vol. 51, pp. 793-804.

Hamilton, D. G. and Gallucci, R. R. 1993, *Journal of Applied Polymer Science*, vol. 48, pp. 2249-2252.

Hanrahan, B. D., Angeli, S. R., and Runt, J. 1985, *Polymer Journal*, vol. 17, p. 297.

He, T. and Becker, K. D. 1997, *Solid State Ionics*, vol. 101-103, pp. 337-342.

Hegedus, C. R. and Kamel, I. L. 1993b, *Journal of Coatings Technology*, vol. 65, no. 820, pp. 23-30.

Hegedus, C. R. and Kamel, I. L. 1993a, *Journal of Coatings Technology*, vol. 65, no. 820, pp. 31-43.

Herrero, C. R., Morales, E., and Acosta, J. L. 1994, *Journal of Applied Polymer Science*, vol. 51, pp. 1189-1197.

Hobbs, S. Y., Dekkers, M. E. J., and Watkins, V. H. 1987, *Polymer Bulletin*, vol. 17, pp. 341-345.

Hobbs, S. Y., Dekkers, M. E. J., and Watkins, V. H. 1988a, *Polymer*, vol. 29, pp. 1598-1602.

Hobbs, S. Y., Dekkers, M. E. J., and Watkins, V. H. 1988b, *Journal of Materials Science*, vol. 23, pp. 1219-1224.

Hobbs, S. Y., Groshans, V. L., Dekkers, M. E. J., and Shultz, A. R. 1987, *Polymer Bulletin*, vol. 17, pp. 335-339.

Hopfe, I., Pompe, G., and Eichhorn, K. J. 1997, *Polymer*, vol. 38, no. 10, pp. 2321-2327.

Hopfe, I., Pompe, G., Eichhorn, K. J., and Haubler, L. 1995, *Journal of Molecular Structure*, vol. 349, pp. 443-446.

Howelton, R. and Letton, A. 1991, *Polymeric Materials Science and Engineering*, vol. 64, pp. 391-392.

Huang, C.-C. and Chang, F.-C. 1997, *Polymer*, vol. 38, no. 9, pp. 2135-2141.

Huang, Y. C., Fowkes, F. M., and Lloyd, T. B. 1991, "Acidic and basic nature of ferric oxide surfaces. Adsorption, adhesion, zeta potentials and dispersibility in magnetic inks for hard disks," in *Acid-Base Interactions: Relevance to Adhesion Science and Technology*, K. L. Mittal and J. Anderson, eds., VSP, Utrecht, The Netherlands, pp. 363-380.

Huyskens, P. L., Luck, W. A. P., and Zeegers-Huyskens, T. 1991, *Intermolecular Forces, An Introduction to Modern Methods and Results* Springer-Verlag, London.

Imken, R. L., Paul, D. R., and Barlow, J. W. 1976, *Polymer Engineering and Science*, vol. 16, pp. 593-601.

Iriyama, Y. and Ikeda, S. 1994, *Polymer Journal*, vol. 26, no. 1, pp. 109-111.

Ishida, H. 1984, *Polymer Composites*, vol. 5, pp. 101-123.

Israelachvili, J. N. 1991, *Intermolecular and Surface Forces*, 2nd edn, Academic Press, London.

Ito, K. and Guillet, J. E. 1979, *Macromolecules*, vol. 12, no. 6, pp. 1163-1167.

Jackson, P. L., Huglin, M. B., and Cervenka, A. 1994, *Polymer International*, vol. 35, pp. 119-133.

Jacobson, W. H. and Wilmington, D. E. 1995, *Polymer-coated inorganic particles*, US5562978, E.I.Du Pont de Nemours and Company, (patent).

Jagur-Grodzinski, J. 1999, in *Heterogeneous Modification of Polymers, Matrix and Surface Reactions*, John Wiley and Sons, New York.

Jensen, W. B. 1991, "The Lewis acid-base concepts: recent results and prospects for the future," in *Acid-Base Interactions: Relevance to Adhesion Science and Technology*, K. L. Mittal and J. Anderson, eds., VSP, Utrecht, The Netherlands, pp. 3-23.

Jones, R. A. L. and Kramer, E. J. 1993, *Polymer*, vol. 34, no. 1, pp. 115-118.

Joshi, M., Misra, A., and Maiti, S. N. 1991, *Journal of Applied Polymer Science*, vol. 43, pp. 311-328.

Kakarala, N. 1999, "Trends in Automotive Plastics".

Kamdem, D. P., Bose, S. K., and Luner, P. 1993, *Langmuir*, vol. 9, no. 11, pp. 3039-3044.

Kamdem, D. P. and Riedl, B. 1992, *Journal of Colloid and Interface Science*, vol. 150, no. 2, pp. 507-516.

Keskula, H. and Paul, D. R. 1994, "Toughening agents for engineering polymers," in *Rubber Thoughened Engineering Plastics*, A. A. Collyer, ed., Chapman and Hall, London, pp. 137-165.

Kim, H., Keskkula, H., and Paul, D. R. 1991, *Polymer*, vol. 32, p. 1447.

Kim, J. K. and Mai, Y. W. 1998, *Engineered Interfaces in Fiber Reinforced Composites* Elsevier, Amsterdam, Oxford.

Kim, W. N. and Burns, C. M. 1989, *Makromolekulare Chemie*, vol. 190, pp. 661-676.

Kirk, O. 1978, *Encyclopedia of Chemical Technology*, 3rd edn, John Wiley, New York.

Klemberg-Sapieha, J. E., Martinu, L., Sapieha, S., and Wertheimer, M. R. 1993, "Control and Modification of Surfaces and Interfaces by Corona and Low Pressure Plasma," in *The Interfacial Interactions in Polymeric Composites*, G. Akovali, ed., Kluwer Academic Publishers, The Netherlands, pp. 201-222.

Klotz, S. and al., e. 1989, "Estimation of Free Energy of Polymers," in *Inverse Gas Chromatography, Characterization of Polymers and Other Materials*, D. R. Lloyd, T. C. Ward, and H. P. Schreiber, eds., A.C.S., Washington, pp. 135-154.

Kloubek, J. and Schreiber, H. P. 1993, *Journal of Adhesion*, vol. 42, pp. 87-90.

Kong, Y. and Hay, J. N. 2002a, *Polymer*, vol. 43, pp. 3873-3878.

Kong, Y. and Hay, J. N. 2002b, *Polymer*, vol. 43, pp. 1805-1811.

kumar, S. K. and Yoon, D. Y. 1989, *Macromolecules*, vol. 22, pp. 4098-4101.

Lambla, M. and Schreiber, H. P. 1980, *European Polymer Journal*, vol. 16, pp. 211-218.

Lara, J. and Schreiber, H. P. 1991a, *Journal of Coatings Technology*, vol. 63, pp. 81-90.

Lara, J. and Schreiber, H. P. 1991b, *Journal of Coatings Technology*, vol. 63, no. 801, pp. 81-90.

Lara, J. and Schreiber, H. P. 1996, *Journal of Polymer Science: Part B: Polymer physics*, vol. 34, pp. 1733-1740.

Lavielle, L. and Schultz, J. 1991, *Langmuir*, vol. 7, no. 5, pp. 978-981.

Lavielle, L., Schultz, J., and Nakajima, K. 1991, *Journal of Applied Polymer Science*, vol. 42, pp. 2825-2831.

Leclair, A. and Favis, B. D. 1996, *Polymer*, vol. 37, no. 21, pp. 4723-4728.

Lee, L. H. 1991, "Relevance of the density-functional theory to acid-base interactions and adhesion in solids," in *Acid-Base Interactions: Relevance to Adhesion Science and Technology*, K. L. Mittal and J. Anderson, eds., VSP, Utrecht, The Netherlands, pp. 25-46.

Lee, M. H., Fleicher, C. A., Morales, A. R., Koberstein, J. T., and Koningsveld, R. 2001, *Polymer*, vol. 42, pp. 9163-9172.

Lee, Y. J., Manas-Zloczower, I., and Feke, D. L. 1992, *Powder Technology*, vol. 73, pp. 139-146.

Lenglet, M. and Lefez, B. 1996, *Solid State Communications*, vol. 98, no. 8, pp. 689-694.

Li, B. 1996, *Rubber Chemistry and Technology*, vol. 69, no. 3, pp. 347-376.

Liang, H., Xu, R., Favis, B. D., and Schreiber, H. P. 1999, *Polymer*, vol. 40, pp. 4419-4423.

Liang, H., Xu, R., Favis, B. D., and Schreiber, H. P. 2000, *Journal of Polymer Science: Part B: Polymer physics*, vol. 38, pp. 2096-2104.

Lipatov, Y. S., Nesterov, A. E., Ignatova, T. D., and Nesterov, D. A. 2002, *Polymer*, vol. 43, pp. 875-880.

Lipson, J. E. G. and Guillet, J. E. 1982, *Dev.Poly.Char.*, vol. 3, pp. 33-71.

Liston, E. M. 1993, "Plasmas and Surfaces - A practical Approach to Good Composites," in *The Interfacial Interactions in Polymeric Composites*, G. Akovali, ed., Kluwer Academic Publishers, The Netherlands, pp. 223-268.

Luxgrant, R. and Vesey, D. 1998, *SAE SP*, vol. 1340, pp. 11-23.

Lyngaae-Jorgensen, J. 1993, "Rheology of polymer blends," in *Polymer Blends and Alloys*, M. J. Folkes and P. S. Hope, eds., Blackie Academic and Professional, London, pp. 75-102.

Ma, D., Johns, W. E., Dunker, A. K., and Bayoumi, A. E. 1991, "The effect of donor-acceptor interactions on the mechanical properties of wood," in *Acid-Base Interactions: Relevance to Adhesion Science and Technology*, K. L. Mittal and J. Anderson, eds., VSP, Utrecht, The Netherlands, pp. 343-361.

Malik, T. M., Carreau, P. J., Grmela, M., and Dufresne, A. 1988, *Polymer Composites*, vol. 9, pp. 412-418.

Mandak, B. M., Bhattcharya, C., and Bhattacharya, S. N. 1989, *Macromol.SCI.-Chem.*, vol. A26, no. 1, pp. 175-212.

Marosi, G., Bertalan, G., Rusznak, I., and Anna, P. 1987, *Colloids and Surfaces*, vol. 23, pp. 185-198.

McGrath, G. C. 1994, "Fracture and toughening in fibre reinforced polymer composites," in *Rubber Toughened Engineering Plastics*, A. A. Collyer, ed., Chapman and Hall, London, pp. 57-137.

McKie, D. and McKie, C. 1974, *Crystalline Solids* Nelson, London.

Memon, N. A. 1994, *Journal of Applied Polymer Science*, vol. 54, pp. 1059-1072.

Mishra, S. P. and Venkidusamy, P. 1995, *Journal of Applied Polymer Science*, vol. 58, pp. 2229-2234.

Mizobuchi, Y. and Freed, R. 1996, US6103782, Marconi Data Systems, Inc., (patent).

Montaudo, G., Puglisi, C., and Samperi, F. 1998, *Macromolecules*, vol. 31, pp. 650-661.

Mukhopadhyay, P. and Schreiber, H. P. 1993, *Macromolecules*, vol. 26, pp. 6391-6396.

Mukhopadhyay, P. and Schreiber, H. P. 1994, *Journal of Polymer Science: Part B: Polymer physics*, vol. 32, pp. 1653-1656.

Mukhopadhyay, P. and Schreiber, H. P. 1995, *Colloids and Surfaces A: Physicochem.Eng.Aspects*, vol. 100, pp. 47-71.

Murakami, Y. 1994, *Polymer Journal*, vol. 26, no. 5, pp. 607-612.

Nadkarni, V. M. and Jog, J. P. 1991, "Crystallization Behaviour in Polymer Blends," in *Two-Phase Polymer Systems*, L. A. Utracki, ed., Hanser, Munich, pp. 213-239.

Nakatsuka, T. 1985, in *Molecular Characterisation of Composite Interfaces*, H. Ishida and G. Kumar, eds., Plenum Press, London, pp. 51-75.

Namhata, S. P., Santolini, L., and Locati, G. 1990, *Polymer Testing*, vol. 9, pp. 75-89.

Nardin, M., Asloun, E. M., and Schultz, J. 1990, in *Controlled Interfaces in Composite Materials*, H. Ishida, ed., Elsevier Science Publishing Co., Inc., pp. 285-293.

Nardin, M. and Schultz, J. 1993a, *Composite Interfaces*, vol. 1, pp. 177-192.

Nardin, M. and Schultz, J. 1993b, "Interactions and Properties of Composites: a) fibre-matrix adhesion measurements," in *The Interfacial Interactions in Polymeric Composites*, G. Akovali, ed., Kluwer Academic Publishers, The Netherlands, pp. 81-93.

Nardin, M. and Schultz, J. 1993c, "Interactions and Properties of Composites: b) adhesion-compostes properties relationships," in *The Interfacial Interactions in Polymeric Composites*, G. Akovali, ed., Kluwer Academic Publishers, The Netherlands, pp. 95-105.

Nishimoto, M., Keskkula, H., and Paul, D. R. 1991, *Polymer*, vol. 32, no. 2, pp. 272-278.

O'Neill, H. 1994, *European Journal of Mineralogy*, vol. 6, no. 5, pp. 603-609.

Okamoto, M. and Inoue, T. 1994, *Polymer*, vol. 35, no. 2, pp. 257-261.

Panzer, U. and Schreiber, H. P. 1992, *Macromolecules*, vol. 25, pp. 3633-3637.

Papirer, E., Balard, H., Brendle, E., and Lignieres, J. 1996, *J.Adhesion Sci.Technol.*, vol. 10, no. 12, pp. 1401-1411.

Papirer, E., Balard, H., and Vidal, A. 1988a, *Eur.Polym.J.*, vol. 24, no. 8, pp. 783-790.

Papirer, E., Balard, H., and Vidal, A. 1988b, *Eur.Polym.J.*, vol. 24, pp. 783-790.

Papirer, E., Perrin, J.-M., Siffert, B., and Philopponneau, G. 1991, *Journal of Colloid and Interface Science*, vol. 144, no. 1, pp. 263-270.

Pellow-Jarman, M. and Hetem, M. 1995, *Plastics, Rubber and Composites Processing and Applications*, vol. 23, pp. 31-41.

Pickett, J. E. 2001, *Polymer Preprints*, vol. 42, no. 1, pp. 424-425.

Pillin, I., Pimbert, S., Feller, J. F., and Levesque, G. 2001, *Polymer Engineering and Science*, vol. 41, no. 2, pp. 178-191.

Plueddemann, E. P. 1985, in *Molecular Characterisation of Composite Interfaces*, H. Ishida and G. Kumar, eds., Plenum Press, London, pp. 13-23.

Pompe, G. 1997, *Recent Research developments in Polymer Science*, vol. 1, pp. 109-147.

Pompe, G. and Haubler, L. 1997, *Jounal of Polymer Science: Part B: Polymer Physics*, vol. 35, pp. 2161-2168.

Pompe, G., Haubler, L., and Winter, W. 1996, *Journal of Polymer Science: Part B: Polymer physics*, vol. 34, pp. 211-219.

Pompe, G., Meyer, E., Komber, H., and Hamann, H. 1991, *Thermochimia Acta*, vol. 187, pp. 185-200.

Ponec, V., Knor, Z., and Cerny, S. 1974, *Adsorption on Solids* Butterworths, London.

Premphet, K. and Horanont, P. 2000, *Polymer*, vol. 41, pp. 9283-9290.

Price, G. J. 1989, "Calculation of Solubility Parameters by IGC," in *Inverse Gas Chromatography, Characterization of Polymers and Other Materials*, D. R. Lloyd, T. C. Ward, and H. P. Schreiber, eds., A.C.S., Washington, pp. 48-57.

Prolongo, M. G., Masegosa, R. M., and Horta, A. 1989, *Macromolecules*, vol. 22, pp. 4346-4351.

Pyke, D., Mallick, K. K., Reynolds, R., and Bhattacharya, A. K. 1998, *J.Mater.Chem.*, vol. 8, no. 4, pp. 1095-1098.

Qin, R. Y. and Schreiber, H. P. 1994, *Langmuir* , vol. 10, pp. 4153-4156.

Radusch, H. J. and Androsch, R. 1994, *Angew.Makromol.Chem.*, vol. 214, p. 179.

Ratzsch, M., Haudel, G., Pompe, G., and Meyer, E. 1990, *Journal of Macromolecular Science A Chemistry*, vol. A27, no. 13and14, pp. 1631-1655.

Reading, M. 1992, "Thermomechanical Analysis and Dynamic Mechanical Analysis," in *Thermal Analysis, Techniques and Applications*, E. L. Charsley and S. B. Warrington, eds., Thermal Analysis Consultancy Service, pp. 109-125.

Richard, C., Hing, K., and Schreiber, H. P. 1985, *Polymer Composites*, vol. 6, no. 4, pp. 201-208.

Riddle, J. and Fowkes, F. M. 1990, *J.Am.Chem.Soc.*, vol. 112, no. 9, pp. 3259-3264.

Riedl, B. and Kamdem, D. P. 1992, *J.Adhesion Sci.Technol.*, vol. 6, no. 9, pp. 1053-1067.

Rodriguez, J. L., Eguiazabal, J. I., and Nazabal, J. 1997, *Journal of Macromolecular Science B Physics*, vol. 36, no. 6, pp. 773-787.

Ryan, A. J. 2002, *Nature Materials*, vol. 1, no. September, pp. 8-10.

Ryan, A. J., Stanford, J. L., and Still, R. H. 1988, *Polymer Communications*, vol. 29, pp. 196-198.

Sadowski, G., Mokrushina, L. V., and Arlt, W. 1997, *Fluid Phase Equilibria*, vol. 139, pp. 391-403.

Saini, D. R., Shenoy, A. V., and Nadkarni, V. M. 1984, *Journal of Applied Polymer Science*, vol. 29, pp. 4123-4143.

Sanchez, P., Remiro, P. M., and Nazabal, J. 1993, *Journal of Applied Polymer Science*, vol. 50, pp. 995-1005.

Santos, J. M. R. C. A., Fagelman, K., and Guthrie, J. T. 2002a, "Characterisation of the surface Lewis acid-base properties of the components of pigmented, impact-modified, bisphenol A polycarbonate-poly(butylene terephthalate) blends by inverse gas chromatography", *Journal of Chromatography A*, vol. 969, no. 1-2, pp. 119-132.

Santos, J. M. R. C. A., Fagelman, K., and Guthrie, J. T. 2002b, "Characterisation of the surface Lewis acid–base properties of poly(butylene terephthalate) by inverse gas chromatography", *Journal of Chromatography A*, vol. 969, no. 1-2, pp. 11-118.

Santos, J. M. R. C. A., Gil, M. H., Portugal, A., and Guthrie, J. T. 2001, "Characterisation of the surface of a cellulosic multi-purpose office paper by inverse gas chromatography", *Cellulose*, vol. 8, pp. 217-224.

Scherbakoff, N. and Ishida, H. 1997, *Journal of Adhesion*, vol. 64, pp. 203-228.

Schreiber, H. P. 1993, "Aspects of Component Interactions in Polymer Systems," in *The Interfacial Interactions in Polymeric Composites*, G. Akovali, ed., Kluwer Academic Publishers, The Netherlands, pp. 21-59.

Schreiber, H. P. and et.al. 1994, *Journal of Adhesion Science and Technology*, vol. 8, pp. 1383-1394.

Schreiber, H. P. and Germain, F. S. 1990, *Journal of Adhesion Science and Technology*, vol. 4, pp. 319-331.

Schreiber, H. P. and Germain, F. S. 1991, "Specific interactions and their effect on the properties of filled polymers," in *Acid-Base Interactions: Relevance to Adhesion Science and Technology*, K. L. Mittal and J. Anderson, eds., VSP, Utrecht, The Netherlands, pp. 273-285.

Schreiber, H. P. and Lloyd, D. R. 1989, ""Overview of Inverse Gas Chromatography"," in *Inverse Gas Chromatography, Characterization of Polymers and Other Materials*, D. R. Lloyd, T. C. Ward, and H. P. S. (Eds.), eds., A.C.S., Washington, pp. 1-10.

Schreiber, H. P., Richard, C., and Wertheimer, M. R. 1983, in *Physicochemical Aspects of Polymer Surfaces*, K. L. Mittal, ed., Plenum Press, New York, pp. 739-748.

Schreiber, H. P., Viau, J. M., Fetoui, A., and Deng, Z. 1990, *Polymer Engineering and Science* pp. 263-269.

Schreiber, H. P., Wertheimer, M. R., and Lambla, M. 1982, *Journal of Applied Polymer Science*, vol. 27, pp. 2269-2280.

Schroder, J. 1988, *Progress in Organic Coatings*, vol. 16, pp. 3-17.

Schultz, J. and Lavielle, L. 1989, "Interfacial Properties of Carbon Fiber-Epoxy," in *Inverse Gas Chromatography, Characterization of Polymers and Other Materials*, D. R. Lloyd, T. C. Ward, and H. P. Schreiber, eds., A.C.S., Washington, pp. 185-202.

Sepe, M. P. 1995, *ANTEC*, vol. 53, no. 2, pp. 3131-3138.

Shi, Z. H. and Schreiber, H. P. 1991, *Macromolecules*, vol. 24, pp. 3522-3527.

Shi, Z. H. and Schreiber, H. P. 1992, *Journal of Applied Polymer Science*, vol. 46, pp. 787-796.

Solomon, D. H. and Hawthorne, D. G. 1983, *Chemistry of Pigments and Fillers* John Wiley and Sons, New York.

Stone, A. J. 1998, *The Theory of Intermolecular Forces* Claredon Press, Oxford.

Stori, A. and Dahl, I. M. 1990, in *Controlled Interfaces in Composite Materials*, H. Ishida, ed., Elsevier Science Publishing Co., Inc., pp. 321-333.

Su, C. S., Patterson, D., and Schreiber, H. P. 1976, *Journal of Applied Polymer Science*, vol. 20, pp. 1025-1034.

Tamura, H., Tanaka, A., Mita, K. Y., and Furuichi, R. 1999, *Journal of Colloid and Interface Science*, vol. 209, pp. 225-231.

Tattum, S. B., Cole, D., and Wilkinson, A. N. 1993, *The Effects of Transesterification on Structure Development In Polycarbonate - Polyester Blends* Manchester.

Tattum, S. B., Cole, D., and Wilkinson, A. N. 2000, *Journal of Macromolecular Science B Physics*, vol. 39, no. 4, pp. 459-479.

Tiburcio, A. C. and Manson, J. A. 1991a, *Journal of Applied Polymer Science*, vol. 42, pp. 427-438.

Tiburcio, A. C. and Manson, J. A. 1991b, "The effects of filler/polymer acid-base interactions in model coating systems," in *Acid-Base Interactions: Relevance to Adhesion Science and Technology*, K. L. Mittal and J. Anderson, eds., VSP, Utrecht, The Netherlands, pp. 313-328.

Timmerman, T., Grimm, A., Lillie, T., and Hurst, J. 2001, Private Communications, G. E. Plastics, 1 Plasticslaan, Bergen op Zoom, The Netherlands.

Tjong, S. C. and Meng, Y. Z. 1999, *Journal of Applied Polymer Science*, vol. 74, pp. 1827-1835.

Trujillo, E., Richard, C., and Schreiber, H. P. 1988, *Polymer Composites*, vol. 9, pp. 426-433.

Tseng, W. T. and Lee, J. S. 2000a, *Journal of Applied Polymer Science*, vol. 76, pp. 1280-1284.

Tseng, W. T. W. and Lee, J. S. 2000b, *Journal of Applied Polymer Science*, vol. 76, pp. 1280-1284.

Tsobokawa, N., Hamada, H., and Fujiki, K. 1994, *Polymer*, vol. 35, no. 5, pp. 1084-1089.

Tsubokawa, N. and Kogure, A. 1991, *Journal of Polymer Science: Part A: Polymer Chemistry*, vol. 29, pp. 697-702.

Tsubokawa, N., Maruyama, K., Sone, Y., and Shimomura, M. 1989, *Colloid and Polymer Science*, vol. 267, pp. 511-515.

Umamaheswaran, V. and Bax, F. 1999, "High-performance Thermoplastic Extrior Body Panels", *Plastic Components, Processes, and Technology, Society of Automotive Engineers*.

Usaka, K. and Shibayama, K. 1978, *Journal of Applied Polymer Science*, vol. 22, pp. 3135-3143.

Utracki, L. A. 1998, "PEST/PC Blends," in *Commercial Polymer Blends*, L. A. Utacki, ed., Chapman and Hall, London.

Utracki, L. A., Walsh, D. J., and Weiss, R. A. 1989, "Polymer Alloys, Blends, and Ionomers," in *Multiphase Polymers: Blends and Ionomers*, ACS, ed., ACS, pp. 1-35.

van Bennekom, A. C. M. and Gaymans, R. J. 1997, *Polymer*, vol. 38, no. 3, pp. 657-665.

Vesely, D. 1993, "Practical techniques for studying blend microstructure," in *Polymer Blends and Alloys*, M. J. Folkes and P. S. Hope, eds., Blackie Academic and Professional, London, pp. 103-125.

Voelkel, A., Andrzejewska, E., Maga, R., and Andrzejewski, M. 1996a, *Polymer*, vol. 37, no. 3, pp. 455-462.

Voelkel, A., Andrzejewska, E., Maga, R., and Andrzejewski, M. 1996b, *Polymer*, vol. 37, no. 19, pp. 4333-4344.

Vollenberg, P. and Heikens, D. 1989, *Polymer*, vol. 30, pp. 1656-1662.

Vollenberg, P., Heikens, D., and Ladan, H. C. B. 1988, *Polymer Composites*, vol. 9, pp. 382-388.

Wahrmund, D. C., Paul, D. R., and Barlow, J. W. 1978, "(Polyester-polycarbonate blends. I. Poly(butylene terephthalate)", *J.Appl.Polym.Sci.*, vol. 22, pp. 2155-2164.

Walker, I. and Collyer, A. A. 1994, "Rubber toughening mechanisms in polymeric materials," in *Rubber Toughened Engineering Plastics*, A. A. Collyer, ed., Chapman and Hall, London, pp. 29-55.

Wang, W., Liang, H., Favis, B. D., and Schreiber, H. P. 2001, *Journal of Applied Polymer Science*, vol. 81, pp. 1891-1901.

Wang, W., Schreiber, H. P., Yu, Y., and Eisenberg, A. 1997, *Journal of Polymer Science: Part B: Polymer physics*, vol. 35, pp. 1793-1805.

Ward, T. C., Sheehy, D. P., and McGrath, J. E. 1980, *Polym.Prepr., Am.Chem.Soc., Div.Polym.Chem.*, vol. 21, p. 70.

Ward, T. C., Sheehy, D. P., Riffle, J. S., and McGrath, J. E. 1981, *Macromolecules*, vol. 14, pp. 1791-1797.

Weber, H. 1978, *14th FATIPEC Congress* pp. 697-704.

Wertheimer, M. R., Klemberg-Sapieha, J. E., and Schreiber, H. P. 1984, *Thin solid films*, vol. 115, pp. 109-124.

Wetton, R. E. and Corish, P. J. 1989, *Polymer Testing*, vol. 8, pp. 303-312.

Wetton, R. E., Marsh, R. D. L., and Van-de-Velde, J. G. 1991, *Thermochimia Acta*, vol. 175, no. 1, pp. 1-11.

Wilkinson, A. N., Cole, D., and Tattum, S. B. 1995, *Polymer Bulletin*, vol. 35, no. 6, pp. 751-757.

Wilkinson, A. N., Tattum, S. B., and Ryan, A. J. 1997, *Polymer*, vol. 38, no. 8, pp. 1923-1928.

Wilkinson, A. N., Tattum, S. B., and Ryan, A. J. 2002, " Inhibition of crystalline structure development in a reactive polycarbonate-poly(butyleneterephthalate) blend", *Polymer Bulletin*, vol. 48, pp. 199-206.

Wu, J. and Mai, Y. W. 1993, *Journal of Materials Science*, vol. 28, pp. 6167-6177.

Wu, J., Mai, Y. W., and Cotterell, B. 1992, *Mat.REs.Soc.Symp.Proc.*, vol. 274, pp. 3-9.

Wu, J., Mai, Y. W., and Cotterell, B. 1993, *Journal of Materials Science*, vol. 28, pp. 3373-3384.

Wu, J., Mai, Y. W., and Yee, A. F. 1994, *Journal of Materials Science*, vol. 29, pp. 4510-4522.

Wu, J., Yu, D. M., Mai, Y.-W., and Yee, A. F. 2000, *Jounal of Materials Sciences*, vol. 35, pp. 307-315.

Wu, J. S. and Mai, Y. W. 1998, *Key Engineering Materials*, vol. 145-149, pp. 793-798.

Wu, S. 1982, *Polymer Interface and Adhesion* Marcel Dekker, Inc., New York.

Xu, R. and Schreiber, H. P. 1998, *Journal of Applied Polymer Science*, vol. 70, pp. 1597-1604.

Xu, R., Tovar, G., and Schreiber, H. P. 1999, *J.Adhesion*, vol. 71, pp. 153-165.

Xue, G., Ji, G., Cai, S., and Fang, J. 1990, in *Controlled Interfaces in Composite Materials*, H. Ishida, ed., Elsevier Science Publishing Co., Inc., pp. 147-156.

Zhang, R., Jagiello, J., Hu, J. F., Huang, Z. Q., and Schwarz, J. A. 1992, *Applied Catalysis A: General*, vol. 84, pp. 123-139.

Zhang, W. and Leonov, A. I. 2000, *Journal of Applied Polymer Science*, vol. 81540, pp. 2517-2530.

Ziani, A., Xu, R., Schreiber, H. P., and Kobayashi, T. 1999, *Journal of Coatings Technology*, vol. 71, no. 893, pp. 53-60.

Phase Separation and Phase Preferences

in

Pigmented, Impact-Modified, PC/PBT Blends

VOLUME II

by

José Manuel Ribeiro Correia Afonso dos Santos

Submitted in accordance with the requirements for the degree of

Doctor of Philosophy

The University of Leeds

Department of Colour Chemistry

June 2003

TABLE OF CONTENTS

APPENDIX A. Error Propagation in IGC Calculations

When experimental results are subject to a series of mathematical operations, the corresponding experimental error is determined by a function:

$R = f(x_1,x_2,x_3,.....,x_k,A,B,C,.....)$

Being $x_1,x_2,x_3,\ldots x_k$, factors and A, B, C, …., parameters

To determine the experimental error expression, the partial derivatives for each variable of the function where the experimental data is being introduced, must be determined.

$$d_i = \left\{ \frac{\partial f}{\partial d_i} \right\}_{i = 1, ..., k} \tag{A-1}$$

The linear terms of the full expression of df/dx are then used to determine the experimental variance (e^2_R):

$$e_R^2 = \sum (d_i \times e_i)^2 \tag{A-2}$$

e_i can be a standard deviation or a confidence limit.

For the energy of adsorption (see Section 1.2.5.3., for further details):

$$V_n = (t_r - t_o).\ F.\ C.\ J \tag{A-3}$$

$$\Delta G_a = -RT \ln(V_n) + K \tag{A-4}$$

Using the above described mathematical procedure, one gets:

$$\frac{\partial f}{\partial F} = RT \frac{JC(t_r - t_o)}{JCF(t_r - t_o)} = \frac{RT}{F} \tag{A-5}$$

$$\frac{\partial f}{\partial t_r} = RT \frac{JCF}{JCF(t_r - t_o)} = \frac{RT}{(t_r - t_o)} \tag{A-6}$$

$$\frac{\partial f}{\partial F} = RT \frac{-JCF}{JCF(t_r - t_o)} = \frac{-RT}{(t_r - t_o)} \tag{A-7}$$

$$e^2 = \left(RT \frac{1}{JC\bar{F}(\bar{t}_r - \bar{t}_o)} \times \sqrt{\left((JC(\bar{t}_r - \bar{t}_o) \times e_F)^2 + (JC\bar{F}e_{t_r})^2 + (JC\bar{F}e_{to})^2 \right)} \right)^2 \tag{A-8}$$

This expression quantifies the variance associated with the determination of the energy of adsorption. The terms $\bar{F}$, $\bar{t}_R$ and $\bar{t}_0$ are average values of, at least, three measurements, and the terms e_F, e_{t_R} and e_{t_o} are the corresponding standard deviations.

APPENDIX B. Tables concerning IGC

B.1. Study of the Reproducibility of the Retention Time, determined using different IGC units

Table B-1. Retention time, t_r, net retention volume, V_n, and energy of adsorption, RTLn(V_n), of n-alkanes on the surface of Chromosorb® W AW DCMS, at T = 313 K, F = 21.25 cm^3/min, J = 0.95, C = 0.97, P_{in} = 110.90 kPa, P_{out} = 100.56 kPa, and $T_{flow\ meter}$ = 296 K.

Probe molecule	t_r (s)	V_g (cm^3/g)	RTLn(V_g) (kJ/mol)
CH_4	29.8	n/a	n/a
C_6H_{14}	32.7	1.0	0.1
C_7H_{16}	38.5	2.9	2.7
C_8H_{18}	49.3	6.4	4.8
C_9H_{20}	81.3	16.9	7.4
$C_{10}H_{22}$	167.5	45.1	9.9

B.2. IGC Study of C. I. Pigment Blue 28

B.2.1. Effect of the Carrier Gas Flow Rate on the Retention Times of the Probe Molecules

Table B-2. Retention time, t_r, specific retention volume, V_g, and energy of adsorption, RTLn(V_g) of $C_{10}H_{22}$ on the surface of C. I. Pigment Blue 28, at T = 313 K, F = 9.83 cm^3/min, J = 0.94, C = 0.98, P_{in} = 115.41 kPa, P_{out} = 101.62 kPa, and $T_{flow\ meter}$ = 293 K.

Probe molecule	t_r (s)	V_g (cm^3/g)	RTLn(V_g) (kJ/mol)
CH_4	44.7	n/a	n/a
$C_{10}H_{22}$	391.5	402.5	15.6

Table B-3. Retention time, t_r, specific retention volume, V_g, and energy of adsorption, RTLn(V_g) of $C_{10}H_{22}$ on the surface of C. I. Pigment Blue 28, at T = 313 K, F = 15.05 cm^3/min, J = 0.90, C = 0.97, P_{in} = 120.31 kPa, P_{out} = 99.62 kPa, and $T_{flow\ meter}$ = 298 K.

Probe molecule	t_r (s)	V_g (cm^3/g)	RTLn(V_g) (kJ/mol)
CH_4	33.8	n/a	n/a
$C_{10}H_{22}$	311.3	472.5	16.0

Table B-4. Retention time, t_r, specific retention volume, V_g, and energy of adsorption, RTLn(V_g) of $C_{10}H_{22}$ on the surface of C. I. Pigment Blue 28, at T = 313 K, F = 20.55 cm^3/min, J = 0.89, C = 0.98, P_{in} = 126.39 kPa, P_{out} = 102.25 kPa, and $T_{flow\ meter}$ = 294 K.

Probe molecule	t_r (s)	V_g (cm^3/g)	RTLn(V_g) (kJ/mol)
CH_4	28.5	n/a	n/a
$C_{10}H_{22}$	271.7	561.7	16.5

Table B-5. Retention time, t_r, specific retention volume, V_g, and energy of adsorption, RTLn(V_g) of $C_{10}H_{22}$ on the surface of C. I. Pigment Blue 28, at T = 313 K, F = 24.93 cm^3/min, J = 0.85, C = 0.97, P_{in} = 135.80 kPa, P_{out} = 101.33 kPa, and $T_{flow\ meter}$ = 296 K.

Probe molecule	t_r (s)	V_g (cm^3/g)	RTLn(V_g) (kJ/mol)
CH_4	20.0	n/a	n/a
$C_{10}H_{22}$	202.8	486.1	16.1

Table B-6. Retention time, t_r, specific retention volume, V_g, and energy of adsorption, RTLn(V_g) of $C_{10}H_{22}$ on the surface of C. I. Pigment Blue 28, at T = 333 K, F = 9.66 cm^3/min, J = 0.94, C = 0.97, P_{in} = 115.42 kPa, P_{out} = 101.63 kPa, and $T_{flow\ meter}$ = 296 K.

Probe molecule	t_r (s)	V_g (cm^3/g)	RTLn(V_g) (kJ/mol)
CH_4	57.0	n/a	n/a
$C_{10}H_{22}$	163.9	121.4	13.3

Table B-7. Retention time, t_r, specific retention volume, V_g, and energy of adsorption, RTLn(V_g) of $C_{10}H_{22}$ on the surface of C. I. Pigment Blue 28, at T = 333 K, F = 15.05 cm^3/min, J = 0.90, C = 0.97, P_{in} = 120.31 kPa, P_{out} = 99.62 kPa, and $T_{flow\ meter}$ = 298 K.

Probe molecule	t_r (s)	V_g (cm^3/g)	RTLn(V_g) (kJ/mol)
CH_4	34.5	n/a	n/a
$C_{10}H_{22}$	141.0	181.3	14.4

Table B-8. Retention time, t_r, specific retention volume, V_g, and energy of adsorption, RTLn(V_g) of $C_{10}H_{22}$ on the surface of C. I. Pigment Blue 28, at T = 333 K, F = 20.86 cm^3/min, J = 0.86, C = 0.97, P_{in} = 132.35 kPa, P_{out} = 101.33 kPa, and $T_{flow\ meter}$ = 296 K.

Probe molecule	t_r (s)	V_g (cm^3/g)	RTLn(V_g) (kJ/mol)
CH_4	25.3	n/a	n/a
$C_{10}H_{22}$	91.3	149.2	13.9

Table B-9. Retention time, t_r, specific retention volume, V_g, and energy of adsorption, $RTLn(V_g)$ of $C_{10}H_{22}$ on the surface of C. I. Pigment Blue 28, at T = 333 K, F = 23.14 cm^3/min, J = 0.85, C = 0.97, P_{in} = 135.80 kPa, P_{out} = 101.33 kPa, and $T_{flow\ meter}$ = 296 K.

Probe molecule	t_r (s)	V_g (cm^3/g)	$RTLn(V_g)$ (kJ/mol)
CH_4	19.5	n/a	n/a
$C_{10}H_{22}$	79.0	146.9	13.8

Table B-10. Retention time, t_r, specific retention volume, V_g, and energy of adsorption, $RTLn(V_g)$ of $C_{10}H_{22}$ on the surface of C. I. Pigment Blue 28, at T = 353 K, F = 9.66 cm^3/min, J = 0.94, C = 0.97, P_{in} = 115.42 kPa, P_{out} = 101.63 kPa, and $T_{flow\ meter}$ = 296 K.

Probe molecule	t_r (s)	V_g (cm^3/g)	$RTLn(V_g)$ (kJ/mol)
CH_4	48.0	n/a	n/a
$C_{10}H_{22}$	93.0	45.0	11.6

Table B-11. Retention time, t_r, specific retention volume, V_g, and energy of adsorption, $RTLn(V_g)$ of $C_{10}H_{22}$ on the surface of C. I. Pigment Blue 28, at T = 353 K, F = 14.80 cm^3/min, J = 0.90, C = 0.97, P_{in} = 121.66 kPa, P_{out} = 100.97 kPa, and $T_{flow\ meter}$ = 293 K.

Probe molecule	t_r (s)	V_g (cm^3/g)	$RTLn(V_g)$ (kJ/mol)
CH_4	83.3	n/a	n/a
$C_{10}H_{22}$	22.5	83.6	13.0

Table B-12. Retention time, t_r, specific retention volume, V_g, and energy of adsorption, $RTLn(V_g)$ of $C_{10}H_{22}$ on the surface of C. I. Pigment Blue 28, at T = 353 K, F = 20.79 cm^3/min, J = 0.85, C = 0.97, P_{in} = 135.80 kPa, P_{out} = 101.33 kPa, and $T_{flow\ meter}$ = 296 K.

Probe molecule	t_r (s)	V_g (cm^3/g)	$RTLn(V_g)$ (kJ/mol)
CH_4	22.5	n/a	n/a
$C_{10}H_{22}$	55.7	73.6	12.6

Table B-13. Retention time, t_r, specific retention volume, V_g, and energy of adsorption, $RTLn(V_g)$ of $C_{10}H_{22}$ on the surface of C. I. Pigment Blue 28, at T = 353 K, F = 23.15 cm^3/min, J = 0.85, C = 0.97, P_{in} = 135.80 kPa, P_{out} = 101.33 kPa, and $T_{flow\ meter}$ = 296 K.

Probe molecule	t_r (s)	V_g (cm^3/g)	$RTLn(V_g)$ (kJ/mol)
CH_4	22.0	n/a	n/a
$C_{10}H_{22}$	46.0	59.3	12.0

B.2.2. Effect of the Pigment Loading on the Retention Times of the Probe Molecules

Table B-14. Retention time, t_r, net retention volume, V_n, specific retention volume, V_g, and energy of adsorption, RTLn(V_n) and RTLn(V_g) of C_{10} H_{22} relating to column RefW, at T = 313 K, F = 20.62 cm^3/min, J = 0.89, C = 0.97, P_{in} = 123.13 kPa, P_{out} = 99.00 kPa, and $T_{flow\ meter}$ = 297 K.

Probe molecule	t_r (s)	V_n (cm^3)	V_g (cm^3/g)	RTLn(V_n) (kJ/mol)	RTLn(V_g) (kJ/mol)
CH_4	17.0	n/a	n/a	n/a	n/a
C_{10} H_{22}	148.7	39.0	n/a	9.5	n/a

Table B-15. Retention time, t_r, net retention volume, V_n, specific retention volume, V_g, and energy of adsorption, RTLn(V_n) and RTLn(V_g) of $C_{10}H_{22}$ relating to column 1, at T = 313 K, F = 18.22 cm^3/min, J = 0.85, C = 0.98, P_{in} = 133.53 kPa, P_{out} = 99.06 kPa, and $T_{flow\ meter}$ = 290 K.

Probe molecule	t_r (s)	V_n (cm^3)	V_g (cm^3/g)	RTLn(V_n) (kJ/mol)	RTLn(V_g) (kJ/mol)
CH_4	20.8	n/a	n/a	n/a	n/a
$C_{10}H_{22}$	189.3	42.4	329.0	9.8	15.1

Table B-16. Retention time, t_r, net retention volume, V_n, specific retention volume, V_g, and energy of adsorption, RTLn(V_n) and RTLn(V_g) of $C_{10}H_{22}$ relating to column 2, at T = 313 K, F = 19.89 cm^3/min, J = 0.69, C = 0.97, P_{in} = 182.53 kPa, P_{out} = 99.80 kPa, and $T_{flow\ meter}$ = 298 K.

Probe molecule	t_r (s)	V_n (cm^3)	V_g (cm^3/g)	RTLn(V_n) (kJ/mol)	RTLn(V_g) (kJ/mol)
CH_4	24.9	n/a	n/a	n/a	n/a
$C_{10}H_{22}$	414.0	85.9	352.1	11.6	15.3

Table B-17. Retention time, t_r, net retention volume, V_n, specific retention volume, V_g, and energy of adsorption, RTLn(V_n) and RTLn(V_g) of $C_{10}H_{22}$ relating to column 3, at T = 313 K, F = 18.99 cm^3/min, J = 0.65, C = 0.97, P_{in} = 196.36 kPa, P_{out} = 99.83 kPa, and $T_{flow\ meter}$ = 296 K.

Probe molecule	t_r (s)	V_n (cm^3)	V_g (cm^3/g)	RTLn(V_n) (kJ/mol)	RTLn(V_g) (kJ/mol)
CH_4	17.5	n/a	n/a	n/a	n/a
$C_{10}H_{22}$	174.2	31.4	448.6	9.0	15.9

Table B-18. Retention time, t_r, net retention volume, V_n, specific retention volume, V_g, and energy of adsorption, RTLn(V_n) and RTLn(V_g) of $C_{10}H_{22}$ relating to column 4, at T = 313 K, F = 19.09 cm^3/min, J = 0.83, C = 0.97, P_{in} = 137.99 kPa, P_{out} = 100.07 kPa, and $T_{flow\ meter}$ = 295 K.

Probe molecule	t_r (s)	V_n (cm^3)	V_g (cm^3/g)	RTLn(V_n) (kJ/mol)	RTLn(V_g) (kJ/mol)
CH_4	17.5	n/a	n/a	n/a	n/a
$C_{10}H_{22}$	140.0	31.6	1128.6	9.00	18.3

Table B-19. Retention time, t_r, net retention volume, V_n, specific retention volume, V_g, and energy of adsorption, RTLn(V_n) and RTLn(V_g) of $C_{10}H_{22}$ relating to column 5, at T = 313 K, F = 22.01 cm^3/min, J = 0.85, C = 0.97, P_{in} = 134.54 kPa, P_{out} = 100.07 kPa, and $T_{flow\ meter}$ = 295 K.

Probe molecule	t_r (s)	V_n (cm^3)	V_g (cm^3/g)	RTLn(V_n) (kJ/mol)	RTLn(V_g) (kJ/mol)
CH_4	17.0	n/a	n/a	n/a	n/a
$C_{10}H_{22}$	159.0	42.9	340.5	9.8	15.2

B.2.3. Determination of the Dispersive Component of the Surface Tension

Table B-20. Retention time, t_r, specific retention volume, V_g, and energy of adsorption, RTLn(V_g), for C. I. Pigment Blue 28, at T = 323 K, F = 21.77 cm^3/min, J = 0.85, C = 0.98, P_{in} = 134.31 kPa, P_{out} = 99.84 kPa, $T_{flow\ meter}$ = 291 K.

Probe molecule	t_r (s)	V_g (cm^3/g)	RTLn(V_g) (kJ/mol)
CH_4	24.8	n/a	n/a
C_6H_{14}	28.3	11.4	6.5
C_7H_{16}	37.8	19.5	8.0
C_8H_{18}	61.3	41.8	10.0
C_9H_{20}	122.3	96.7	12.3
$C_{10}H_{22}$	24.8	238.9	14.7

Table B-21. Retention time, t_r, specific retention volume, V_g, and energy of adsorption, RTLn(V_g), for C. I. Pigment Blue 28, at T = 333 K, F = 20.98 cm^3/min, J = 0.84, C = 0.97, P_{in} = 139.31 kPa, P_{out} = 101.38 kPa, $T_{flow\ meter}$ = 295 K.

Probe molecule	t_r (s)	V_g(cm^3/g)	RTLn(V_g) (kJ/mol)
CH_4	25.0	n/a	n/a
C_6H_{14}	29.8	9.9	6.4
C_7H_{16}	32.6	16.3	7.7
C_8H_{18}	39.5	31.4	9.6
C_9H_{20}	57.1	70.4	11.8
$C_{10}H_{22}$	95.0	154.0	14.0

Table B-22. Retention time, t_r, specific retention volume, V_g, and energy of adsorption, $RTLn(V_g)$, for C. I. Pigment Blue 28, at T = 343 K, F = 19.19 cm^3/min, J = 0.84, C = 0.98, P_{in} = 140.36 kPa, P_{out} = 102.43 kPa, $T_{flow\ meter}$ = 294 K.

Probe molecule	t_r (s)	V_g (cm^3/g)	$RTLn(V_g)$ (kJ/mol)
CH_4	21.2	n/a	n/a
C_6H_{14}	23.9	5.5	4.8
C_7H_{16}	27.8	13.3	7.4
C_8H_{18}	29.3	16.4	8.0
C_9H_{20}	41.3	40.7	10.6
$C_{10}H_{22}$	64.1	87.1	12.7

Table B-23. Retention time, t_r, specific retention volume, V_g, and energy of adsorption, $RTLn(V_g)$, for C. I. Pigment Blue 28, at T = 353 K, F = 19.50 cm^3/min, J = 0.83, C = 0.98, P_{in} = 135.93 kPa, P_{out} = 98.01 kPa, $T_{flow\ meter}$ = 291 K.

Probe molecule	t_r (s)	V_g (cm^3/g)	$RTLn(V_g)$ (kJ/mol)
CH_4	19.5	n/a	n/a
C_6H_{14}*	26.4	5.6	5.1
C_7H_{16}	23.6	8.5	6.3
C_8H_{18}	39.0	40.1	10.8
$C_{10}H_{22}$	45.8	54.0	11.7

* F = 16.81 cm^3/min, J = 0.85, C = 0.97, P_{in} = 134.23 kPa, P_{out} = 99.76 kPa, $T_{flow\ meter}$ = 296 K, $t_{r\ (methane)}$ = 23.3 s

B.2.4. Determination of the Energy, the Enthalpy and the Entropy of Adsorption of Polar Probes

Table B-24. Retention time, t_r, specific retention volume, V_g, energy of adsorption, $RTLn(V_g)$, and corresponding dispersive and specific components, $RTln(V^d_{g,ref})$ and $RTln(V^s_g)$, respectively, for C. I. Pigment Blue 28, at T = 323 K, F = 21.05 cm^3/min, J = 0.85, C = 0.98, P_{in} = 134.32 kPa, P_{out} = 99.85 kPa, $T_{flow\ meter}$ = 294 K.

Probe molecule	t_r (s)	V_g (cm^3/g)	$RTLn(V_g)$ (kJ/mol)	$RT\ln\left(V^d_{g,ref}\right)$ (kJ/mol)	$RT\ln\left(V^s_g\right)$ (kJ/mol)
CH_4	20.4	n/a	n/a	n/a	n/a
DCM	24.4	9.0	5.9	2.9	3.0
DEE	68.3	107.7	12.6	3.9	8.7
Acet	582.0	1263.0	19.2	3.4	15.8
THF	480.0	1033.6	18.6	5.7	12.9
EtAcet	643.0	1400.1	19.5	4.7	14.8

Table B-25. Retention time, t_r, specific retention volume, V_g, energy of adsorption, RTLn(V_g), and corresponding dispersive and specific components, RTln($V^d_{g,ref}$) and RTln(V^s_g), respectively, for C. I. Pigment Blue 28, at T = 333 K, F = 20.00 cm^3/min, J = 0.84, C = 0.97, P_{in} = 137.58 kPa, P_{out} = 101.38 kPa, $T_{flow\ meter}$ = 295 K.

Probe molecule	t_r (s)	V_g (cm^3/g)	RTLn(V_g) (kJ/mol)	$RT\ln\left(V^d_{g,ref}\right)$ (kJ/mol)	$RT\ln\left(V^s_g\right)$ (kJ/mol)
CH_4	23.6	n/a	n/a	n/a	n/a
DCM	27.2	7.6	5.6	3.0	2.6
DEE	56.0	68.7	11.7	3.9	7.8
Acet	505.5	1022.0	19.2	3.4	15.8
THF	379.5	754.8	18.4	5.6	12.8
EtAcet	370.5	735.7	18.3	4.6	13.7

* F = 19.70 cm^3/min, J = 0.83, C = 0.98, P_{in} = 137.67 kPa, P_{out} = 99.75 kPa, $T_{flow\ meter}$ = 293 K, $t_{r\ (methane)}$ = 24.2 s

Table B-26. Retention time, t_r, specific retention volume, V_g, energy of adsorption, RTLn(V_g), and corresponding dispersive and specific components, RTln($V^d_{g,ref}$) and RTln(V^s_g), respectively, for C. I. Pigment Blue 28, at T = 353 K, F = 20.74 cm^3/min, J = 0.84, C = 0.98, P_{in} = 132.49 kPa, P_{out} = 98.01 kPa, $T_{flow\ meter}$ = 291 K.

Probe molecule	t_r (s)	V_g (cm^3/g)	RTLn(V_g) (kJ/mol)	$RT\ln\left(V^d_{g,ref}\right)$ (kJ/mol)	$RT\ln\left(V^s_g\right)$ (kJ/mol)
CH_4	21.8	n/a	n/a	n/a	n/a
DCM	23.8	4.5	4.4	2.1	2.4
DEE	36.0	31.1	10.1	2.9	7.2
Acet	237.0	470.4	18.1	2.5	15.6
THF*	157.0	239.1	16.1	4.5	11.6
EtAcet	187.5	362.2	17.3	3.6	13.7

* F = 16.81 cm^3/min, J = 0.85, C = 0.97, P_{in} = 134.23 kPa, P_{out} = 99.76 kPa, $T_{flow\ meter}$ = 296 K, $t_{r\ (methane)}$ = 23.3 s

B.3. IGC Study of the MBS Rubber

B.3.1. Effect of the Polymer Loading and of the Carrier Gas Flow Rate on the Retention Times of the Probe Molecules

Table B-27. Retention time, t_r, specific retention volume, V_g, and energy of adsorption, RTLn(V_g) of C_8H_{18} relating to column 6, at T = 343 K, F = 29.41 cm^3/min, J = 0.94, C = 0.98, P_{in} = 115.13 kPa, P_{out} = 101.34 kPa, and $T_{flow\ meter}$ = 293 K.

Probe molecule	t_r (s)	V_g (cm^3/g)	RTLn(V_g) (kJ/mol)
CH_4	21.8	n/a	n/a
C_8H_{18}	40.3	151.4	14.3

Table B-28. Retention time, t_r, specific retention volume, V_g, and energy of adsorption, $RTLn(V_g)$ of C_8H_{18} relating to column 6, at T = 343 K, F = 35.47 cm^3/min, J = 0.92, C = 0.98, P_{in} = 118.58 kPa, P_{out} = 101.34 kPa, and $T_{flow\ meter}$ = 293 K.

Probe molecule	t_r (s)	V_g (cm^3/g)	$RTLn(V_g)$ (kJ/mol)
CH_4	18.6	n/a	n/a
C_8H_{18}	33.7	145.8	14.2

Table B-29. Retention time, t_r, specific retention volume, V_g, and energy of adsorption, $RTLn(V_g)$ of C_8H_{18} relating to column 6, at T = 343 K, F = 41.38 cm^3/min, J = 0.90, C = 0.98, P_{in} = 122.03 kPa, P_{out} = 101.34 kPa, and $T_{flow\ meter}$ = 293 K.

Probe molecule	t_r (s)	V_g (cm^3/g)	$RTLn(V_g)$ (kJ/mol)
CH_4	17.3	n/a	n/a
C_8H_{18}	29.3	134.0	14.0

Table B-30. Retention time, t_r, specific retention volume, V_g, and energy of adsorption, $RTLn(V_g)$ of C_8H_{18} relating to column 6, at T = 343 K, F = 50.99 cm^3/min, J = 0.89, C = 0.98, P_{in} = 125.47 kPa, P_{out} = 101.34 kPa, and $T_{flow\ meter}$ = 293 K.

Probe molecule	t_r (s)	V_g (cm^3/g)	$RTLn(V_g)$ (kJ/mol)
CH_4	14.8	n/a	n/a
C_8H_{18}	25.3	142.3	14.1

Table B-31. Retention time, t_r, specific retention volume, V_g, and energy of adsorption, $RTLn(V_g)$ of C_8H_{18} relating to column 7, at T = 343 K, F = 29.65 cm^3/min, J = 0.80, C = 0.98, P_{in} = 149.62 kPa, P_{out} = 101.35 kPa, and $T_{flow\ meter}$ = 297 K.

Probe molecule	t_r (s)	V_g (cm^3/g)	$RTLn(V_g)$ (kJ/mol)
CH_4	27.8	n/a	n/a
C_8H_{18}	100.3	204.2	15.2

Table B-32. Retention time, t_r, specific retention volume, V_g, and energy of adsorption, $RTLn(V_g)$ of C_8H_{18} relating to column 7, at T = 343 K, F = 37.27 cm^3/min, J = 0.76, C = 0.98, P_{in} = 159.96 kPa, P_{out} = 101.35 kPa, and $T_{flow\ meter}$ = 297 K.

Probe molecule	t_r (s)	V_g (cm^3/g)	$RTLn(V_g)$ (kJ/mol)
CH_4	23.8	n/a	n/a
C_8H_{18}	87.8	216.7	15.3

Table B-33. Retention time, t_r, specific retention volume, V_g, and energy of adsorption, $RTLn(V_g)$ of C_8H_{18} relating to column 7, at T = 343 K, F = 42.96 cm^3/min, J = 0.74, C = 0.98, P_{in} = 166.85 kPa, P_{out} = 101.35 kPa, and $T_{flow\ meter}$ = 297 K.

Probe molecule	t_r (s)	V_g (cm^3/g)	$RTLn(V_g)$ (kJ/mol)
CH_4	23.6	n/a	n/a
C_8H_{18}	76.0	198.5	15.1

Table B-34. Retention time, t_r, specific retention volume, V_g, and energy of adsorption, $RTLn(V_g)$ of C_8H_{18} relating to column 7, at T = 343 K, F = 54.22 cm^3/min, J = 0.71, C = 0.98, P_{in} = 178.92 kPa, P_{out} = 101.35 kPa, and $T_{flow\ meter}$ = 297 K.

Probe molecule	t_r (s)	V_g (cm^3/g)	$RTLn(V_g)$ (kJ/mol)
CH_4	17.8	n/a	n/a
C_8H_{18}	68.7	231.2	15.5

Table B-35. Retention time, t_r, specific retention volume, V_g, and energy of adsorption, $RTLn(V_g)$ of C_8H_{18} relating to column 8, at T = 343 K, F = 22.57 cm^3/min, J = 0.86, C = 0.98, P_{in} = 132.38 kPa, P_{out} = 101.35 kPa, and $T_{flow\ meter}$ = 297 K.

Probe molecule	t_r (s)	V_g (cm^3/g)	$RTLn(V_g)$ (kJ/mol)
CH_4	19.9	n/a	n/a
C_8H_{18}	113.3	192.4	15.0

Table B-36. Retention time, t_r, specific retention volume, V_g, and energy of adsorption, $RTLn(V_g)$ of C_8H_{18} relating to column 8, at T = 343 K, F = 35.43 cm^3/min, J = 0.85, C = 0.98, P_{in} = 135.83 kPa, P_{out} = 101.36 kPa, and $T_{flow\ meter}$ = 299 K.

Probe molecule	t_r (s)	V_g (cm^3/g)	$RTLn(V_g)$ (kJ/mol)
CH_4	16.0	n/a	n/a
C_8H_{18}	90.8	195.0	15.0

Table B-37. Retention time, t_r, specific retention volume, V_g, and energy of adsorption, $RTLn(V_g)$ of C_8H_{18} relating to column 8, at T = 343 K, F = 39.74 cm^3/min, J = 0.84, C = 0.98, P_{in} = 139.27 kPa, P_{out} = 101.35 kPa, and $T_{flow\ meter}$ = 297 K.

Probe molecule	t_r (s)	V_g (cm^3/g)	$RTLn(V_g)$ (kJ/mol)
CH_4	21.3	n/a	n/a
C_8H_{18}	86.7	188.2	14.9

Table B-38. Retention time, t_r, specific retention volume, V_g, and energy of adsorption, $RTLn(V_g)$ of C_8H_{18} relating to column 8, at T = 343 K, F = 48.78 cm^3/min, J = 0.80, C = 0.98, P_{in} = 149.62 kPa, P_{out} = 101.35 kPa, and $T_{flow\ meter}$ = 298 K.

Probe molecule	t_r (s)	V_g (cm^3/g)	$RTLn(V_g)$ (kJ/mol)
CH_4	18.2	n/a	n/a
C_8H_{18}	72.3	182.7	14.9

Table B-39. Retention time, t_r, specific retention volume, V_g, and energy of adsorption, $RTLn(V_g)$ of C_8H_{18} relating to column 9, at T = 343 K, F = 28.75 cm^3/min, J = 0.89, C = 0.98, P_{in} = 125.49 kPa, P_{out} = 101.36 kPa, and $T_{flow\ meter}$ = 300 K.

Probe molecule	t_r (s)	V_g (cm^3/g)	$RTLn(V_g)$ (kJ/mol)
CH_4	24.8	n/a	n/a
C_8H_{18}	124.5	180.1	14.8

Table B-40. Retention time, t_r, specific retention volume, V_g, and energy of adsorption, $RTLn(V_g)$ of C_8H_{18} relating to column 9, at T = 343 K, F = 34.82 cm^3/min, J = 0.88, C = 0.98, P_{in} = 128.94 kPa, P_{out} = 101.36 kPa, and $T_{flow\ meter}$ = 300 K.

Probe molecule	t_r (s)	V_g (cm^3/g)	$RTLn(V_g)$ (kJ/mol)
CH_4	20.9	n/a	n/a
C_8H_{18}	107.5	186.3	14.9

Table B-41. Retention time, t_r, specific retention volume, V_g, and energy of adsorption, $RTLn(V_g)$ of C_8H_{18} relating to column 9, at T = 343 K, F = 42.16 cm^3/min, J = 0.86, C = 0.98, P_{in} = 134.10 kPa, P_{out} = 101.36 kPa, and $T_{flow\ meter}$ = 300 K.

Probe molecule	t_r (s)	V_g (cm^3/g)	$RTLn(V_g)$ (kJ/mol)
CH_4	19.0	n/a	n/a
C_8H_{18}	92.7	187.4	14.9

Table B-42. Retention time, t_r, specific retention volume, V_g, and energy of adsorption, $RTLn(V_g)$ of C_8H_{18} relating to column 9, at T = 343 K, F = 53.10 cm^3/min, J = 0.82, C = 0.98, P_{in} = 142.73 kPa, P_{out} = 101.36 kPa, and $T_{flow\ meter}$ = 299 K.

Probe molecule	t_r (s)	V_g (cm^3/g)	$RTLn(V_g)$ (kJ/mol)
CH_4	16.3	n/a	n/a
C_8H_{18}	80.3	197.4	15.1

B.3.2. Determination of the Dispersive Component of the Surface Tension

Table B-43. Retention time, t_r, specific retention volume, V_g, and energy of adsorption, $RTLn(V_g)$, of the n-alkanes on the surface of the MBS rubber, at T = 333 K, F = 25.54 cm^3/min, J = 0.85, C = 0.97, P_{in} = 135.73 kPa, P_{out} = 101.26 kPa, and $T_{flow\ meter}$ = 298 K.

Probe molecule	t_r (s)	V_g (cm^3/g)	$RTLn(V_g)$ (kJ/mol)
CH_4	22.7	n/a	n/a
C_6H_{14}	39.5	31.5	9.6
C_7H_{16}	60.3	70.4	11.8
C_8H_{18}	133.8	207.7	14.8
C_9H_{20}	277.5	476.2	17.1

Table B-44. Retention time, t_r, specific retention volume, V_g, and energy of adsorption, $RTLn(V_g)$, for the MBS rubber, at T = 343 K F = 28.62 cm^3/min, J = 0.82, C = 0.97, P_{in} = 142.62 kPa, P_{out} = 101.25 kPa, $T_{flow\ meter}$ = 295 K.

Probe molecule	t_r (s)	V_g (cm^3/g)	$RTLn(V_g)$ (kJ/mol)
CH_4	25.3	n/a	n/a
C_6H_{14}	37.0	23.7	9.0
C_7H_{16}	51.5	53.1	11.3
C_8H_{18}	98.0	147.5	14.2
C_9H_{20}	207.5	369.7	16.9

Table B-45. Retention time, t_r, specific retention volume, V_g, and energy of adsorption, $RTLn(V_g)$, for the MBS rubber, at T = 353 K, F = 30.93 cm^3/min, J = 0.85, C = 0.97, P_{in} = 135.73 kPa, P_{out} = 101.25 kPa, $T_{flow\ meter}$ = 297 K.

Probe molecule	t_r (s)	V_g (cm^3/g)	$RTLn(V_g)$ (kJ/mol)
CH_4	22.2	n/a	n/a
C_6H_{14}	30.3	18.3	8.5
C_7H_{16}	39.2	38.5	10.7
C_8H_{18}	78.2	126.7	14.2
C_9H_{20}	136.0	257.6	16.3

Table B-46. Retention time, t_r, specific retention volume, V_g, and energy of adsorption, RTLn(V_g), for the MBS rubber, at T = 363 K, F = 30.15 cm^3/min, J = 0.85, C = 0.97, P_{in} = 135.73 kPa, P_{out} = 101.26 kPa, $T_{flow\ meter}$ = 300 K.

Probe molecule	t_r (s)	V_g (cm^3/g)	RTLn(V_g) (kJ/mol)
CH_4	21.8	n/a	n/a
C_6H_{14}	26.5	10.5	7.1
C_7H_{16}	37.0	33.6	10.6
C_8H_{18}	63.5	92.1	13.7
C_9H_{20}	104.0	181.5	15.7

Table B-47. Retention time, t_r, specific retention volume, V_g, and energy of adsorption, RTLn(V_g), for the MBS rubber, at T = 373 K, F = 29.22 cm^3/min, J = 0.84, C = 0.98, P_{in} = 139.16 kPa, P_{out} = 101.24 kPa, $T_{flow\ meter}$ = 293 K.

Probe molecule	t_r (s)	V_g (cm^3/g)	RTLn(V_g) (kJ/mol)
CH_4	22.6	n/a	n/a
C_6H_{14}	26.9	9.0	6.8
C_7H_{16}	36.7	29.6	10.5
C_8H_{18}	55.3	68.9	13.1
C_9H_{20}	80.33	121.6	14.9

B.3.3. Determination of the Energy, the Enthalpy and the Entropy of Adsorption of Polar Probes

Table B-48. Retention time, t_r, specific retention volume, V_g, energy of adsorption, RTLn(V_g), and corresponding dispersive and specific components, RTln($V^d_{g,ref}$) and RTln(V^s_g), respectively, for the MBS rubber, at T = 343 K, F = 29.32 cm^3/min, J = 0.86, C = 0.97, P_{in} = 131.18 kPa, P_{out} = 100.16 kPa, $T_{flow\ meter}$ = 296 K.

Probe molecule	t_r (s)	V_g (cm^3/g)	RTLn(V_g) (kJ/mol)	$RT\ln(V^d_{g,ref})$ (kJ/mol)	$RT\ln(V^s_g)$ (kJ/mol)
CH_4	22.7	n/a	n/a	n/a	n/a
DCM	43.5	45.3	10.9	4.8	6.1
Acet	77.5	119.3	13.6	5.4	8.3
THF*	81.5	128.0	13.8	8.3	5.5
EtAcet	63.8	89.6	12.8	7.0	5.8

Table B-49. Retention time, t_r, specific retention volume, V_g, energy of adsorption, RTLn(V_g), and corresponding dispersive and specific components, RTln($V^d_{g,ref}$) and RTln(V^s_g), respectively, for the MBS rubber, at T = 353 K, F = 30.31 cm^3/min, J = 0.85, C = 0.97, P_{in} = 134.64 kPa, P_{out} = 100.16 kPa, $T_{flow\ meter}$ = 298 K.

Probe molecule	t_r (s)	V_g (cm^3/g)	RTLn(V_g) (kJ/mol)	$RT\ln\left(V^d_{g,ref}\right)$ (kJ/mol)	$RT\ln\left(V^s_g\right)$ (kJ/mol)
CH_4	23.8	n/a	n/a	n/a	n/a
DCM	37.0	29.1	9.9	4.3	5.6
Acet	55.2	69.1	12.4	4.9	7.6
THF*	60.7	81.3	12.9	7.9	5.1
EtAcet	51.5	61.0	12.1	6.5	5.6

Table B-50. Retention time, t_r, specific retention volume, V_g, energy of adsorption, RTLn(V_g), and corresponding dispersive and specific components, RTln($V^d_{g,ref}$) and RTln(V^s_g), respectively, for the MBS rubber, at T = 363 K, F = 29.85 cm^3/min, J = 0.85, C = 0.98, P_{in} = 134.62 kPa, P_{out} = 100.15 kPa, $T_{flow\ meter}$ = 293 K.

Probe molecule	t_r (s)	V_g (cm^3/g)	RTLn(V_g) (kJ/mol)	$RT\ln\left(V^d_{g,ref}\right)$ (kJ/mol)	$RT\ln\left(V^s_g\right)$ (kJ/mol)
CH_4	17.9	n/a	n/a	n/a	n/a
DCM	26.8	19.5	9.0	3.4	5.5
Acet	37.0	41.8	11.3	4.0	7.2
THF*	43.2	55.3	12.1	7.0	5.1
EtAcet	36.0	39.6	11.1	5.7	5.4

Table B-51. Retention time, t_r, specific retention volume, V_g, energy of adsorption, RTLn(V_g), and corresponding dispersive and specific components, RTln($V^d_{g,ref}$) and RTln(V^s_g), respectively, for the MBS rubber, at T = 373 K, F = 28.99 cm^3/min, J = 0.83, C = 0.98, P_{in} = 138.07 kPa, P_{out} = 100.15 kPa, $T_{flow\ meter}$ = 293 K.

Probe molecule	t_r (s)	V_g (cm^3/g)	RTLn(V_g) (kJ/mol)	$RT\ln\left(V^d_{g,ref}\right)$ (kJ/mol)	$RT\ln\left(V^s_g\right)$ (kJ/mol)
CH_4	22.8	n/a	n/a	n/a	n/a
DCM	30.0	15.2	8.4	3.2	5.3
Acet	37.2	30.2	10.6	3.8	6.8
THF*	42.3	41.0	11.5	6.8	4.8
EtAcet	37.3	30.6	10.6	5.4	5.2

B.4. IGC Study of the PC 125

B.4.1. Effect of the Polymer Loading and of the Carrier Gas Flow Rate on the Retention Times of the Probe Molecules

Table B-52. Retention time, t_r, specific retention volume, V_g, and energy of adsorption, $RTLn(V_g)$ of C_6H_{14} relating to column 10, at T = 353 K, F = 10.14 cm^3/min, J = 0.89, C = 0.97, P_{in} = 124.41 kPa, P_{out} = 100.27 kPa, and $T_{flow\ meter}$ = 295 K.

Probe molecule	t_r (s)	V_g (cm^3/g)	$RTLn(V_g)$ (kJ/mol)
CH_4	30.5	n/a	n/a
C_6H_{14}	240.5	127.1	14.2

Table B-53. Retention time, t_r, specific retention volume, V_g, and energy of adsorption, $RTLn(V_g)$ of C_6H_{14} relating to column 10, at T = 353 K, F = 14.59 cm^3/min, J = 0.87, C = 0.97, P_{in} = 127.85 kPa, P_{out} = 100.27 kPa, and $T_{flow\ meter}$ = 295 K.

Probe molecule	t_r (s)	V_g (cm^3/g)	$RTLn(V_g)$ (kJ/mol)
CH_4	19.0	n/a	n/a
C_6H_{14}	160.0	120.7	14.1

Table B-54. Retention time, t_r, specific retention volume, V_g, and energy of adsorption, $RTLn(V_g)$ of C_6H_{14} relating to column 10, at T = 353 K, F = 20.18 cm^3/min, J = 0.81, C = 0.98, P_{in} = 127.85 kPa, P_{out} = 100.27 kPa, and $T_{flow\ meter}$ = 295 K.

Probe molecule	t_r (s)	V_g (cm^3/g)	$RTLn(V_g)$ (kJ/mol)
CH_4	11.8	n/a	n/a
C_6H_{14}	117.0	115.4	13.9

Table B-545 Retention time, t_r, specific retention volume, V_g, and energy of adsorption, $RTLn(V_g)$ of C_6H_{14} relating to column 10, at T = 353 K, F = 25.00 cm^3/min, J = 0.82, C = 0.97, P_{in} = 142.19 kPa, P_{out} = 100.82 kPa, and $T_{flow\ meter}$ = 296 K.

Probe molecule	t_r (s)	V_g (cm^3/g)	$RTLn(V_g)$ (kJ/mol)
CH_4	12.0	n/a	n/a
C_6H_{14}	114.8	141.5	14.5

Table B-56. Retention time, t_r, specific retention volume, V_g, and energy of adsorption, $RTLn(V_g)$ of C_6H_{14} relating to column 10, at T = 353 K, F = 30.82 cm^3/min, J = 0.80, C = 0.97, P_{in} = 149.09 kPa, P_{out} = 100.82 kPa, and $T_{flow\ meter}$ = 296 K.

Probe molecule	t_r (s)	V_g (cm^3/g)	$RTLn(V_g)$ (kJ/mol)
CH_4	8.8	n/a	n/a
C_6H_{14}	75.5	109.9	13.8

Table B-57 Retention time, t_r, specific retention volume, V_g, and energy of adsorption, $RTLn(V_g)$ of C_6H_{14} relating to column 11, at T = 353 K, F = 10.73 cm^3/min, J = 0.92, C = 0.97, P_{in} = 117.19 kPa, P_{out} = 99.96 kPa, and $T_{flow\ meter}$ = 295 K.

Probe molecule	t_r (s)	V_g (cm^3/g)	$RTLn(V_g)$ (kJ/mol)
CH_4	21.8	n/a	n/a
C_6H_{14}	201.8	93.3	13.3

Table B-58. Retention time, t_r, specific retention volume, V_g, and energy of adsorption, $RTLn(V_g)$ of C_6H_{14} relating to column 11, at T = 353 K, F = 15.31 cm^3/min, J = 0.90, C = 0.97, P_{in} = 120.64 kPa, P_{out} = 99.96 kPa, and $T_{flow\ meter}$ = 296 K.

Probe molecule	t_r (s)	V_g (cm^3/g)	$RTLn(V_g)$ (kJ/mol)
CH_4	21.5	n/a	n/a
C_6H_{14}	157.5	102.5	13.6

Table B-59. Retention time, t_r, specific retention volume, V_g, and energy of adsorption, $RTLn(V_g)$ of C_6H_{14} relating to column 11, at T = 353 K, F = 20.64 cm^3/min, J = 0.87, C = 0.97, P_{in} = 127.54 kPa, P_{out} = 99.96 kPa, and $T_{flow\ meter}$ = 296 K.

Probe molecule	t_r (s)	V_g (cm^3/g)	$RTLn(V_g)$ (kJ/mol)
CH_4	13.0	n/a	n/a
C_6H_{14}	97.5	80.4	12.9

Table B-60. Retention time, t_r, specific retention volume, V_g, and energy of adsorption, $RTLn(V_g)$ of C_6H_{14} relating to column 11, at T = 353 K, F = 25.07 cm^3/min, J = 0.85, C = 0.97, P_{in} = 134.43 kPa, P_{out} = 99.96 kPa, and $T_{flow\ meter}$ = 296 K.

Probe molecule	t_r (s)	V_g (cm^3/g)	$RTLn(V_g)$ (kJ/mol)
CH_4	12.5	n/a	n/a
C_6H_{14}	90.0	87.9	13.1

Table B-61. Retention time, t_r, specific retention volume, V_g, and energy of adsorption, $RTLn(V_g)$ of C_6H_{14} relating to column 11, at T = 353 K, F = 31.04 cm^3/min, J = 0.81, C = 0.97, P_{in} = 144.78 kPa, P_{out} = 99.96 kPa, and $T_{flow\ meter}$ = 297 K.

Probe molecule	t_r (s)	V_g (cm^3/g)	$RTLn(V_g)$ (kJ/mol)
CH_4	9.0	n/a	n/a
C_6H_{14}	58.5	65.9	12.3

Table B-62. Retention time, t_r, specific retention volume, V_g, and energy of adsorption, $RTLn(V_g)$ of C_6H_{14} relating to column 12, at T = 353 K, F = 10.73 cm^3/min, J = 0.93, C = 0.98, P_{in} = 116.95 kPa, P_{out} = 101.44 kPa, and $T_{flow\ meter}$ = 293 K.

Probe molecule	t_r (s)	V_g (cm^3/g)	$RTLn(V_g)$ (kJ/mol)
CH_4	28.5	n/a	n/a
C_6H_{14}	298.5	94.4	13.4

Table B-63. Retention time, t_r, specific retention volume, V_g, and energy of adsorption, $RTLn(V_g)$ of C_6H_{14} relating to column 12, at T = 353 K, F = 15.31 cm^3/min, J = 0.92, C = 0.98, P_{in} = 118.68 kPa, P_{out} = 101.44 kPa, and $T_{flow\ meter}$ = 295 K.

Probe molecule	t_r (s)	V_g (cm^3/g)	$RTLn(V_g)$ (kJ/mol)
CH_4	18.8	n/a	n/a
C_6H_{14}	240.0	109.1	13.8

Table B-64. Retention time, t_r, specific retention volume, V_g, and energy of adsorption, $RTLn(V_g)$ of C_6H_{14} relating to column 12, at T = 353 K, F = 20.64 cm^3/min, J = 0.89, C = 0.97, P_{in} = 125.58 kPa, P_{out} = 101.44 kPa, and $T_{flow\ meter}$ = 295 K.

Probe molecule	t_r (s)	V_g (cm^3/g)	$RTLn(V_g)$ (kJ/mol)
CH_4	18.0	n/a	n/a
C_6H_{14}	190.0	110.7	13.8

Table B-65. Retention time, t_r, specific retention volume, V_g, and energy of adsorption, $RTLn(V_g)$ of C_6H_{14} relating to column 12, at T = 353 K, F = 25.07 cm^3/min, J = 0.86, C = 0.97, P_{in} = 132.48 kPa, P_{out} = 101.44 kPa, and $T_{flow\ meter}$ = 296 K.

Probe molecule	t_r (s)	V_g (cm^3/g)	$RTLn(V_g)$ (kJ/mol)
CH_4	15.0	n/a	n/a
C_6H_{14}	122.3	81.0	12.9

Table B-66. Retention time, t_r, specific retention volume, V_g, and energy of adsorption, RTLn(V_g) of C_6H_{14} relating to column 12, at T = 353 K, F = 31.04 cm^3/min, J = 0.84, C = 0.97, P_{in} = 139.37 kPa, P_{out} = 101.45 kPa, and $T_{flow\ meter}$ = 296 K.

Probe molecule	t_r (s)	V_g (cm^3/g)	RTLn(V_g) (kJ/mol)
CH_4	10.0	n/a	n/a
C_6H_{14}	116.3	96.3	13.4

B.4.2. Determination of the Dispersive Component of the Surface Tension

Table B-67. Retention time, tr, specific retention volume, V_g, and energy of adsorption, RTLn(V_g), for the adsorption of n-alkanes on the surface of PC 125, at T = 353 K, F = 44.89 cm^3/min, J = 0.90, C = 0.98, P_{in} = 122.01 kPa, P_{out} = 101.32 kPa and $T_{flow\ meter}$ = 293 K.

Probe molecule	t_r (s)	V_g (cm^3/g)	RTLn(V_g) (kJ/mol)
CH_4	9.1	n/a	n/a
C_6H_{14}	55.0	101.5	13.6
C_7H_{16}	115.5	235.4	16.0
C_8H_{18}	230.0	488.8	18.2
C_9H_{20}	625.0	1363.0	21.2

Table B-68. Retention time, t_r, specific retention volume, V_g, and energy of adsorption, RTLn(V_g), for PC 125, at T = 363 K, F = 45.34 cm^3/min, J = 0.92, C = 0.98, P_{in} = 116.00 kPa, P_{out} = 98.76 kPa, $T_{flow\ meter}$ = 293 K.

Probe molecule	t_r (s)	V_g (cm^3/g)	RTLn(V_g) (kJ/mol)
CH_4	11.4	n/a	n/a
C_6H_{14}	35.8	55.4	12.1
C_7H_{16}	73.8	141.4	14.9
C_8H_{18}*	143.5	298.6	17.2
C_9H_{20}*	386.7	849.1	20.4

* F = 45.11 cm^3/min, J = 0.92, C = 0.98, P_{in} = 117.28 kPa, P_{out} = 100.05 kPa, $T_{flow\ meter}$ = 292 K, $t_{r\ (methane)}$ = 11.6 s

Table B-69. Retention time, t_r, specific retention volume, V_g, and energy of adsorption, RTLn(V_g), for PC 125, at T = 373 K, F = 46.64 cm^3/min, J = 0.92, C = 0.98, P_{in} = 117.78 kPa, P_{out} = 100.55 kPa, $T_{flow\ meter}$ = 292 K.

Probe molecule	t_r (s)	V_g (cm^3/g)	RTLn(V_g) (kJ/mol)
CH_4	11.8	n/a	n/a
C_6H_{14}	26.7	34.7	11.0
C_7H_{16}	40.3	66.4	13.0
C_8H_{18}	71.5	139.4	15.3
C_9H_{20}	155.5	335.7	18.0
$C_{10}H_{22}$	362.5	819.5	20.8

Table B-70. Retention time, t_r, specific retention volume, V_g, and energy of adsorption, RTLn(V_g), for PC 125, at T = 383 K, F = 45.69 cm^3/min, J = 0.92, C = 0.98, P_{in} = 117.44 kPa, P_{out} = 100.20 kPa, $T_{flow\ meter}$ = 293 K.

Probe molecule	t_r (s)	V_g (cm^3/g)	RTLn(V_g) (kJ/mol)
CH_4	11.8	n/a	n/a
C_6H_{14}	18.5	15.4	8.7
C_7H_{16}	28.8	38.9	11.7
C_8H_{18}	45.3	76.6	13.8
C_9H_{20}	91.5	182.4	16.6
$C_{10}H_{22}$	161.8	343.1	18.6

Table B-71. Retention time, t_r, specific retention volume, V_g, and energy of adsorption, RTLn(V_g), for PC 125, at T = 393 K, F = 46.04 cm^3/min, J = 0.92, C = 0.98, P_{in} = 117.39 kPa, P_{out} = 100.15 kPa, $T_{flow\ meter}$ = 294 K.

Probe molecule	t_r (s)	V_g (cm^3/g)	RTLn(V_g) (kJ/mol)
CH_4	9.9	n/a	n/a
C_6H_{14}	16.5	15.1	8.9
C_7H_{16}	25.3	35.2	11.6
C_8H_{18}	29.0	43.8	12.4
C_9H_{20}*	47.5	84.1	14.5

* F = 45.00 cm^3/min, J = 0.92, C = 0.98, P_{in} = 117.59 kPa, P_{out} = 100.35 kPa, $T_{flow\ meter}$ = 293 K, $t_{r\ (methane)}$ = 10.5 s

B.4.3. Determination of the Energy, the Enthalpy and the Entropy of Adsorption of Polar Probes

Table B-72. Retention time, t_r, specific retention volume, V_g, energy of adsorption, RTLn(V_g), and corresponding dispersive and specific components, RTln($V^d_{g,ref}$) and RTln(V^s_g), respectively, for PC 125, at T = 363 K, F = 46.04 cm^3/min, J = 0.92, C = 0.98, P_{in} = 117.29 kPa, P_{out} = 100.05 kPa, $T_{flowmeter}$ = 293 K.

Probe molecule	t_r (s)	V_g (cm^3/g)	RTLn(V_g) (kJ/mol)	$RT\ln\left(V^d_{g,ref}\right)$ (kJ/mol)	$RT\ln\left(V^s_g\right)$ (kJ/mol)
CH_4	9.3	n/a	n/a	n/a	n/a
TCM	68.5	136.5	14.8	12.5	2.3
DCM	35.1	59.6	12.3	8.2	4.2
DEE	29.3	46.3	11.6	9.5	2.1
Acet*	86.0	169.8	15.5	8.8	6.7
THF**	120.0	247.5	16.6	11.7	4.9
EtAcet	92.3	191.2	15.9	10.4	5.5

*F = 45.80 cm^3/min, J = 0.92, C = 0.97, P_{in} = 118.54 kPa, P_{out} = 101.30 kPa, $T_{flow\ meter}$ = 296 K, $t_{r\ (methane)}$ = 11.7 s

Table B-73. Retention time, t_r, specific retention volume, V_g, energy of adsorption, RTLn(V_g), and corresponding dispersive and specific components, RTln($V^d_{g,ref}$) and RTln(V^s_g), respectively, for PC 125, at T = 373 K, F = 45.57 cm^3/min, J = 0.92, C = 0.98, P_{in} = 117.79 kPa, P_{out} = 100.55 kPa, $T_{flowmeter}$ = 294 K.

Probe molecule	t_r (s)	V_g (cm^3/g)	RTLn(V_g) (kJ/mol)	$RT\ln\left(V^d_{g,ref}\right)$ (kJ/mol)	$RT\ln\left(V^s_g\right)$ (kJ/mol)
CH_4	9.9	n/a	n/a	n/a	n/a
TCM	43.2	75.8	13.4	10.9	2.5
DCM	25.0	34.4	11.0	6.8	4.1
DEE	20.3	23.8	9.8	8.0	1.8
Acet	53.0	98.3	14.2	7.4	6.9
THF*	69.0	134.7	15.2	10.1	5.1
EtAcet*	64.2	117.1	14.8	8.9	5.9

* F = 45.92 cm^3/min, J = 0.92, C = 0.98, P_{in} = 117.43 kPa, P_{out} = 100.20 kPa, $T_{flow\ meter}$ = 292 K, $t_{r\ (methane)}$ = 13.3 s

Table B-74. Retention time, t_r, specific retention volume, V_g, energy of adsorption, RTLn(V_g), and corresponding dispersive and specific components, RTln($V^d_{g,ref}$) and RTln(V^s_g), respectively, for PC 125, at T = 383 K, F = 45.23 cm^3/min, J = 0.92, C = 0.98, P_{in} = 117.39 kPa, P_{out} = 100.15 kPa, $T_{flowmeter}$ = 295 K.

Probe molecule	t_r (s)	V_g (cm^3/g)	RTLn(V_g) (kJ/mol)	$RT\ln\left(V^d_{g,ref}\right)$ (kJ/mol)	$RT\ln\left(V^s_g\right)$ (kJ/mol)
CH4	13.1	n/a	n/a	n/a	n/a
TCM	30.0	38.1	11.6	9.2	2.4
DCM	20.6	17.0	9.0	5.1	4.0
DEE	18.3	11.8	7.9	6.3	1.6
Acet	33.8	46.6	12.2	5.6	6.6
THF	43.3	68.1	13.4	8.4	5.1
EtAcet	36.3	52.3	12.6	7.2	5.5

Table B-75. Retention time, t_r, specific retention volume, V_g, energy of adsorption, RTLn(V_g), and corresponding dispersive and specific components, RTln($V^d_{g,ref}$) and RTln(V^s_g), respectively, for PC 125, at T = 393 K, F = 46.16 cm^3/min, J = 0.92, C = 0.98, P_{in} = 117.59 kPa, P_{out} = 100.35 kPa, $T_{flowmeter}$ = 294 K.

Probe molecule	t_r (s)	V_g (cm^3/g)	RTLn(V_g) (kJ/mol)	$RT\ln\left(V^d_{g,ref}\right)$ (kJ/mol)	$RT\ln\left(V^s_g\right)$ (kJ/mol)
CH_4	11.5	n/a	n/a	n/a	n/a
TCM	20.5	20.9	9.9	7.7	2.2
DCM	16.3	11.3	7.9	3.9	4.0
DEE	14.5	7.0	6.4	5.0	1.4
Acet	24.3	29.7	11.1	4.4	6.7
THF	28.5	39.3	12.0	7.0	5.0
EtAcet	24.3	29.7	11.1	5.8	5.3

B.5. IGC Study of the PBT 195

B.5.1. Effect of the Carrier Gas Flow Rate on the Retention Times of the Probe Molecules

Table B-76. Retention time, t_r, specific retention volume, V_g, and energy of adsorption, RTLn(V_g) of $C_{10}H_{22}$ relating to column 14, at T = 303 K, F = 5.14 cm^3/min, J = 0.98, C = 0.97, P_{in} = 105.09 kPa, P_{out} = 101.64 kPa, and $T_{flow\ meter}$ = 295 K.

Probe molecule	t_r (s)	V_g (cm^3/g)	RTLn(V_g) (kJ/mol)
CH_4	67.5	n/a	n/a
$C_{10}H_{22}$	218.7	2.7	2.5

Table B-77. Retention time, t_r, specific retention volume, V_g, and energy of adsorption, RTLn(V_g) of $C_{10}H_{22}$ relating to column 14, at T = 303 K, F = 9.94 cm^3/min, J = 0.98, C = 0.97, P_{in} = 105.09 kPa, P_{out} = 101.64 kPa, and $T_{flow\ meter}$ = 296 K.

Probe molecule	t_r (s)	V_g (cm^3/g)	RTLn(V_g) (kJ/mol)
CH_4	38.7	n/a	n/a
$C_{10}H_{22}$	117.0	2.7	2.5

Table B-78. Retention time, t_r, specific retention volume, V_g, and energy of adsorption, RTLn(V_g) of $C_{10}H_{22}$ relating to column 14, at T = 303 K, F = 15.69 cm^3/min, J = 0.98, C = 0.97, P_{in} = 105.09 kPa, P_{out} = 101.64 kPa, and $T_{flow\ meter}$ = 297 K.

Probe molecule	t_r (s)	V_g (cm^3/g)	RTLn(V_g) (kJ/mol)
CH_4	26.0	n/a	n/a
$C_{10}H_{22}$	77.7	2.8	2.6

Table B-79. Retention time, t_r, specific retention volume, V_g, and energy of adsorption, RTLn(V_g) of $C_{10}H_{22}$ relating to column 14, at T = 303 K, F = 20.27 cm^3/min, J = 0.98, C = 0.97, P_{in} = 105.09 kPa, P_{out} = 101.64 kPa, and $T_{flow\ meter}$ = 298 K.

Probe molecule	t_r (s)	V_g (cm^3/g)	RTLn(V_g) (kJ/mol)
CH_4	20.0	n/a	n/a
$C_{10}H_{22}$	60.0	2.8	2.6

Table B-80. Retention time, t_r, specific retention volume, V_g, and energy of adsorption, RTLn(V_g) of $C_{10}H_{22}$ relating to column 14, at T = 303 K, F = 30.87 cm^3/min, J = 0.97, C = 0.97, P_{in} = 108.55 kPa, P_{out} = 101.64 kPa, and $T_{flow\ meter}$ = 298 K.

Probe molecule	t_r (s)	V_g (cm^3/g)	RTLn(V_g) (kJ/mol)
CH_4	14.7	n/a	n/a
$C_{10}H_{22}$	40.4	2.7	2.5

Table B-81. Retention time, t_r, specific retention volume, V_g, and energy of adsorption, RTLn(V_g) of $C_{10}H_{22}$ relating to column 14, at T = 313 K, F = 3.68 cm^3/min, J = 0.98, C = 0.98, P_{in} = 105.34 kPa, P_{out} = 101.89 kPa, and $T_{flow\ meter}$ = 294 K.

Probe molecule	t_r (s)	V_g (cm^3/g)	RTLn(V_g) (kJ/mol)
CH_4	80.7	n/a	n/a
$C_{10}H_{22}$	190.8	1.4	0.9

Table B-82. Retention time, t_r, specific retention volume, V_g, and energy of adsorption, $RTLn(V_g)$ of $C_{10}H_{22}$ relating to column 14, at T = 313 K, F = 10.42 cm^3/min, J = 0.98, C = 0.97, P_{in} = 105.34 kPa, P_{out} = 101.90 kPa, and $T_{flow\ meter}$ = 296 K.

Probe molecule	t_r (s)	V_g (cm^3/g)	$RTLn(V_g)$ (kJ/mol)
CH_4	38.1	n/a	n/a
$C_{10}H_{22}$	74.2	1.3	0.7

Table B-83. Retention time, t_r, specific retention volume, V_g, and energy of adsorption, $RTLn(V_g)$ of $C_{10}H_{22}$ relating to column 14, at T = 313 K, F = 15.35 cm^3/min, J = 0.98, C = 0.97, P_{in} = 105.35 kPa, P_{out} = 101.90 kPa, and $T_{flow\ meter}$ = 297 K.

Probe molecule	t_r (s)	V_g (cm^3/g)	$RTLn(V_g)$ (kJ/mol)
CH_4	26.2	n/a	n/a
$C_{10}H_{22}$	50.0	1.3	0.6

Table B-84. Retention time, t_r, specific retention volume, V_g, and energy of adsorption, $RTLn(V_g)$ of $C_{10}H_{22}$ relating to column 14, at T = 313 K, F = 21.05 cm^3/min, J = 0.98, C = 0.97, P_{in} = 105.35 kPa, P_{out} = 101.90 kPa, and $T_{flow\ meter}$ = 298 K.

Probe molecule	t_r (s)	V_g (cm^3/g)	$RTLn(V_g)$ (kJ/mol)
CH_4	19.0	n/a	n/a
$C_{10}H_{22}$	37.5	1.3	0.8

Table B-85. Retention time, t_r, specific retention volume, V_g, and energy of adsorption, $RTLn(V_g)$ of $C_{10}H_{22}$ relating to column 14, at T = 313 K, F = 29.65 cm^3/min, J = 0.98, C = 0.97, P_{in} = 105.35 kPa, P_{out} = 101.90 kPa, and $T_{flow\ meter}$ = 298 K.

Probe molecule	t_r (s)	V_g (cm^3/g)	$RTLn(V_g)$ (kJ/mol)
CH_4	15.0	n/a	n/a
$C_{10}H_{22}$	28.0	1.3	0.7

B.5.2. Determination of the Dispersive Component of the Surface Tension

Table B-86. Retention time, t_r, specific retention volume, V_g, and energy of adsorption, $RTLn(V_g)$, for the n-alkanes on the surface of PBT 195, at T = 298 K, F = 13.21 cm^3/min, J = 0.95, C = 0.98, P_{in} = 111.59 kPa, P_{out} = 101.25 kPa, and $T_{flow\ meter}$ = 294 K.

Probe molecule	t_r (s)	V_g (cm^3/g)	$RTLn(V_g)$ (kJ/mol)
CH_4	33.8	n/a	n/a
C_6H_{14}	38.0	0.2	-4.0
C_7H_{16}	46.7	0.6	-1.3
C_8H_{18}	72.7	1.8	1.5
C_9H_{20}	156.0	5.7	4.3
$C_{10}H_{22}$	432.3	18.5	7.2

Table B-87. Retention time, t_r, specific retention volume, V_g, and energy of adsorption, $RTLn(V_g)$, for PBT 195, at T = 303 K, F = 12.06 cm^3/min, J = 0.95, C = 0.98, P_{in} = 111.59 kPa, P_{out} = 101.25 kPa, $T_{flow\ meter}$ = 294 K.

Probe molecule	t_r (s)	V_g (cm^3/g)	$RTLn(V_g)$ (kJ/mol)
CH_4	34.5	n/a	n/a
C_6H_{14}	37.3	0.1	-5.4
C_7H_{16}	45.0	0.5	-2.0
C_8H_{18}	63.5	1.2	5.2
C_9H_{20}	114.2	3.4	3.1
$C_{10}H_{22}$	290.2	10.8	6.0

Table B-88. Retention time, t_r, specific retention volume, V_g, and energy of adsorption, $RTLn(V_g)$, for PBT 195, at T = 308 K, F = 12.74 cm^3/min, J = 0.95, C = 0.97, P_{in} = 111.59 kPa, P_{out} = 101.25 kPa, $T_{flow\ meter}$ = 296 K.

Probe molecule	t_r (s)	V_g (cm^3/g)	$RTLn(V_g)$ (kJ/mol)
CH_4	34.2	n/a	n/a
C_6H_{14}	36.7	0.1	-5.6
C_7H_{16}	40.0	0.3	-3.4
C_8H_{18}	52.8	0.8	-0.5
C_9H_{20}	91.8	2.6	2.4
$C_{10}H_{22}$	207.8	7.8	5.3

Table B-89. Retention time, t_r, specific retention volume, V_g, and energy of adsorption, $RTLn(V_g)$, for PBT 195, at T = 313 K, F = 12.08 cm^3/min, J = 0.95, C = 0.98, P_{in} = 111.59 kPa, P_{out} = 101.25 kPa, $T_{flow\ meter}$ = 294 K.

Probe molecule	t_r (s)	V_g (cm^3/g)	$RTLn(V_g)$ (kJ/mol)
CH_4	34.2	n/a	n/a
C_6H_{14}	36.0	0.1	-6.7
C_7H_{16}	38.8	0.2	-4.2
C_8H_{18}	47.7	0.6	-1.5
C_9H_{20}	75.8	1.8	1.5
$C_{10}H_{22}$	151.5	5.0	4.2

Table B-90. Retention time, t_r, specific retention volume, V_g, and energy of adsorption, $RTLn(V_g)$, for PBT 195, at T = 318 K, F = 11.97 cm^3/min, J = 0.95, C = 0.97, P_{in} = 111.59 kPa, P_{out} = 101.25 kPa, $T_{flow\ meter}$ = 295 K.

Probe molecule	t_r (s)	V_g (cm^3/g)	$RTLn(V_g)$ (kJ/mol)
CH_4	37.5	n/a	n/a
C_7H_{16}	41.0	0.2	-5.1
C_8H_{18}	45.2	0.3	-3.0
C_9H_{20}	66.3	1.2	0.5
$C_{10}H_{22}$	120.7	3.5	3.3

B.5.3. Determination of the Energy, the Enthalpy and the Entropy of Adsorption of Polar Probes

Table B-91. Retention time, t_r, specific retention volume, V_g, energy of adsorption, $RTLn(V_g)$, and corresponding dispersive and specific components, $RTln(V^d_{g,ref})$ and $RTln(V^s_g)$, respectively, for PBT 195, at T = 303 K, F = 12.49 cm^3/min, J = 0.95, C = 0.97, P_{in} = 111.59 kPa, P_{out} = 101.25 kPa, $T_{flow\ meter}$ = 296 K.

Probe molecule	t_r (s)	V_g (cm^3/g)	$RTLn(V_g)$ (kJ/mol)	$RT\ln\left(V^d_{g,ref}\right)$ (kJ/mol)	$RT\ln\left(V^s_g\right)$ (kJ/mol)
CH_4	34.5	n/a	n/a	n/a	n/a
TCM	87.7	2.3	2.1	-4.9	7.1
DCM	113.7	3.5	3.1	-9.6	12.9
DEE	40.4	0.3	-3.4	-8.2	4.8
Acet	65.0	1.3	0.7	-8.9	9.7
THF*	54.3	0.9	-0.3	-5.8	5.4
EtAcet	70.8	1.6	1.2	-7.2	8.4

Table B-92. Retention time, t_r, specific retention volume, V_g, energy of adsorption, RTLn(V_g), and corresponding dispersive and specific components, RTln($V^d_{g,ref}$) and RTln(V^s_g), respectively, for PBT 195, at T = 308 K, F = 12.14 cm^3/min, J = 0.95, C = 0.98, P_{in} = 111.58 kPa, P_{out} = 101.24 kPa, $T_{flow\ meter}$ = 293 K.

Probe molecule	t_r (s)	V_g (cm^3/g)	RTLn(V_g) (kJ/mol)	$RT\ln\left(V^d_{g,ref}\right)$ (kJ/mol)	$RT\ln\left(V^s_g\right)$ (kJ/mol)
CH_4	34.3	n/a	n/a	n/a	n/a
TCM	85.3	2.2	2.0	-5.7	7.7
DCM	107.3	3.1	2.9	-10.2	13.1
DEE	39.7	0.2	-3.8	-8.9	5.1
Acet	60.5	1.1	0.3	-9.6	9.9
THF*	52.7	0.8	-0.6	-6.5	5.9
EtAcet	69.0	1.5	1.0	-7.9	8.9

Table B-93. Retention time, t_r, specific retention volume, V_g, energy of adsorption, RTLn(V_g), and corresponding dispersive and specific components, RTln($V^d_{g,ref}$) and RTln(V^s_g), respectively, for PBT 195, at T = 313 K, F = 13.14 cm^3/min, J = 0.95, C = 0.97, P_{in} = 111.59 kPa, P_{out} = 101.25 kPa, $T_{flow\ meter}$ = 295 K.

Probe molecule	t_r (s)	V_g (cm^3/g)	RTLn(V_g) (kJ/mol)	$RT\ln\left(V^d_{g,ref}\right)$ (kJ/mol)	$RT\ln\left(V^s_g\right)$ (kJ/mol)
CH_4	34.2	n/a	n/a	n/a	n/a
TCM	80.3	2.1	2.0	-6.6	8.5
DCM	99.3	3.0	2.9	-11.1	14.0
DEE	38.8	0.2	-4.0	-9.8	5.8
Acet	59.3	1.2	0.4	-10.5	10.9
THF*	52.2	0.8	-0.5	-74.1	6.9
EtAcet	67.0	1.5	1.1	-8.8	9.9

Table B-94. Retention time, t_r, specific retention volume, V_g, energy of adsorption, RTLn(V_g), and corresponding dispersive and specific components, RTln($V^d_{g,ref}$) and RTln(V^s_g), respectively, for PBT 195, at T = 318 K, F = 12.41 cm^3/min, J = 0.95, C = 0.97, P_{in} = 111.59 kPa, P_{out} = 101.25 kPa, $T_{flow\ meter}$ = 296 K.

Probe molecule	t_r (s)	V_g (cm^3/g)	RTLn(V_g) (kJ/mol)	$RT\ln\left(V^d_{g,ref}\right)$ (kJ/mol)	$RT\ln\left(V^s_g\right)$ (kJ/mol)
CH_4	35.5	n/a	n/a	n/a	n/a
TCM	84.3	2.1	2.0	-8.0	10.0
DCM	100.0	2.8	2.7	-12.7	15.5
DEE	39.5	0.2	-4.6	-11.4	6.8
Acet	58.2	1.0	-0.03	-12.1	12.1
THF*	56.5	0.9	-0.2	-8.9	8.6
EtAcet	75.7	1.8	1.5	-10.3	11.8

B.5.4. Determination of the Energy, the Enthalpy, and the Entropy of Adsorption on the Bulk PBT 195

Table B-95. Retention time, t_r, specific retention volume, V_g, and energy of adsorption, $RTLn(V_g)$ of $C_8\ H_{18}$ on the bulk PBT 195, at T = 353 K, F = 7.79 cm^3/min, J = 0.98, C = 0.98, P_{in} = 104.69 kPa, P_{out} = 101.35 kPa, $T_{flow\ meter}$ = 295 K.

Probe molecule	t_r (s)	V_g (cm^3/g)	$RTLn(V_g)$ (kJ/mol)
CH_4	45.3	n/a	n/a
$C_8\ H_{18}$	68.2	0.7	-1.3

Table B-96. Retention time, t_r, specific retention volume, V_g, and energy of adsorption, $RTLn(V_g)$ of $C_8\ H_{18}$ on the bulk PBT 195, at T = 353 K, F = 10.16 cm^3/min, J = 0.97, C = 0.98, P_{in} = 108.14 kPa, P_{out} = 101.35 kPa, $T_{flow\ meter}$ = 294 K.

Probe molecule	t_r (s)	V_g (cm^3/g)	$RTLn(V_g)$ (kJ/mol)
CH_4	35.7	n/a	n/a
$C_8\ H_{18}$	46.5	0.4	-2.7

Table B-97. Retention time, t_r, specific retention volume, V_g, and energy of adsorption, $RTLn(V_g)$ of $C_8\ H_{18}$ on the bulk PBT 195, at T = 353 K, F = 13.57 cm^3/min, J = 0.95, C = 0.98, P_{in} = 111.59 kPa, P_{out} = 101.25 kPa, $T_{flow\ meter}$ = 296 K.

Probe molecule	t_r (s)	V_g (cm^3/g)	$RTLn(V_g)$ (kJ/mol)
CH_4	24.5	n/a	n/a
$C_8\ H_{18}$	29.5	0.2	-4.2

Table B-98. Retention time, t_r, specific retention volume, V_g, and energy of adsorption, $RTLn(V_g)$ of $C_8\ H_{18}$ on the bulk PBT 195, at T = 353 K, F = 15.34 cm^3/min, J = 0.95, C = 0.98, P_{in} = 111.59 kPa, P_{out} = 101.25 kPa, $T_{flow\ meter}$ = 295 K.

Probe molecule	t_r (s)	V_g (cm^3/g)	$RTLn(V_g)$ (kJ/mol)
CH_4	23.3	n/a	n/a
$C_8\ H_{18}$	26.2	0.2	-5.5

Table B-99. Retention time, t_r, specific retention volume, V_g, and energy of adsorption, $RTLn(V_g)$ of polar probes on the bulk PBT 195, at T = 353 K, F = 7.92 cm^3/min, J = 0.98, C = 0.97, P_{in} = 104.70 kPa, P_{out} = 101.25 kPa, $T_{flow\ meter}$ = 297 K.

Probe molecule	t_r (s)	V_g (cm^3/g)	$RTLn(V_g)$ (kJ/mol)
CH_4	44.7	n/a	n/a
DCM	212.5	4.8	4.6
DEE	67.8	0.7	-1.2
Acet	131.7	2.5	2.7
EtAcet	166.7	3.5	3.7

Table B-100. Retention time, t_r, specific retention volume, V_g, and energy of adsorption, $RTLn(V_g)$ of polar probes on the bulk PBT 195, at T = 353 K, F = 10.58 cm^3/min, J = 0.96, C = 0.97, P_{in} = 109.87 kPa, P_{out} = 101.25 kPa, $T_{flow\ meter}$ = 296 K.

Probe molecule	t_r (s)	V_g (cm^3/g)	$RTLn(V_g)$ (kJ/mol)
CH_4	33.8	n/a	n/a
DCM	152.3	4.5	4.4
DEE	36.8	0.1	-6.4
Acet	89.8	2.1	2.2
EtAcet	108.3	2.8	3.0

Table B-101. Retention time, t_r, specific retention volume, V_g, and energy of adsorption, $RTLn(V_g)$ of polar probes on the bulk PBT 195, at T = 353 K, F = 13.33 cm^3/min, J = 0.95, C = 0.97, P_{in} = 111.59 kPa, P_{out} = 101.25 kPa, $T_{flow\ meter}$ = 297 K.

Probe molecule	t_r (s)	V_g (cm^3/g)	$RTLn(V_g)$ (kJ/mol)
CH_4	26.7	n/a	n/a
DCM	104.2	3.6	3.8
DEE	29.0	0.1	-6.5
Acet	70.0	2.0	2.1
EtAcet	86.2	2.8	3.0

Table B-102. Retention time, t_r, specific retention volume, V_g, and energy of adsorption, RTLn(V_g), for PBT 195, at T = 353 K, F = 7.66 cm^3/min, J = 0.97, C = 0.97, P_{in} = 108.24 kPa, P_{out} = 101.35 kPa, $T_{flow\ meter}$ = 296 K.

Probe molecule	t_r (s)	V_g (cm^3/g)	RTLn(V_g) (kJ/mol)
CH_4	20.7	n/a	n/a
TCM	194.2	4.8	4.6
THF	141.7	3.3	3.5

Table B-103. Retention time, t_r, specific retention volume, V_g, and energy of adsorption, RTLn(V_g), for PBT 195, at T = 353 K, F = 9.66 cm^3/min, J = 0.95, C = 0.97, P_{in} = 111.69 kPa, P_{out} = 101.35 kPa, $T_{flow\ meter}$ = 296 K.

Probe molecule	t_r (s)	V_g (cm^3/g)	RTLn(V_g) (kJ/mol)
CH_4	38.0	n/a	n/a
TCM	135.0	3.3	3.5
THF*	95.0	2.1	2.2

* F = 10.35 cm^3/min, J = 0.95, C = 0.98, P_{in} = 111.69 kPa, P_{out} = 101.34 kPa, $T_{flow\ meter}$ = 294 K, $t_{r\ (methane)}$ = 37.0 s

Table B-104. Retention time, t_r, specific retention volume, V_g, and energy of adsorption, RTLn(V_g), for PBT 195, at T = 353 K, F = 13.54 cm^3/min, J = 0.95, C = 0.97, P_{in} = 111.69 kPa, P_{out} = 101.35 kPa, $T_{flow\ meter}$ = 296 K.

Probe molecule	t_r (s)	V_g (cm^3/g)	RTLn(V_g) (kJ/mol)
CH_4	26.0	n/a	n/a
TCM	90.0	3.1	3.3
THF	52.5	1.3	0.7

Table B-105. Retention time, t_r, specific retention volume, V_g, and energy of adsorption, RTLn(V_g), for PBT 195, at T = 353 K, F = 21.00 cm^3/min, J = 0.94, C = 0.98, P_{in} = 113.41 kPa, P_{out} = 101.34 kPa, $T_{flow\ meter}$ = 294 K.

Probe molecule	t_r (s)	V_g (cm^3/g)	RTLn(V_g) (kJ/mol)
CH_4	17.0	n/a	n/a
TCM	37.3	1.5	1.2
THF	31.0	1.0	0.1

Table B-106. Retention time, t_r, specific retention volume, V_g, and energy of adsorption, $RTLn(V_g)$, for PBT 195, at T = 353 K, F = 24.23 cm^3/min, J = 0.94, C = 0.97, P_{in} = 115.14 kPa, P_{out} = 101.35 kPa, $T_{flow\ meter}$ = 297 K.

Probe molecule	t_r (s)	V_g (cm^3/g)	$RTLn(V_g)$ (kJ/mol)
CH_4	15.2	n/a	n/a
TCM	33.2	1.5	1.2
THF	23.0	0.7	-1.2

Table B-107. Retention time, t_r, specific retention volume, V_g, and energy of adsorption, $RTLn(V_g)$, for PBT 195, at T = 353 K, F = 29.13 cm^3/min, J = 0.92, C = 0.97, P_{in} = 118.59 kPa, P_{out} = 101.35 kPa, $T_{flow\ meter}$ = 297 K.

Probe molecule	t_r (s)	V_g (cm^3/g)	$RTLn(V_g)$ (kJ/mol)
CH_4	13.0	n/a	n/a
TCM	22.3	0.9	-0.2
THF	18.3	0.5	-1.9

Table B-108. Retention time, t_r, specific retention volume, V_g, and energy of adsorption, $RTLn(V_g)$, for PBT 195, at T = 373 K, F = 7.02 cm^3/min, J = 0.97, C = 0.97, P_{in} = 108.25 kPa, P_{out} = 101.35 kPa, $T_{flow\ meter}$ = 298 K.

Probe molecule	t_r (s)	V_g (cm^3/g)	$RTLn(V_g)$ (kJ/mol)
CH_4	48.8	n/a	n/a
TCM	266.7	5.5	5.3
THF	195.8	3.7	4.0

Table B-109. Retention time, t_r, specific retention volume, V_g, and energy of adsorption, $RTLn(V_g)$, for PBT 195, at T = 373 K, F = 9.90 cm^3/min, J = 0.97, C = 0.97, P_{in} = 108.24 kPa, P_{out} = 101.35 kPa, $T_{flow\ meter}$ = 295 K.

Probe molecule	t_r (s)	V_g (cm^3/g)	$RTLn(V_g)$ (kJ/mol)
CH_4	33.0	n/a	n/a
TCM	173.3	5.0	5.0
THF	131.7	3.5	3.9

Table B-110. Retention time, t_r, specific retention volume, V_g, and energy of adsorption, RTLn(V_g), for PBT 195, at T = 373 K, F = 14.68 cm^3/min, J = 0.95, C = 0.97, P_{in} = 111.69 kPa, P_{out} = 101.35 kPa, $T_{flow\ meter}$ = 297 K.

Probe molecule	t_r (s)	V_g (cm^3/g)	RTLn(V_g) (kJ/mol)
CH_4	23.2	n/a	n/a
TCM	109.7	4.5	4.6
THF	83.5	3.1	3.5

Table B-111. Retention time, t_r, specific retention volume, V_g, and energy of adsorption, RTLn(V_g), for PBT 195, at T = 373 K, F = 20.71 cm^3/min, J = 0.94, C = 0.97, P_{in} = 115.14 kPa, P_{out} = 101.35 kPa, $T_{flow\ meter}$ = 298 K.

Probe molecule	t_r (s)	V_g (cm^3/g)	RTLn(V_g) (kJ/mol)
CH_4	16.1	n/a	n/a
TCM	58.0	3.0	3.4
THF	43.3	1.9	2.1

Table B-112. Retention time, t_r, specific retention volume, V_g, and energy of adsorption, RTLn(V_g), for PBT 195, at T = 373 K, F = 23.69 cm^3/min, J = 0.94, C = 0.97, P_{in} = 115.14 kPa, P_{out} = 101.35 kPa, $T_{flow\ meter}$ = 298 K.

Probe molecule	t_r (s)	V_g (cm^3/g)	RTLn(V_g) (kJ/mol)
CH_4	14.3	n/a	n/a
TCM	42.5	2.3	2.6
THF	34.3	1.6	1.5

Table B-113. Retention time, t_r, specific retention volume, V_g, and energy of adsorption, RTLn(V_g), for PBT 195, at T = 373 K, F = 29.41 cm^3/min, J = 0.92, C = 0.97, P_{in} = 118.59 kPa, P_{out} = 101.35 kPa, $T_{flow\ meter}$ = 298 K.

Probe molecule	t_r (s)	V_g (cm^3/g)	RTLn(V_g) (kJ/mol)
CH_4	12.4	n/a	n/a
TCM	30.2	1.8	1.8
THF	25.5	1.3	0.8

Table B-114. Retention time, t_r, specific retention volume, V_g, and energy of adsorption, RTLn(V_g), for PBT 195, at T = 393 K, F = 5.40 cm^3/min, J = 0.98, C = 0.97, P_{in} = 104.80 kPa, P_{out} = 101.35 kPa, $T_{flow\ meter}$ = 297 K.

Probe molecule	t_r (s)	V_g (cm^3/g)	RTLn(V_g) (kJ/mol)
CH_4	48.3	n/a	n/a
TCM	383.3	6.6	6.2
THF	305.8	5.1	5.3

Table B-115. Retention time, t_r, specific retention volume, V_g, and energy of adsorption, RTLn(V_g), for PBT 195, at T = 393 K, F = 10.01 cm^3/min, J = 0.95, C = 0.97, P_{in} = 111.69 kPa, P_{out} = 101.35 kPa, $T_{flow\ meter}$ = 296 K.

Probe molecule	t_r (s)	V_g (cm^3/g)	RTLn(V_g) (kJ/mol)
CH_4	2.8	n/a	n/a
TCM	4.3	5.5	5.6
THF	2.9	4.4	4.8

Table B-116. Retention time, t_r, specific retention volume, V_g, and energy of adsorption, RTLn(V_g), for PBT 195, at T = 393 K, F = 13.72 cm^3/min, J = 0.94, C = 0.97, P_{in} = 115.14 kPa, P_{out} = 101.35 kPa, $T_{flow\ meter}$ = 297 K.

Probe molecule	t_r (s)	V_g (cm^3/g)	RTLn(V_g) (kJ/mol)
CH_4	21.5	n/a	n/a
TCM	131.7	5.2	5.4
THF	109.2	4.2	4.7

B.6. IGC Study of the PBT 315

B.6.1. Determination of the Dispersive Component of the Surface Tension

Table B-117. Retention time, t_r, specific retention volume, V_g, and energy of adsorption, RTLn(V_g), of the n-alkanes on the surface of PBT 315, at T = 298 K, F = 12.25 cm^3/min, J = 0.97, C = 0.98, P_{in} = 108.13 kPa, P_{out} = 101.24 kPa, and $T_{flow\ meter}$ = 292 K.

Probe molecule	t_r (s)	V_g (cm^3/g)	RTLn(V_g) (kJ/mol)
CH_4	38.0	n/a	n/a
C_7H_{16}	49.2	0.5	-2.0
C_8H_{18}	69.2	1.3	0.6
C_9H_{20}	144.2	4.3	3.6
$C_{10}H_{22}$	389.5	14.1	6.5

Table B-118. Retention time, t_r, specific retention volume, V_g, and energy of adsorption, RTLn(V_g), for PBT 315, at T = 303 K, F = 12.75 cm^3/min, J = 0.97, C = 0.98, P_{in} = 108.14 kPa, P_{out} = 101.25 kPa, $T_{flow\ meter}$ = 294 K.

Probe molecule	t_r (s)	V_g (cm^3/g)	RTLn(V_g) (kJ/mol)
CH_4	36.7	n/a	n/a
C_7H_{16}	46.0	0.4	-2.4
C_8H_{18}	59.0	0.9	-0.2
C_9H_{20}	109.7	3.1	2.8
$C_{10}H_{22}$	250.0	8.9	5.5
$C_{11}H_{24}$	720.0	28.6	8.5

Table B-119. Retention time, t_r, specific retention volume, V_g, and energy of adsorption, RTLn(V_g), for PBT 315, at T = 308 K, F = 12.46 cm^3/min, J = 0.97, C = 0.98, P_{in} = 108.14 kPa, P_{out} = 101.24 kPa, $T_{flow\ meter}$ = 293 K.

Probe molecule	t_r (s)	V_g (cm^3/g)	RTLn(V_g) (kJ/mol)
CH_4	35.5	n/a	n/a
C_8H_{18}	51.0	0.6	-1.2
C_9H_{20}	92.0	2.3	2.2
$C_{10}H_{22}$	181.7	6.0	4.6
$C_{11}H_{24}$	478.0	18.11	7.4

Table B-120. Retention time, t_r, specific retention volume, V_g, and energy of adsorption, RTLn(V_g), for PBT 315, at T = 313 K, F = 10.84 cm^3/min, J = 0.97, C = 0.98, P_{in} = 107.45 kPa, P_{out} = 101.25 kPa, $T_{flow\ meter}$ = 294 K.

Probe molecule	t_r (s)	V_g (cm^3/g)	RTLn(V_g) (kJ/mol)
CH_4	40.2	n/a	n/a
C_8H_{18}	56.5	0.6	-1.4
C_9H_{20}	91.2	1.8	1.6
$C_{10}H_{22}$	174.0	4.8	4.1
$C_{11}H_{24}$	428.2	13.9	6.9

Table B-121. Retention time, t_r, specific retention volume, V_g, and energy of adsorption, $RTLn(V_g)$, for PBT 315, at T = 318 K, F = 9.61 cm^3/min, J = 0.98, C = 0.98, P_{in} = 106.08 kPa, P_{out} = 101.25 kPa, $T_{flow\ meter}$ = 296 K.

Probe molecule	t_r (s)	V_g (cm^3/g)	$RTLn(V_g)$ (kJ/mol)
CH_4	45.2	n/a	n/a
C_8H_{18}	56.8	0.4	-2.6
C_9H_{20}	84.3	1.3	0.6
$C_{10}H_{22}$	141.0	3.1	3.0
$C_{11}H_{24}$	322.0	8.8	5.8

B.6.2. Determination of the Energy, the Enthalpy and the Entropy of Adsorption of Polar Probes

Table B-122. Retention time, t_r, specific retention volume, V_g, energy of adsorption, $RTLn(V_g)$, and corresponding dispersive and specific components, $RTln(V^d_{g,ref})$ and $RTln(V^s_g)$, respectively, for PBT 315, at T = 303 K, F = 12.77 cm^3/min, J = 0.97, C = 0.97, P_{in} = 108.14 kPa, P_{out} = 101.25 kPa, $T_{flow\ meter}$ = 295 K.

Probe molecule	t_r (s)	V_g (cm^3/g)	$RTLn(V_g)$ (kJ/mol)	$RT\ln(V^d_{g,ref})$ (kJ/mol)	$RT\ln(V^s_g)$ (kJ/mol)
CH_4	34.7	n/a	n/a	n/a	n/a
TCM	63.2	1.2	0.5	-5.1	5.6
DCM	95.0	2.5	2.4	-9.7	12.0
Acet	63.5	1.2	0.5	-9.0	9.5
THF	52.8	0.8	-0.7	-6.0	5.3
EtAcet	75.0	1.7	1.3	-7.4	8.7

Table B-123. Retention time, t_r, specific retention volume, V_g, energy of adsorption, $RTLn(V_g)$, and corresponding dispersive and specific components, $RTln(V^d_{g,ref})$ and $RTln(V^s_g)$, respectively, for PBT 315, at T = 308 K, F = 12.61 cm^3/min, J = 0.97, C = 0.98, P_{in} = 108.14 kPa, P_{out} = 101.25 kPa, $T_{flow\ meter}$ = 295 K.

Probe molecule	t_r (s)	V_g (cm^3/g)	$RTLn(V_g)$ (kJ/mol)	$RT\ln(V^d_{g,ref})$ (kJ/mol)	$RT\ln(V^s_g)$ (kJ/mol)
CH_4	35.5	n/a	n/a	n/a	n/a
TCM	64.3	1.2	0.5	-6.3	6.8
DCM	97.8	2.6	2.4	-11.0	13.4
Acet	59.3	1.0	-0.024	-10.4	10.3
THF*	49.5	0.6	-1.4	-7.2	5.8
EtAcet*	67.8	1.3	0.8	-8.6	9.4

* F = 12.46 cm^3/min, J = 0.97, C = 0.98, P_{in} = 108.14 kPa, P_{out} = 101.24 kPa, $T_{flow\ meter}$ = 293 K, $t_{r\ (methane)}$ = 35.2 s

Table B-124. Retention time, t_r, specific retention volume, V_g, energy of adsorption, RTLn(V_g), and corresponding dispersive and specific components, RTln($V^d_{g,ref}$) and RTln(V^s_g), respectively, for PBT 315, at T = 313 K, F = 12.89 cm^3/min, J = 0.97, C = 0.98, P_{in} = 108.13 kPa, P_{out} = 101.24 kPa, $T_{flow\ meter}$ = 292 K.

Probe molecule	t_r (s)	V_g (cm^3/g)	RTLn(V_g) (kJ/mol)	$RT\ln\left(V^d_{g,ref}\right)$ (kJ/mol)	$RT\ln\left(V^s_g\right)$ (kJ/mol)
CH_4	33.2	n/a	n/a	n/a	n/a
TCM	66.3	1.4	0.9	-6.5	7.4
DCM	91.0	2.5	2.4	-11.0	13.3
Acet	58.3	1.1	0.2	-10.4	10.5
THF*	47.0	0.6	-1.4	-7.3	5.9
EtAcet	64.7	1.3	0.8	-8.7	9.5

Table B-125. Retention time, t_r, specific retention volume, V_g, energy of adsorption, RTLn(V_g), and corresponding dispersive and specific components, RTln($V^d_{g,ref}$) and RTln(V^s_g), respectively, for PBT 315, at T = 318 K, F = 13.13 cm^3/min, J = 0.97, C = 0.98, P_{in} = 108.14 kPa, P_{out} = 101.24 kPa, $T_{flow\ meter}$ = 293 K.

Probe molecule	t_r (s)	V_g (cm^3/g)	RTLn(V_g) (kJ/mol)	$RT\ln\left(V^d_{g,ref}\right)$ (kJ/mol)	$RT\ln\left(V^s_g\right)$ (kJ/mol)
CH_4	32.8	n/a	n/a	n/a	n/a
TCM	63.0	1.3	0.7	-7.7	8.4
DCM	79.0	2.0	1.8	-12.2	14.0
Acet	55.2	1.0	-0.08	-11.6	11.5
THF*	47.2	0.6	-1.2	-8.5	7.3
EtAcet	58.3	1.1	0.3	-9.9	10.2

B.7. IGC Study of the Pigment Hiwre

B.7.1. Determination of the Dispersive Component of the Surface Tension

Table B-126. Retention time, t_r, specific retention volume, V_g, and energy of adsorption, RTLn(V_g), for the surface-modified pigment (hiwre), at T = 323 K, F = 90.46 cm^3/min, J = 0.78, C = 0.98, P_{in} = 154.68 kPa, P_{out} = 101.25 kPa, $T_{flow\ meter}$ = 294 K.

Probe molecule	t_r (s)	V_g (cm^3/g)	RTLn(V_g) (kJ/mol)
CH_4	11.5	n/a	n/a
C_8H_{18}	65.3	414.6	16.2
C_9H_{20}	168.7	1210.5	19.1
$C_{10}H_{22}$	525.0	3954.9	22.3

Table B-127. Retention time, t_r, specific retention volume, V_g, and energy of adsorption, $RTLn(V_g)$, for the surface-modified pigment (hiwre), at T = 333 K, F = 66.67 cm^3/min, J = 0.79, C = 0.98, P_{in} = 152.96 kPa, P_{out} = 101.25 kPa, $T_{flow\ meter}$ = 294 K.

Probe molecule	t_r (s)	V_g (cm^3/g)	$RTLn(V_g)$ (kJ/mol)
CH_4	14.8	n/a	n/a
C_8H_{18}	53.0	218.8	14.9
C_9H_{20}	132.5	673.4	18.0
$C_{10}H_{22}$	366.3	2010.2	21.1

Table B-128. Retention time, t_r, specific retention volume, V_g, and energy of adsorption, $RTLn(V_g)$, for the surface-modified pigment (hiwre), at T = 343 K, F = 51.28 cm^3/min, J = 0.82, C = 0.98, P_{in} = 142.61 kPa, P_{out} = 101.25 kPa, $T_{flow\ meter}$ = 295 K.

Probe molecule	t_r (s)	V_g (cm^3/g)	$RTLn(V_g)$ (kJ/mol)
CH_4	16.3	n/a	n/a
C_8H_{18}	48.2	146.5	14.2
C_9H_{20}	112.0	440.2	17.4
$C_{10}H_{22}$	258.8	1115.5	20.0

Table B-129. Retention time, t_r, specific retention volume, V_g, and energy of adsorption, $RTLn(V_g)$, for the surface-modified pigment (hiwre), at T = 353 K, F = 47.01 cm^3/min, J = 0.82, C = 0.98, P_{in} = 142.61 kPa, P_{out} = 101.24 kPa, $T_{flow\ meter}$ = 293 K.

Probe molecule	t_r (s)	V_g (cm^3/g)	$RTLn(V_g)$ (kJ/mol)
CH_4	18.0	n/a	n/a
C_7H_{16}	26.8	37.0	10.6
C_8H_{18}	34.2	68.3	12.4
C_9H_{20}	69.2	216.3	15.8
$C_{10}H_{22}$	148.3	550.9	18.5
$C_{11}H_{24}$	380.0	1530.2	21.5

Table B-130. Retention time, t_r, specific retention volume, V_g, and energy of adsorption, $RTLn(V_g)$, for the surface-modified pigment (hiwre), at T = 363 K, F = 45.34 cm^3/min, J = 0.82, C = 0.98, P_{in} = 142.61 kPa, P_{out} = 101.24 kPa, $T_{flow\ meter}$ = 294 K.

Probe molecule	t_r (s)	V_g (cm^3/g)	$RTLn(V_g)$ (kJ/mol)
CH_4	18.0	n/a	n/a
C_8H_{18}	28.2	48.6	11.7
C_9H_{20}	50.0	137.5	14.9
$C_{10}H_{22}$	97.5	331.1	17.5
$C_{11}H_{24}$	220.0	859.3	20.4

* F = 46.75 cm^3/min, J = 0.82, C = 0.97, P_{in} = 142.62 kPa, P_{out} = 101.25 kPa, $T_{flow\ meter}$ = 295 K, $t_{r\ (methane)}$ = 15 s

Table B-131. Retention time, t_r, specific retention volume, V_g, and energy of adsorption, RTLn(V_g), for the surface-modified pigment (hiwre), at T = 373 K, F = 42.25 cm^3/min, J = 0.82, C = 0.97, P_{in} = 142.62 kPa, P_{out} = 101.25 kPa, $T_{flow\ meter}$ = 295 K.

Probe molecule	t_r (s)	V_g (cm^3/g)	RTLn(V_g) (kJ/mol)
CH_4	17.3	n/a	n/a
C_8H_{18}	25.8	31.9	10.7
C_9H_{20}	38.3	79.2	13.6
$C_{10}H_{22}$	72.5	209.0	16.6
$C_{11}H_{24}$	141.3	469.4	19.1

B.7.2. Determination of the Energy, the Enthalpy and the Entropy of Adsorption of Polar Probes

Table B-132. Retention time, t_r, specific retention volume, V_g, energy of adsorption, RTLn(V_g), and corresponding dispersive and specific components, RTln($V^d_{g,ref}$) and RTln(V^s_g), respectively, for the surface-modified pigment (hiwre), at T = 323 K, F = 22.17 cm^3/min, J = 0.90, C = 0.98, P_{in} = 120.84 kPa, P_{out} = 110.15 kPa, $T_{flow\ meter}$ = 294 K.

Probe molecule	t_r (s)	V_g (cm^3/g)	RTLn(V_g) (kJ/mol)	$RT\ln\left(V^d_{g,ref}\right)$ (kJ/mol)	$RT\ln\left(V^s_g\right)$ (kJ/mol)
CH_4	47.7	n/a	n/a	n/a	n/a
DCM	90.5	93.7	12.2	5.5	6.7

Table B-133. Retention time, t_r, specific retention volume, V_g, energy of adsorption, RTLn(V_g), and corresponding dispersive and specific components, RTln($V^d_{g,ref}$) and RTln(V^s_g), respectively, for the surface-modified pigment (hiwre), at T = 333 K, F = 22.14 cm^3/min, J = 0.90, C = 0.98, P_{in} = 120.84 kPa, P_{out} = 100.15 kPa, $T_{flow\ meter}$ = 294 K.

Probe molecule	t_r (s)	V_g (cm^3/g)	RTLn(V_g) (kJ/mol)	$RT\ln\left(V^d_{g,ref}\right)$ (kJ/mol)	$RT\ln\left(V^s_g\right)$ (kJ/mol)
CH_4	40.7	n/a	n/a	n/a	n/a
DCM	70.0	64.1	11.5	4.1	7.4

Table B-134. Retention time, t_r, specific retention volume, V_g, energy of adsorption, RTLn(V_g), and corresponding dispersive and specific components, RTln($V^d_{g,ref}$) and RTln(V^s_g), respectively, for the surface-modified pigment (hiwre), at T = 343 K, F = 17.84 cm^3/min, J = 0.93, C = 0.98, P_{in} = 113.94 kPa, P_{out} = 100.15 kPa, $T_{flow\ meter}$ = 294 K.

Probe molecule	t_r (s)	V_g (cm^3/g)	RTLn(V_g) (kJ/mol)	$RT\ln\left(V^d_{g,ref}\right)$ (kJ/mol)	$RT\ln\left(V^s_g\right)$ (kJ/mol)
CH_4	33.2	n/a	n/a	n/a	n/a
DCM	52.2	34.6	10.1	4.1	6.0

Table B-135. Retention time, t_r, specific retention volume, V_g, energy of adsorption, RTLn(V_g), and corresponding dispersive and specific components, RTln($V^d_{g,ref}$) and RTln(V^s_g), respectively, for the surface-modified pigment (hiwre), at T = 333 K, F = 100.00 cm^3/min, J = 0.76, C = 0.97, P_{in} = 158.76 kPa, P_{out} = 100.16 kPa, $T_{flow\ meter}$ = 295 K.

Probe molecule	t_r (s)	V_g (cm^3/g)	RTLn(V_g) (kJ/mol)	$RT\ln\left(V^d_{g,ref}\right)$ (kJ/mol)	$RT\ln\left(V^s_g\right)$ (kJ/mol)
CH_4	10.2	n/a	n/a	n/a	n/a
THF	895.0	7334.7	24.7	8.2	16.4

Table B-136. Retention time, t_r, specific retention volume, V_g, energy of adsorption, RTLn(V_g), and corresponding dispersive and specific components, RTln($V^d_{g,ref}$) and RTln(V^s_g), respectively, for the surface-modified pigment (hiwre), at T = 343 K, F = 86.14 cm^3/min, J = 0.77, C = 0.97, P_{in} = 157.04 kPa, P_{out} = 100.16 kPa, $T_{flow\ meter}$ = 295 K.

Probe molecule	t_r (s)	V_g (cm^3/g)	RTLn(V_g) (kJ/mol)	$RT\ln\left(V^d_{g,ref}\right)$ (kJ/mol)	$RT\ln\left(V^s_g\right)$ (kJ/mol)
CH_4	12.2	n/a	n/a	n/a	n/a
THF	603.3	4252.8	23.8	8.0	15.9

Table B-137. Retention time, t_r, specific retention volume, V_g, energy of adsorption, RTLn(V_g), and corresponding dispersive and specific components, RTln($V^d_{g,ref}$) and RTln(V^s_g), respectively, for the surface-modified pigment (hiwre), at T = 363 K, F = 62.72 cm^3/min, J = 0.80, C = 0.98, P_{in} = 146.69 kPa, P_{out} = 100.15 kPa, $T_{flow\ meter}$ = 295 K.

Probe molecule	t_r (s)	V_g (cm^3/g)	RTLn(V_g) (kJ/mol)	$RT\ln\left(V^d_{g,ref}\right)$ (kJ/mol)	$RT\ln\left(V^s_g\right)$ (kJ/mol)
CH_4	12.2	n/a	n/a	n/a	n/a
THF	265.0	1387.0	16.4	5.5	10.9

Table B-138. Retention time, t_r, specific retention volume, V_g, energy of adsorption, RTLn(V_g), and corresponding dispersive and specific components, RTln($V^d_{g,ref}$) and RTln(V^s_g), respectively, for the surface-modified pigment (hiwre), at T = 373 K, F = 62.29 cm^3/min, J = 0.80, C = 0.98, P_{in} = 148.42 kPa, P_{out} = 100.15 kPa, $T_{flow\ meter}$ = 295 K.

Probe molecule	t_r (s)	V_g (cm^3/g)	RTLn(V_g) (kJ/mol)	$RT\ln\left(V^d_{g,ref}\right)$ (kJ/mol)	$RT\ln\left(V^s_g\right)$ (kJ/mol)
CH_4	14.7	n/a	n/a	n/a	n/a
THF	160.5	788.4	15.1	4.6	10.5

B.8. IGC Study of the Pigment Hiwren

B.8.1. Determination of the Dispersive Component of the Surface Tension

Table B-139. Retention time, t_r, specific retention volume, V_g, and energy of adsorption, $RTLn(V_g)$, for the surface-modified pigment (hiwren), at T = 323 K, F = 86.13 cm^3/min, J = 0.80, C = 0.98, P_{in} = 149.51 kPa, P_{out} = 101.25 kPa, $T_{flow\ meter}$ = 294 K.

Probe molecule	t_r (s)	V_g (cm^3/g)	$RTLn(V_g)$ (kJ/mol)
CH_4	15.3	n/a	n/a
C_7H_{16}	26.3	101.6	12.4
C_8H_{18}	47.0	292.5	15.3
C_9H_{20}	125.7	1019.1	18.6
$C_{10}H_{22}$	275.3	2401.5	20.9

Table B-140. Retention time, t_r, specific retention volume, V_g, and energy of adsorption, $RTLn(V_g)$, for the surface-modified pigment (hiwren), at T = 333 K, F = 91.38 cm^3/min, J = 0.79, C = 0.98, P_{in} = 151.23 kPa, P_{out} = 101.25 kPa, $T_{flow\ meter}$ = 294 K.

Probe molecule	t_r (s)	V_g (cm^3/g)	$RTLn(V_g)$ (kJ/mol)
CH_4	14.7	n/a	n/a
C_7H_{16}	22.5	76.2	12.0
C_8H_{18}	37.3	219.6	14.9
C_9H_{20}	73.5	572.2	17.6
$C_{10}H_{22}$	177.5	1583.6	20.4

Table B-141. Retention time, t_r, specific retention volume, V_g, and energy of adsorption, $RTLn(V_g)$, for the surface-modified pigment (hiwren), at T = 343 K, F = 51.87 cm^3/min, J = 0.86, C = 0.98, P_{in} = 134.00 kPa, P_{out} = 101.25 kPa, $T_{flow\ meter}$ = 295 K.

Probe molecule	t_r (s)	V_g (cm^3/g)	$RTLn(V_g)$ (kJ/mol)
CH_4	17.0	n/a	n/a
C_7H_{16}	25.7	51.7	11.3
C_8H_{18}	45.3	168.4	14.6
C_9H_{20}	77.0	357.6	16.8
$C_{10}H_{22}$	167.5	897.0	19.4

Table B-142. Retention time, t_r, specific retention volume, V_g, and energy of adsorption, $RTLn(V_g)$, for the surface-modified pigment (hiwren), at T = 353 K, F = 52.17 cm^3/min, J = 0.85, C = 0.98, P_{in} = 135.72 kPa, P_{out} = 101.25 kPa, $T_{flow\ meter}$ = 295 K.

Probe molecule	t_r (s)	V_g (cm^3/g)	$RTLn(V_g)$ (kJ/mol)
CH_4	16.5	n/a	n/a
C_8H_{18}	30.2	81.3	12.9
C_9H_{20}	52.2	212.1	15.7
$C_{10}H_{22}$	100.8	501.6	18.3
$C_{11}H_{24}$	241.7	1339.1	21.1

Table B-143. Retention time, t_r, specific retention volume, V_g, and energy of adsorption, $RTLn(V_g)$, for the surface-modified pigment (hiwren), at T = 363 K, F = 52.17 cm^3/min, J = 0.85, C = 0.98, P_{in} = 135.72 kPa, P_{out} = 101.25 kPa, $T_{flow\ meter}$ = 295 K.

Probe molecule	t_r (s)	V_g (cm^3/g)	$RTLn(V_g)$ (kJ/mol)
CH_4	16.5	n/a	n/a
C_8H_{18}	25.0	50.6	11.8
C_9H_{20}	41.8	150.2	15.1
$C_{10}H_{22}$	72.5	333.1	17.5
$C_{11}H_{24}$	140.0	734.5	19.9

B.8.2. Determination of the Energy, the Enthalpy and the Entropy of Adsorption of Polar Probes

Table B-144. Retention time, t_r, specific retention volume, V_g, energy of adsorption, $RTLn(V_g)$, and corresponding dispersive and specific components, $RTln(V^d_{g,ref})$ and $RTln(V^s_g)$, respectively, for the surface-modified pigment (hiwren), at T = 323 K, F = 27.40 cm^3/min, J = 0.92, C = 0.98, P_{in} = 117.39 kPa, P_{out} = 100.15 kPa, $T_{flow\ meter}$ = 294 K.

Probe molecule	t_r (s)	V_g (cm^3/g)	$RTLn(V_g)$ (kJ/mol)	$RT\ln\left(V^d_{g,ref}\right)$ (kJ/mol)	$RT\ln\left(V^s_g\right)$ (kJ/mol)
CH_4	27.0	n/a	n/a	n/a	n/a
DCM	45.5	62.6	11.1	5.0	6.1

Table B-145. Retention time, t_r, specific retention volume, V_g, energy of adsorption, $RTLn(V_g)$, and corresponding dispersive and specific components, $RTln(V^d_{g,ref})$ and $RTln(V^s_g)$, respectively, for the surface-modified pigment (hiwren), at T = 323 K, F = 91.38 cm^3/min, J = 0.79, C = 0.98, P_{in} = 150.14 kPa, P_{out} = 100.15 kPa, $T_{flow\ meter}$ = 295 K.

Probe molecule	t_r (s)	V_g (cm^3/g)	$RTLn(V_g)$ (kJ/mol)	$RT\ln\left(V^d_{g,ref}\right)$ (kJ/mol)	$RT\ln\left(V^s_g\right)$ (kJ/mol)
CH_4	11.7	n/a	n/a	n/a	n/a
THF	718.3	6849.0	23.7	8.9	14.8

Table B-146. Retention time, t_r, specific retention volume, V_g, energy of adsorption, RTLn(V_g), and corresponding dispersive and specific components, RTln($V^d_{g,ref}$) and RTln(V^s_g), respectively, for the surface-modified pigment (hiwren), at T = 333 K, F = 23.87 cm^3/min, J = 0.92, C = 0.98, P_{in} = 117.39 kPa, P_{out} = 100.15 kPa, $T_{flow\ meter}$ = 294 K.

Probe molecule	t_r (s)	V_g (cm^3/g)	RTLn(V_g) (kJ/mol)	$RT\ln\left(V^d_{g,ref}\right)$ (kJ/mol)	$RT\ln\left(V^s_g\right)$ (kJ/mol)
CH_4	28.0	n/a	n/a	n/a	n/a
DCM	40.7	37.4	10.0	4.9	5.1

Table B-147. Retention time, t_r, specific retention volume, V_g, energy of adsorption, RTLn(V_g), and corresponding dispersive and specific components, RTln($V^d_{g,ref}$) and RTln(V^s_g), respectively, for the surface-modified pigment (hiwren), at T = 333 K, F = 86.54 cm^3/min, J = 0.78, C = 0.98, P_{in} = 151.86 kPa, P_{out} = 100.15 kPa, $T_{flow\ meter}$ = 294 K.

Probe molecule	t_r (s)	V_g (cm^3/g)	RTLn(V_g) (kJ/mol)	$RT\ln\left(V^d_{g,ref}\right)$ (kJ/mol)	$RT\ln\left(V^s_g\right)$ (kJ/mol)
CH_4	12.3	n/a	n/a	n/a	n/a
THF	518.3	4616.7	23.4	8.7	14.7

Table B-148. Retention time, t_r, specific retention volume, V_g, energy of adsorption, RTLn(V_g), and corresponding dispersive and specific components, RTln($V^d_{g,ref}$) and RTln(V^s_g), respectively, for the surface-modified pigment (hiwren), at T = 343 K, F = 18.91 cm^3/min, J = 0.93, C = 0.98, P_{in} = 113.94 kPa, P_{out} = 100.15 kPa, $T_{flow\ meter}$ = 295 K.

Probe molecule	t_r (s)	V_g (cm^3/g)	RTLn(V_g) (kJ/mol)	$RT\ln\left(V^d_{g,ref}\right)$ (kJ/mol)	$RT\ln\left(V^s_g\right)$ (kJ/mol)
CH_4	31.3	n/a	n/a	n/a	n/a
DCM	43.2	28.01	9.5	4.7	4.8

Table B-149. Retention time, t_r, specific retention volume, V_g, energy of adsorption, RTLn(V_g), and corresponding dispersive and specific components, RTln($V^d_{g,ref}$) and RTln(V^s_g), respectively, for the surface-modified pigment (hiwren), at T = 343 K, F = 78.96 cm^3/min, J = 0.79, C = 0.98, P_{in} = 150.14 kPa, P_{out} = 100.15 kPa, $T_{flow\ meter}$ = 295 K.

Probe molecule	t_r (s)	V_g (cm^3/g)	RTLn(V_g) (kJ/mol)	$RT\ln\left(V^d_{g,ref}\right)$ (kJ/mol)	$RT\ln\left(V^s_g\right)$ (kJ/mol)
CH_4	13.0	n/a	n/a	n/a	n/a
THF	236.7	1874.6	21.5	8.3	13.2

Table B-150. Retention time, t_r, specific retention volume, V_g, energy of adsorption, RTLn(V_g), and corresponding dispersive and specific components, RTln($V^d_{g,ref}$) and RTln(V^s_g), respectively, for the surface-modified pigment (hiwren), at T = 363 K, F = 77.59 cm^3/min, J = 0.78, C = 0.97, P_{in} = 151.87 kPa, P_{out} = 100.16 kPa, $T_{flow\ meter}$ = 295 K.

Probe molecule	t_r (s)	V_g (cm^3/g)	RTLn(V_g) (kJ/mol)	$RT\ln\left(V^d_{g,ref}\right)$ (kJ/mol)	$RT\ln\left(V^s_g\right)$ (kJ/mol)
CH_4	14.2	n/a	n/a	n/a	n/a
THF	98.3	686.9	19.7	6.2	13.5

APPENDIX C. Figures concerning DSC Studies

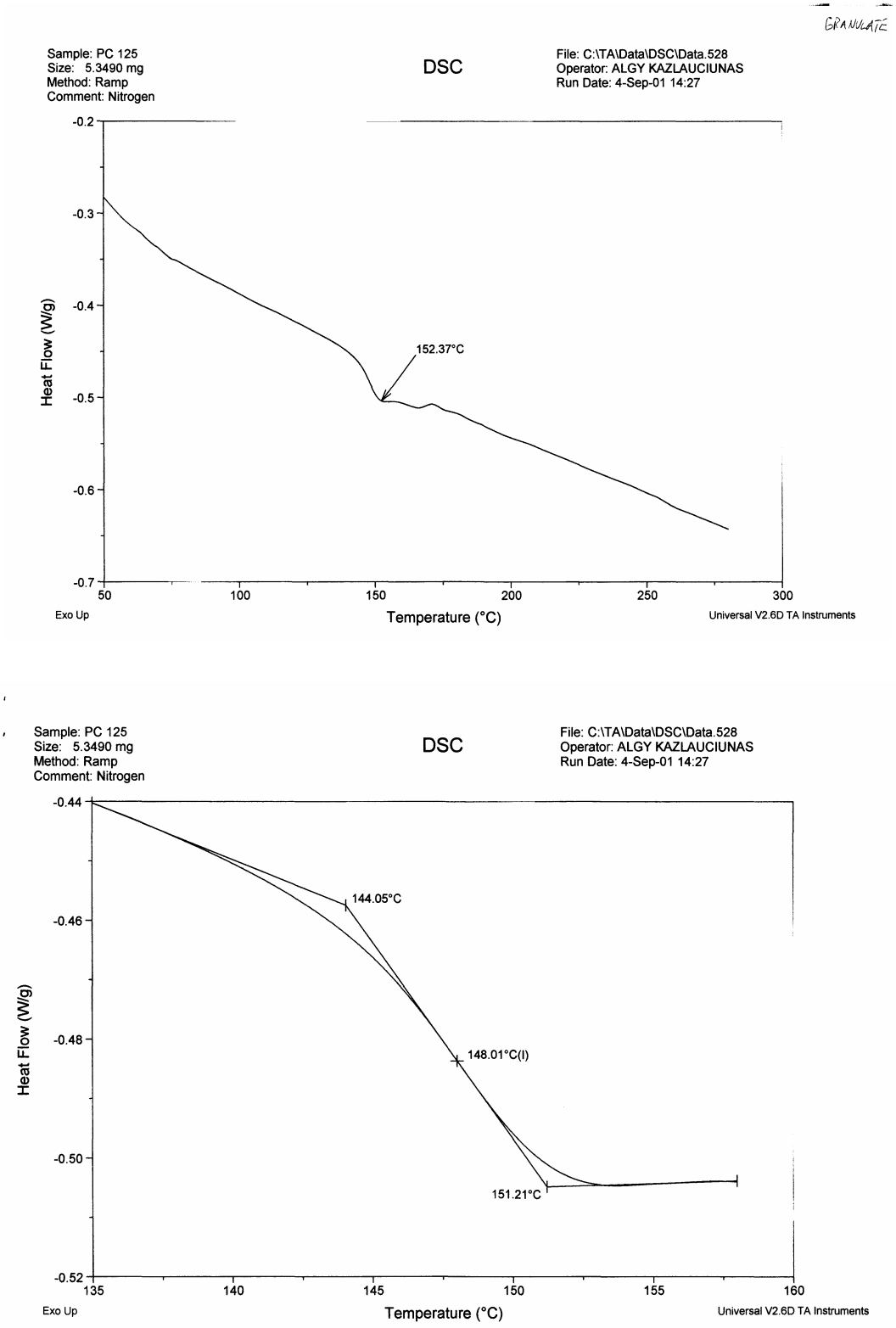

Figure C-1. DSC thermograms of a sample of PC 125.

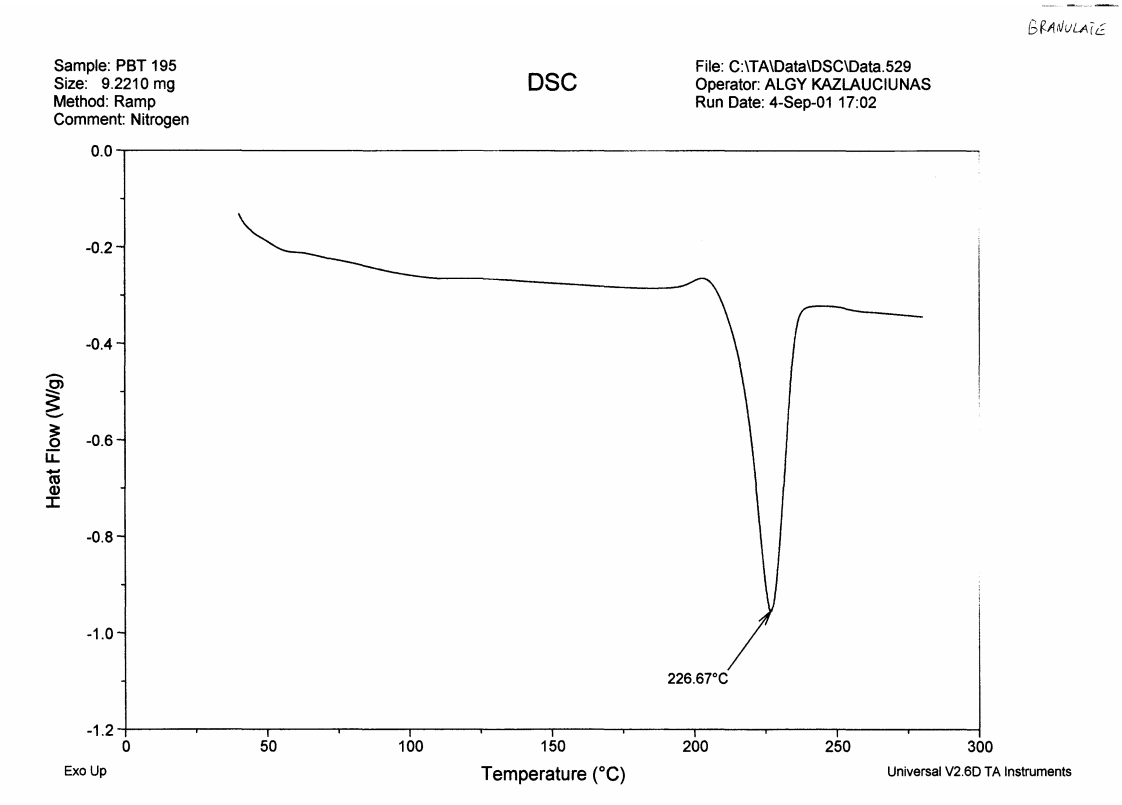

Figure C-2. DSC thermogram of a sample of PBT 195.

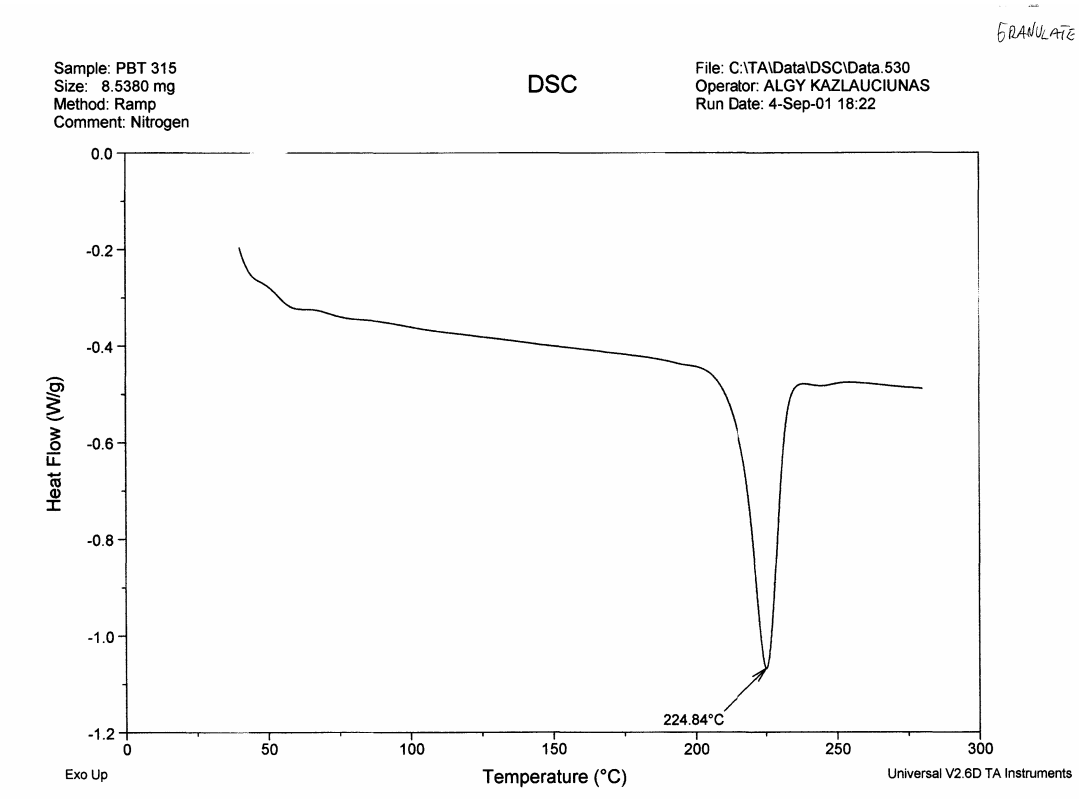

Figure C-3. DSC thermogram of a sample of PBT 315.

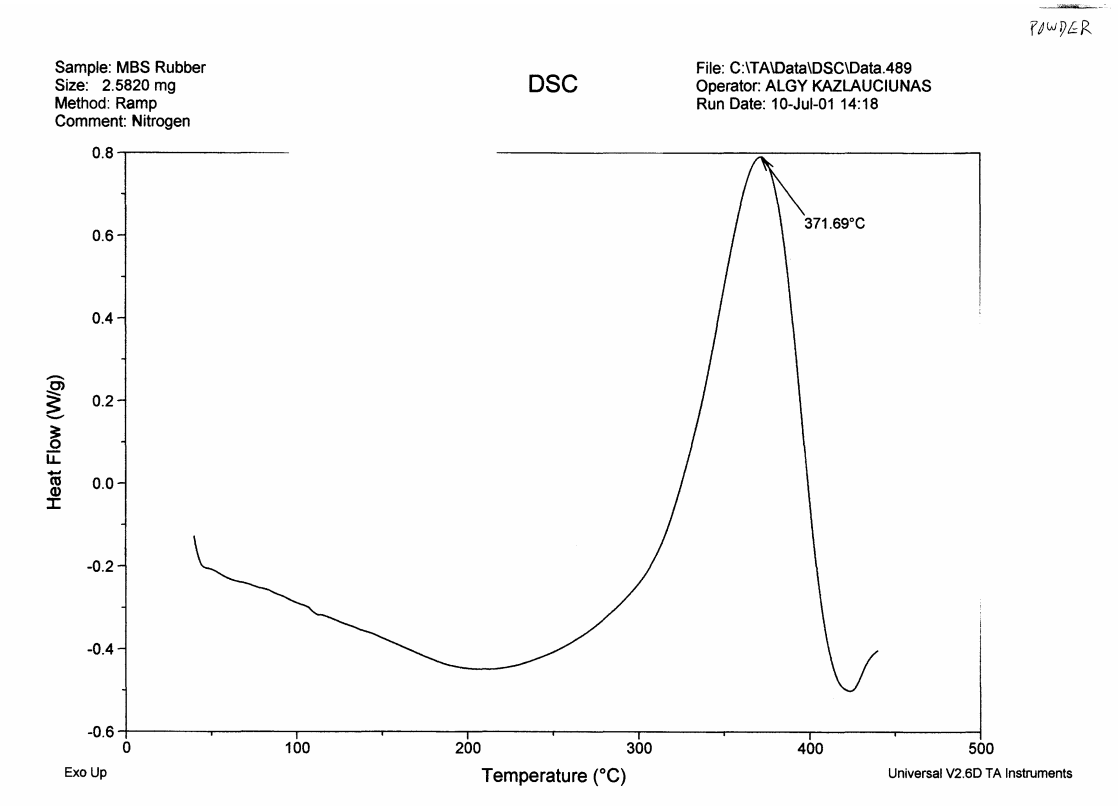

Figure C-4. DSC thermogram of a sample of MBS rubber.

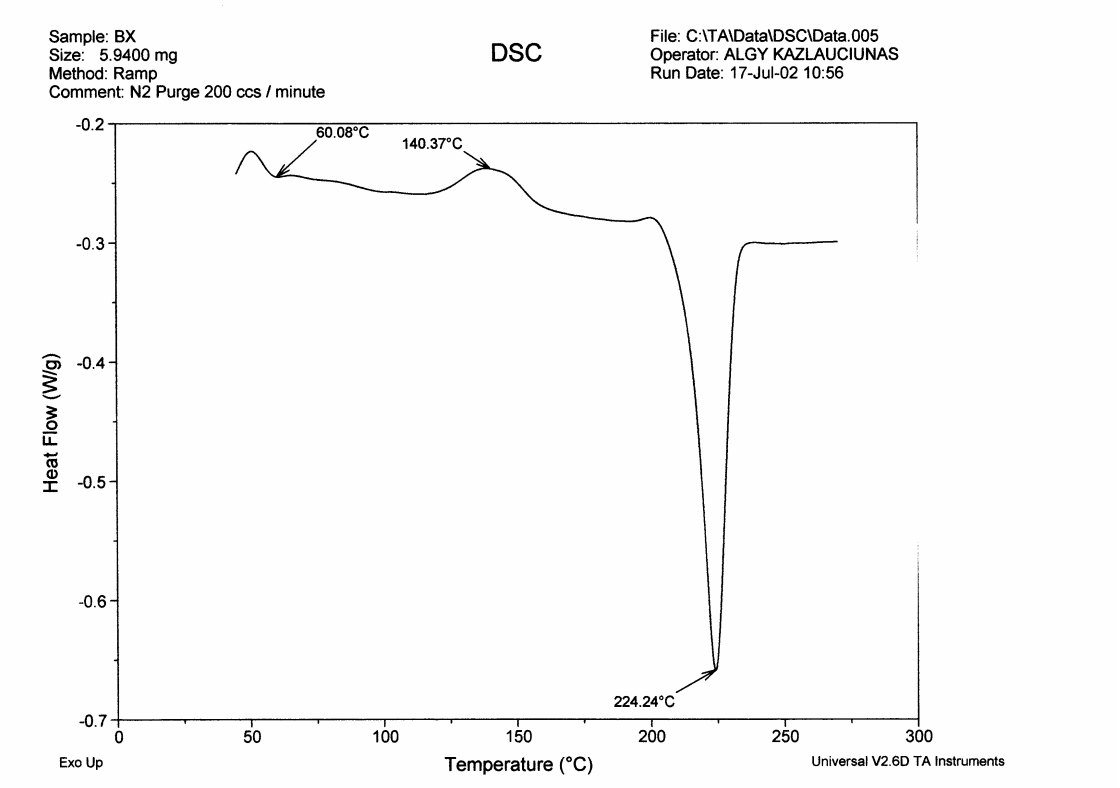

Figure C-5. DSC thermogram of a sample of batch BX (heating run).

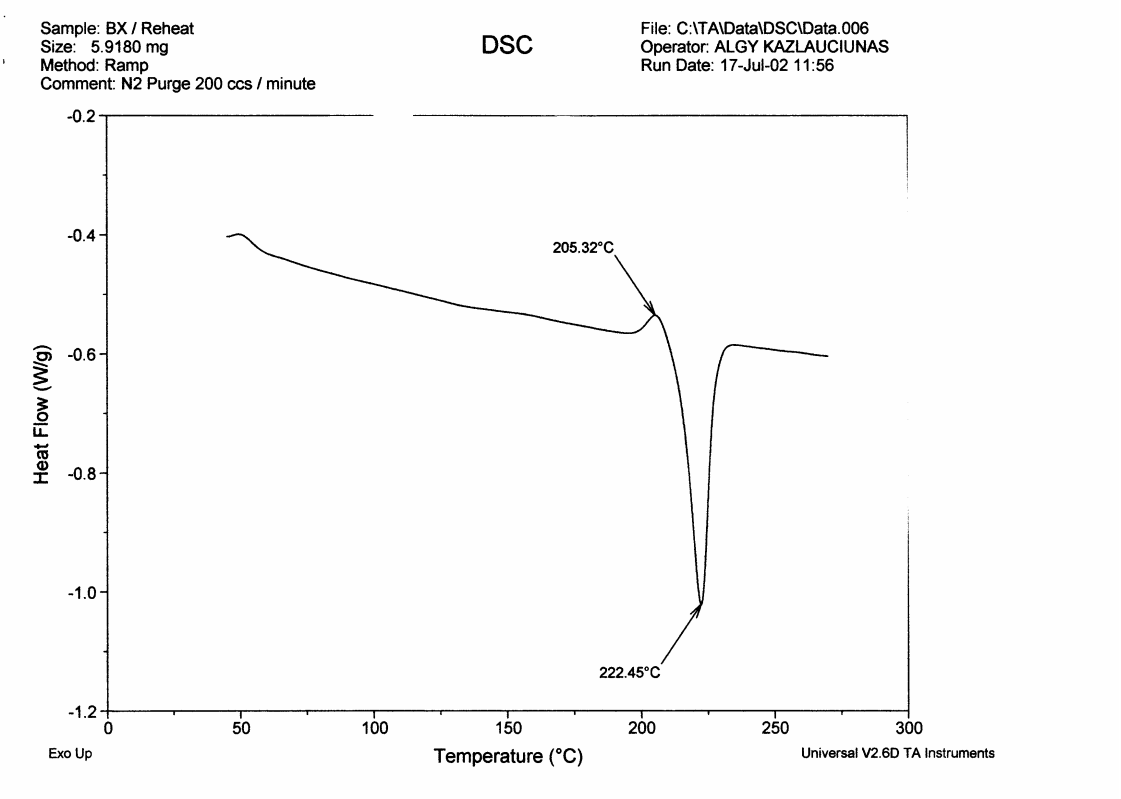

Figure C-6. DSC thermogram of a sample of batch BX (reheating run).

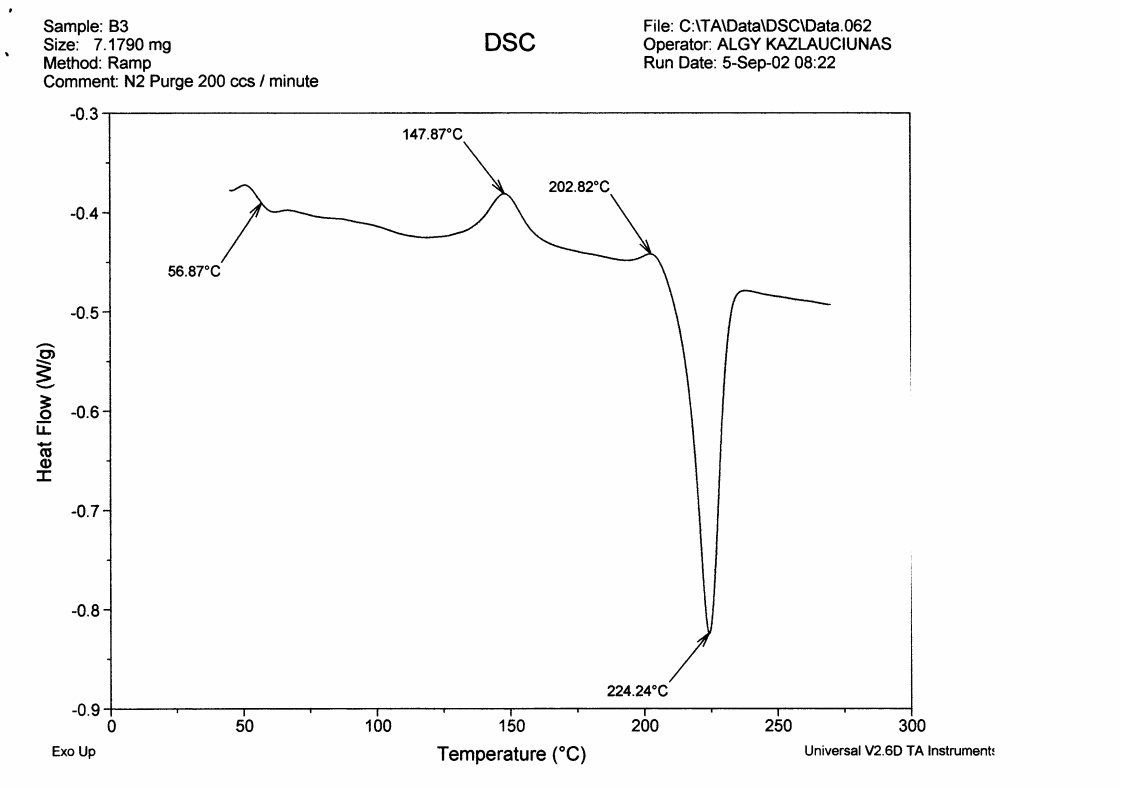

Figure C-7. DSC thermogram of a sample of batch B3 (heating run).

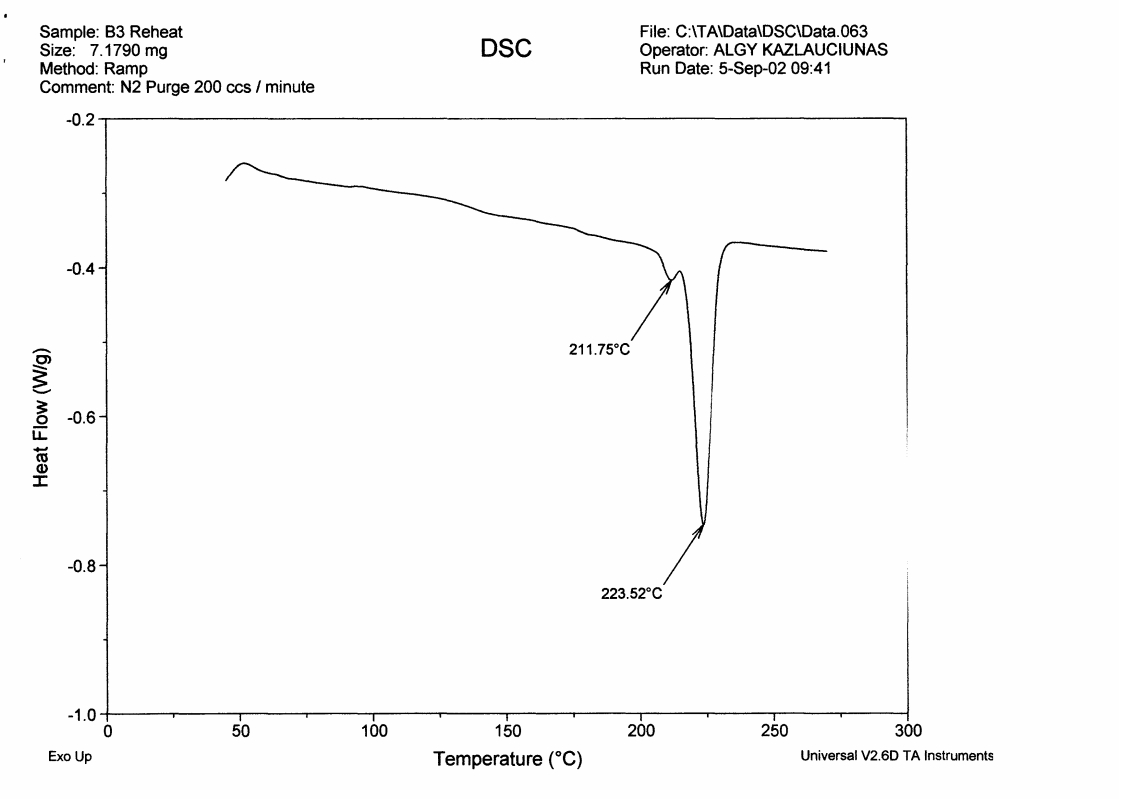

Figure C-8. DSC thermogram of a sample of batch B3 (reheating run).

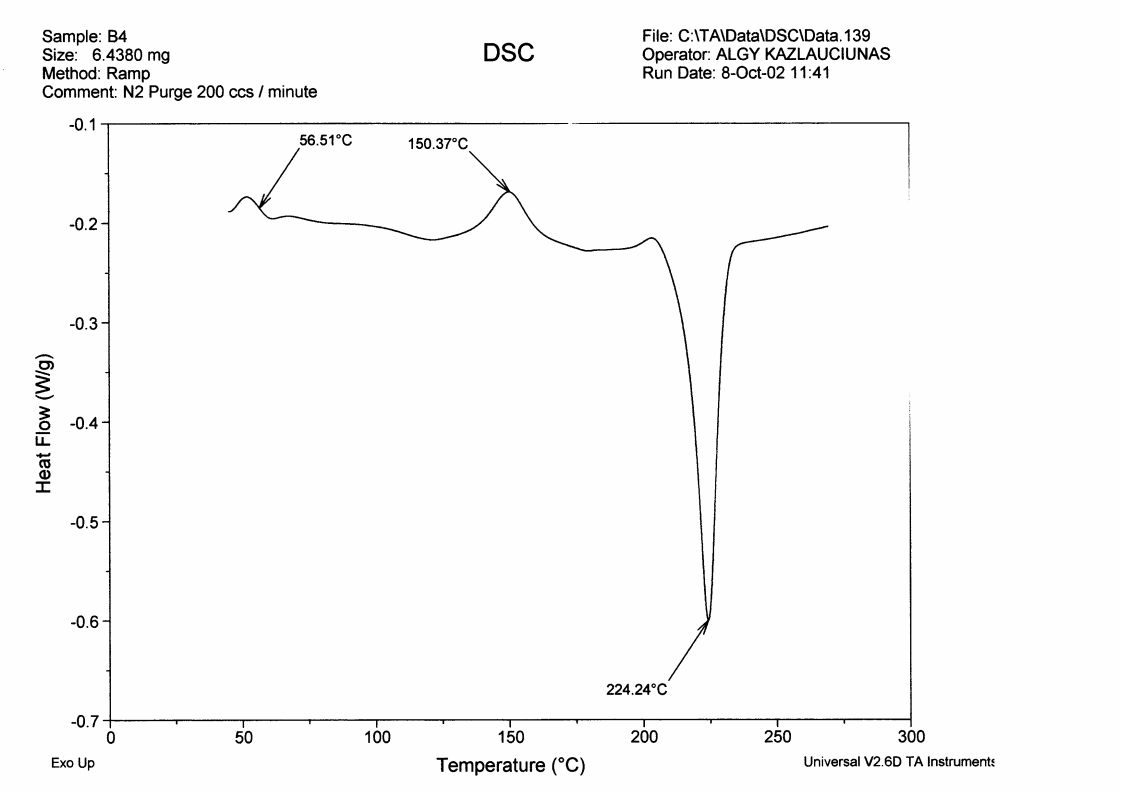

Figure C-9. DSC thermogram of a sample of batch B4 (heating run).

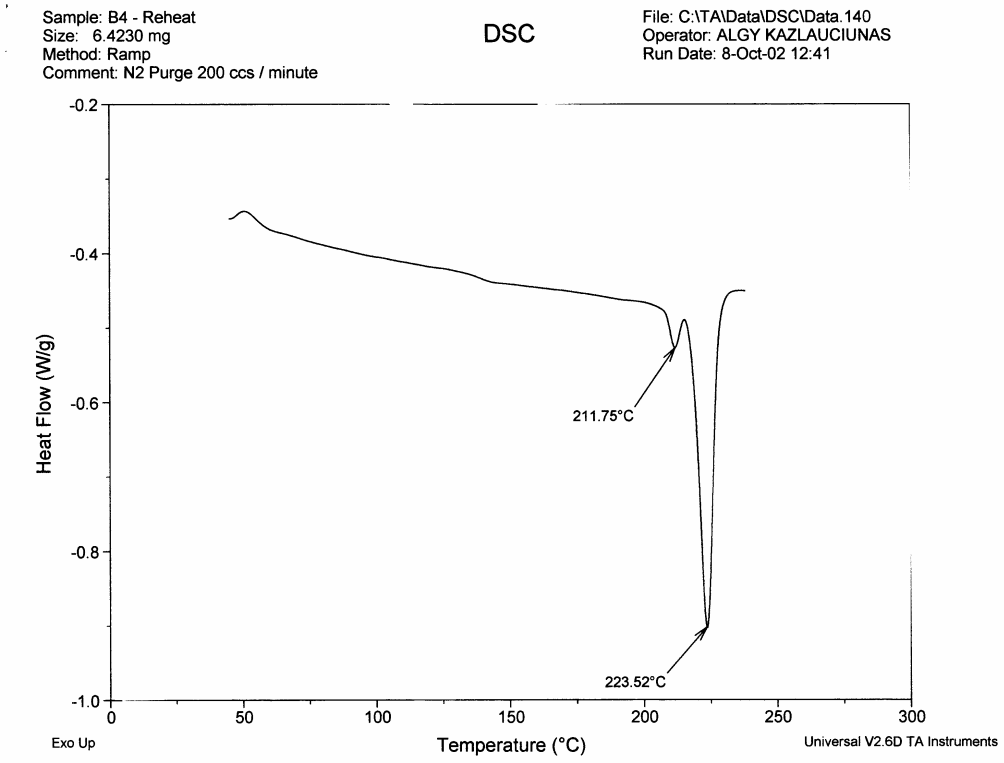

Figure C-10. DSC thermogram of a sample of batch B4 (reheating run).

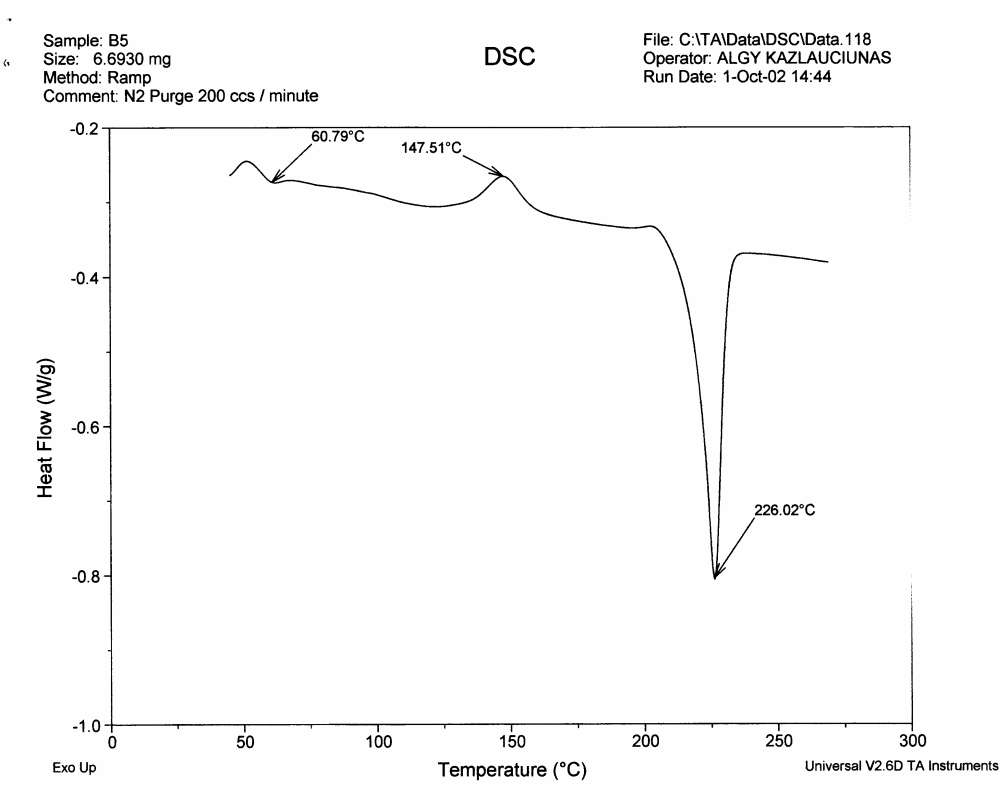

Figure C-11. DSC thermogram of a sample of batch B5 (heating run).

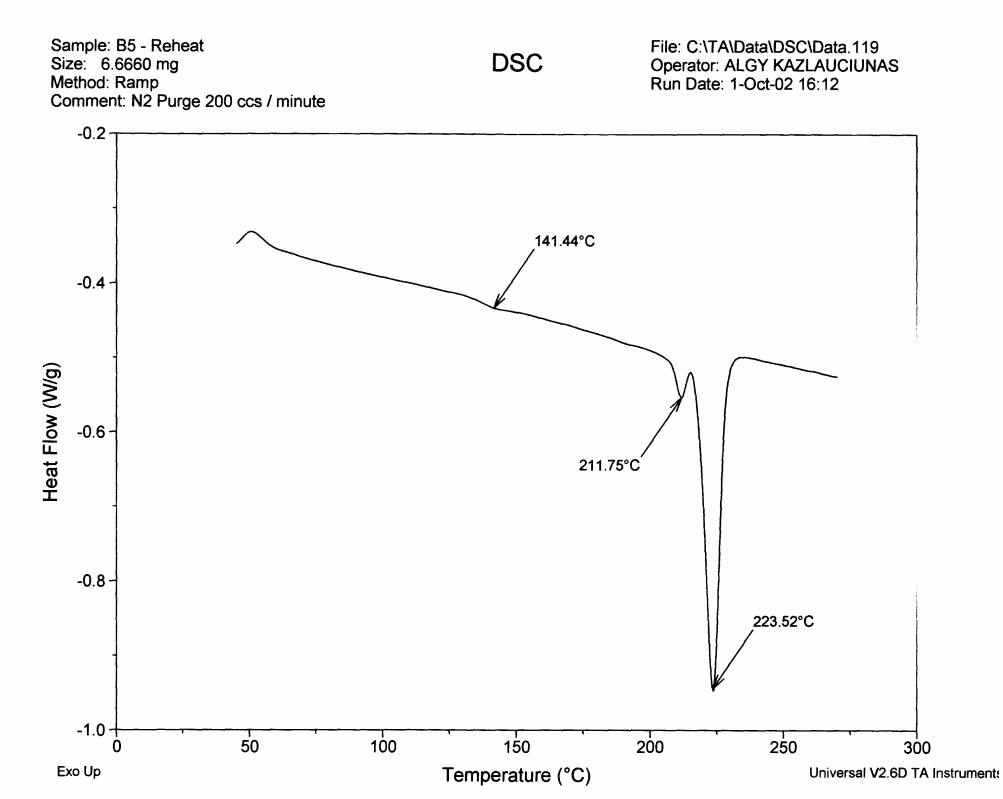

Figure C-12. DSC thermogram of a sample of batch B5 (reheating run).

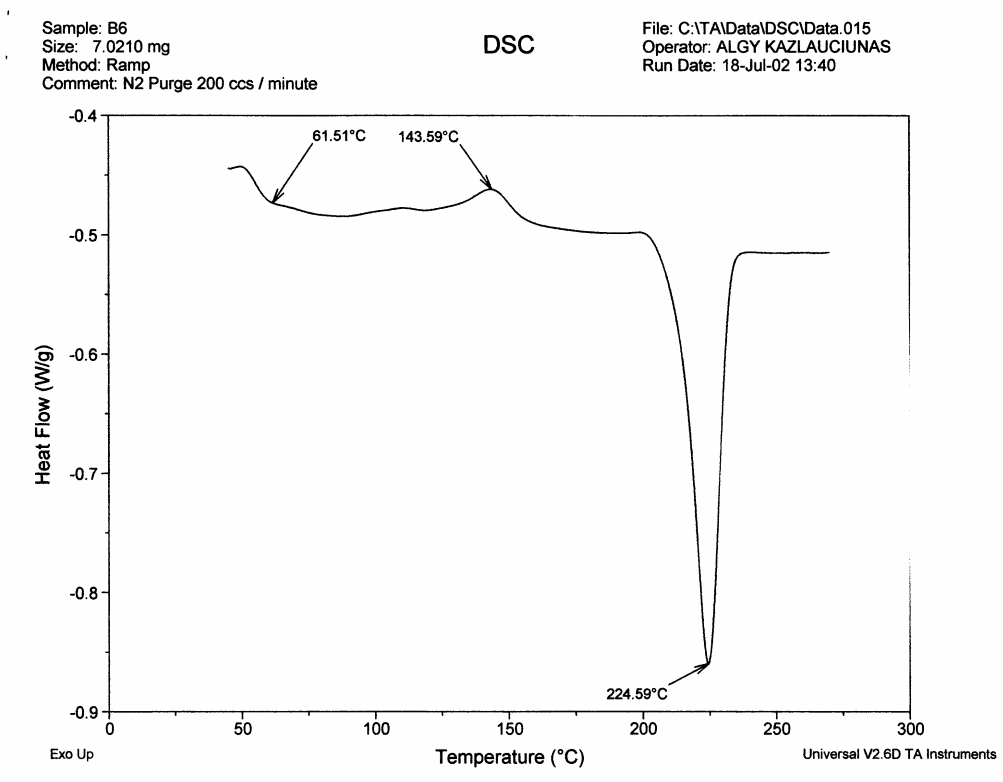

Figure C-13. DSC thermogram of a sample of batch B6 (heating run).

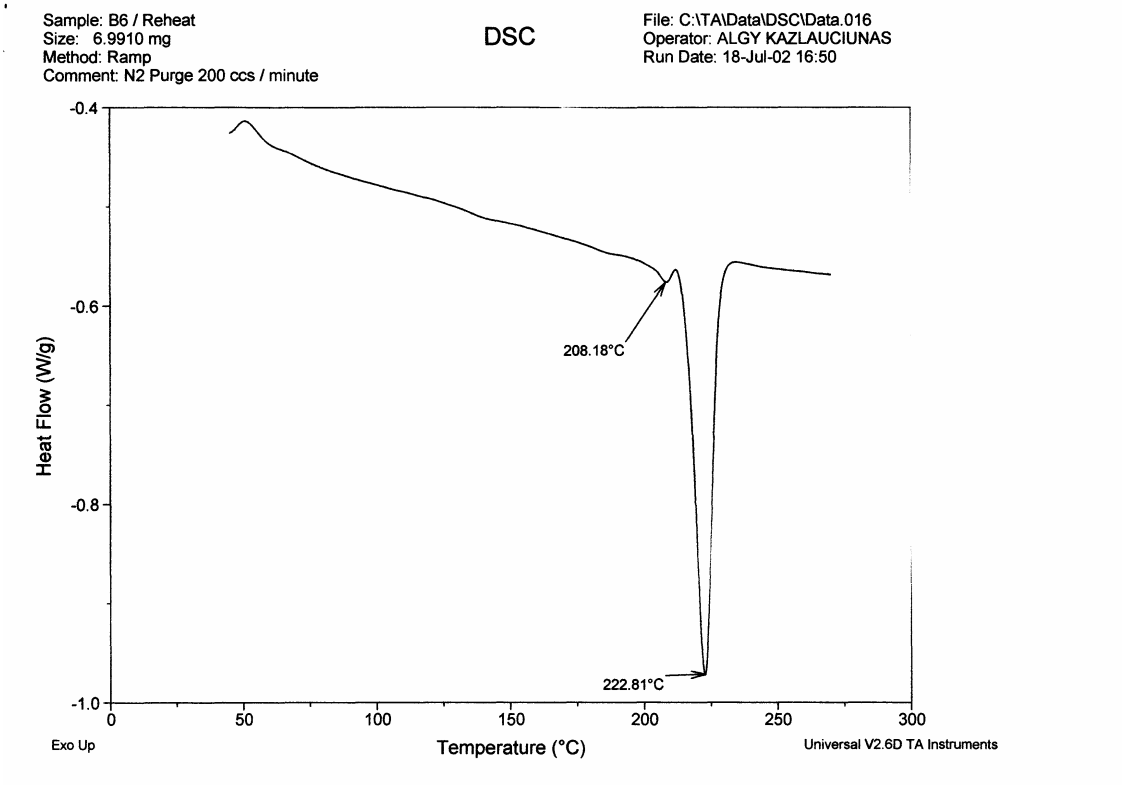

Figure C-14. DSC thermogram of a sample of batch B6 (reheating run).

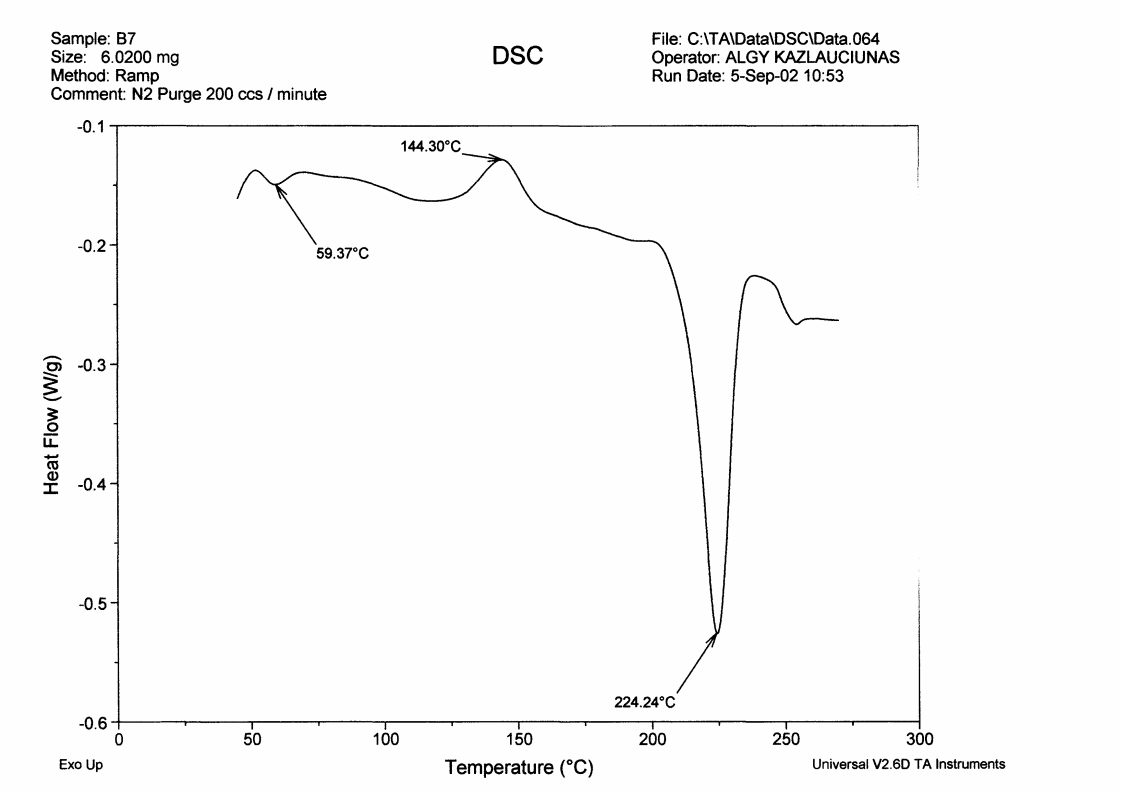

Figure C-15. DSC thermogram of a sample of batch B7 (heating run).

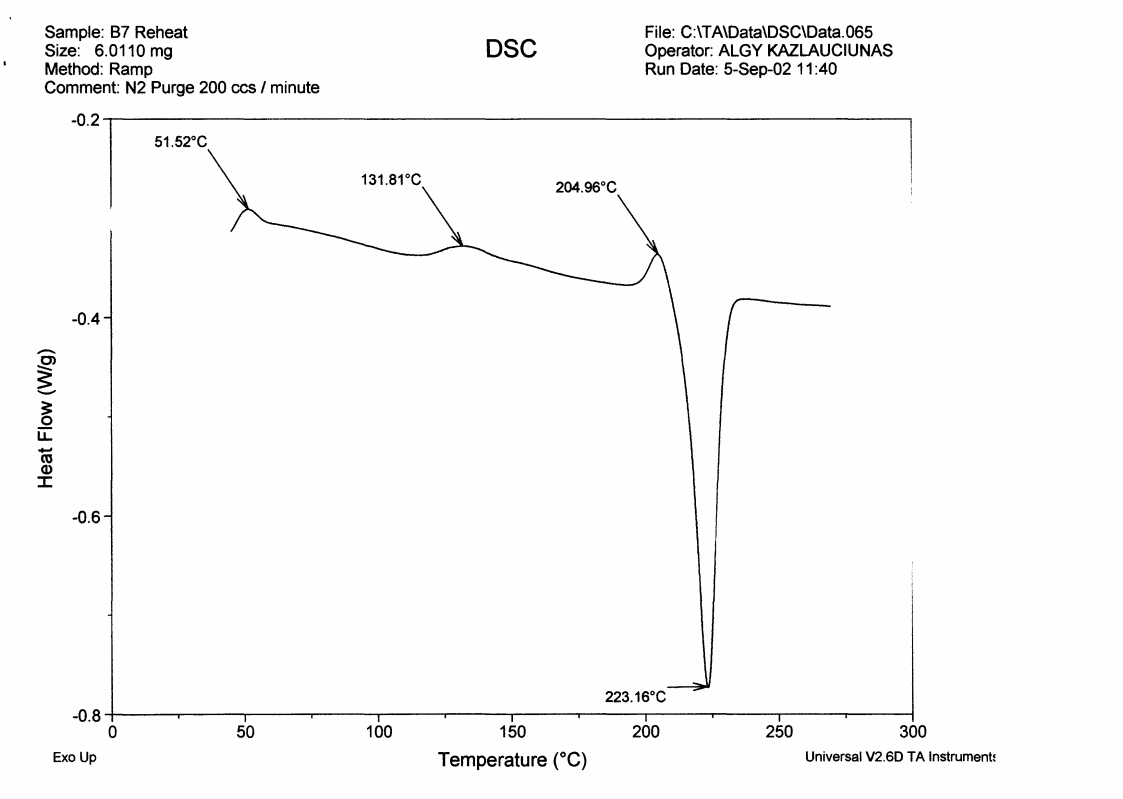

Figure C-16. DSC thermogram of a sample of batch B7 (reheating run).

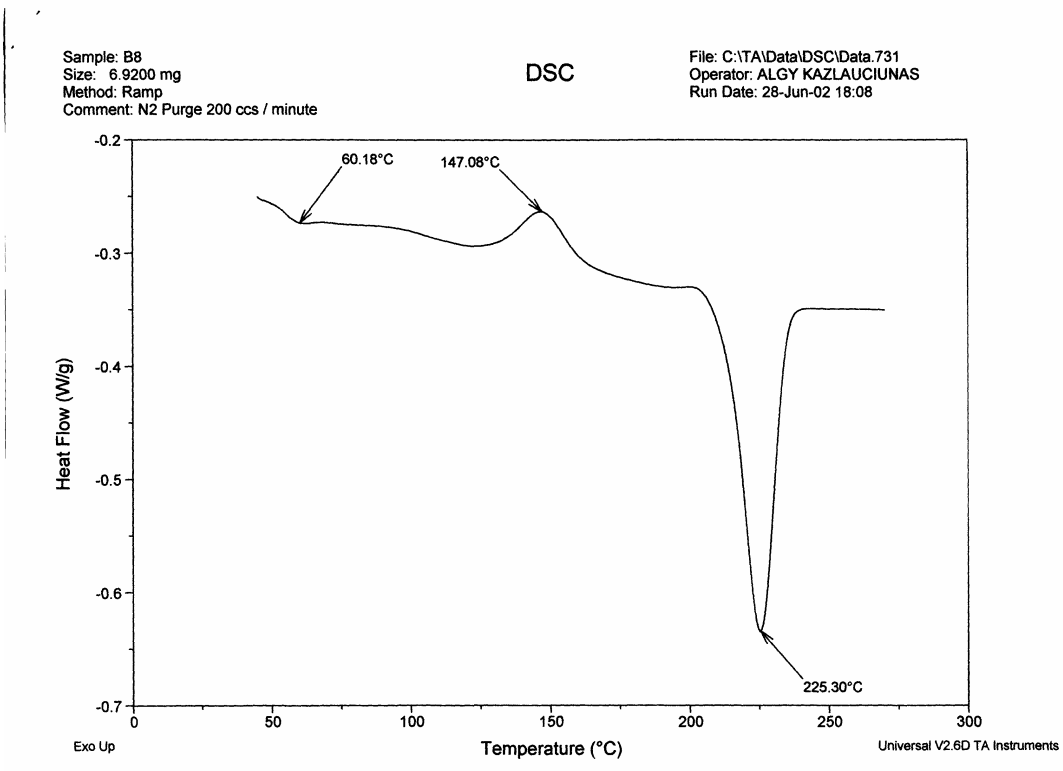

Figure C-17. DSC thermogram of a sample of batch B8 (heating run).

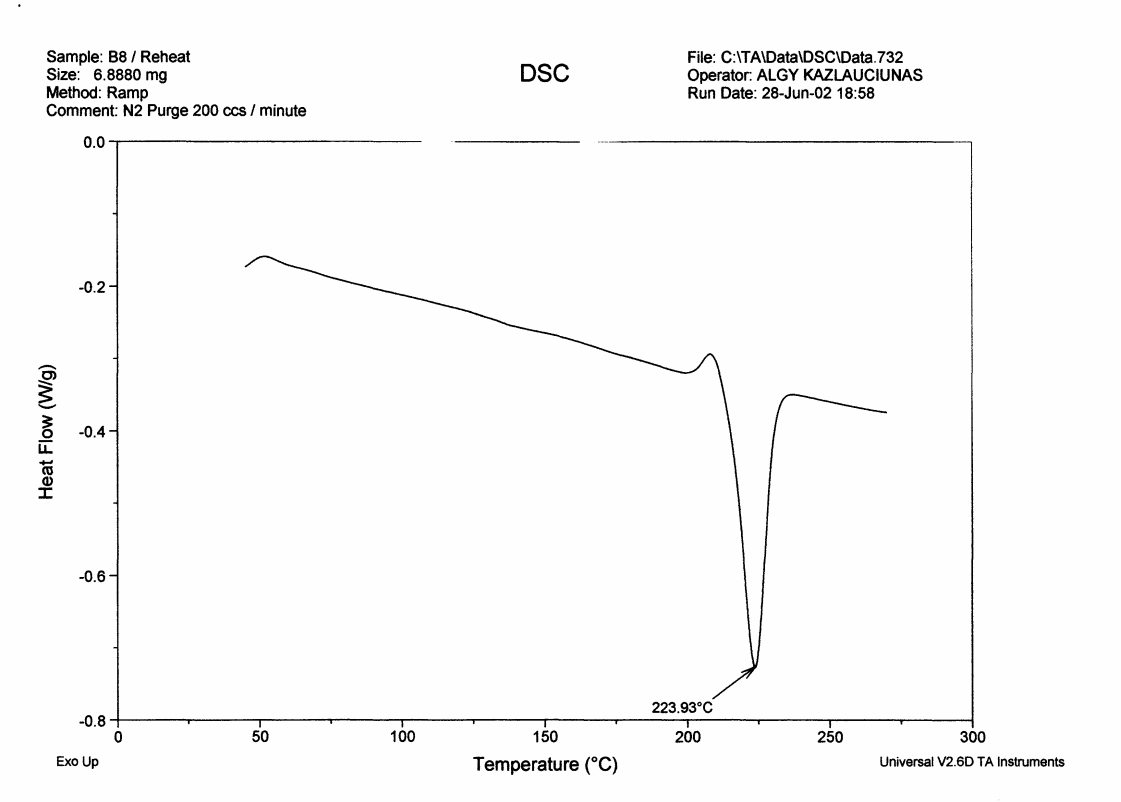

Figure C-18. DSC thermogram of a sample of batch B8 (reheating run).

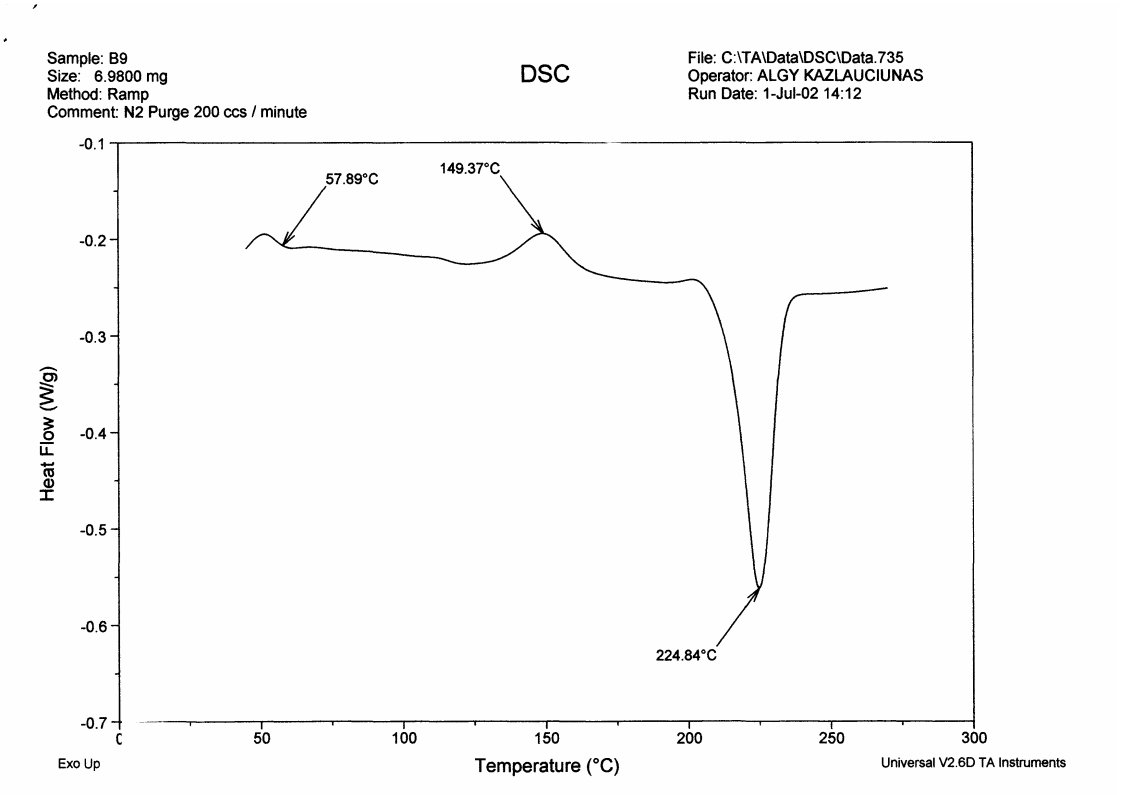

Figure C-19. DSC thermogram of a sample of batch B9 (heating run).

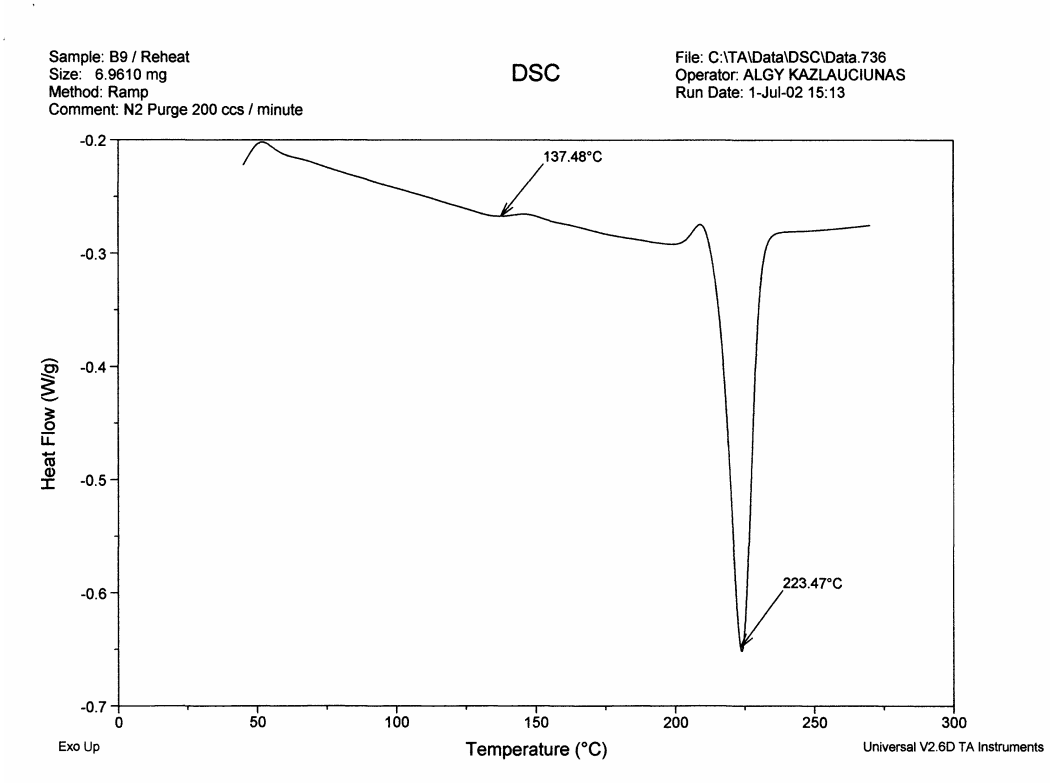

Figure C-20. DSC thermogram of a sample of batch B9 (reheating run).

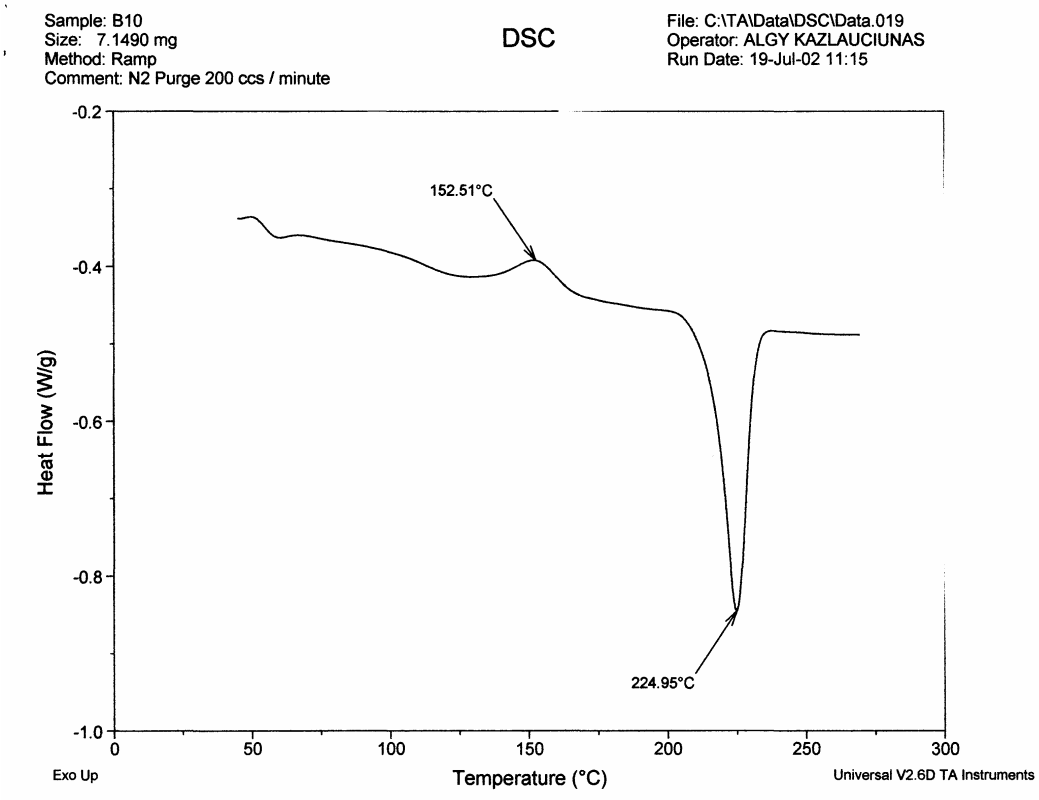

Figure C-21. DSC thermogram of a sample of batch B10 (heating run).

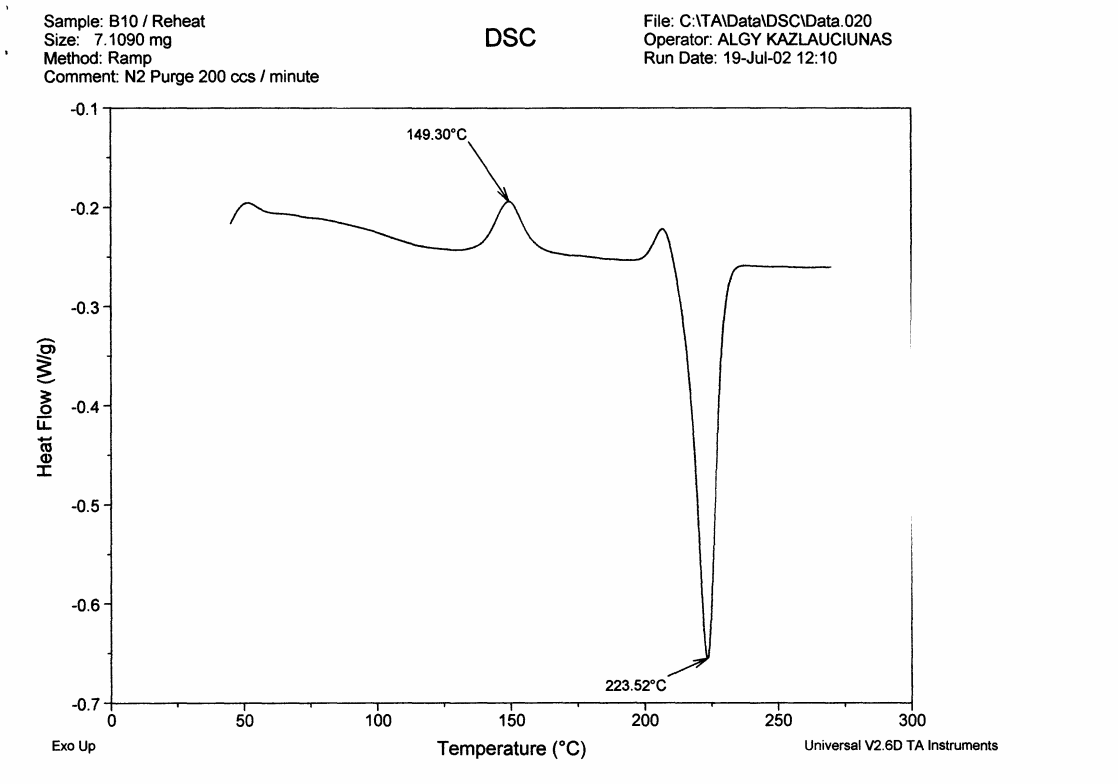

Figure C-22. DSC thermogram of a sample of batch B10 (reheating run).

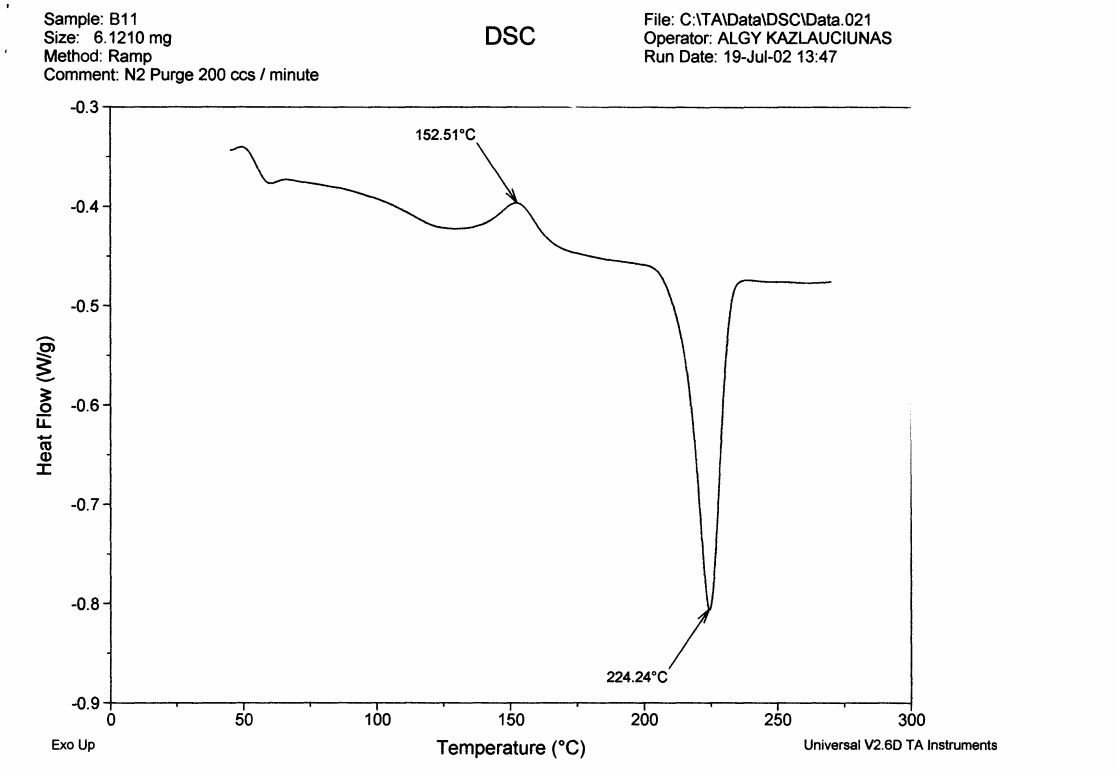

Figure C-23. DSC thermogram of a sample of batch B11 (heating run).

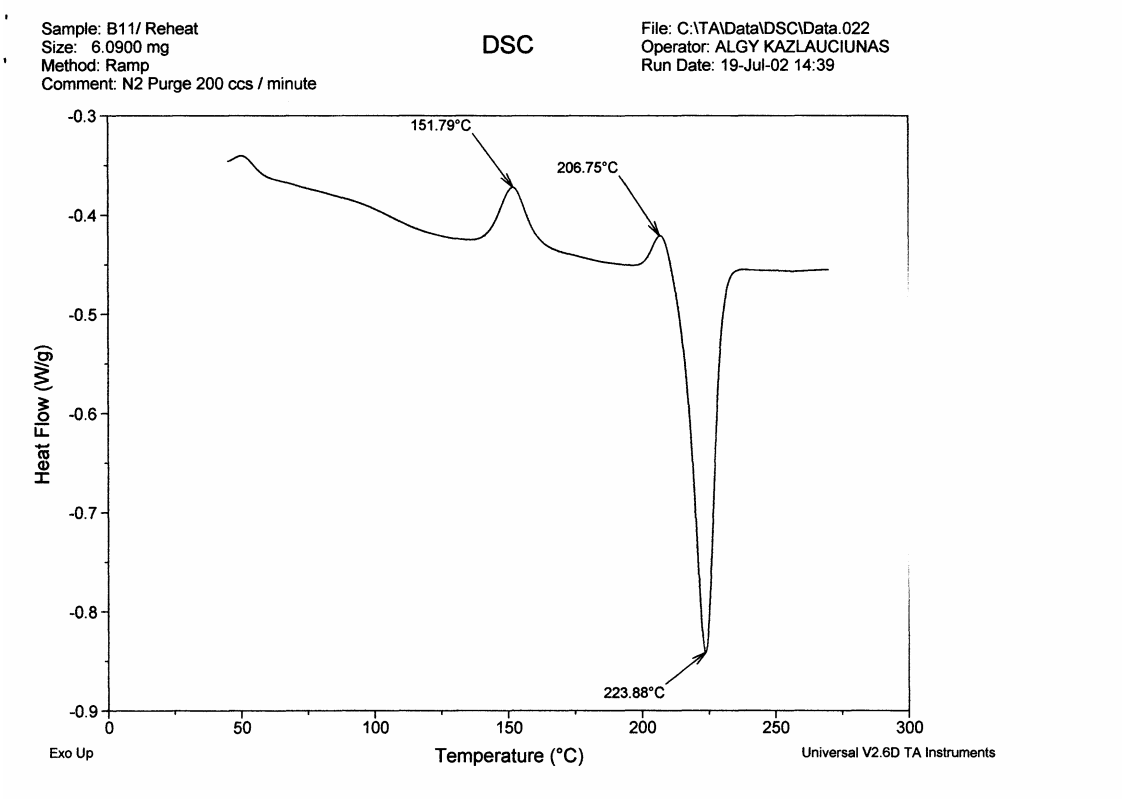

Figure C-24. DSC thermogram of a sample of batch B11 (reheating run).

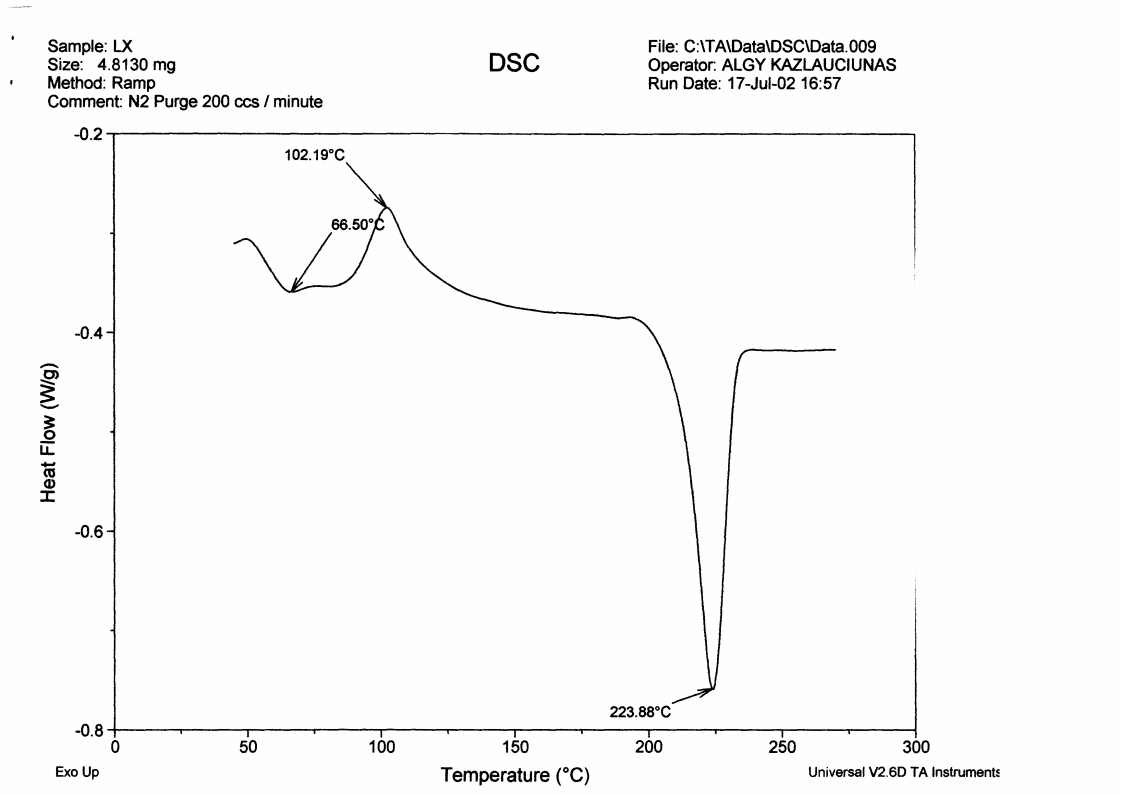

Figure C-25. DSC thermogram of a sample of batch LX (heating run).

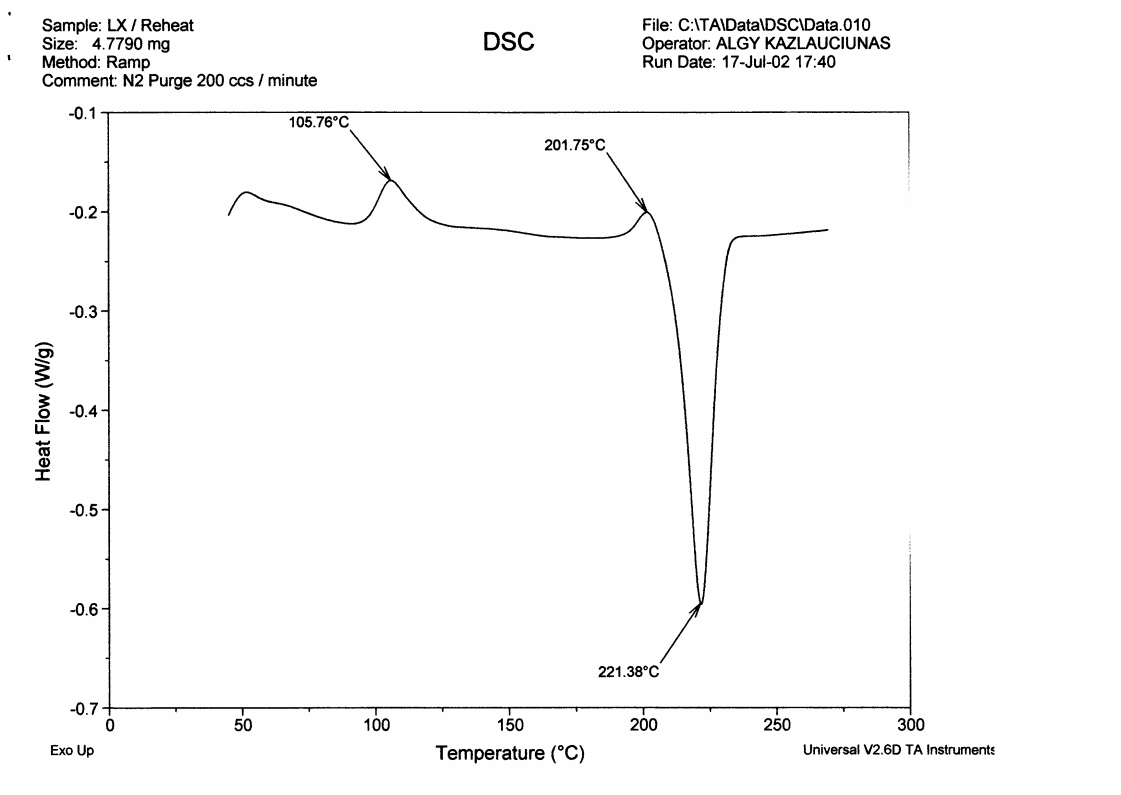

Figure C-26. DSC thermogram of a sample of batch LX (reheating run).

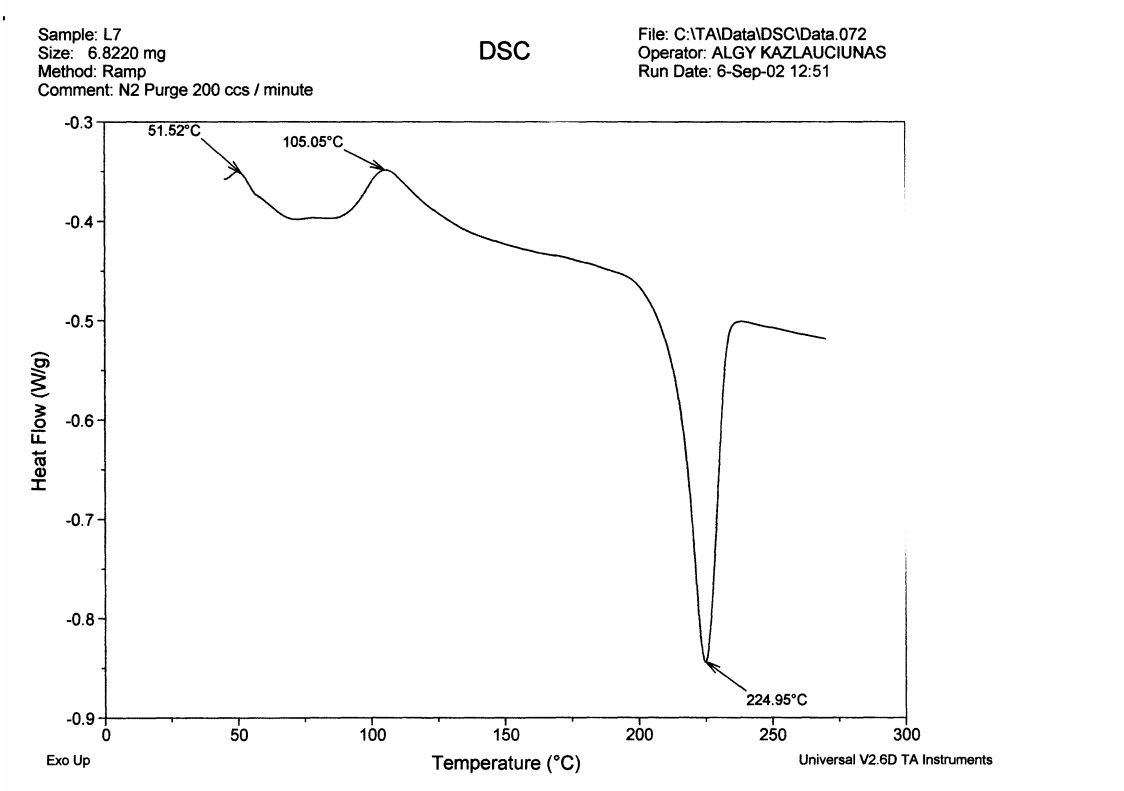

Figure C-27. DSC thermogram of a sample of batch L7 (heating run).

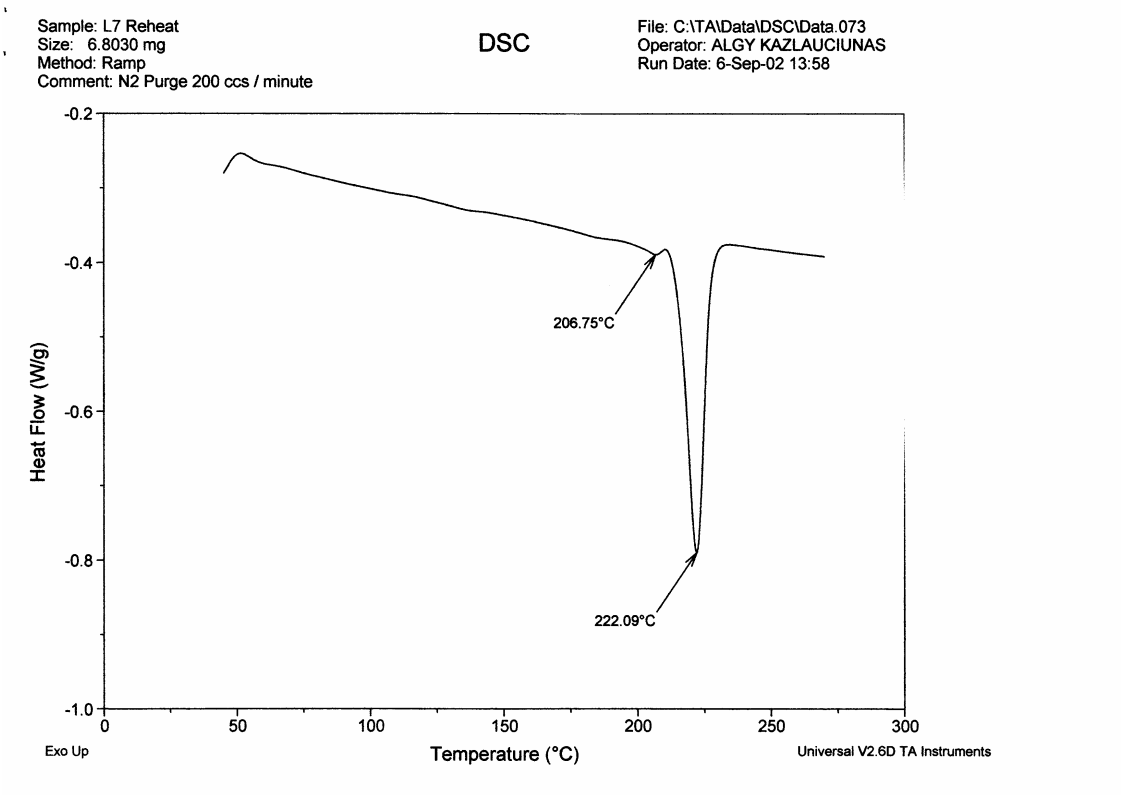

Figure C-28. DSC thermogram of a sample of batch L7 (reheating run).

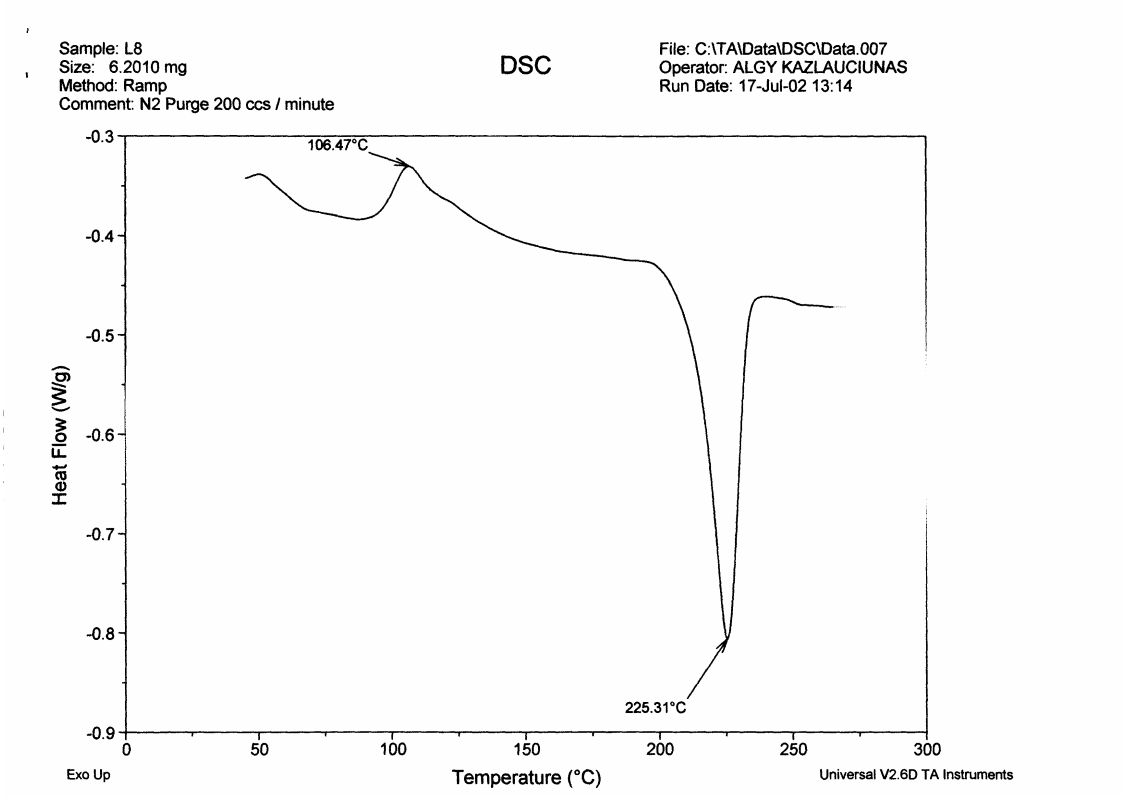

Figure C-29. DSC thermogram of a sample of batch L8 (heating run).

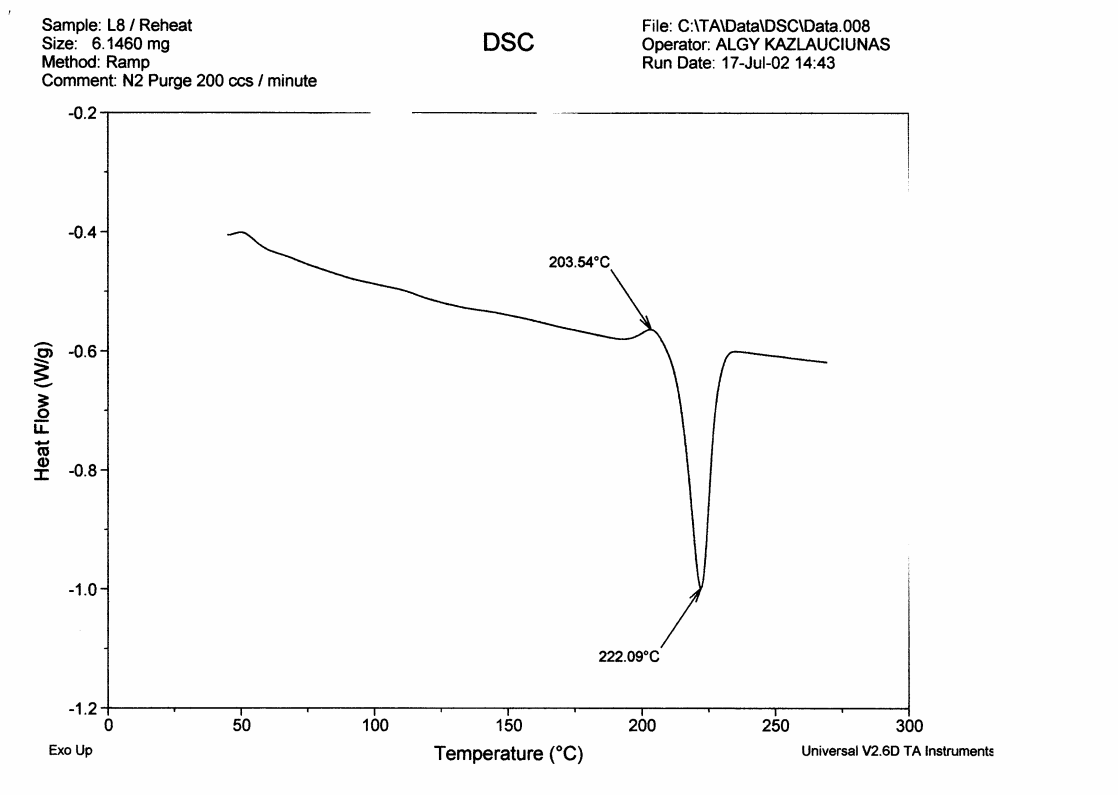

Figure C-30. DSC thermogram of a sample of batch L8 (reheating run).

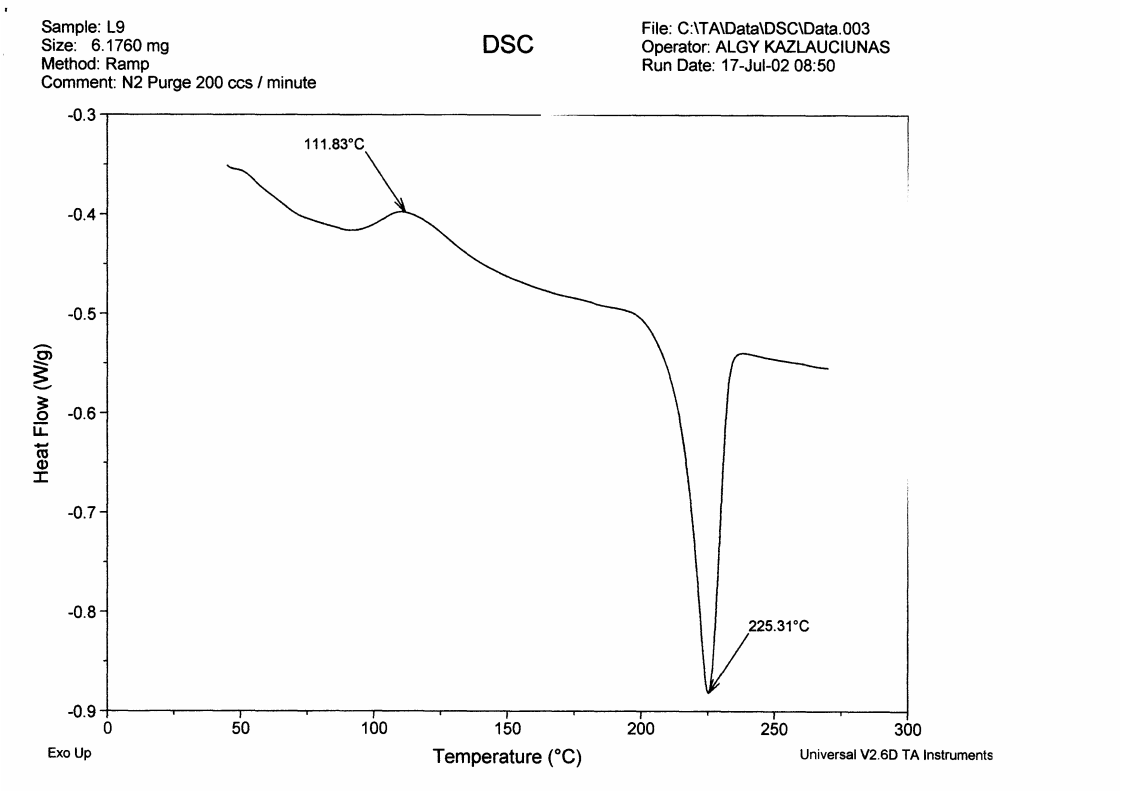

Figure C-31. DSC thermogram of a sample of batch L9 (heating run).

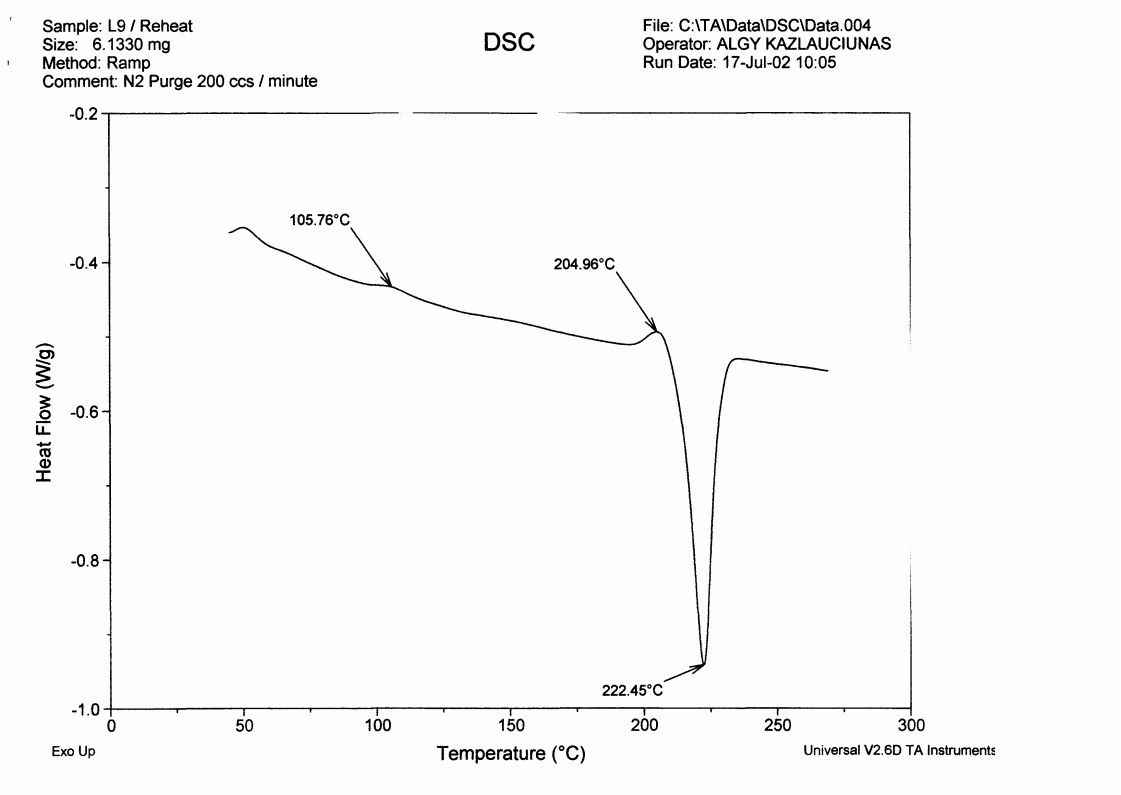

Figure C-32. DSC thermogram of a sample of batch L9 (reheating run).

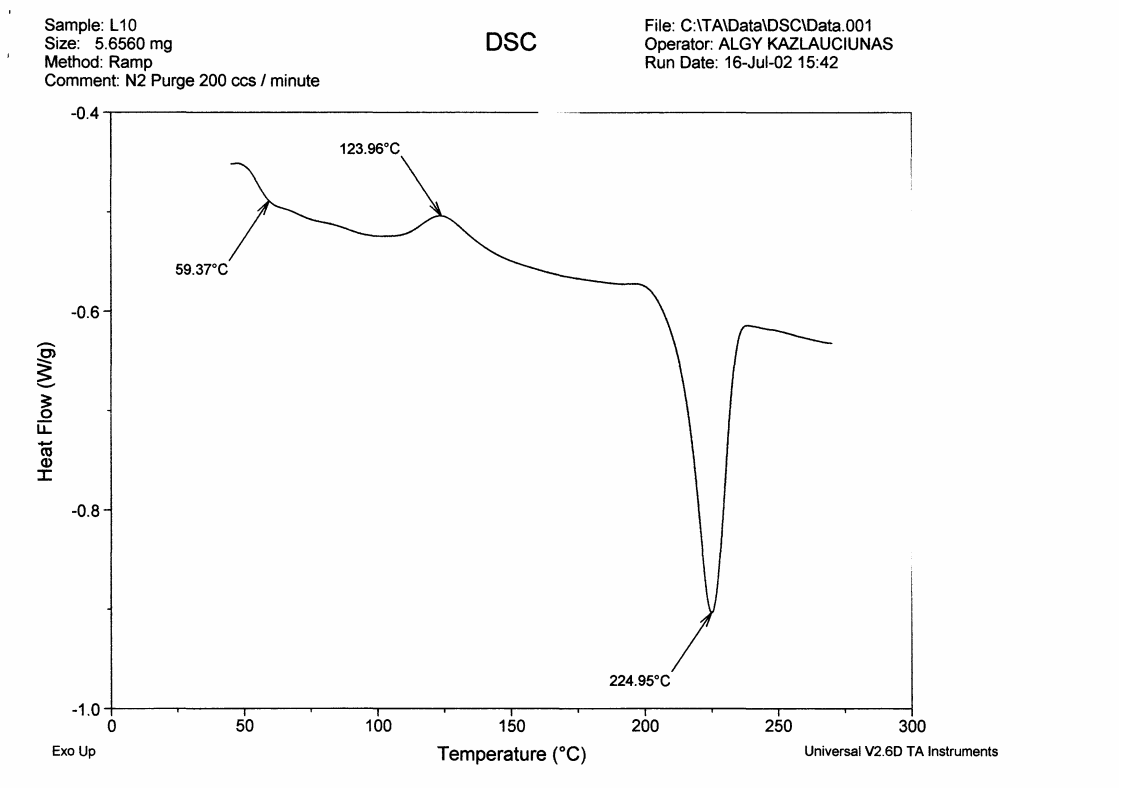

Figure C-33. DSC thermogram of a sample of batch L10 (heating run).

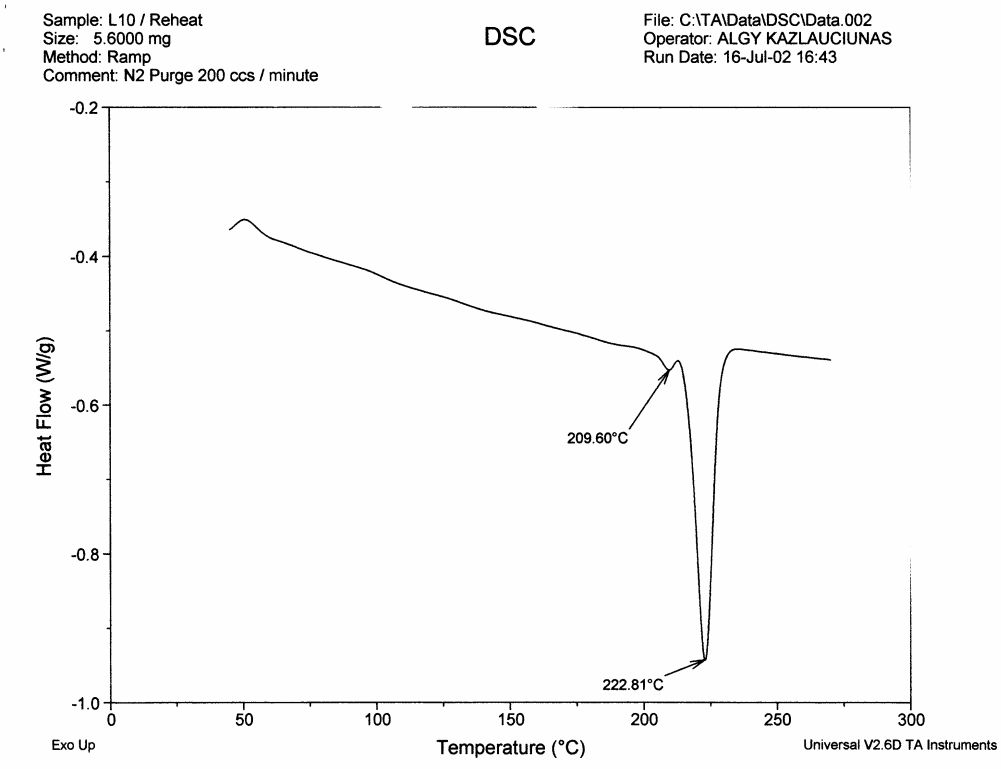

Figure C-34. DSC thermogram of a sample of batch L10 (reheating run).

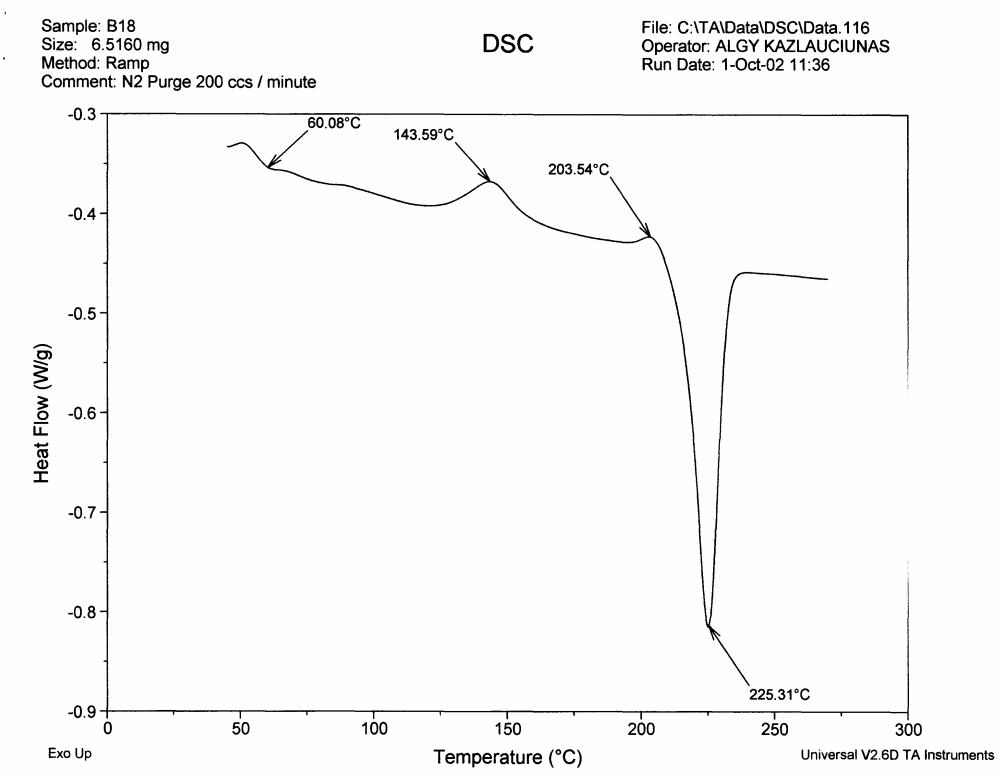

Figure C-35. DSC thermogram of a sample of batch B18 (heating run).

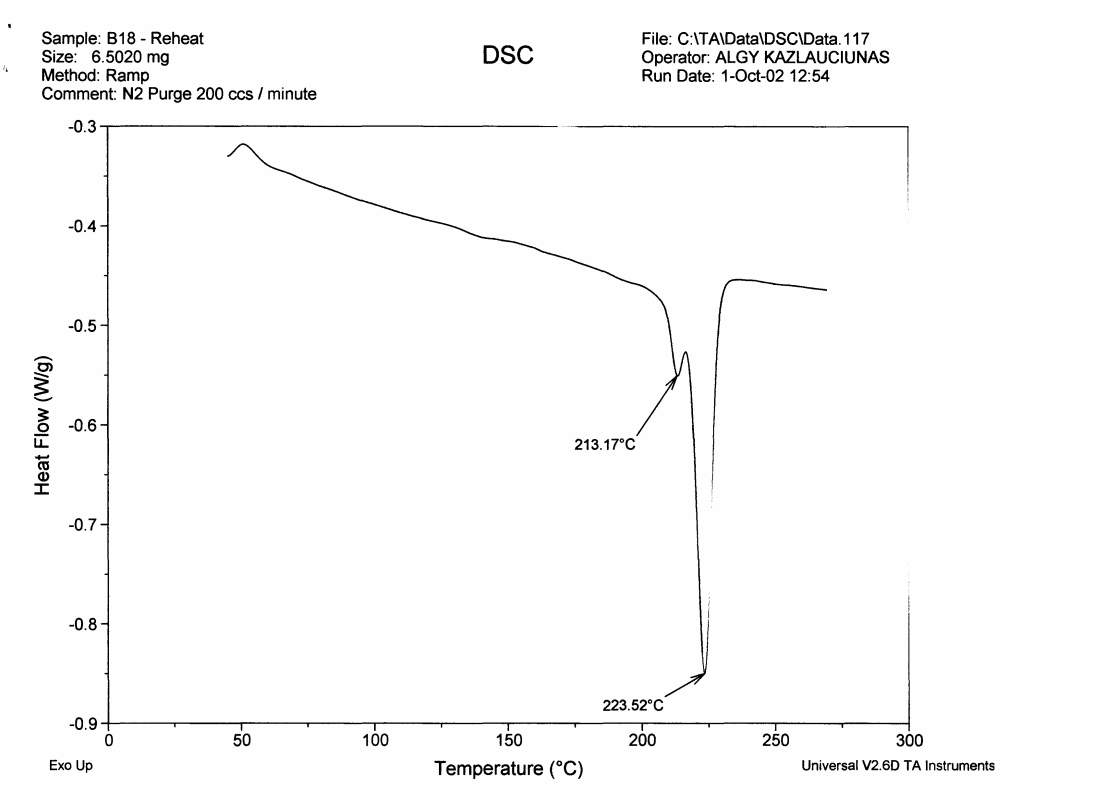

Figure C-36. DSC thermogram of a sample of batch B18 (reheating run).

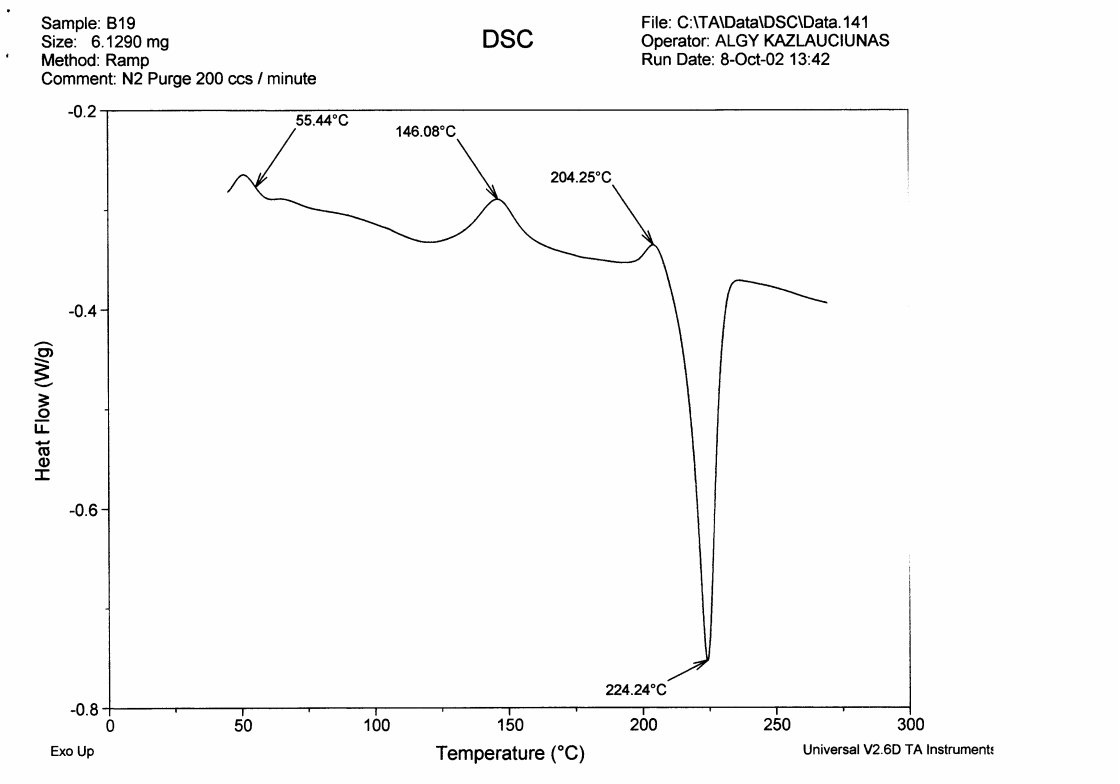

Figure C-37. DSC thermogram of a sample of batch B19 (heating run).

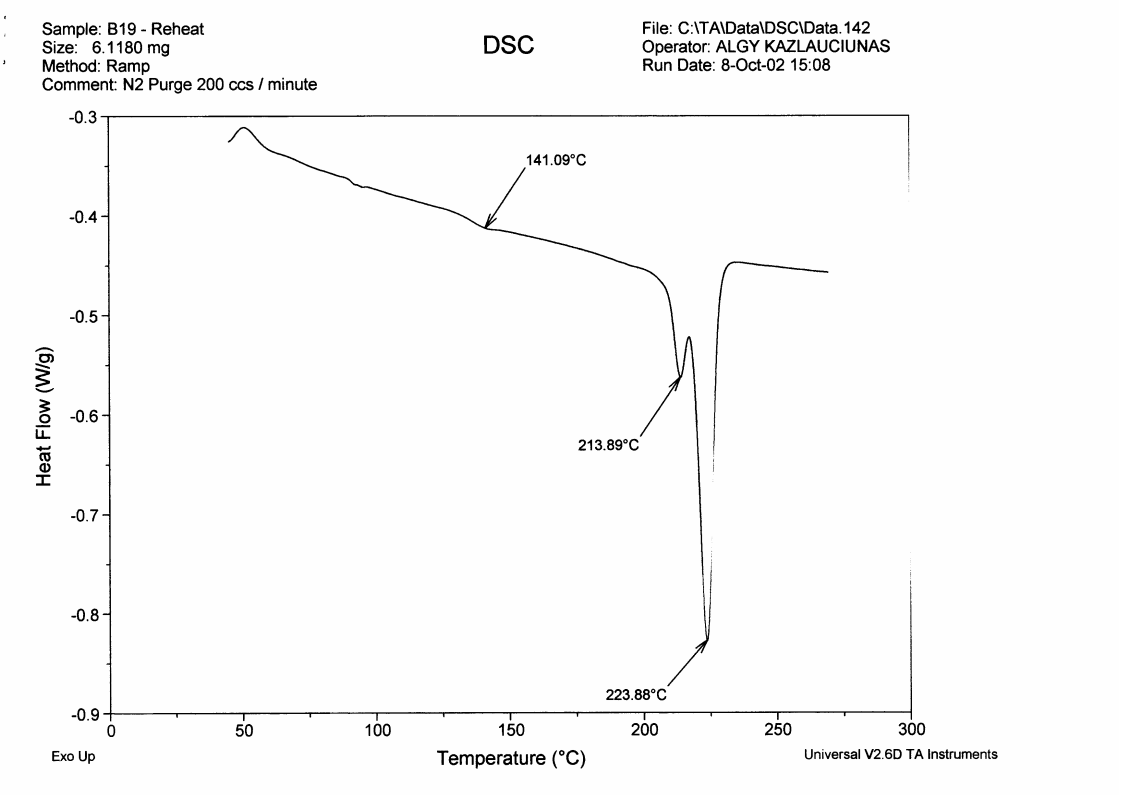

Figure C-38. DSC thermogram of a sample of batch B19 (reheating run).

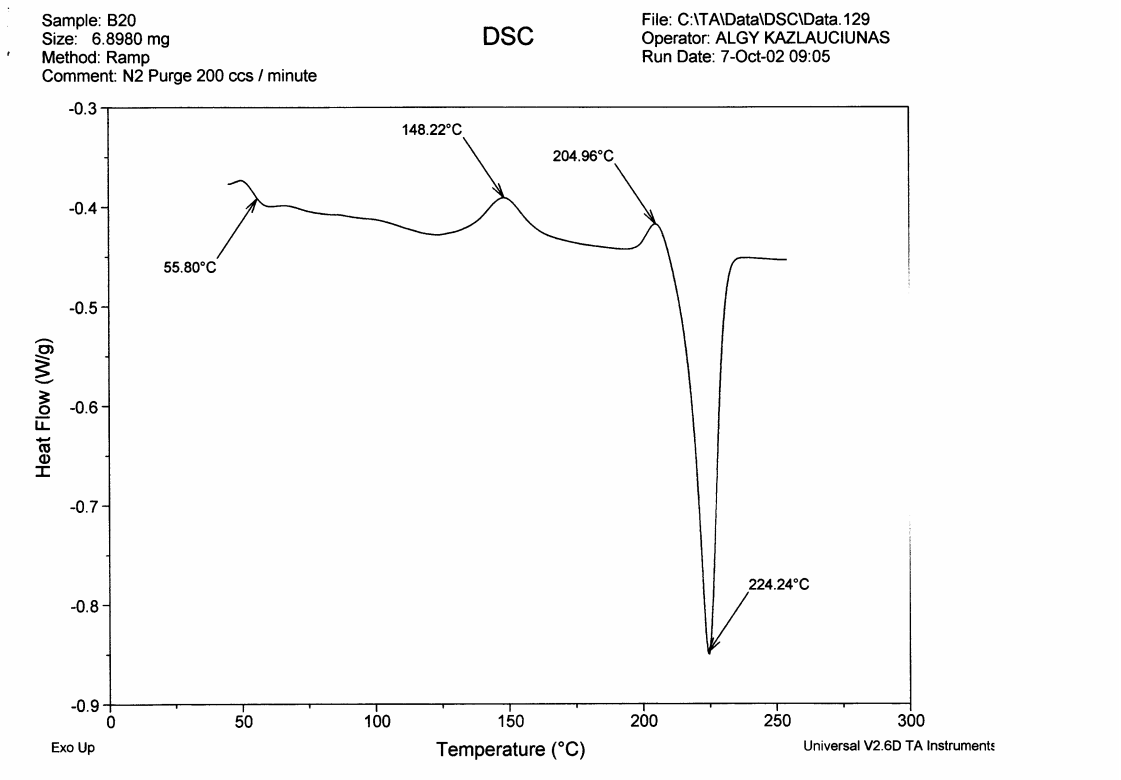

Figure C-39. DSC thermogram of a sample of batch B20 (heating run).

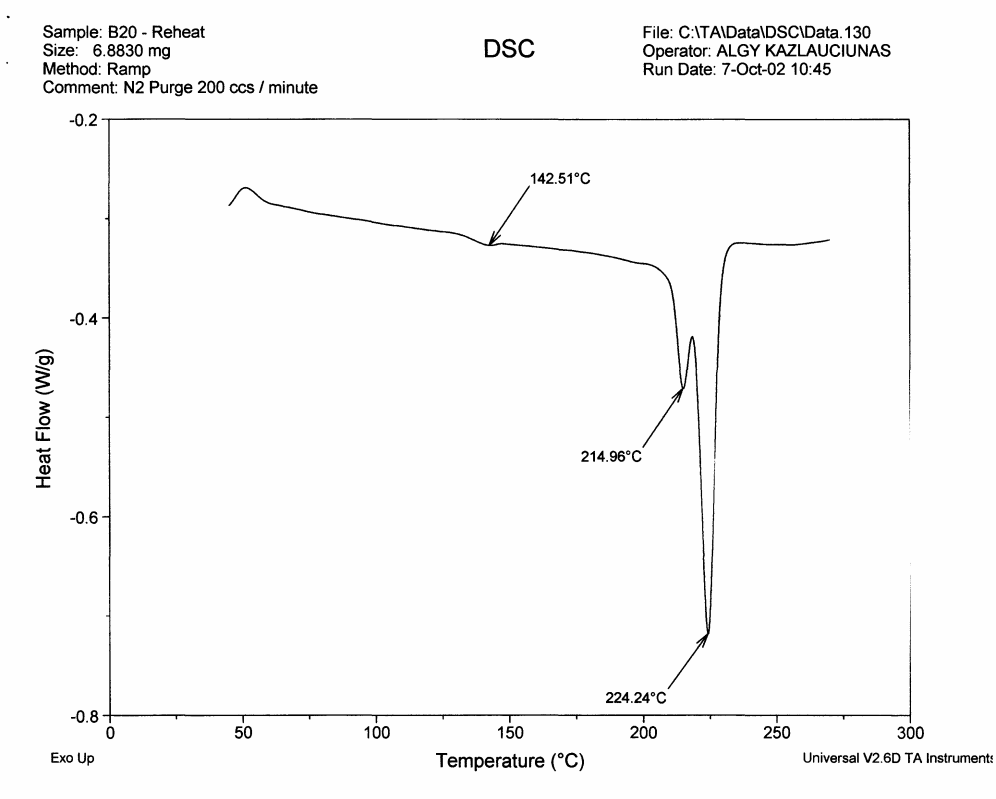

Figure C-40. DSC thermogram of a sample of batch B20 (reheating run).

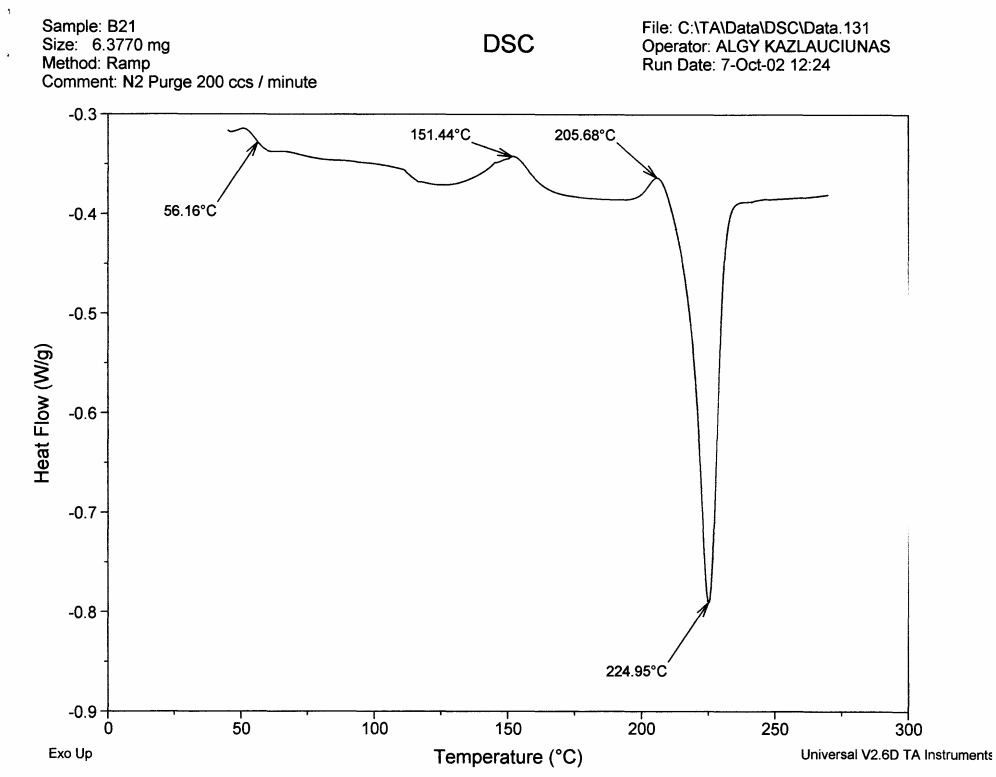

Figure C-41. DSC thermogram of a sample of batch B21 (heating run).

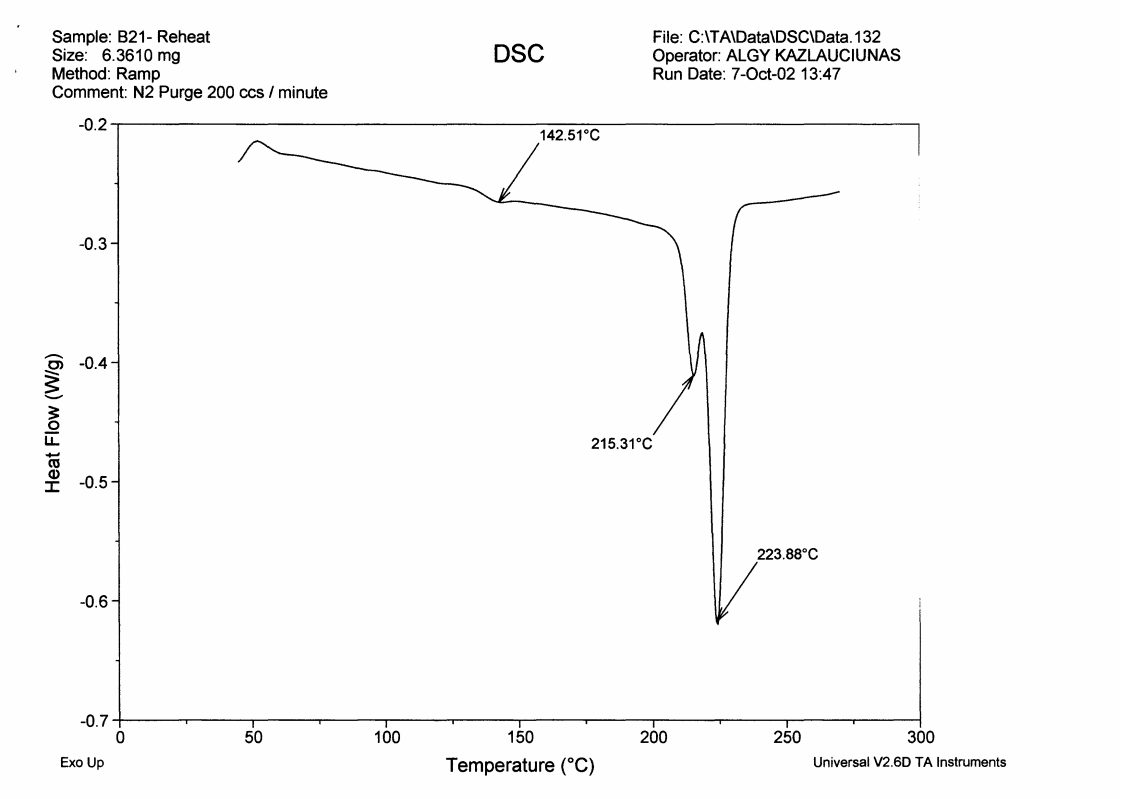

Figure C-42. DSC thermogram of a sample of batch B21 (reheating run).

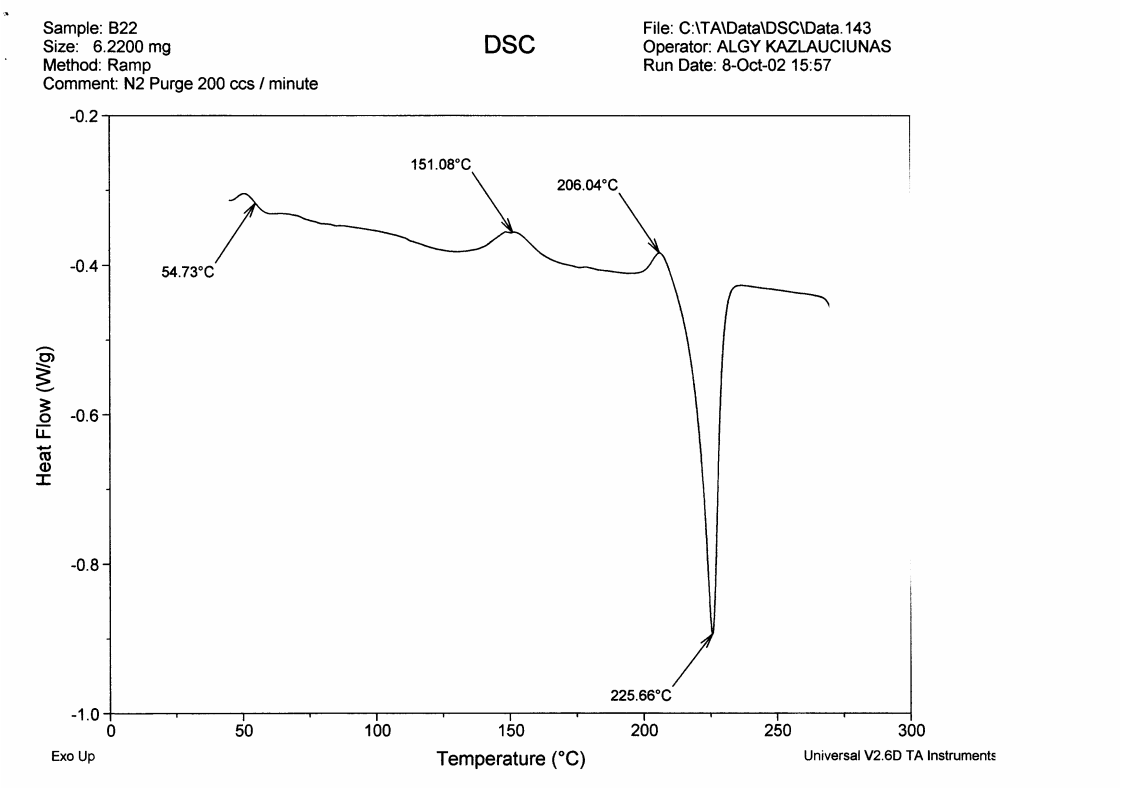

Figure C-43. DSC thermogram of a sample of batch B22 (heating run).

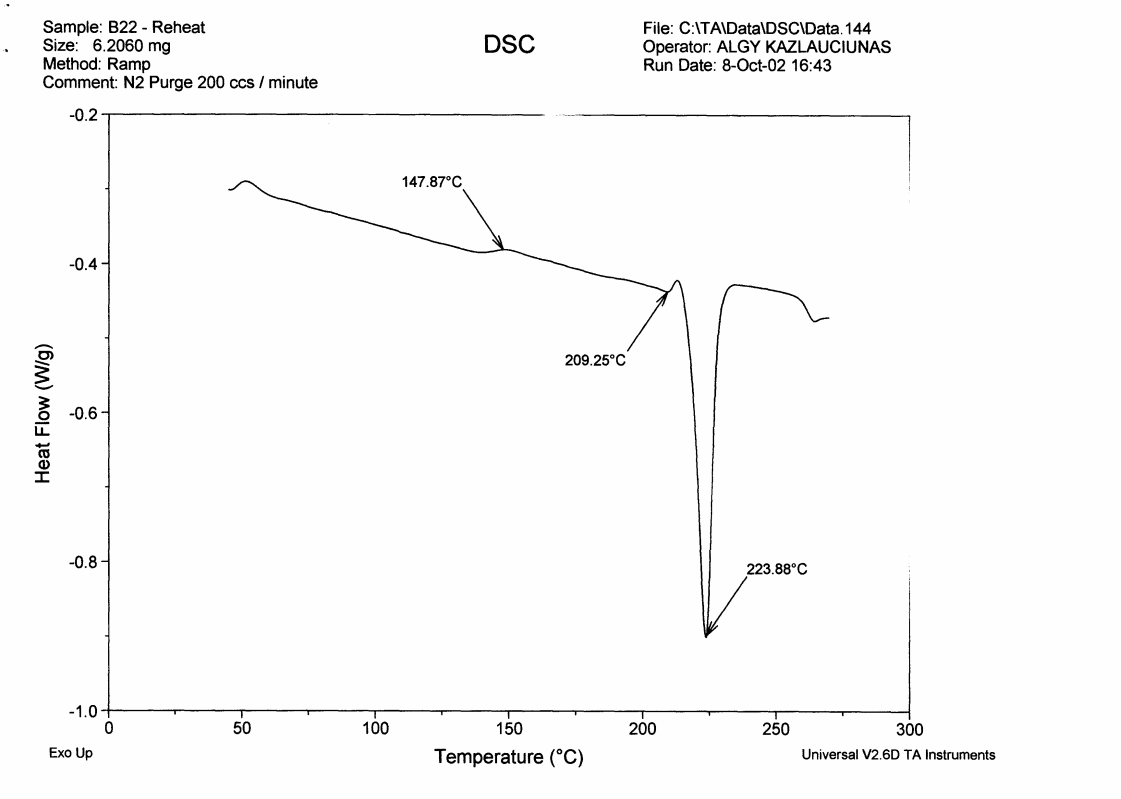

Figure C-44. DSC thermogram of a sample of batch B22 (reheating run).

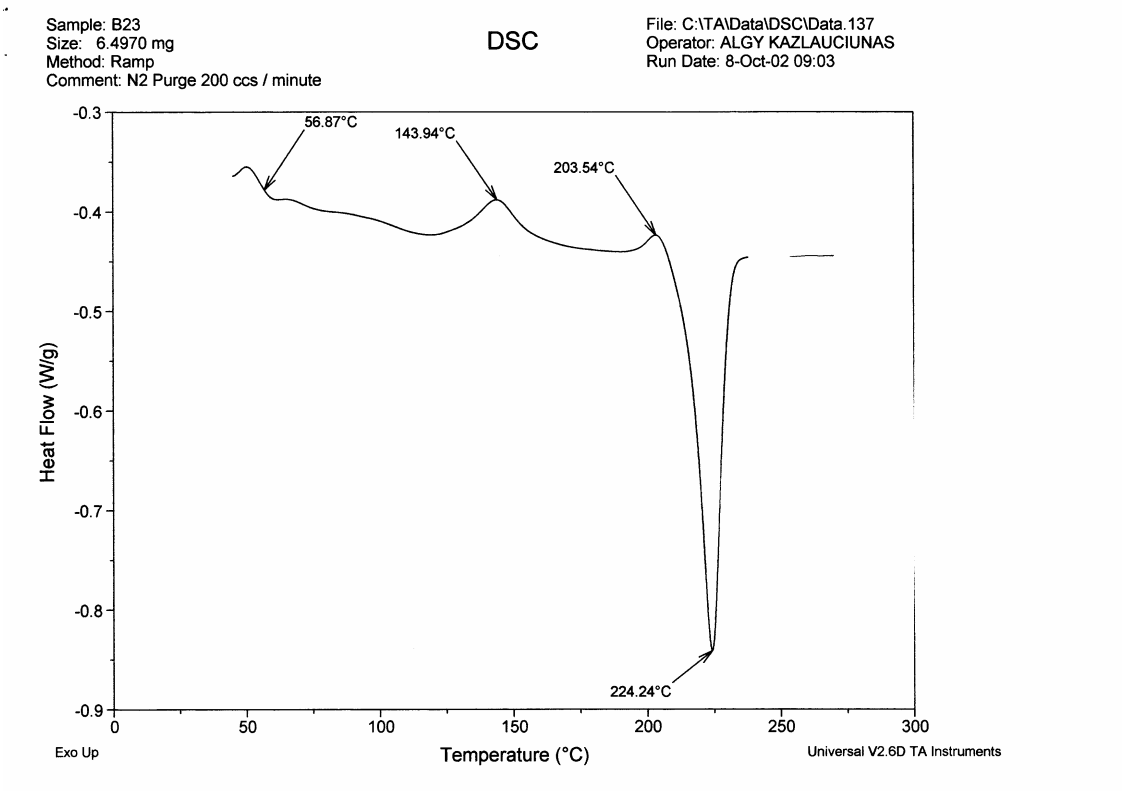

Figure C-45. DSC thermogram of a sample of batch B23 (heating run).

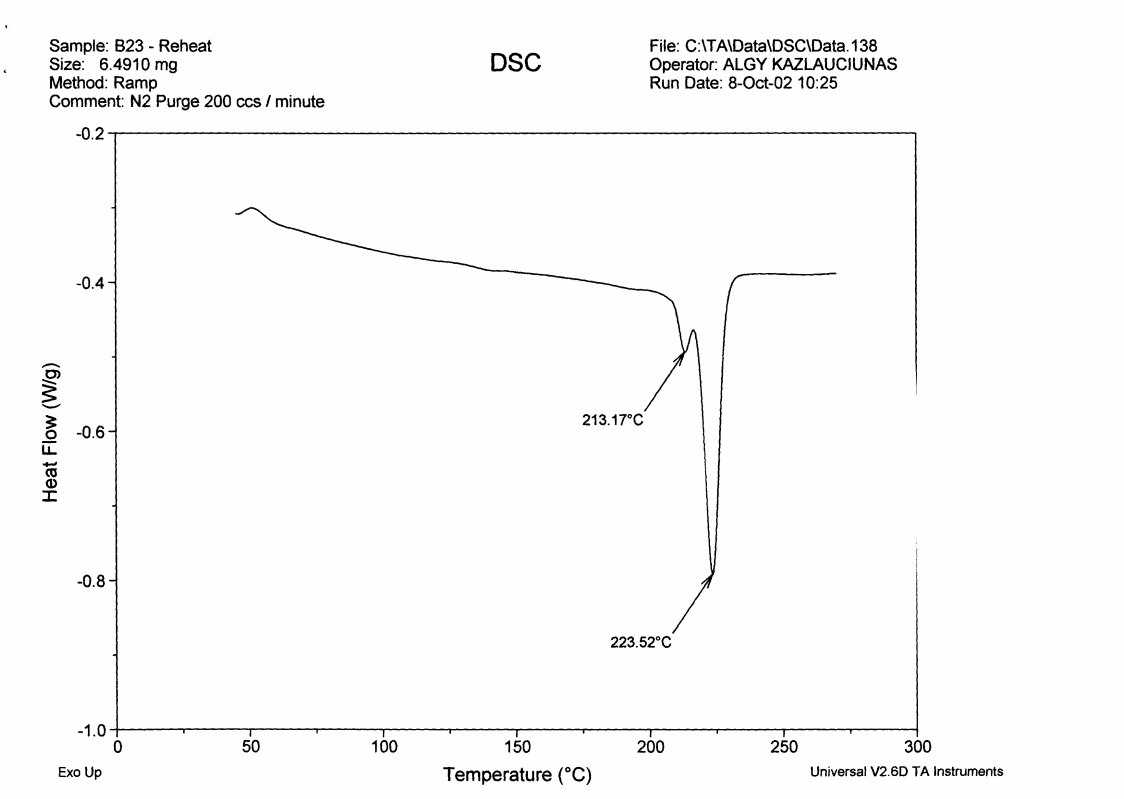

Figure C-46. DSC thermogram of a sample of batch B23 (reheating run).

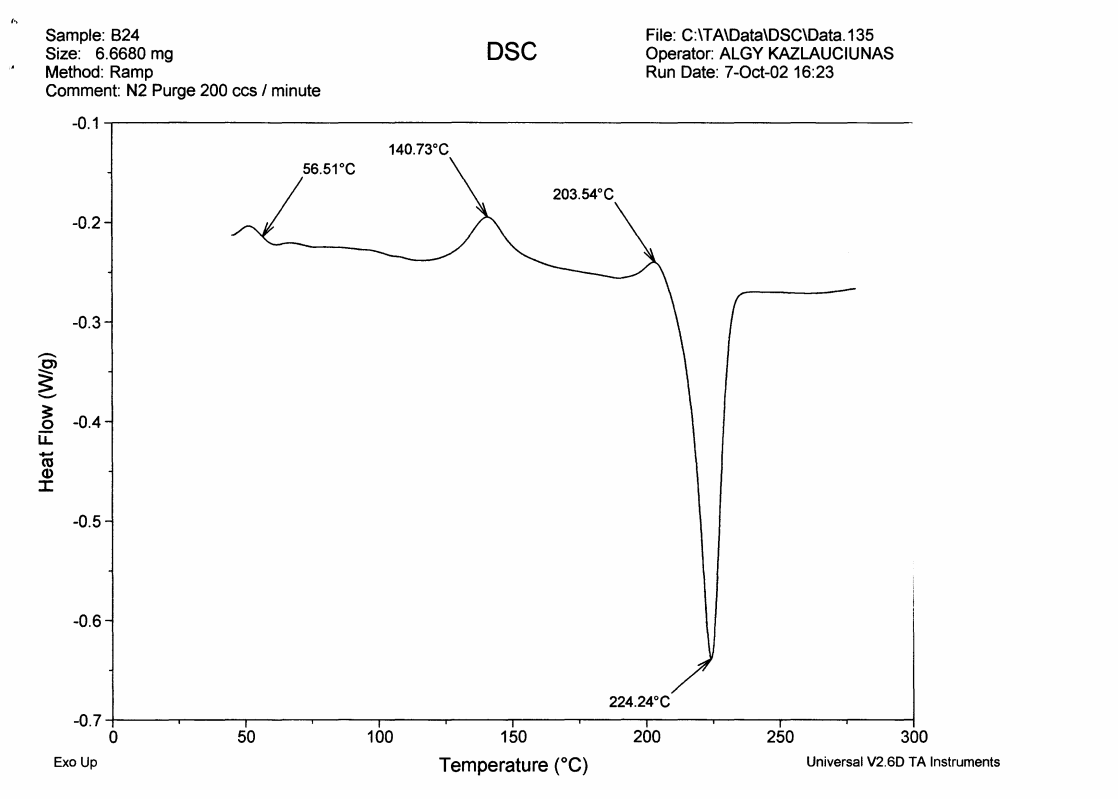

Figure C-47. DSC thermogram of a sample of batch B24 (heating run).

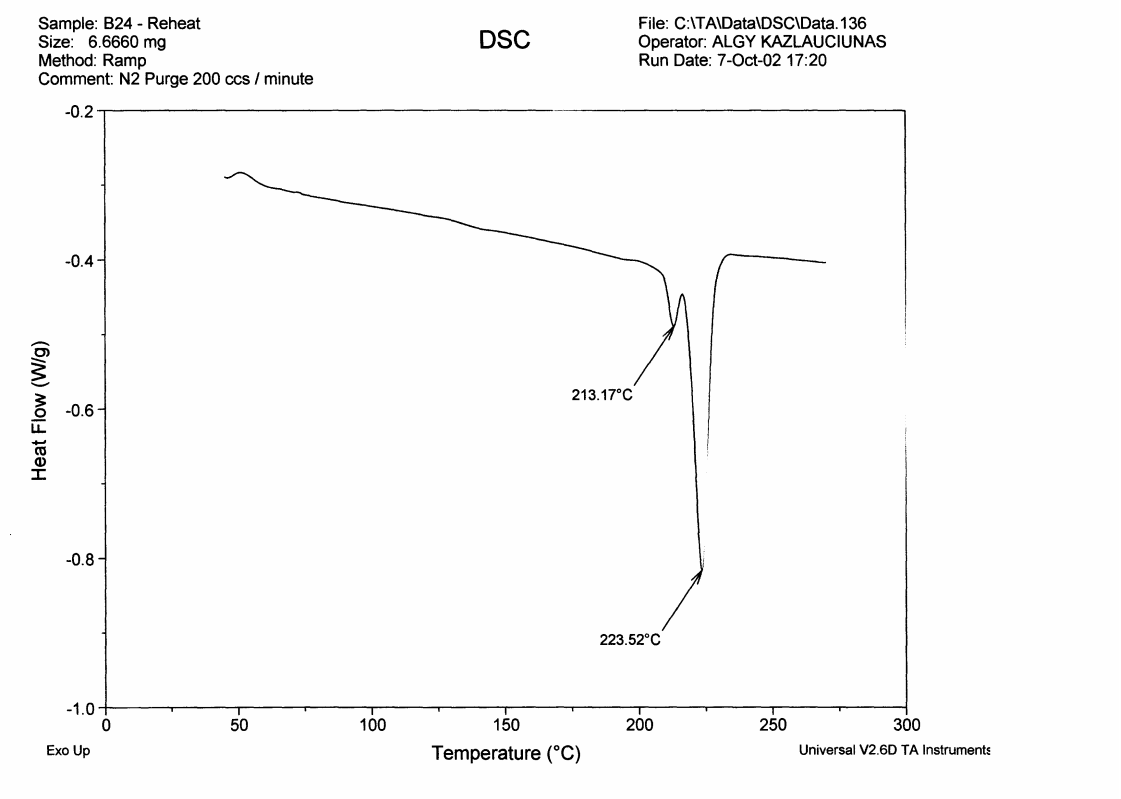

Figure C-47. DSC thermogram of a sample of batch B24 (reheating run).

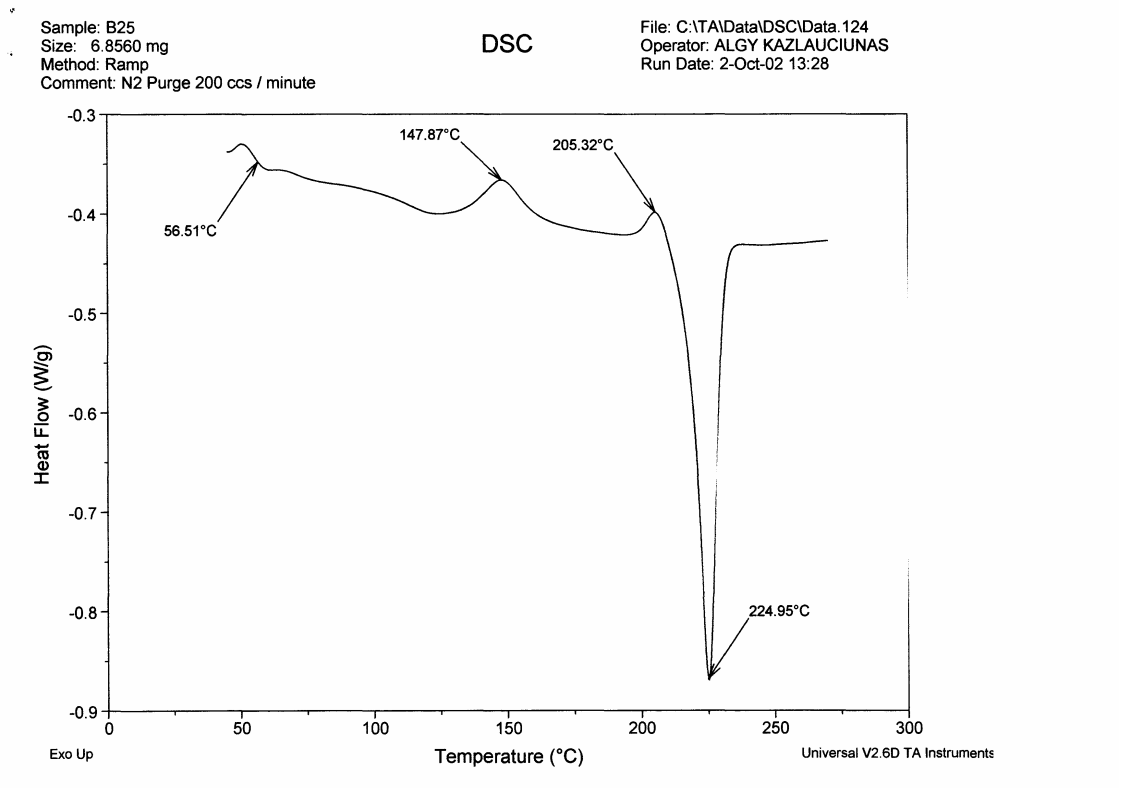

Figure C-48. DSC thermogram of a sample of batch B25 (heating run).

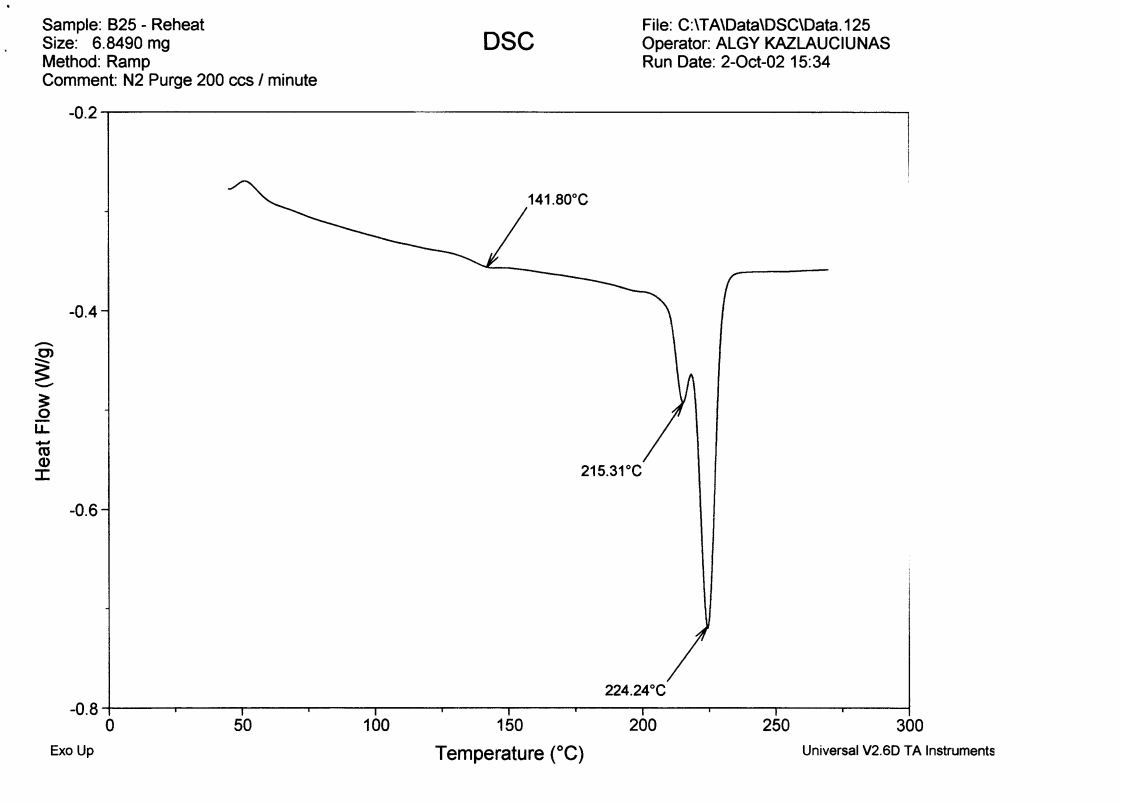

Figure C-49. DSC thermogram of a sample of batch B25 (reheating run).

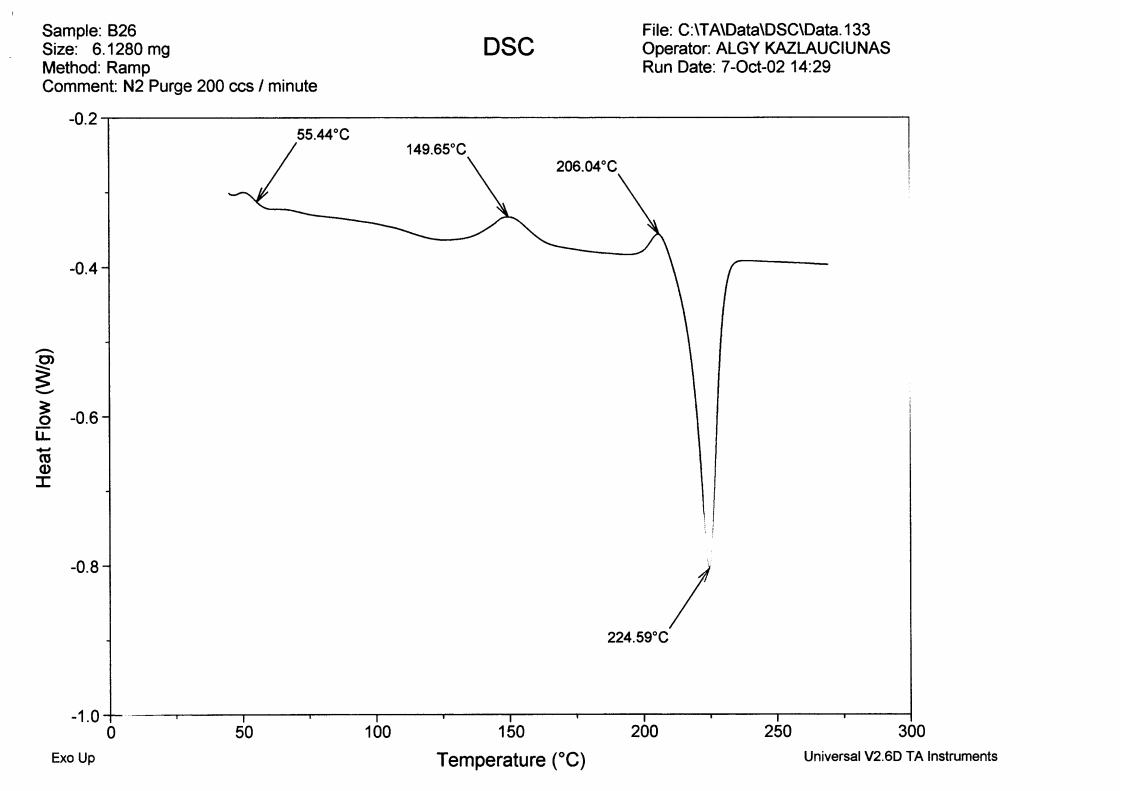

Figure C-50. DSC thermogram of a sample of batch B26 (heating run).

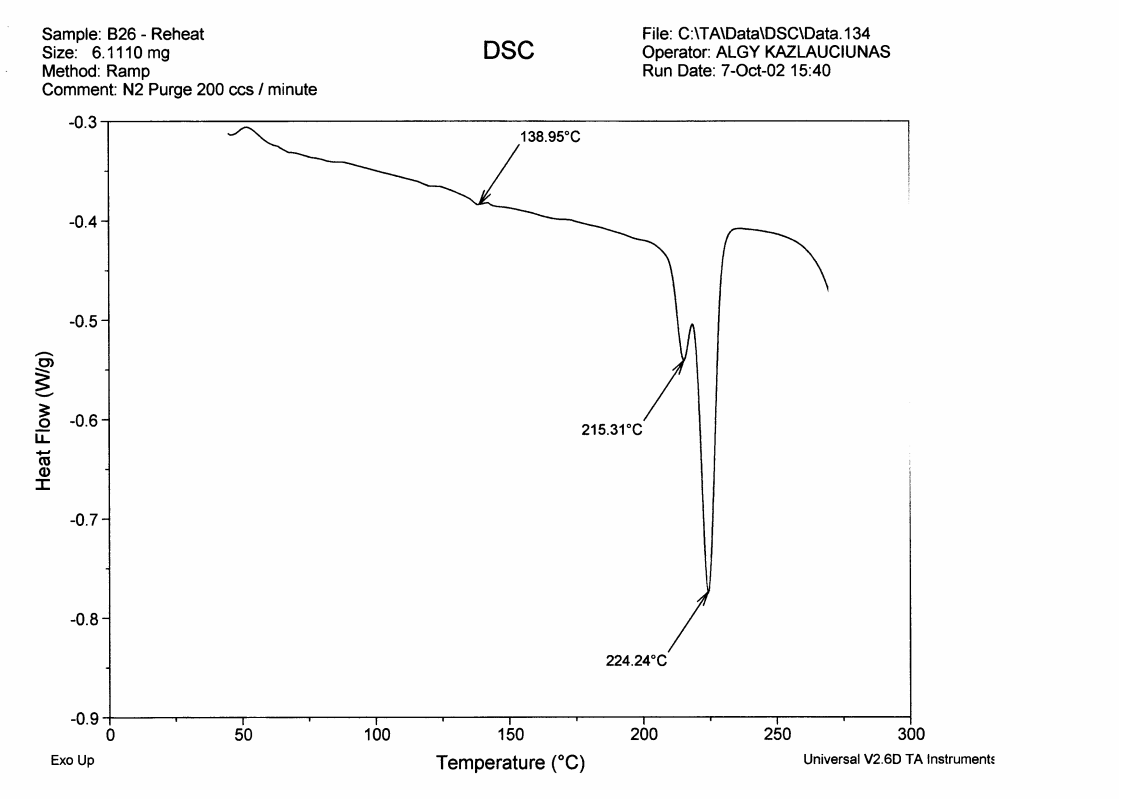

Figure C-51. DSC thermogram of a sample of batch B26 (reheating run).

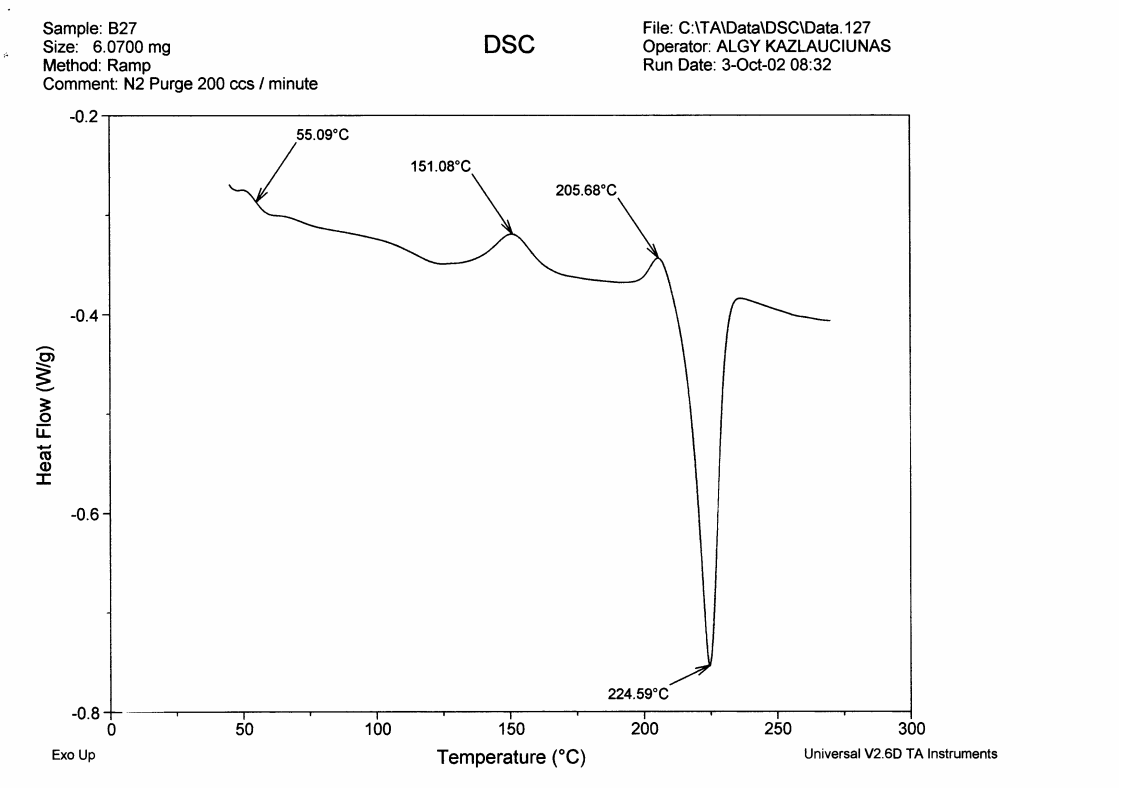

Figure C-52. DSC thermogram of a sample of batch B27 (heating run).

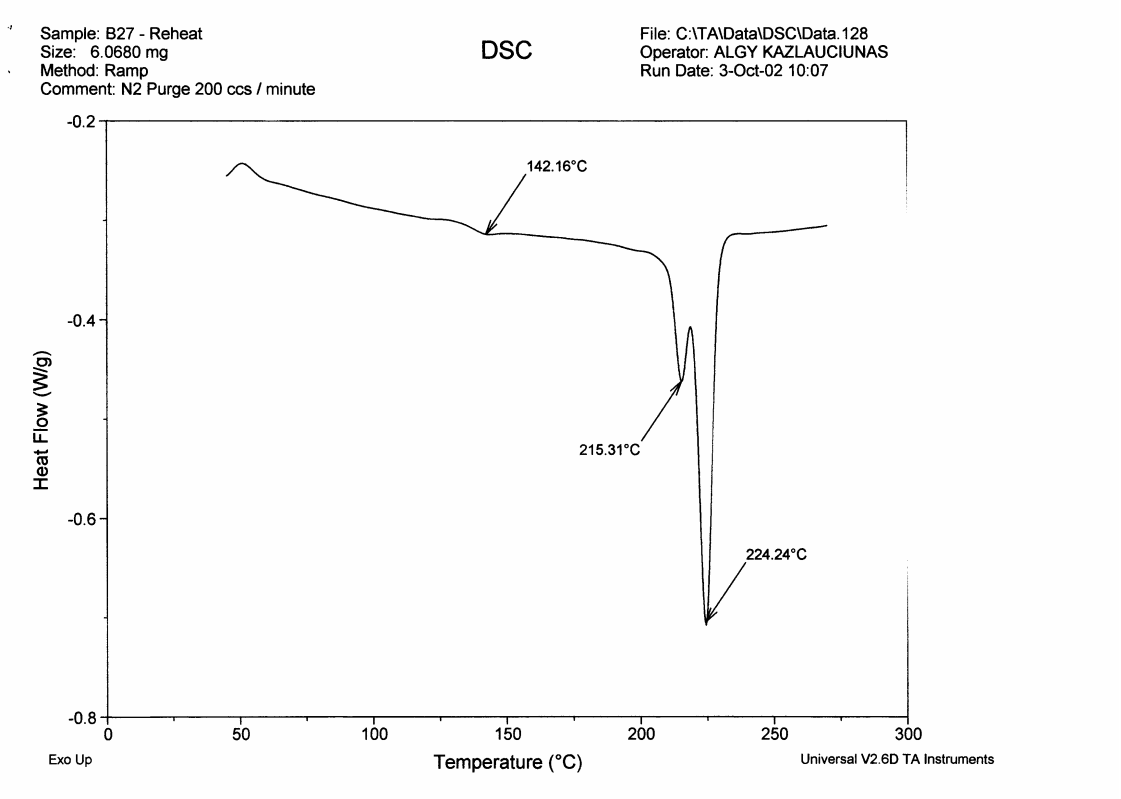

Figure C-53. DSC thermogram of a sample of batch B27 (reheating run).

APPENDIX D. Figures concerning TGA Studies

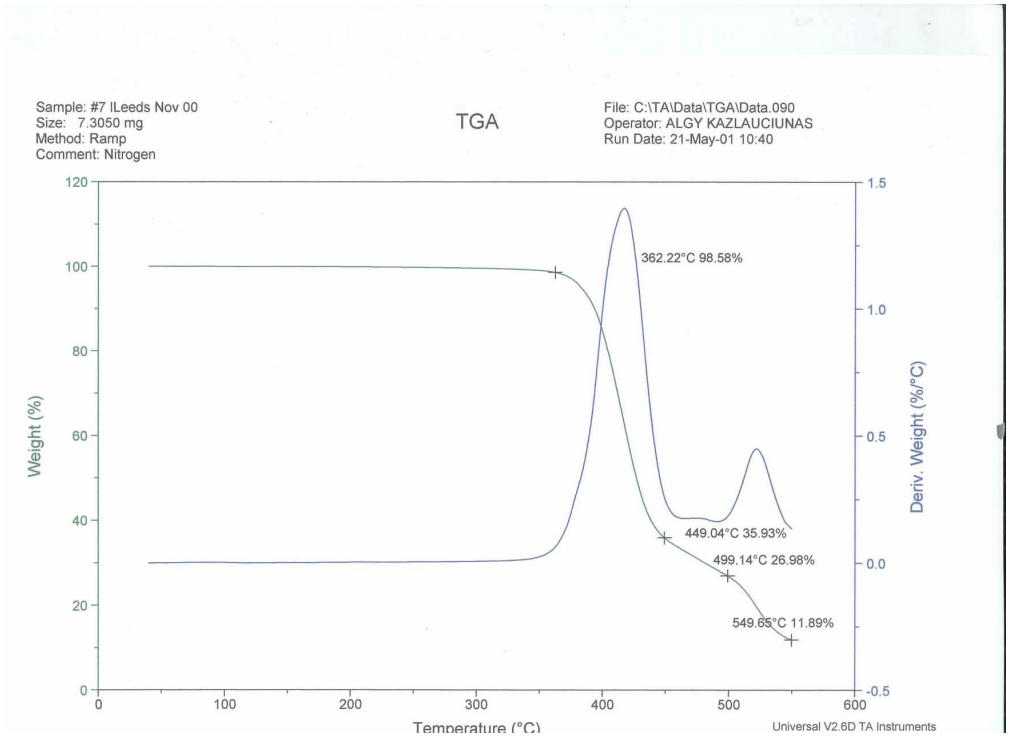

Figure D-1. TGA thermogram of a sample of batch L7.

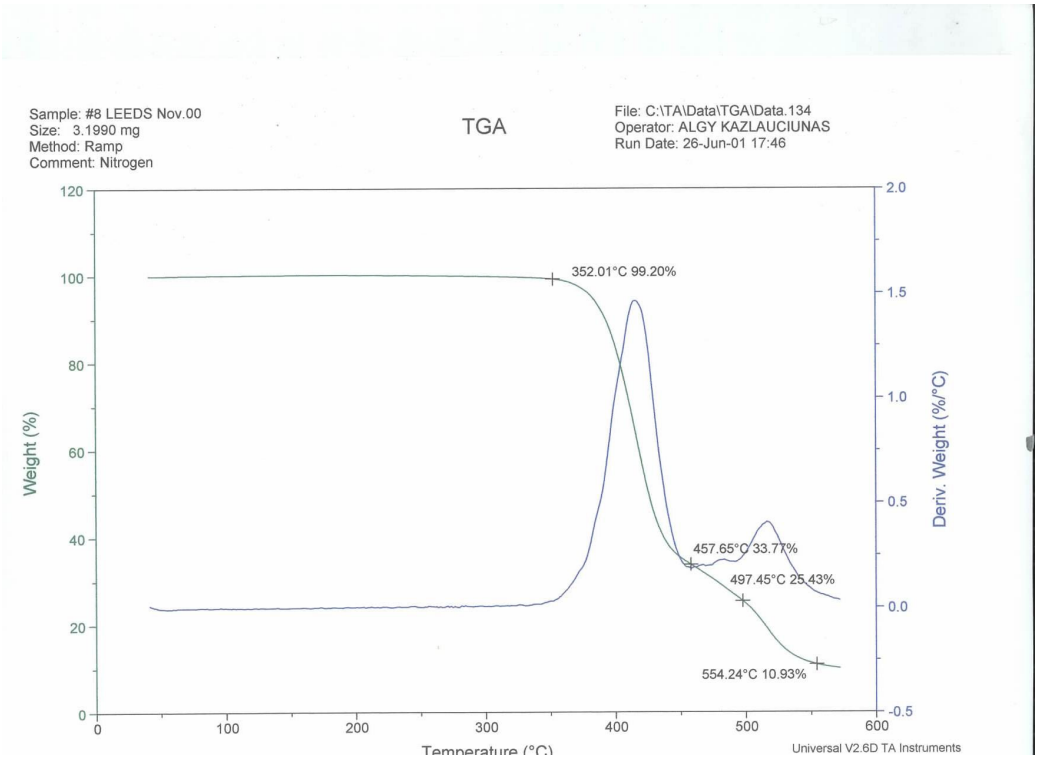

Figure D-2. TGA thermogram of a sample of batch L8.

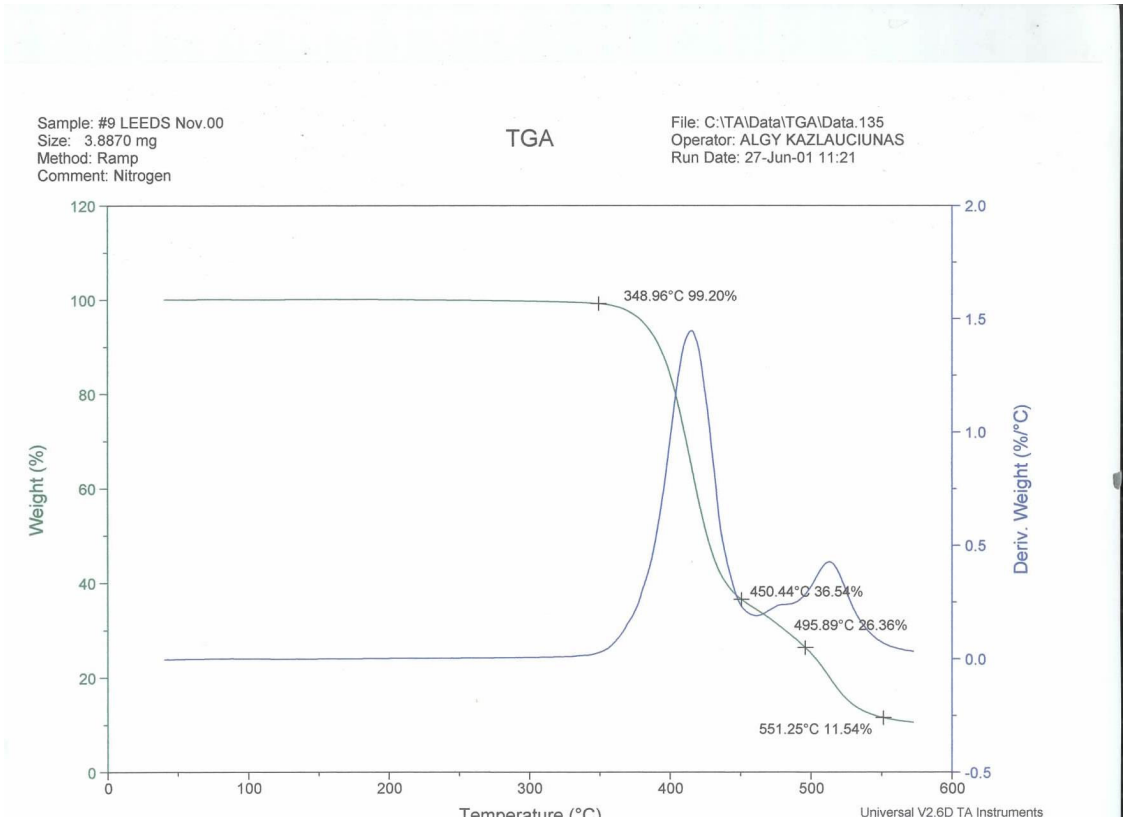

Figure D-3. TGA thermogram of a sample of batch L9.

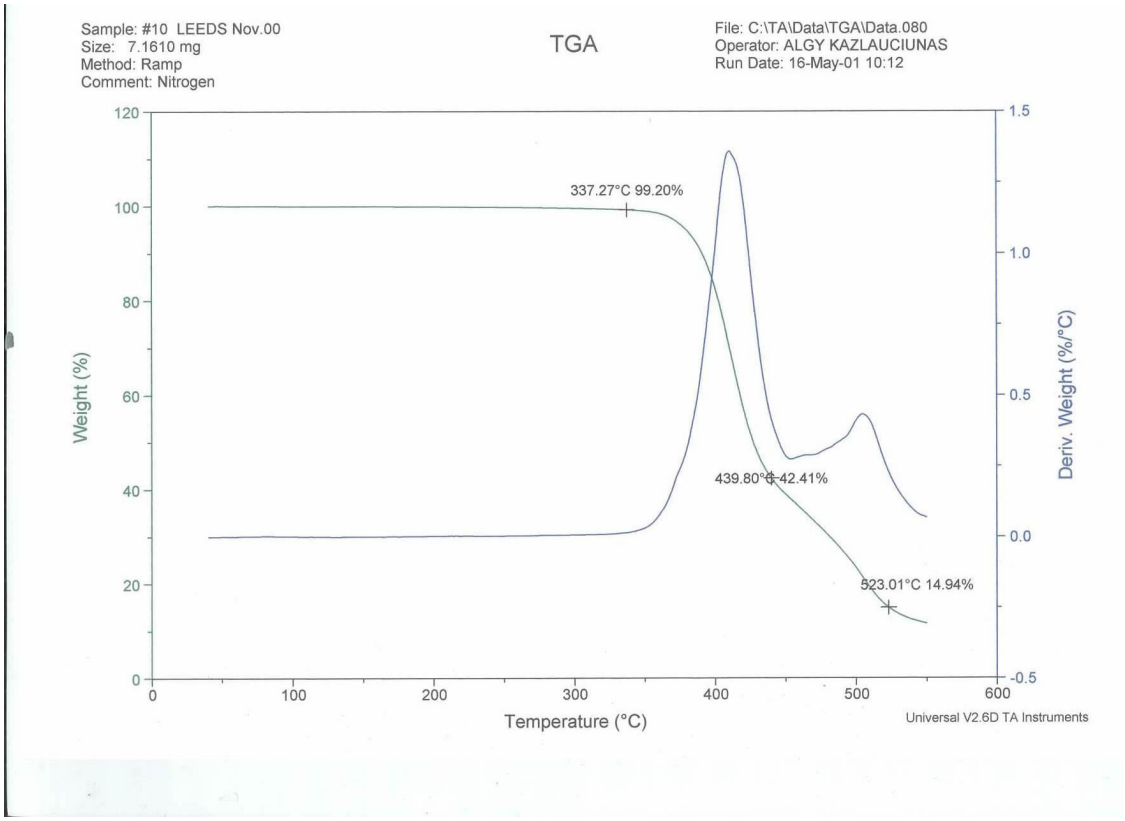

Figure D-4. TGA thermogram of a sample of batch L10.

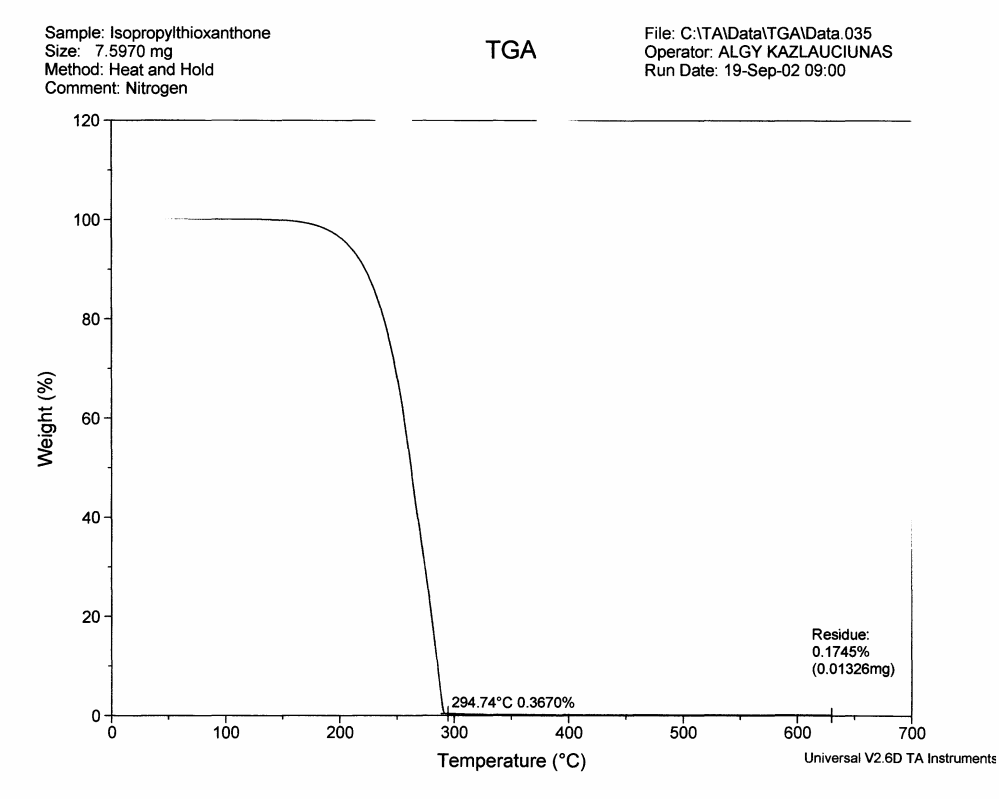

Figure D-5. TGA thermogram of the photoinitiator (ITX).

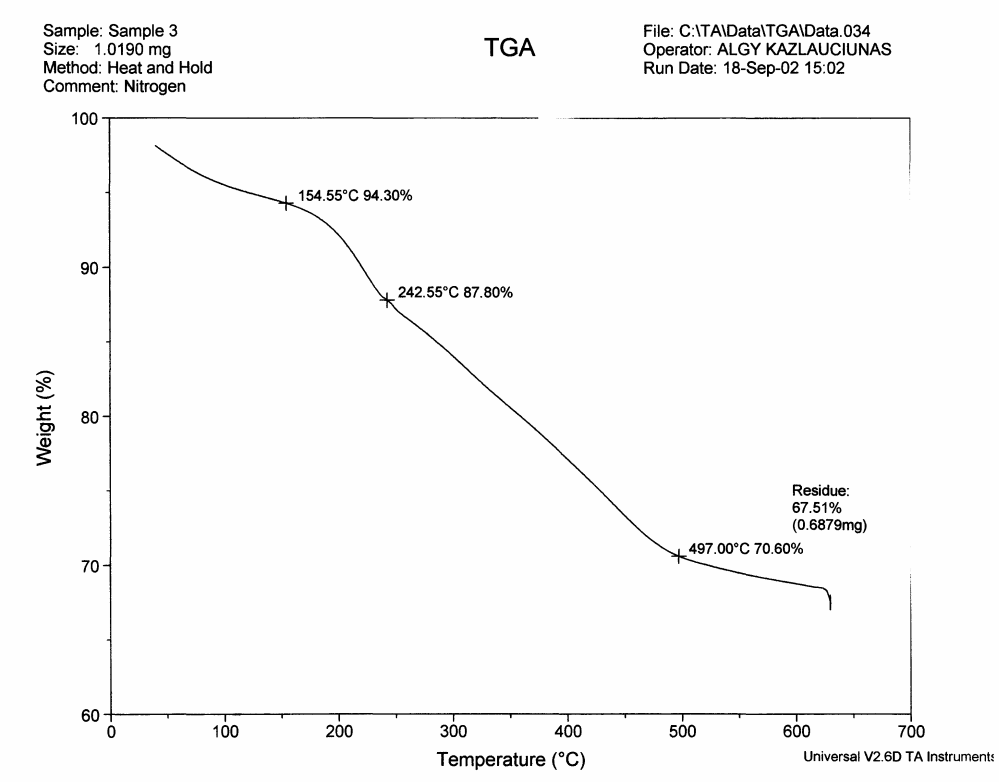

Figure D-6. TGA thermogram of PMMA.

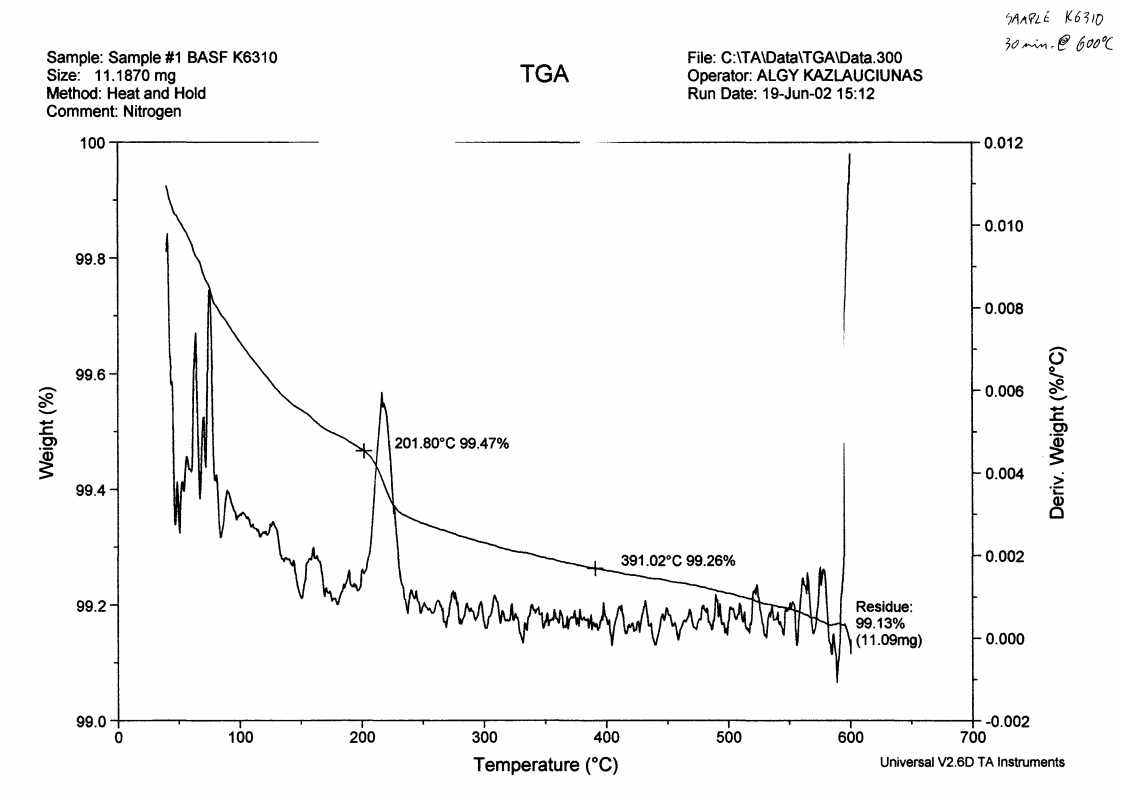

Figure D-7. TGA thermogram of the control pigment (C. I. Pigment Blue 28).

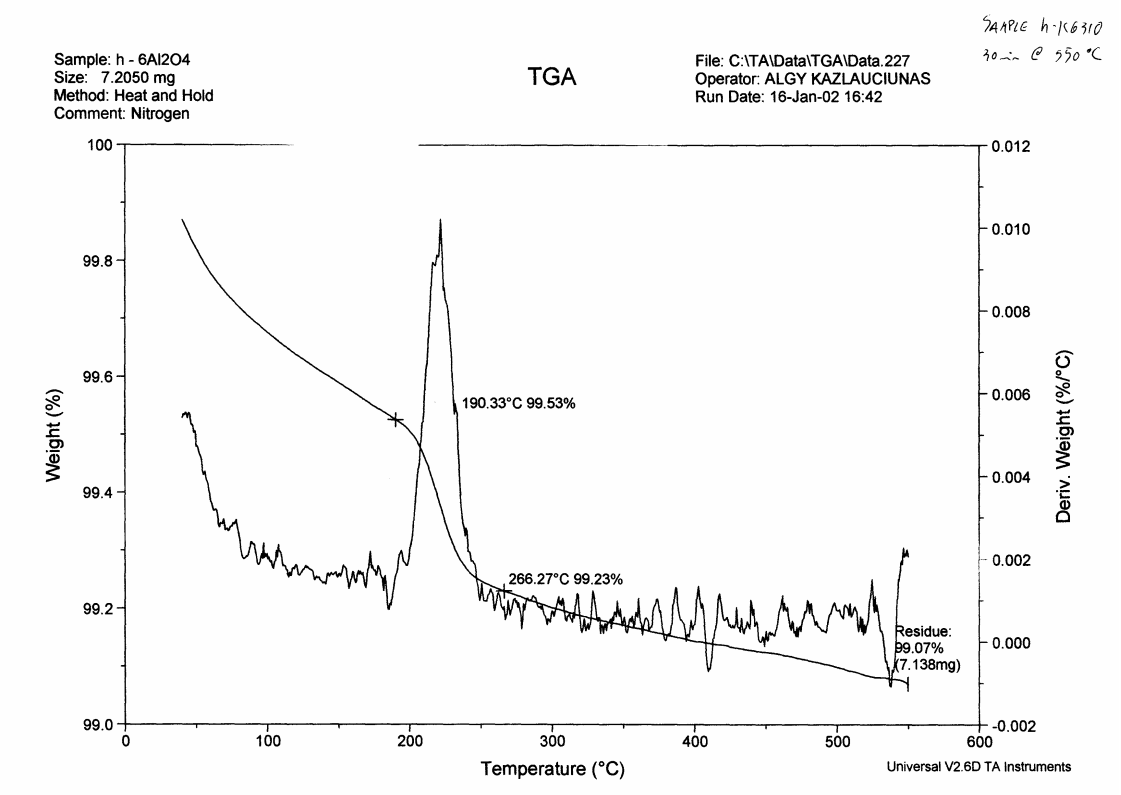

Figure D-8. TGA thermogram of the control hydrated pigment (C. I. Pigment Blue 28).

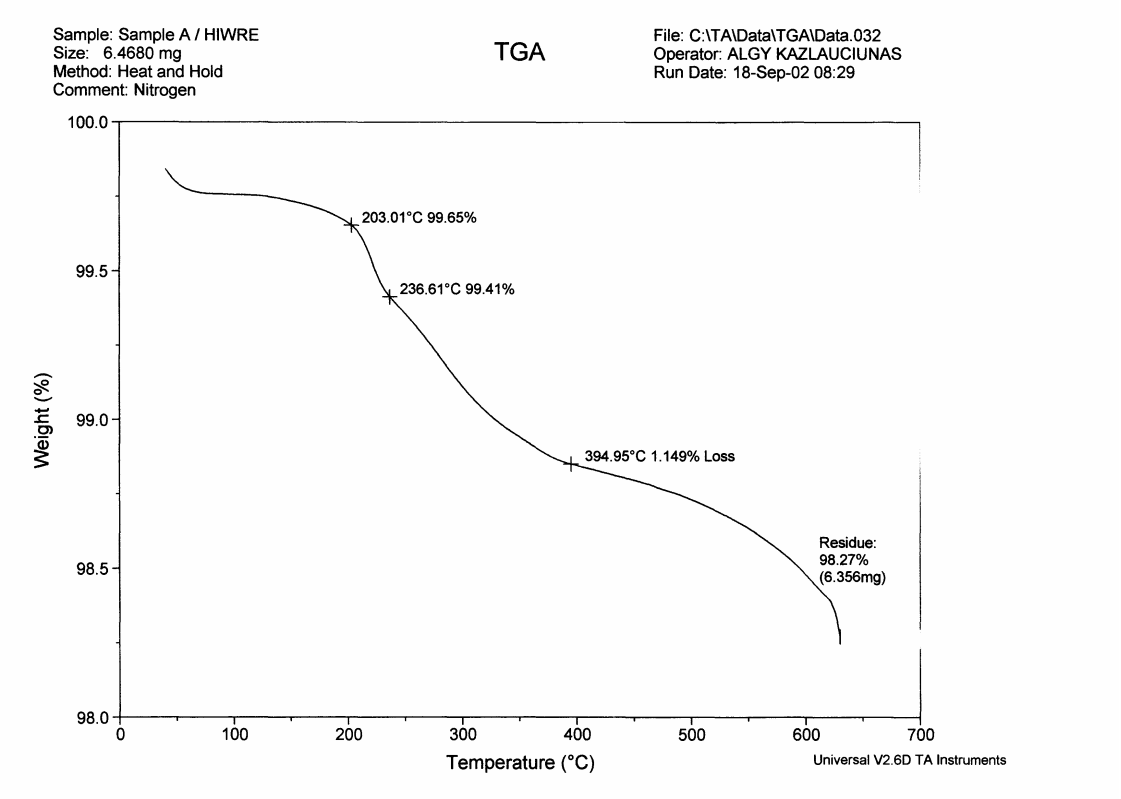

Figure D-9. TGA thermograms of the pigment hiwre (sample 1).

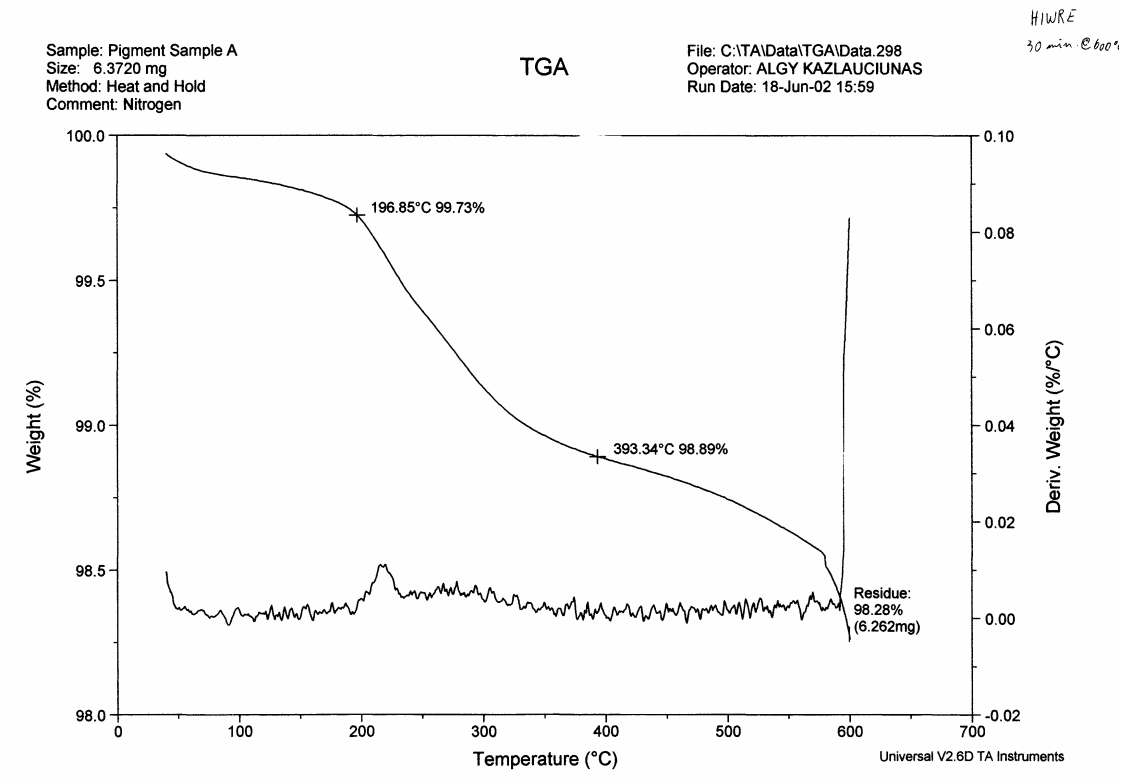

Figure D-10. TGA thermograms of the pigment hiwre (sample 2).

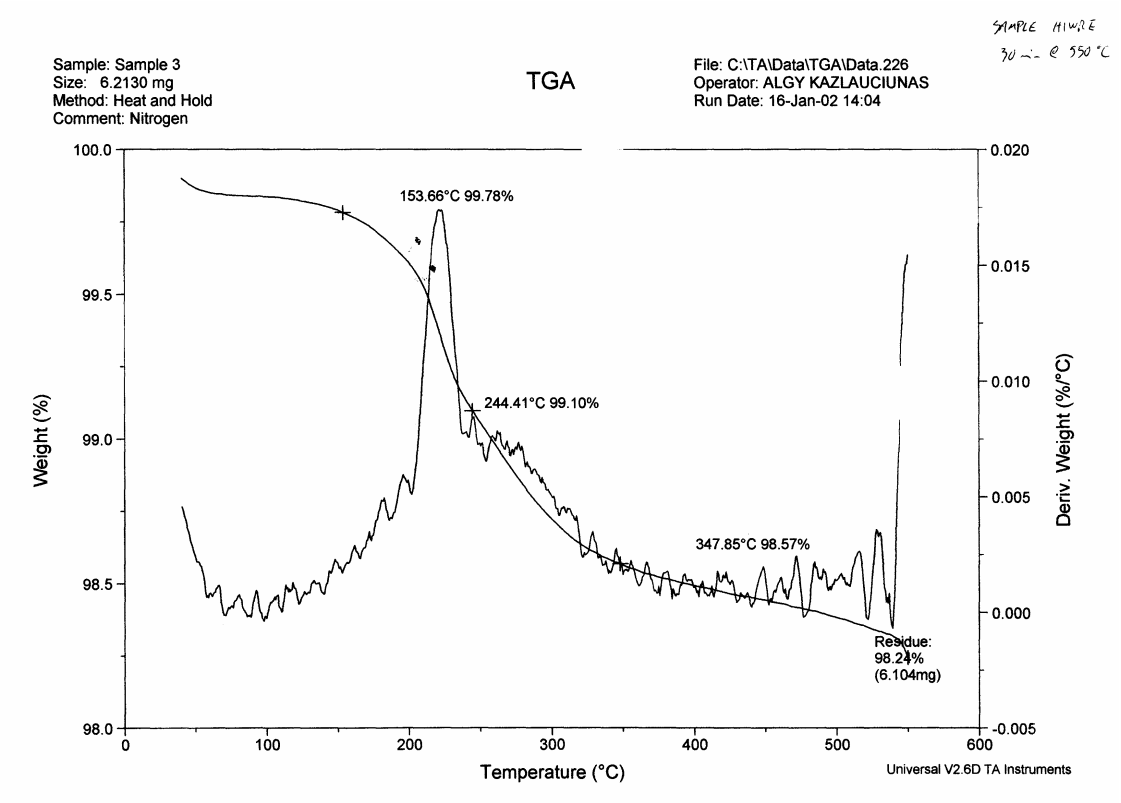

Figure D-11. TGA thermograms of the pigment hiwre (sample 3).

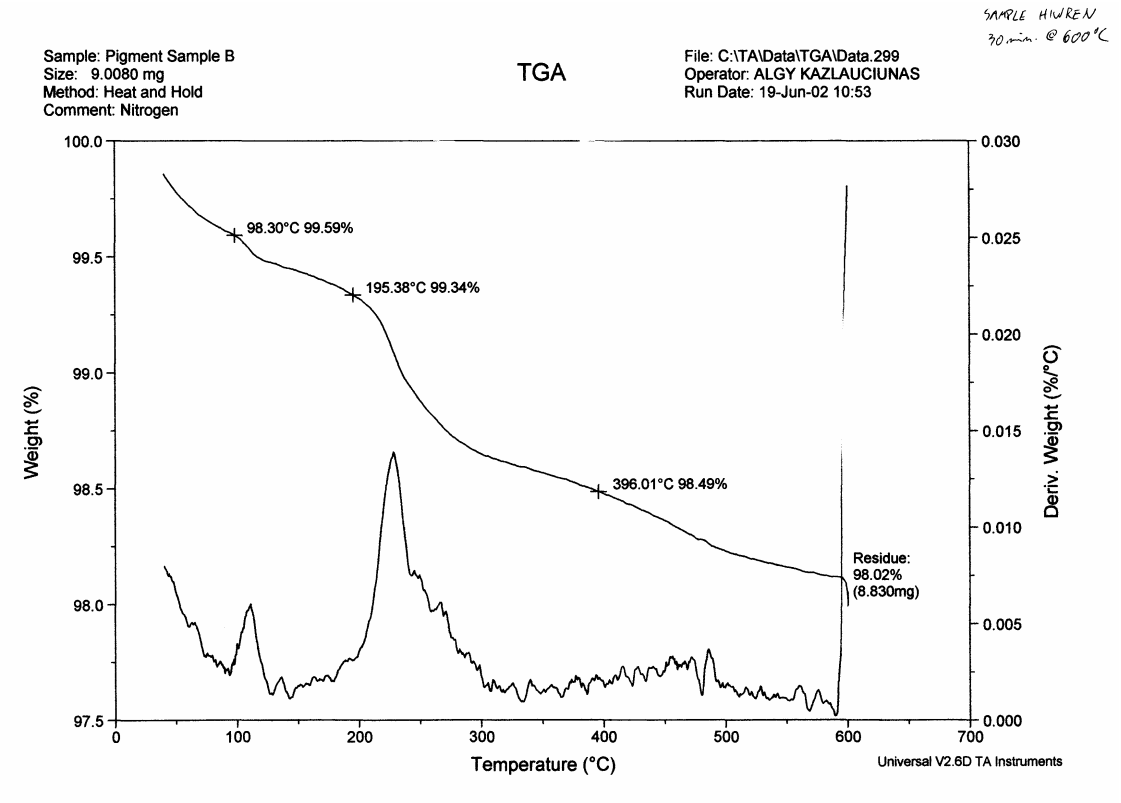

Figure D-12. TGA thermograms of the pigment hiwren.

APPENDIX E. Figures concerning EDXA Studies

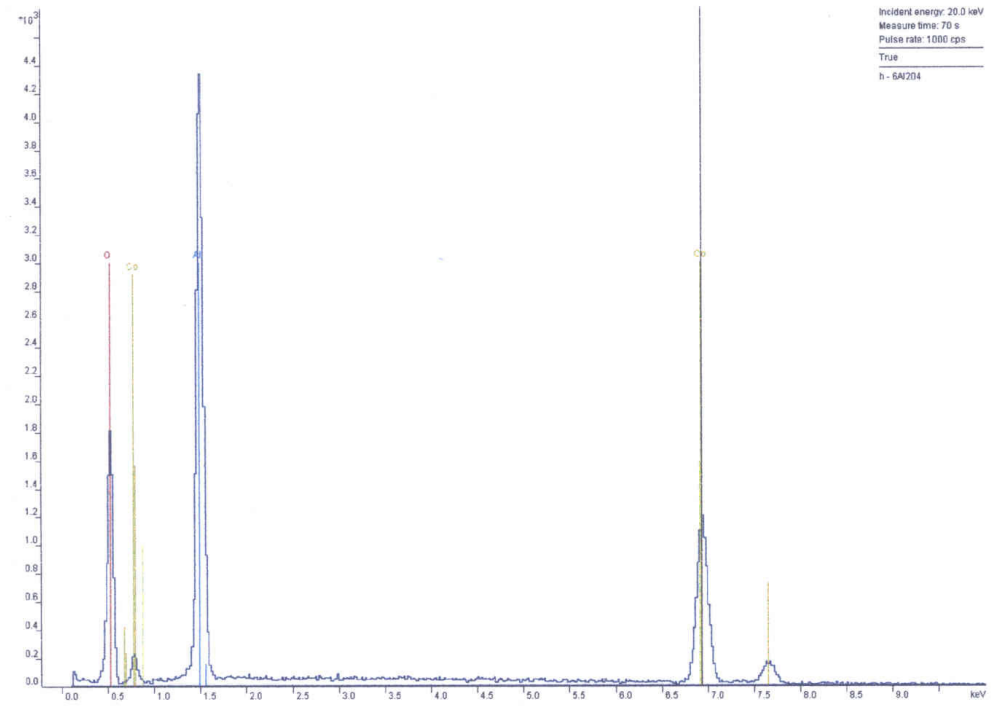

RONTEC EDWIN WinTools	H-6AL204 22.01.2002 (11:13)
NT vers: 3.2 eng	Eo:20.0 keV (TO:35.0 TI: 0.0)

*** PUzaf results ***

elem/line	P/B	B	F	c	c(100%)	confid.	h
O K-ser		1.00000	1.00000	56.15	51.48	+- 8.90	n
Co K-alpha	275.5	1.03200	1.05350	24.96	22.89	+- 4.32	
Al K-ser	236.0	1.00834	1.00322	27.96	25.63	+- 3.68	*
standardless				109.07	100.00	[2s]	

Figure E-1. EDXA results for the control sample (unmodified pigment).

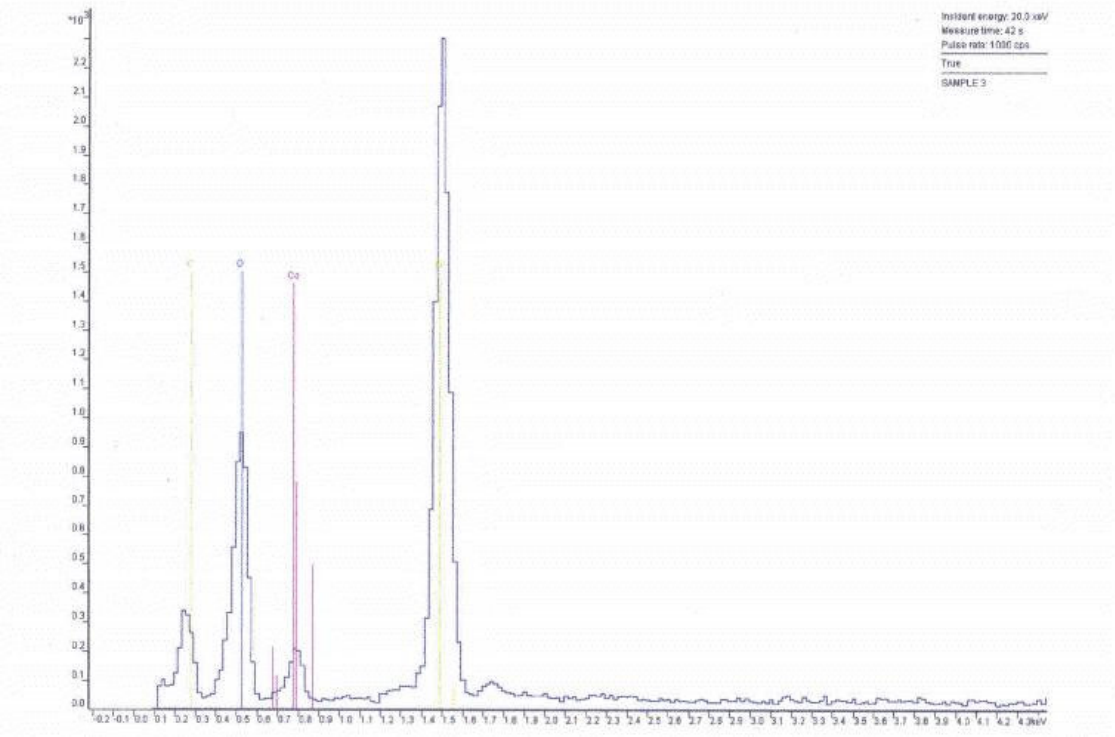

Figure E-2. EDXA results for pigment hiwre.

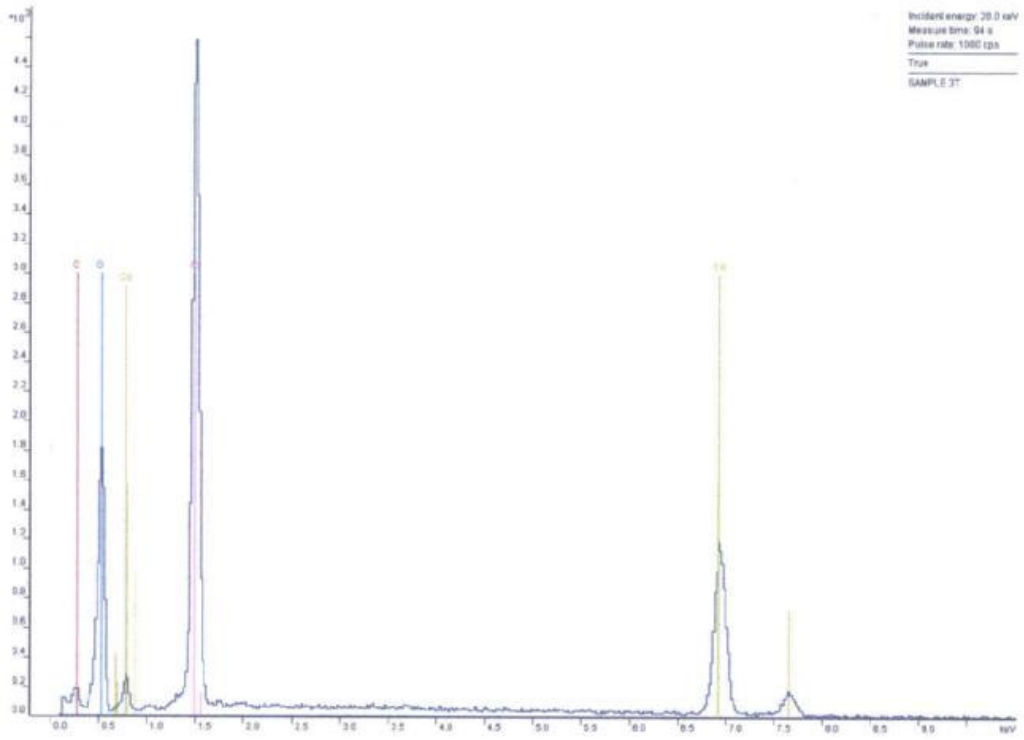

```
================================   ================================
    RONTEC EDWIN WinTools          SAMPLE3T    18.01.2002 (14:47)
================================   ================================
      NT vers: 3.2 eng             Eo:20.0 keV  (TO:35.0  TI: 0.0)
```

*** PUzaf results ***

elem/line	P/B	B	F	c	c(100%)	confid.	h
C K-ser	Coat?	1.00000	1.00000	5.24	5.74	+- 1.16	n
O K-ser		1.00000	1.00000	33.06	36.27	+- 6.22	n
Co K-alpha	276.1	1.03412	1.04695	27.03	29.65	+- 5.81	
Al K-ser	204.6	1.00889	1.00336	25.82	28.33	+- 4.50	*
standardless				91.14	100.00	[2s]	

Figure E-2. EDXA results for pigment hiwren.

APPENDIX F. Figures concerning DMTA Studies

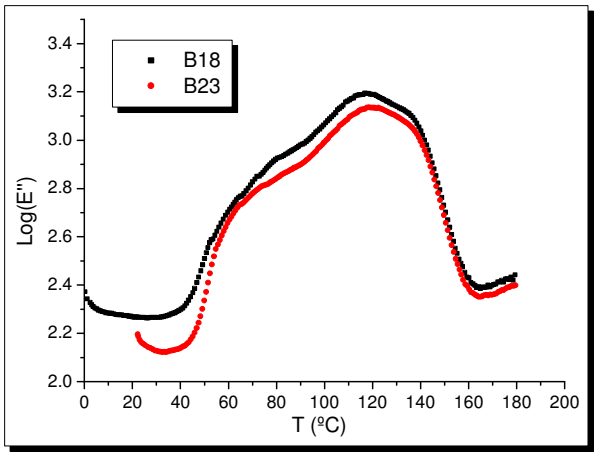

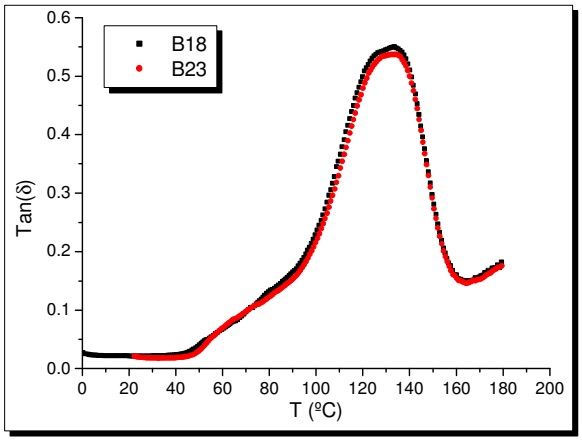

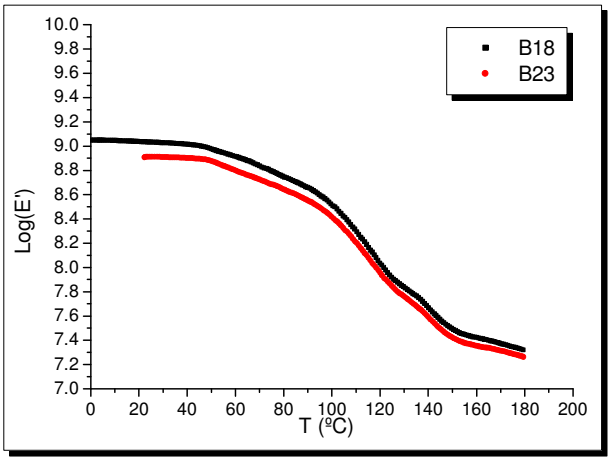

Figure F-1. Loss modulus, loss tangent, and storage modulus *versus* temperature, for samples of batches B18 and B23.

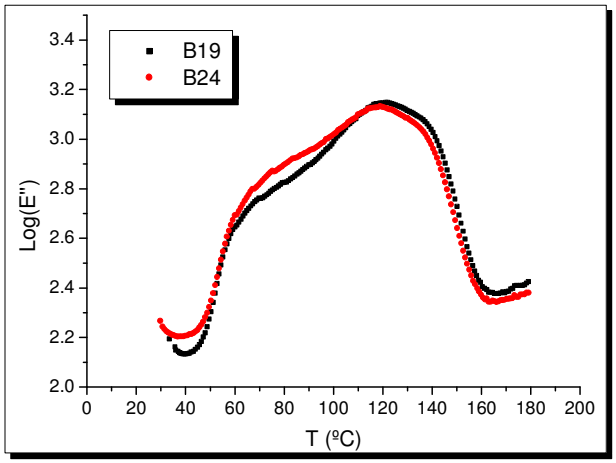

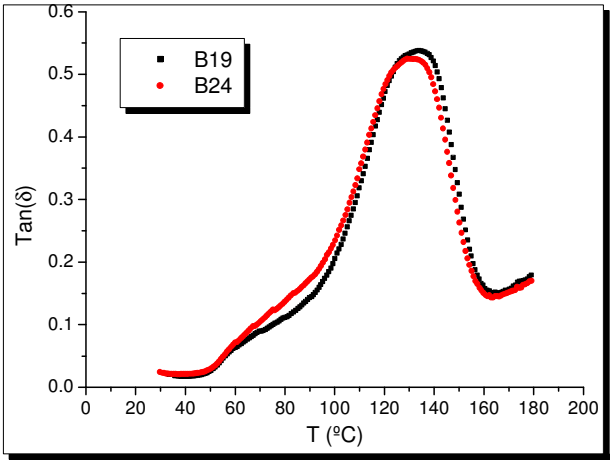

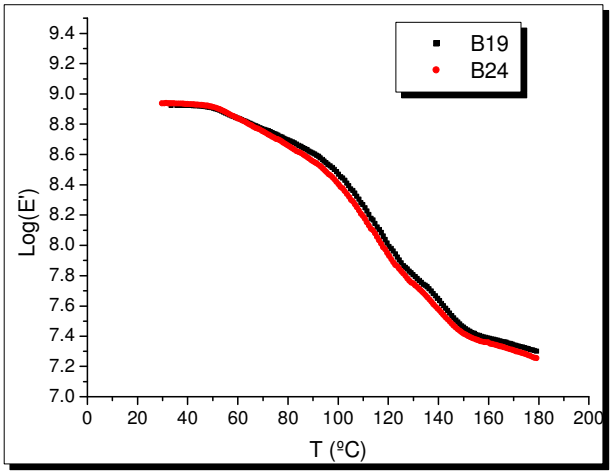

Figure F-2. Loss modulus, loss tangent, and storage modulus *versus* temperature, for samples of batches B19 and B24.

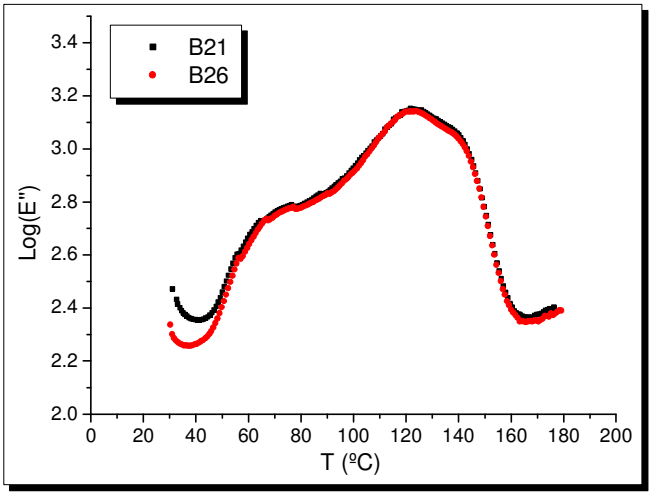

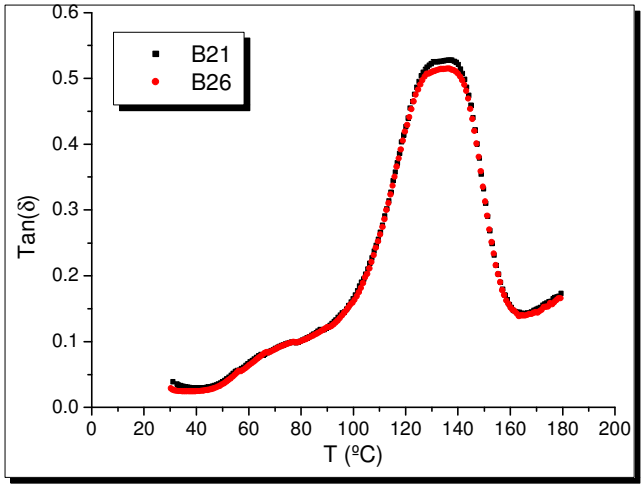

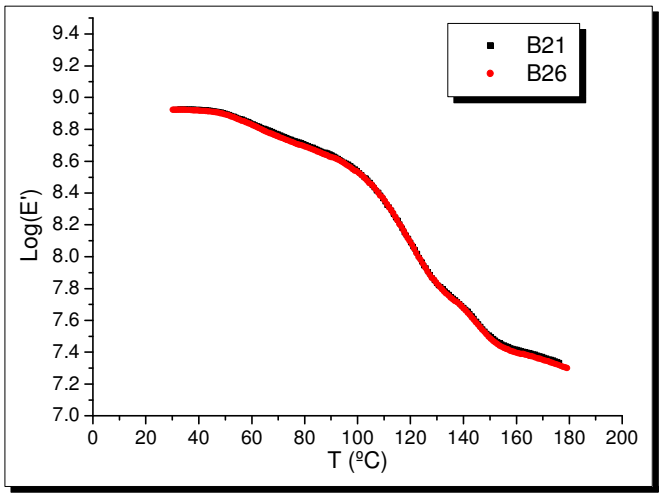

Figure F-3. Loss modulus, loss tangent, and storage modulus *versus* temperature, for samples of batches B21 and B26.

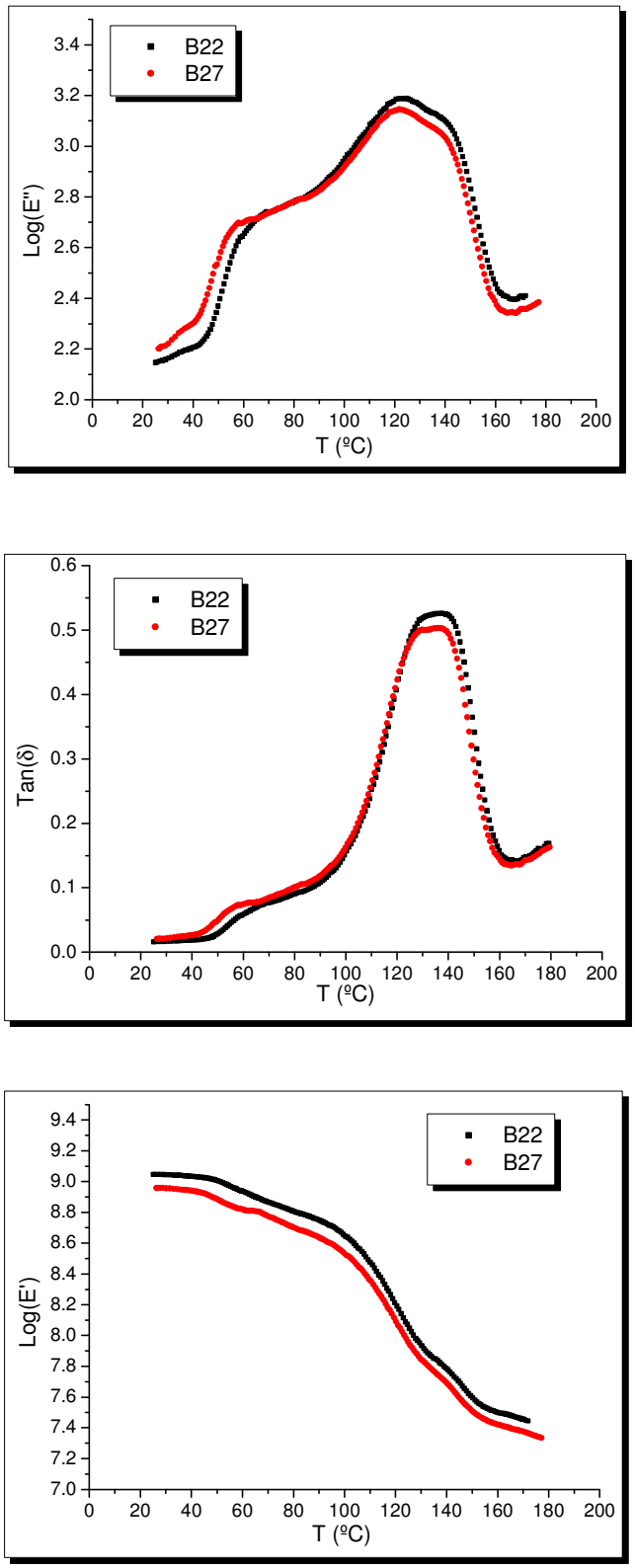

Figure F-4. Loss modulus, loss tangent, and storage modulus *versus* temperature, for samples of batches B22 and B27.

APPENDIX G. Izod Notched Impact Test Information

The notched Izod test is best applied to the determination of the impact resistance for parts with many sharp corners, such as ribs, intersecting walls and other stress risers. Impact properties can be very sensitive to test specimen thickness and molecular orientation.

In this approach, the specimen is clamped upright in the vice of the impact machine (Figure G-1).

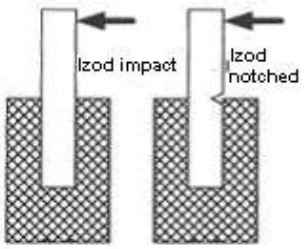

Figure G-1. Izod impact and Izod notched impact testing.

The pendulum hammer, with a hardened steel striking edge of specified radius, is released from a predefined height, leading to shear of the specimen due to the abrupt load. The residual energy in the pendulum hammer moves it upwards (Figure 2-6), and the difference in the drop height (h_1) and return height (h_2) is proportional to the energy necessary to break the test bar. The test can be carried out at room temperature, or at lower temperatures (to test cold-temperature embrittlement). The results are defined as the impact energy in Joules needed to break the test specimen, divided by the specimen area at the notch. Results are reported in kJ/m^2.

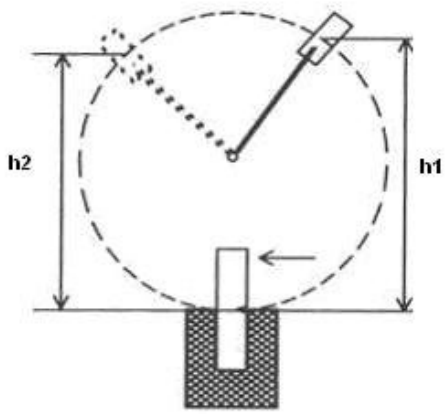

Figure G-2. Sketch of the Izod test.

APPENDIX H. Tensile Test Information

The elastic modulus (or tensile modulus) is the ratio of stress to strain below the proportional limit of the material (Figure 2-7). Moulded parts must be designed such that, in real situations, they are able to accommodate stress levels below those used in the tensile testing. Tensile stress-strain representations are the most widely reported mechanical property for comparing plastic materials or for designing a plastic part. The mechanical properties determined are (Figure 2-7):

Stress = load/(original cross sectional area), MPa (H-1)

Strain = (elongation/(original length))*100, % (H-2)

Modulus = stress/strain, MPa (H-3)

Stress at yield = initial maximum stress, MPa (H-4)

Strain at yield = initial maximum strain, % (H-5)

Stress at break = stress at failure, MPa (H-6)

Strain at break = strain at failure, % (H-7)

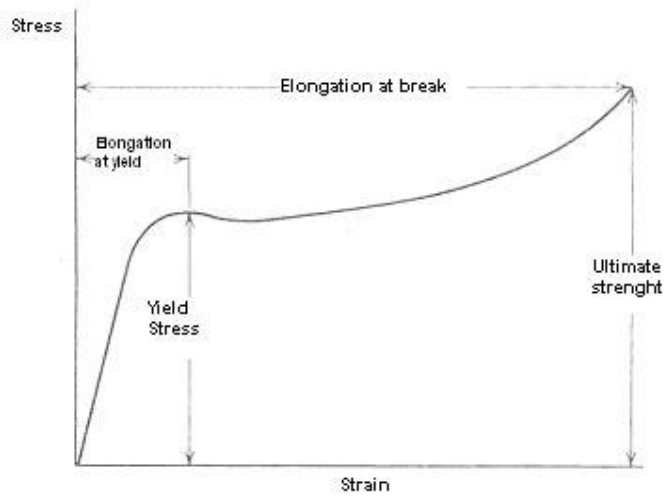

Figure H-1. Generalised tensile-strain curve for plastics.

In applications where rubbery elasticity is of interest, a high elongation at break is desirable. In the case of rigid plastic parts, there is significant advantage in having moderate elongation, as this characteristic benefits impact energy absorption. On the other hand, a material that is characterised by high tensile modulus, and low elongation at break, would tend to be brittle when in use.

APPENDIX I. Dynamic Mechanical Thermal Analysis Information

When a sinusoidal stress is applied to a perfectly elastic solid, the deformation (and, thus, the strain) occurs exactly in phase with the applied stress. A completely viscous material will respond with the deformation lagging 90º behind the applied stress (Figure I-1)

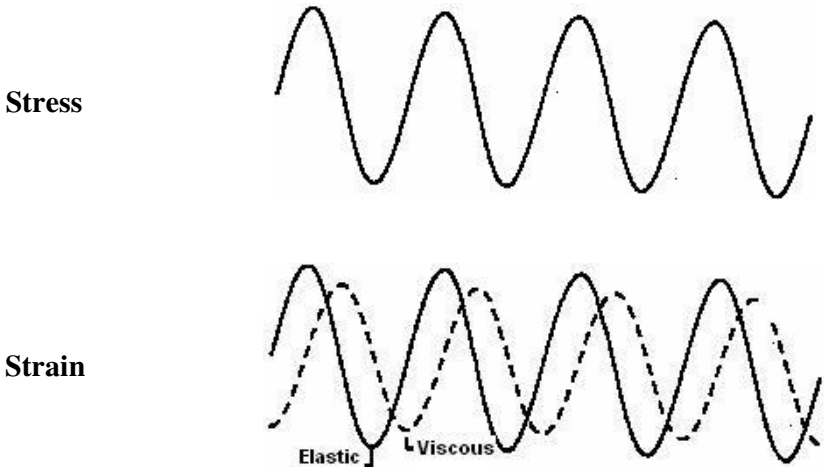

Figure I-1. Schematic representation of the response of perfectly elastic materials and of perfectly viscous materials to an applied stress.

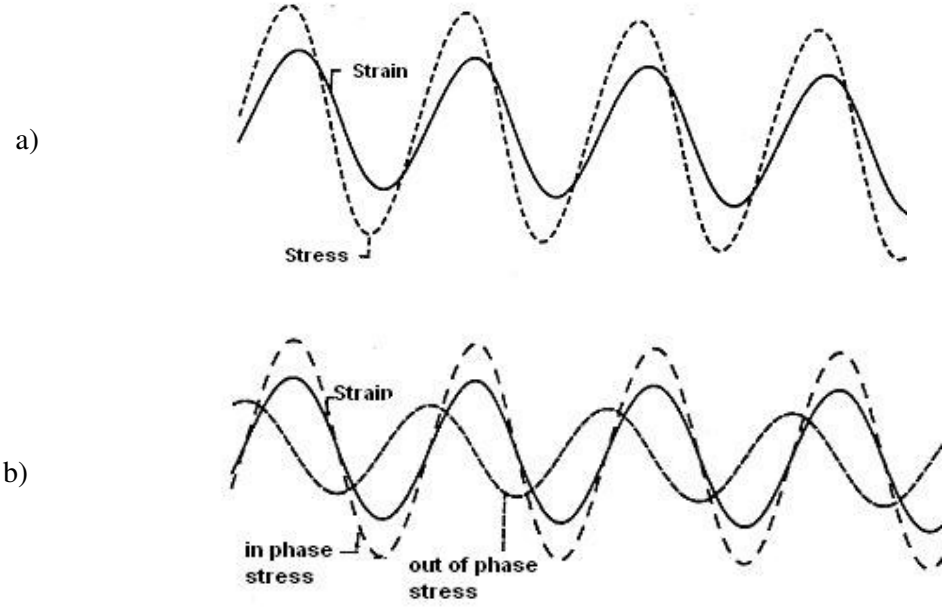

Figure I-2. a) Schematic representation of the response of a viscoelastic material to an applied sinusoidal stress. b) Schematic representation of the resolution of the in phase stress component and of the out of phase stress component.

In real situations, when a sinusoidal stress is applied to a viscoelastic material, the material will behave neither as a perfectly elastic nor as perfectly viscous material. The resultant strain will lag behind the stress by an angle δ where δ< 90º (Figure I-2). The magnitude of the loss angle is dependent upon the amount of internal motion that occurs in the same frequency range as the imposed stress.

The complex dynamic modulus (E* for bending or tensile measurements, G* for shear measurements) is defined as:

$$E^* = \text{stress amplitude/strain amplitude} \tag{2-9}$$

The complex modulus, however, does not take into account the phase and it is, therefore, useful to define completely elastic component of the deformation and completely viscous component of the deformation.

The storage modulus, E' (or G' in shear) is defined as:

$$E' = \frac{\text{amplitude of the in phase stress component}}{\text{strain amplitude}} \tag{2-10}$$

And the loss modulus, E'' (or G'') is defined as:

$$E'' = \frac{\text{amplitude of the out of phase stress component}}{\text{strain amplitude}} \tag{2-11}$$

The storage modulus is the elastic response and corresponds to completely recoverable energy, whereas the loss modulus is the viscous response corresponding to energy lost through internal motion.

The tangent of the loss angle, tan δ, is dimensionless and is equal to the ratio of energy lost (dissipated as heat) to energy stored per cycle:

$$Tan\delta = \frac{\text{loss modulus}}{\text{storage modulus}} \tag{2-12}$$

The DMTA instrument can impose a sinusoidal stress on a sample, by various modes, depending on the instrument model: bending mode, shear mode, compression mode, or tensile mode, and determines the sample modulus, and tan δ, as a function of temperature and/or frequency. The bending mode is the most widely used. For large samples (e.g. ASTM bars) the cantilever accessory is used. For very stiff samples (e.g. metallic/ceramic materials) the three-point accessory is used. The tension mode is used for thin films and fibres and for elastomers below T_g. The shear mode is used or weaker samples such as gels, elastomers above T_g, and for the curing of epoxies. The compression mode is used for weak, but elastic materials, such as foams and elastomers.

If soft materials, such as rubbers and adhesives, are to be analysed, the shear sandwich geometry should be used. In this configuration, a disc or plate is affixed to the drive clamp and the sample is sandwiched between the disc and studs that are mounted on the fixed clamps. In this arrangement, he faces may be horizontal or vertical. The tensile mode utilises additional control of the static stress in the sample and can accommodate samples which relax with temperature, such as films and fibres. In this mode, the sample is mounted such that its length is parallel to the drive direction.

APPENDIX J. Rheological Assessment (Melt Volume Rate) Information

The instrument consists of a vertical cylinder with a small die of 2 mm at the bottom and a removable piston at the top (Figure J-1). A charge of material is placed in the cylinder and preheated for several minutes. The piston is placed on top of the molten polymer and its weight forces the polymer through the die and on to a collecting plate. The amount of polymer collected after a specific interval is weighed and normalised to the number of grams that would have been extruded in 10 minutes. Thus, the melt flow rate is expressed in grams per reference time. Knowing the mean cross-sectional area of the piston and the cylinder, one can obtain the MVR value (cm^3/10 min).

The melt flow rate of polymers is dependent on the rate of shear. The shear rates in this test are much smaller than those that are used under normal conditions of processing. Therefore, data obtained by this method may not always correlate with the behaviour of the polymers in actual use. The melt flow rate concept (in volume or mass) was originally designed for simple homopolymers, such as polyethylene and polypropylene. Nevertheless, this technique has been widely used to characterize a variety of materials, including filled systems and blend systems.

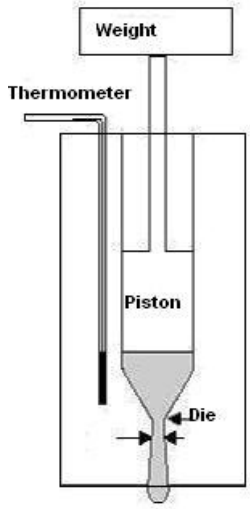

Figure J-1. Schematic representation of the melt flow testing.

APPENDIX K. Nomenclature

Section 1.1.1.:

PC – Polycarbonate

PBT - Poly(butylene terephthalate)

PC/PBT - polycarbonate/poly(butylene terephthalate)

MBS – methyl methacrylate-butadiene-styrene

Section 1.2.1.

LCST - lower critical solution temperature

ΔG_{mix} - Gibbs free energy of mixing

ΔH_{mix} - enthalpy of mixing

ΔS_{mix} - entropy of mixing

ϕ - molar fraction

UCST - upper critical solution temperature

R – ideal gas constant

T – temperature

n_i - number of moles of molecules of component i

Section 1.2.2.

δ_T - solubility parameter

ΔH_v - molar vaporisation energy

V - molar volume

δ_d – dispersive component of the solubility parameter

δ_T – specific component of the solubility parameter

Section 1.2.3.

χ – Flory-Huggins interaction parameter

μ - chemical potential

φ - volume fraction

Section 1.2.4.

W_a - thermodynamic adhesion energy

γ - surface tension

γ_{12} - interfacial tension

γ_d - dispersive component of the surface tension

γ_p - polar component of the surface tension

W_{ab} – Lewis acid/base component of the work of adhesion

W_d – dispersive component of the work of adhesion

γ^+ - acidic component of the surface tension

γ^- - basic component of the surface tension

Section 1.2.5.

IGC – inverse gas chromatography

GC – gas chromatography

t_r – retention time of probe molecules

T_g – glass transition temperature

T_m – melting temperature

Section 1.2.5.1.

PE – poly(ethylene)

PVC – poly(vinyl chloride)

Section 1.2.5.2.

V_n – net retention volume

v_2 – specific volume

p_1^0 - saturation vapour pressure of the molecular probe

B_{11} - second virial coefficient of the probe

χ_s - entropic contribution to χ

Section 1.2.5.3.

t_o - retention time of a non-interacting probe species

F - carrier gas flow rate

J - term correcting for the compressibility of the carrier gas

P_i - inlet pressure of the carrier gas

P_o - outlet pressure of the carrier gas

C - correction factor, allowing for the vapour pressure of the water at the temperature of the bubble flow meter

P_{H_2O} - the vapour pressure of the water in the flow meter, at the temperature of measurement

V_g – specific retention volume

m – mass of interacting stationary phase

k_s - partition coefficient for the surface adsorption

k_a - partition coefficient for the bulk absorption

V - volume of the adsorbate

A - area of the adsorbate

c – concentration of the probe molecules on the gas phase

Γ - partition function that accounts for the probe excess concentration on the surface

p - partial pressure of the probe molecules

K - term that includes all the constants that are present in Equation 1-31

π - pressure of the probe on the surface

ΔG_a – energy of adsorption

P_g^s - pressure of a reference gas phase

P_s^s - pressure of a reference adsorption phase

γ_s^d - dispersive component of the surface free energy of a solid

γ_l^d - dispersive component of the surface free energy of a liquid

N_A - Avogadro's constant

a - molecular surface area of the adsorbed species

T_b - boiling point of the probe molecules

ΔG_a^d - term that represents the dispersive Lifshitz-van der Waals contribution to the total free energy of adsorption

ΔG_a^s - term that represents the Lewis acid/base contribution to the total free energy of adsorption

$V_{n,ref}^{d}$ - retention volume that is derived from the n-alkanes reference line

ΔH_a – enthalpy of adsorption

ΔS_a – entropy of adsorption

ΔH_a^s - specific component of the enthalpy of adsorption

ΔS_a^s - specific component of the entropy of adsorption

ΔH_a^d - dispersive component of the enthalpy of adsorption

ΔS_a^d - dispersive component of the entropy of adsorption

K_a – Lewis acidity constant

K_b – Lewis basicity constant

DN - Gutmann's donor number

AN - Gutmann's acceptor number

AN^d - dispersive contribution to AN

AN – modified Gutmann's acceptor number

C and E – Drago parameters expressing covalent and electrostatic contributions, respectively, to the acidity and to the basicity of a substance

I_{sp1}, I_{sp2} and I_{sp3} – Lewis acid/base interaction parameters

Section 1.3.1.

PET – poly(ethylene terephthalate)

EVA – ethylene-vinyl acetate copolymer

LLDPE – low pressure, low-density poly(ethylene)

EPR – ethylene-propylene rubber

EPDM – ethylene-propylene-diene rubber

NBR – nitrile rubber

Section 1.3.2.1.

ΔH_f^o - enthalpy of fusion

Section 1.3.2.2.

DMTA - dynamic mechanical thermal analysis

Section 1.3.2.3.

PMMA – poly(methyl methacrylate)

MMA – methyl methacrylate

Section 1.4.

T_c – crystallisation temperature

DSC – Differential scanning calorimetry

TGA – thermogravimetric analysis

SEM – scanning electron microscopy

TEM –transmission electron microscopy

OM – optical microscopy

FTIR – Fourier transform infra-red spectroscopy

NMR – nuclear magnetic resonance

Section 1.4.3.

DTA – dynamic thermal analysis

DMA – dynamic mechanical analysis

WAXS - wide angle X-ray scattering

Section 1.4.4.

IM – impact modifier

Section 1.6.2.

$CoAl_2O_4$ – cobalt aluminate

λ - order parameter (degree of inversion)

XRD – X-ray difraction

EDX – Energy Dispersive X-ray Spectrometry

Section 2.1.

PELTP – [pentaerythritol tetrakis(3-n-dodexyl thiopropionate)]

MZP - monozinc phosphate

$\bar{M}_w$ - weight-average molecular weight

$\bar{M}_n$ - number-average molecular weight

D – polydispersity

rpm – rotations per minute

Section 2.3.3.

MAI – multi-axial impact

$T_{c,on-set}$ - crystallisation on-set temperature

$T_{c,off-set}$ - crystallisation off-set temperature

T_c – enthalpy of crystallisation

$-\Delta H_c$ – enthalpy of crystallisation

C - heat capacity

q - heat flow

c – cooling rate

x_{PBT} - mass fraction of PBT

m – mass of sample

Section 2.4.3.

E* - complex dynamic modulus

E' – strorage modulus

E'' – loss modulus

tan δ – loss tangent

Section 1.3.2.1.

C6 – n-hexane

C7 – n-heptane

C8 – n-octane

C9 – n-nonane

C10 – n-decane

C11 – n-undecane

TCM – trichloromethane

DCM – dichloromethane

DEE – diethyl ether

THF – tetrahydrofuran

Acet – acetone

EtAcet – ethyl acetate

Section 2.7.

GPC – gel permeation chromatography

PS – poly(styrene)

Section 2.9.

MVR – melt volume rate

Section 2.10.

VST – Vicat softening temperature

Section 2.13.

hiwre – “Lewis acidic” pigment

hiwren – “neutralized” hiwre pigment

MAA – methacrylic acid

TEA – triethylaluminium

Section 3.3.3.

E - surface modification effectiveness

pH_{H_2O} - pH value for the dispersion medium

Section 3.3.3.

W_f - mass of dried, extracted, surface-treated pigment

W_c - the mass of pigment prior to the surface treatment